Metabolic dependencies of breast cancer cells

Franziska Baenke

University College London
and
Cancer Research UK London Research Institute

Primary Supervisor: Dr. Almut Schulze
Secondary Supervisor: Prof. Julian Downward
Tertiary Supervisor: Dr. Michael Howell

A thesis submitted for the degree of Doctor of Philosophy
University College London

December 2012

Declaration

I, Franziska Baenke, confirm that the work presented in this thesis is my own. Where information has been derived from other sources, I confirm that this has been indicated in the thesis.

Abstract

Metabolic dependencies of breast cancer cell lines under normoxia and hypoxia

Cellular metabolism is one of the core processes for cell growth and proliferation. This process is altered in cancer cells as most solid tumours exhibit increased glucose uptake and lactate secretion, a feature known as the Warburg effect. These metabolic changes are the consequence of oncogene activation, loss of tumour suppressor function and/or mutations in metabolic enzymes. However, cancer cell metabolism is not limited to the Warburg effect and the exact role the metabolic machinery plays in facilitating proliferation and cell survival in different cancer types is still poorly understood and requires further study.

Breast cancer is a complex and heterogeneous disease at the molecular level. In addition, the PI3K/AKT signalling pathway is frequently activated in breast cancers due to loss of the PTEN tumour suppressor, oncogenic activation of *PIK3CA* or overexpression of certain growth factor receptors.

This study aimed to investigate whether the metabolic requirements of breast cancer cell lines are determined by their molecular alterations. By using RNA interference (siRNA), the expression of 231 metabolic enzymes, transporters and metabolic regulators of the cellular glucose and lipid metabolism were ablated in a panel of 14 breast cancer cell lines and 3 non-malignant breast cell lines with distinct molecular characteristics.
Solid breast tumours are known to have regions of high/low delivery of nutrients and oxygen that facilitate changes in the metabolic dependencies of cancer cells that reside within these areas. Moreover, these solid tumours that contain regions of poor oxygen delivery are associated with cancers refractive to treatment and that have poorer overall survival. Thus, to examine the metabolic dependencies of cells that reside in these regions, an environment of low oxygen was recapitulated and the effect of silencing of metabolic genes on cell survival was assessed. Crucially, this approach has led to the identification of previously known and novel metabolic genes that are essential for survival of breast cancer cells for each of the defined breast cancer subgroups.

In addition, the characterisation of the metabolic requirements and processes revealed that each subgroup displays a distinct metabolic phenotype that might provide potential novel molecular targets that could be exploited therapeutically.

Acknowledgement

Firstly, and most importantly, I would like to thank my supervisor, Dr. Almut Schulze for giving me the opportunity to be a PhD student in her lab. Thank you for your help, advice and patience over the last four years.

I would also like to thank all of the past and present members of the Gene Expression laboratory. Beatrice, for sharing all your technical knowledge with me and helping me during my PhD years. Emma, Barrie, Heike, Susana, Caroline and Claudio I feel so fortunate that I was able to work with and learn from you all. Thank you for teaching me so much and for always being so supportive (even after some of you left the lab).

Thank you to Dr. Nicola Zamboni, Sebastien Dubuis, Dr. Alan Mackay, Prof. Gordon Stamp and Prof. Jorge Reis-Filho for their willingness to collaborate and sharing their knowledge and expertise with me. I would like to acknowledge the members of my thesis committee, Prof. Julian Downward and Dr. Michael Howell, for guiding my project. I am also very grateful to Dr. Britta Weigelt for helping me to understand the complexity of breast cancer and sharing her broad knowledge with me.

There are many LRI services that have contributed to the work presented in this thesis. Special thanks goes to Ming and Mike of the High Throughput Screening laboratory, everyone in the Equipment Park, especially to Dave who was patient and helpful during all my mini-prep and sequencing samples, Andy of the FACS facility, Bradley and Richard for making it possible to perform Immunohistochemistry on the fiddly spheroids. I would also like to thank our lab aides, Chris and Ian, for keeping the 1st floor, organised, tidy and being always pleasant.

I would also like to thank Dr. Sally Leevers, Dr. Sophie Lutter, Sabina Ebbols and David Bacon, for making the LRI graduate program work so smoothly and for creating such a great student community.

Thank you to all of my friends for helping and encouraging me during my PhD (Sophie Z, Sophie L, Christoph, Sandra and Nancy). Special thanks goes to my always optimistic PhD buddy and friend, Hollie, and to my long time friend Ivonne - this PhD would have been so tough without you guys. Moreover I would like to thank Britta for

all her support often over a shared love of bento box.

Ein riesengroßes Dankeschön an meine Eltern Reinhard und Christine, meine Großeltern und meiner ganzen Familie für die unendliche Unterstützung, Liebe und den Versuch meine Arbeit/Experimente zu verstehen.

Above all, I would like to thank Garry who has been supportive, understanding and patient. During my PhD Garry became a very good presenter of cancer metabolism through osmosis, after listening to many of my practice talks!

Finally, I would like to thank CRUK for funding my placement as a graduate student and the generosity of the public for donating to such an amazing charity.

Table of Contents

Table of figures

List of tables

Abbreviations

2D	Two-dimensional
2-DG	2-Deoxyglucose
2-HG	2-Hydroxyglutarate
3D	Three-dimensional
3BP	3-Bromopyruvate
ACC	Acetyl-CoA carboxylase
ACLY	Acetyl-CoA
ACSS2	Acetyl-CoA synthase 2
AKT	Protein Kinase B
ALDOA	Aldolase A
AML	Acute myeloid leukemia
AMP	Adenosine monophosphate
AMPK	AMP kinase
amu	Atomic mass unit
ARNT	Aryl hydrocarbon receptor nuclear translocator
ATCC	American Type Culture Collection
ATP	Adenosine triphosphate
BDT	Big dye terminator
BRCA1	Breast cancer type 1
BRCA2	Breast cancer type 2
BSA	Bovine serum albumine
BSG	Basigin
CAF	Cancer associated fibroblasts
CAIX	Carbonic anhydrase 9
ccRCC	Clear cell renal cell carcinoma
cDNA	Complementary DNA
CGH	Comparative genomic hybridization
CHREBP	Carbohydrate Response Element Binding Protein
CT	Cholera toxin
DAPI	4’,6-Diamidine-2’-phenylindole dihydrochloride
DCA	Dichloroacetate
DMSO	Dimethyl sulfoxide
dNTP	Deoxyribonucleotide triphosphate
dox	Doxycycline
dsRNA	Double-stranded RNA
ECAR	Extracellular acidification rate
ECM	Extracellular matrix
EcoR	Ecotropic receptor
EGF	Epidermal growth factor
EGFR	Epidermal growth factor receptor
ENO	Enolase
EPO	Erythropoietin
ER	Estrogen receptor
ERE	Estrogen response element
ETC	Electron transport chain
EtOH	Ethanol

FACS	Fluorescence-activated cell sorting
FASN	Fatty acid synthase
FBS	Fetal bovine serum
FCCP	Carbonylcyanide-p-trifluoromethoxyphenylhydrazone
FDG	Fluorodeoxyglucose
FIH	Factor inhibiting HIF-1
FOXO1	Forkhead box O1
G6PD	Glucose-6-phosphate dehydrogenase
GLS2	Glutaminase 2
GLUT	Glucose transporter
GOF	Gain-of-function
GPX	Glutathione peroxidase
GSH	Glutathione, reduced
h	Hour(s)
H_2O_2	Hydrogen peroxide
HBSS	Hank's Balanced Salt Solution
HC	Hydrocortisone
HCl	Hydrogen chloride
HEK	Human embryo kidney cells
HER2	Human epidermal growth factor receptor 2
HIF	Hypoxia inducible factor
HTS	High Throughput Screening
IRS1	Insulin receptor substrate 1
KEGG	Kyoto Encyclopedia of Genes and Genomes
LDHA	Lactate dehydrogenase A
LDHB	Lactate dehydrogenase B
LOF	Loss-of-function
LPP	Lipid phosphatase phosphate
MAD	Median absolute deviation
MAPK	Mitogen activated protein kinase
MCT1	Monocarboxylate transporter 1
MCT4	Monocarboxylate transporter 4
ME1	Malic enzyme 1
ME2	Malic enzyme 2
MEF	Mouse embryo fibroblast
min	Minute(s)
MMP	Metallomatrixproteinases
mTOR	Mammalian target of rapamycin
MWU	Mann-Whitney-U test
NAC	N-acetyl cysteine
NAD+	Nicotinamide adenine dinucleotide
NADP+	Nicotinamide adenine dinucleotide phosphate
NGS	Normal goat serum
OCR	Oxygen consumption rate
ODD	Oxygen-dependent degradation domain
OS	Overall survival
PA	Phosphatidic acid
PCAF	P300/CBP-associated factor

PDGF	Platelet-derived growth factor
PET	Positron emission tomography
PFA	Paraformaldehyde
PFK	Phosphofructokinase
PHD	Prolyl-hydroxylase domain enzymes
pH_e	Extracellular pH
PHGDH	Phopshoglycerate dehydrogenase
pH_i	Intracellular pH
PK	Pyruvate kinase
PI	Phosphatidyl-inositol
PI3K	Phosphoinositol-3-kinase
PIP	Phosphatidyl-inositol-phosphate
PPP	Pentose phosphate pathway
PR	Progesterone receptor
PTEN	Phosphatase and tensin homolog
RNAi	RNA interference
ROS	Reactive oxygen species
RFU	Relative fluorescent unit
S6K	S6-kinase
SCO	Cytochrome c oxidase
SD	Standard deviation
SDS	Sodium dodecyl sulfate
sec	Second(s)
SEM	Standard error of mean
SERM	Selective ER modulators
shRNA	Short-hairpin RNA
siRNA	Small interfering RNA
TBS	Tris-Buffered Saline
TBST	Tris-Buffered Saline and Tween 20
TCA	Tricarboxylic acid cycle
TEMPOL	4-Hydroxy-TEMPO
TKTL	Transketolase like
TMA	Tissue microarray
TNBC	Triple negative breast cancer
UPGMA	Unweighted Pair Group Method with Arithmetic Mean
VEGFA	Vascular endothelial growth factor A

1 Introduction

1.1 Cancer

Cancer is defined as not one but an array of diseases with more than 200 different types depending on the cell and tissue of origin. The latest research studies show that the incidence rates for cancer are increasing and that by 2040 one in four people aged over 65 in the United Kingdom will be cancer survivors (Maddams et al., 2012), making cancer one of the most significant causes of mortality not only in the UK, but throughout the developed world. This underlines the importance of continuing the efforts to get a better understanding of the complexity of cancer and to discover novel therapeutic strategies.

The progression from a normal cell to a cancerous cell is a multistep process that reflects the accumulation of genetic and epigenetic alterations within a cell's genome. In general, high-frequency mutations in cancer are mainly found in proto-oncogenes and tumour suppressor genes. Gain-of-function (GOF) mutations in proto-oncogenes result in hyperactive forms, termed oncogenes that can promote cell transformation. Conversely, loss-of-function (LOF) mutations in tumour suppressor genes, expression of which usually restricts cell transformation, result in a hypoactive or inactive state of the respective gene. Complex alterations occur during the process of transformation and some cancer cells become dependent on the continued activation of a single gene/pathway. This dependence is termed 'oncogene addiction' (Weinstein and Joe, 2008). In addition to high-frequency mutations, recent sequencing studies show that cancer cells harbour a large number of low-frequency aberrations (Kan et al., 2010; Shah et al., 2012).

The common phenotypes that contribute to the transformation process from a normal cell to a cancerous cell have been described as the 12 hallmarks of cancer (Hanahan and Weinberg, 2011). These hallmarks are depicted in Figure 1.1. One of these hallmarks is the independency from external proliferative signals due to upregulation of growth factor receptors, or mutations in growth factor signalling cascades. Moreover, cancer cells resist inhibitory signals that would normally halt proliferation and cell growth.

Furthermore, cancer cells have the ability to evade stimuli that lead to the induction of apoptosis. Another hallmark of cancer is the ability to overcome the limited number of replication cycles that normal cells are restricted to, giving cancer cells unlimited replicative potential.

Another important hallmark of cancer is the activation of cell migration and invasion that is a prerequisite of metastasis formation. Cancer cells lose the expression of certain cell/cell and cell/matrix adhesion molecules and become able to invade into local blood or lymph vessels and disseminate to distant tissues (Hanahan and Weinberg, 2011). The proliferation and growth advantage of cancer cells is often associated with the deregulation of metabolic processes. The metabolic reprogramming of cancer cells allows them to not only survive but also grow under conditions of stress, such as nutrient and oxygen starvation, which contributes to tumorigenic potential. In addition, the deprivation of oxygen is a common feature of the tumour microenvironment and leads to the induction of new blood vessels, a process termed 'tumour angiogenesis'. Tumour angiogenesis supports the supply of oxygen and nutrients to the growing tumour and facilitates invasion and metastasis.

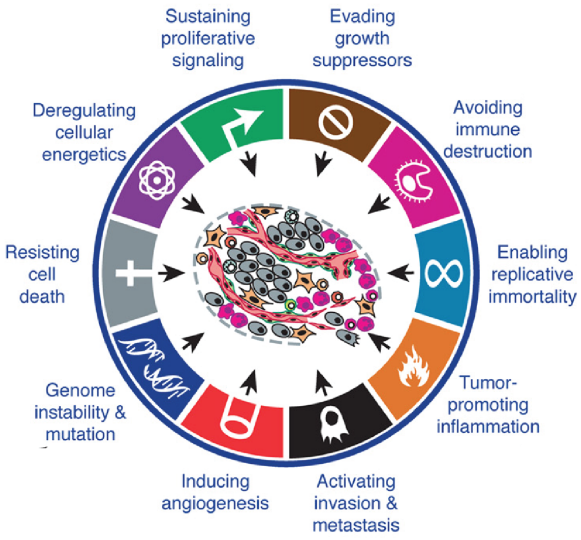

Figure 1-1 The hallmarks of cancer

This schematic overview is adapted from (Hanahan and Weinberg, 2011) and illustrates the hallmarks of cancer. These hallmarks are defined by intracellular processes (e.g. genome instability), intercellular signalling between tumour cells and/or other cell types (e.g. cancer-associated fibroblasts, immune cells) and extracellular interactions between tumour cells and the microenvironment.

1.2 Breast Cancer

1.2.1 Incidence

Breast cancer is the most common type of cancer occurring in women of the developed and developing world, comprising 16 % of all mortality cases in cancer. In 2010, 49,961 new breast cancer cases and 11,633 breast cancer-related deaths were reported in the United Kingdom alone (source Office of National Statistics http://www.ons.gov.uk).

In recent years, despite the increase in breast cancer incidence, mortality rates have decreased. This has been attributed to screening programmes and earlier detection of the disease, the advances in the understanding of the biology of breast cancer, and the development of novel therapeutic strategies for the treatment of patients with this disease (www.cancerresearchuk.org/cancerinfo/cancerstats/types/breast/incidence).

Most cases of breast cancer occur sporadically. However, approximately 5-10% of all breast cancers are hereditary and develop in individuals who have a breast cancer predisposition due to germline gene mutations (Scheuner et al., 2010; Slattery and Kerber, 1993). The genes most frequently linked to hereditary breast cancer are breast cancer type 1 (BRCA1) and breast cancer type 2 (BRCA2) susceptibility proteins, which together account for approximately 2% of all breast cancers (Malone et al., 2006; Papelard et al., 2000).

Historically, breast cancer was defined as a single disease, but it is now appreciated that breast cancer is a heterogeneous and complex disease and in fact encompasses multiple diseases in the same anatomical site.

1.2.2 Breast cancer treatment

Successful cancer treatment requires the complete eradication of tumour cells to prevent recurrence, which is the main cause of mortality. The current standard of care for patients with primary breast cancer is local management, including surgery and radiotherapy, and adjuvant systemic treatment (i.e. endocrine therapy and/or chemotherapy and/or molecularly targeted therapies) to reduce the risk of disease relapse. Treatment decisions are based on a number of clinical parameters, including age of the patient, tumour size, regional and lymph node metastasis, and histological

parameters, including histological grade and expression of hormone receptors (estrogen receptor (ER) and progesterone receptor (PR)) and the Human Epidermal Growth Factor Receptor 2 (HER2).

Patients with ER-positive/HER2-negative breast cancers tend to have a better prognosis and outcome than patients with ER-negative/HER2-negative or *HER2*-amplified breast cancers (Fan et al., 2006). As ER-positive/HER2-negative tumours are dependent on estrogen for proliferation, therapeutic intervention with selective ER modulators (SERMs) have been proven successful in the clinic. Approaches to target ER signalling in ER-positive breast cancers include anti-estrogens (such as Tamoxifen and Fulvestrant), which bind to the ER and inhibit its function, and aromatase inhibitors, which block estrogen synthesis thereby depriving the tumour of this important growth-promoting signal (Johnston, 2010).

HER2-positive breast cancer cells depend on the activation of the HER2 onco-protein, and multiple strategies to inhibit this molecular target have been developed. To date, the most successful strategy produced the humanised monoclonal antibody Trastuzumab (also known as Herceptin), which binds to the extracellular domain of HER2 and inhibits its function as an activator of intracellular signalling pathways that drive proliferation (Hudis, 2007). Trastuzumab has been shown to improve overall survival (OS) by 33-35% of breast cancer patients with HER2-positive tumours in combination with chemotherapeutic drugs such as paclitaxel (Perez et al., 2008; Romond et al., 2005). An alternative approach to treat HER2-positive tumours is to inhibit HER2 activity by targeting the intracellular tyrosine kinase domain. The most established small molecule inhibitor targeting HER2 is Lapatinib, an orally administered dual inhibitor that blocks the activity of HER2 and epidermal growth factor receptor (EGFR) through reversible binding (Burris, 2004). Lapatinib is currently approved for the treatment of patients with metastatic breast cancer (Opdam et al., 2012).

Breast tumours that do not express hormone receptors or HER2, i.e. the ER-negative/HER2-negative cancers, do not benefit from the endocrine and anti-HER2 therapies mentioned above and are treated using conventional cytotoxic and/or spindle-

poison agents (e.g. paclitaxel, docetaxel, capecitabine, gemcitabine) (Foulkes et al., 2010).

The genetic heterogeneity of breast cancer is an ongoing challenge for clinicians as patients that have breast cancer with identical clinicopathological characteristics may have markedly distinct outcomes. There is therefore a clear need to identify additional markers to help selecting those patients that may benefit from a certain type of therapy.

1.2.3 Breast cancer classification

To account for the heterogeneity and reduce the complexity of breast cancer, different classification systems have been introduced. These include a) a histological classification (Lakhani et al., 2012), b) a clinical classification system based on the expression of hormone receptors and HER2, the predictive markers and targets of endocrine and anti-HER2 treatments, and c) a molecular classification system based on gene expression profiling.
Recent sequencing studies analysing the entire genome or exome (only the coding regions of the genome) of breast tumours, as well as comparative genomic hybridization (CGH) that detect gene copy number and changes using single nucleotide polymorphism (SNPs), revealed that breast cancers can also be classified depending on their repertoire of genetic aberrations (CancerGenomeAtlasNetwork, 2012; Curtis et al., 2012; Shah et al., 2012). The genetic landscape of breast cancer is discussed in section 1.2.4.

1.2.3.1 Molecular classification

The molecular classification of breast cancer is based on gene expression profiling by using complementary DNA (cDNA) microarrays (DeRisi et al., 1996). Such profiling has unravelled breast cancer as a disease with multiple transcriptional subtypes. Using so called ‘intrinsic gene lists’ and hierarchical clustering analyses, it has been found that ER-positive and ER-negative breast cancers differed significantly at the transcriptional level (Perou et al., 2000; Sorlie et al., 2001). Within the ER-positive and ER-negative subgroups at least five molecular subtypes have been identified: Two ER-positive subtypes termed luminal A and luminal B, and three ER-negative subtypes termed

basal-like, ERBB2-enriched and normal-like breast cancers (Cheang et al., 2008; Hu et al., 2006; Parker et al., 2009; Reis-Filho and Pusztai, 2011; Sorlie et al., 2003). Importantly, these molecular subtypes have been shown to be associated with distinct outcomes. Women with luminal A breast cancers have the best prognosis while patients with a basal-like or ERBB2-enriched breast cancer have the worst outcome (Hu et al., 2006; Parker et al., 2009). However, this molecular classification system is still evolving as additional ER-negative molecular subtypes have been identified, including the molecular apocrine subtype (Doane et al., 2006; Farmer et al., 2005; Guedj et al., 2012) and claudin-low breast cancers (Prat et al., 2010).

1.2.3.2 Clinical classification

The clinical classification of breast cancer is based on the expression of the hormone receptors, which predict response to endocrine therapy, and growth factor receptor HER2, which is the molecular target of Trastuzumab and is used as a predictive marker for the response to this drug.

1.2.3.2.1 Estrogen receptor-positive, HER2-negative breast cancer

The majority of breast cancers (approximately 70%) express estrogen receptor α (ERα) and are sensitive to estrogen. Estrogen diffuses through the plasma membrane and binds to the ER within the cytoplasm. This complex then translocates to the nucleus where it binds to estrogen responsive element (ERE) sequences in the promoter regions of its target genes. In addition, estrogen can also bind to ER molecules that are located in or close to the plasma membrane. ERα and ERβ are the two main forms of ER and are encoded by different genes: *ESR1* and *ESR2*, respectively. These receptors display some differences in their tissue specific expression pattern, but can also be co-expressed within the same tissue (Deroo and Korach, 2006).

1.2.3.2.2 *HER2*-amplified/HER2-positive breast cancer

HER2-amplified breast cancers are characterised by the amplification of the *ERBB2* gene locus on chromosome 17q12-q21, which codes for the receptor tyrosine kinase HER2 (Arriola et al., 2008). Amplification or overexpression of HER2 is observed in 15-20% of all breast cancer cases. This subtype is a more aggressive form of breast

cancer and leads to a worse outcome compared to ER-positive breast cancers (Slamon et al., 1987).

HER2-positive breast cancers can be further classified by the expression of ER (Marchio et al., 2008). HER2-positive breast cancers positive for ER expression belong to the luminal B gene expression subtype, whereas HER2-positive breast cancers with less than 1% ER expression belong to the ERBB2-enriched gene expression subtype.

1.2.3.2.3 ER-negative, HER2-negative breast cancer

Breast tumours that lack expression of ER, PR and HER2 belong to the subtype of ER-negative/HER2-negative breast cancer. This group has also been termed triple negative breast cancer (TNBC) and accounts for approximately 15-20% of all breast cancer cases (Foulkes et al., 2010). The clinical definition suggests that this cancer type cannot be treated with Trastuzumab or endocrine therapy given that it is not driven by, and that lacks the expression of, the respective molecular markers HER2 and ER/PR. The TNBC subtype is a heterogeneous subtype and is comprised of different subgroups such as basal-like breast cancer (75%) with minor groups including claudin-low breast cancers (Foulkes et al., 2010; Lehmann et al., 2011). TNBCs display the worst OS with very limited treatment options (Foulkes et al., 2010; Perou, 2011).

1.2.4 Genetic landscape of breast cancer

The genetic alterations in breast cancer are defined by only a few highly recurrent mutations. These mutations mostly affect well-established oncogenes and tumour suppressors including *TP53*, *PIK3CA*, and *PTEN*. Recent studies investigated the genetic composition of thousands of breast tumours by sequencing, CGH, and gene expression profiling (Curtis et al., 2012; Marcotte et al., 2012) and revealed numerous additional mutations that are rare and affect less than 3% of breast cancer patients (i.e. non-recurrent mutations). Interestingly, 50% of these mutations affect the JUN signalling cascade (Hartmaier et al., 2012).

1.2.4.1 The PI3K pathway

The most prevalent genetic alterations in breast cancer affect the phosphatidylinositol-3-kinase (PI3K) signalling pathway. This signalling pathway consists of a family of

proteins regulating multiple cellular processes such as cell growth, cell motility, cell differentiation and cell survival (Baselga, 2011). The PI3K pathway can be activated in breast cancer through several mechanisms: constitutive signalling by growth factor receptors such as HER2 (overexpressed in 15-20%) (Slamon et al., 1987) or EGFR (overexpressed in 6-36%) (Bhargava et al., 2005; Harris et al., 1989; Walker and Dearing, 1999), activating mutations in *PIK3CA* (30%) or loss of function of PTEN (16%) (source: catalogue of somatic mutations in cancer (COSMIC)).

1.2.4.2 HER2

The receptor tyrosine kinase HER2 (*ERBB2*) is one of four members of the epidermal growth factor (EGF) receptor family (Yarden and Pines, 2012). Members of this family are expressed in multiple tissues. HER2 and EGFR (*ERBB1*) have been implicated in tumorigenesis (Hynes and Stern, 1994; Moscatello et al., 1995; Slamon et al., 1989; Sunpaweravong et al., 2005). HER2 signalling is activated by homodimer formation or by heterodimerisation with other members of the HER family (e.g. HER3 (*ERBB3*) and EGFR) in a ligand-dependent or ligand-independent manner. Overexpression of HER2 can result in ligand-independent activation of HER2 signalling due to the close proximity of receptors (Graus-Porta et al., 1997). Ligand-dependent activation results in various combinations of HER dimerisation through binding of certain ligands (e.g. EGF, neuregulin) (Olayioye et al., 2000). The extracellular domain of HER2 shows low affinity towards these ligands (Alroy and Yarden, 2000).
Activated HER2 promotes the activity of two main downstream signalling cascades; the mitogen activated protein kinase (MAPK) pathway and the PI3K pathway (Yarden and Sliwkowski, 2001). Interestingly, the activation of the ER can also activate ERBB signalling through stimulation of matrix metalloproteinases (MMP) to release EGF (Razandi et al., 2003).

1.2.4.3 PI3Ks

All enzymes of the PI3K family are heterodimers that consists of a catalytic and a regulatory subunit. They catalyse the phosphorylation of the 3'-hydroxyl group of different phosphatidylinositol phosphates (PIPs) or phosphatidylinositol (PI). Class IA PI3Ks selectively phosphorylate phosphatidylinositol-4,5-bisphosphate (PIP_2) to

generate phosphatidylinositol-3,4,5-trisphosphate (PIP_3). PIP_3 acts as a second messenger and is important for the activation of specific signalling cascades. Under resting conditions, cellular PIP_3 levels are very low due to the negative regulation of the PI3K pathway by the phosphatase and tensin homolog on chromosome 10 (PTEN), a lipid phosphatase that removes the 3'-phosphate group from PIP_3 (Vanhaesebroeck et al., 2010).

Class I PI3Ks are mostly activated in response to growth factor receptor signalling (Katso et al., 2001). Class IA consists of three isoforms of the catalytic subunit p110 (α, β and δ) and three isoforms of the regularly subunit p85 (α, β and δ). The proto-oncogene p110α is encoded by the *PIK3CA* gene and is frequently mutated in human cancer. In common tumour types including breast cancer, 80% of these gain of function mutations occur in exons 9 and 20, in particular in two hot spots within the catalytic domain of p110α (E545 and H1047) (Samuels et al., 2004). One of the downstream targets of class I PI3Ks is the threonine/serine kinase AKT, which regulates numerous cellular processes including cell growth, motility, proliferation and cell survival (Engelman et al., 2006; Vanhaesebroeck et al., 2010).

1.2.4.4 Tumour suppressor PTEN

PTEN was first identified as a potential tumour suppressor in 1997 when deletions of the gene were found in brain, breast and prostate cancer (Li et al., 1997). *PTEN* is now established as one of the most frequently mutated tumour suppressor genes in sporadic cancer. Germline mutations of *PTEN* have been found in patients with Cowden disease, a genetic disorder that leads to a higher risk of cancer (Sansal and Sellers, 2004).

PTEN is both a lipid and a protein phosphatase. PTEN acting as a lipid phosphatase de-phosphorylates the 3' position on PIP_3, thereby negatively regulating the downstream effectors of PI3K, including PDK1 and AKT. The protein phosphatase activity of PTEN has been shown to regulate cyclin D and the family members of the family of SRC kinases (Hollander et al., 2011). Loss of PTEN activity results in hyperactive PI3K/AKT signalling and can contribute to tumour development and progression. According to the COSMIC database, *PTEN* is mutated in only 6% of all breast cancers. However, approximately 40% of all breast cancer tissue samples show loss of PTEN expression (Perez-Tenorio et al., 2007). This is due to mechanisms (such as microRNA

targeting of PTEN mRNA or protein degradation pathways) that result in downregulation of PTEN expression. Of note, mutations in *PTEN* and *PIK3CA* are generally mutually exclusive in breast cancer (Saal et al., 2005).

1.2.4.5 TP53

The *TP53* gene encodes the transcription factor, which is activated in response to various cellular stresses, including hypoxia and DNA damage (Vogelstein, 2000). Under non-stressed conditions, p53 is expressed at low levels due to its relatively short protein half-life of about 30 minutes (Maltzman and Czyzyk, 1984). Stress signals activate p53 mostly by translational or posttranslational modifications that lead to stabilisation and nuclear accumulation of the protein. A major regulator of p53 stability is the ubiquitin ligase MDM2, which inhibits p53 by mediating its ubiquitination and proteasomal degradation (Michael and Oren, 2003). Activated p53 controls the transcription of numerous targets genes that regulate cell cycle arrest (e.g. p21) and apoptotic cell death pathways (e.g. BAX, NOXA, PUMA) (Riley et al., 2008).
Functional p53 can suppress cell proliferation and induce cell death in response to anti-proliferative stimuli. Loss of p53 promotes uncontrolled proliferation of cancer cells and promotes genetic instability. p53 is one of the most important tumour suppressors and is mutated in up to 50% of sporadic human cancers (Soussi and Lozano, 2005). The rate of p53 mutations in breast cancer is 50%-74% (Forbes et al., 2011; Kan et al., 2010). Moreover, p53 status in breast cancer can influence the clinical response to chemotherapy (Jackson et al., 2012).

1.2.4.6 Additional mutations in breast cancer

Recent studies by the Cancer Genome Atlas Network (CancerGenomeAtlasNetwork, 2012), the Cancer Genome Project (Nik-Zainal et al., 2012a; Nik-Zainal et al., 2012b; Stephens et al., 2012) and the groups of Caldas and Aparicio (Curtis et al., 2012; Shah et al., 2012) analysed between 21 and 2000 primary breast cancer by using next-generation sequencing. These studies provide a comprehensive overview of the mutational landscape of breast cancer, identifying previously unrecognised mutations, describing novel drivers of tumour development and resulting in the classification of additional clinical subtypes. These studies also confirmed the existence of multiple sub-

clones of cells within a tumour population (intra-tumoural heterogeneity). Furthermore, these studies confirmed that mutations in *TP53*, *PIK3CA* and *PTEN* were the most prevalent mutations found in breast cancer. *TP53* mutations occurred most frequently in TNBC. *PIK3CA* mutations were prevalent in the ERBB2-enriched and luminal A type, whereas *PTEN* mutations were enriched in the luminal B and basal-like subgroups. The basal-like subtype displayed the highest rate of genome instability, as determined by their CGH profiles. In addition, mutations in *ERBB2* were found in TNBC.

1.2.5 Tumour microenvironment

In addition to the genetic alterations in cancer cells, environmental factors provided by the tissue context also contribute to disease development. In particular, interactions with the microenvironment play an important role in determining how oncogenes and tumour suppressors regulate cell transformation in a tissue-specific context (Bissell et al., 2002). The microenvironment consists of different cell types such as fibroblasts, macrophages and other immune cells, extracellular matrix (ECM) components, such as collagen and fibronectin fibres, and small molecules including nutrients, ions and oxygen (discussed in more detail in 1.3.10). The 3-dimensional (3D) tissue architecture is mainly determined by cell-cell and cell-ECM interactions. During early tumorigenesis, tissue architecture remains intact. However, even occult tumour cells influence the ECM by secreting enzymes, growth factors and cytokines. These factors affect the behaviour of stromal cells and contribute to the generation of cancer-associated fibroblasts (CAF) from normal fibroblasts. The altered phenotype of CAFs influences the structure of the ECM and contributes to tumour progression and metastasis formation (Bissell et al., 2002; Xing et al., 2010).

It has been suggested that breast cancers can be classified into four different groups according to their ECM composition. The ECM type 1 is characterised by high expression of metallopeptidases and integrins and has the least favourable outcome. In contrast, ECM type 4, characterised by overexpression of serpin family members, shows a good prognosis (Bergamaschi et al., 2008).

Over the last couple of years, the importance of tumour-stroma interactions has received increasing interest. It has emerged that in addition to the important role that the tumour microenvironment plays during tumour formation and tumour progression; it can also determine the clinical response to cancer therapeutics. Straussman and colleagues investigated the sensitivities of 45 different cancer cell lines towards multiple drugs when co-cultured with 23 different stromal cell lines (Straussman et al., 2012). This study demonstrated that stromal-mediated resistance is common, particularly towards targeted agents. Moreover, a recent study in a xenograft breast cancer mouse model revealed that the chemokines CXCL1 and CXCL2 are highly expressed in tumours that have developed resistance to chemotherapy. This study showed that myeloid cells secrete inflammatory proteins that upregulated CXCL1 and CXCL2 in tumour cells (Acharyya et al., 2012). Taken together, these studies underline the importance of understanding the communication between tumour and stromal cells to improve the design of suitable therapeutic strategies.

1.3 Metabolism

1.3.1 Metabolism of quiescent and normal proliferating cells

The metabolic requirements of non-transformed (normal) cells depend on their differentiation state. Quiescent cells are metabolically active to fulfil their physiological function and to maintain their structural integrity as well as redox and energy balance. Proliferating normal cells require molecular building blocks in the form of amino acids, fatty acids and nucleotides to generate macromolecules for cell growth and division (Thompson et al., 2005; Vander Heiden et al., 2011). All cellular processes, including metabolic reactions, are tightly regulated through control systems that ensure normal cell function and maintain cell and tissue integrity. These control systems are mediated by cellular signalling processes. These signalling networks contain many of the proto-oncogenes and tumour suppressors that are also involved in cell transformation and tumour development. Any abnormal signalling cues transmitted intra- or intercellular, may result in cell cycle arrest and/or programmed cell death.

Normal cells in resting tissue are in close proximity to blood vessels that usually provide sufficient nutrients and oxygen levels for normal cell function. Cells utilise sugars, fatty acids and amino acids that are present within their environment. These nutrients have to be transported across the plasma membrane by specialised transporters and can be catabolised to provide cellular energy in the form of adenosine triphosphate (ATP). Most normal cells generate ATP through their mitochondrial metabolism, which generates NADH to drive the electron transport chain (ETC) and oxidative phosphorylation (Fig 1.2). In contrast, proliferating cells rely on glycolysis for a significant proportion of their ATP demand (Vander Heiden et al., 2009). Proliferating cells also use some nutrients directly for anabolic reactions to synthesise macromolecules. Mitochondrial respiration in normal cells recycles NADH to NAD^+ thereby coupling energy production with cofactor supply. However, in proliferating normal cells, the regeneration of NAD^+ can be achieved through both mitochondrial respiration and lactate production (Fig 1.2).

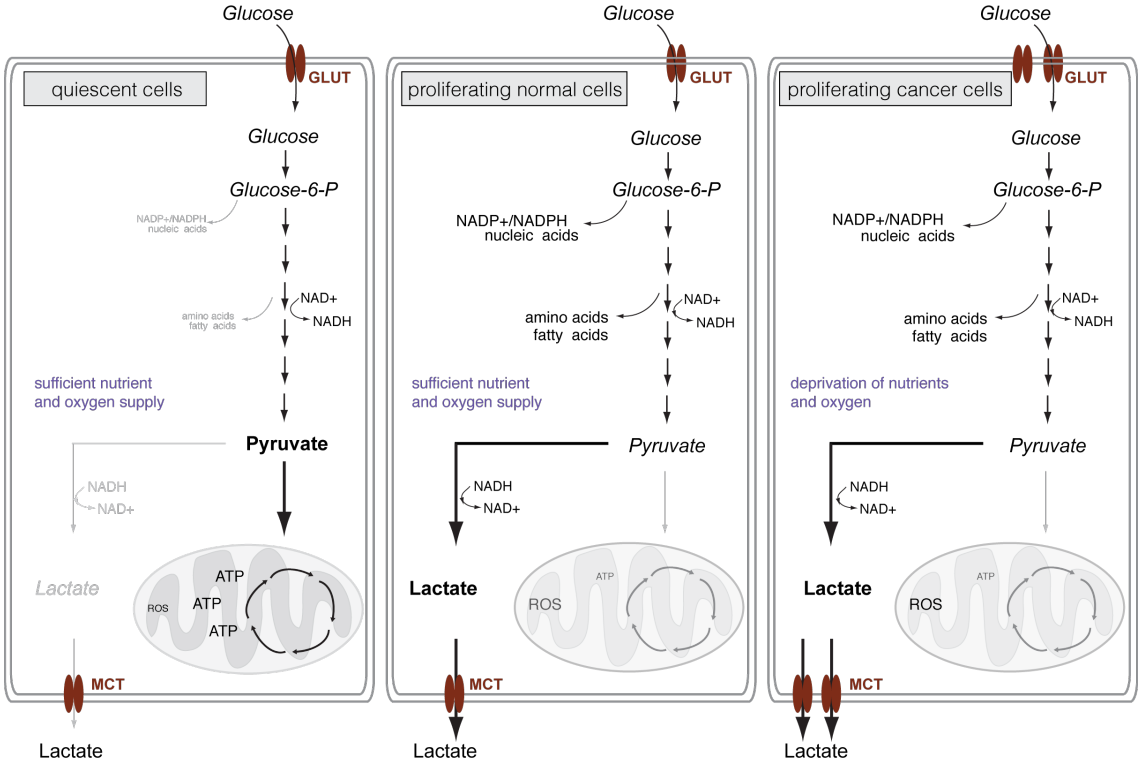

Figure 1-2 Overview of metabolic activity in quiescent and proliferating cells

Schematic representation of the metabolism in quiescent cells, proliferating normal cells and proliferating cancer cells. Quiescent cells rely mainly on mitochondrial respiration for ATP production. Proliferating cells use glucose for the conversion to pyruvate-derived lactate. They also divert carbons from glycolysis to accumulate building blocks for macromolecule biosynthesis and to maintain their redox potential. Non-malignant cells are embedded in and environment that provides sufficient nutrients and oxygen for normal cell function. In contrast, cancer cells may be exposed to nutrient and oxygen withdrawal during same stages of tumorigenesis.

1.3.2 Rewiring of cellular metabolism in cancer

Historically, the field of cancer metabolism has been dominated by the discoveries by the German biochemist Otto Warburg in the 1920s. He and his colleagues observed that malignant rodent liver cells use glycolysis for ATP production even in the presence of oxygen (Warburg, 1956; Warburg et al., 1927). This increase in glycolytic activity was accompanied by enhanced lactate secretion and was termed aerobic glycolysis, also known as the ‘Warburg effect’. These findings led to Warburg’s hypothesis that inhibition of mitochondrial respiration is the cause of cancer development, a theory that was proven wrong when the genetic contribution to cancer development was established in the 1960s.

However, the question as to why cancer cells favour the much less efficient process of aerobic glycolysis over oxidative phosphorylation remained open. One explanation for this phenomenon is that many important metabolic processes required for macromolecule biosynthesis depend on intermediates of the glycolytic pathway. Recent work in the field of cancer metabolism has demonstrated that increased glycolytic flux in cancer cells is the consequence of activation of proto-oncogenes and loss of tumour suppressors, and not impaired mitochondrial function. Cancer cells may also favour aerobic glycolysis over mitochondrial respiration to minimise the generation of reactive oxygen species (ROS). The metabolic re-programming in cancer is essential for redox balance and the synthesis of fatty acids, amino acids and nucleotides to generate macromolecules for cell growth (Fantin et al., 2006; Lunt and Vander Heiden, 2011; Moreno-Sanchez et al., 2007).

Cancer cells also influence the metabolite composition of the immediate tumour environment. The increased nutrient influx into cancer cells and their enhanced metabolic rate also leads to an increase in metabolic by-products that are secreted into the surrounding tissue. Therefore, tumour cells also need to secure mechanisms that can remove any toxic by-products in order to stabilise their intracellular as well as their extracellular environment. The following chapter will discuss core processes of metabolism in the context of the genetic and non-genetic factors that contribute to metabolic reprogramming in cancer.

1.3.2.1 Glycolysis

Glycolysis is the a metabolic process that converts 1 mole of glucose into 2 moles of pyruvate, resulting in a net gain of two moles of ATP and two moles of NADH. The fate of glucose-derived pyruvate depends on the cell type and on environmental conditions. In well-oxygenated, differentiated tissue, pyruvate enters the mitochondria and is completely oxidised to CO_2, a process that generates approximately 36 moles of ATP per mole of glucose. Under oxygen deprivation, pyruvate is converted to lactic acid. This reaction is catalysed by lactate dehydrogenase (LDH) and facilitates the conversion of NADH to NAD^+, which is a necessary cofactor for the glycolytic flux (Fig 1.3). In proliferating tissue, pyruvate is mainly converted to lactate regardless of

the oxygen concentration. Lactate produced by muscle during anaerobic exercise is converted back to pyruvate and glucose by the liver, a process of metabolic coupling known as the Cori Cycle (Cori, 1981). Pyruvate can also be converted to alanine by alanine transaminase, which connects glycolysis with amino acid metabolism (Berg et al., 2002). It is evident that pyruvate occupies a central position within the cellular energy metabolism. The different fates of pyruvate are determined by the relative needs of the cells for ATP generation and the requirement of anabolic processes for cell growth.

Many glycolytic enzymes have been shown to be upregulated during tumorigenesis. The increased glucose uptake in cancer cells is due to the upregulation of glucose transporters. There are five glucose transporters (GLUTs) in the mammalian system. GLUT1 and GLUT3 are expressed in most tissues whereas GLUT2, GLUT4 and GLUT5 show tissue specific expression patterns. GLUT1 and GLUT3 are overexpressed in many different cancer types (Yamamoto et al., 1990) and GLUT1 expression in primary tumours has been correlated to poor clinical outcome (Macheda et al., 2005). The irreversible conversion of glucose to glucose 6-phosphate (G-6-P) is catalysed by hexokinase. There are four isoforms of hexokinase (*HK1-3* and *GCK*). Hexokinase 2 (*HK2*) is upregulated in many cancers and its ablation in U87, a glioblastoma cell line, decreased cell viability (Wolf et al., 2011). HK1 and HK2 can be found in close proximity to the mitochondria and have been implicated in the prevention of intrinsic apoptotic cell death (Gottlob et al., 2001; Majewski et al., 2004).

A rate-limiting step in glycolysis is the conversion of fructose-6-phosphate (F-6-P) to fructose-1,6-bisphosphate (F-1,6-BP) regulated by phosphofructokinase1 (PFK1). The activity of PFK1 is tightly regulated through several allosteric mechanisms. High levels of ATP or citrate inhibit the activity of PFK1 and block the generation of F-1,6-BP. This results in an accumulation of upstream intermediates that can be used for other biosynthetic pathways, such as the pentose phosphate pathway (PPP) (see 1.3.2.4). Another allosteric regulator of PFK1 is fructose-2,6-bisphosphate (F-2,6-BP). This metabolite is generated from F-6-P by the activity of 6-phosphofructo-2-kinase/fructose-2,6-bisphosphatases (PFK2/FBPases). F-2,6-BP is an allosteric activator of PFK1 and high levels of this metabolite overcome the ATP-mediated inhibition of

PFK1 (Telang et al., 2006). The mammalian genome encodes four PFK2 isoforms (*PFKFB1-4*) and two of these, *PFKFB3* and *PFKFB4*, have been implicated in cancer (Bando et al., 2005; Minchenko et al., 2002). *PFKFB3* is required for anchorage-independent growth of RAS-transformed cells (Telang et al., 2006), and its inhibition impaired glycolytic flux and reduced viability of cancer cells (Clem et al., 2008). *PFKFB4* has been shown to be important for the survival of metastatic prostate cancer cells. In this context, it mainly functioned as FBPases and balanced the glycolytic flux with the production of NADPH by the PPP thereby maintaining cellular redox balance (Ros et al., 2012). *PFKFB4* is also overexpressed in primary human glioblastomas and is associated with a poor clinical outcome. The ablation of *PFKFB4* in brain cancer stem-like cells *in-vitro* caused reduction in cell number (Goidts et al., 2012). A recent finding underlined the importance of the regulation of PFK1 activity by post-translational modification. High levels of PFK1 glycosylation were observed in cancer cell lines and tumour tissues. PFK1 glycosylation was mainly mediated by O-linked β-N-acetylglucosamine (O-GlcNAc) transferase and resulted in reduced PFK1 activity. This decreased the glycolytic flux and redirected the flux of glucose to the PPP, thereby providing a selective growth advantage to cancer cells (Yi et al., 2012).

A recent study by Muller and colleagues found that a passenger mutation in enolase 1 (ENO1) renders glioblastoma cells vulnerable to ablation of enolase 2 (ENO2) and caused enhanced sensitivity towards enolase inhibition. This finding illustrates the importance of isoform compensation. Importantly, this study demonstrated that passenger mutations in non-essential genes cause cancer specific therapeutic vulnerabilities (Muller et al., 2012).

Another key player in glycolysis is pyruvate kinase (PK), which coordinates the conversion of phosphoenolpyruvate (PEP) to pyruvate. In mammals, two genes encode PK isoforms (*PKM* and *PKLR*) and the *PKM* gene can give rise to two isoforms, PKM1 and PKM2, through alternative splicing. PKM2 can adapt its activity in response to extracellular stimuli, thereby influencing the glycolytic flux. PKM2 can assemble into two different catalytically active complexes: a less active homo-dimer with low affinity to PEP and a homo-tetramer with high affinity to PEP resulting in high enzymatic activity. The conversion from a tetramer to the dimeric form is induced by binding of

PKM2 to viral oncoproteins (Zwerschke et al., 1999), the presence of phosphotyrosine-containing peptides (Christofk et al., 2008b), phosphorylation (Hitosugi et al., 2009) and the presence of ROS (Anastasiou et al., 2011). Expression of the PKM2 isoform enables cells to accumulate glycolytic intermediates upstream of PEP for biosynthetic processes. The conformational switch of PKM2 also allows cells to regulate their glycolytic flux depending on the energy demand of the cell. The expression of PKM2 is upregulated in proliferating and cancer cells (Christofk et al., 2008a). Importantly, expression of the PKM2 isoform supports tumour formation (Christofk et al., 2008a).

Some cancers, including lung and breast cancer, show a high expression of lactate dehydrogenase A (LDHA), and abrogation of LDHA compromises the proliferation of tumour cells under hypoxic conditions (Fantin et al., 2006). Furthermore, inhibition of LDHA results in a switch from aerobic glycolysis to oxidative phosphorylation and is accompanied by increased ATP production. Interestingly, the inhibition of LDHA reduces tumour formation (Fantin et al., 2006), suggesting that LDHA function is crucial for cancer cells. Recently, another isoform of LDH, LDHB, has been shown to be important for ER-negative/HER2-negative breast cancers. The ablation of LDHB impaired cell proliferation *in-vitro* and caused tumour regression *in-vivo* (McCleland et al., 2012).

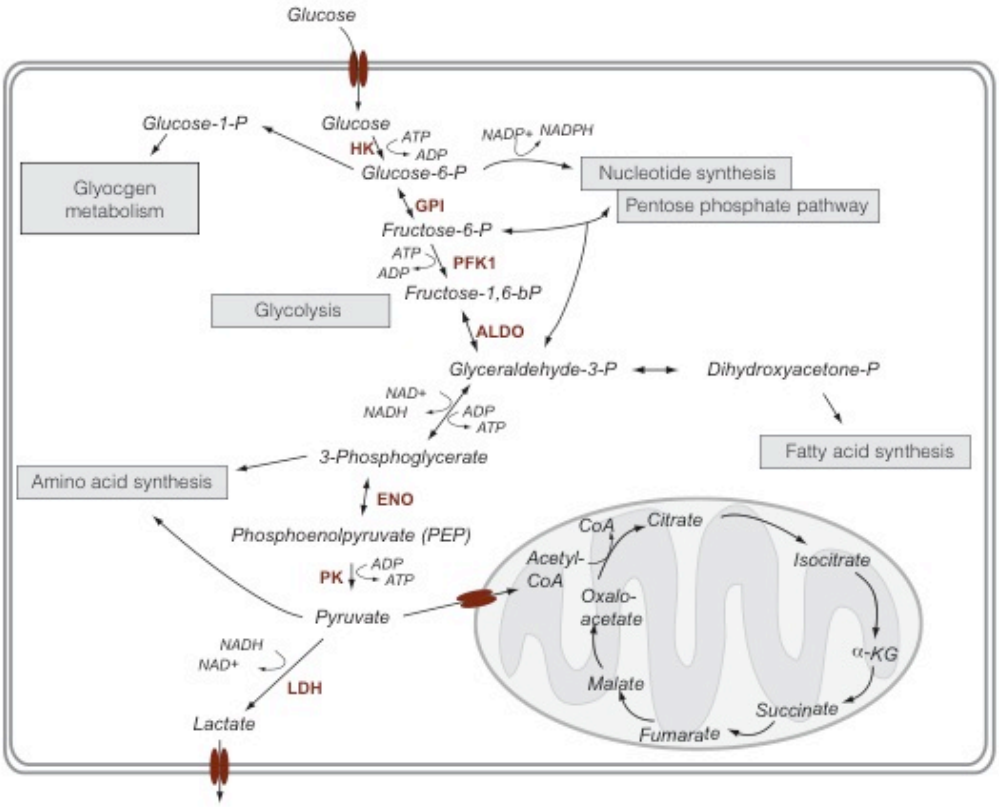

Figure 1-3 Overview of glycolysis

Schematic overview of the metabolic reactions that are required to convert glucose into pyruvate as part of glycolysis. Many glycolytic intermediates are precursors for other metabolic processes such as fatty acid and amino acid synthesis. Under resting conditions, glucose is catabolised to CO_2 by mitochondrial processes resulting in the production of ATP. Cancer cells use aerobic glycolysis, where approximately 90% of all glucose-derived carbons are converted to lactate. Lactate is then secreted out of the cell.

1.3.2.2 Glutaminolysis

Glutaminolysis is defined as a metabolic process where glutamine is converted to α-ketoglutarate via glutamate (Fig 1.4). Glutamine is an important source for cellular carbon and nitrogen and is required for the biosynthesis of macromolecules and the regulation of the cellular redox potential. Glutamine is the most abundant amino acid in human serum (Stein and Moore, 1954). Glutamine-derived carbons are not only used for amino acid and nucleotide synthesis but also to replenish metabolites of the tricarboxylic acid (TCA) cycle, a process termed anaplerosis (DeBerardinis et al., 2007). Glutamine can also generate lactate via oxidative carboxylation of malate to pyruvate thereby supporting NADPH production. Recent studies have shown that glutaminolysis is regulated by the proto-oncogene *c-MYC*, which is overexpressed or amplified in multiple cancers (Dang, 2012). MYC overexpressing cells strongly depend on glutamine, which is known as 'glutamine addiction' (Dang, 2009). Glutamine-addicted cells alter their transcriptional programme to upregulate the expression of glutamine transporters and enzymes within the glutaminolysis pathway (Wise et al., 2008). The depletion of glutamine prevents the replenishment of TCA cycle metabolites and induces cells to undergo MYC-dependent apoptosis (Yuneva et al., 2007).

Glutamine metabolism also substantially contributes to lipogenesis (DeBerardinis et al., 2007; Mullen et al., 2012). Flux studies with isotope-labelled glucose and glutamine have revealed that hypoxic cancer cells, or clear cell renal carcinoma (ccRCC) cells harbouring deletions in the Von Hippel-Lindau gene (*VHL*), use reductive glutamine metabolism to generate cytosolic citrate for lipid synthesis (Metallo et al., 2012; Wise et al., 2008). Moreover, cancer cells with dysfunctional mitochondria also use reductive decarboxylation of glutamine to compensate for the lack of mitochondrial metabolism (Mullen et al., 2012).

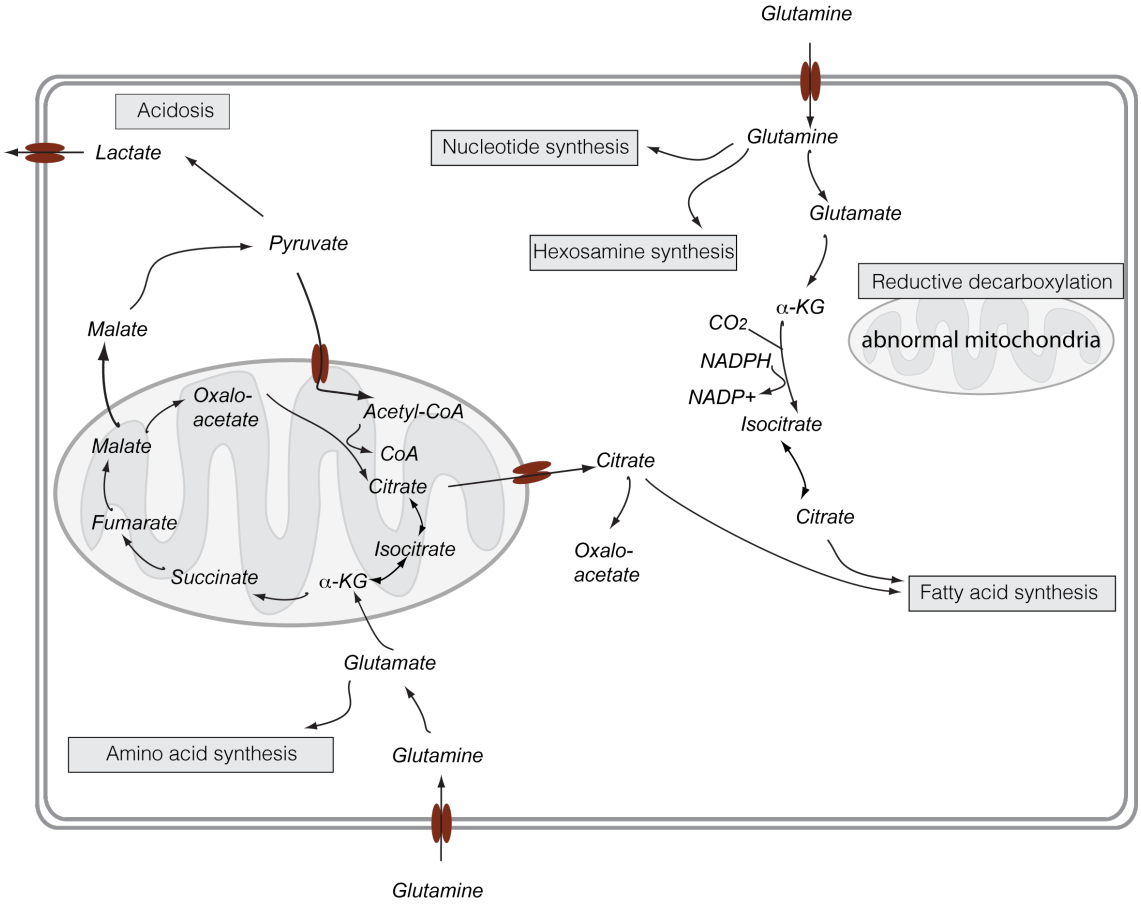

Figure 1-4 Overview of Glutaminolysis

Schematic overview of glutaminolysis. Glutamine addiction is observed in many cancer cells that use glutamine as a substrate for anaplerosis of the TCA cycle, as well as nucleotide and hexosamine synthesis. However, in cancer cells with dysfunctional mitochondria, glutamine-derived carbons are used for lipid synthesis.

1.3.2.3 Amino acid synthesis

Amino acids are the building blocks for proteins and can be mostly provided by the cell environment (essential amino acids). However, some amino acids are synthesised by intracellular reactions (non-essential amino acids). The major pathways involved in amino acid synthesis are glycolysis, the TCA cycle and glutaminolysis (Fig 1.5).

Recently, the synthesis of the amino acid serine via the serine pathway has been demonstrated to be important in cancer. The serine synthesis pathway diverts from the glycolytic intermediate 3-phosphoglycerate, and all three metabolic enzymes of this pathway are often overexpressed in cancer. The first step of the serine biosynthesis pathway is catalysed by the enzyme 3-phosphoglycerate dehydrogenase (PHGDH) and amplifications of the *PHGDH* gene have been found in melanoma and breast cancer (Locasale et al., 2011; Possemato et al., 2011). Furthermore, ablation of PHGDH expression with shRNA leads to decreased cancer cell survival and flux analysis studies showed that serine biosynthesis is tightly coupled to glutaminolysis and that the serine synthesis pathway contributes up to 50% of the glutamate to α-ketoglutarate conversion (Possemato et al., 2011).

Not only is serine important for the cell, but it can also be converted to the amino acids cysteine and glycine. Together with glutamine, these two amino acids are required for the synthesis of glutathione, an important antioxidant system that counteracts the effect of ROS. Several antioxidant systems ensure the removal of hydrogen peroxide (H_2O_2) and other free radicals from cells. These include catalases, peroxiredoxins and glutathione peroxidases (GPX). GPX proteins become oxidised by H_2O_2 followed by a recycling reaction that requires the reduced form of glutathione (GSH). The removal of ROS by the glutathione system protects cell from oxidative damage (Sena and Chandel, 2012).

Glutaminolysis is also important for amino acid synthesis. Glutamine can be used to generate the amino acids arginine and proline. In addition to their function as precursors for protein synthesis, arginine is involved in nitric oxide signalling (Cendan et al., 1996; Lala and Chakraborty, 2001), and proline can also act as an antioxidant (Phang et al.,

2012). Moreover, glutamine shuttling across the plasma membrane is necessary for the import of essential amino acids such as phenylalanine (Nicklin et al., 2009).

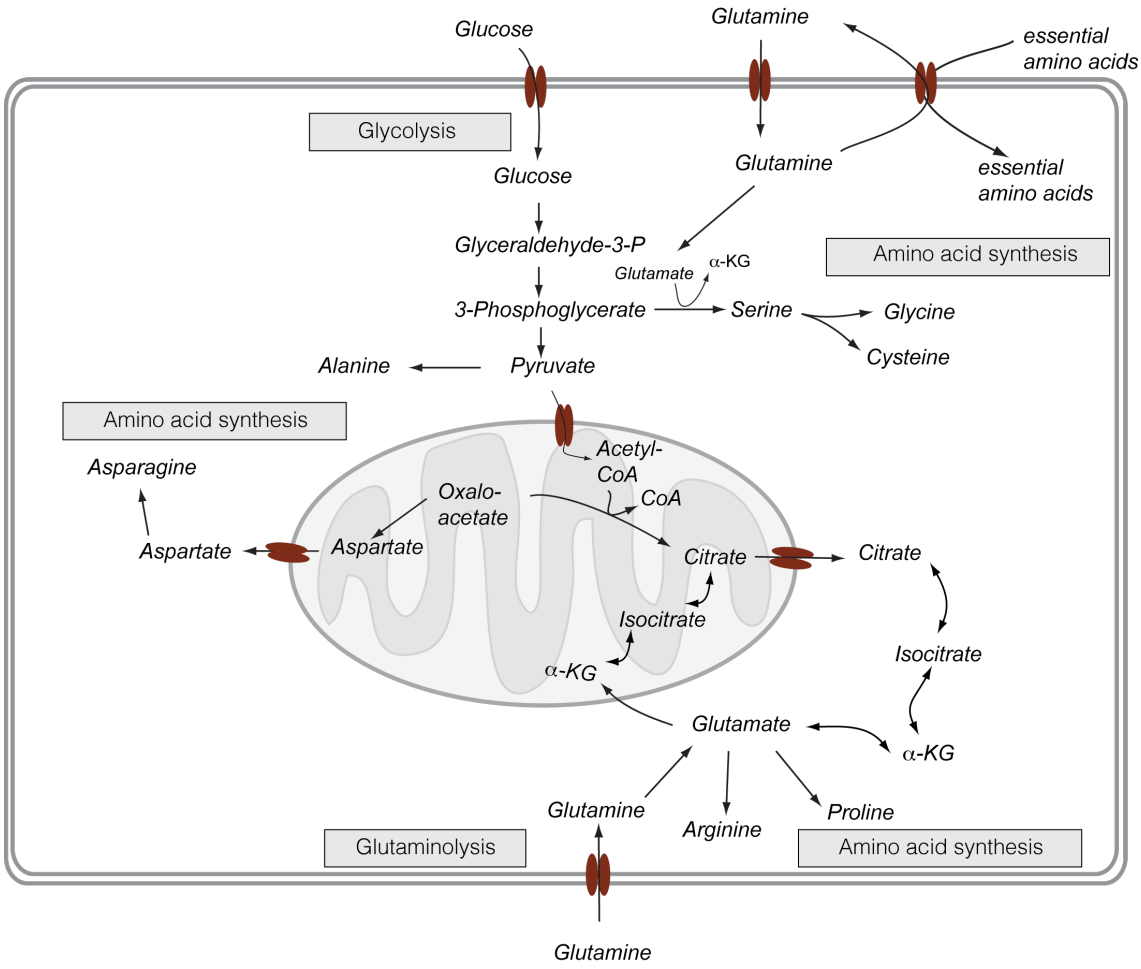

Figure 1-5 Overview of amino acid synthesis

Schematic overview of metabolites that are precursors for the biosynthesis of non-essential amino acids. Glutamine plays an important role in amino acid synthesis as a precursor to arginine, proline and the serine biosynthesis pathway as well as being involved in the import of essential amino acids.

1.3.2.4 Fatty acid synthesis

Fatty acids are carboxylic acids containing a long hydrocarbon chain and are the precursors of phospholipids, cholesterol-esters and triacylglycerides. Most cells in the adult body rely on lipids to be provided by their environment. In contrast, tumour cells re-activate *de-novo* lipogenesis. Indeed, early experiments using ^{14}C-labelled glucose showed that neoplastic tissue slices synthesise lipids regardless of abundant extracellular lipids (Medes et al., 1953). While the role of *de-novo* lipogenesis in cancer cells is not fully understood, several potential benefits for cancer cells have been proposed (Menendez and Lupu, 2007). Importantly, the increased rate of fatty acid synthesis supports cell growth in multiple ways: it provides lipids for membrane biogenesis, it provides cancer cells with fuel that can be mobilised in times of nutrient deprivation through fatty acid oxidation and lipid synthesis precursors and these products can also function as second messengers and signalling molecules.

The primary source for fatty acid biosynthesis is citrate, which is synthesised in the mitochondria in a two-step process: decarboxylation of pyruvate to form acetyl-CoA, followed by the condensation of the acetyl-group with oxaloacetate to form citrate. Fatty acid biosynthesis is a cytosolic process and therefore citrate needs to be transported from the mitochondria to the cytoplasm. Mitochondrial citrate transporters such as SLC25A1 have been shown to be important for citrate efflux from the mitochondria, especially in prostate tissue (Mycielska et al., 2009).

The first step of fatty acid biosynthesis involves the transfer of an acetyl-group from citrate to form acetyl-CoA and oxaloacetate by ATP citrate lyase (ACLY) in the cytoplasm. The metabolite oxaloacetate can re-enter the mitochondria or be converted into pyruvate and NADPH by malic enzyme. Acetyl-CoA, which can also be synthesised in the cytoplasm by acetyl-CoA synthetase (ACSS2) (Yoshii et al., 2009), is further converted to fatty acids and/or cholesterol. The first step in fatty acid synthesis is the carboxylation of acetyl-CoA to malonyl-CoA by acetyl-CoA carboxylase (ACC). This highly regulated enzyme has two isoforms, which differ in their ability to become allosterically activated by citrate (Locke et al., 2008). Malonyl-CoA is converted to palmitate, a saturated fatty acid of 16-carbons, by fatty acid synthase (FASN) via repeated condensation reactions of acyl-groups. This saturated fatty acid is the origin of

many saturated and unsaturated fatty acids containing more than 16-carbons. The desaturation process is catalysed by stearoyl-CoA desaturase (SCD) (Ntambi and Miyazaki, 2004) (Fig 1.6).

As mentioned above, acetyl-CoA can also be used to generate cholesterol, an important building block for steroid synthesis and membranes. The condensation of acetyl-CoA with acetoacyl-CoA generates 3-hydroxy-3-methylglutaryl-CoA (HMG-CoA), a reaction that is catalysed by HMG-CoA synthase (HMGCS). HMG-CoA is further converted to mevalonate by HMG-CoA reductase (Goldstein et al., 2006).

Not only is lipogenesis a process that generates different intermediates for biosynthetic processes, it also requires intermediates from other metabolic processes to maintain the generation of lipids (e.g. glycolysis, PPP) (Fig 1.6). Increased expression of metabolic enzymes involved in lipogenesis such as *ACLY*, *ACC* and *FASN* have been reported across different malignancies (e.g. breast and hepatocellular cancer) (Menendez and Lupu, 2007; Yahagi et al., 2005; Yoon et al., 2007). The inhibition or ablation of these enzymes leads to decreased proliferation and tumour growth and is accompanied by increased cell death (Hatzivassiliou et al., 2005; Lupu and Menendez, 2006).

Important regulators of lipogenesis are the transcription factors of the sterol regulatory element binding protein (SREBP) family. SREBPs induce the transcription of multiple genes involved in fatty acid and sterol synthesis. The regulation of the activity of SREBP involves sensing of intracellular sterol concentrations. Low sterol levels result in the induction of the transcription of SREBP target genes. In contrast, high sterol levels prevent SREBP processing and inhibit SREBP mediated transcription (Bengoechea-Alonso and Ericsson, 2007). It has been demonstrated that SREBP1 is also a downstream target of the mammalian target of rapamycin complex 1 (mTORC1) (Porstmann et al., 2008). Dysregulation of mTORC1 by oncogenic signalling or loss of tumour suppressors during tumorigenesis can therefore enhance *de-novo* lipogenesis.

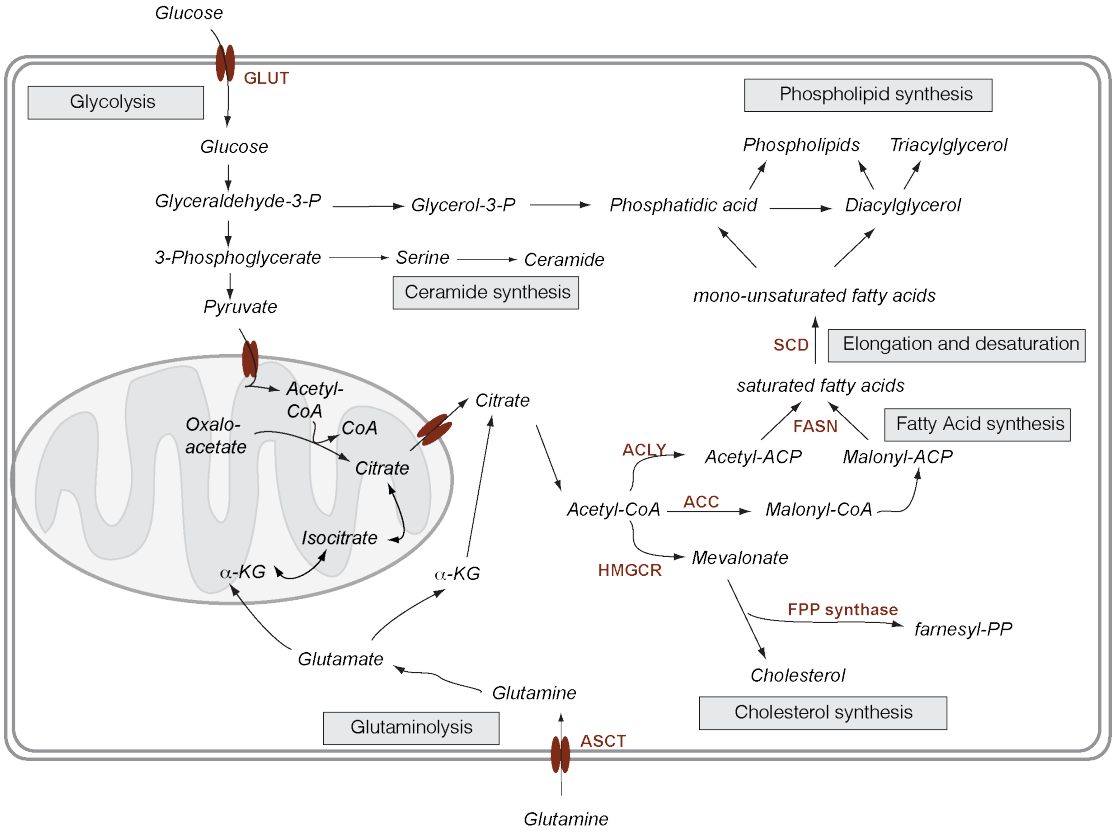

Figure 1-6 Overview of fatty acid synthesis

Schematic overview of lipid biosynthesis. Glucose-derived pyruvate or glutamine-derived α-Ketoglutarate is used for the production of citrate. Citrate is converted to acetyl-CoA, which either acts as substrate for fatty acid synthesis via malonyl-CoA or is used as precursor for cholesterol biosynthesis. Lipogenic enzymes such as FASN, ACC and ACLY have been found to be overexpressed in cancer.

1.3.2.5 Pentose phosphate pathway

The pentose phosphate pathway (PPP) is a metabolic pathway that uses glucose-derived and glutamine-derived molecules for purine and pyrimidine biosynthesis. The PPP, is also a major source of NADPH. NADPH is required for the production of antioxidants, which are important to counteract ROS. The PPP is branched into an oxidative and non-oxidative pathway. The oxidative pathway is important for the synthesis of NADPH and produces the 5-carbon sugar, ribulose-5-phosphate (R-5-P). R-5-P is a precursor for nucleic acid synthesis by the oxidative pathway (Fig 1.7). Moreover, R-5-P can be converted to the glycolytic intermediates F-6-P and glyceraldehyde-3-phosphate via the activity of transketolases and transaldolases of the non-oxidative pathway. This allows cells to adapt their metabolism according to the relative demands for NADPH, riboses and ATP (Berg et al., 2002).

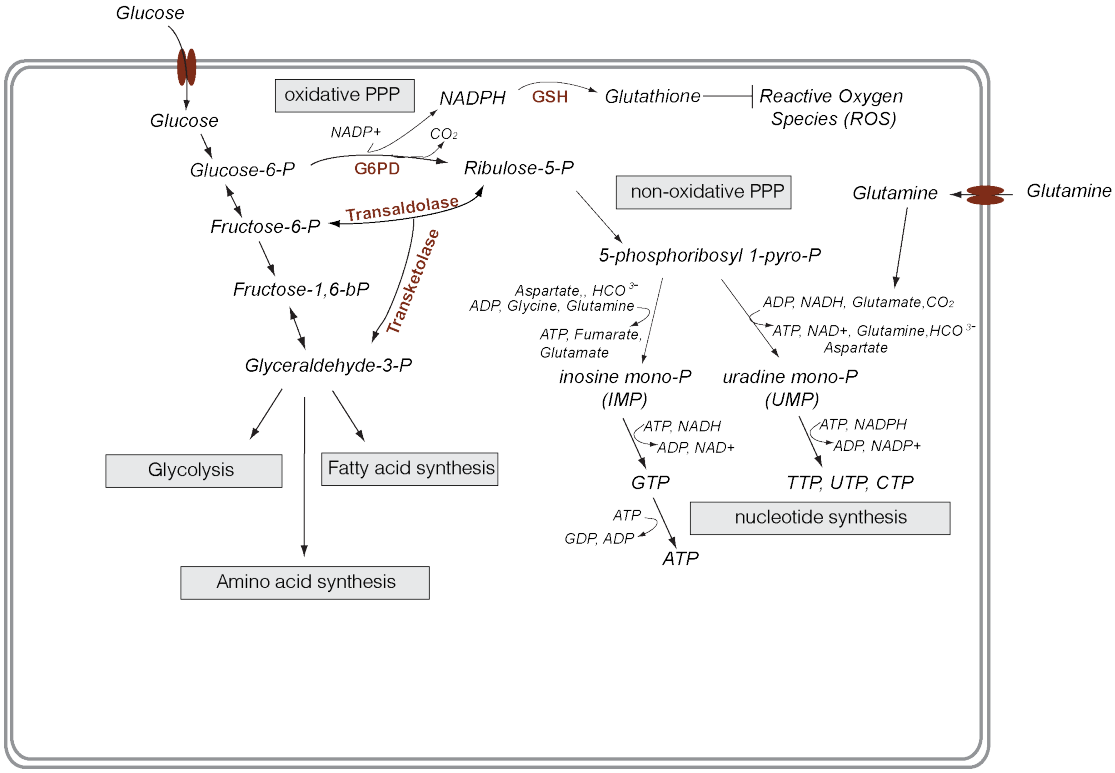

Figure 1-7 Overview of the pentose phosphate pathway

Schematic overview of the oxidative and non-oxidative PPP. Glucose and glutamine contribute to the production of important macromolecules via PPP. NADPH generation is necessary for redox balance and ribose-5-phosphate is an important intermediate for other metabolic synthesis processes (e.g. nucleotides, amino acids and lipid synthesis)

1.3.2.6 NADH and NADPH production

Besides generating macromolecules for cell growth and proliferation, cancer cells also require sufficient amounts of the cofactors nicotinamide adenine dinucleotide (NADH) and nicotinamide adenine dinucleotide phosphate (NADPH) for energy transduction and biosynthetic processes. The relative abundance of the oxidised and reduced forms of these cofactors is also an important regulator of metabolic activity (Feron, 2009).

NAD^+/NADH ratios are important for the catabolism of glucose and fatty acids as well as energy production (Chiarugi et al., 2012). Moreover, the relative NAD^+/NADH levels regulate the activity of many metabolic enzymes. Highly glycolytic cells display increased NADH levels relative to NAD^+ levels. This leads to a constraint in their metabolic activity and cancer cells need to regenerate NAD^+ to maintain a balanced NAD^+/NADH ratio. Cells possess different mechanisms to regenerate NAD^+. One mechanism is the conversion of pyruvate to lactate by LDH. In oxidative cells, the electron transport chain accepts electrons from NADH to regenerate NAD^+. NADH generated by glycolysis has to be transferred to the mitochondria by the malate-aspartate shuttle. However, this process is slower than the conversion of pyruvate into lactate. (Canto et al., 2009; Canto et al., 2012).

The other cofactor important for biosynthetic processes and redox regulation is NADPH. It has been suggested that the production of NADPH is a rate-limiting factor in cancer metabolism (Vander Heiden et al., 2009). This can be partially explained by the high demand of NADPH for lipogenesis (14 molecules NADPH are needed per molecule palmitoyl-CoA) (Vander Heiden et al., 2009). NADPH can be generated through three different metabolic processes: the oxidative arm of the PPP via glucose-6-phosphate dehydrogenase (G6PD); the conversion of malate to pyruvate by the cytosolic isoform of malic enzyme (ME1); and the conversion of isocitrate to α-ketoglutarate by the cytosolic isoform of isocitrate dehydrogenase (IDH1). Depending on the context, cells may prefer one mechanism of NADPH production over another. Glutamine-dependent cells have been suggested to produce NADPH by converting glutamine-derived malate to pyruvate by ME1 (DeBerardinis et al., 2007). However, cancer cells with a less pronounced glutamine addiction or those that use glutamine for reductive decarboxylation to form citrate might show a stronger dependence on the PPP

enzyme G6PD for NADPH production. However, it should be noted that inherited mutations in G6PD, that result in reduced activity of this enzyme, have not yet been linked to reduced cancer risk.

A recent study has provided evidence that the AMP-activated protein kinase (AMPK) regulates NADPH levels during metabolic stress situations in cancer cells. Under metabolic stress situations, such as nutrient deprivation, energy-consuming processes, such as lipid biosynthesis, need to be inhibited while energy production through glycolysis and oxidative phosphorylation are activated. Since cells also need to counteract ROS, AMPK maintains NADPH levels via inhibition of lipid biosynthesis through phosphorylation of acetyl carboxylases 1 and 2 (Jeon et al., 2012).

In conclusion, NADPH is an important cofactor for biosynthetic processes and also essential to maintain redox balance in proliferating and cancer cells.

1.3.3 Mutations in metabolic genes regulate cancer metabolism

Recent discoveries have shown that metabolic genes themselves can harbour LOF or GOF mutations. The metabolic phenotype of cancer cells with these genetic alterations in metabolic genes can accumulate metabolites resulting in their selective dependency on additional metabolic pathways and enzymes. This 'non-oncogene addiction' can be found in cells harbouring mutations in the mitochondrial enzymes fumarate hydratase (*FH*) and succinate dehydrogenase (*SDH*), which are part of the tricarboxylic acid cycle (Frezza et al., 2010).

LOF mutations in *SDH* and *FH* lead to an accumulation of their substrates, fumarate and succinate (Fig 1.8). These metabolites can act as onco-metabolites by inducing specific changes to cellular signalling that promote tumorigenesis. Tumours deficient in *FH* exhibit a strong hypoxic gene expression signature due to activation of HIF1α and induction of HIF1α target genes (Ashrafian et al., 2010). Increased succinate levels inhibit the activity of prolyl hydroxylases (PHDs) that negatively regulate HIF1α (Selak et al., 2005). A similar mechanism was found for *FH*-deficient tumours (Isaacs et al., 2005; Pollard et al., 2005). Cells that lack functional FH or SDH elicit glycolytic phenotypes. Moreover, it has been suggested that *FH*-deficient cells rely on the urea cycle (Frezza et al., 2011).

A genome wide screen by Parsons and colleagues initially demonstrated the occurrence of mutations in the cytoplasmic form of isocitrate dehydrogenase (IDH1) (Parsons et al., 2008). This was supported by other studies identifying IDH1 as well as IDH2 mutations in acute myeloid leukaemia (AML) and glioblastomas (Marcucci et al., 2010; Yan et al., 2009). The mutation always resulted in a single amino acid change within the active centre of the enzyme (arginine 132 in IDH1 and arginine 172 in IDH2). There are three isoforms of IDH (IDH1, IDH2 and IDH3). IDH1 and IDH2 are $NADP^+$-dependent enzymes whereas IDH3 is NAD^+-dependent. These enzymes differ in their localisation within the cell. The isoforms IDH2 and IDH3 are part of the mitochondrial metabolism whereas IDH1 is localised in the cytoplasm. Metabolite analyses in glioblastomas and AML has revealed that mutant forms of IDH1 or IDH2 acquire a neomorphic activity and generate the metabolite 2-hydroxyglutarate (2-HG) from α-ketoglutarate (Dang et

al., 2009). Increased levels of 2-HG influence histone modifications via the DNA and histone demethylase TET2 (Xu et al., 2011), and the jumonji domain containing protein 2A (JMJD2A) (Chowdhury et al., 2011); thereby linking cellular metabolism to epigenetic regulation (Fig 1.8).

Other genetic alterations of metabolic enzymes in cancer mainly affect gene copy number or expression levels. Overexpression of metabolic enzymes has been observed in melanoma, prostate and breast cancers. The *FASN* gene locus is amplified in prostate cancer (Migita et al., 2009). Moreover, the metabolite sarcosine is enriched in metastatic prostate cancer (Sreekumar et al., 2009). ER-negative/HER2-negative breast cancer and melanoma depend on increased flux through the serine/glycine pathway due to amplifications in the phosphoglycerate dehydrogenase (*PHGDH*) gene (Locasale et al., 2011; Possemato et al., 2011).

Together these studies demonstrate that the metabolic adaptations of cancer cells are not only the consequence of oncogenic signalling events but can be causally involved in the transformation process. It appears that selective pressure can not only alter the activity of metabolic enzymes to optimise the survival of cancer cells, but can even lead to the production of onco-metabolites that may drive tumorigenesis. Metabolic enzymes are important to support proliferation and survival of transformed cells and promote tumour growth. The dependency of cancer cells on these metabolic activities and enzymatic functions leads to non-oncogene addiction and can be explored therapeutically. It is likely that further studies exploring other cancer types might uncover additional metabolic oncogenes and onco-metabolites.

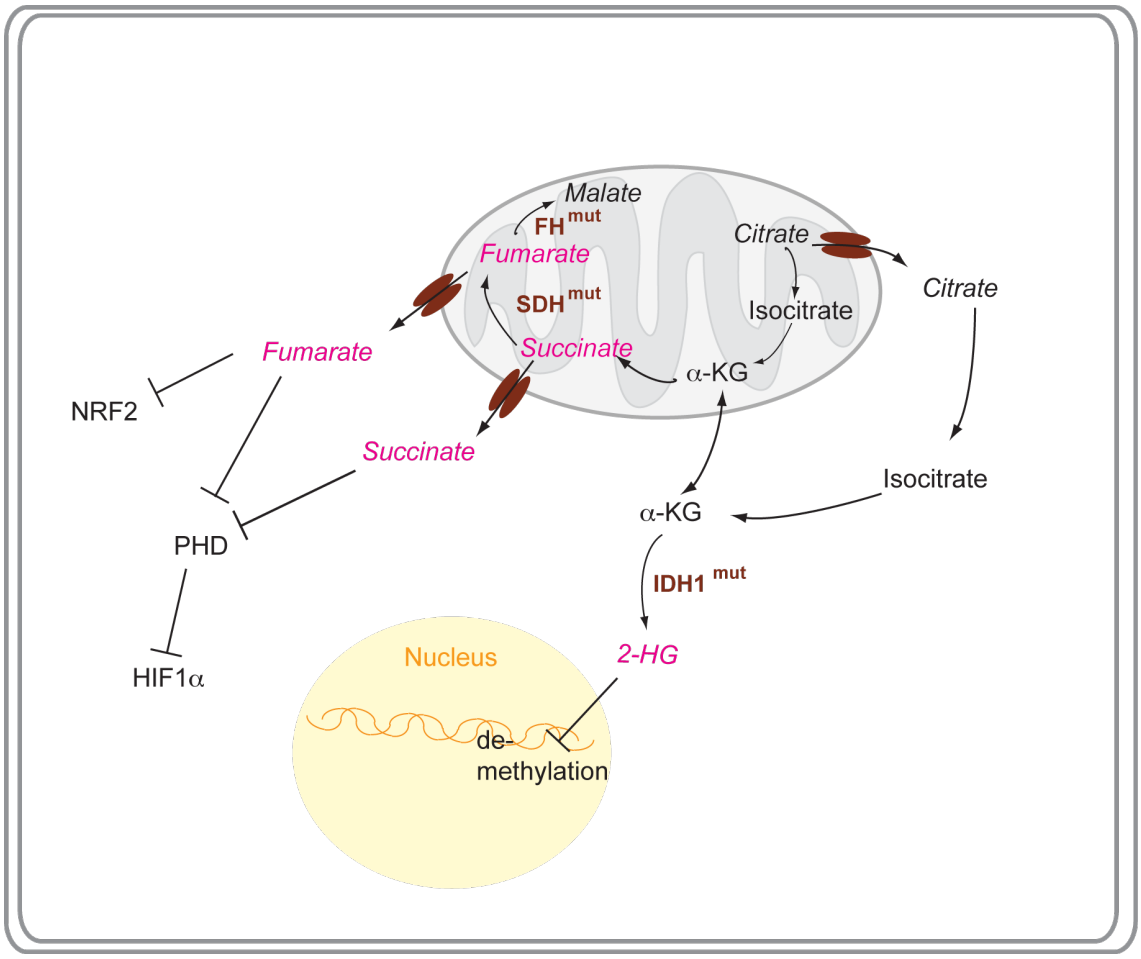

Figure 1-8 Oncometabolites in cancer cells

Schematic overview of oncometabolites in cancer cells. Oncometabolites accumulate due to genetic alterations in IDH, SDH and FH that regulate a specific reaction. Succinate and fumarate, both mitochondrial metabolites, inhibit PHDs, resulting in a pseudo-hypoxic state mediated by HIFα stabilisation. 2-HG, generated through mutated IDH, affects DNA methylation.

1.3.4 Regulation of metabolism by tumour suppressors and oncogenes

1.3.4.1 p53

p53 has also been identified as a key player in the regulation of cellular metabolism and reactive oxygen species (Vousden and Ryan, 2009). p53 promotes mitochondrial respiration through inducing the expression of an assembly factor of cytochrome c oxidase (SCO2). SCO2 is an important regulator of the mitochondrial complex IV, which is part of the respiratory chain and required for oxidative phosphorylation (Matoba et al., 2006). p53 has also been shown to dampen glycolytic flux though several mechanisms. The expression of GLUT1 and GLUT4 are decreased by p53 (Schwartzenberg-Bar-Yoseph et al., 2004) and p53 downregulates the expression of the glycolytic enzyme phosphoglycerate mutase (PGM) (Kondoh et al., 2005). In addition, p53 directly increases the expression of the glycolytic regulator TIGAR (*TP53*-induced glycolysis and apoptosis regulator). *TIGAR* displays sequence homology to *FBPases* and reduces glycolytic activity by lowering F-2,6-BP levels (Bensaad et al., 2006). This results in increased entry of G-6-P into the PPP and increases the synthesis of riboses and NADPH for nucleotide biosynthesis. However, p53 can also act as a negative regulator of the PPP by direct inhibition of G6PD, leading to a decrease in the generation of NADPH (Jiang et al., 2011). This can affect overall cellular ROS levels due to the antioxidant role of NADPH. ROS levels are balancing many cellular processes, such as apoptosis and autophagy. TIGAR also has a p53-independent function; being involved in the control of autophagy (Bensaad et al., 2009).

Another direct p53 target is glutaminase 2 (GLS2). GLS2 is a mitochondrial glutaminase that produces glutamate from glutamine. Glutamine can then be converted into α-ketoglutarate for mitochondrial respiration. This enzyme promotes an antioxidant defence mechanism by increasing reduced glutathione (GSH) and blocking ROS accumulation (Hu et al., 2010). These studies underline the importance of p53 in the regulation of metabolic processes. Loss of p53 supports the glycolytic phenotype by reducing mitochondrial respiration. Moreover, loss of p53 results in increased ROS levels that can promote genomic instability and cellular stress. Another mechanism for the modulation of energy production by p53 is via the nuclear factor-kappaB (NFκB) pathway. p53 expression inhibits the activity of IκB kinases (IKK) that are required for

NFκB activation. NFκB increases the expression of GLUT3 and thereby increases glucose uptake and glycolysis (Kawauchi et al., 2008).

p53 also communicates with other tumour suppressors such as AMPK and PTEN to coordinate the response of cell growth and proliferation during stress situations such as nutrient and oxygen deprivation. p53 has been demonstrated to be essential for AMPK-mediated fatty acid catabolism (β-oxidation). In a study by Buzzai and colleagues, treatment of p53-deficient tumours with metformin, an indirect activator of AMPK, resulted in tumour regression. Loss of p53 sensitised cancer cells to metformin by preventing the degradation of fatty acids for energy production via autophagy (Buzzai et al., 2007). Intriguingly, p53 is also involved in the regulation of lipogenesis. Freed-Pastor and colleagues showed that cancer-specific mutant forms of p53, which have lost their ability to bind to DNA, control the activity of the mevalonate pathway (cholesterol biosynthesis) in breast cancer cells. Ablation of mutant p53 led to repression of genes such as *DHCR7*, *HMGCR* and *MVD*. The altered expression of these genes resulted in morphological changes in the breast cancer cell lines MDA-MB-231 and MDA-MB-468 cultured in a 3D matrix (matrigel). The cells adopted a more acinar architecture usually found in 3D-cultures of non-malignant MCF10A cells. This suggests a potential mechanism of how mutant p53 contributes to cell transformation through metabolic rewiring (Freed-Pastor et al., 2012).

1.3.4.2 PI3K/AKT pathway

One important signalling pathway in the regulation of metabolic processes is the PI3K/AKT pathway. This pathway is activated in cancer cells through aberrant activation of receptor tyrosine kinases (Moasser, 2007; Sauter et al., 1996), loss of PTEN or by activating mutations in *PIK3CA* (Zhao et al., 2005), *AKT* (Carpten et al., 2007) or *RAS* (Pylayeva-Gupta et al., 2011). Activation of the PI3K/AKT pathway can drive metabolic reprogramming in cancer cells. AKT has been suggested to be the 'Warburg kinase' due to its critical role in promoting glycolysis in cancer cells (Robey and Hay, 2009).

AKT stimulates glycolytic flux through upregulation of multiple glycolytic enzymes. Activated AKT promotes glucose uptake via GLUT1 (Barthel et al., 2001) and GLUT4

(Kohn et al., 1998) and promotes localisation of HK2 to the mitochondrial membrane for the conversion of glucose to G-6-P (Robey and Hay, 2006). Glycolysis is further influenced by another downstream effector of AKT, forkhead box O1 (FOXO1), which is directly phosphorylated by AKT resulting in the suppression of enzymes involved in gluconeogenesis (Nakae et al., 2001). Fatty acid synthesis is stimulated by AKT via phosphorylation of ACLY, which catalyses the production of acetyl-CoA from citrate in the cytoplasm (Berwick et al., 2002) and by induction of expression of genes within the lipid biosynthesis pathway (Porstmann et al., 2005).

However, the most prominent role of AKT is the regulation of cell growth by activating mTORC1 signalling. The inhibition of the tuberous sclerosis complex proteins 1 and 2 (TSC1/2), negative regulators of mTORC1, via AKT-mediated phosphorylation activates mTORC1. This enables cells to induce the synthesis of lipids and proteins (Inoki et al., 2002). In addition, AKT can also directly phosphorylate Pro-rich AKT substrate (PRAS40), a component of mTORC1. This prevents PRAS40 from inhibiting mTORC1 (Kovacina et al., 2003). Moreover glycogen synthase kinase 3β (GSK3β), which is negatively regulated by AKT (Cross et al., 1995), can also inhibit mTORC1 activity by phosphorylating TSC2 (Inoki et al., 2006). mTORC1 can also induce activation of other important players in tumorigenesis, such as HIF, SREBP (Duvel et al., 2010; Porstmann et al., 2008) and c-Myc. mTORC1 has been shown to play a dominant role during nutrient stress and oxygen withdrawal. S6 kinase (S6K), a downstream target of mTORC1, can elicit a negative feedback response to control for aberrant mTORC1 activity. S6K thereby dampens AKT activity through the insulin receptor substrate 1 (IRS1) (Nakae et al., 2001).

1.3.4.3 PTEN

The tumour suppressor PTEN, a negative regulator of PI3K/AKT signalling, regulates cellular homeostasis by controlling processes involved in cell growth, proliferation and survival. Many cancers including breast cancer, endometrial cancer, prostate cancer, melanoma, and glioblastoma harbour inactivating mutations in *PTEN*, which highlights the importance of this gene in cellular signalling processes (Salmena et al., 2008).

Overexpression of PTEN in a transgenic mouse models leads to a decrease in body size caused by a reduction of cell number. Mouse embryo fibroblasts (MEFs) isolated from PTEN overexpressing mice (referred as Super-PTEN) are resistant to oncogenic transformation and Super-PTEN mice show reduced tumour formation after treatment with a chemical carcinogen (Garcia-Cao et al., 2012). The effects of PTEN overexpression on metabolism included a reduction in body fat accumulation without affecting expression of key enzymes of the fatty acid metabolism. The contribution of glucose-derived carbons to fatty acids was significantly decreased, pointing to decreased glucose uptake. This study further showed that overexpression of PTEN leads to an increase in mitochondrial respiration for energy production and an increased number of mitochondria. This creates a metabolic state that is not favourable for tumour formation by negatively regulating glucose and glutamine consumption, which are necessary for anabolic processes (Garcia-Cao et al., 2012). However, the mechanism by which PTEN modulates metabolic enzymes independently of PI3K/AKT still needs to be investigated.

1.3.4.4 AMPK

AMPK is a sensor for nutrient and oxygen deprivation (Hardie, 2011). It consists of a hetero-trimeric protein complex formed by three subunits (α, β and γ). The γ-subunit is the sensor for the detection of energy stress and binds to AMP and ADP. In non-stressed situations where nutrients and oxygen are abundant, AMP levels are low. During nutrient and energy stress, AMP levels are increased as two moles of ADP are converted into one mole of ATP and one mole of AMP to provide energy. AMP binds to the γ-subunit and induces a conformational change in the AMPK complex. This exposes the catalytic domain located on the α-subunit, which is phosphorylated on threonine 172 by AMPK-kinases (LKB1, STRAD and MO25).

AMPK is a regulator of glucose and lipid metabolism. It activates glucose transporter and induces glycolytic flux by phosphorylating PFKFB3 (Mendoza et al., 2012). The lipid metabolism enzymes ACC, PLD1, HMGCR are direct downstream targets of AMPK and become inactivated during nutrient stress and oxygen deprivation (Mihaylova and Shaw, 2011). AMPK influences not only metabolic enzymes but also

signalling components that are important for cell growth. One of its downstream targets, the TSC1/2 complex, a negative regulator of mTORC1, is phosphorylated to minimise energy-consuming and growth-promoting processes such as protein and lipid synthesis (Shackelford et al., 2009). AMPK can also phosphorylate and inhibit RAPTOR, one of the components of mTORC1 (Gwinn et al., 2008). AMPK also influences the activity of several transcription factors. AMPK phosphorylates SREBP and thereby prevents its cleavage and nuclear localisation (Li et al., 2011). The crosstalk between p53 and AMPK was mentioned earlier (see 1.3.4.1). A recent study has also linked AMPK to the regulation of NADPH (Jeon et al., 2012).

1.3.5 Regulation of metabolic processes by the microenvironment

Tumour growth is not only characterised by uncontrolled proliferation but also by changes in the microenvironment of the cancer cells. Moreover, the tumour microenvironment itself can impact tumour metabolism and affect the metabolic activity of cancer cells. Interestingly, cancers with the same genetic aberrations exhibit different metabolic signatures depending on the tissues they arise in (Yuneva et al., 2012).

As a tumour increases in size, cancer cells face an increasing challenge to ensure their supply of nutrients and oxygen, provided by the vasculature, are obtained. This challenge exists because the tumour starts to outgrow the diffusion limit of these metabolites (100-200μm distance from blood vessel). These microenvironmental conditions, in combination with the genetic instability of cancer cells, can give rise to heterogeneous cell populations within the tumour. Some specific challenges of the tumour microenvironment that cancer cells have to overcome to sustain growth and cell proliferation are discussed below.

1.3.5.1 Hypoxia

Hypoxia is defined as a reduction in the partial pressure of oxygen and can cause cell or tissue damage if the oxygen deprivation is severe or prolonged. The architecture of normal tissues consists of ordered structures, which are usually well vascularized. When solid tumours arise from a particular tissue (such as breast epithelium), the rapid

proliferation of transformed cells disrupts the normal tissue architecture. The developing tumour demands increasing amounts of nutrients and oxygen in an environment where the ability to deliver these is decreasing. To survive in this unfavourable environment, hypoxic tumour cells need to undergo genetic and metabolic reprogramming. Recent research has shown that the degree of intra-tumour hypoxia has become an important predictor for the OS of cancer patients in the clinic (Horsman et al., 2012). Interestingly, cells that occupy hypoxic niches are known to be resistant to radiotherapy and chemotherapy, due to inefficient drug delivery. The cells within hypoxic niches can also show increased invasive and metastatic potential and develop genetic instability (Wilson and Hay, 2011).

1.3.5.1.1 Hypoxia inducible factors (HIF) and its regulation

HIF was first described as the transcriptional regulator of the erythropoietin gene (EPO) in renal fibroblasts. HIF activation resulted in increased EPO production when the oxygen concentration was low (Wang and Semenza, 1995). A large number of transcriptional targets of HIF have now been described. These include many genes involved in the regulation of angiogenesis and metabolism (Keith et al., 2012; Semenza, 2010a). At the molecular level, HIF consists of a heterodimeric complex that contains an oxygen sensitive α-subunit and an oxygen-insensitive β-subunit. The latter is the aryl hydrocarbon receptor nuclear translocator (ARNT), which is ubiquitously expressed. There are three genes that encode α-subunits of HIF in mammals: HIF1α, HIF2α and HIF3α. Historically, most research has been focussed on HIF1α but, more recently the specific targets and roles of HIF2α have become well understood. HIF1α is expressed in most tissues, whereas HIF2α expression is mainly restricted to the vascular endothelium, renal cells, liver parenchyma and lung type II pneumocytes. HIF3α is much less well characterised. However, HIF3α seems to act as negative regulator to HIF1α– and HIF2α-induced gene transcription and is found in the corneal epithelium of the eye, the thymus and cerebellum (Majmundar et al., 2010).

HIFα subunits can sense oxygen through an oxygen-dependent degradation domain (ODD) that consists of a region of 200 amino acids. In oxygen-rich tissues (2-9% O_2), HIFα is targeted for degradation by the VHL ubiquitin ligase. Binding of VHL to the

ODD requires the hydroxylation of two proline residues (P402 and P564) by one of three prolyl hydroxylases (PHD1-3). These modifications are then recognised by the VHL-elongin complex that acts as an E3 ubiquitin ligase and marks HIFα for ubiquitination. The ubiquitinated HIF α-subunit is then recognised by the 26S proteasome, resulting in its degradation (Jaakkola et al., 2001). Another regulatory modification of HIFα is the hydroxylation of the asparagine residue N803 by the factor inhibiting HIF (FIH). This modification influences HIFα activity rather than stability by interrupting its interaction with the co-activator p300/CREB (Mahon et al., 2001).

Several studies have shown that HIFα is also regulated by acetylation. Park and colleagues have shown that a member of NAD^+ dependent histone deacetylases termed Sirtuin 1 (SIRT1) can bind to HIFα. This leads to the deacetylation of lysine residue 674 and the inactivation of HIFα transcriptional activity. In contrast, acetylation of HIFα by the acetyltransferase p300/CREB associated factor (PCAF) promotes HIF1α activity (Lim et al., 2010).

In oxygen-deprived tissue (below 2% O_2), HIF α-subunits become stabilised or activated due to the diminished activity of PHDs and FIH, as well as decreased levels of NAD^+ and hetero-dimerise with ARNT. These heterodimers recognise and bind to specific genomic sequences, termed hypoxia response elements (HRE) (5'-[AG]CGTG-3'), that lie within target gene promoters. This leads to changes in the transcription of genes that are necessary to overcome oxygen deprivation.
The stability and activity of HIFα can also be affected by other mechanisms. ROS, metabolic intermediates such as succinate, fumarate and α-ketoglutarate, and genetic alterations of upstream regulators, including the proto-oncogenes RAS, PI3K and HER2/ERBB2 and the PTEN tumour suppressor, have been shown to influence the activity and/or stability of HIFα (Bardos and Ashcroft, 2004).

1.3.5.1.2 Hypoxia and HIF function in tumour progression

Numerous studies have investigated the role of hypoxia during tumour initiation and progression (Semenza, 2010a). Many of these studies have focussed on HIF1α.

However, it is now clear that only a small subset of genes are regulated by both HIF1α and HIF2α, suggesting that they regulate specific transcriptional programmes that influence the cellular phenotype in a differential manner (Keith et al., 2012). The distinct roles of HIF1α- and HIF2α-specific target genes in tumour progression are emerging as a key area of study in the hypoxia field. For example, the opposing effects of HIF1α and HIF2α on the activity of c-Myc have been investigated (Keith et al., 2012). Furthermore, there is evidence that HIF1α is more important for metabolic regulation in cancer cells, while HIF2α is thought to mainly act on the regulation of angiogenic and metastatic processes (Qing and Simon, 2009).

1.3.5.1.3 HIF regulates metabolic processes

HIF directly regulates glycolysis by inducing the expression of glucose transporters (GLUT1 and GLUT3) thereby increasing the efficiency of glucose uptake (Chen et al., 2001; Mimura et al., 2012). HIF1α also increases the expression of glycolytic enzymes, including enolase 1 and aldolase, which are essential for the conversion of glucose to pyruvate (Marin-Hernandez et al., 2009). Moreover, HIF1α activation leads to increased expression of PFKFB3, which controls the levels of F-2,6-BP. PFKFB3 acts as an allosteric activator of PFK1 thereby contributing to the increased glycolytic flux in malignant cells (Minchenko et al., 2002).

HIF1α is also an important inducer of an overall shift in energy production by reducing mitochondrial respiration and increasing glycolysis. This is mediated by upregulation of pyruvate dehydrogenase kinase 1 (PDHK1, also known as PDK1), which phosphorylates and inhibits pyruvate dehydrogenase (PDH), the enzyme that converts pyruvate into acetyl-CoA (Kim et al., 2006). As a result, pyruvate is mainly converted to lactate by the HIF1α dependent induction of lactate dehydrogenase A (LDHA). In addition, HIF1α reduces mitochondrial biogenesis by inhibiting c-Myc (Zhang et al., 2007a).

HIF1α induces regulators of cellular pH control, including transporters such as monocarboxylate transporter 4 (MCT4) and carbonic anhydrase 9 (CAIX). These factors enable hypoxic tumour cells to maintain an alkaline intracellular pH and to

survive and proliferate under the acidic conditions imposed by oxygen deprivation (discussed in more detail in 1.3.5.2). The secretion of lactate leads to increased acidification of the extracellular environment, which can promote tumour cell invasion and metastasis. Conversion of pyruvate to lactate and its removal by lactate transporters allows the cancer cells to regenerate NAD^+ and maintain glycolytic flux in hypoxia (Feron, 2009).

The metabolic reprogramming by HIFs enables cancer cells to survive in hypoxic conditions. However, these cancer cells might become dependent on HIF signalling for survival and are potentially more sensitive towards metabolic perturbations.

1.3.5.1.4 Clinical relevance of HIF and hypoxia

The molecular findings of how hypoxia and HIF influence cellular and metabolic signalling pathways have been also visualised by studying numerous human tissue biopsies. Tumours exhibit heterogeneity due to highly proliferative cancer cells growing into surrounding healthy tissue accompanied by limited access to the vascular system for certain areas of the tumour. This also leads to heterogeneity in hypoxic regions. These hypoxic regions correlate with increased HIF1α and HIF2α levels and have been associated with a poor OS signature in malignancies of breast, brain, pancreas, colon and many others (Semenza, 2010a).

HIF stabilisation and activity have also been described in context of certain genetic alterations, such as loss of VHL in ccRCC and mutations in the WNT/β-catenin signalling in colon cancer (Majmundar et al., 2010). Genes regulated by HIF are also involved in other aspects of cancer biology, such as proliferation (c-MYC, p53), genetic instability (GADD45a), apoptosis (BNIP3), evasion of the immune response, angiogenesis (VEGFA), invasion and metastasis (CXCR4, MMP1, LOX) as well as resistance to radiotherapy. Collectively, these observations show a crucial role of hypoxia and HIF in tumour growth and progression. This has led to the development of numerous drugs and compounds targeting HIF stabilisation and HIF target genes (Semenza, 2010a). However, in some cancers, HIF1α expression correlates with a lower mortality rate. This has been shown for several cancer types including non-small-

cell lung cancer, colorectal cancer and head and neck squamous cell carcinoma. In these cancer types, HIF2α expression is believed to be more relevant (Keith et al., 2012; Yoshimura et al., 2004). Surprisingly, both HIF1α and HIF2α may therefore have tumour suppressor function in certain cancer types and HIF1α has been identified as a tumour suppressor in clear cell renal carcinoma (Keith et al., 2012).

Bevacizumab, a monoclonal antibody targeting VEGFA, and Sorafenib, an inhibitor of VEGFA receptor tyrosine kinase, have shown some promising effects in certain cancers such as metastatic colorectal cancer and renal cancer. However, in other cancers such as breast cancer the promised benefits were disappointing (Rapisarda and Melillo, 2012). Only in combination with chemotherapeutics was an OS effect observed. It has been demonstrated that hypoxic breast tumours predominantly show poorer clinical outcome. Also, hypoxic tumours do no respond well to established therapeutics (as compared to well oxygenated ER positive tumours), so identifying novel targets within these tumours is a worthwhile endeavour.

1.3.5.2 pH regulation

One hallmark of the tumour microenvironment is extracellular acidosis. In contrast to quiescent cells with an intracellular pH (pH_i) of ~7.2 and an extracellular pH (pH_e) of ~7.4, tumour cells exhibit altered pH levels ($pH_i \geq 7.4$ and pH_e~6.7-7.1). It is astonishing that these cancer cells display a reversed pH gradient compared to quiescent cells (Vaupel et al., 1989). This can be explained by increased secretion of protons (H^+) and acidic metabolites (e.g. lactate) from the cancer cells. The different pH regulation systems display tissue specificity and might also compensate for each other.

Some proton transporters are overexpressed in certain cancer, for example, the sodium/hydrogen exchanger NHE1 (SLC9A1), carbonic anhydrase 9 and 12 (CAIX, CAXII) and monocarboxylate transporter 1-4 (MCT1-4) (Fig 1.9) These transporters have been implicated in cancer progression, cancer cell invasion and metastasis formation. The acidic conditions influence the ECM resulting in degradation of certain components by matrix metalloproteinases (such as MMP9) (Wolf and Friedl, 2009). Cellular pH regulation also influences the activity of lyosomal proteins such as cathepsins (Rafn et al., 2012; Rozhin et al., 1994), and activates hyaluronidase

(Jacobetz et al., 2012) and the hyaluronan receptor CD44 (Montgomery et al., 2012). These degradation systems restructure the ECM leading to a environment that is more permissive for cancer cell invasion (Borsi et al., 1996).

The regulation of pH is essential in order to prevent the disruption of metabolic processes that are regulated by pH sensitive enzymes. Any perturbations in pH homeostasis can affect many cellular processes (metabolism, protein synthesis, proliferation and apoptosis). A number of the pH regulation systems are modulated in response to hypoxia. For example, NHE1, which extrudes H^+ ions in exchange for the cation Na^+, is induced by hypoxia (Shimoda et al., 2006). Its abrogation caused drastic tumour shrinkage, thereby underlining the importance of pH regulation in tumour cells (Lagarde et al., 1988).

Carbonic anhydrases catalyse the hydration of CO_2 to HCO_3^- and H^+. This reaction is reversible and depends on the substrate/product equilibrium. This family consists of 16 members in the mammalian system, and the isoforms differ in their tissue specific expression and subcellular localisation. The expression of CAIX and CAXII, which are plasma membrane-bound transporters, is regulated by oxygen levels and it is not surprising that CAIX is a downstream target of HIF. In contrast, the transcriptional regulation of CAXII is still unclear. *In-vivo* ablation of these two carbonic anhydrases results in intracellular acidosis and reduced tumour growth (Chiche et al., 2009; Lock et al., 2012). Other studies have also demonstrated CAIX's role in the pH regulation of cancer cells (Chiche et al., 2010b; Swietach et al., 2010).

Another important pH regulating system involves four members of the monocarboxylate transporter family. MCT1-4 facilitate the transport of lactate, pyruvate, and other monocarboxylates linked with H^+ exchange across membranes. Intriguingly, MCT1 and MCT4 are overexpressed in breast, prostate, colorectal and ovarian cancers (Pinheiro et al., 2010a; Pinheiro et al., 2008a; Pinheiro et al., 2008b). The effect of inhibiting MCT1 was tested in lung and colorectal tumour models. Ablation of MCT1 induced tumour regression and caused an increase in mitochondrial respiration

(Sonveaux et al., 2008). Despite their potential role in tumorigenesis, the specific functions of individual MCTs in different tissues have not been fully characterised.

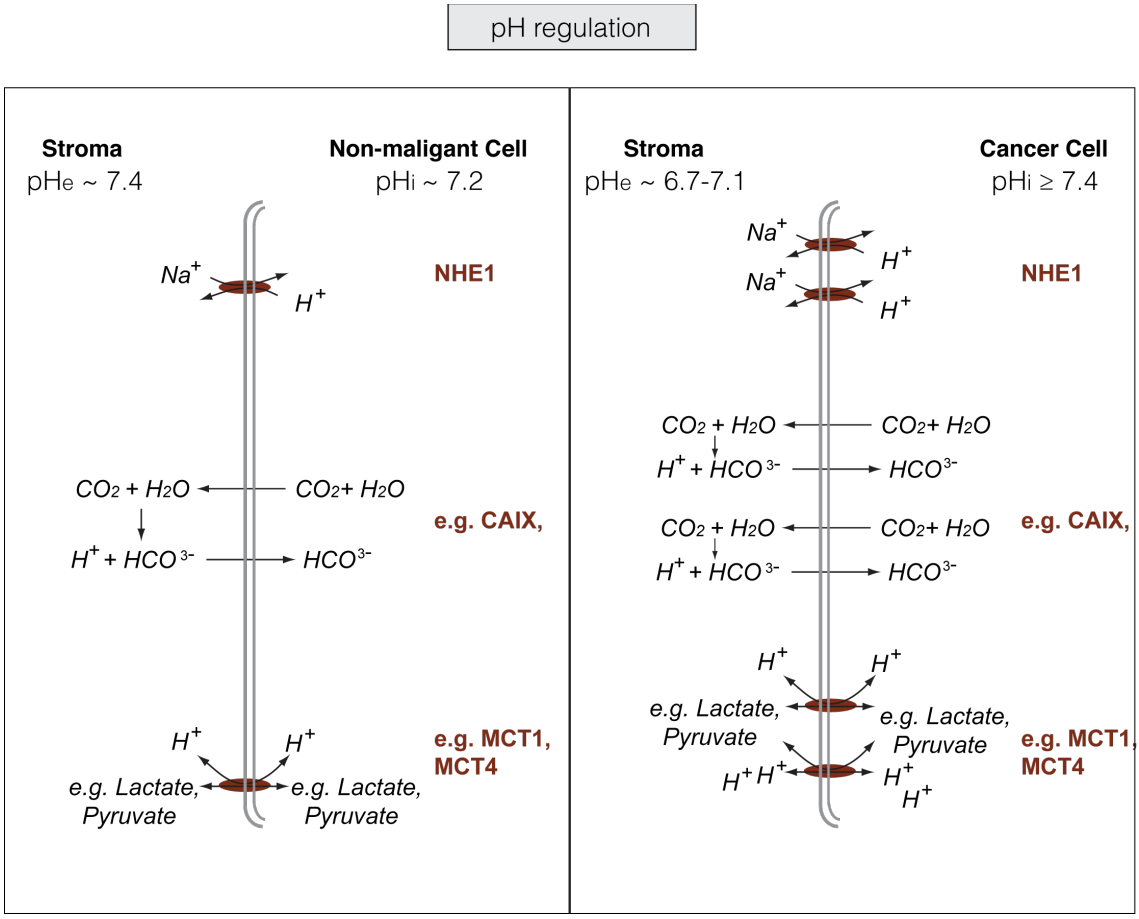

Figure 1-9 pH regulation in non-malignant and cancer cells

Schematic overview of pH regulation in normal and cancer cells. Normal cells exhibit a lower intracellular pH (pH_i) than their extracellular pH (pH_e) of the microenvironment. However in cancer cells the pH gradient is reversed with a higher pH_i. This is caused by overexpression of different pH regulation systems (e.g. NHE1, MCT and CA).

1.4 Targeting altered cellular metabolism in cancer

In recent years it has become clear that the altered metabolism in transformed cells could be used to develop new therapeutic approaches to increase the OS of cancer patients. The increased biosynthetic activity of rapidly proliferating cancer cells provides an 'Achilles heel', as cells depend on the biosynthesis of macromolecules, such as nucleotides, amino acids and fatty acids. However, the subtle difference between the metabolism of proliferating normal cells and cancer cells presents the significant challenge of developing such therapeutics that only target cancer cells. Different therapeutic options for the targeting of cancer metabolism have been discussed (Dang et al., 2011; Jones and Schulze, 2012; Tennant et al., 2010; Vander Heiden, 2010, 2011).

Targeting glucose metabolism

Many tumours show a high level of glucose uptake, which can be visualised by fluorodeoxyglucose positron emission tomography (FDG-PET). An inhibitor of glucose metabolism called 2-deoxy-d-glucose (2-DG) was developed in the 1950s (Ely, 1954). This component repressed the activity of HK2 and initially showed promising effects *in-vitro* and *in-vivo* studies. Cells exposed to sufficient amounts of 2-DG showed impaired cell growth by undergoing cell cycle arrest or cell death. Despite these promising results, treatment with glycolytic inhibitors (e.g. Lonidamine, 2-DG) alone was not efficient enough for therapeutic benefit (Maschek et al., 2004; Papaldo et al., 2003). Clinical trials are currently evaluating the impact of 2-DG on prolonged survival in breast, ovarian and lung cancer in combination with different chemotherapeutic drugs. Another inhibitor of HK2, 3-bromopyruvate has also been shown to cause a reduction in cell viability in multiple studies (Pedersen, 2012) but has only been used in pre-clinical studies to date.

Targeting nucleotide metabolism

Cytotoxic agents such as 5-flurоucil and gemcitabine belong to the class of antimetabolite chemotherapeutics targeting nucleotide biosynthesis (Ewald et al., 2008). They are used across many different cancer types and cause improved survival.

However, these agents do not display tumour specificity and target all highly proliferative cells. This explains the frequently observed side effects of nausea and hair loss, which are due to their effects in proliferating normal cells. However, these agents may be highly useful as a proof-of-principle for targeting nucleotide biosynthesis (Tennant et al., 2010).

Targeting lactate metabolism

Increased lactate secretion is another typical characteristic of cancer cell metabolism and drug development efforts have focussed on targeting lactate transporters (MCTs). Blocking lactate transport should cause intracellular acidosis due to lactate and proton accumulation. Inhibition of lactate transport could also prevent metabolic coupling of cancer cells, a mechanism by which cells within hypoxic tumour areas secrete lactate, which is then used for energy production by better oxygenated cancer cells. This metabolic coupling of glycolytic and oxidative cells has been shown *in-vitro* and *in-vivo* (Sonveaux et al., 2008). Another approach is to target LDH, the enzyme that converts pyruvate into lactate. *In-vitro* studies demonstrated a reduction in cell viability after ablation of LDHA (Fantin et al., 2006). This isoform is specifically upregulated in cancer cells compared to normal proliferating cells and compounds targeting LDHA could be taken forward to clinical trials.

Targeting mutated enzymes

Some cancers harbour specific GOF or LOF mutations in metabolic enzymes (*IDH1*, *IDH2, FH* and *SDH* discussed above). These mutations lead to specific alterations in cancer metabolism and cancer cells can become highly dependent on these alterations. 2-HG is a metabolite that is generated by mutant forms of *IDH1* and *IDH2* and has been shown to promote tumorigenesis (Dang et al., 2010). Detection of 2-HG can also be used for diagnostic purposes. The metabolic dependencies of cancers harbouring specific mutations could be used to develop inhibitors that should be highly selective for cancer cells and not affect normal proliferating cells.

Targeting mitochondrial metabolism

Metformin is an approved drug for the treatment of diabetes and has been considered for use in cancer. It is an inhibitor of complex I of the respiratory chain, and reduces circulating glucose levels in the blood by activating AMPK. (Gallagher and LeRoith, 2011). Trials in diabetic breast cancer patients that were treated either with neoadjuvant chemotherapy alone or received a combination of metformin and neoadjuvant chemotherapy, demonstrated that patients on combination therapies showed increased pathological complete response compared to the diabetic breast cancer patients with only neoadjuvant treatment (Guppy et al., 2011; Jiralerspong et al., 2009)

A small molecule inhibitor termed Dichloroacetate (DCA) has been used for treatment of lactic acidosis in patients with inborn defects of mitochondrial metabolism (Stacpoole et al., 2003). DCA inhibits PDHK, which is overexpressed in many cancer cells because of its induction by HIF. PDHK supports the glycolytic phenotype by inhibiting PDH, which catalyses the oxidative decarboxylation of pyruvate to mitochondrial acetyl-CoA. Treatment of cancer cells with DCA causes a shift from a glycolytic phenotype to mitochondrial respiration, resulting in increased oxidative stress and cell death (Michelakis et al., 2008). This study sets the president that differences in metabolism between tumour cells and normal proliferating cells can be therapeutically targeted.

Targeting lipogenesis

The observation that cancer cells depend on *de-novo* lipogenesis suggests that enzymes of the fatty acid synthesis pathway might be suitable therapeutic targets. Endogenous fatty acid synthesis is driven by cytosolic citrate that is secreted from the mitochondria. The conversion of citrate to acetyl-CoA is mediated by ACLY. Pre-clinical data suggests that ablation of ACLY results in decreased survival of cancer cells (Hatzivassiliou et al., 2005). Another lipogenic enzyme, FASN, is overexpressed in many cancers (Kuhajda, 2000) and treatment with FASN inhibitors (orlistat, cerulenin and C75) reduced cancer cell survival. However, FASN inhibitors have shown dramatic effects on whole body metabolism causing substantial weight loss in mice (Loftus et al.,

2000). It is therefore unclear whether inhibition of lipogenesis will be suitable as anti-cancer therapy.

Targeting the tumour microenvironment

The altered metabolic flux in cancer cells also leads to intra- and intercellular changes. The growing tumour mass depends on the diffusion of oxygen and nutrients for cell survival. One of the most studied antibodies to inhibit VEGFA-mediated angiogenesis is currently part of different clinical trials. Previous studies with bevacizumab alone have shown no OS benefits for breast cancer patients (Kerbel, 2009). However in other types of cancer, bevacizumab shows promising results. Current studies are investigating bevacizumab in combination with other chemotherapeutics to observe increased recurrence free and overall survival benefits.

To investigate the contribution of altered pH regulation in cancer cells to tumour development, Robey and colleagues explored the effect of systemic treatment with bicarbonate. Treatment with administered orally bicarbonate has counteracted acidosis in a mouse model and reduced metastasis formation of orthotopically injected MDA-MB-231 cells. However, the primary tumour showed no response to bicarbonate treatment (Robey et al., 2009). Recent studies have also investigated the inhibition of regulators of intracellular pH. Cariporide, an inhibitor of NHE1, has been shown to decrease viability in HeLa cells (Lin et al., 2011) as well as in combination with another inhibitor in glioma cell lines (Harley et al., 2010). These studies are all restricted to pre-clinical work *in-vitro*, but phase II/III clinical trials for carbonic anhydrases inhibitors are underway (Tennant et al., 2010).

In summary these different approaches provide evidence that targeting cancer metabolism is a promising therapeutic strategy. However, current clinical trials might not yield significant increase in overall survival due to non-specific patient selection. It has been recently acknowledged that pre-selection of patients in clinical trials should be based on the tumour genotype. Moreover, targeting cancer metabolism might be more effective when used in combination with other drugs. Identifying cohorts of patients that are likely to benefit from these treatments is of great importance. Suitable screens or genetic tests (e.g. detection of IDH mutations or FASN overexpression) have to be

employed to identify patients that are more likely to show a response in targeted clinical trials.

1.5 Aim of thesis

The aim of this thesis was to investigate the importance of metabolic enzymes, metabolite transporters and metabolic regulators for the survival of genetically diverse breast cancer cell lines. Not only is it important to identify the metabolic dependencies of each breast epithelial cell line but it is also important to identify their potential 'Achilles heel'. The following chapters will outline efforts to address the following aims of this thesis. These aims were:

- To characterise the metabolic phenotype of different breast cancer subtypes in a panel of genetically diverse breast epithelial cell lines.
- To identify metabolic enzymes, metabolite transporters and metabolic regulators that are selectively important for the survival of specific subsets of breast cancer cell lines by using a functional genetics approach.
- To analyse the mechanism by which these enzymes support the growth and survival of specific subtypes of breast cancer cell lines *in-vitro* and *in-vivo*.
- To explore mechanisms of deregulation of these enzymes in different subtypes of breast cancer.

2 Materials & Methods

2.1 Reagents and chemicals

2.1.1 Enzymes

Enzymes were used according to the manufacturer's instructions.

- Reverse transcriptase "Superscript II" (Invitrogen; Carlsbad, CA, USA).
- Restriction enzymes (New England Biolabs Inc, Ipswich, MA, USA)
- PfuUltra high-fidelity DNA polymerase (Agilent, Wokingham, UK)

2.1.2 Buffers and solutions

The use of commercially available as well as common solutions and buffers are mentioned below. Buffers and solutions for specific experiments are mentioned in the relevant sections. Solutions and buffers were prepared with ddH_2O and HCl or NaOH was used to adjust the pH.

2.1.3 Molecular weight marker

- 100 bp DNA ladder (New England Biolabs Inc)
- 1Kbp DNA ladder (New England Biolabs Inc)
- Full-range Rainbow molecular marker (RPN800E) (GE Healthcare, Chalfont, UK)

2.1.4 Bacterial strains

Escherichia coli (E.coli) strain DH5α (ThermoFisher Scientific, Loughborough, UK)

The *E.coli* strain DH5α strain is commonly used for cloning and propagating plasmid DNA. Genotype: F^-, φ80d*lacZ*ΔM15, Δ(*lacZYA-argF*)U169, *deoR*, *recA*1, *endA*1, *hsdR*17(rk^-, mk^+), *phoA*, *supE*44, λ^-, *thi*-1, *gyrA*96, *relA*1.

Ultracompetent XL-10 Gold (Agilent)

This strain is commonly used for cloning and propagating large plasmid DNA

Genotype: TetrD(mcrA)183, D(mcrCB-hsdSMR-mrr)173, endA1, supE44, thi-1, recA1, gyrA96, relA1, lac Hte [F´ proAB lacIqZDM15 Tn10 (Tetr) Amy Camr].

2.1.5 Plasmids

pCl-neo human monocarboxylate transporter 4 (h*SLC16A3*)

The pCl-neo h*SLC16A3* construct was kindly provided by Prof. Andrew Halestrap (University of Bristol). The genomic DNA sequence of *SLC16A3* was subcloned into the pCl-neo vector via the EcoRI restriction site. The vector contains two selectable markers, a puromycin resistance gene for selection of transduced mammalian cells and an ampicillin resistance gene for selection of transformed *E. coli.* The construct was digested with EcoRI to separate the h*SLC16A3* insert from the pCl-neo backbone.

pWZL-neo-ecotropic retroviral receptor (EcoR)

The pWZL-neo-EcoR construct was kindly provided by the Signal Transduction Laboratory, Cancer Research UK (CR UK). The construct is a retroviral expression vector coding for an ecotropic retroviral receptor. It contains two selectable markers, a neomycin resistance gene for selection of transduced mammalian cells and an ampicillin resistance gene for selection of transformed *E. coli*

pBABE puro3

The pBABE puro3 vector was kindly provided by Prof. Hartmut Land (Morgenstern and Land, 1990). This vector is a retroviral expression vector and it contains two selectable markers, a puromycin resistance gene for selection of transduced mammalian cells and an ampicillin resistance gene for selection of transformed *E. coli.*

pBABE puro3 h*SLC16A3*

The pBABE puro3 h*SLC16A3* construct was generated by cloning the h*SLC16A3* sequence of the pCl-neo h*SLC16A3* into a pBABE puro3 vector for rescue experiments.

Tet-pLKO-puro

The Tet-pLKO-puro construct was purchased from Addgene (Cambridge, MA, USA). This is a lentiviral expression vector containing two selectable markers: puromycin and ampicillin (Wiederschain et al., 2009). This construct also allows inducible expression of a gene of interest by the Tet repressor protein (TetR) cassette. In the absence of a tetracycline (e.g. doxycycline), the TetR is repressed, whereas in the presence of a tetracycline TetR and the gene of interest are expressed.

2.1.6 Cell lines

293T:

The 293T cell line is a derivative of the human embryonic kidney (HEK) 293 cells. 293T cells constitutively express the SV40 large T-antigen and are commonly used for generation of retroviral and lentiviral particles following transfection of the cells with retroviral and lentiviral plasmid constructs (Pear et al., 1993).

Phoenix cell line (amphotropic and ecotropic):

These cell lines are a derivative of the 293T cells and contain packaging genes gag-pol and envelope gene VSV-G. Phoenix ampho cells were used as amphotropically for gene delivery of the EcoR to all dividing cells. Phoenix Eco cells were used for gene delivery of pBABE puro3 *SLC16A3* constructs to all dividing cells containing an Eco receptor to allow virus production.

Breast cell line panel

The breast cell lines were obtained from American Type Culture Collection (ATCC) and CR UK Cell Services.

Table 2-1 Breast epithelial cell lines used in this study.

Cell line	Source
184B5	ATCC
AU-565	ATCC
BT-20	CR UK cell services
BT-549	CR UK cell services
HCC38	ATCC
HCC1806	ATCC
HCC1954	ATCC
HS-578T	ATCC
MCF7	CR UK cell services
MCF10A	ATCC
MCF12A	ATCC
MDA-MB-231	CR UK cell services
MDA-MB-436	ATCC
MDA-MB-468	CR UK cell services
SK-BR-3	CR UK cell services
T-47D	CR UK cell services
ZR-75-1	ATCC

2.1.7 Xenograft experiment

Immunodeficient 8-week old female mice (nu/nu) were injected orthotopically into the mammary fat pad with $1.5x10^6$ MDA-MB-468 cells that were stably transduced with TET-pLKO-SLC16A3 #88. After initial tumour formation (day 10), mice were divided into two cohorts, a cohort on a standard diet and the other cohort on a doxycycline diet.

The doxycycline containing food (0.2g/kg food pellets, TD.98186, Harlan Laboratories, Indianapolis, Indiana, USA) induced depletion of SLC16A3 and mice were monitored. Tumour measurements was carried out two times a week and tumour volume was determined by use of the ellipsoidal volume formula: ½ x length x $(width)^2$. All animal experiments were carried out according to the UK Home Office guidelines.

2.1.8 Antibiotics, inhibitors and other chemicals used in this study

All inhibitors were were solubilised in dimethyl sulfoxide (DMSO), double distilled water (ddH_2O) or ethanol (EtOH) and stored at 4ºC or -20ºC.

Table 2-2 Dilutions of antibiotics used:

Reagent	Supplier	Solvent	Stock solution	Final concentration	Type
Ampicillin	Sigma-Aldrich (St. Louis, MO, USA)	ddH_2O	1M	100μg/ml	Cell membrane synthesis inhibitor
Doxycycline	BD Biosciences (San Jose, CA, USA)	EtOH	1mg/ml	1μg/ml	Protein synthesis inhibitor
Geneticin (G418)	Invitrogen	ddH_2O	100mg/ml	100μg/ml	Protein synthesis inhibitor
Oligomycin	Sigma-Aldrich	DMSO	5mg/ml	0.05μg/ ml	Mitochondrial ATP synthase inhibitor
Puromycin	Sigma-Aldrich	ddH2O	1mM	2μg/ ml	Protein synthesis inhibitor

Table 2-3 Dilutions of inhibitors and activators used:

Reagent	Supplier	Solvent	Stock solution	Final concentration	Type
2-deoxy-D -glucose (2-DG)	Sigma-Aldrich	ddH_2O	2mM	2M	Inhibitor of glycolysis
AZD3965	AstraZeneca (London, UK)	DMSO	10mM	0.1μM-10μM	Monocarboxylate transporter 1inihibitor
Complete, Mini (EDTA free)	Roche (Basel, Switzerland)	DMSO	1mM	1μM	Protease inhibitor cocktail
Dichloroacetate (DCA)	Sigma-Aldrich	DMSO	0.4M	0.4mM	Inhibitor of pyruvate dehydrogenase kinase
Etoposide	Sigma-Aldrich	ddH_2O	10mM	2μM	Topoisomerase II inhibitor
Lapatinib	Provided by Dr. Eric Sahai	DMSO	200μM	1μM	Dual inhibitor of EGFR and HER2
PhosSTOP	Roche	-	20 tablets	1 tablet per 10ml	Phosphatase inhibitor
RNaseOUT	Invitrogen	-	200 units	1 unit	Recombinant Ribonuclease inhibitor

Table 2-4 Chemicals used:

Reagent	Supplier	Solvent	Stock solution	Final concentration	Type
Albumin from Bovine serum (BSA)	Sigma-Aldrich	ddH_2O	30%	3%	Blocking reagent
Ammonium carbonate	Sigma-Aldrich	ddH_2O	75mM	75mM	Washing buffer
Caspase-3 substrate IX	Merck Millipore (Darmstadt, Germany)	DMSO	1mg/ml	1μg/ml	Fluorogenic salt
CellTiter Blue	Promega (Fitchburg, WI, USA)	ddH_2O	100%	10%	Fluorescent dye
Cholera toxin (CT)	Sigma-Aldrich	ddH_2O	1mg/ml	100ng/ml	Growth factor
Crystal Violet	Sigma-Aldrich	ddH_2O	100%	0.10%	Dye
Deoxynucleotide (dNTP) mix	Invitrogen	ddH_2O	100mM	25mM	dNTP
EGF, murine	Merck Millipore	ddH_2O	50μg/ml	20ng/ml	Growth factor
FCCP	Sigma-Aldrich	DMSO	20mM	2μM	Uncoupling agent
Formaldehyde	Sigma-Aldrich	ddH_2O	37%	3.70%	Fixation reagent
Formic acid	Sigma-Aldrich	ddH_2O	98%	n.a.	Buffer
Goat serum	Sigma-Aldrich	TBST	100%	3%	Blocking agent
Hydrocortisone (HC)	Sigma-Aldrich	EtOH	10mg/ml	5μg/ml	Growth factor
Dithiothreitol (DTT)	Invitrogen	ddH_2O	1M	1mM	Redox agent
Insulin, bovine	Sigma-Aldrich	ddH_2O	10mg/ml	10μg/ml	Growth factor
N-Acetyl-L-cysteine (NAC)	Sigma-Aldrich	ddH_2O	100mM	5-20μM	Anti-oxidant
Orange G sodium salt	Sigma-Aldrich	Sucrose	30%	0.18%	tracking dye for nucleic acids
Protein assay	Bio-Rad (Hercules, CA, USA)	ddH_2O	100%	20%	Protein dye
Sodium L-Lactate	Sigma-Aldrich	ddH_2O	10M	10mM	Metabolite
4-hydroxy-2,2,6,6-tetramethylpiperidine-N-oxyl(Tempol)	Sigma-Aldrich	ddH_2O	10mM	1-2μM	Antioxidant
Tween 20	ThermoFisher Scientific	ddH_2O	100%	0.1%	Detergent

2.1.9 Media

Medium for culturing *E. coli* DH5α (ThermoFisher Scientific) and XL-10 Gold (Agilent):

The medium preparation and sterilisation process was performed by CR UK Cell Services.

Medium for in vitro culture of breast cancer cell lines:

Table 2-5 Media composition for breast cancer cell lines.

Media Components	Amount
D-MEM/F-12 (1:1) (Invitrogen)	500ml
Penicillin/Streptomycin (Gibco, Carlsbad, CA, USA)	1%
L-Glutamine stock solution (Invitrogen)	100units/ml
FBS (Gibco)	10%

Medium for in vitro culture of non-malignant breast cell lines:

Table 2-6 Media composition for non-malignant breast cell lines.

Media Components	Amount
D-MEM/F-12 (1:1) (Invitrogen)	500ml
Penicillin/Streptomycin (Gibco)	1%
L-Glutamine stock solution (Invitrogen)	100units/ml
Horse Serum (Gibco)	5%
Insulin (Sigma-Aldrich)	10μg/ml
Cholera toxin (Sigma-Aldrich)	100ng/ml
Epidermal growth factor (Merck Millipore)	20ng/ml
Hydrocortisone (Sigma)	5μg/ml

2.1.10 Antibodies

Antibodies for immunoblotting were stored and used according to manufacturer's instructions. Briefly, primary antibodies were diluted 1:1000 in 3% BSA/Tris buffered saline Tween 20 (TBST) blocking solution, except beta-actin-horse radish peroxidase (HRP) (1:10000) and HIF2α (1:500) in 5% milk/TBST. Phospho-specific primary antibodies were diluted in 3% BSA/TBST due to interference by milk as blocking solution. Secondary antibodies were diluted 1:2000 in 5% milk/TBST.

Table 2-7 Primary antibodies used in this study

Primary Antibody	Host	Clonality	Clone	Manufacturer	Catalog number
Acetyl CoA Carboxylase (ACC)	Rabbit	Polyclonal		Cell Signaling (Boston, MA, USA)	3662
AKT	Rabbit	Polyclonal		Cell Signaling	9272
Aldolase A	Mouse	Monoclonal	3D9-6F3	Novus Biologicals (Littleton, CO, USA)	H00000226-M01
AMPKα	Rabbit	Polyclonal		Cell Signaling	2532
Anti-β-Actin HRP	Mouse	Monoclonal	AC-15	Sigma-Aldrich	A3854
ATP- Citrate Lyase (ACLY)	Rabbit	Polyclonal		Cell Signaling	4332
CD147 (Q370)	Rabbit	Polyclonal		Novus Biologicals	NBP1-19677
Cleaved Caspase-3 (Asp175)	Rabbit	Polyclonal		Cell Signaling	9661
HIF1α	Mouse	Monoclonal	54/HIF1α	BD Biosciences	610959
HIF2α	Rabbit	Polyclonal		Novus Biologicals	NB100-122
MCT1	Rabbit	Polyclonal		Merck Millipore	AB3538P
MCT4	Rabbit	Polyclonal		Santa Cruz (Santa Cruz, CA, USA)	sc-50329
Malic enzyme 1	Mouse	Monoclonal	3H5	Novus Biologicals	H00004199-M03
Malic enzyme 2	Rabbit	Polyclonal		Novus Biologicals	NBP1-82434
PARP	Rabbit	Polyclonal		Cell Signaling	9542
Phospho-AMPKα (Thr172)	Rabbit	Polyclonal		Cell Signaling	2531
Phospho-ACC (Ser79)	Rabbit	Polyclonal		Cell Signaling	3661
Phospho-ACLY(Ser454)	Rabbit	Polyclonal		Cell Signaling	4331
Phospho-AKT (Ser473)	Rabbit	Polyclonal		Cell Signaling	9271
Phospho-AKT (Thr308)	Rabbit	Polyclonal		Cell Signaling	9275
Phospho-EGFR(Tyr992)	Rabbit	Polyclonal		Cell Signaling	2235
EGFR	Rabbit	Polyclonal		Cell Signaling	2232
Phospho- p44/42 MAPK (Thr202/Tyr204)	Mouse	Monoclonal	E10	Cell Signaling	9106
p44/42 MAPK	Rabbit	Polyclonal		Cell Signaling	9102
Fatty Acid Synthase	Mouse	Monoclonal	23	BD Biosciences	610963
p53	Mouse	Monoclonal	DO-7	Dako (Cambridgeshire,UK)	610984
p21 (C-19)	Rabbit	Polyclonal		Santa Cruz	sc-397
PTEN	Rabbit	Polyclonal		Cell Signaling	9552
HER2/ErbB2	Rabbit	Polyclonal		Cell Signaling	2242
TKTL1	Mouse	Monoclonal	JFC12T10	R-Biopharm (Darmstadt, Germany)	T-001

Table 2-8 Secondary antitbodies used in this study.

Secondary Antibody	Host	Clonality	Clone	Manufacturer	Catalog number
ECL Anti-rabbit IgG HRP	Donkey	Polyclonal		GE Healthcare	NA934V
ECL Anti-mouse IgG HRP	Sheep	Polyclonal		GE Healthcare	NA931V

2.1.11 Transfection reagents

Different transfection reagents were purchased to test and optimise the transfection efficiency for each of the breast cell lines used. The test amount was 0.1µl and 0.3µl of each reagent

Table 2-9 Transfection reagents used in this study

Transfection Reagent	Manufacturer
CodeBreaker™	Promega
DharmaFect 1	ThermoFisher Scientific
DharmaFect 2	ThermoFisher Scientific
DharmaFect 3	ThermoFisher Scientific
DharmaFect 4	ThermoFisher Scientific
DreamFect Gold	Oz Biosciences (Marseille, France)
FuGENE®	Promega
GeneEraser™	Agilent
GeneSilencer®	Genlantis (San Diego, CA, USA)
HiPerFect®	Qiagen (Germantwon, MD, USA)
INTERFERin®	Polyplus (Illkirch, France)
Lipofectamine	Invitrogen
Lipofectamine™ 2000	Invitrogen
Lipofectamine™ RNAiMAX	Invitrogen
Lullaby®	Oz Biosciences
METAFECTENE®	Cambio (Cambridge, UK)
N-TER™ Nanoparticle	Sigma-Aldrich
Oligofectamine™	Invitrogen
RiboJuice™	Merck Millipore
siIMPORTER™	Merck Millipore
siPORT™ Amine	Ambion
siPORT™ NeoFX™	Ambion
TransIT-siQUEST®	Mirusbio (Madison, Wi, USA)
TransIT-TKO®	Mirusbio
TransPass R1	New England Biolabs, Inc.
Plus Reagent	Invitrogen

2.1.12 RNA interference (RNAi) oligonucleotides

The small interference RNA (siRNA) oligonucleotides used for the small screen siRNA library and siRNA upgrades for deconvolution studies and follow up studies were purchased from ThermoFisher Scientific (siGenome series). Further information can be found in Appendix table 2.

2.1.13 Primers

Primers were ordered as desalted oligonucleotides and used for DNA sequencing and PCR amplification. Primer information is mentioned in the relevant method section.

Table 2-10 Sequencing and mutagenesis primers used in this study.

Gene	Nucleotides	Sequence 5'-3'	Orientation	Purpose
SLC16A3_oligo 3F	40	GCTGCTGGGCAAACTTCTTTTGGATTAGGAA GAAGCCCAAA	forward	site directed mutagenesis
SLC16A3_oligo 3R	40	TTTGGGCTTCTTCCTAATCCAAAAGAAGTTG CCCAGCAGC	reverse	site directed mutagenesis
SLC16A3_oligo 4F	34	CTCCTGGATGCGACGCACGTGTACATGTACG TGTT	forward	site directed mutagenesis
SLC16A3_oligo 4R	34	AACACGTACATGTACACGTGCGTCGCATCCA GGAG	reverse	site directed mutagenesis
SLC16A3_oligo 5F	35	GCGTCGCTGGGCATGGTAGCAGCATCCTTTT GCCG	forward	site directed mutagenesis
SLC16A3_oligo 5R	35	CGGCAAAAGGATGCTGCTACCATGCCCAGCG ACGC	reverse	site directed mutagenesis
SLC16A3_oligo 6F	35	CGAGGTTGCTCACCTCGTCGCTGATTTTGCTG CTG	forward	site directed mutagenesis
SLC16A3_oligo 6R	35	CAGCAGCAAAATCAGCGACGAGGTGAGCAC CTCG	reverse	site directed mutagenesis
SLC16A3_221-239F	20	ACAGGTCCGCTCTGCAGTGT	forward	sequencing
SLC16A3_396-415R	20	GGTTCAGCATGATGAGCGAG	reverse	sequencing
SLC16A3_1061-1080F	20	GTGCCATTGGCCTGGTGCTG	forward	sequencing
SLC16A3 1290-1309R	20	CCGAGTCTGCAGGAGGCTTG	reverse	sequencing
pBABE_ F	27	CCTCTTTCGACCCCGCCTCAATCCTCC	forward	sequencing
pBABE_ R	30	CCTGTGGAATGTGTGTCAGTTAGGGTGTGG	reverse	sequencing

2.2 Experimental procedures

2.2.1 Mammalian cell culture manipulations

2.2.1.1 Cell culture

184B5, AU-565, HCC38, HCC1806, HCC1954, HS-578T, MCF10A, MCF12A, MDA-MB-436 and ZR-75-1 were kindly provided from Dr. Britta Weigelt (CR UK, LRI), who obtained them from ATCC. BT-20, BT-549, MDA-MB-231, MDA-MB-468, MCF7, SK-BR-3 and T-47D were obtained from the CR UK Cell Services facility. The 293T cell line was obtained from the Signal Transduction Lab (CR UK, LRI). Phoenix cells were obtained from ATCC. All cell lines were grown in a monolayer and maintained in D-MEM/F-12 (1:1) (breast cell line panel) or DMEM (293T and Phoenix cells) media supplemented with 2mM L-glutamine and 100units/ml penicillin/ 100μg/ml streptomycin. The breast cancer cell lines, 293T and Phoenix cells were cultured in 10% foetal bovine serum (FBS). The three non-malignant cell lines MCF10A, MCF12A and 184B5 were maintained in 5% horse serum (HS), EGF, insulin,

hydrocortisone and cholera toxin. Cells were kept in a 5% CO_2 atmosphere at 37ºC and passaged approximately every 2-3 days when confluent according to ATCC's instructions. Briefly, the supernatant was aspirated, cell were rinsed once with PBS and then incubated with a 1:3 mix of trypsin/ versene at 37ºC until the cells detached. Next, the cells were resuspended in their designated media to neutralise trypsin. The non-malignant cells were centrifuged at 650 x g for 5 minutes (min) to remove remaining trypsin, the supernatant was aspirated and cells were resuspended in fresh media. For experimental purposes, the cells were counted and then seeded.

Table 2-11 Culturing overview of cell lines used in this study.

Cell line	Split ratio	Comments
184B5	1/3	spin after trypsin
AU-565	1/3	
BT-20	1/2-1/3	
BT-549	1/4-1/5	
HCC38	1/3	
HCC1806	1/6	
HCC1954	1/3-1/4	
HS-578T	1/3-1/4	
MCF7	1/5	
MCF10A	1/9	spin after trypsin
MCF12A	1/9	spin after trypsin
MDA-MB-231	1/5	
MDA-MB-436	1/2	no trypsin
MDA-MB-468	1/4	
SK-BR-3	1/2	
T-47D	1/4	
ZR-75-1	1/3	

2.2.1.2 Culture of cell lines under hypoxic conditions

For cell culture of breast cell lines under hypoxic conditions, cells were placed into a hypoxia chamber (Ruskinn Invivo$_2$ 500, Bridgend, UK). All breast cell lines were cultured under ≤0.5% oxygen conditions. For siRNA transfection experiments cells were transferred directly after seeding to the hypoxic chamber for 96 hours (h), whereas for protein and RNA extraction experiments cells were seeded 24 h prior to hypoxic exposure of 24 h.

2.2.1.3 Cryopreservation cells of cell lines

Exponentially growing cells were collected and pelleted as described above. Cells were then resuspended in freezing media (40% culture media, 50% FCS and 10% DMSO) and 1.5ml aliquots were gradually frozen in cryo vials (Nunc, ThermoFisher Scientific) and stored in a freezing container (Nalgene, ThermoFisher Scientific) at -80ºC for at least 24 h before being transferred to a liquid nitrogen tank for long term storage.

2.2.1.4 Recovery of cryopreserved cell lines

Frozen vials of cells were quickly thawed in a 37°C water bath. The thawed cell suspension of 1.5ml was added to 3ml pre-warmed culture medium in a 15ml falcon tube. The cells were then centrifuged for 5 min at 650 x g. The cell pellet was resuspended in 6ml fresh media and transferred to 25cm^3 culture dish for standard cell culture. Cells were incubated overnight before fresh media was added. Experiments with freshly thawed cells were set up after at least two passages.

2.2.1.5 Determination of cell number with Countess automated cell counter

The cells were counted using the Cell Countess (Invitrogen). Briefly, 10μl of a single cell suspension was mixed with 10μl trypan blue stain (0.4%). Next, 10 μl of the cell/trypan blue mix was pipetted into a disposable Countess chamber slide. Then, the Countess chamber slide was inserted into the instrument and the counting program was started. The principle of the Countess is similar to that of a hemacytometer, but it gives additional information such as average cell size of live, dead and total cells as well as the proportion of single cells versus multiple cells.

2.2.1.6 Reverse siRNA transfection of breast cell lines using Lullaby reagent

siRNA oligonucleotides of genes to be targeted were obtained from ThermoFisher Scientific. The lyophilized siRNA siGenome upgrades (2nmoles) were dissolved in 100μl 1x siRNA-buffer (Ambion). The silencing experiments were performed using a reverse transfection protocol with 37.5nM siRNA per well of a 96-well plate. Briefly, for a 96-well format 3,75μl of siRNA (1μM) were mixed with 6,25μl OptiMEM (Invitrogen) and incubated for 5 min. Meanwhile, 0,1μl of Lullaby transfection reagent (TF) from Oz Biosciences was mixed with 9,9μl of OptiMEM and then added to the siRNA/OptiMEM and incubated for 20 min. In parallel, cells were trypsinised and counted and then the optimised concentration of cells (see 2.2.17) was resuspended in a total of 80μl media. The 20μl transfection mixes were transferred to each well of a 96-well plate and the cell suspension was added on top to yield a final volume of 100μl. The plates were either incubated at a 20% or 0.5% oxygen atmosphere at 37ºC. The media was topped up to 200μl 24 h post transfection. Cells were analysed 96 h post transfection.

2.2.1.7 siRNA screening in breast cell panel

For each cell line, a transfection protocol was established during the optimization process.

Table 2-12 Overview of cell plating densities for transfections.

Cell line	Cells plated per well	TF reagent
184B5	5000 per 80µl	0.1µl
AU-565	7500 per 80µl	0.1µl
BT-20	6000 per 80µl	0.1µl
BT-549	3500 per 80µl	0.1µl
HCC1806	3000 per 80µl	0.1µl
HCC1954	5000 per 80µl	0.2µl
HCC38	8500 per 80µl	0.1µl
HS-578T	4000 per 80µl	0.1µl
MCF10A	4000 per 80µl	0.1µl
MCF12A	6000 per 80µl	0.1µl
MCF7	4000 per 80µl	0.1µl
MDA-MB-231	4000 per 80µl	0.1µl
MDA-MB-436	8500 per 80µl	0.1µl
MDA-MB-468	5000 per 80µl	0.1µl
SK-BR-3	7500 per 80µl	0.1µl
T-47D	7000 per 80µl	0.1µl
ZR-75-1	10000 per 80µl	0.1µl

2.2.1.8 Primary siRNA screen

Three days prior to screen:

All eighteen cell lines used for the siRNA screen were passaged under standard tissue culture such that they would be 90-95% confluent on the day of the experiment (e.g. screen day).

One day prior to screen:

Medium of all cell lines was refreshed 24 h prior to the experiment.

Screen day:

The aliquoted siRNA library containing 10µl of 375nM siRNA/Hank's Buffer Salt Solution (HBSS) mix were thawed for 20 min at room temperature (RT) and centrifuged for 1 min at 3000 x g. Next, 10µl of the transfection reagent mix (Lullaby/HBSS) was added to each well of each plate using an 8-channel multichannel pipette. The 20µl siRNA/Lullaby/HBSS mixes were left to incubate for 20 min at RT. Meanwhile the cells were rinsed with PBS once before trypsination. The cells were counted with the Cell Countess and for each cell line the optimised number of cells

were resuspended in 200ml freshly prepared media. A cell suspension of 80µl was then added to each well of the eighteen 96-well plates (9 plates each for normoxic and hypoxic culturing) per cell line by using the WellMate 8-channel microplate dispenser (ThermoFisher Scientific). This led to a total volume of 100µl per well with a final siRNA concentration of 37.5nM. The plates were then stacked into 2 groups (3 plates each of siRNA library plates 1,2 and 3 per oxygen condition). The plates for hypoxia were wrapped with aluminium foil to prevent evaporation before being placed into the hypoxic chamber (Ruskinn Invivo$_2$ 500), whereas the normoxic plates were placed in a standard incubator with 5% CO_2 atmosphere. Media for the hypoxic plates were prepared and incubated overnight to equilibrate in the hypoxic chamber to diminish as much oxygen possible within the media.

Day 1:

After 24 h, 100µl of the media was added to each plate. The cells were then incubated for a further 72 h.

Day 4:

The plates were processed in two batches of 9 plates (first normoxia, then hypoxia). The WellMate 8-channel microplate dispenser was programmed to remove the media first, and then the cells were fixed by adding 100µl of 80% ice-cold EtOH to each well. The plates were sealed with foil and stored at 4ºC until the next day.

Day 5:

The DAPI solution (1µg/ml) was prepared before the plates were de-sealed. The WellMate 8-channel microplate dispenser aspirated the EtOH, washed the fixed cells three times with 100µl PBS before adding 30µl of DAPI (1:5000 in PBS) was added for 1 h before aspirating the solution and adding 100µl of PBS. The plates were then sealed and read by the Acumen X^3 (TTP Labtech, Hertfordshire, UK), a laser scanning imaging cytometer to determine DAPI staining intensity as a readout for cell number.

2.2.1.9 Fixation and cell number quantification of cells

Cells were fixed in 80% EtOH (-20ºC) and stored for a minimum of 3 h at -20ºC, then fixed cells were washed three times with PBS before staining with 1µg/ml DAPI (Roche Diagnostics GmBH) to visualise stained cell nuclei, the Acumen X^3 (TTP Labtech) was used.

2.2.1.10 Viability assays

Trypan blue staining:

This is a standard method in cell culture to easily discriminate viable cells from non-viable cells. Briefly, 10µl of 0.4 % trypan blue solution (Invitrogen) was applied to 10µl of cell suspension and mixed carefully by pipetting up and down. After an incubation of 2 min, cells were counted using a Cell Countess (Invitrogen). Living cells appeared unstained due to their intact cell membrane, whereas dead cells were stained a blue colour.

Cell Titer blue:

This assay is based on a fluorescent method to monitor cell viability. Viable cells are able to convert the redox dye called resazurin into resofurin, a reaction which features auto fluorescence. Non-viable cells are not capable of generating this fluorescent end product given that these cells have lost the metabolic capacity to convert resazurin. The Cell Titer blue solution (Promega) is applied directly to cells cultured in serum-supplemented media and incubated for 1-3 h depending on the metabolic activity of each cell line (according to the manufacturers). This assay was used for assessing the viability of 3D cultures by adding 50µl Cell titer blue to 800µl media in each well of a 24-well plate. The fluorescent signal was measured with an EnVision fluorescence plate reader (PerkinElmer).

2.2.1.11 Generation of stably transfected cell lines expressing different SLC16A3 constructs using retroviral transduction

The pWZL construct containing EcoReceptor (5µg) was transfected into Phoenix amphotropic packaging cells using Lipofectamine™ PLUS™ (Invitrogen). Supernatant containing pseudotyped retroviruses were collected 72 h after transfection, filtered through a 0.45µm sterile filter (Merck Millipore) and used for transduction. Breast cancer cell lines were cultured 12 h prior to transduction in 100mm- dishes to obtain 25-35% confluent cells. Transduction was carried out with 100% retroviral supernatant plus hexadimethrine bromide (polybrene - at a final concentration 8µg/ml) (Abe et al., 1998). Cells were then incubated for 6 h after which virus-containing supernatant was replaced with fresh media after 6 h. The selection for infected cells started 36 h later with media supplemented with 0.5µg/ml G418 (Invitrogen). After a two-week selection

process, these cells were then infected with ecotropic retroviruses carrying pBABE puro3, pBABE puro3 h*SLC16A3* wildtype and the different pBABE-puro3 h*SLC16A3* constructs that have been mutated by site directed mutagenesis (see 2.2.2.6). After 24 h post infection, the cells were exposed to media supplemented with puromycin (1μg/ml) for selection of cells containing the pBABE puro3 constructs.

2.2.1.12 Generation of stably transfected cell lines expressing Tet-pLKO-shRNA constructs using lentiviral transduction

Cells stably expressing inducible short hairpin RNA (shRNA) targeting malic enzyme 1 (ME1), monocarboxylate transporter 4 (MCT4) and a non-targeting control (scrambled) were generated according to the Tet-pLKO-on manual found on the Addgene website (http://www.addgene.org/21915/). The shRNA sequences were obtained from the Mission system (Sigma-Aldrich) and cloned into the empty Tet-pLKO-puro vector. HEK-293-TLA cells were seeded at $4x10^6$ cells in 100mm dishes to reach confluency the following day. The transfection of HEK-293-TLA cells was achieved by co-transfecting 10μg plasmid DNA containing the shRNA sequence, 7.5μg of the gag-polyprotein encoding vector pCMVΔR8.91 and 2.5μg of the envelope encoding vector VSV-G using Lipofectamine2000^{TM}. Briefly, 80μl of Lipofectamine2000^{TM} was added to 520μl OptiMEM and incubated for 5 min. Meanwhile, the different plasmids DNAs (vsv-g, pCMVDR8.91 and shRNA containing plasmid DNA) were diluted together in a total of 600μl OptiMEM. Next, the Transfection reagent mix was added to the DNA mix and incubated for 30 min at RT. The HEK-293-TLA cells were carefully washed twice with OptiMEM before adding 4ml OptiMEM to the cells. The transfection reagent/ DNA mix was then drop wise added to the cells and left overnight. The following morning, the breast epithelial cells to be infected were then seeded to reach 40% confluency the next day. In parallel, 5ml media with 10% heat-inactivated serum was added to the HEK-293-TLA cells and incubated for another 24- 36 h. The next day, the lentivirus-containing supernatant from the HEK-293-TLA cells was collected, spun at 650 x g for 5 min and filtered through a 0.45μm sterile filter. The breast epithelial cells were washed once with D-MEM/F-12 (1:1) media before adding 5ml of a 1:1 lentivirus/media mix supplemented with 8μg/ml polybrene. The cells were incubated overnight before adding fresh media. The selection process with puromycin was started

36 h post-transfection and was stopped when the control cells were dead. Once the selection was complete, the cells were maintained puromycin free. Doxycycline was used at a final concentration of 1μg/ml to induce the expression of the shRNA and due to the half-life of doxycycline, it was re-added every 48 h. For RNA extraction, doxycycline was applied for 72 h. For protein analysis, doxycycline was added for 5 days and 9 days for cell viability/ clonogenic assays.

Table 2-13 shRNA sequences used in this study.

Gene symbol	Sequence	Orientation
Sh Scrambled	CCGGCCTAAGGTTAAGTCGCCCTCGCTCGAGCGAGGGCGACTTAACCTTAGG	forward
Sh Scrambled	AATTCCTAAGGTTAAGTCGCCCTCGCTCGAGCGAGGGCGACTTAACCTTAGG	reverse
SLC16A3	CCGGCGTCTACATGTACGTGTTCATCTCGAGATGAACACGTACATGTAGACGTTTTTG	forward
SLC16A3	AATTCAAAAACGTCTACATGTACGTGTTCATCTCGAGATGAACACGTACATGTAGACG	reverse
SLC16A3	CCGGGCTCATACAGGAGTTTGGGATCTCGAGATCCCAAACTCCTGTATGAGCTTTTTG	forward
SLC16A3	AATTCAAAAAGCTCATACAGGAGTTTGGGATCTCGAGATCCCAAACTCCTGTATGAGC	reverse
SLC16A3	CCGGCGTCTACATGTACGTGTTCATCTCGAGATGAACACGTACATGTAGACGTTTTTG	forward
SLC16A3	AATTCAAAAACGTCTACATGTACGTGTTCATCTCGAGATGAACACGTACATGTAGACG	reverse
SLC16A3	CCGGGCTCATCATGCTGAACCGCTACTCGAGTAGCGGTTCAGCATGATGAGCTTTTTG	forward
SLC16A3	AATTCAAAAAGCTCATCATGCTGAACCGCTACTCGAGTAGCGGTTCAGCATGATGAGC	reverse
ME1	CCGGGCCTTCAATGAACGGCCTATTCTCGAGAATAGGCCGTTCATTGAAGGCTTTTTG	forward
ME1	AATTCAAAAAGCCTTCAATGAACGGCCTATTCTCGAGAATAGGCCGTTCATTGAAGGC	reverse
ME1	CCGGGCTGAGGTTATAGCTCAGCAACTCGAGTTGCTGAGCTATAACCTCAGCTTTTTG	forward
ME1	AATTCAAAAAGCTGAGGTTATAGCTCAGCAACTCGAGTTGCTGAGCTATAACCTCAGC	reverse
ME1	CCGGGCTTCCTTAACACAAGAGAAACTCGAGTTTCTCTTGTGTTAAGGAAGCTTTTTG	forward
ME1	AATTCAAAAAGCTTCCTTAACACAAGAGAAACTCGAGTTTCTCTTGTGTTAAGGAAGC	reverse
ME1	CCGGCCTGTGGGTAAATTGGCTCTACTCGAGTAGAGCCAATTTACCCACAGGTTTTTG	forward
ME1	AATTCAAAAACCTGTGGGTAAATTGGCTCTACTCGAGTAGAGCCAATTTACCCACAGG	reverse

2.2.1.13 Clonogenic assay

To determine the effect of specific shRNAs on cell viability, shRNA expressing cells were plated in the presence or absence of doxycycline in 12-well plates in duplicates at a density of 10,000 cells per well. After 12 h, doxycycline (1μg/ml) or EtOH as control was added to the assigned wells. After 8 days, cells were washed twice in PBS before fixation with 4% paraformaldehyde (PFA) for 15 min at RT. Then, cells were stained with 0.05% crystal violet for 30 min on a rocker before being washed with distilled

water. Plates were dried overnight at RT. After 12 h, the dye was extracted by adding 0.5ml methanol per well and the OD was measured at 560 nm to determine relative proliferation.

2.2.1.14 Three-dimensional (3D) matrigel cultures and spheroids

For 3D cultures, the on-top matrigel assay was performed (Lee et al., 2007). Cells were reverse transfected with the siRNA of interest and seeded as a monolayer (2D culture) for 24 h. The next day, matrigel (BD Biosciences, phenol-red-free, growth-factor reduced) was thawed on ice and 200µl were used to coat one well of a 24-well plate, and incubated for at least 20 min at 37ºC to allow the matrigel to solidify. The transfected cells were detached with trypsin to generate a single-cell suspension and the cell number was determined by the Cell Countess System (Invitrogen).

Table 2-14 Cell suspensions used for three- dimensional growth studies:

Cell line	Cell number for on-top matrigel (24-well plate)	Number of cells plated for spheroid formation assay (96-well plate)
MCF10A	20,000	-
MDA-MB-231	20,000	2000
MDA-MB-468	30,000	1000
HCC1954	20,000	2000

The number of cells for 3D matrigel cultures used for seeding was diluted to a total volume of 600µl and put on ice for 5-10 min. Next, 35µl matrigel was added to the cells, mixed and carefully transferred on top of the solified matrigel in the plates.

For spheroid formation, the optimised cell number for each cell line tested was diluted in 100µl media. Prior to plating in a 96-well format, cells were incubated on ice for 5-10 min. Next, 2% matrigel was added before the cells were seeded in a 96-well plate and centrifuged for 10 min at 650 x g at RT.

2.2.1.15 Fluorescence-activated cell sorting (FACS) analysis for cell cycle

Flow cytometry was used to analyse cell cycle, reactive oxygen species (ROS) and intracellular pH. All cells used were reverse transfected with the siRNA duplexes of interest for 72 h. The labelled cells were transferred to polystyrene tubes (BD Falcon) and analysed by laser emission in the mentioned flow cytometer (BD Bioscience).

Cell cycle analysis

Cells were washed once in PBS (1x) before being harvested and fixed with ice-cold 70% EtOH and stored at 4ºC for at least two hours or up to a month. Then cells were

washed twice in ice-cold PBS. To ensure that only DNA was stained, cells were treated with 50µl ribonuclease (100µg/ml) for 5 min. After the digestion step, 200µl of propidium iodide (50µg/ml) were added and samples were immediately analysed on the flow cytometer.

Reactive oxygen species (ROS) detection

An h prior to starting the experimental analysis, 1µM H_2O_2 was added to the assigned positive control well. Then, cells were incubated with 5µM 6-carboxy-2',7'-dichlorodihydrofluorescein diacetate, a chemically reduced, acetylated form of fluorescein that is used as an indication of the presence of reactive oxygen species (ROS) (Carboxy-H_2DCFDA, Molecular Probes) for 30 min at 37ºC. Excess H_2DCFDA was removed and the labelled cells were then trypsinised, cells were suspended in PBS, centrifuged at 650 x g for 5 min and rinsed twice with ice cold PBS and resuspended in 400µl PBS. The cell suspension was immediately analysed on the LSRIIb flow cytometer.

pH detection

Intracellular pH was determined with 10µM SNARF-4F 5-(and-6)-Carboxylic Acid (Molecular probes). Briefly, cells were harvested and washed once in PBS, before being incubated with SNARF-4F for 30 min at RT. Excess dye was removed by centrifugation and two washing steps with ice cold PBS. Cells were resuspended in 400µl PBS and measured on the Fortessa cytometer (BD Biosciences)

2.2.1.16 Measurement of rate of glycolysis with tritiated glucose

The uptake of radioactively labelled glucose and the rate of glycolysis was measured by monitoring the conversion of 5-^{3}H-glucose to ^3H_2O. Briefly, cells were washed once in PBS prior to incubating them in 0.5ml of glucose free DMEM media (CR UK Cell Services) for 30 min at 37°C. Cells were then exposed to DMEM media containing glucose (10mM) spiked with 10µCi of 5-^{3}H-glucose. Following incubation for 1 h at 37°C, triplicates of 50µl aliquots in DMEM media were transferred to uncapped PCR tubes containing 50µl of 0.2N hydrogen chloride (HCl), and the PCR tube was carefully transferred to a scintillation vial containing 0.5ml of H_2O. The scintillation vial was then sealed and incubated for 24 h at RT to enable diffusion of the contents of the PCR

tube into the H_2O. The amounts of diffused and un-diffused ^3H were then determined by scintillation counting. ^3H-glucose-only and ^3H_2O-only controls were included in each experiment to enable the calculation of ^3H_2O per sample, as well as the rate of glycolysis.

2.2.1.17 Detection of cleaved caspase 3/7 activity

Apoptotic cell death was determined using the Apo-ONE assay based on that from Promega, which allows fluorometric measurement of the activity of caspases 3 and 7. Cells were cultured in a 96-well format for allocated times in a total volume of 100μl. For each well, 100μl of the buffer mix containing the light sensitive pro-fluorescent caspases 3/7 substrate (Z-DEVD-R110) were prepared and added for 1.5 h incubation in the dark at RT. Samples with active caspase 3/7 allowed cleavage of the c-terminal part of the DEVD substrate, and the resulting R110 (Rhodamine 110) fluorescence was measured at a wavelength of 485 nm using an EnVision Mulitlabel plate reader (Perkin Elmer). The amount of fluorescence generated is representative of the amount of cleaved caspases 3/7 in each sample. To normalise each value to the total protein content of the cells, a sulforhodamine B assay was performed afterwards.

Table 2-15 Apo-One buffer pH7.3

Components	Concentrations
HEPES	25mM
EDTA	1mM
NaCl	10mM
DTT	5mM
CHAPS	0.10%
Z-DEVD R110 substrate	0.01mg/ml

2.2.2 Nucleic acid manipulations

2.2.2.1 Extraction of total RNA

Total RNA was extracted from cells using the RNeasy Mini Kit (Qiagen) according to the manufacturer's instructions for extraction of animal tissues. Briefly, cells were disrupted with RLT buffer and the mixture was transferred to shredder columns (QIAshredder, Qiagen). The additional step with DNAse was also performed. The RNA was eluted in 20-40μl of nuclease-free water (Ambion) depending on the input of cells used for RNA extraction. The RNA concentration was measured using the NanoDrop spectrophotometer (ThermoFisher Scientific). The RNA was stored at -80ºC.

2.2.2.2 Complementary DNA synthesis

Total RNA was used to generate its complementary DNA (cDNA) with SuperScript II reverse transcriptase, Oligo dT_{12-18} and RNaseOUT (Invitrogen). Reverse transcription was performed according to the first-strand cDNA synthesis protocol (Invitrogen). Briefly, 1µg RNA was mixed with 1µl of 10mM dNTPs and 1µl Oligo dT_{12-18} primer (500µg/ml) up to a total volume of 12µl and the mix was heated for 5 min at 65ºC. Then, the samples were cooled for 5 min on ice before adding 8µl SuperScript II mix to each sample (5x first strand buffer, 0.1M DTT, 1µl RNAseOUT (40units/µl), 1µl SuperScript II reverse transcriptase (200units/µl). The RNA/ SuperScript mixes were incubated for 90 min at 42ºC to generate cDNA.

2.2.2.3 Nucleic acid quantification

RNA and DNA concentrations were quantified using the NanoDrop spectro-photometer (ThermoFisher Scientific). Briefly, 2µl of nucleic acid solution was used for each measurement. The RNA and DNA were always eluted in nuclease free water and nuclease free water was used as blank.

2.2.2.4 Quantitative real time PCR (RT-PCR)

Quantitative RT-PCR is based on a PCR, where the amplified product is measured after each cycle by a fluorescence detector for amplification (7900HT Fast Real-Time PCR System, Applied Biosystems). Here, the SYBR Green I dye (Platinum® SYBR® Green qPCR SuperMix-UDG with ROX, Invitrogen) was used as the fluorescent dye, which binds to double-stranded DNA during the elongation phase (Ponchel et al., 2003). The disadvantage of this method is that each double-stranded product, whether specific or non-specific, emits a signal. To confirm the presence of a single double-stranded PCR-product, and confirming the specificity of the RT-PCR performed, a dissociation curve was created using the standard melting-curve program (90ºC-65ºC) of SDS2.3 software. For every single PCR product, the ratio of fluorescence intensity and temperature is displayed via a peak. The more identical products are present in the PCR reaction, the higher is the peak of the melting curve. Therefore a melting curve can be used as internal quality control that provides information on how many double-stranded products are in a given sample and if primer dimers are present and influenced the cycle threshold (C_T) obtained for a sample.

Each reaction included 12.5µl Platinum® SYBR® Green qPCR SuperMix-UDG with

ROX, 2.5µl QuantiTect Primer (10pmol/µl) and 100ng cDNA. Negative controls such as non-template controls were always included in each run.

The analysis of the quantitative RT-PCR is based on the number of PCR cycles where a certain level of fluorescence needs to be present. The C_T value is fixed at the exponential phase of the PCR curve. The C_T is proportional to the logarithm of initial amount of the mRNA/cDNA of the gene of interest in a sample. To compare the relative concentration of a gene of interest among different samples, the control gene β-actin was determined in each sample to reflect the difference in cycle number (ΔC_T) for normalisation of the samples (Livak and Schmittgen, 2001).

Table 2-16 RT-PCR conditions.

Temperature	Time	Cycle(s)
50ºC	2 min	1x
95°C	5 min	1x
95°C	15 sec	40x
60°C	1 min	

Table 2-17 Qiagen QuantiTect Primer used in this study.

Gene symbol	Gene	Catalog number
ACTB	β-Actin	QT01680476
ALDOA	Aldolase A	QT00082460
ALDOB	Aldolase B	QT00094038
ALDOC	Aldolase C	QT00996786
BSG	Basigin	QT00074564
CAD	Carbamoyl-phosphate synthetase 2, aspartate transcarbamylase, dihydroorotase	QT00057603
CHPT1	Choline phosphotransferase 1	QT00038549
EPAS1	Endothelial PAS domain-containing protein 1	QT00069587
G6PD	Glucose-6-phosphate dehydrogenase	QT00071596
HIF1α	Hypoxia inducible factor 1 alpha	QT00083664
HK2	Hexokinase 2	QT00013209
LDHA	Lactate dehydrogenase A	QT00001687
LDHB	Lactate dehydrogenase B	QT00071512
ME1	Malic enzyme 1	QT00005943
ME2	Malic enzyme 2	QT00031962
OXCT2	3-oxoacid CoA transferase	QT02318729
PPAP2A	Phosphatidic acid phosphatase type 2A	QT00067193
PPAP2B	Phosphatidic acid phosphatase type 2B	QT00052836
PPAP2C	Phosphatidic acid phosphatase type 2C	QT00064372
SLC16A1	Monocarboxylate transporter 1	QT00012838
SLC16A3	Monocarboxylate transporter 4	QT00085855
SLC2A1	Glucose transporter 1	QT00068957
TKTL1	Transketolase 1	QT00017402
VEGFA	Vascular endothelial growth factor A	QT01682072

2.2.2.5 DNA restriction digestions

To confirm that plasmid DNA contains the expected insert or to insert a sequence into a plasmid, the DNA was digested. For this, 1-5µg DNA per reaction were used for digestion with 1µl of each restriction enzyme, 2µl restriction enzyme buffer (10x), 0.2µl BSA (100x) in a total volume of 20µl using ddH_2O. The mix was incubated for either 2

h or overnight at 37°C. All restriction enzymes and buffers were purchased from New England Biolabs. A sample of the reaction product was used for analysis by agarose gel electrophoresis (see 2.2.8).

2.2.2.6 PCR based site directed mutagenesis

The mutagenesis of the complementary sequence of the h*SLC16A3* plasmid that can be targeted by the *SLC16A3* siRNAs has been carried out according to the QuikChange site directed mutagenesis protocol (Agilent).

2.2.2.7 DNA sequencing

To determine a DNA sequence, Sanger sequencing was performed using specific primers and the ABI PRISM® dGTP BigDye® Terminator v3.0 mix (Applied Biosystems). The reaction mix consisted of 200-500ng plasmid DNA, 8µl BigDye Terminator (BDT) mix and 5pmol primer containing nuclease free water (Ambion) to a total volume of 20µl. After the sequencing PCR, the samples were purified with the DyeEx 2.0 spin kit (Qiagen) according to manufacturer's instruction to remove unincorporated dye. The centrifugation steps were carried out at 750 x g for 3 minutes. David Philips, a member of the CR UK LRI equipment park, carried out the sequencing experiments. The sequence analysis was performed by using SeqMan Pro 8.1.5 (Lasergene).

Table 2-18 Sequencing PCR condition.

Temperature	Time	Cycle(s)
96ºC	10 sec	25x
55°C	5 sec	
60°C	4 min	
12°C	∞	1x

2.2.2.8 Agarose gel electrophoresis

To confirm the digestion of plasmids and insertion of sequences, UltraPure™ Agarose (Invitrogen) for a 1-2% gel (depending on size of DNA fragments) prepared with 1x TAE buffer to separate DNA samples were run for 1 h at 120 V. Ethidium bromide was added to the gel and to the TAE running buffer at a final concentration of 0.5µg/ml to visualise DNA under UV light. DNA samples were mixed with 6x DNA loading dye to load them into the wells of the agarose gel. The size of the DNA fragment(s) was established by using 100bp or 1Kbp DNA ladder on the same gel.

2.2.2.9 Purification of DNA fragments from agarose gel

To extract and purify a given DNA sample from an agarose gel, the designated band was extracted with a scalpel under longwave UV light and transferred into a 1.7 ml reaction tube. Next, the DNA was eluted using the QIAquick Gel Extraction kit protocol (Qiagen) according to the instructions. The elution step was carried out with 40µl ddH_2O rather than buffer EB.

2.2.2.10 Transformation of E.coli DH5α with plasmids

An aliquot of chemically competent *E.coli DH5α* was thawed slowly on ice. 100-500ng of plasmid DNA was added to 50µl competent *E.coli DH5α* cells gently mixed and incubated for 30 min on ice. The mixture was then incubated at 42°C for 45 seconds (sec) and immediately after the heat-shock placed on ice for 5 min. Then, 900µl of pre-warmed liquid LB media without antibiotics was added and the bacterial suspension was incubated at 37°C at shaking at 225 rpm for 60 min in a shaking incubator. 100µl of bacteria suspension was plated on solid LB media agar plates containing ampicillin, incubated for 10 min at RT followed by an overnight incubation at 37°C. Transformed colonies were picked and grown for isolation of plasmids by Mini and/or Maxi-prep kits (Qiagen).

2.2.2.11 Transformation of XL10-Gold with ligation reactions

The protocol for transforming XL-10-Gold bacteria with Tet-pLKO-puro constructs was followed according to the Agilent's instruction. Briefly, an aliquot of chemically ultracompetent XL10-Gold was thawed slowly on ice. Next, 4µl β- mercaptoethanol was added to 100µl competent cells and incubated for 10 min prior to adding 4µl of ligation mixture and, gently mixed and incubated for 30 min on ice. The mixture was then incubated at 42°C for 30 sec and immediately after the heat-shock placed on ice for 2 min. Then, 900µl of pre-warmed liquid LB media (42ºC) without antibiotics was added and the bacterial suspension was incubated at 37°C shaking at 225 rpm for 60 min in a shaking incubator. A bacterial suspension of 100µl was plated onto solid LB media agar plates containing 75µg/ml ampicillin, incubated for 10 min at RT followed by an overnight incubation at 37°C. Transformed colonies were grown and picked for isolation of plasmids by Mini and/or Maxi-preparation (Qiagen).

2.2.2.12 Preparation of plasmid DNA

To isolate plasmid DNA from *E.coli DH5α* or *XL-10-Gold* colonies, multiple clones were picked from the LB-agarose plates and cultured in a total volume of 6ml LB medium. After 12-16 h, mini-cultures were used for plasmid DNA extraction or if larger quantities were required, the mini culture was used to inoculate 400ml of LB medium supplemented with ampicillin (50μg/ml) and incubated overnight at 37°C. The isolation of the plasmid DNA was carried out by using the Qiagen Mini/ Maxiprep Kit (Qiagen) according to the manufacturer's instructions. The air- dried DNA pellets were dissolved in ddH_2O and the purity was measured by spectrometry ($Abs_{280/260}$).

2.2.3 Protein manipulations

2.2.3.1 Preparation of cell lysates for immunoblots

The following procedure was used to extract proteins from adherent cells. Briefly, the medium was aspirated and cells were washed with 1x cold PBS prior to lysis with cold TNET buffer supplemented with protease (Complete, EDTA free) and phosphatase (PhosStop, Roche) inhibitors and DTT. After incubation on ice for 10 min, a cell scraper (Sarstedt; Newton, NC USA) was used to collect cell lysates. The cell/protein lysates were transferred to 1.7ml reaction tubes and centrifuged at maximum speed for 10 min at 4°C. The supernatants were then carefully transferred into new 1.7ml tubes. Protein lysates were stored at -80°C until further use.

Table 2-19 TNET lysis buffer

Components	Concentrations
NP-40	1%
Tris-HCL (pH8.0)	20mM
NaCl	137mM
Glycerol	10%
EDTA	2mM
DTT	1mM
Sodium orthovanadate	

2.2.3.2 Protein quantification using Bradford assay

In order to load equal amounts of protein samples on SDS- polyacrylamide gels, the protein concentration was determined using Bradford reagent (Bio-Rad Protein Assay). BSA was used to generate a standard curve. The procedure was performed according to the manufacturer's protocol in a 96-well plate. After 5 min incubation period of each sample at RT, the absorbance at 595nm was determined on a SpectraMax 190 plate reader using the SoftMax Pro software (Molecular devices).

Table 2-20 Dilution of BSA to generate standard curve

µg/µl BSA	µl BSA (0.025µg/µl)	Bradford reagent (µl)
0	0	250
0.4	2	250
0.8	4	250
1.2	6	250
1.6	8	250
2.0	10	250
2.4	12	250
2.8	14	250

NuPage loading dye (4x) was added to 15-20µg protein lysates to denature the proteins. TNET buffer was used to equalise total volumes of cell lysates used for separation on sodium dodecyl sulphate (SDS)-gels. The mixture was vortexed followed by a 10 min incubation period at 70°C. For this study only 4-12% gradient gels were used to separate the proteins (see 2.2.3.3).

Table 2-21 Recipe for 4x NuPage Loading Dye

Components	Concentrations
SDS	8%
Tris Base	200mM
Glycerol	40%
Bromphenol Blue	0.01g/L
β-mercaptoethanol	2%

2.2.3.3 Sodium dodecyl sulphate-page

SDS-page is a common method used to analyse proteins as this technique allows the separation of proteins based on molecular weight (Laemmli, 1970). The detergent SDS is not only used to denature the proteins into subunits but also imparts a uniform charge to them. Therefore, proteins will separate solely based on size and not charge. The 15-30 µg of protein lysates of interest were loaded in the pockets of a pre-cast 4-12% Novex®- NuPage TRIS-glycine SDS-page gels (Invitrogen). The MOPS SDS running buffer was purchased from Invitrogen. Pre-stained protein markers RPN800E full-range (Amersham) were used as a molecular size standard to determine the approximate size of the proteins in the protein lysates. The protein lysates loaded on the gel were separated at 150 V for 60-90 min.

Table 2-22 Recipe for NuPAGE® MOPS SDS Running Buffer pH7.7 (20X) (500ml)

Components	Concentrations
MOPS	50mM
TRIS base	50mM
SDS	0.10%
EDTA	1mM

2.2.3.4 Immunoblotting procedure

Immunoblotting is a commonly used method to transfer proteins separated by denaturing gel electrophoresis onto a membrane. To transfer the proteins from a 4-12% gradient gel onto a Immobilon-P membrane (Merck Millipore) an electrophoretic transfer cell (Bio-RAD) was used according to the manufacturer's instructions. Briefly, the PVDF membrane was prepared by activating it for 15 sec in methanol followed by a quick wash with transfer buffer. All other components for the blot were equilibrated in transfer buffer. The SDS-gel was gently removed from the plastic and rinsed in transfer buffer for 1 min. Then the gel was loaded onto the membrane and the transfer was carried out at 250 mA for 120 min. To prevent unspecific binding of the antibodies to the membrane, membranes were then blocked in 5% milk or 3% BSA for 1 h at RT. A primary antibody against a specific protein of interest on the membrane was diluted according to the manufacturer's instructions and incubated overnight at 4°C on a shaker (see Table 2.7). The following day the antibody solution was removed and washing steps were carried out by rinsing the membrane twice and washing the membrane for 2 x 5 min with 5% milk/TBST and 4 x 5 min in 0.1% TBST on a shaker. After the washing steps, a secondary antibody conjugated to horseradish-peroxidase (HRP) were used to visualise the primary antibody bound to the protein of interest on the membrane (see Table 2.8). The secondary antibody was diluted 1:2000 in 5% milk/TBST and incubated for 45 min at RT on a platform shaker. The secondary antibody was then visualised by chemiluminescence using the Amersham ECL detection kit (GE Healthcare) and detected by Medical X-ray film (Hyperfilm, GE Healthcare). The film was developed with an automatic X-ray film processor (JP-33, *JPI* Healthcare Solutions, Planview, NY, USA) after different exposure times depending on the signal intensity.

Table 2-23 Transfer buffer

Components	Concentrations
Glycine	250mM
Tris Base	25mM
Methanol	10%

Table 2-24 Tris-buffered saline (TBS) pH7.4

Components	Concentrations
NaCL	137mM
Tris Base	25mM

Table 2-25 Blocking solution

Components	Concentrations
Milk powder or BSA	5%
TBS	500ml
Tween 20	0.10%

Table 2-26 TBST- washing buffer

Components	Concentrations
TBS	500ml
Tween 20	0.10%

2.2.3.5 Sulforhodamine B assay

To determine the protein content of cell lines used for metabolic and cleaved caspase activity assays, a sulforhodamine B staining was performed. This method was adapted from (Vichai and Kirtikara, 2006). Supernatant/ media was aspirated from the cells, which were then fixed with cold 10% tri-chloro-acetic acid (TCA) in PBS and incubated for 1 h at 4ºC. Next the cells were washed twice with 100µl/well ddH_2O and air-dried at RT overnight. The following day, 50µl/well of a 0.4% Sulforhodamine B in 1% acetic acid solution was added and incubated on a rocking platform for 30 min at RT. The stained and fixed cells were then washed twice in 1% acetic acid. Cells were dried for 1 h before adding 100µl/well 10mM TRIS pH8 to re-solubilise the Sulforhodamine B dye for 5 min on a rocking platform at RT. For quantification of the protein content, a colorimetric measurement was performed at three different wavelengths 530, 565 and 690nm using a SpectraMax 190 plate reader (Molecular Devices, Sunnyvale, CA, USA) and analysis was determined by SoftMax Pro software.

2.2.3.6 Immunofluorescence

Glass coverslips were placed in 12-well plates and cells were directly seeded onto these coverslips (13mm, ThermoFisher Scientific). Three days post-seeding, cells were fixed with 3.7% PFA for 15 min at RT followed by two wash steps with PBS. Then, the cells were permeabilised using 0.1%Triton- X 100 for 15 min at RT. Cells were blocked for 1 h in 3% normal goat serum (NGS) before adding anti-MCT4 antibody (see 2.1.9) diluted in 3% NGS (1:300) for 2 h at room temperature. After exposure to the primary antibody, coverslips were washed twice with PBS. Then the secondary antibody Alexa Fluor 633-conjugated anti-rabbit (Molecular probes) diluted in 3% BSA (1:500) was added to the cells for 1 h. Cells were then washed with PBS and nuclei were stained with DAPI (1µg/ml) for 30 min. Following two washes with PBS, the coverslips were mounted on a microscope slide (ThermoFisher Scientific) with 40µl Mowiol

(Calbiochem) and dried overnight. The image acquisation was obtained by using a LSM 710 Upright Confocal microscope (Carl Zeiss) with a 63x Plan APOCHROMAT 1.4 Oil immersion objective (Carl Zeiss) at RT. Image capture was achieved with the ZEN2009 software. All images were processed according to the LRI image processing guidelines.

2.2.3.7 Immunohistochemistry

All immunohistochemical staining was performed by the LRI Experimental Histopathology Laboratory (Prof. Gordon Stamp and Dr Bradley Spencer-Dene).

Tissue microarray (TMA) slides BR1503 were purchased from US Biomax, Inc. (Rockville, MD, USA). Each contained cores in duplicates of three normal breast tissue, three fibrocystic adenomas, two cystosarcoma phyllodes, seven intraductal carcinomas and sixty invasive ductal carcinomas. All tissues were neutral buffered formalin (NBF) fixed and paraffin embedded. The thickness of each section was 5μM. To remove paraffin from the TMA, slides were incubated for 2 x 3 min in xylene, then for 2 x 3 min in 100% industrial methylated spirit (IMS) and rehydrated in 70% IMS and distilled water. For antigen retrieval, slides were microwaved in 0.01M sodium citrate (pH6) for 15 min (900W oven, on medium setting), and then cooled for 20 min. To block endogenous peroxidase activity slides were incubated for 10 min in 1.6% H_20_2/PBS. After brief washes in distilled water and PBS, slides were blocked in 10% normal goat or horse serum in 1% BSA/PBS for 30 min before the primary antibody was applied. Primary antibodies were all diluted in 1% BSA/PBS and incubated for 1 h at RT in a humid chamber (dilutions are shown in table 2.26). After primary incubation slides were washed 3 x 2 min in PBS and incubated in biotinylated goat anti rabbit IgG (1/250 in 1%BSA/PBS) or biotinylated horse anti mouse IgG (1/400 in 1%BSA/PBS) for 45 min at RT. After 3 x 2 min PBS washes slides were incubated in Avidin-Biotin-Complex (Vector Labs) for 30 min washed again in PBS then developed with Diaminobenzidine (DAB). After washing in distilled water, slides were counterstained with haematoxylin, washed in tap water, dehydrated, cleared and finally mounted in DPX mountant. As positive controls, different tissues were the protein of interest is expressed, were used. Moreover, secondary antibody only stain as negative control was performed on some tissue samples to check for unspecific binding.

For immunohistochemical staining of spheroids grown in vitro, spheroids were collected with a cut 200ml pipette tip and fixed in 3.7% PFA for 16h at 4ºC. The spheroids were then centrifuged and washed with 70% EtOH for short-term storage. To facilitate handling and sectioning, spheroids were rehydrated in distilled water and transferred into liquid molten 2% agarose in a petri dish and then, when cooled, a small block of agarose containing the spheroids was isolated and paraffin processed. After embedding, serial 4μm sections were cut onto positively charged slides and dried overnight at 37^{o}C. Each set of spheroids was processed in a serial and stained histologically for haematoxylin and eosin. For immunohistochemical staining the same protocol used for the TMA sections was followed.

Table 2-27 Primary antibodies used in this study:

Primary Antibody	Dilution
MCT4	1/300
cleaved caspase 3	1/900
Hydroxyprobe 1	1/100

2.2.4 Metabolic Manipulations

2.2.4.1 Oxygen measurement

Measurements of cellular oxygen consumption rates were determined with the BD Oxygen Biosensor system (BD Biosciences). This system is based on oxygen sensitive fluorophore (tris 4,7 diphenyl- 1,10-phenanthroline ruthenium (II) chloride), which is quenched when oxygen is present (Rolo et al., 2009). 96-well plates coated with this fluorophore embedded into a silicone rubber matrix were used. Empty plates were measured on the EnVision™ Multilabel Plate Reader (excitation=485nm, emission=630nm) prior to use to compare levels of autofluorescence. Cells to be analysed for oxygen consumption were harvested after trypsination and counted. Then, 1x10^{6} cells were plated in a total volume of 200μl of media per well in these 96-well plates. Three independent measurements were performed for each cell line. Standard cell culture medium was used to determine the basal oxygen consumption rate of the cells analysed, and addition of the uncoupling agent carbonyl cyanide *p*-(trifluoromethoxy) phenylhydrazone (FCCP) (Sigma-Aldrich) to the media at a final concentration of 2μM was used to establish the maximal oxygen capacity. The ATP synthase inhibitor oligomycin (Sigma-Aldrich) inhibits respiration and was added to the media at a final concentration of 0.05μg/ml. The plates were sealed prior to the

measurements. After an incubation time of 15 min, the plates were scanned and measurements taken every 2 min for 2 h on the EnVision™ Multilabel Plate Reader (excitation= 485nm, emission= 630nm). The time profile was then analysed with Excel software, where the values were normalised to measurements from wells containing medium only. The slope of the fluorescence signal was calculated within the dynamic range of the measurements to compare it to the oxygen consumption profile of other cell lines. As a positive control, the oxygen scavenger agent sodium sulphite was used.

2.2.4.2 Cell proliferation assay

Cell lines were plated in 96-well plates using the cell number established for the siRNA screens (see Table 2.12). After 24 h, cells were washed once in PBS before adding complete culture media consisting of DMEM supplemented with 10% dialysed FCS, either in the presence or absence of glucose and/or glutamine. DMEM was used here, because DMEM/F12 was not available without glucose and glutamine. Cells were fixed in 80% EtOH 72 h later and cell number was determined with Acumen X^3.

2.2.4.3 Measurement of intracellular lactate

Intracellular lactate concentrations of the breast cell lines MCF10A, HCC1954, MDA-MB-231 and MDA-MB-468 were measured. Briefly, cells were washed in PBS twice before being harvested. The cells were then collected after the centrifugation step, resuspended in ice cold PBS and counted. Next, $0.5x10^6$ cells were centrifuged, and then lysed with 200µl dH_2O using a 21G syringe. After 20 min incubation on ice, the cell suspension was centrifuged for 5 min at 650 x g. The analysis of the lactate levels was carried out with the lactate kit from BioVision (Milpitas, CA, USA), according to the manufacturer's instruction.

2.2.4.4 Measurement of utilised glucose

Glucose uptake of breast cell lines were measured after 1 h starvation in glucose- and glutamine-free DMEM before adding complete culture media for 1 h. The glucose changes after addition of complete media were measured with the Glucose kit (BioVision) according to the manufacturer's instructions and the values were normalised to cell mass. To be within the linear range of glucose levels determined by the glucose standard curve, 10 µl of the supernatant were diluted 1:10 in glucose assay buffer and then 5µl of this dilution were used for establishing the glucose amount utilised.

2.2.4.5 Measurement of secreted lactate

Lactate secretion of breast cell lines were measured after 1 h starvation in glucose and glutamine free DMEM before adding complete culture media for a further hour. The amount of secreted lactate after addition of complete media was measured with a BioVision kit according to the manufacturer ‘s instructions and the values were normalised to cell mass (see 2.2.3.5). For this, 10 µl of the supernatant of the incubated complete media was diluted 1:10 in lactate assay buffer and then 10µl of this dilution were used for establishing the secreted amount of lactate. The amount of diluted supernatant was determined to make sure to be within the linear range of the lactate standard curve.

2.2.4.6 Measurement of NAD+/NADH ratio

To determine the redox-potential of chosen breast epithelial cell lines, cells were reverse transfected with siRNA duplexes of interest and cultured for 72 h. Next, cells were trypsinised, counted and $2x10^5$ cells were used for the experiment. The NAD+/NADH kit (Biovision) was used and the protocol was followed according to the manufacturer’s instruction.

2.2.4.7 Measurements of extracellular flux

To determine cellular bioenergetics of the two main metabolic processes: mitochondrial respiration (OCR) and extracellular acidification (ECAR) simultaneously in breast epithelial cell lines, a XF96^e Extracellular Flux Analyser (Seahorse Biosciences, North Billerica, MA, USA) for 96-well plates was used. Real-time measurements of the OCR and ECAR were directly measured over a period of time after injection of different metabolites such as glucose, L-glutamine, Sodium L-lactate and methyl-pyruvate. A flux analyser kit consisted of a dual-analyte sensor XF^{e}96 cartridge plate and a XF^{e}96-well microplate. Briefly, cells were plated in a volume of 80µl per well of a XF^{e}96-well microplate in their normal medium conditions 24 h prior to the experiment. The XF^{e}96 flux cartridge plate includes a hydrogen and oxygen sensor that needed calibration for at least 6 h in the XF^{e}96 flux analyser. On the day of the experiment, the injection ports of the XF^{e}96 flux assay cartridge plate were loaded with different metabolite solutions (pH7.4). The cartridge plate was then loaded into the flux analyser. The cells were then rinsed once with assay medium pH7.4 before cultured in 200µl assay medium. The cells were incubated for 25 min before plate was loaded onto the analyser. The standard

protocol included three readings of 3 min each per treatment. Between each reading there was a 3 min waiting time. The values were normalised to protein content of the cells.

2.2.4.8 Preparation of metabolite samples for mass spectrometry analysis

Metabolic profiling by analysing metabolites extracted from cells may provide information about the metabolic state of a given cell line. To analyse the metabolites of the breast cell line panel, the cells were plated 48 h in 6-well plates prior to the metabolite extraction at a density that on the day of extraction the confluency of the cell was approximately 80-90%. The media were then aspirated and the cells were quickly rinsed twice with 37ºC warm 75mM ammonium carbonate (Sigma-Aldrich) dissolved in ddH_2O that had been adjusted to pH7.4 by the addition of formic acid (Sigma-Aldrich). Then the plates with cells were snap-frozen in liquid nitrogen and stored at -80ºC. The extraction of metabolites was performed in a fume hood. Next, a frozen 6-well plate was placed on a heated magnetic stirrer plate that had been preheated to 90ºC. Then, 600µl of 80% hot EtOH (preheated to 90ºC) was added to each well of the 6-well plate and incubated for 1 min, while the plate was constantly shaken by hand. The cells were then scraped and transferred into a 15ml Falcon tube that was placed in a 90ºC water bath and incubated for 2 min with a vortex step every 30 sec. Another 600µl of 90ºC EtOH was added to the plate followed by scraping. The cell suspension was then transferred to the same 15ml tube and incubated for another 2 min at 90ºC. The cell suspension/ EtOH mixes were spun for 3 min at -10ºC at 3000 x g. The supernatant was then transferred into a 1.7ml reaction tube. The pellet was re-extracted and homogenised with a syringe/ needle containing 600µl 90ºC EtOH. The homogenate was incubated for 1 min at 90ºC before being spun again. The supernatant was added to a 1.7ml reaction tube with the supernatant collected earlier and stored at -80ºC. Analyses were carried out by Dr. Nicola Zamboni's group at ETH Zurich, Switzerland (Buscher et al., 2009). Briefly, extracts were dried with a vacuum centrifuge at 30°C and stored at -80°C. Prior to measurement the extracts were resuspended in 100µl *Nanopure*® water (ThermoFisher Scientific). The samples were then injected in an Agilent 6520 Q-TOF or an Agilent 6550 iFunnel Q-TOF according to (Fuhrer et al., 2011).

2.2.5 Data analysis

Data are usually presented as mean or median values and the error bars represent either the standard deviation (SD) or standard error of the mean (SEM) as described in the figure legend. The quantitative data are depicted using GraphPad Prism 5.0 (GraphPad software). All experiments have been preformed at least twice independently from each other with multiple replicates for each experiment or otherwise indicated.

The p-values were obtained by using a two-tailed paired/unpaired student t-test. P-values smaller than 0.05 were considered to be statistically significant.

For the analysis of the screen the raw data was pre-processed by cellHTS. Z-scores were calculated by and normalised on the basis of the median cell number within each plate in the screen of one cell line/ condition using cellHTS. The Z-scores of candidate genes were defined as those siRNA pools, which had an adjusted Z-score of less than -1.7. Z-score results were symbol annotated to 231 metabolic genes. The Z-score replicates of each cell line under normoxia and hypoxia were combined. The data was then processed into an annotated Z-score matrix. This matrix was subjected to unsupervised hierarchical clustering based upon Pearson correlation distance measure with a ward-clustering algorithm. The candidate genes were defined with a Z-score less than -1.7. Phenotype and genotype information of breast cell line panel was provided and implemented into the R-script. All Z-scores, which separated different phenotypes/genotypes as defined by the Mann-Whitney-U test were created and displayed in heat maps for each phenotype/genotype under normoxic and hypoxic conditions. The heat maps show the significant genes ranked row-wise according to their median difference and column-wise ordered for their phenotype/genotype. The analysis was performed in R2.9.0 using the script by Dr. Alan Mackay.

2.3 Reference List for Material and Methods

Abe, A., Miyanohara, A., and Friedmann, T. (1998). Polybrene increases the efficiency of gene transfer by lipofection. Gene therapy *5*, 708-711.
Fuhrer, T., Heer, D., Begemann, B., and Zamboni, N. (2011). High-throughput, accurate mass metabolome profiling of cellular extracts by flow injection-time-of-flight mass spectrometry. Anal Chem *83*, 7074-7080.
Laemmli, U.K. (1970). Cleavage of structural proteins during the assembly of the head of bacteriophage T4. Nature *227*, 680-685.
Lee, G.Y., Kenny, P.A., Lee, E.H., and Bissell, M.J. (2007). Three-dimensional culture models of normal and malignant breast epithelial cells. Nat Methods *4*, 359-365.
Livak, K.J., and Schmittgen, T.D. (2001). Analysis of relative gene expression data using real-time quantitative PCR and the 2(-Delta Delta C(T)) Method. Methods (San Diego, Calif *25*, 402-408.
Morgenstern, J.P., and Land, H. (1990). Advanced mammalian gene transfer: high titre retroviral vectors with multiple drug selection markers and a complementary helper-free packaging cell line. Nucleic Acids Res *18*, 3587-3596.
Pear, W.S., Nolan, G.P., Scott, M.L., and Baltimore, D. (1993). Production of high-titer helper-free retroviruses by transient transfection. Proceedings of the National Academy of Sciences of the United States of America *90*, 8392-8396.
Ponchel, F., Toomes, C., Bransfield, K., Leong, F.T., Douglas, S.H., Field, S.L., Bell, S.M., Combaret, V., Puisieux, A., Mighell, A.J.*, et al.* (2003). Real-time PCR based on SYBR-Green I fluorescence: an alternative to the TaqMan assay for a relative quantification of gene rearrangements, gene amplifications and micro gene deletions. BMC biotechnology *3*, 18.
Rolo, A.P., Palmeira, C.M., and Cortopassi, G.A. (2009). Biosensor plates detect mitochondrial physiological regulators and mutations in vivo. Anal Biochem *385*, 176-178.
Vichai, V., and Kirtikara, K. (2006). Sulforhodamine B colorimetric assay for cytotoxicity screening. Nat Protoc *1*, 1112-1116.
Wiederschain, D., Wee, S., Chen, L., Loo, A., Yang, G., Huang, A., Chen, Y., Caponigro, G., Yao, Y.M., Lengauer, C.*, et al.* (2009). Single-vector inducible lentiviral RNAi system for oncology target validation. Cell Cycle *8*, 498-504.

3 ER-negative/HER2-negative breast cancer cells differ in their metabolic phenotype from other subtypes

3.1 Introduction

Breast cancer can be classified into different subtypes according to their molecular profiles, clinically based upon the expression of predictive markers (i.e. ER, PR and HER2) and histological features. There have been numerous studies published providing evidence to suggest that these breast cancer subtypes differ in their metabolic phenotypes (McCleland et al., 2012; Possemato et al., 2011). For example, using ^{18}F-FDG-PET imaging of primary breast tumours in female cancer patients showed differences in the uptake rate of ^{18}F- FDG, an analogue of glucose, especially in women diagnosed with the ER-negative/HER2-negative breast cancer compared to the other subtypes (Basu et al., 2008; Tchou et al., 2010).

Alterations of metabolic processes occur during the transformation process from a normal to a cancerous cell. This metabolic reprogramming can be influenced by certain genetic aberrations such as activating mutations in *PIK3CA* (Engelman et al., 2006) or overexpression/amplification of HER2 (Schafer et al., 2009). Even the selection pressure from the microenvironment such as hypoxia or nutrient stress might influence the metabolic phenotype of cancer cells. It has been repeatedly observed that solid tumours utilise more glucose concurrent with lactate secretion even in the presence of oxygen (Gambhir et al., 2001). This hallmark has been termed aerobic glycolysis or Warburg effect (Warburg et al., 1927). Although aerobic glycolysis is not as effective in energy production as oxidative phosphorylation, cancer cells favour glycolysis over oxidative phosphorylation, given that other important metabolic processes branch from the glycolytic pathway. These processes are necessary for cells to produce and accumulate building blocks such as fatty acids, amino acids and nucleic acids for the biosynthesis of lipids, proteins and nucleotides (Vander Heiden et al., 2012).

The molecular heterogeneity of human primary breast cancer (Neve et al., 2006) can be recapitulated *in-vitro* by the use of not a single but a panel of established breast epithelial cell lines. Here, a panel of 17 breast epithelial cell lines to account for the

heterogeneity of breast cancer was chosen. This panel of cell lines used is characterised by distinct gene expression profiles and was established from patients with breast tumours of different clinical subtypes, from benign breast lesions (MCF10A, MCF12A) and normal breast epithelium (184B5) (Fig 3.1A). These cell lines also showed differences in growth patterns and morphologies when grown as two-dimensional (2D) monolayers (Fig 3.1B). This, however, was much more prominent when cells were grown in 3D cell cultures. It has been shown previously that breast cell lines when cultured in 3D extracellular matrix (ECM) cultures adopt either mass, grape-like and stellate morphologies (Kenny et al., 2007).

Not only the genetic background of cells has an impact on metabolic reprogramming, but also the tumour microenvironment with its nutrient and oxygen gradients. To mimic one of these conditions, the breast cell lines used in this study were cultured either under normoxic (20% oxygen) or hypoxic (≥0.5% oxygen) conditions. Different metabolic assays were then performed to metabolically phenotype the cell lines and to determine whether this could be attributed to their receptor status (i.e. ER-positive/HER2-negative, HER2-positive, ER-negative/HER2-negative and non-malignant breast cells) and or genetic aberrations (e.g. PTEN loss, *PIK3CA* mutations).

3.2 Breast cancer cell lines show different dependency on growth factors

The PI3K/AKT signalling pathway is frequently activated in human cancers, including breast cancer. Amplification of genes encoding for receptor tyrosine kinases, such as HER2 and EGFR, mutations in *PIK3CA*, the catalytic subunit p110α of PI3K, and loss of PTEN expression lead to an increased activation of PI3K downstream components such as AKT (Baselga, 2011). These aberrations facilitate breast cancer cell survival and render cells to be less dependent on growth factor stimulation.

To determine the levels of expression of key components of the PI3K/AKT pathway, HER2 and PTEN protein analyses were performed in all 17 breast cell lines included in this study (Fig 3.2A). As expected, the HER2-positive breast cancer cell lines SK-BR-3, AU-565 and HCC1954 showed high levels of expression of HER2, whereas the *EGFR*-amplified MDA-MB-468 showed increased EGFR protein expression levels (Fig 3.2A).

Five cell lines had lost expression of PTEN (BT-549, ZR-75-1, MDA-MB-468, HCC38 and MDA-MB-436) (Fig. 3.2A), which is consistent with previous reports (Neve et al., 2006; Weigelt et al., 2011).

To assess whether the PI3K/AKT signalling pathway is activated in the breast cell line panel, cells were cultured under full medium, reduced serum and serum-deprived media conditions for 24 hours and whole cell lysates were analysed by western blotting. Activation of the PI3K/AKT pathway was determined by the ratio of phosphorylated AKT over total AKT protein expression levels, quantified using Image J. Under serum-starved conditions, growth factors in the cell culture medium are reduced leading to a decrease in AKT activation. Cells with an activated PI3K/AKT pathway, however, are expected to retain high levels of phosphorylated AKT even under serum withdrawal. This analysis revealed substantial diversity of AKT activation among the breast cell lines studied (Fig 3.2B). Remarkably, some (HCC1954 and T-47D) but not all cell lines harbouring activating *PIK3CA* mutations (Barretina et al., 2012; Weigelt et al., 2011) showed elevated AKT activity (MCF7 and BT-20). In contrast, PTEN-deficiency and *HER2*-amplification were associated with increased AKT activation ($p=0.0274$) (Fig. 3.2B). The non-malignant breast cell lines were highly sensitive to serum withdrawal regarding their AKT activity (Fig 3.2B)

Taken together, these findings, in line with previous observations (Stemke-Hale et al., 2008), suggest that activation of the PI3K/AKT pathway, as assessed by AKT phosphorylation, is associated with PTEN LOF rather than *PIK3CA* GOF mutations in the breast cell lines studied. Based on the differential activation of AKT observed in these cells, one can hypothesise that there may also be different metabolic activities in breast cell lines with high vs low levels of AKT activation.

3.3 Glutamine and glucose are crucial for the proliferation of ER-negative/HER2-negative breast cancer cell lines under hypoxic conditions

Glucose and glutamine are the two main carbon sources available for tumour cells to maintain cell growth and proliferation (DeBerardinis et al., 2007). Numerous studies have reported the effects of oncogenes and tumour suppressors influencing glycolysis

and glutaminolysis in cancer cells (Gaglio et al., 2011; Le et al., 2012; Wise and Thompson, 2010; Yuneva et al., 2007). However, cancer cells showed varied glucose and glutamine utilisation dependent on the genetic alteration they harboured and/or the tumour microenvironment (Yuneva et al., 2012). Under low oxygen conditions, cancer cells have been shown to utilise increased amounts of glucose for energy production to compensate for the decreased mitochondrial respiration (Semenza, 2010b). Recent studies have also implicated a role for glutamine under low oxygen conditions to replenish parts of the TCA cycle for fatty acid synthesis (Gaglio et al., 2011; Metallo et al., 2012; Soh et al., 2007).

To determine the substrate dependency of the breast cell lines, cells were deprived of glucose, glutamine or both for 72 hours under normoxic and hypoxic conditions. To assess differences in cell viability between reduced and depleted glucose and glutamine conditions, cell number changes were investigated using normal serum (Fig. 3.3) or dialysed serum (Fig 3.4) under both oxygen conditions. The breast cancer cells (Fig 3.3A-C) cultured in standard serum exhibited no decrease in cell number after glutamine withdrawal under normoxic conditions compared to the non-malignant cells (Fig 3.3D). However, withdrawal of glucose resulted in reduced cell numbers in all breast epithelial cell lines under normoxia (Fig 3.3). Under hypoxic conditions, ER-positive/HER2-positive breast cancer subtypes became more dependent on glutamine as well as glucose. However, the ER-negative/HER2-negative subtype showed no growth impairment under hypoxic conditions in the presence of both carbon sources (glucose and glutamine) as well as after glutamine deprivation (Fig 3.3C) compared to the other breast cancer subtypes and the non-malignant cell lines (Fig 3.3).

Cell lines cultured with dialysed serum showed a severe impairment in proliferation after glutamine withdrawal under normoxic conditions compared to normal serum (Fig 3.4). Interestingly, glucose withdrawal in the non-malignant cell lines showed better survival compared to glutamine depletion under normoxic conditions (Fig 3.4D) Under hypoxic conditions, the effect after glutamine depletion was similar to the effects observed under normoxia. Of note, the ER-negative/HER2-negative cell lines showed only a minor effect under hypoxia when cultured in complete medium (Fig 3.4C). While it cannot be ruled out that the effects observed are due to different batches of

serum, this finding may indicate that traces of glutamine in the normal serum are sufficient to rescue cell proliferation.

In summary, these results demonstrate that glucose and glutamine dependencies differ between breast cell lines. The results of the dialysed serum compared to the normal serum suggest that small amounts of glutamine are sufficient to sustain cell proliferation of breast cancer cells. In addition, the non-malignant breast cell lines appear to be highly sensitive to any perturbations in nutrient and oxygen availability.

3.4 Only ER-negative/HER2-negative breast cancer cells display features of the Warburg effect

Increased glucose utilisation is a feature of aerobic glycolysis in cancer cells, where glucose is mainly fermented to lactate even in the presence of oxygen (Warburg, 1956). The different dependencies on glucose in the breast cell lines suggest that their glucose consumption rate may also differ.

To test this hypothesis, the panel of breast epithelial cell lines was assessed for the phenotype of aerobic glycolysis. To determine glucose uptake and lactate secretion, sensitive fluorescent assays were used to measure glucose and lactate levels in the supernatant of cultured cells. To control for differences in proliferation, the glucose and lactate levels of each culture were normalised to their protein content.

Under normoxic conditions, the non-malignant cell lines depleted less glucose from the media compared to the majority of cancer cell lines. By contrast, only the non-malignant cell lines displayed significantly higher glucose consumption ($p=0.0042$) than the breast cancer cells under hypoxic conditions (Fig 3.5A). Of note, cell lines with increased glucose uptake rates also exhibited enhanced lactate secretion. In general, breast cancer cells showed higher levels of lactate secretion as the non-malignant cell lines both under normoxia and hypoxia (Fig 3.5B). Surprisingly, the ER-negative/HER2-negative subgroup showed a more pronounced effect of lactate secretion under both oxygen conditions compared to the other cancer cells ($p=0.0121$), while HER2-positive cancer cells only showed a significant difference only under hypoxia (Fig 3.5B).

Taken together, these data suggests that only the ER-negative/HER2-negative cell lines display features of aerobic glycolysis. The non-malignant cell lines exhibit a more glycolytic phenotype under oxygen deprivation, which reaches a level similar to that observed in the ER-positive/HER2-negative and HER2-positive breast cancer cell lines under normoxic conditions. However, no changes in the level of secreted lactate was observed, suggesting that the non-malignant cell lines do not possess the capacity to export lactate under conditions of low oxygen levels. This could limit their survival under hypoxic conditions, which is consistent with the observation of the dramatic reduction of cell number in low oxygen of the non-malignant cells. To survive and maintain a glycolytic phenotype, cancer cells need to overcome this toxicity, particularly under low oxygen conditions.

3.5 ER-negative/HER2-negative breast cancer cell lines show low oxygen consumption and reduced mitochondrial oxidative capacity

Glycolytic cancer cells use pyruvate preferentially for lactate production, which has been suggested to result in decreased mitochondrial respiration due to diminished levels of pyruvate available for the transport into the mitochondria (Cairns et al., 2011). In fact, some cancer cells lines have been described to show HIF1α stabilisation and/or harbour genetic alterations affecting genes with mitochondrial function (Semenza, 2010a). Together, this results in decreased mitochondrial activity.

To test the extent to which the breast cell lines use mitochondrial metabolism and oxidative phosphorylation, basal oxygen consumption was determined. Mitochondrial oxidative capacity was measured in the presence of the uncoupling agent FCCP. FCCP is a lipid-soluble acid that disturbs the pH gradient across the mitochondrial membrane, which results in disruption of the mitochondrial membrane potential and rapid respiration independent of ATP synthesis. Moreover, oligomycin, an inhibitor of mitochondrial ATP synthase, was used to block ATP synthesis and abolish ADP-stimulated respiration in intact mitochondria.

The non-malignant cell lines displayed high basal oxygen consumption as well as high maximal mitochondrial oxidative capacity (Fig 3.6A). Both, the cancer and the non-malignant breast cell lines responded to oligomycin treatment leading to a reduction in

their oxygen consumption. Residual oxygen consumption in the presence of oligomycin is caused by proton leakage, which was observed in some of the breast cancer cell lines studied (e.g. HCC1954 and SK-BR-3, Fig 3.6A). In general, breast cancer cell lines showed lower oxygen consumption rates compared to the highly oxidative non-malignant cell lines. Remarkably, the majority of ER-negative/HER2-negative breast cancer cell lines showed a strong reduction in their basal oxygen consumption (Fig 3.6B) and a severe impairment in spare mitochondrial capacity (Fig 3.6A) as compared to the ER-positive/HER2-negative ($p=0.0242$), HER2-positive ($p=0.0242$) and non-malignant cell lines ($p=0.0121$).

Taken together, the highly glycolytic phenotype of ER-negative/HER2-negative cell lines in combination with impaired mitochondrial oxidative activity may suggest that these cell lines may harbour genetic alterations affecting the TCA cycle and/or the electron transport chain.

3.6 ER-negative/HER2-negative breast cancer cells show increased survival under hypoxic conditions

Based on the findings above, one could hypothesise that breast cancer cells with high glycolytic flux and low oxygen consumption may be able to survive better under hypoxic conditions than those with low glycolytic flux and high oxygen consumption. To test this, the impact of hypoxia on proliferation of the 17 breast cell lines was investigated. Under hypoxic conditions, the non-malignant cell lines MCF10A, MCF12A and 184B5 showed a severe decrease in their proliferation rates compared to normoxic conditions ($p<0.0001$) (Fig. 3.7A). In general, breast cancer cell lines were less affected when cultured under hypoxic conditions as similar growth rates compared to the normal oxygen conditions were observed (Fig 3.7B). Some cancer cell lines, however, in particular HER2-positive cell lines (i.e. SK-BR-3) were sensitive to the reduced oxygen conditions and showed decreased proliferation rates. In contrast, ER-negative/HER2-negative breast cancer cell lines were only marginally affected by hypoxia and showed significantly increased proliferation rates under hypoxic conditions as compared to the non-malignant cell lines ($p=0.0121$) (Fig. 3.7B). In fact, ER-negative/HER2-negative breast cancer cell lines which show features of epithelial to

mesenchymal transition, in particular the breast cancer cell lines HS-578T, BT-549, MDA-MB-231 and MDA-MB-436 (Bae et al., 1993; Neve et al., 2006), showed the highest tolerance to low oxygen conditions. A gene signature of hypoxia has been shown to correlate with poor clinical outcome in patients with ER-negative/HER2-negative breast cancer (Favaro et al., 2011).

HIF1α is overexpressed in many human cancers including colon, kidney and breast malignancies compared to non-malignant tissue samples (Zhong et al., 1999). To further investigate the difference in growth observed under hypoxic conditions, the levels of HIF1α and HIF2α expression were determined in the different breast cell lines. Western blot analysis of HIF1α and HIF2α protein revealed that all cancer cell lines, with the exception of SK-BR-3, showed elevated levels of HIF1α under hypoxia compared to the non-malignant cell lines (Fig 3.7C). The non-malignant cell lines showed relatively low levels of HIF1α expression even under hypoxic conditions. Furthermore, three ER-negative/HER2-negative breast cancer cell lines displayed HIF1α stabilisation under normoxia, MDA-MB-231, HS-578T and BT-549. Given that these cell lines do not harbour mutations in VHL (according to the COSMIC database and Broad-Novartis Cell Line Encyclopaedia (Barretina et al., 2012)), these findings suggest that other genetic alterations may contribute to HIF1α stabilisation in these cells.

To summarise, proliferation in the non-malignant breast cell lines is strongly affected in hypoxic conditions, suggesting that they are highly dependent on mitochondrial metabolism. The breast cancer cell lines, however, exhibit varied responses to hypoxia. Proliferation in the ER-negative/HER2-negative breast cancer cell lines with high levels of aerobic glycolysis (chapter 3.4) was found to be affected under low oxygen conditions. This might indicate that these ER-negative/HER2-negative cancer cell lines already display pseudo-hypoxic characteristics. This is supported by the observation that some of these cancer cells lines stabilised HIF1α even in the presence of oxygen.

3.7 Metabolite analysis divides breast cell lines into new subgroups

The metabolome of a cell/organism comprises all small molecules with low molecular weight. The abundance of these molecules or metabolites has been shown to be

influenced by the microenvironment and the activity of intracellular enzymes (Oliver, 2002). The abundance of enzymes as determined by their gene expression levels, CGH, or substrate/product balance modifies the metabolic flux (Griffin and Shockcor, 2004). Metabolite concentrations can be quantified and changes in metabolites may be used in the diagnostic setting (Sreekumar et al., 2009).

Given that the panel of breast epithelial cell lines studied here exhibited differences in their metabolic phenotype, it is likely that they also show differences in their intracellular metabolite concentrations, hence in their metabolome. To investigate this, metabolites were extracted from all cell lines under normoxic and hypoxic conditions and their mass and relative abundance was measured by mass spectrometry (in collaboration with Dr. Nicola Zamboni, ETH Zurich, Switzerland). In normoxia, 2875 ions of good quality, meaning good signal-noise ratios, were detected. 320 ions could be annotated based on the measured molecular weight and compared to the list of human metabolites listed by the Kyoto Encyclopaedia of Genes and Genomes (KEGG) (Kanehisa et al., 2012) within a tolerance of 0.001 atomic mass units (amu). Because of isomers with identical mass, the 320 ions can be associated to up to 628 compounds. In the samples generated under hypoxia, 1539 ions of good quality were detected. After KEGG annotation, 202 ions representing 429 compounds were obtained.

To identify cell lines with a similar metabolome, metabolite profiles of all cell lines were analysed in an unbiased fashion, using an unsupervised clustering analysis of the annotated ions under normoxia (Fig 3.8A) and hypoxia (Fig 3.8B). In general, all biological and technical replicates clustered together, confirming the quality of the data. An exception were the data of the non-malignant cell line 184B5, which was excluded from further analysis due to poor reproducibility between replicates.
In normoxia, the non-malignant cell lines MCF10A and MCF12A and the ER-positive/HER2-negative cell line MCF7 displayed a similar metabolome as their results clustered together (cluster I) (Fig 3.8A). All remaining 14 breast cancer cell lines clustered together in a separate second cluster of the dendrogram (Cluster II). This cluster was further divided into 2 branches: The ER-positive/HER2-negative cell line ZR-75-1 (IIa) followed by a separate second branch (IIb). The latter one included the

ER-positive/HER2-negative cell line T-47D and the HER2-positive cell lines in one sub-branch (b_i) and the ER-negative/HER2-negative cell lines in a second sub-branch (b_{ii}) (Fig 3.8A).

Hierarchical clustering of the metabolomic data from cells grown under hypoxic conditions revealed that the ER-positive/HER2-negative cell lines MCF7 and ZR-75-1 formed a cluster (cluster I) that was distinct from that of the remaining breast epithelial cell lines (cluster II) (Fig 3.8B). The second cluster consisted of two sub-clusters: cluster IIa consisted of BT-20 that is distinguished from the remaining cell lines (IIb). This sub-branch (IIb) could be further divided into the ER-negative/HER2-negative non-malignant cell lines, HER2-positive cell line HCC1954 and the other ER-negative cell lines (HER2-positive cell lines SK-BR-3 and AU-565 as well as the other six ER-negative/HER2-negative cell lines including the ER-positive/HER2-negative cell line T-47D (b_i) and MDA-MB-436 as only cell line (b_{ii}) (Fig 3.8B).

These data suggest that ER-negative/HER2-negative breast cancer cell lines may harbour a specific hypoxic signature given that they are within one sub-cluster (see Fig 3.8B). Data from Chi and colleagues stated that ER-negative breast epithelial cell lines express a hypoxia response signature on gene expression level that correlated with a poorer prognosis (Chi et al., 2006).

To identify certain metabolic process that are significantly enriched in the different types of breast epithelial cell lines, a pathway enrichment analysis was performed using hypergeometric testing in matrix laboratory (MATLAB). An overview of all the metabolic processes is shown in Figure 3.9. Pathway enrichment analysis was performed for both oxygen conditions. Two main subgroups of cell lines based on gene expression profiling (luminal versus basal) (Neve et al., 2006), the subgroups based on different clinical classifiers (ER-positive and HER2-positive versus non-malignant or ER-negative/HER2-negative versus non-malignant) and non-malignant versus cancer cell lines were compared.

Under both oxygen conditions, it is obvious that the comparison between the gene expression subtypes showed only minor pathway enrichment. This might be explained by the importance of posttranslational processes that override gene expression. Moreover, fatty acid related metabolic processes displayed no substantial differences,

which can be explained by the limited detection of lipid compounds with the method used. Under normoxia, most of the enriched pathways are involved in the amino acid metabolism such as arginine and proline metabolism (arrow 1), aromatic amino acid metabolism (arrow 2), beta alanine metabolism (arrow 3), cyanoamino acid metabolism (arrow 4) as well as starch and sucrose metabolism (arrow 5) (Fig 3.9A). Under hypoxia, the only enriched pathways involve the metabolism of arginine, proline and aromatic amino acids (1,2) (Fig 3.9B). The strongest difference between the different groups was observed between cancer and non-malignant cell lines under normoxic conditions and ER-negative/HER2-negative versus non-malignant cell lines under hypoxia.

Amino acid metabolism influences metabolic and signalling processes of the cell such as arginine regulating nitrite oxide production and proline and serine being part of the cellular redox regulation. The differences in the pathway enrichment studies could suggest that the non-malignant cells show distinct metabolic features, that are different from the cancer cell lines regarding their amino acid metabolism. Tumour progression changes the proline and glycine metabolism in breast cancer cells (Richardson et al., 2008). Furthermore, many cancer cells show increase in glycine metabolism (Jain et al., 2012).

In conclusion, the metabolome analysis revealed that the metabolite levels under normoxic conditions are distinct between breast cancer and non-malignant cell lines. Under hypoxic conditions, ER-positive and ER-negative cell lines showed a distinctive metabolomic pattern, with the exception of the ER-positive T-47D cells. These findings indicate that the non-malignant cell lines may compensate oxygen deprivation through changes in their metabolism. The observed changes in activity of certain metabolites in ER-negative cell lines also indicate potentially selective dependencies of these cell lines for proliferation and survival. It is therefore of great interest to investigate whether perturbations of genes involved in these processes differentially affect the cell lines.
These preliminary results will be further investigated by the group of Dr Nicola Zamboni (ETH Zurich, Switzerland). The aim of this work is to identify different ‘metabo-types’ of breast epithelial cell lines, and to investigate how the ‘metabo-types’

of non-malignant cell lines and cancer cells influence their metabolic activity in response to perturbations such as treatment with inhibitors of selected enzymes.

3.8 Discussion

Breast cancer is a collection of different diseases that can be defined according to histological appearance, molecular and clinical features. The different molecular subtypes are predominantly divided by ER status. Molecular gene expression profiling demonstrated that ER-positive and ER-negative breast cancer are two different diseases (Hu et al., 2006; Perou et al., 2000). This is also recapitulated in their clinical classification. ER-positive breast cancers have a better prognosis and OS rates compared to ER-negative breast cancer (Fan et al., 2006). Certain genetic alterations are more prevalent in one subtype compared to another (Curtis et al., 2012; Shah et al., 2012).

Here, it was aimed to investigate the metabolic phenotype of breast cancer cells of different genetic composition. To recapitulate this diversity, 17 breast epithelial cell lines were chosen for this study. These cell lines harbour frequent genetic alterations that are outlined in Figure 3.1. One of the most altered signalling pathway in breast cancer is the PI3K/AKT signalling pathway cascade (Baselga, 2011). Therefore to assess PI3K activity in these cells we analysed the phosphorylation status - activity - of the PI3K effector kinase AKT, as well as the expression of other key components of the pathway. It was established that these breast epithelial cell lines differ in their levels of AKT activation (pAKT/AKT ratio). Increased AKT activity after growth factor withdrawal was associated with loss of PTEN, a negative regulator of the PI3K/AKT pathway, and interestingly with amplified HER2, an upstream activator of the PI3K/AKT signalling. This has been recently demonstrated by a Cancer Genome Atlas Network study, where they examined the relationship between *PIK3CA* mutation, PTEN loss, and activities of certain pathways. Levels of pAKT and pS6 as markers of activated PI3K signalling were not increased in *PIK3CA*-mutated breast cancer specimen. Instead, pAKT and pS6 were elevated in basal-like and *ERBB2*-enriched subtypes. This correlated strongly with PTEN loss (CancerGenomeAtlasNetwork, 2012). Constitutive HER2 signalling through the activation of downstream kinases, i.e. p110α (*PIK3CA*), have been also mentioned (Stemke-Hale et al., 2008). These and other

signalling cascades influence metabolic processes and it is important to determine how these genetic aberrations feed into the metabolic phenotypes of cancer cells. Therefore, the metabolic phenotype of 17 breast epithelial cell lines was investigated. The dependency of the two main carbon sources glutamine and glucose was established, demonstrating that all cell lines exhibited to a certain extent glucose and glutamine dependency, and that traces of glutamine in glucose-supplemented medium protected cell proliferation (see Fig 3.3-3.4). The Warburg effect or aerobic glycolysis was only detected in ER-negative/HER2-negative breast cancer cell lines, suggesting that this subtype could be more dependent on glycolysis than oxidative phosphorylation, which is in line with previous reports (Groheux et al., 2011; Ramanathan et al., 2005), explaining the here-observed low mitochondrial oxidative capacities of these cell lines. McCleland and colleagues used publically available data from the Broad institute and showed that basal-like and *ERBB2*-enriched cells are not using oxidative phosphorylation (McCleland et al., 2012). The high export to lactate was mostly limited to the ER-negative cell lines. In agreement with the findings of this study ER-negative/HER2-negative are the only subtype that displayed the Warburg effect with increased glucose utilisation, lactate export and low mitochondrial activity which is thought to facilitate their high proliferative capacity. These cells might have adapted and optimised their metabolic network to support rapid proliferation.

Contribution of tumorigenic capacity of cancer cells is also defined by the microenvironment. Cancer cells experience oxygen and nutrient fluctuations in different areas of their tumour due to the close proximity to blood vessels. Areas of low oxygen produce more chemo-resistant cells that are difficult to treat (Horsman et al., 2012). The process of adaptation is integral to how cells can survive under these unfavourable conditions. This study investigated the survival of breast epithelial cells belonging to different subtypes in hypoxia and their ability to handle low oxygen. Here, it was shown that non-malignant breast epithelial cells are least able to survive low oxygen, whereas most cancer cells showed a degree of adaption, especially the ER-negative/HER2-negative cell lines. These cells have the best survival under hypoxia (see Fig 3.7) and exhibited a pseudo-hypoxic phenotype even under normoxic conditions.

Central to the survival in hypoxia, is the upregulation of the hypoxic downstream effector HIF. Most of the cancer cells showed high expression of HIF1α/HIF2α under

hypoxia. Mesenchymal breast cancer exhibited stabilisation of HIF1α/HIF2α even under normoxic conditions. Moreover, another possible explanation could be that defects in mitochondrial activity lead to an activation of AKT by inhibiting PTEN through an increase in NADH levels (Pelicano et al., 2006). Activated AKT signals to its downstream target mTORC1, which upregulates HIF (Majumder et al., 2004).

To continue the metabolic characterisation of breast epithelial cell lines, metabolic profiling of each cell line under normoxic and hypoxic conditions was assessed. The metabolic profiles showed a clear distinction between non-malignant and breast cancer cells. Under hypoxia, the ER-negative/HER2-negative breast cancer cell lines had metabolite features distinct from the ER-positive/HER2-negative and HER2-positive cell lines. In particular, metabolic pathways including amino acid metabolism, were enriched in these cells compare to the other subgroups (see Fig 3.9). The neoplastic transformation to cancer cells can also change the repertoire of carbon sources and amino acids especially glycine and proline are important in tumorigenesis (Jain et al., 2012; Richardson et al., 2008).
Although ER-negative/HER2-negative can be further divided into more subclasses, this study here suggests that the metabolic phenotype observed unifies the ER-negative/HER2-negative subtype. However, this might be due to different metabolic adaptations caused by the heterogenic genetic composition of these cells that then feed into the same biological processes.

A potential limitation of this study is that the intracellular metabolism of these cell lines was only investigated under 2D cell culture conditions. As numerous studies have shown that 3D culture models create a more physiological environment (Yamada and Cukierman, 2007), which may also affect the metabolic features assessed here. However, the physiological oxygen environment of breast cancer was recapitulated by culturing the cells under low oxygen conditions.

In summary, this study determined that the genotypic and histological diversity of breast cell lines mirror metabolic diversity and dependencies. The established clinical subtypes show different metabolic features. The ER-positive/HER2-negative cells are

more oxidative, while the ER-negative/HER2-negative showed strong aerobic glycolysis and a hypoxic phenotype. This suggests that different subtypes can be susceptible to different perturbations in the metabolic machinery. Particularly interesting are metabolic dependencies of HER2-positive and ER-negative/HER2-negative breast cancer. These breast cancer subtypes encounter for aggressive diseases with poor prognosis in the clinic (Parker et al., 2009). Finding a distinct metabolic dependency that could be exploited therapeutically would be of significant interest and could display considerable patient benefit.

Figure 3.1

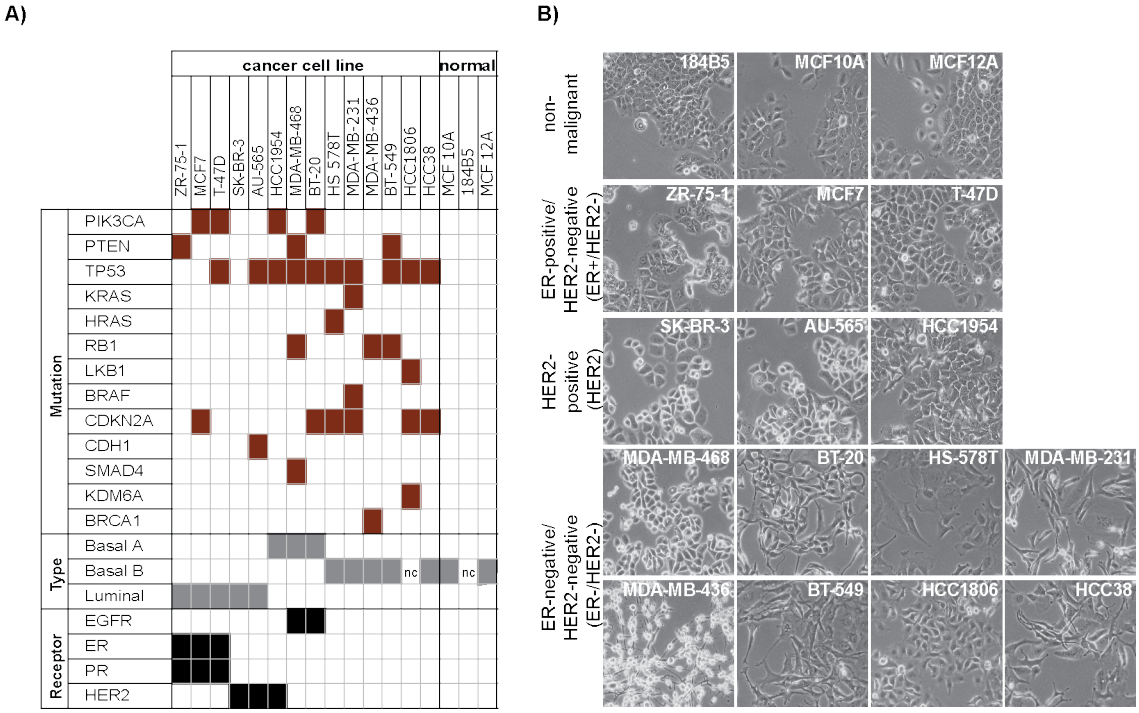

Figure 3-1 Panel of breast epithelial cell lines

(A) Overview of 17 breast epithelial cells lines consisting of fourteen breast cancer cell lines and three non-malignant breast epithelial cell lines that were selected for this study. These cell lines can be classified according to their genetic alterations (Mutation), gene expression profile (Type) and receptor status (Receptor). The data were collected and merged from ATCC, COSMIC database and published data (Neve et al., 2006). The cell lines 184B5 and HCC1806 are not classified regarding their gene expression profile (nc). (B) Representative pictures of the three non-malignant cell lines 184B5, MCF10A and MCF12A, the three ER-positive/HER2-negative breast cancer cell lines ZR-75-1, MCF7 and T-47D, the three HER2-positive breast cancer cell lines SK-BR-3, AU-565 and HCC1954, and the eight ER-negative/HER2-negative breast cancer cell lines HS-578T, MDA-MB-231, MDA-MB-436, BT-549, HCC1806, HCC38 including the EGFR overexpressing cell lines MDA-MB-468 and BT-20, are shown.

Figure 3.2

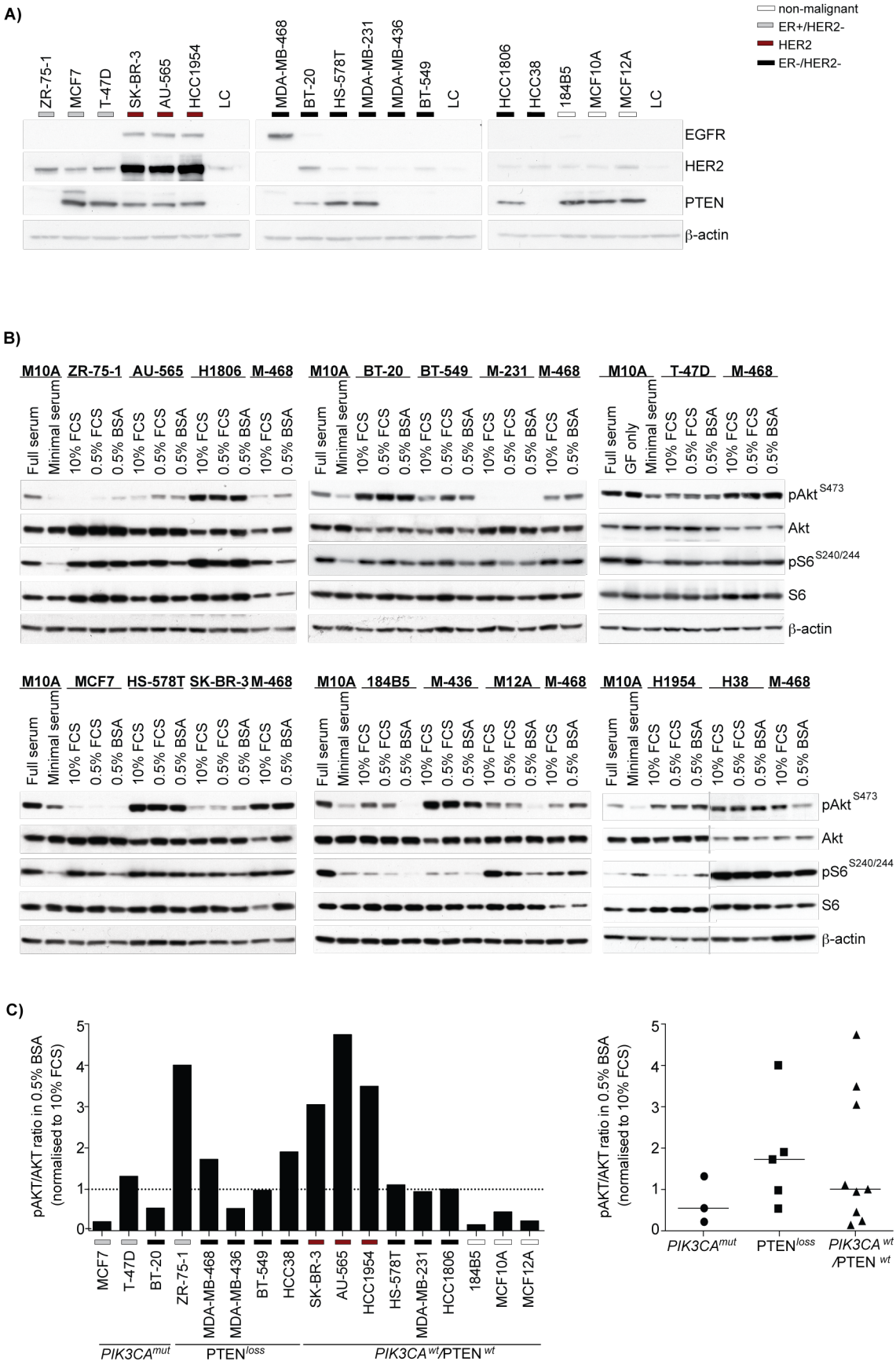
A)
non-malignant
ER+/HER2-
HER2
ER-/HER2-
ZR-75-1
MCF7
T-47D
SK-BR-3
AU-565
HCC1954
LC
MDA-MB-468
BT-20
HS-578T
MDA-MB-231
MDA-MB-436
BT-549
LC
HCC1806
HCC38
184B5
MCF10A
MCF12A
LC
EGFR
HER2
PTEN
β-actin
B)
M10A
ZR-75-1
AU-565
H1806
M-468
BT-20
BT-549
M-231
T-47D
Full serum
Minimal serum
GF only
10% FCS
0.5% FCS
0.5% BSA
pAkt S473
Akt
pS6 S240/244
S6
β-actin
MCF7
HS-578T
SK-BR-3
184B5
M-436
M12A
H1954
H38
C)
pAKT/AKT ratio in 0.5% BSA (normalised to 10% FCS)
PIK3CA mut
PTEN loss
PIK3CA wt /PTEN wt

Figure 3-2 Signalling in breast epithelial cell lines

(A) Seventeen breast epithelial cell lines were seeded in full medium. After 24 hours, whole cell protein lysates were harvested and analysed for the stated signalling molecules. (B) Seventeen breast epithelial cell lines were seeded in full medium. After 12 hours, cells were washed once with PBS and in medium containing 10% FCS, 0.5% FCS and 0.5% BSA. Whole cell protein lysates were analysed for phosphorylation of AKT and S6. Cell line names were shortened: H38=HCC38, M10A=MCF10A, M-468=MDA-MB-468, H1806=HCC1806, H1954=HCC1954, M-231=MDA-MB-231, M12A=MCF12A and M-436=MDA-MB-436 (C) Quantitative analysis using Image J of pAKT/AKT ratio in 17 breast epithelial cell lines. Cell lines were divided according to their PIK3CA and PTEN status.

Figure 3.3

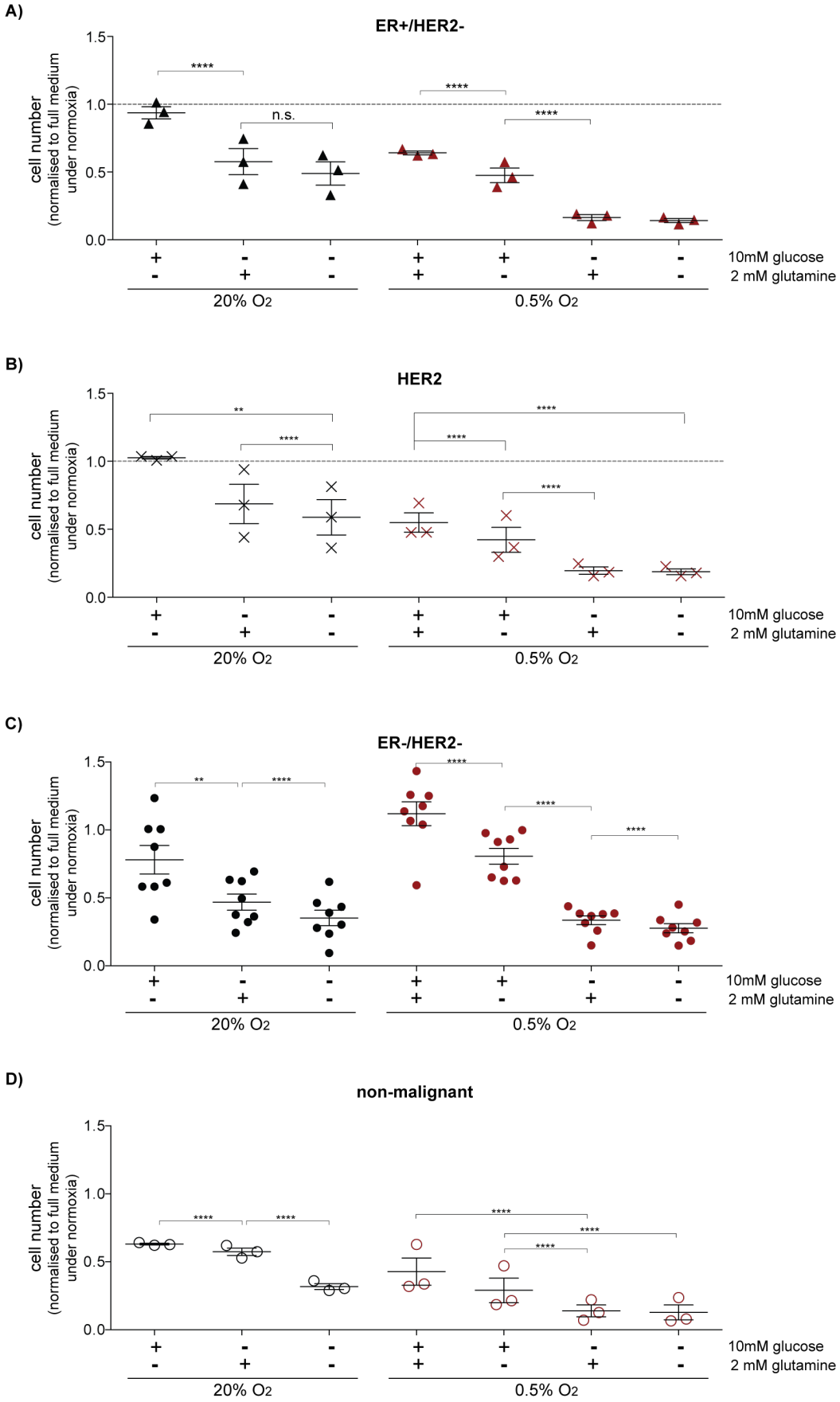
A)
ER+/HER2-
cell number (normalised to full medium under normoxia)
1.5
1.0
0.5
0.0
****
n.s.
****
****
10mM glucose
2 mM glutamine
20% O2
0.5% O2
B)
HER2
**
****
****
****
****
C)
ER-/HER2-
**
****
****
****
****
D)
non-malignant
****
****
****
****

Figure 3-3 Breast cancer cell lines are highly glucose dependent in standard serum conditions

Seventeen breast epithelial cell lines were seeded in full medium. After 24 hours complete medium was changed to medium containing glucose and/or glutamine under normoxic (black symbols) and hypoxic conditions (red symbols). Results are shown for the (A) ER-positive/HER2-negative, (B) HER2-positive, (C) ER-negative/HER2-negative subtype and the non-malignant cell lines (D). Two independent experiments with 3 replicates each were performed and p-values were calculated using the unpaired parametric t-test. The mean of each condition is displayed. (**=p ≤0.01; ***=p≤0.001; ****=p≤0.0001)

Figure 3.4

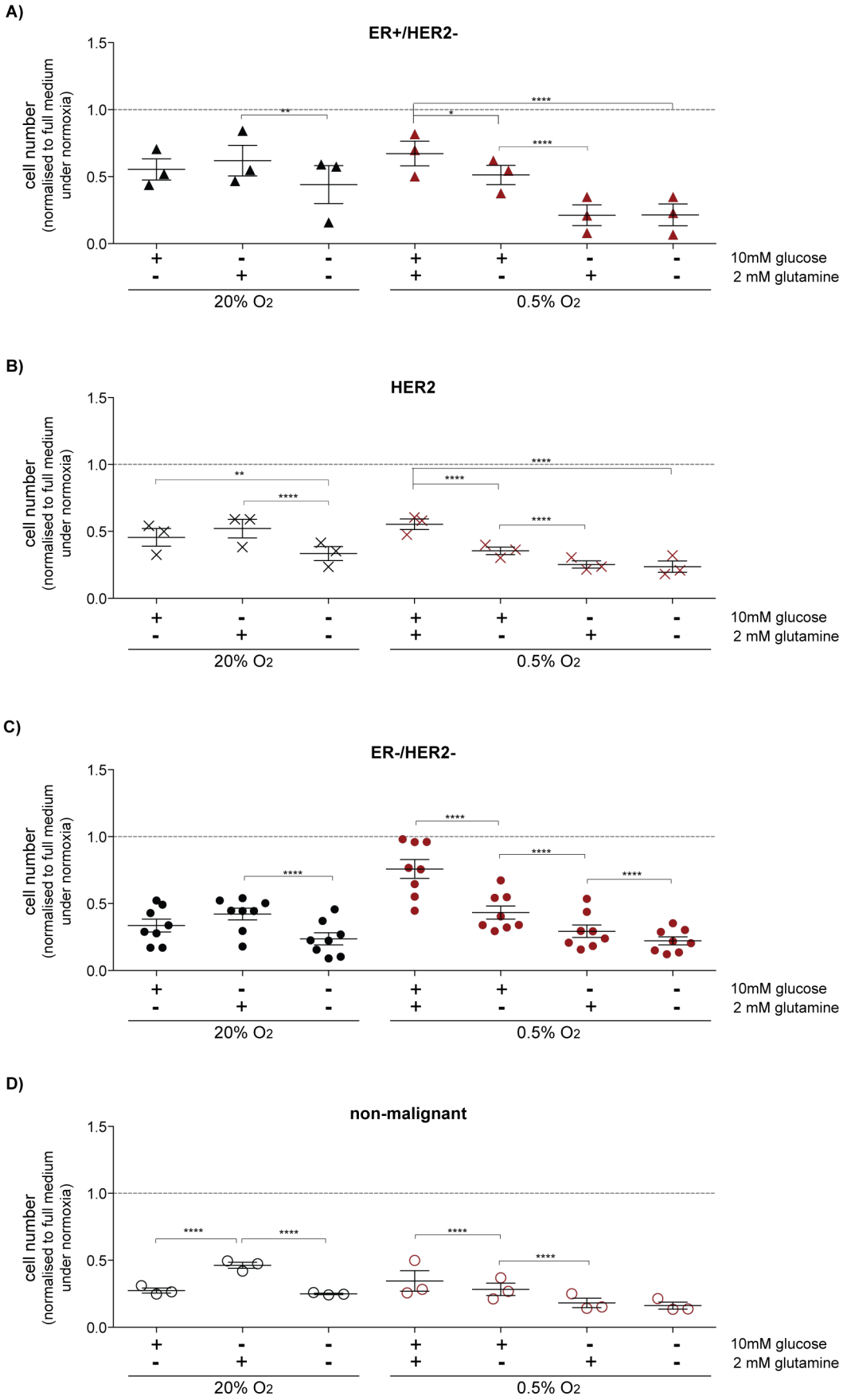
A)
ER+/HER2-
B)
HER2
C)
ER-/HER2-
D)
non-malignant
cell number
(normalised to full medium
under normoxia)
1.5
1.0
0.5
0.0
10mM glucose
2 mM glutamine
20% O2
0.5% O2

Figure 3-4 Breast epithelial cell lines are glucose and glutamine dependent under dialysed serum conditions

Seventeen breast epithelial cell lines were seeded in full medium. After 24 hours complete medium was changed to medium containing dialysed serum with glucose and/or glutamine under normoxic (black symbols) and hypoxic conditions (red symbols). Results are shown for the (A) ER-positive/HER2-negative, (B) HER2-positive, (C) ER-negative/HER2-negative subtype and the non-malignant cell lines (D). Two independent experiments with 3 replicates each were performed and p-values were calculated using the unpaired parametric t-test. The mean of each condition is displayed. (*=p-value ≤0.05, **=p-value≤0.01,***=p-value≤0.001, ****=p-value≤0.0001)

Figure 3.5

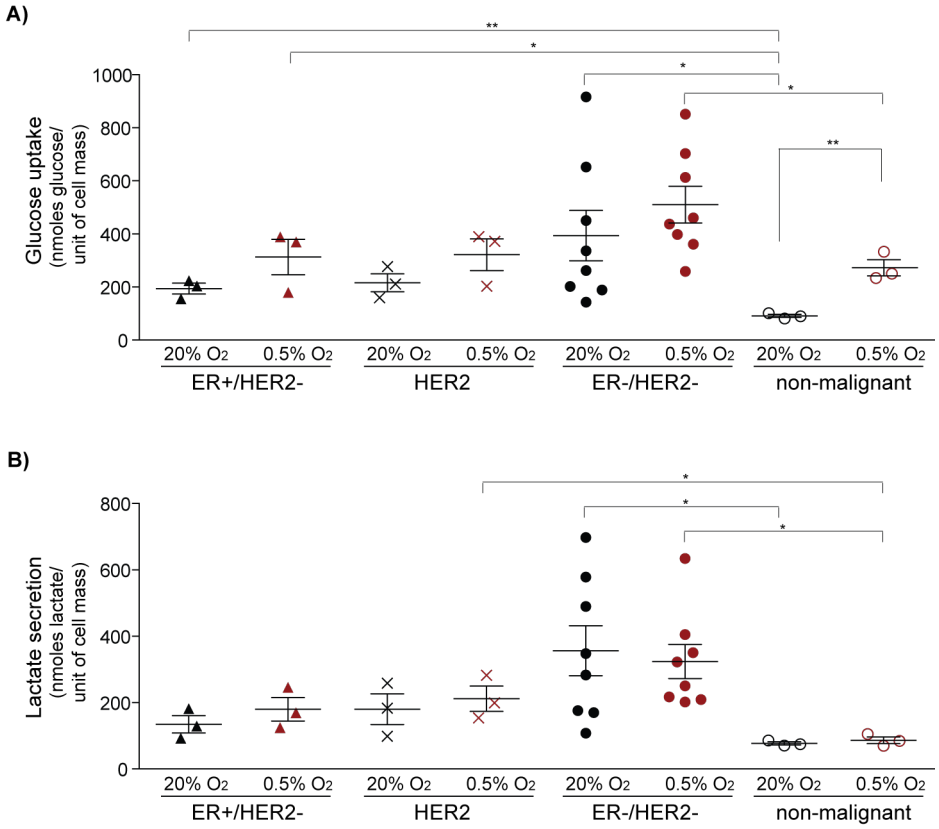

Figure 3-5 Glucose uptake and Lactate secretion in different breast cell lines

Cells from seventeen breast epithelial cell lines were seeded in full medium. After 24 hours medium was changed and cells were cultured for a further 48 hours. Then, cells were starved in glucose and glutamine free DMEM for 1 hour prior to a further hour of full medium. Medium was then analysed for glucose uptake (A) and lactate secretion (B) under normoxic (black) and hypoxic (red) conditions. The raw values were normalised to the accumulation of protein content. The mean values of 2 independent experiments with three replicates each are displayed. The mean of each condition is displayed and p-values were calculated using the unpaired t-test. Parametric comparison was used for the comparison of ER-positive/HER2-negative, HER2-positive and non-malignant cell lines, whereas the non-parametric MWU test was used for the comparison with the ER-negative/HER2-negative cell lines. (*=p≤0.05, **=p≤0.01)

Figure 3.6

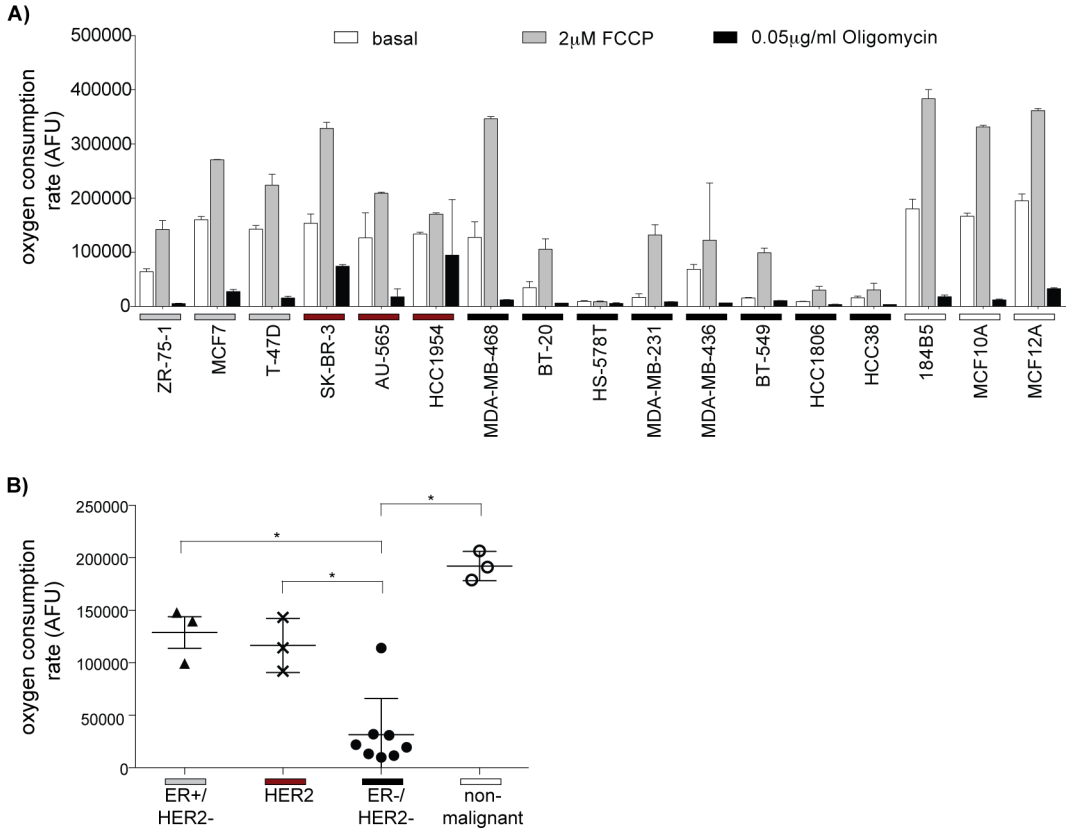

Figure 3-6 Oxygen consumption and mitochondrial oxidative capacity in a panel of breast cell lines

(A) Cell lines were cultured for 48 hours in full medium before oxygen consumption of one million cells was determined. Oxygen consumption was measured with BD oxygen biosensor plates (BD Biosciences) for a 2 hours period. (B) Overview of basal oxygen consumption in different subtypes. Each dot represents mean of a representative of 3 experiments performed in triplicate. The error bars display the standard error of the mean. (*=p≤0.05)

Figure 3.7

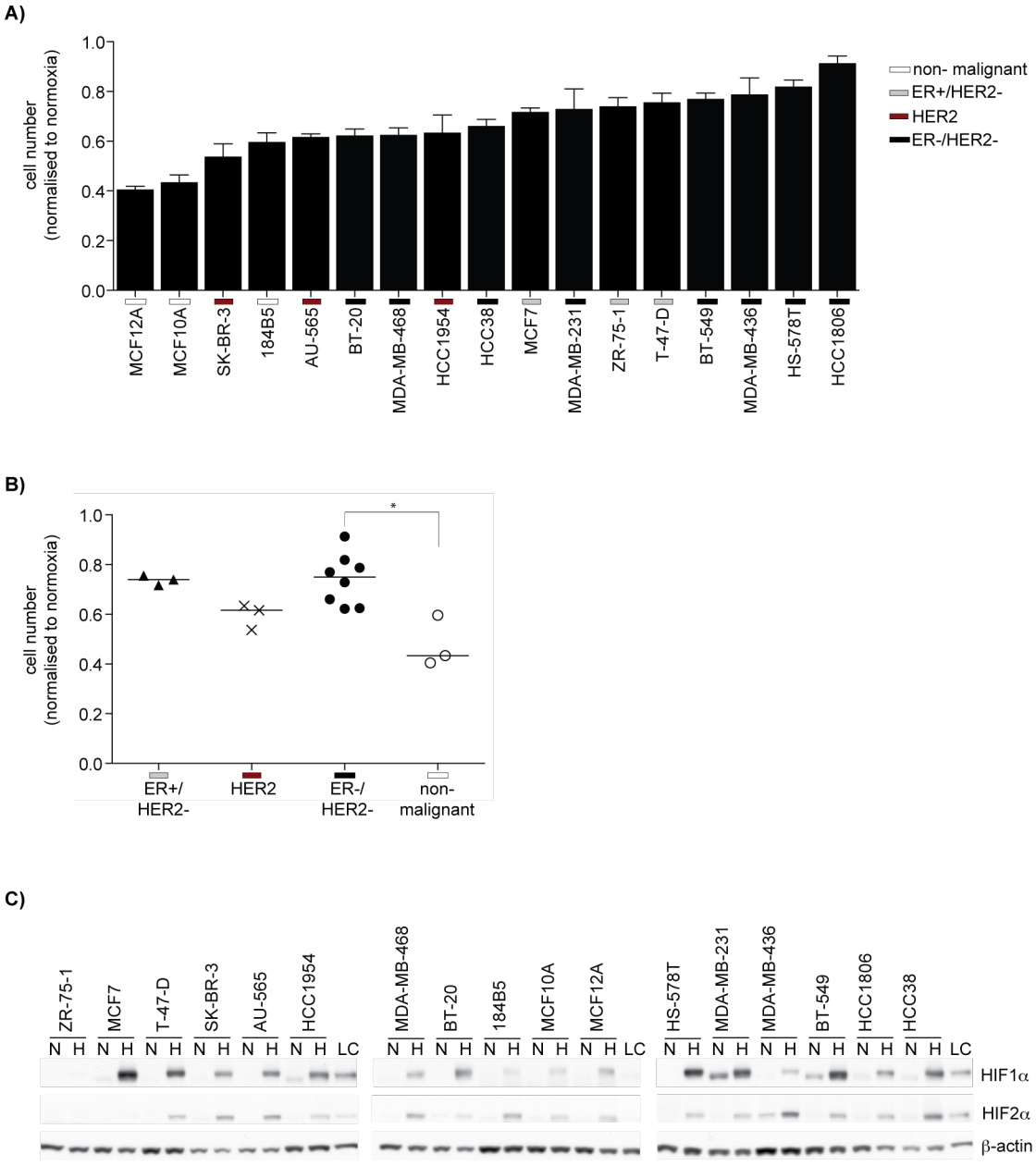

Figure 3-7 ER-negative/HER2-negative breast cancer cells are pseudo-hypoxic

(A) Cells of seventeen breast epithelial cell lines were seeded in triplicates in 96-well plates, cultured under normoxic and hypoxic conditions (O_2≤0.5%) for 96 hours. After fixation and staining with DAPI, cell number was determined by the Acumen X^3. Here shown is the cell number of each breast cell line under hypoxic conditions normalised to its normoxic cell number values. (B) Overview of cell number under hypoxia for the different subtypes. Three independent experiments were performed and the median of the cell number per subgroup is displayed (*=p≤0.05). (C) Cells were seeded for 24 hours under normoxic conditions prior to the exposure to hypoxia (O_2≤0.5%). Whole cell protein lysates were harvested and analysed for HIF1α and HIF2α expression. N=Normoxia, H=Hypoxia.

Figure 3.8

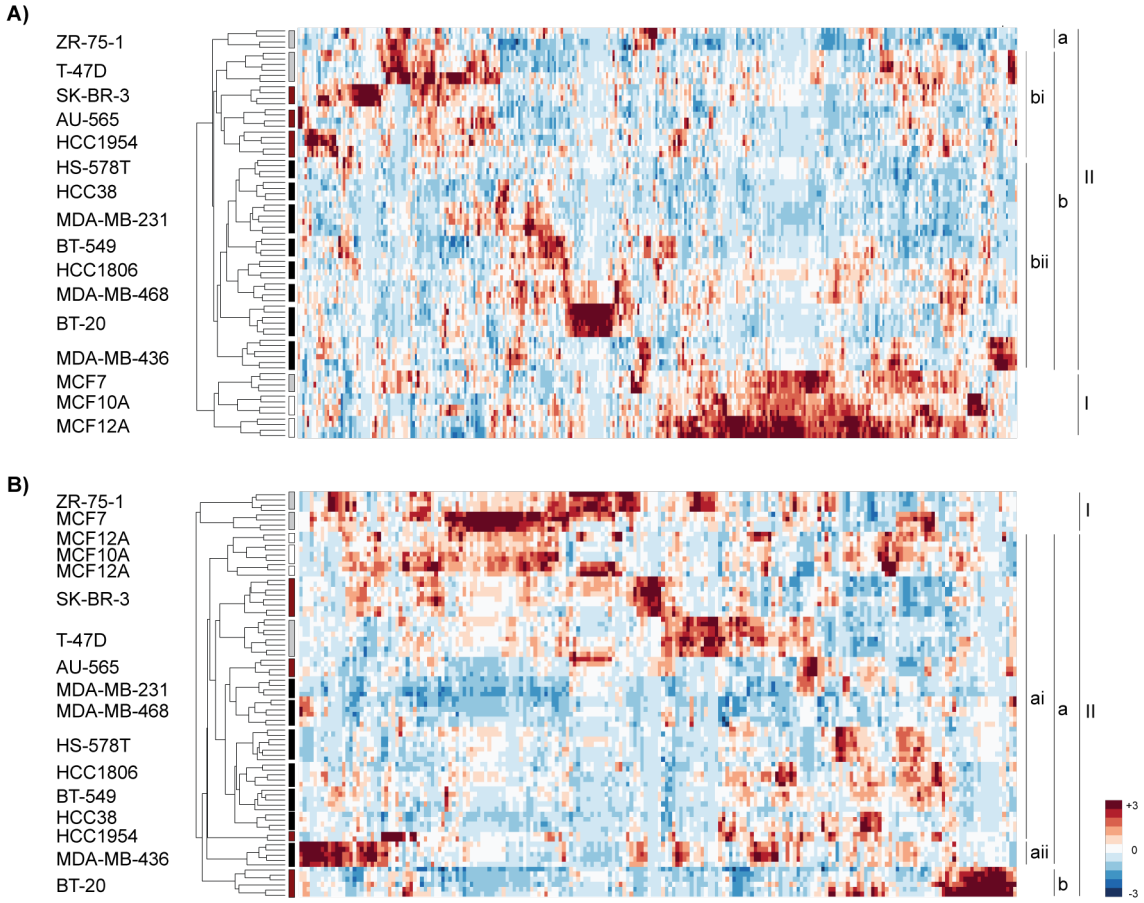

Figure 3-8 Breast epithelial cell lines show differences in their metabolites

Cells from seventeen breast epithelial cell lines were seeded in 6-well plates in full medium in triplicates. After 24 hours, cells were snap frozen in liquid nitrogen. Metabolites were extracted and analysed by mass spectrometry. Unsupervised clustering using the euclidean distance and average linkage (UPGMA) method of the normalised intensity of the annotated ions of all cell lines under normoxia (A) and under hypoxia (B). Colour bars display the affiliation of the cell line with a specific subtype (grey=ER+/HER2-; red=HER2; black=ER-/HER2- and white=non-malignant cell lines. Width of the colour bar indicates number of samples replicate (1-6), each with 3 independent replicates.

Figure 3.9

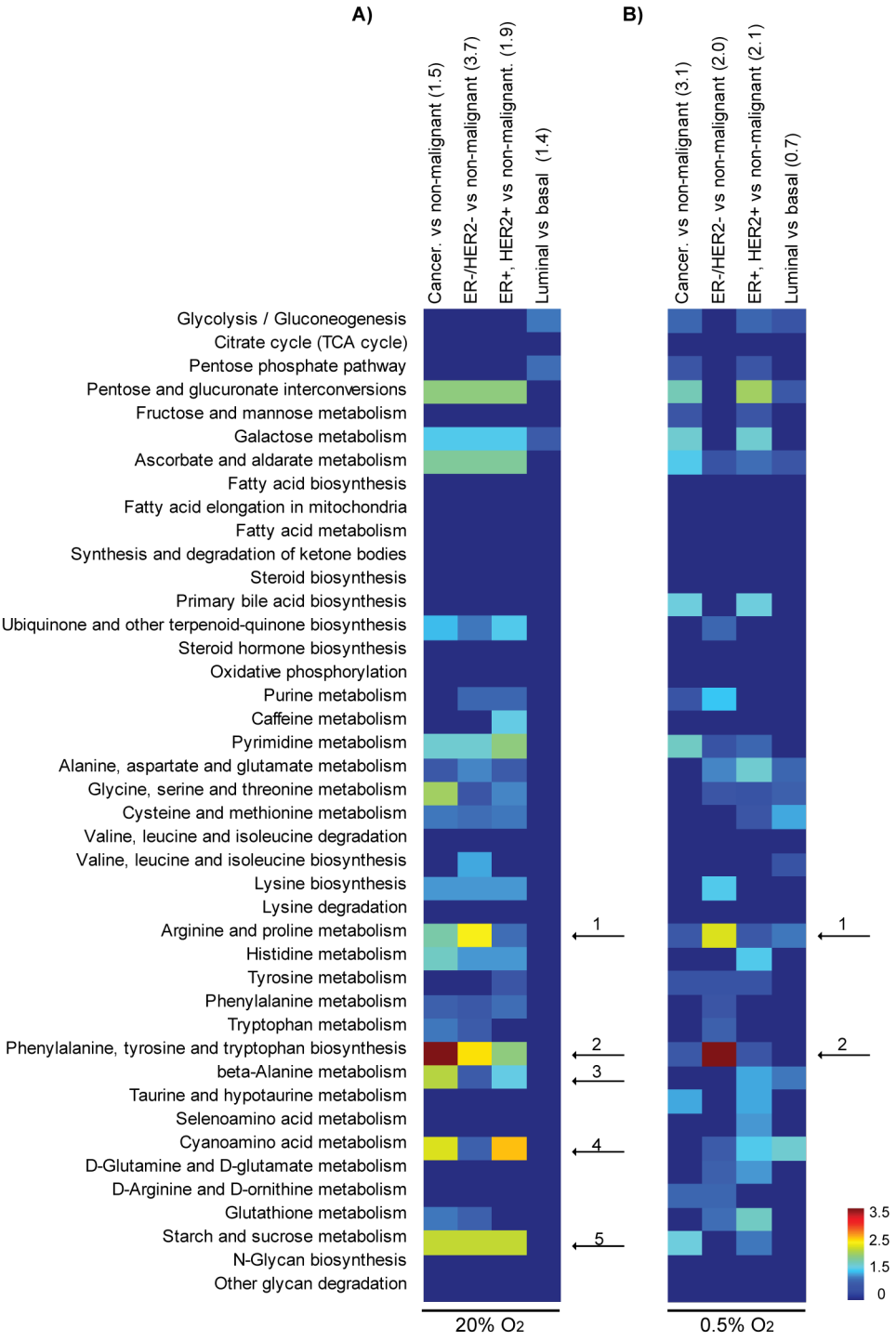

Figure 3-9 Subtypes of breast cancer cells show enrichment in amino acid metabolism

Metabolite data from seventeen breast epithelial cell lines were analysed with MATLAB using a hypergeometric test to compute the p-values. Gene pathway enrichment analyses were performed for all metabolites under normoxia (A) and hypoxia (B). Heat maps show log10 of p-values indicating that a pathway is different between the two groups within the comparison.

4 Identification of metabolic enzymes essential for breast cancer cell survival by using RNA interference (RNAi)

1.1 Introduction

RNA interference (RNAi) is an important endogenous pathway that modulates the expression of genes. The generation of small non-coding RNAs involves the processing of long double-stranded RNA (dsRNA) molecules into 21-25 nucleotide long dsRNAs by the endoribonuclease DICER in the cytoplasm. The 'guide'-strand, which is a template for the mRNA to be repressed, will then be recognised by the RNA induced silencing complex (RISC), whereas the 'non-guide' or passenger strand is degraded by RISC. The RISC complex with the guided strand will then bind to the complementary sequence of its target mRNA. The recognition of the target mRNA by the guide-strand occurs through the base-pairing model of Watson and Crick. This catalyses the slicing or degradation of the target RNA leading to its repression/ablation, which results in a LOF phenotype in the cell system used (Hannon, 2002). The recognition of target mRNA in the presence of synthetic small-interfering RNA molecules (siRNA) also involves RISC (Fig 4.1).

The discovery of RNAi in the early 1990s has changed the approach of how to study gene functions in model organisms such as *Drosophila*, *Caenorhabitis elegans* (*C.elegans)* and mammalian cell systems (Fire et al., 1998). Since then, RNAi has been utilised as an efficient and effective research tool for the depletion of genes at the mRNA level. Today, RNAi is being employed to screen small-scale (e.g. gene family networks such as metabolic pathways or kinases) or large-scale gene sets (whole genome) in a high-throughput manner. RNAi libraries for mammalian genes are commercially available and consist of either siRNAs or vectors expressing short-hairpin RNAs (shRNAs) that can be experimentally introduced into different cell systems (Carpenter and Sabatini, 2004).

The screening of RNAi libraries using different cell systems allows for functional analysis of the dependencies on certain pathways within cell systems that differ in their genetic background or tissue of origin. This technique has led to the identification of novel components of various signalling pathways and has increased our understanding of how genes affect the viability of cancer cells. Recent RNAi studies integrated data

obtained from siRNA/shRNA screens with other datasets such as gene copy number changes or gene expression profiles. This has revealed novel insights into the effects of single genes within a specific cellular context (Brough et al., 2011; Marcotte et al., 2012). RNAi screens are highly sensitive to experimental variation and to increase the likelihood of identifying biologically relevant candidate genes, RNAi screens need to be thoroughly designed and optimised.

4.1 Optimisation and setup of screen

To introduce synthetic siRNA oligonucleotides efficiently and effectively into multiple cell lines, initial experiments were carried out to optimise RNAi screening conditions. Numerous key factors had to be considered during the optimisation process: selection of cell lines, optimisation of cell density, choice of transfection reagent, identification of the optimal concentration of transfection reagent and targeting siRNA duplexes, duration of the assay, the choice of positive and negative controls as well as the biological nature of the screen (normoxic and hypoxic conditions).

4.1.1 Cell number optimisation

The aim of the siRNA screen of 17 breast epithelial cell lines was to identify metabolic genes whose ablation caused marked changes in cell number. Therefore, determining the cell density at time of seeding was crucial for detecting changes in cell number at the end of the experiment. Given that different cell lines have different growth kinetics and conditions, initial cell number seeding experiments for each cell line were carried out to define the number of cells to be plated in a well of a 96-well plate, so that at the endpoint of the screen (96 hours) a confluency of 80-90% was reached. Each of the 17 breast cell lines was plated at different cell densities ranging from 1000 up to 6000 cells per well of a 96-well plate. After 96 hours, the cells were fixed and two different fixation methods (4% PFA or 80% ice-cold EtOH for 12 h at 4ºC) were compared. Cells were stained with DAPI and the numbers of nuclei, representative of cell number, were detected using the laser imaging scanner Acumen X^3 (Fig 4.2A). The different fixation methods resulted in comparable cell numbers. However, the quality of the cell cycle profile that can be established with the Acumen X^3, showed marked differences (Fig 4.2B). Fixation of cells with 80% EtOH and subsequent DAPI staining resulted in a

clear distinction of the different cell cycle phases compared to the 4% PFA fixation. Fixation with 80% EtOH was subsequently used for determining the plating cell density of all cell lines, and three independent experiments were performed for the 17 cell lines (see 2.2.1.7).

4.1.2 Transfection reagent optimisation

The delivery of siRNA into cells is normally performed using liposomal reagents (Elbashir et al., 2001). The choice of the transfection reagent is crucial for the optimal silencing efficiency with minimal toxicity. To achieve optimal transfection, several reagents from different suppliers were tested in the chosen panel of breast cell lines. The cytoskeleton protein LAMIN A/C was used as a positive control during the optimisation procedure (Elbashir et al., 2001). Based on previous experiences by the High Throughput Screening (HTS) laboratory (CR UK, LRI), it was decided to perform a reverse transient transfection of siRNA duplexes targeting the non-essential gene LAMIN A/C. Cells were incubated for a total of 96 hours. To determine the correct volume of transfection reagent, two concentrations (1μl/ml and 3μl/ml) of the 23 different transfection reagents to be tested were used. The knockdown efficiency was determined using a fluorescently labelled antibody detecting the amount of LAMIN A/C protein in each well. Cell number and LAMIN A/C intensity for all the different transfection reagents for each cell line are listed in Appendix Figure 3.

The transfection reagents RNAiMAX, DharmaFect2, Lullaby and siPORT Amine showed the most promising results across the panel of cell lines during the initial tests (Fig 4.3A) and were taken forward for a second round to test the toxicity of each transfection reagent (Fig 4.3A) and the LAMIN A/C knockdown efficiency (Fig 4.3B). Two cell lines are shown to summarise the results. MCF10A cells showed minimal reduction in cell number when 1μl/ml transfection reagent was used compared to higher doses. However, the knockdown efficiency was only sufficient in Lullaby treated samples (60% of LAMIN A/C knockdown). For MDA-MB-468 cells, loss of cell number was reduced when increased cell numbers were used. The corresponding knockdown efficiency showed that most conditions displayed efficient knockdown of 60-70%, except for 1μl/ml siPORT Amine.

Next, the transfection efficiency was tested by using GAPDH siRNA duplexes in all of the cell lines to quantify the knockdown efficiency by immunoblotting (Fig 4.3C). At the time these follow-up experiments were performed, RNAiMAX was no longer commercially available. Therefore DharmaFect1 was included in the study. Lullaby and DharmaFect1 transfection reagents showed repression of GAPDH on protein level whereas siPORT Amine knockdown efficiency was lower. Taken together, Lullaby was the best transfection reagent across the panel of breast epithelial cell lines tested with low toxicity and sufficient delivery of siRNA. All following siRNA transfections were carried out using this transfection reagent.

4.1.3 Transfection controls

Choosing the right transfection controls are essential for evaluating the efficiency of RNAi delivery. Initial experiments were carried out to test if Lullaby shows the desired effect using negative and positive controls for the siRNA screen. Negative controls are siRNA duplexes that have no homology to the human genome, and should not have any effect on cell number. The negative controls used for testing under hypoxic and normoxic conditions included mock transfected cells, cells transfected with siRNA duplexes chemically modified to impair recognition by the RISC complex (RISCfree) and cells transfected with four siRNA duplexes that consist of non-targeting sequences (siControl1-4 and siOTP1-4). The positive controls are siRNAs that cause loss of cell viability and indicate the efficiency of siRNA transfection such as polo-like-kinase 1 (PLK1) and ubiquitin B (UBB). PLK1 encodes a regulator of mitosis and its loss results in apoptosis (Spankuch-Schmitt et al., 2002). UBB belongs to the ubiquitin family and encodes a polyubiquitin precursor. Ubiquitin is essential for the activation of some kinases as well as the unfolded protein response, where ubiquitin is a marker for degradation of misfolded proteins. Loss of UBB leads to apoptosis (Song et al., 2003). In Figure 4.4, all breast cell lines used in this study were reverse transfected with four negative and two positive controls. A good differential between the negative and positive controls was observed across the cell line panel. The non-malignant cell lines as well as the HER2-positive cell lines displayed silencing efficiency that varied on the dependent on oxygen conditions. In contrast, the ER-negative/HER2-negative cells showed similar silencing efficiency under both oxygen conditions. Overall, the negative

controls showed no effect on cell number, whereas the positive controls PLK1 and UBB strongly reduced cell number. Taken together, the difference between negative and positive controls showed a good margin for identification of potential hits. The transfection efficiency between normoxia and hypoxia was also comparable.

4.1.4 Pilot screen

To assess the quality of the optimised RNAi screening conditions, a pilot screen was implemented in 11 out of the 17 breast cell lines with 12 metabolic genes expected to have an effect on cell viability of cancer cells. The chosen genes include those involved in lipogenesis such as fatty acid synthase (*FASN*) (Knowles et al., 2008), mevalonate decarboxylase (*MVD*) (Freed-Pastor et al., 2012), and ATP citrate lyase (*ACLY*) (Hatzivassiliou et al., 2005), as well as genes regulating glycolysis such as *PRKAB1*, a subunit of AMPK, two isoforms of *PFK2 (PFKFB3* and *PFKFB4*) (Ros et al., 2012), and an isoform of pyruvate kinase (*PKM2*) (Christofk et al., 2008a). Moreover, signalling components known to be perturbed in breast cancer such as *PIK3CA* and *AKT* were also chosen. The siRNA for these genes consisted of a pool of four single siRNA duplexes. This pool increases the transfection efficiency and minimises the likelihood of observing off-target effects (Fig 4.5). All cell lines showed some dependencies on a subset of genes. The effect on cell number after the ablation of metabolic genes was not as marked as the strong effect of the positive controls. However, the effect of some siRNAs targeting metabolic genes on cell number compared to the negative control (siControl1-4) was sufficiently strong to be distinguished.

In summary, the optimisation and design of the siRNA screen in combination with a pilot screen in a panel of breast epithelial cell lines revealed that the conditions are suitable for a robust readout. The difference between the negative and positive controls demonstrated a good dynamic range to distinguish potential hits for each cell line. The pilot screen indicates that silencing of the genes in multiple cell lines can show different phenotypes depending on the cell line.

4.2 Primary screen

4.2.1 A functional siRNA screen in breast cancer cell lines

To determine the contribution of metabolic enzymes, nutrient transporters and metabolic regulators to cell proliferation and cell growth in a representative panel of breast cancer cell lines, 17 cell lines were chosen for a functional siRNA screen (see Fig 3.1A). A siRNA library targeting 231 different metabolic genes involved in central carbon metabolism was purchased (Fig 4.6A). The siRNAs of this small-screen library were distributed over three 96-well plates, where the first two rows were always used for the controls (Fig 4.6B). The effect of siRNA transfection on cell growth and survival was studied after culturing the cells for 96 hours under normoxic (20% O_2) and hypoxic (≤0.5% O_2) oxygen conditions using a 96-well format. RNAi screens in each cell line were performed in triplicate (Fig 4.6C). For efficient reverse transfection and silencing conditions, the transfection reagent Lullaby was chosen. Changes in cell number were established using the DNA stain DAPI and measured with a microplate cytometer (Acumen X^3). All RNAi screens were conducted within a three-week period.

4.2.2 Normalisation and Analysis of the screen data

Data was collected from all of the 324 96-well plates. The preliminary analysis of the siRNA screens performed in this study was carried out by Rebecca Saunders of the HTS laboratory (CR UK, LRI) using the Bioconductor software package cellHTS (Boutros et al., 2006). Figure 4.7 shows an overview of the analysis flow.

The readings by the Acumen X^3 represented the total DAPI fluorescence intensity of a given well. The raw data of the cell number derived from the relative fluorescent units (RFU) of each well. RFU is defined as the ratio of the total fluorescence intensity of all cells divided by the fluorescence intensity of a single cell. Figure 4.8A displays an overview of raw cell numbers for all 231 genes targeted by siRNAs and controls in the screen. Because every RNAi screen displays variation within itself due to experimental variability caused by differences in transfection efficiency, fluctuation in the environment or heterogeneity of the cell population (Falschlehner et al., 2010), the raw cell number of each well of a 96-well plate had to be plate-normalised. Therefore, the

raw data scores of each plate were centred to the plate median per plate excluding the negative and positive control values to correct for variations in cell seeding across each well of the plate (Fig 4.8B).

Phenotypes of the same gene in different cells or under different conditions may display small dynamic ranges that are difficult to interpret (Falschlehner et al., 2010). Malo and colleagues have suggested different types of normalisation for RNAi screens such as percentage of negative controls, B-score and Z-score calculations for high-throughput screen analyses (Malo et al., 2006). For this study, the Z-score normalisation was chosen to identify candidate genes resulting in reduced cell number. The Z-score displays the number of standard deviations of a measurement away from the mean of the population. A Z-score of zero represents therefore no changes in cell number, whereas negative values mean a reduction in cell number. Because a relativly small number of siRNA sequences were used in this screen, the Z-score normalisation step becomes sensitive towards outliers. To prevent this, the Z-score calculation of replicate plates was performed with the median absolute deviation of the population (MAD) resulting in the Z-score$_{(MAD)}$ (Chung et al., 2008). For simplicity, Z-score$_{(MAD)}$ will be referred to as Z-score in the following sections. In Figure 4.8C, the Z-score normalisation of a representative cell line is displayed. An overview of the distribution of all replicates of all cell lines is shown in Figure 4.9.

To evaluate if the screen was robust and of good quality, the reproducibility of each replicate with the two other replicates of each breast cell line under both oxygen conditions was calculated using the Spearman correlation. Generally, a Spearman *rho* value above 0.7 is an indicator of correlation, with 0.8 and higher being considered to indicate a very good correlation. Figure 4.10 summarises the correlation analysis. Under normoxic conditions, the four cell lines ZR-75-1, SK-BR-3, BT-20 and MDA-MB-231 showed poor reproducibility with BT-20 being the poorest (*rho*=0.39±0.068). Five cell lines (HCC1954, MDA-MB-468, MDA-MB-436, BT-549 and HCC1806), however, showed a correlation of 0.8 and higher. Under hypoxic conditions, only SK-BR-3, BT-20 and MDA-MB-231 showed less good correlation.

In summary, it can be concluded that the screen showed robust results across the replicates for the majority of the cell lines used in this study. The cell lines showing less robust results were still included in the analysis but the results were treated with caution.

4.2.3 Defining and selection of candidate genes

There are multiple ways to define and select candidate genes that cause a significant reduction in cell number after ablation. The first analysis strategy used unsupervised clustering of the data from all cell lines and siRNAs used in the screen to identify patterns that showed loss of cell number (Kaufman and Rousseeuw, 1990). The different Z-scores of all siRNAs tested for each cell line under normoxic and hypoxic conditions were used to generate hierarchical clusters. The siRNA-mediated depletion of the metabolic genes showed two distinct clusters: I) reduction in cell number and II) increase in cell number (Fig 4.11A). Surprisingly, the hypoxic and normoxic samples of each breast cancer cell line were mostly similar to each other and clustered together, except for HCC38. In addition, normoxic samples of the non-malignant cell lines MCF10A and MCF12A clustered together and away from their respective hypoxic samples. In general, there was no correlation with the clinical classification of the different breast cancer subtypes in this specific analysis (Fig 4.11A).

To investigate whether the siRNA screens revealed potential patterns for the different cell lines under each oxygen condition, the data from each cell line was clustered for the normoxic (Fig 4.11B) and hypoxic (Fig 4.11C) conditions. In general, the non-malignant cell lines built one sub-cluster under both oxygen conditions. Hence, the breast cancer cells showed no separation according to their clinical subtypes. Under normoxia, two distinct clusters were observed, the EGFR amplified cell lines BT-20 and MDA-MB-468 differed from the rest of the cell lines. The second cluster included many sub-clusters and it was observed that HCC1954 and ZR-75-1 are not in the same cluster as the other cell lines belonging to the HER2-positive or ER-positive/HER2-negative subtype, respectively. This was also observed for two cell lines of the ER-negative/HER2-negative subgroup (MDA-MB-231 and HCC38) that differed from the 4 remaining triple negative breast cancer cell lines. Under hypoxia, two main clusters

were determined. The first cluster distinguished between ZR-75-1 and four other cell lines (EGFR-amplified BT-20 and MDA-MB-468 cells, ER-negative/HER2-negative cell line MDA-MB-231 and HER2-positive HCC1954 cells). The second cluster contained a sub-cluster of the non-malignant cell lines and a sub-cluster consisting of the 9 remaining cancer cell lines.

To identify genes that are required for cell viability, a ranking analysis for each cell line was performed. This identified the siRNA duplexes with the lowest Z-score, meaning the strongest reduction in cell number. For each cell line the Z-scores of all 231 experimental siRNAs and controls were ranked. Assuming normally distributed Z-scores (Fig 4.12), a stringent threshold of a Z-score $\leq$ -1.7 was obtained from the F-statistics distribution table to identify siRNAs causing significant changes in cell number with $p \leq 0.05$ (Fig 4.13A). The positive controls were the strongest killers in all cell lines, whereas the negative controls lay within the main population of the distribution (Fig 4.13). In Table 4.1, the 72 candidate genes across all cell lines under normoxic and hypoxic are summarised. These candidate genes are defined as having an effect in more than one cell lines or condition.

To identify genes that are differentially required for the survival of cells of a specific clinical, genetic or metabolic background, a supervised cluster analysis of the Z-score data was carried out. This was performed in collaboration with Dr. Alan Mackay and Prof. Jorge Reis-Filho (Institute of Cancer Research, London, UK). Supervised hierarchical clustering has been used as a tool for the analysis of microarray data. It is a two-step method; at first all genes with a similar behaviour across the cell lines are grouped together using a semi-supervised algorithm. Secondly, genes in clusters showing a differential expression between a given parameter (e.g. ER or PTEN status) are displayed in a heatmap. To test each gene for its significance between the two groups defined by a parameter, the Mann-Whitney-U test (MWU) was used. The heatmaps in Figure 4.14-4.18 show the siRNAs that exhibit significant differences ($p \leq 0.05$) for a given parameter between the groups. All significant siRNAs that caused a reduction in cell number are shown for the comparison between cancer versus non-malignant cell lines (Fig 4.14). Under normoxic and hypoxic conditions, the siRNAs

with the highest differential were the same. *SLC16A3* ablation was more effective in cancer cells, while depletion of *PMVK* was detrimental to the non-malignant cell lines (Fig 4.14). Of note, most of the genes that influenced non-malignant cell survival can be associated with lipid metabolism.

The candidate genes selective towards the different clinical classification (ER, HER2 status) are displayed in Fig 4.15. The comparison between ER-negative and ER-positive breast cell lines under normoxia revealed strong effects of a gene involved in lipid phosphate signalling, *PPAP2A*, in the ER-negative cell lines. In contrast, *OXCT2, WBSCR14* and *AGXT* were mainly important for the ER-positive cell lines (Fig 4.15A). Under hypoxic conditions, the depletion of an isoform of malic enzyme, *ME2*, was important for ER-negative cell lines, whereas ER-positive cell lines were dependent on the function of *TKTL1* and *MT-ND4* (Fig 4.15B). For the comparison between HER2-positive and HER2-negative breast cell lines, *SLC16A3* along with *PIK3CA* and *PRKAB1* built a strong cluster under normoxia for HER2-positive cell lines (Fig 4.15C). Hypoxic conditions however changed most of the genes required for survival (Fig 4.15D). The ER-negative/HER2-negative candidate genes showed *ALDOA* as well as *PPAP2A* are essential for the survival of breast cell lines. However, *PIK3CA* depletion was not tolerated by the cell lines expressing ER or with amplified HER2 (Fig 4.15E). This is in line with a study that investigated the kinome in a panel of breast epithelial cell lines (Brough et al., 2011). The effect of siRNAs on genes important for cell survival under hypoxia for ER-positive or HER2-positive cell lines showed only minor but still significant differences. *GALK2* and *ME2* along with *c-MYC* were essential for the survival of ER-negative/HER2-negative breast cell lines (Fig 4.15F).
When the genetic composition of the three most prevalent mutated genes in breast cancer was used for supervised clustering, it was obvious that fewer genes showed significant differences (*TP53* wt versus mut, *PIK3CA* wt versus mut and *PTEN* wt versus mut) (Fig 4.16).

However, *SLC16A3* and *MT-ND3* were important for the survival of the cell lines that show high levels of AKT phosphorylation (see Fig 3.2) under normoxic conditions (Fig 4.17C). Moreover, under normoxic conditions the transcription factor *SREBF1* is a

candidate gene for cells expressing normal levels of PTEN and showing low AKT activity (Fig 4.17A,C). Cell lines that have lost PTEN expression were more sensitive to the ablation of *H6PD,* a gene that encodes the H form of glucose-6-phosphate dehydrogenases (Fig 4.17B). Depletion of *PIK3CA* was detrimental to cell lines with high AKT activity under both oxygen conditions (Fig 4.17C,D).

The supervised cluster analyses for the metabolic parameters glucose uptake, lactate secretion and oxygen consumption rate showed that more genes are required under hypoxic conditions than normoxic conditions (Fig 4.18). Interestingly, *ALDOA*, two isoforms of ME, *GALK2* and *SLC16A1* were important for the survival of breast cancer cells in hypoxia (Fig 4.18B). In addition, the siRNAs affecting genes important for the survival of high lactate secreting cells were similar to the high glucose consuming cells. However, another member of the SLC16A family, *SLC16A3,* and *ODC1* were essential for high lactate secreting cells (Fig 4.18D). Functional *PIK3CA* was important for high oxygen consuming cells and *SOD1* and *SLC25A10* were selective to cells with low oxygen consumption (Fig 4.18E,F).

In summary, breast epithelial cell lines show differential requirements for metabolic enzymes according to their genotype and phenotypic characterisation. However, some of these enzymes exhibit differential effects in multiple comparisons or under both oxygen conditions.

4.3 Deconvolution screen

A known disadvantage of siRNA is that it might affect the physiology of a cell independently of the repression of its target gene either by sequence dependent or independent off-target effects. Sequence independent off-target effects can be caused by a too high dose of siRNA. Sequence specific off-target effects are often due to mimicking microRNA or high homology between different siRNAs sequences leading to the downregulation of expression of multiple genes. A common method is therefore to pool different siRNA duplexes per gene to reduce the possibility of off-target effects.

In order to confirm that the observed loss of cell number is due to the specific effect of depleting a given target gene, a deconvolution screen was performed. It is known that

the phenotype caused by the pool of four siRNA duplexes is likely to be specific if two or more of the single siRNA duplexes show a similar phenotype. Furthermore, the knockdown efficiency should correlate with the biological effect. This strategy can be used to identify true candidate genes and strengthen the confidence of choosing specific genes for follow-up investigations and to elucidate the mechanism of how these genes influence breast cancer cell survival.

Sets of four single siGenome siRNA duplexes were used and each candidate gene was deconvoluted individually in combination with the negative controls (siControl1-4) and the positive killing control siUBB1 to assure that the transfection conditions were efficient. The results for each gene were normalised to the negative controls and the siRNA pool results were compared to the siControl1-4 normalised values of a given gene in the primary screen.

Deconvolution of a small number of candidate genes was initially performed and assessed on cell number. The most interesting candidate genes from the rank analysis as well as candidate genes that showed a differential in the supervised cluster analysis for a given parameter (e.g. ER status) were selected. A collection of 16 genes was taken forward to test that the loss of cell number was due to silencing of the gene targeted by the siRNA (Fig 4.19). For each gene identified as a potential candidate gene, one representative sensitive and insensitive cell line was chosen to test the ablation of that specific gene. Most of the candidate genes showed a clear distinction between sensitive and insensitive cell lines (Fig 4.19). However, siRNAs targeting *H6PD* or *GPX4* failed to reproduce the effect observed in the screen (Fig 4.19F,H). The genes *PKM2* and *PFKFB1* were not confirmed as candidate genes, because the sensitivity was opposite to the result of the screen data. The resistant cell lines became sensitive after gene ablation, while the sensitive cell lines showed no reduction in cell number (Fig 4.19I,K).

To further confirm that the siRNA-mediated effect was specific, deconvolution was also performed on mRNA level. The silencing efficiency of each gene was confirmed by qPCR after 48 hours of silencing. Some siRNA duplexes showed only minor silencing efficiency. However, 10 out of the 14 candidate genes tested were confirmed as true targets (Fig 4.20). For *ME1* and *ME2,* only 2 out of 4 siRNA duplexes displayed correlation between the effect on cell number and RNA silencing. In contrast, *PPAP2A*

and *PPAP2C* showed efficient knockdown on mRNA level for all four individual siRNA duplexes including the pooled siRNAs (Fig 4.20H,I) but the results showed poor correlation with the observed effect on cell number (Fig 4.19M,N).

4.4 Discussion

In general, RNAi is a useful tool to analyse the specific genetic dependencies of cells, which is pliable to high-throughput technologies for analysing hundreds if not thousands of genes at once. The advantage of using RNAi is that the specific genes that should be inhibited are known beforehand, and the outcome of silencing can be predicted based on their cellular function. However, one of the disadvantages of RNAi is that each siRNA duplex can affect the expression of up to 200 genes or more, which can cause off-target effects (source: Dharmacon website). To minimise off-target effects it is recommended to use siRNA concentrations of less than 50 nM. Off-targets effects are often caused by single siRNA sequences and can be identified by repeating the experiment using several individual sequences including ones from other distributors. In addition, other RNAi constructs such as shRNA (which are comprised of different sequence designs and genetic architecture) and small molecular inhibitors can be used to recapitulate long-term effects of a gene of interest.

Moreover, the use of transfection reagents may cause unwanted side effects such as high toxicity and changes in gene expression profiles. Fedorov and colleagues observed that transfection reagents such as Lipofectamine 2000 induced an immune response, thereby influencing the transcription of 35 out of 65 genes (Fedorov et al., 2005). Therefore, in this study, careful consideration of which reagent and concentration to use minimised unwanted effects caused by transfection reagents. Hence, observed differences to other published studies might be due to different transfection reagents or concentrations of the reagent used and general variation in screen setup and execution.

The plotted frequency of Z-scores presumed a normal distribution scheme, and most cell lines showed robust screening replication shown by the Spearman correlation factor ρ. This quality control is essential for reducing potential false positive or false negative candidate genes or assumptions about screening conditions. Supervised clustering

analysis and rank analysis were used for identification of candidate genes, thereby combining two different analyses to strengthen the selection process for genes essential in breast cancer cell line survival.

In this study, functional cell survival profiles were established for 17 breast epithelial cell lines after the abrogation of 231 genes involved in metabolic processes under normoxic and hypoxic conditions. This led to the identification of 72 potential candidate genes, which significantly impaired survival in at least two cell lines and/or conditions. After careful consideration, 16 genes were taken forward for validation. The approach of a two-step validation process confirming reduction in mRNA expression correlated with reduction in cell number revealed that 10 genes were selectively required for cell survival (see Fig 4.19, Fig 4.20). This screen has the potential to identify metabolic dependencies of genetically diverse breast epithelial cell lines during normal growth conditions and after exposure to hypoxic stress. Most of the essential candidate genes have been identified for the ER-negative cell lines (represented in the screen by HER2-positive and ER-negative/HER2-negative cell lines). This might be explained by the high number of ER-negative cell lines used in this screen (14 cell lines) compared to three ER-positive cell lines. However, given that HER2-positive (of note, in this study only ER-negative cells with amplified HER2 were used) and ER-negative/HER2-negative breast cancers show the poorest prognosis for overall survival, the screen was biased to identify multiple candidate genes that may be essential for the survival of these two subtypes as there is the most need clinically for dependencies that could be exploited therapeutically.

In particular, the genes for malic enzyme (*ME1*, *ME2*), monocarboxylate transporter 4 (*SLC16A3*), transketolase 1 (*TKTL1*), aldolase A (*ALDOA*) and two isoforms of phosphatidic acid phosphatase (*PPAP2A*, *PPAP2C*) were of significant interest. In the following chapters, these six genes will be further investigated.

Figure 4.1

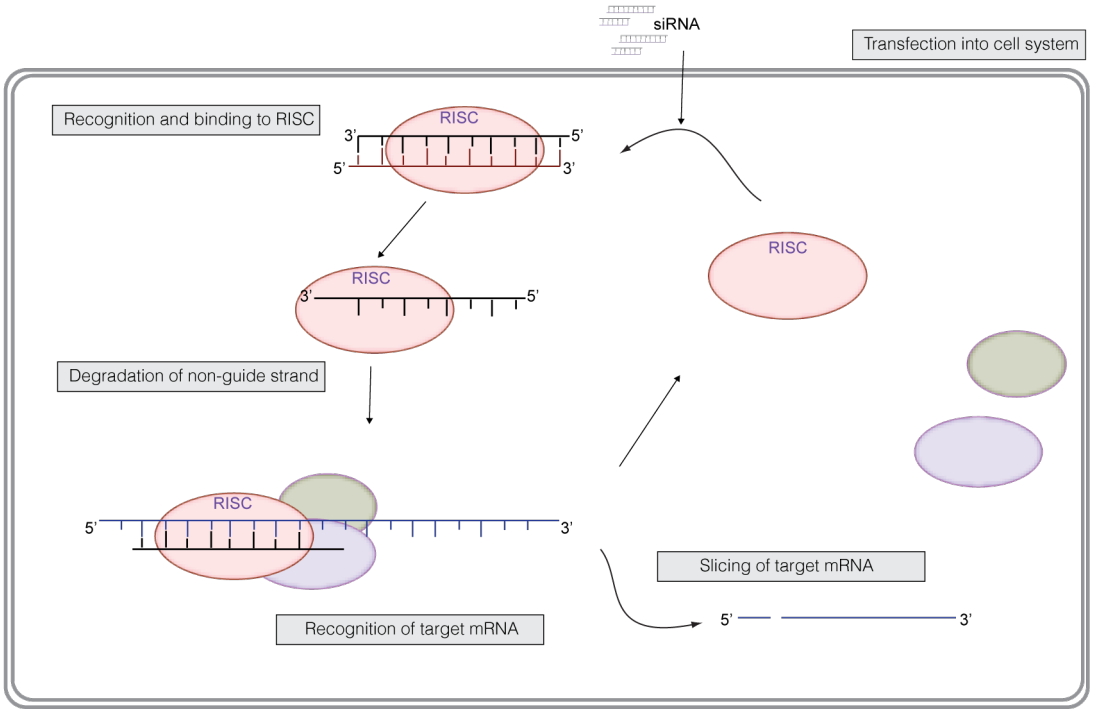

Figure 4-1 Overview of the siRNA mechanism

Schematic overview of the processing of synthetic small-interfering RNAs (siRNA). siRNA is transfected into the cell with lipid based transfection reagents. The recognition of siRNA is mediated by the RISC complex, which binds the siRNA duplex. The guide strand is used as template for recognition of the target mRNA whereas the non-guided strand is degraded. The target mRNA is recognised and bound to the guide strand, which induces the degradation of the sequence.

Figure 4.2

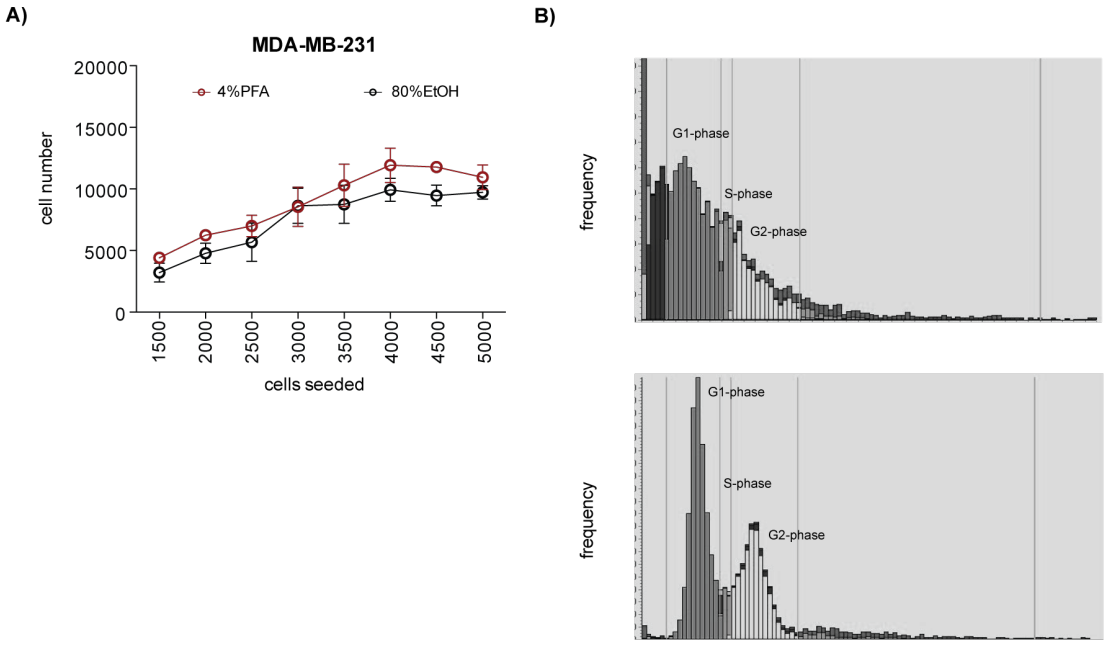

Figure 4-2 Optimisation of cell number for high throughput screening

(A) Growth analysis of MDA-MB-231 cells seeded at the same density, Shown is a representative cell line MDA-MB-231. All cell lines were seeded at different densities (1500-5000 cells per well) for 96 hours culture. Cell number was determined with the Acumen X^3 after fixation with ice-cold 80% EtOH (black line) or 4% PFA (red line). (B) Cell cycle profile of a representative cell line after 4% PFA fixation (upper graph) and 80% EtOH fixation (lower graph).

Figure 4.3

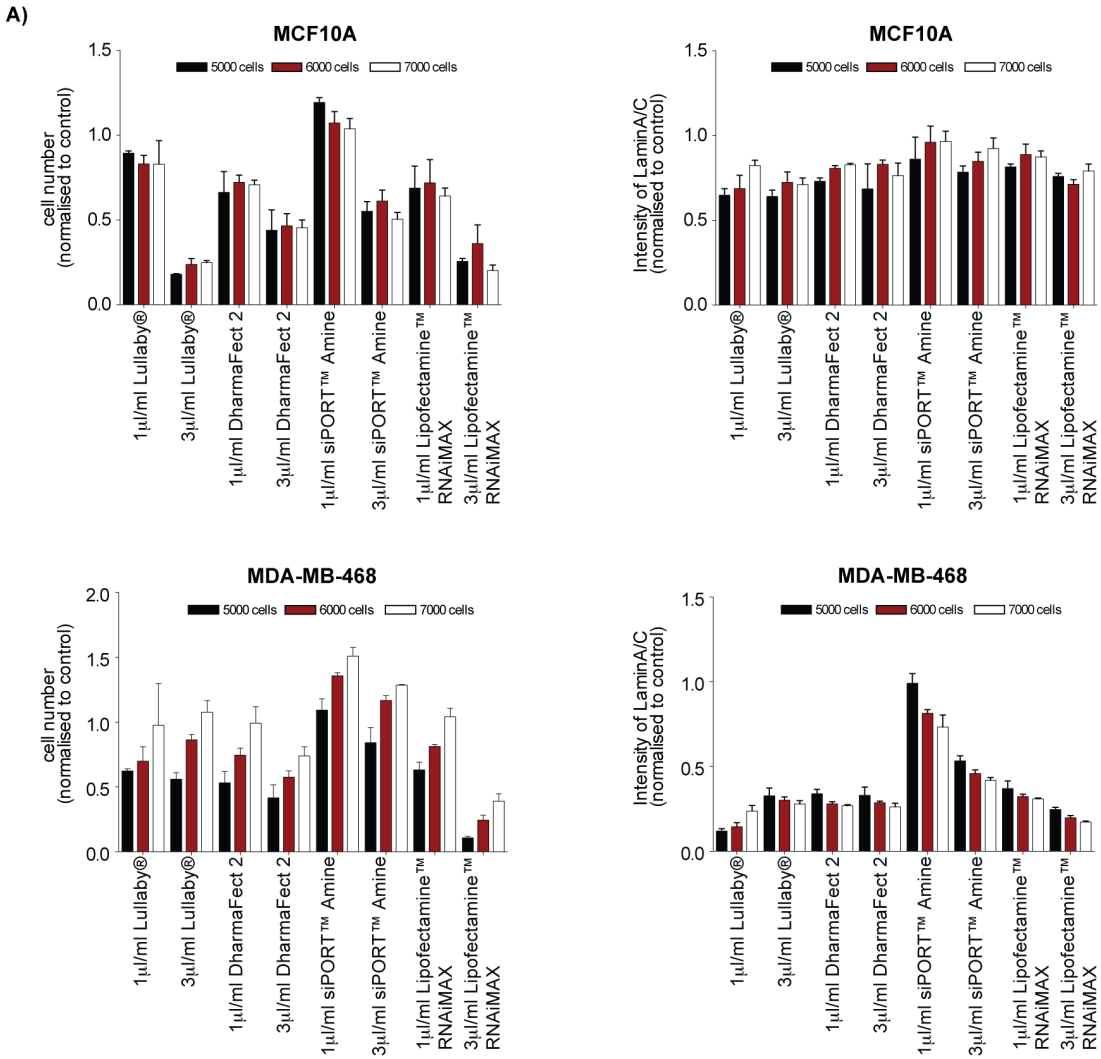
A)
MCF10A
5000 cells
6000 cells
7000 cells
cell number (normalised to control)
Intensity of LaminA/C (normalised to control)
1µl/ml Lullaby®
3µl/ml Lullaby®
1µl/ml DharmaFect 2
3µl/ml DharmaFect 2
1µl/ml siPORT™ Amine
3µl/ml siPORT™ Amine
1µl/ml Lipofectamine™ RNAiMAX
3µl/ml Lipofectamine™ RNAiMAX
MDA-MB-468

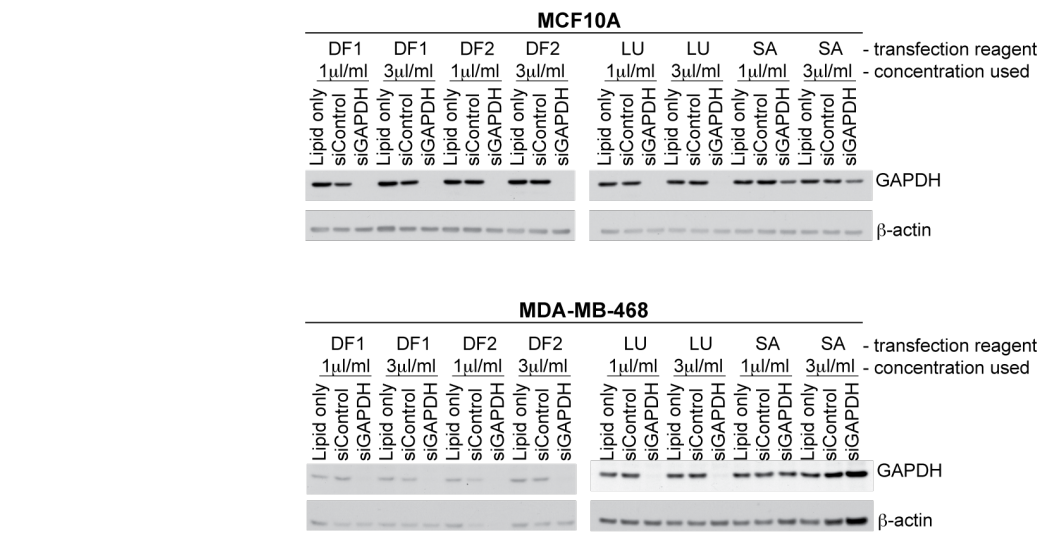
B)
MCF10A
DF1 1µl/ml
DF1 3µl/ml
DF2 1µl/ml
DF2 3µl/ml
LU 1µl/ml
LU 3µl/ml
SA 1µl/ml
SA 3µl/ml
- transfection reagent
- concentration used
Lipid only
siControl
siGAPDH
GAPDH
β-actin
MDA-MB-468

Figure 4-3 Overview of transfection testing

(A) Two representative cell lines (MCF10A and MDA-MB-468) were chosen to demonstrate the effect of 4 transfection reagents on toxicity (left graph) and siRNA delivery (right graph) (B) Immunoblot analysis of GAPDH silencing in the two representative cell lines MCF10A and MDA-MB-468.

Figure 4.4

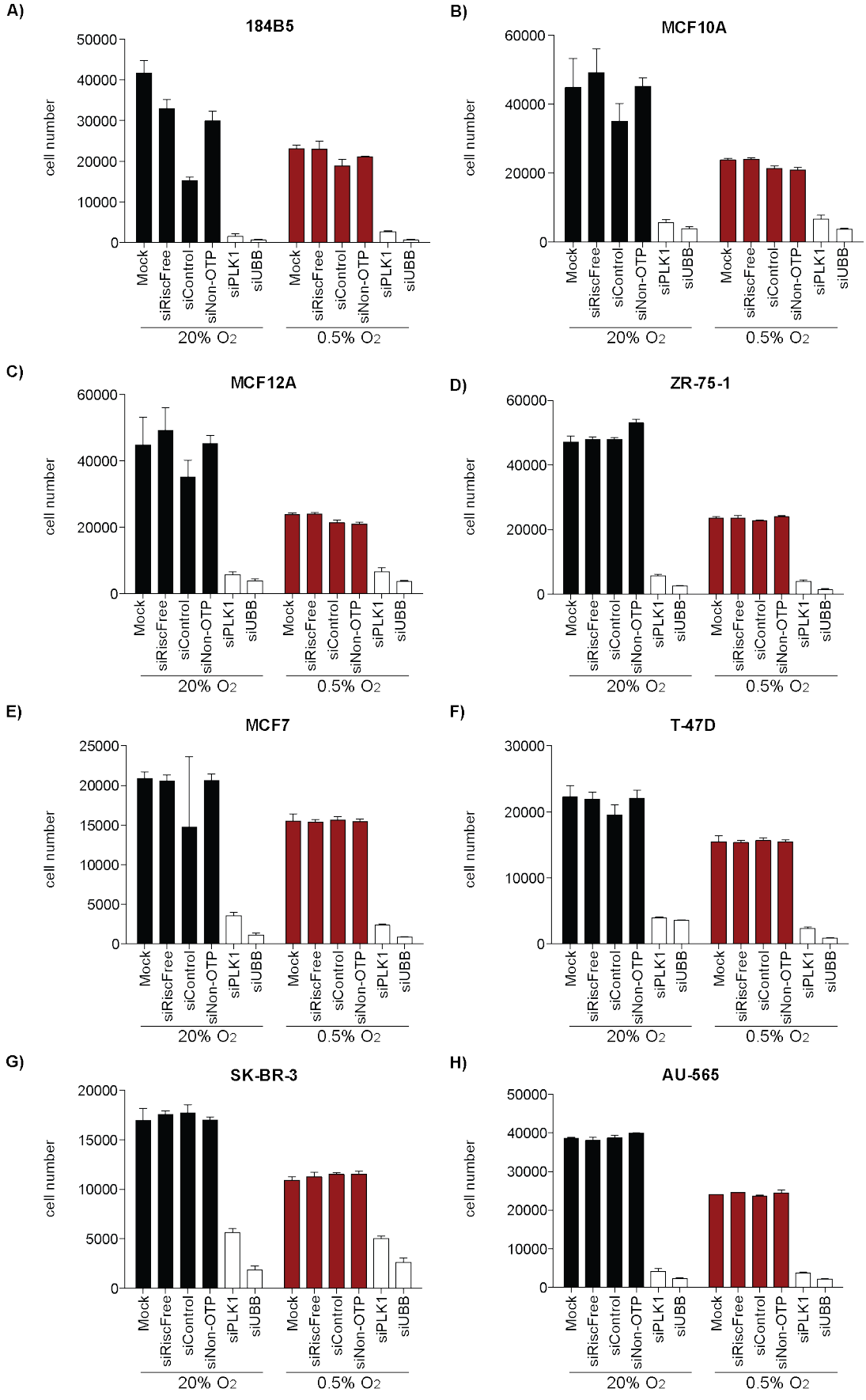
A)
184B5
B)
MCF10A
C)
MCF12A
D)
ZR-75-1
E)
MCF7
F)
T-47D
G)
SK-BR-3
H)
AU-565
cell number
Mock
siRiscFree
siControl
siNon-OTP
siPLK1
siUBB
20% O2
0.5% O2

Figure 4.4

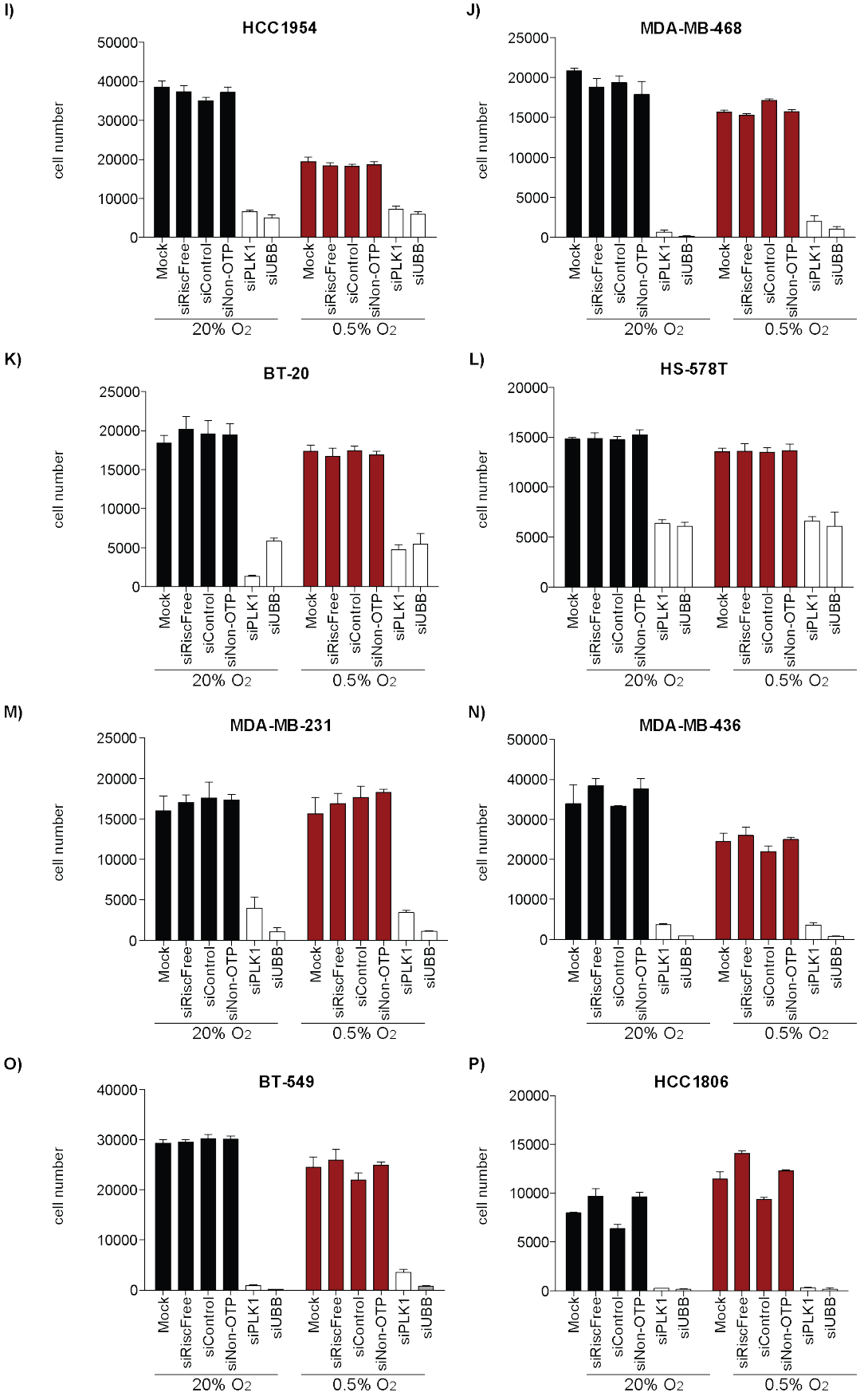
I)
HCC1954
J)
MDA-MB-468
K)
BT-20
L)
HS-578T
M)
MDA-MB-231
N)
MDA-MB-436
O)
BT-549
P)
HCC1806
cell number
Mock
siRiscFree
siControl
siNon-OTP
siPLK1
siUBB
20% O2
0.5% O2

Figure 4.4

Q)

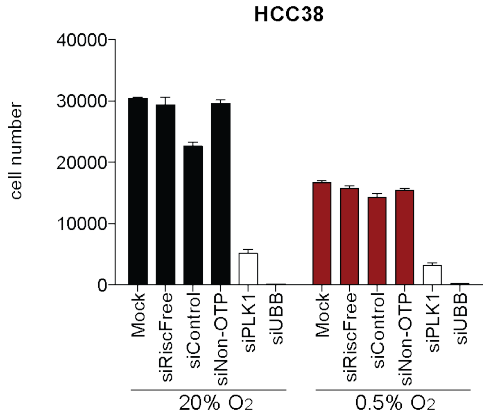

Figure 4-4 Overview of negative and positive controls

Bar graphs indicating cell number of seventeen breast epithelial cell lines reverse transfected with 4 negative controls (black bar=normoxia, red bar=hypoxia) and 2 positive controls (white bars) for each oxygen condition. (A) 184B5, (B) MCF10A, (C) MCF12A, (D) ZR-75-1, (E) MCF7, (F) T-47D, (G) SK-BR-3, (H) AU-565, (I) HCC1954, (J) MDA-MB-468, (K) BT-20, (L) HS-578T, (M) MDA-MB-231, (N) MDA-MB-436, (O) BT-549, (P) HCC1806 and (Q) HCC38.

Figure 4.5

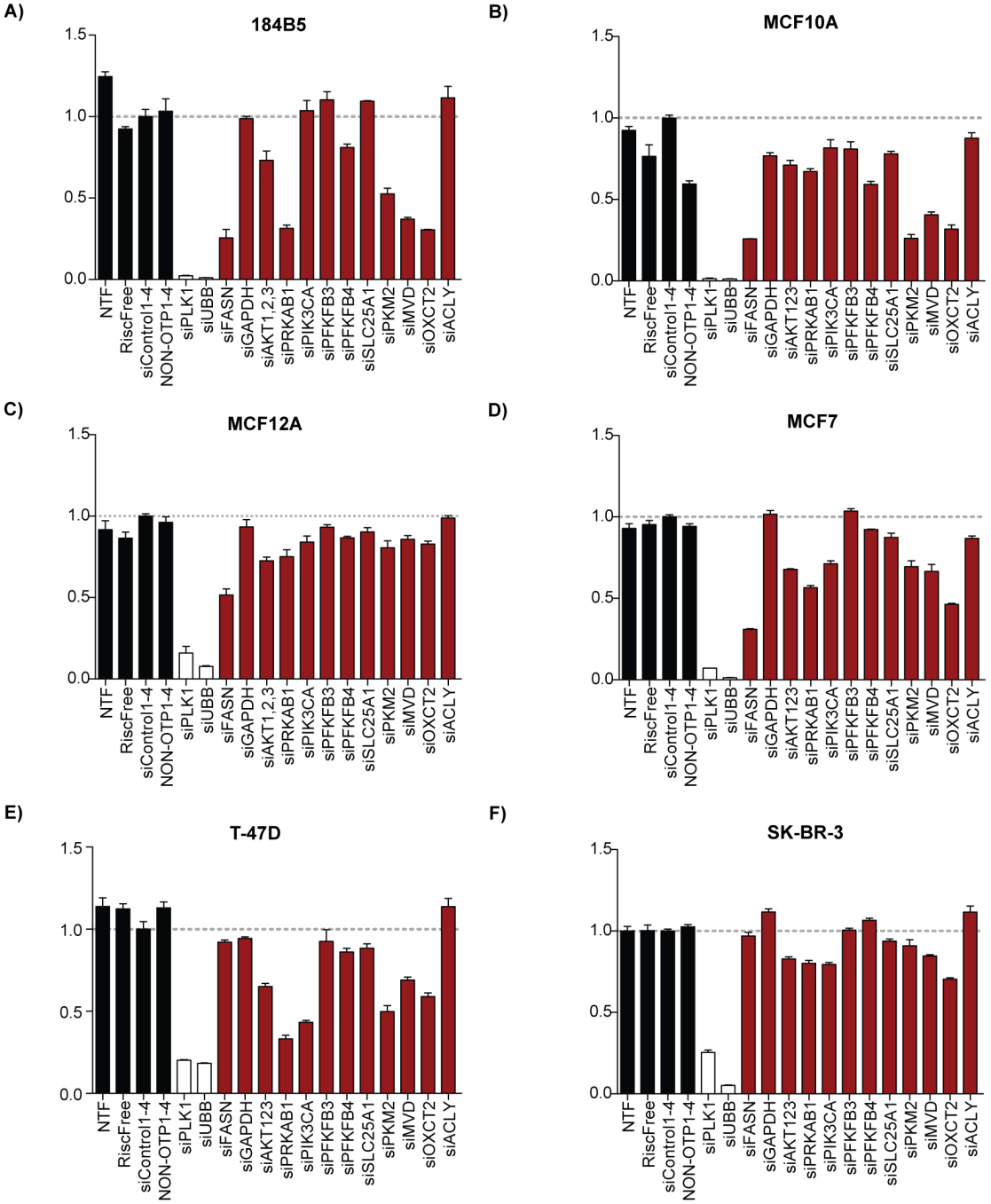
A)
184B5
B)
MCF10A
C)
MCF12A
D)
MCF7
E)
T-47D
F)
SK-BR-3
1.5
1.0
0.5
0.0
NTF
RiscFree
siControl1-4
NON-OTP1-4
siPLK1
siUBB
siFASN
siGAPDH
siAKT1,2,3
siAKT123
siPRKAB1
siPIK3CA
siPFKFB3
siPFKFB4
siSLC25A1
siPKM2
siMVD
siOXCT2
siACLY

Figure 4.5

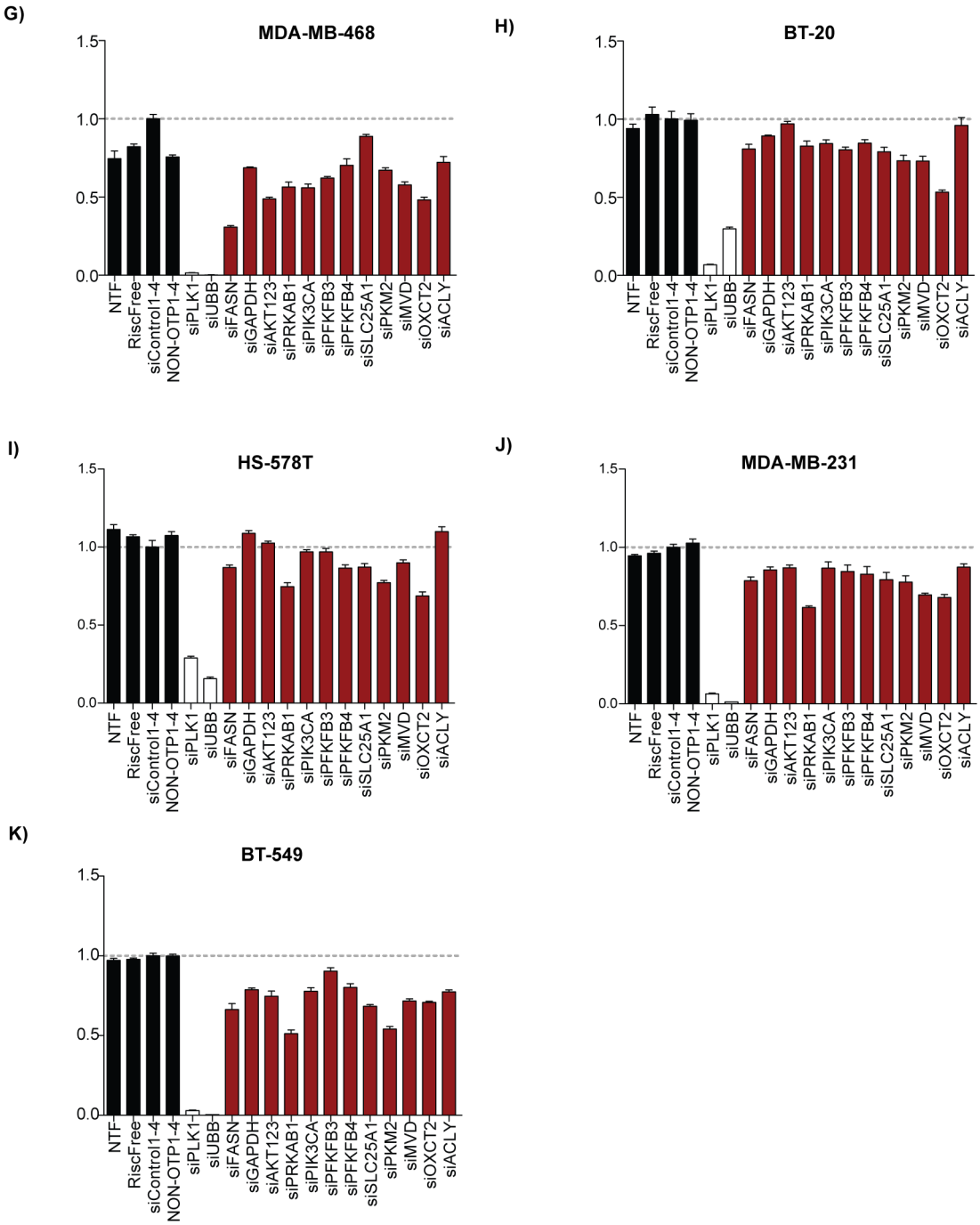

Figure 4-5 Summary of pilot screen

Bar graphs indicating fold change to siControl1-4 transfected cells of eleven breast epithelial cell lines reverse transfected with 4 negative controls (black bars), 2 positive controls (white bars) and 12 metabolic genes known to be important for cancer cell survival. (A) 184B5, (B) MCF10A, (C) MCF12A, (D) MCF7, (E) T-47D, (F) SK-BR-3, (G) MDA-MB-468, (H) BT-20, (I) HS-578T, (J) MDA-MB-231 and (K) BT-549.

Figure 4.6

A)

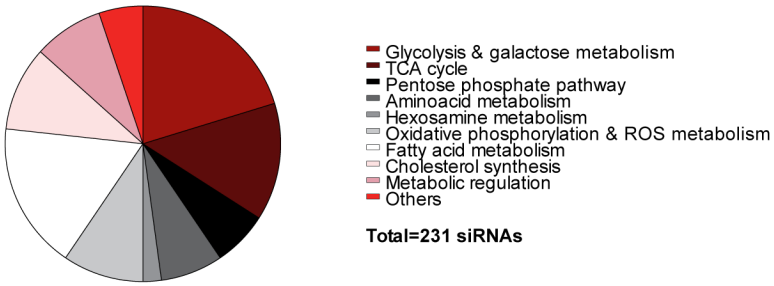

B)

PLATE #1

	1	2	3	4	5	6	7	8	9	10	11	12
A	RF	Control 1-4	HK1	HK2	GCK	PKLR	PKM2	PC	PDHA1	PDHA2	PDHB	DLD
B	NON -OTP	PLK1	DLAT	ACACA	LDHA	LDHB	LDHC	CS	ACLY	G6PD	FASN	CHKA
C	Control 1-4	UBB	CHKB	HMGCS1	HMGCS2	HMGCR	SLC2A4	SLC2A1	SREBF1	SREBF2	PRKAA1	PRKAA2
D	NON -OTP	RF	HIF1A	AKT1	AKT2	AKT3	ILVBL	PHGDH	MDH1	MDH2	GPD1	GPD2
E	Control 1-4	PLK1	PRPS1	PRPS2	PPAT	UMPS	SLC1A5	SLC7A5	PFKL	GAPDH	GAPDS	PGK1
F	RF	UBB	PGK2	ENO1	IDH1	IDH2	OGDH	SDHA	SDHB	SDHC	SDHD	FH
G	UBB	RF	CHPT1	MVK	PMVK	MVD	FDPS	GGPS1	LSS	DHCR7	PRKAG2	PRKAG3
H	NON -OTP	PLK1	PRKAB1	PRKAB2	PRKAG1	EPAS1	MT-ND1	MT-ND2	MT-ND3	MT-ND4	MT-ND5	MT-ND6

PLATE #2

	1	2	3	4	5	6	7	8	9	10	11	12
A	RF	Control 1-4	GALK1	GALK2	GALT	PGM1	PGM3	GLUD1	GLUD2	HK3	GPI	PFKM
B	NON -OTP	PLK1	PFKP	PFKFB1	PFKFB2	PFKFB3	PFKFB4	ALDOA	ALDOB	ALDOC	TPI1	PGAM4
C	Control 1-4	UBB	PGAM1	PGAM2	BPGM	ENO2	ENO3	LDHAL6A	LDHAL6B	PDK3	PDK4	PPM2C
D	NON -OTP	RF	PDP2	ACO1	ACO2	LOC441996	IDH3A	IDH3B	IDH3G	DLST	LOC283398	SUCLG2
E	Control 1-4	PLK1	SUCLG1	SUCLA2	GOT1	GOT2	SLC25A11	GPD1L	ME3	GLUL	GPT	GPT2
F	RF	UBB	DDO	AGXT	AGXT2	PSAT1	CAD	ODC1	SHMT1	SHMT2	TKT	TKTL1
G	UBB	RF	DKFZP434*	PGLS	H6PD	PGD	RPIA	PRPS1L1	GPAM	AGPAT1	AGPAT2	AGPAT6
H	NON -OTP	PLK1	UNQ1849	AGPAT3	AGPAT4	PPAP2A	PPAP2C	PPAP2B	PCYT1A	PCYT1B	PLD1	PLD2

PLATE #3

	1	2	3	4	5	6	7	8	9	10	11	12
A	RF	Control 1-4	ACSS1	ACSS2	ACACB	MT	THEDC1	FLJ20604	ELOVL6	SCD	SCD5	ACAT1
B	NON -OTP	PLK1	ACAT2	AACS	IDI1	IDI2	FDFT1	SQLE	CYP51A1	NSDHL	HSD17B7	EBP
C	Control 1-4	UBB	SC5DL	DHCR24	SOD1	SOD2	SOD3	CAT	GPX6	GPX1	GPX2	GPX3
D	NON -OTP	RF	GPX4	GPX5	GPX7	SCO2	ATPIF1	COX4I1	COX4I2	COX5A	C12ORF5	OXCT1
E	Control 1-4	PLK1	OXCT2	SLC16A7	SLC16A3	SLC16A8	SLC16A4	TALDO1	RPE	GFPT1	GFPT2	GNPNAT1
F	RF	UBB	UAP1	OGT	PGM1	PGM3	CHREBP	SLC25A10	ME1	ME2	GLS	GLS2
G	UBB	RF	PIK3CA	MYLCD	Control 1-4	Control 1-4	LB	IRS1	Control 1-4	Control 1-4	LB	PTEN
H	NON -OTP	PLK1	MYC	RPTOR	RICTOR	SLC16A1	SLC25A1	PDK1	PDK2	CPT1A	CPT1B	Akt pooled

C)

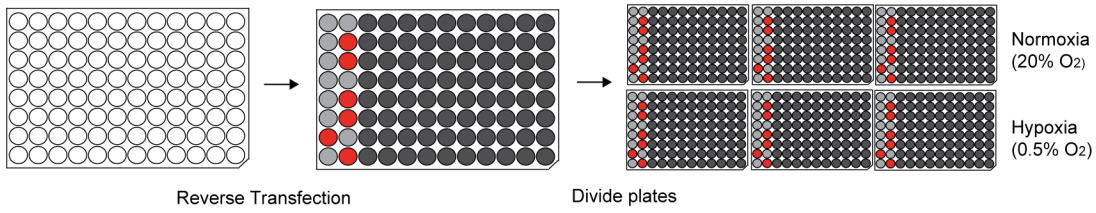

Figure 4-6 Overview of siRNA screen

(A) Pie chart of all the siGenome siRNAs targeting genes representing metabolic processes within the library. (B) Plate layout of small screen siRNA library distributed over three 96-well plates. (C) Reverse transfection of 231 siRNAs (dark grey) including six negative (light grey) or positive (red) controls. Plates were divided after reverse transfection to be cultured under normoxic or hypoxic conditions.

Figure 4.7

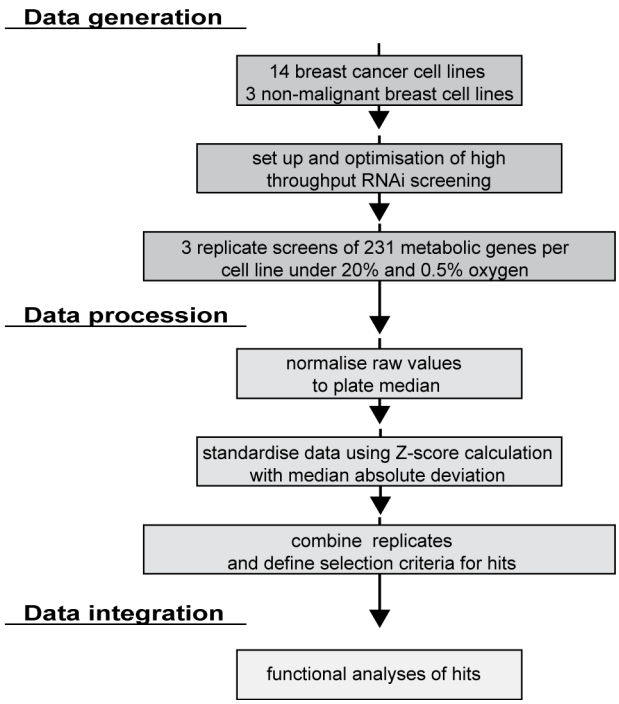

Figure 4-7 Flow diagram of screen analysis strategy to identify metabolic genes essential for survival

Figure 4.8

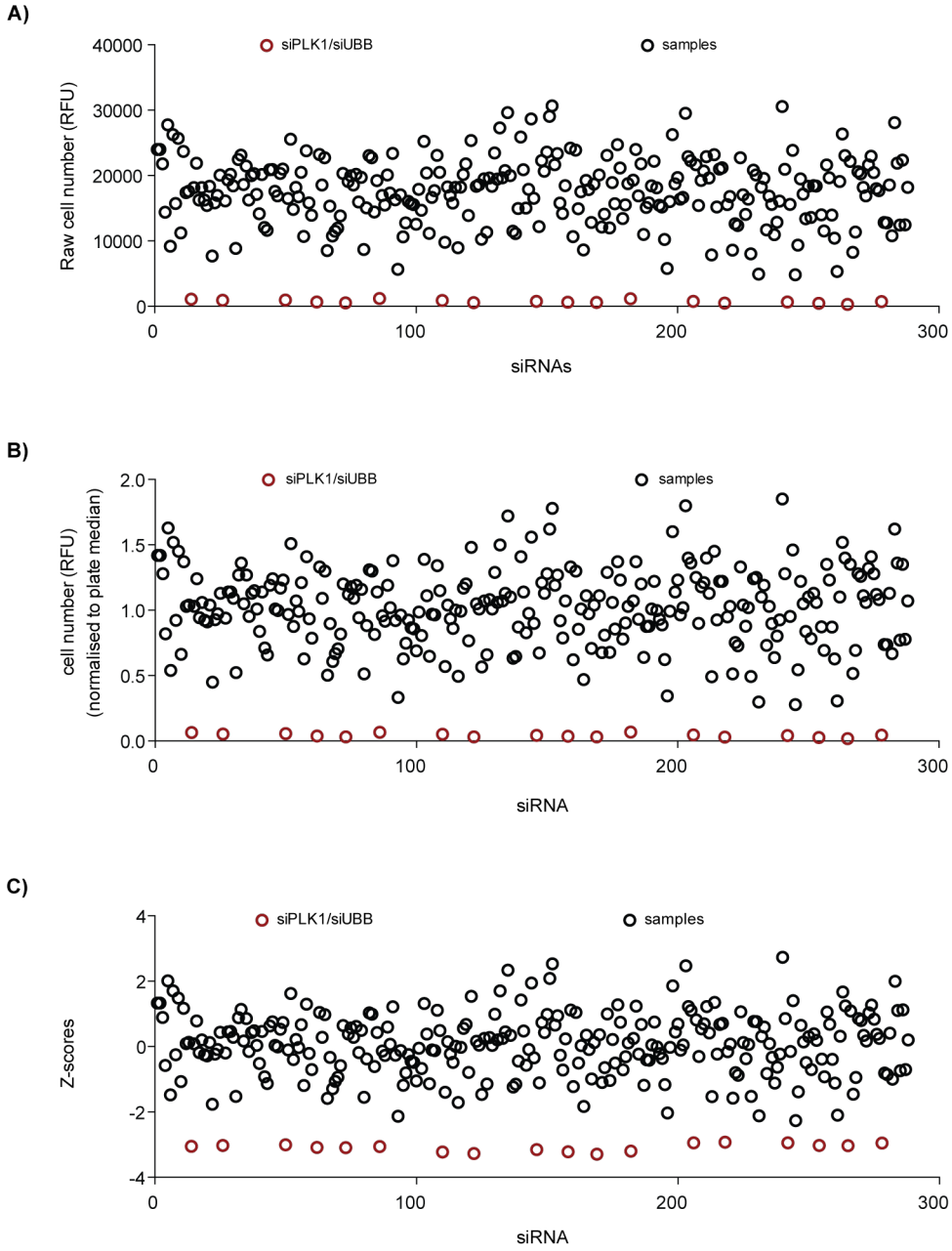

Figure 4-8 Normalisation and analysis of raw data

(A) Overview of the raw cell number data of all 237 genes (231 siRNAs and 6 controls) of a representative sample. The positive controls siPLK1 and siUBB show low relative fluorescent units (RFU) compared to the main population of samples. (B) Overview of the plate normalised data of 237 genes in the screen shown here in a representative sample. (C) Z-score$_{(MAD)}$ normalisation of 237 genes in the screen shown here in a representative sample.

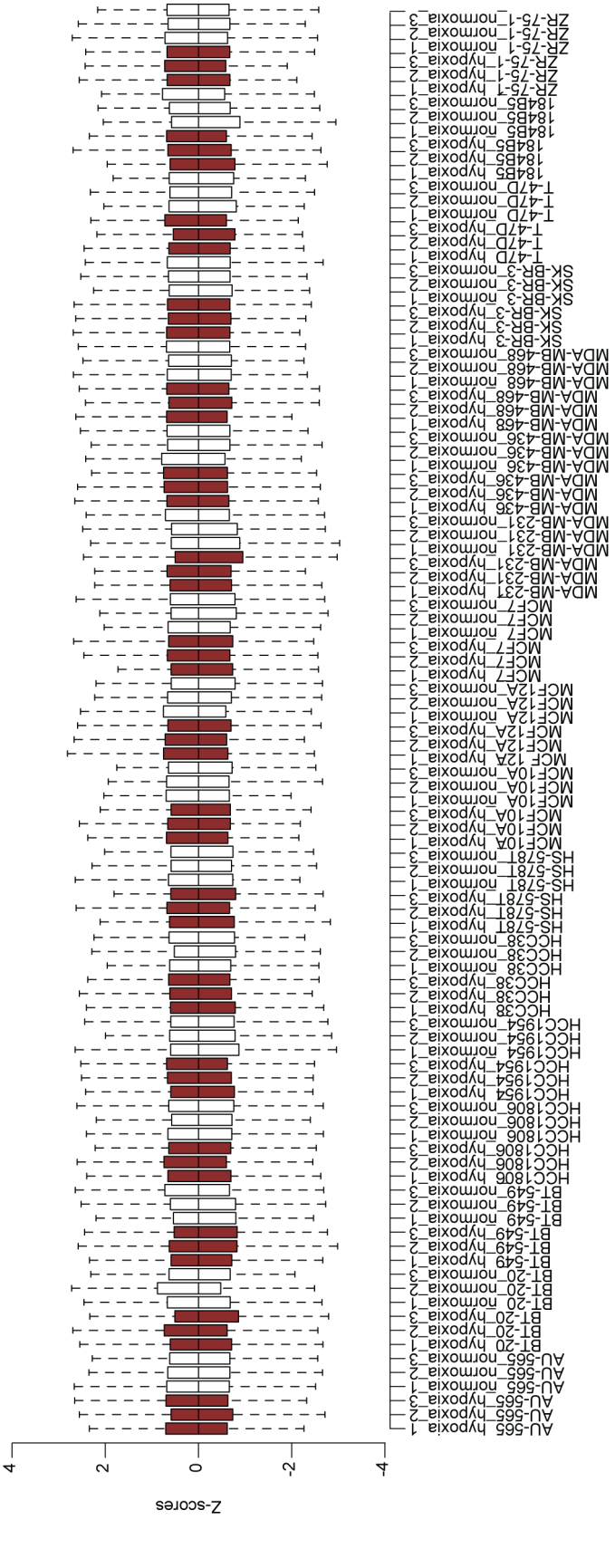
A)
Z-scores
4
2
0
-2
-4
AU-565_hypoxia_1
AU-565_hypoxia_2
AU-565_hypoxia_3
AU-565_normoxia_1
AU-565_normoxia_2
AU-565_normoxia_3
BT-20_hypoxia_1
BT-20_hypoxia_2
BT-20_hypoxia_3
BT-20_normoxia_1
BT-20_normoxia_2
BT-20_normoxia_3
BT-549_hypoxia_1
BT-549_hypoxia_2
BT-549_hypoxia_3
BT-549_normoxia_1
BT-549_normoxia_2
BT-549_normoxia_3
HCC1806_hypoxia_1
HCC1806_hypoxia_2
HCC1806_hypoxia_3
HCC1806_normoxia_1
HCC1806_normoxia_2
HCC1806_normoxia_3
HCC1954_hypoxia_1
HCC1954_hypoxia_2
HCC1954_hypoxia_3
HCC1954_normoxia_1
HCC1954_normoxia_2
HCC1954_normoxia_3
HCC38_hypoxia_1
HCC38_hypoxia_2
HCC38_hypoxia_3
HCC38_normoxia_1
HCC38_normoxia_2
HCC38_normoxia_3
HS-578T_hypoxia_1
HS-578T_hypoxia_2
HS-578T_hypoxia_3
HS-578T_normoxia_1
HS-578T_normoxia_2
HS-578T_normoxia_3
MCF10A_hypoxia_1
MCF10A_hypoxia_2
MCF10A_hypoxia_3
MCF10A_normoxia_1
MCF10A_normoxia_2
MCF10A_normoxia_3
MCF12A_hypoxia_1
MCF12A_hypoxia_2
MCF12A_hypoxia_3
MCF12A_normoxia_1
MCF12A_normoxia_2
MCF12A_normoxia_3
MCF7_hypoxia_1
MCF7_hypoxia_2
MCF7_hypoxia_3
MCF7_normoxia_1
MCF7_normoxia_2
MCF7_normoxia_3
MDA-MB-231_hypoxia_1
MDA-MB-231_hypoxia_2
MDA-MB-231_hypoxia_3
MDA-MB-231_normoxia_1
MDA-MB-231_normoxia_2
MDA-MB-231_normoxia_3
MDA-MB-436_hypoxia_1
MDA-MB-436_hypoxia_2
MDA-MB-436_hypoxia_3
MDA-MB-436_normoxia_1
MDA-MB-436_normoxia_2
MDA-MB-436_normoxia_3
MDA-MB-468_hypoxia_1
MDA-MB-468_hypoxia_2
MDA-MB-468_hypoxia_3
MDA-MB-468_normoxia_1
MDA-MB-468_normoxia_2
MDA-MB-468_normoxia_3
SK-BR-3_hypoxia_1
SK-BR-3_hypoxia_2
SK-BR-3_hypoxia_3
SK-BR-3_normoxia_1
SK-BR-3_normoxia_2
SK-BR-3_normoxia_3
T-47D_hypoxia_1
T-47D_hypoxia_2
T-47D_hypoxia_3
T-47D_normoxia_1
T-47D_normoxia_2
T-47D_normoxia_3
184B5_hypoxia_1
184B5_hypoxia_2
184B5_hypoxia_3
184B5_normoxia_1
184B5_normoxia_2
184B5_normoxia_3
ZR-75-1_hypoxia_1
ZR-75-1_hypoxia_2
ZR-75-1_hypoxia_3
ZR-75-1_normoxia_1
ZR-75-1_normoxia_2
ZR-75-1_normoxia_3

Figure 4.9

Figure 4-9 Overview of Z-scores of all replicates under both oxygen conditions

(A) Boxplot of the median Z-scores of all samples in all replicates under normoxic (white) and hypoxic (red) conditions across the seventeen breast epithelial cell lines.

Figure 4.10

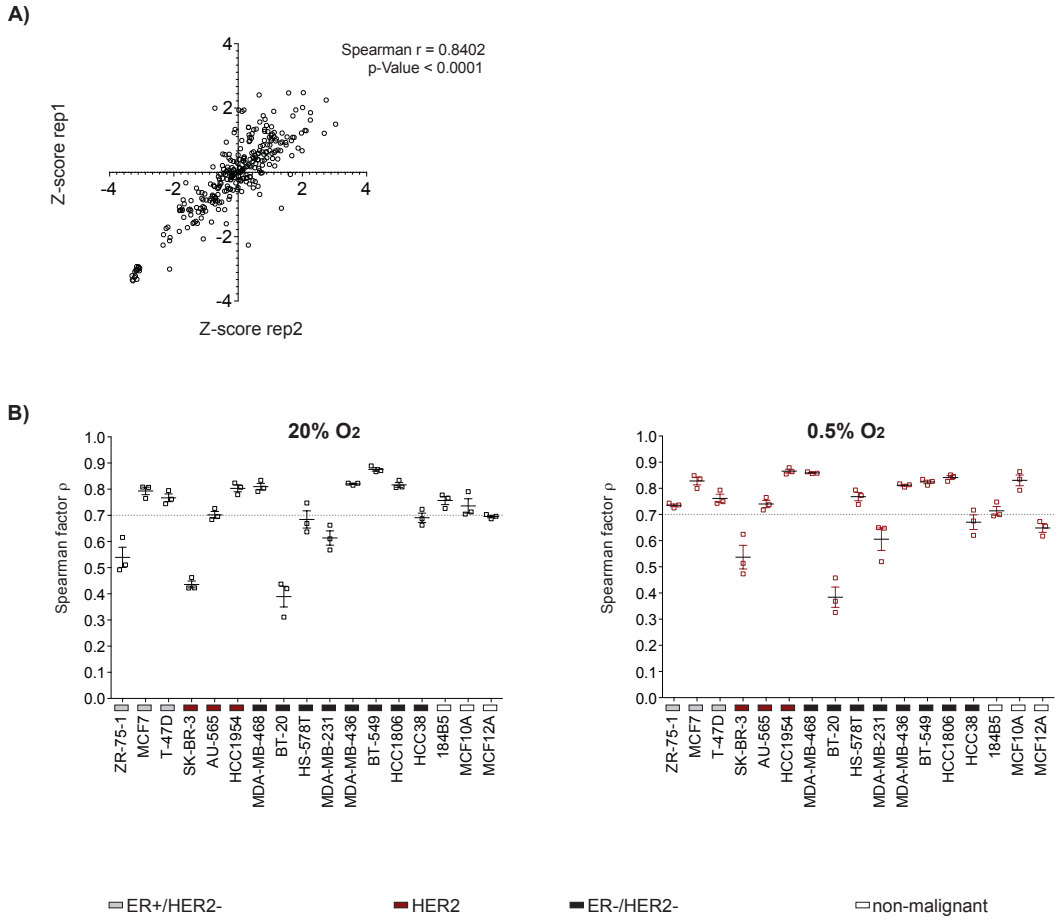

Figure 4-10 Quality control and reproducibility of siRNA screen

(A) Example of the reproducibility of data for one cell line/condition. Correlation of two replicates of a representative cell line within the screen. (B) Spearman correlation of all replicates under normoxic (left) and hypoxic (right) conditions

Figure 4.11

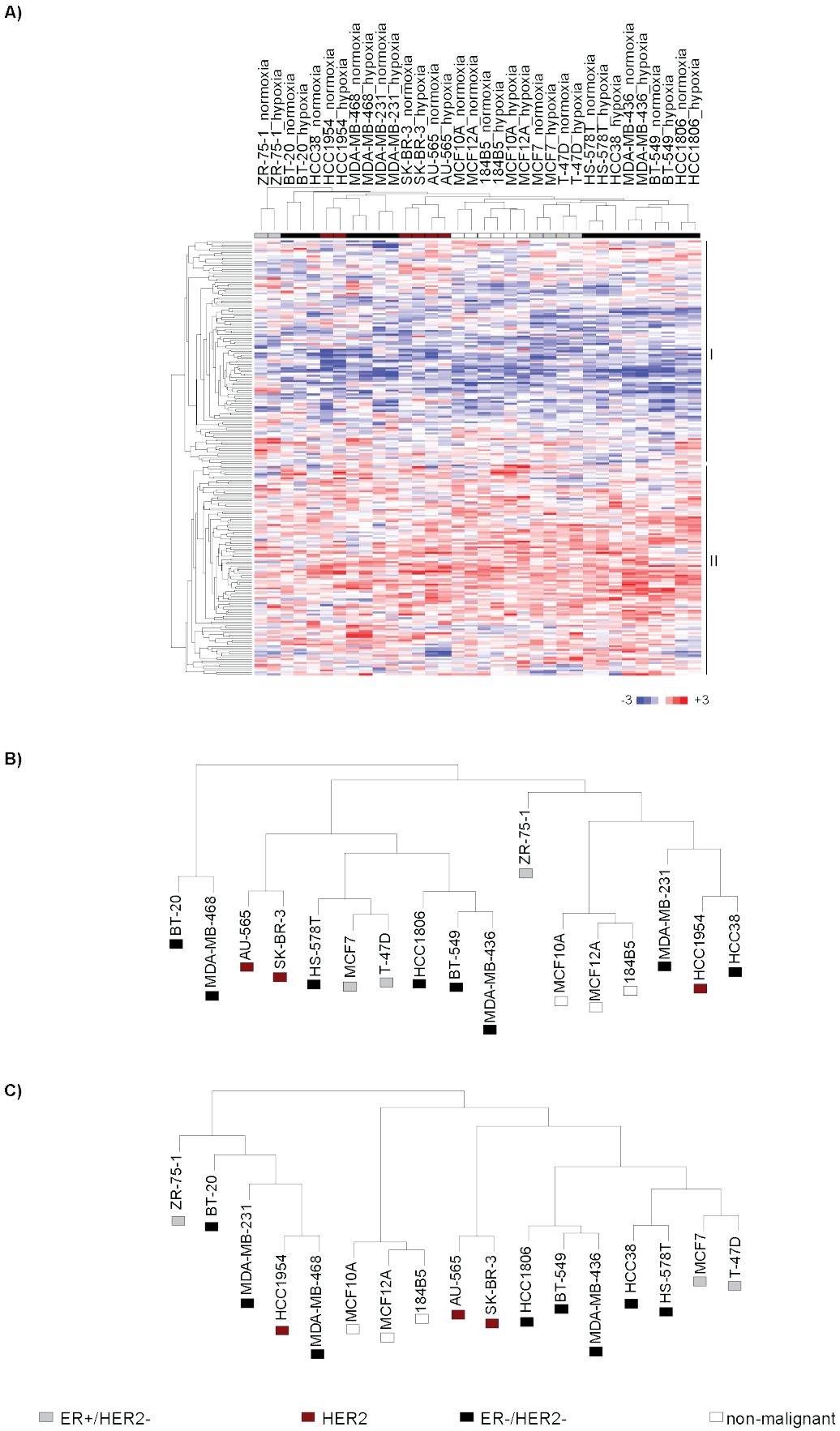
A)
ZR-75-1_normoxia
ZR-75-1_hypoxia
BT-20_normoxia
BT-20_hypoxia
HCC38_normoxia
HCC1954_normoxia
HCC1954_hypoxia
MDA-MB-468_normoxia
MDA-MB-468_hypoxia
MDA-MB-231_normoxia
MDA-MB-231_hypoxia
SK-BR-3_normoxia
SK-BR-3_hypoxia
AU-565_normoxia
AU-565_hypoxia
MCF10A_normoxia
MCF12A_normoxia
184B5_normoxia
184B5_hypoxia
MCF10A_hypoxia
MCF12A_hypoxia
MCF7_normoxia
MCF7_hypoxia
T-47D_normoxia
T-47D_hypoxia
HS-578T_normoxia
HS-578T_hypoxia
HCC38_hypoxia
MDA-MB-436_normoxia
MDA-MB-436_hypoxia
BT-549_normoxia
BT-549_hypoxia
HCC1806_normoxia
HCC1806_hypoxia
I
II
-3
+3
B)
BT-20
MDA-MB-468
AU-565
SK-BR-3
HS-578T
MCF7
T-47D
HCC1806
BT-549
MDA-MB-436
ZR-75-1
MCF10A
MCF12A
184B5
MDA-MB-231
HCC1954
HCC38
C)
ZR-75-1
BT-20
MDA-MB-231
HCC1954
MDA-MB-468
MCF10A
MCF12A
184B5
AU-565
SK-BR-3
HCC1806
BT-549
MDA-MB-436
HCC38
HS-578T
MCF7
T-47D
ER+/HER2-
HER2
ER-/HER2-
non-malignant

Figure 4-11 Hierarchical cluster analysis of RNAi screen data

(A) Hierarchical clustering analysis of 231 genes across the cell lines screened under normoxic and hypoxic conditions. Cluster I represented loss of cell number, whereas cluster II showed gain of cell number. (B) Hierarchical cluster analysis of the data from the experiments performed in normoxia of all cell lines. (C) Hierarchical cluster analysis of the data from the experiments performed in hypoxia of all cell lines.

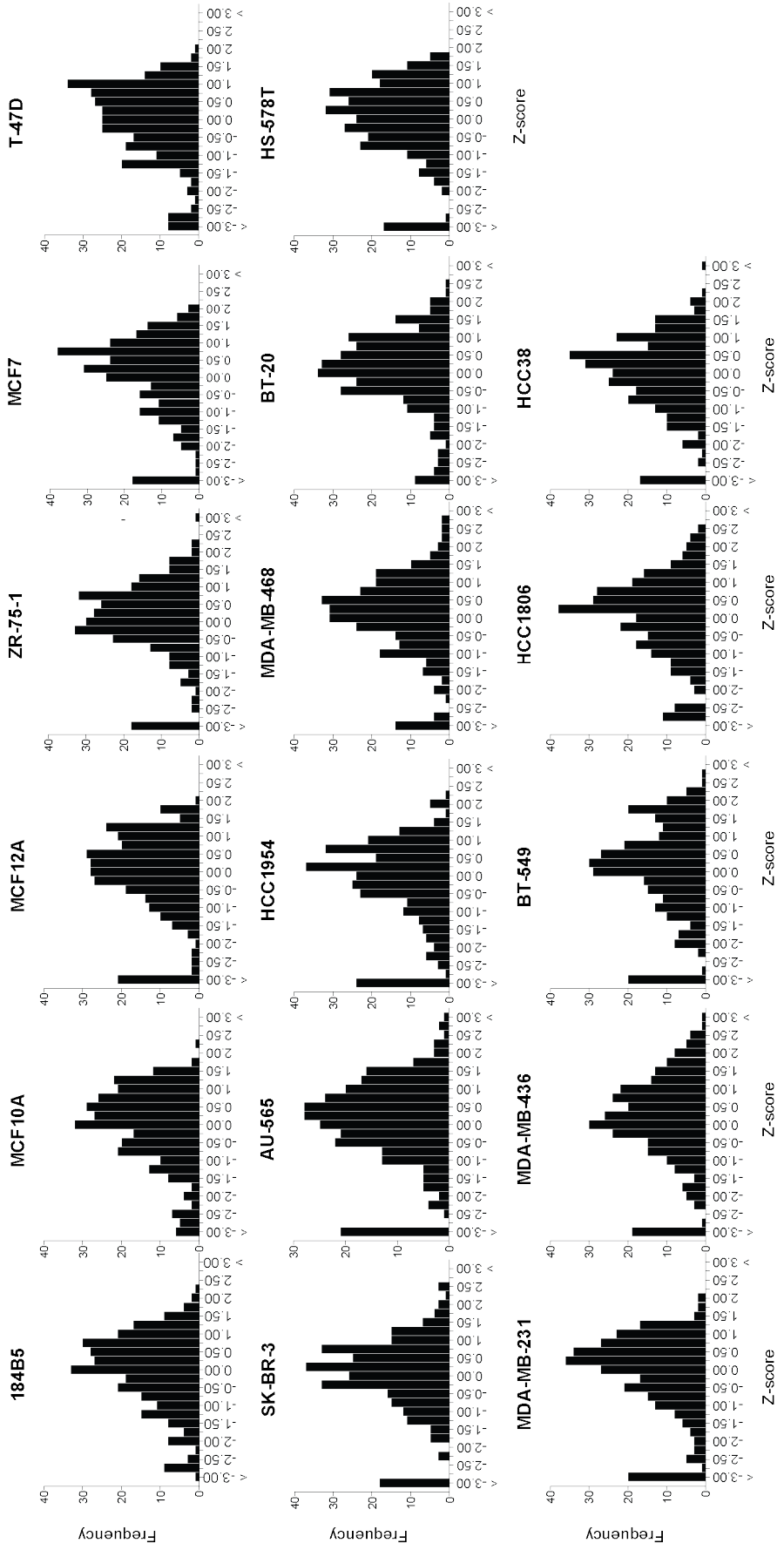
A)
184B5
MCF10A
MCF12A
ZR-75-1
MCF7
T-47D
SK-BR-3
AU-565
HCC1954
MDA-MB-468
BT-20
HS-578T
MDA-MB-231
MDA-MB-436
BT-549
HCC1806
HCC38
Frequency
Z-score

Figure 4.12

Figure 4.12

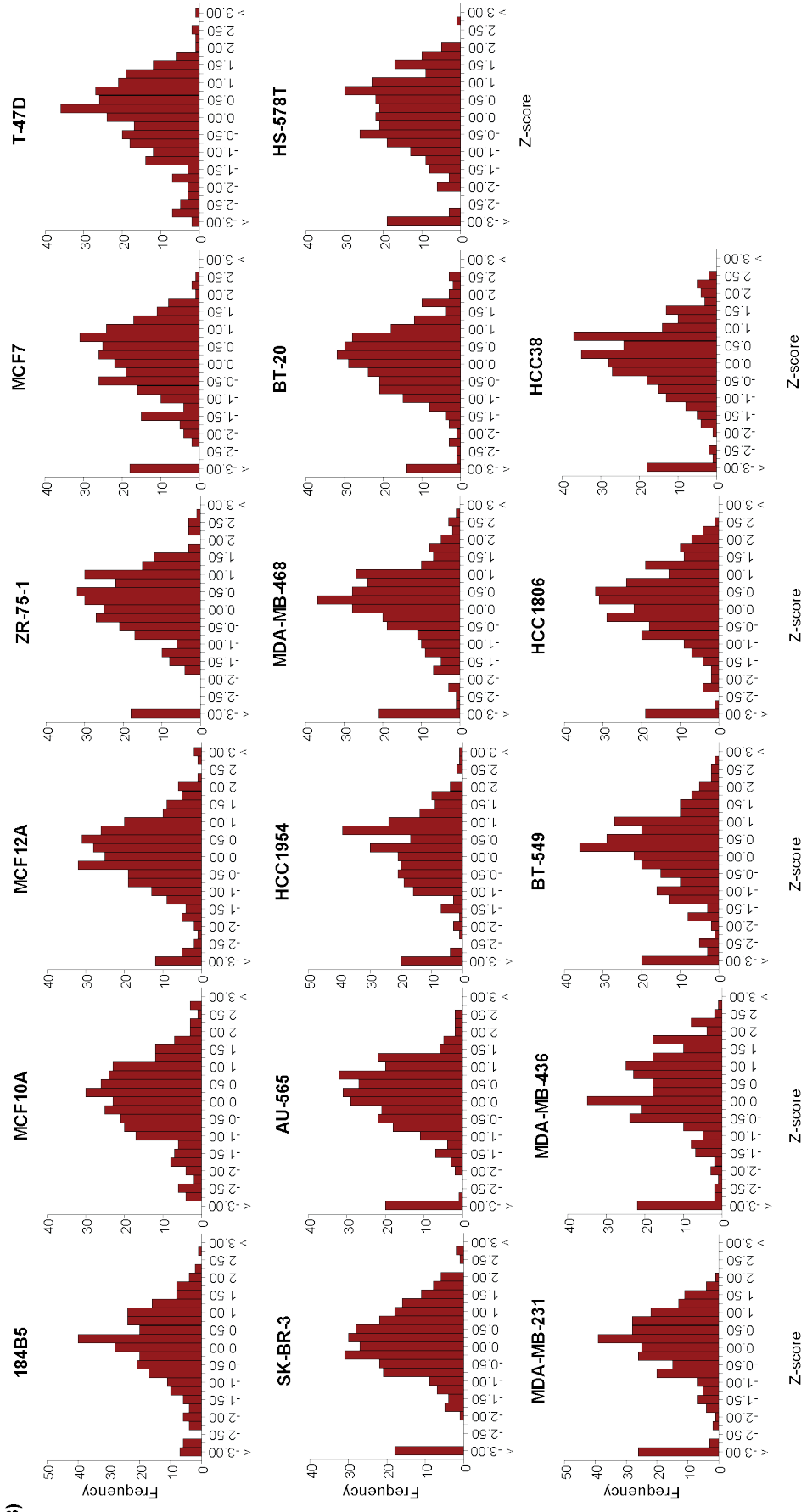
B)
184B5
MCF10A
MCF12A
ZR-75-1
MCF7
T-47D
SK-BR-3
AU-565
HCC1954
MDA-MB-468
BT-20
HS-578T
MDA-MB-231
MDA-MB-436
BT-549
HCC1806
HCC38
Frequency
Z-score

Figure 4-12 Overview of Z-score frequency in the panel of cell lines.

(A) Distribution blot of Z-scores frequencies of all 237 genes across the seventeen cell lines under normoxic conditions. (B) Distribution blot of Z-scores frequencies of all 237 genes across the seventeen cell lines under hypoxic conditions.

Figure 4.13

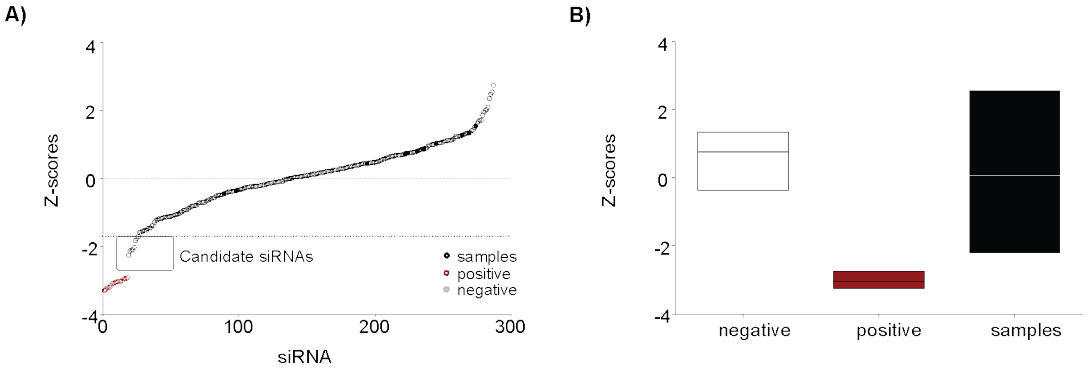

Figure 4-13 Ranking of Z-scores

(A) Scatterplot of ranked Z-scores of a representative cell line. A stringent threshold of a Z-score ≤ -1.7 was applied to identify candidate genes. Red circles indicate positive controls resulting in loss of cell number. Black circles represent 231 genes targeted by the siRNAs and black dots represent negative controls. (B) Boxplot of positive controls, negative controls and sample Z-scores. Negative Z-scores lay within the sample population, whereas the positive controls are showing the strongest negative Z-scores.

Table 4.1

Gene	Gene-ID	Accession number
ACSS2	55902	NM_018677
ACSS1	84532	NM_032501
AGPAT4	56895	NM_020133
AGPAT6	137964	NM_178819.3
AGXT	189	NM_000030
AGXT2	64902	NM_031900
AKT1	207	NM_005163
AKT3	10000	NM_005465
ALDOA	226	NM_000034
CAD	790	NM_004341
CHPT1	56994	NM_020244
DHCR24	1718	NM_014762
DHCR7	1717	NM_001360
DLD	1738	NM_000108
EPAS1	2034	NM_001430
FDFT1	2222	NM_004462
G6PD	2539	NM_000402
GALK1	2584	NM_000154
GALK2	2585	NM_002044
GALT	2592	NM_000155
GAPDHS	26330	NM_014364
GPI	2821	NM_000175
GPX3	2878	NM_002084
GPX4	2879	NM_002085
GPX7	2882	NM_015696
H6PD	9563	NM_004285
HK2	3099	NM_000189
HMGCS2	3158	NM_005518
IDH2	3418	NM_002168
IRS1	3667	NC_000002.11
LDHAL6B	92483	NM_033195
LOC441996	441996	XM_929617
ME1	4199	NC_000006.11
ME2	4200	NC_000018.9
MLYCD	23417	NC_000016.9
MT-ND3	4537	NC_001807_10060
MT-ND6	4541	NC_001807_14150
MVD	4597	NM_002461
MYC	4609	NM_002467.4
ODC1	4953	NM_002539
OGDH	4967	NM_002541
OXCT2	64064	NM_022120
PCYT1B	9468	NM_004845
PDK2	5164	NM_001199898.1
PFKFB1	5207	NM_002625
PFKM	5213	NM_000289
PFKP	5214	NM_002627
PGAM4	441531	NM_001029891
PGD	5226	NM_002631.2
PGM1	5236	NM_002633
PIK3CA	5290	NM_006218.2
PKM2	5315	NM_002654
PLD2	5338	NM_002663
PMVK	10654	NM_006556
PPAP2A	8611	NM_003711
PPAP2B	8613	NM_003713
PPAP2C	8612	NM_003712
PRKAB1	5564	NM_006253
PRKAB2	5565	NM_005399
PRKAG3	53632	NM_017431
RPIA	22934	NM_144563
SCD	6319	NM_005063
SCO2	9997	NM_005138
SDHD	6392	NM_003002
SLC16A3	9123	NM_001042423
SLC16A8	23539	NM_013356
SLC1A5	6510	NM_005628
SLC25A10	1468	NM_001270888.1
SOD1	6647	NM_000454
SUCLG2	8801	NM_003848
TKTL1	8277	NM_012253
UMPS	7372	NM_000373

Table 4-1 Overview of candidate genes

(A) Overview of the 72 candidate genes with a Z-score$_{(MAD)}$ of less than -1.7 in more than one cell line/condition. Indicated in red are the genes taken forward for deconvolution.

Figure 4.14

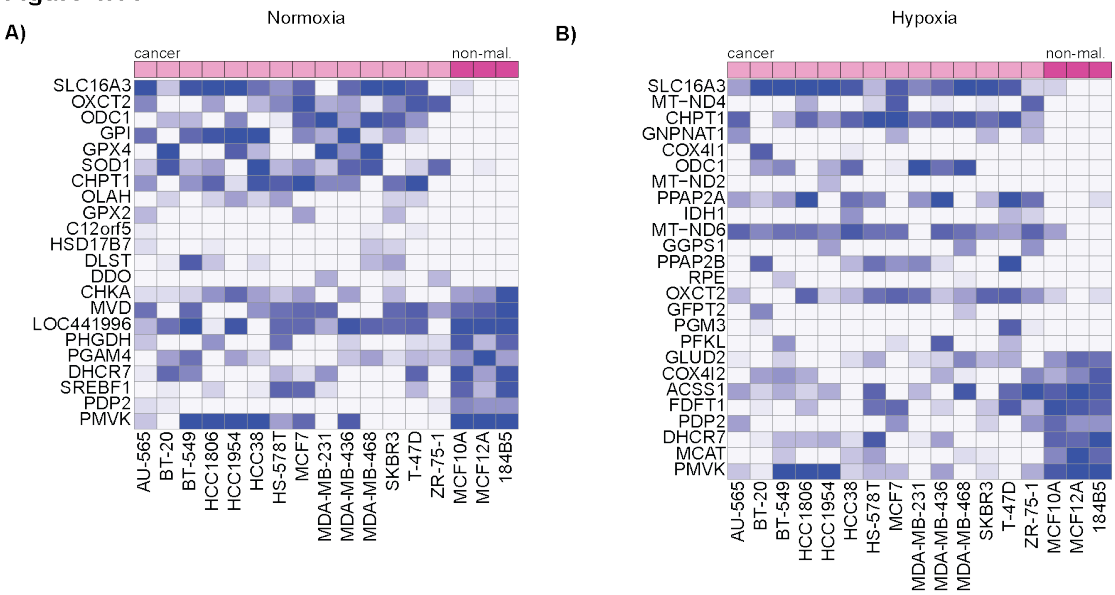

Figure 4-14 Supervised clustering analysis according to malignancy

Supervised cluster analysis of Z-scores according to the malignancy status and differential effects between non-malignant (non-mal.) and cancer cells under (A) normoxia and (B) hypoxia were identified using the Mann-Whitney-U test. Statistically significant effects of siRNAs targeting specific genes are displayed ($p \leq 0.05$).

Figure 4.15

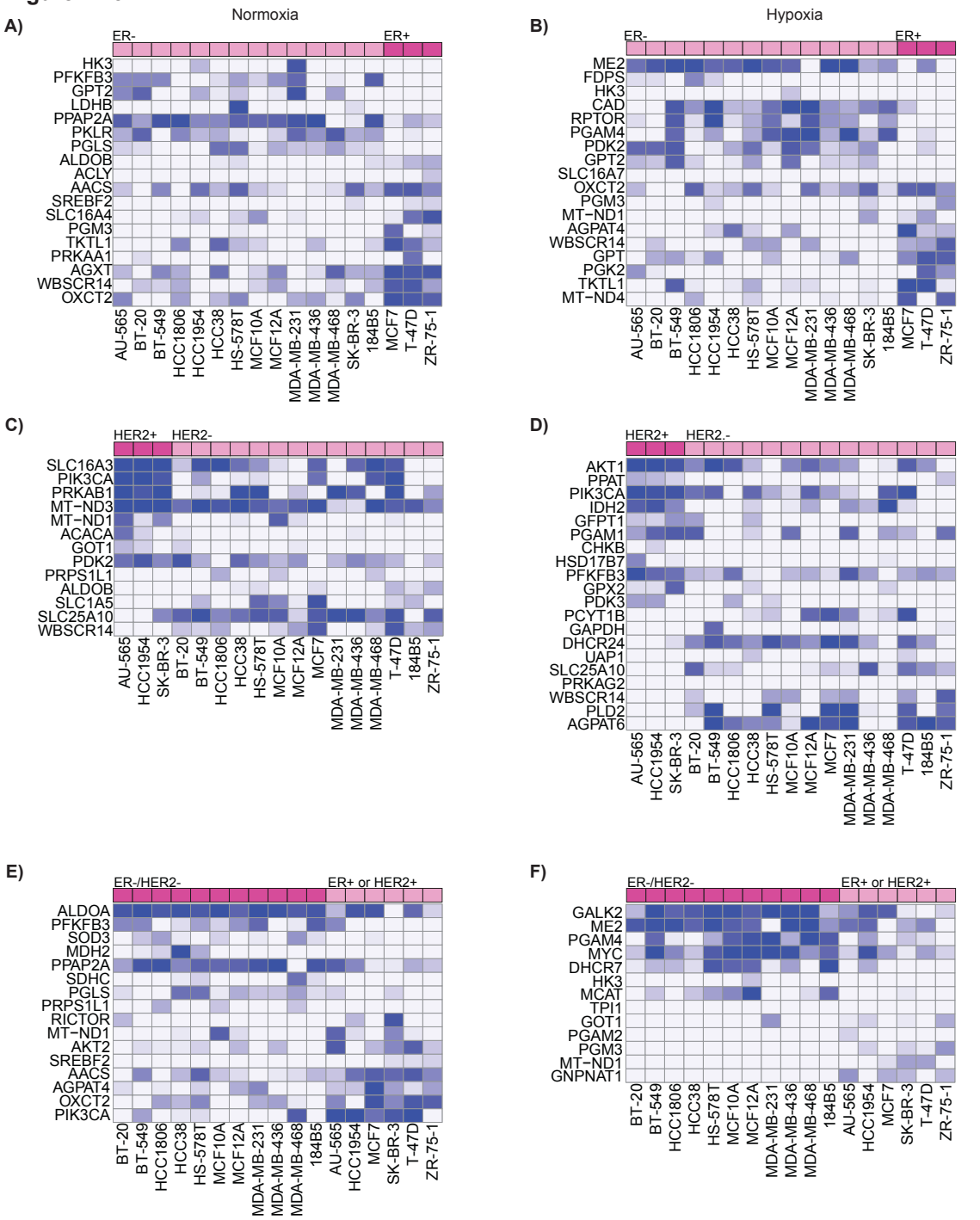
A)
Normoxia
ER-
ER+
HK3
PFKFB3
GPT2
LDHB
PPAP2A
PKLR
PGLS
ALDOB
ACLY
AACS
SREBF2
SLC16A4
PGM3
TKTL1
PRKAA1
AGXT
WBSCR14
OXCT2
AU-565
BT-20
BT-549
HCC1806
HCC1954
HCC38
HS-578T
MCF10A
MCF12A
MDA-MB-231
MDA-MB-436
MDA-MB-468
SK-BR-3
184B5
MCF7
T-47D
ZR-75-1
B)
Hypoxia
ER-
ER+
ME2
FDPS
HK3
CAD
RPTOR
PGAM4
PDK2
GPT2
SLC16A7
OXCT2
PGM3
MT−ND1
AGPAT4
WBSCR14
GPT
PGK2
TKTL1
MT−ND4
AU-565
BT-20
BT-549
HCC1806
HCC1954
HCC38
HS-578T
MCF10A
MCF12A
MDA-MB-231
MDA-MB-436
MDA-MB-468
SK-BR-3
184B5
MCF7
T-47D
ZR-75-1
C)
HER2+
HER2-
SLC16A3
PIK3CA
PRKAB1
MT−ND3
MT−ND1
ACACA
GOT1
PDK2
PRPS1L1
ALDOB
SLC1A5
SLC25A10
WBSCR14
AU-565
HCC1954
SK-BR-3
BT-20
BT-549
HCC1806
HCC38
HS-578T
MCF10A
MCF12A
MCF7
MDA-MB-231
MDA-MB-436
MDA-MB-468
T-47D
184B5
ZR-75-1
D)
HER2+
HER2.-
AKT1
PPAT
PIK3CA
IDH2
GFPT1
PGAM1
CHKB
HSD17B7
PFKFB3
GPX2
PDK3
PCYT1B
GAPDH
DHCR24
UAP1
SLC25A10
PRKAG2
WBSCR14
PLD2
AGPAT6
AU-565
HCC1954
SK-BR-3
BT-20
BT-549
HCC1806
HCC38
HS-578T
MCF10A
MCF12A
MCF7
MDA-MB-231
MDA-MB-436
MDA-MB-468
T-47D
184B5
ZR-75-1
E)
ER-/HER2-
ER+ or HER2+
ALDOA
PFKFB3
SOD3
MDH2
PPAP2A
SDHC
PGLS
PRPS1L1
RICTOR
MT−ND1
AKT2
SREBF2
AACS
AGPAT4
OXCT2
PIK3CA
BT-20
BT-549
HCC1806
HCC38
HS-578T
MCF10A
MCF12A
MDA-MB-231
MDA-MB-436
MDA-MB-468
184B5
AU-565
HCC1954
MCF7
SK-BR-3
T-47D
ZR-75-1
F)
ER-/HER2-
ER+ or HER2+
GALK2
ME2
PGAM4
MYC
DHCR7
HK3
MCAT
TPI1
GOT1
PGAM2
PGM3
MT−ND1
GNPNAT1
BT-20
BT-549
HCC1806
HCC38
HS-578T
MCF10A
MCF12A
MDA-MB-231
MDA-MB-436
MDA-MB-468
184B5
AU-565
HCC1954
MCF7
SK-BR-3
T-47D
ZR-75-1

Figure 4-15 Supervised clustering analysis according to clinical classification

(A, B) Supervised cluster analysis of Z-scores according to the ER status and differential effects between ER-positive and ER-negative breast epithelial cells under (A) normoxia and (B) hypoxia were identified using the Mann-Whitney-U test. Statistically significant effects of siRNAs targeting specific genes are displayed ($p \leq 0.05$). (C, D) Supervised cluster analysis of Z-scores according to the HER2 status and differential effects between HER2-positive and HER2-negative breast epithelial cells under (C) normoxia and (D) hypoxia were identified using the Mann-Whitney-U test. Statistically significant effects of siRNAs targeting specific genes are displayed ($p \leq 0.05$). (E, F) Supervised cluster analysis of Z-scores according to the ER and HER2 status and differential effects between ER-positive or HER2-positive and ER-negative/HER2-negative breast epithelial cells under (E) normoxia and (F) hypoxia were identified using the Mann-Whitney-U test. Statistically significant effects of siRNAs targeting specific genes are displayed ($p \leq 0.05$).

Figure 4.16

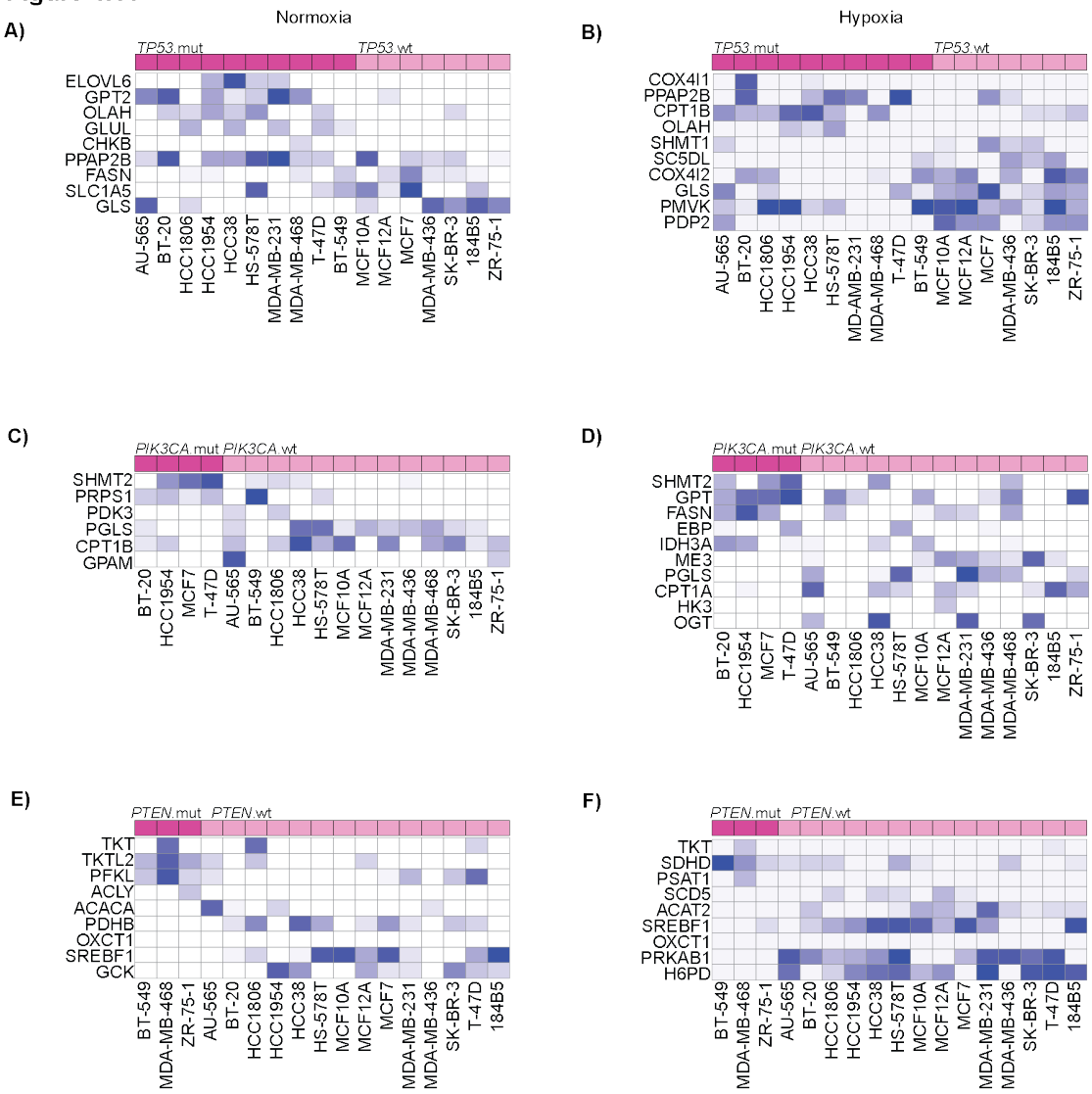

Figure 4-16 Supervised clustering analysis according to genetic aberrations

(A, B) Supervised cluster analysis of Z-scores according to the *TP53* status and differential effects between *TP53* mutant (mut) and *TP53* wildtype (wt) breast epithelial cells under (A) normoxia and (B) hypoxia were identified using the Mann-Whitney-U test. Statistically significant effects of siRNAs targeting specific genes are displayed ($p \leq 0.05$). (C, D) Supervised cluster analysis of Z-scores according to the *PIK3CA* status and differential effects between *PIK3CA* mutant (mut) and *PIK3CA* wildtype (wt) breast epithelial cells under (C) normoxia and (D) hypoxia were identified using the Mann-Whitney-U test. Statistically significant effects of siRNAs targeting specific genes are displayed ($p \leq 0.05$). (E, F) Supervised cluster analysis of Z-scores according to the *PTEN* status and differential effects between *PTEN* mutant (mut) and *PTEN* breast epithelial cells under (E) normoxia and (F) hypoxia were identified using the Mann-Whitney-U test. Statistically significant effects of siRNAs targeting specific genes are displayed ($p \leq 0.05$).

Figure 4.17

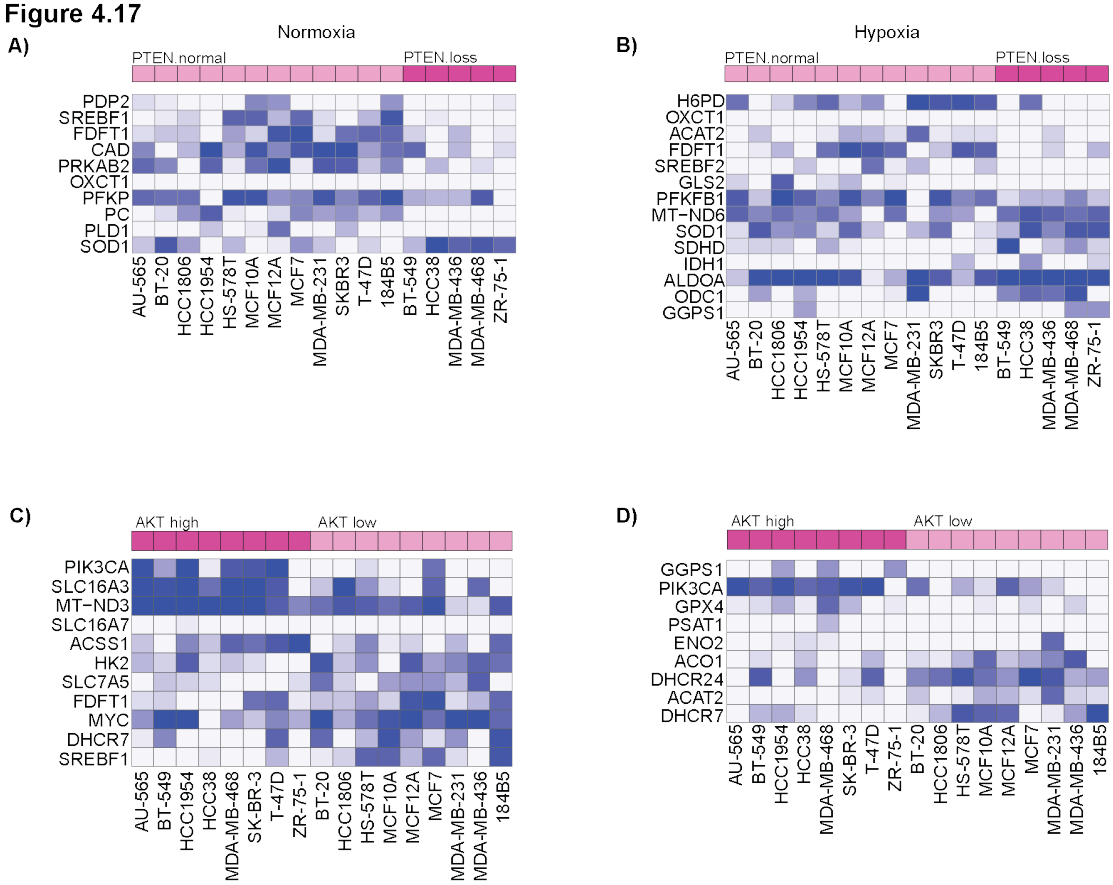

Figure 4-17 Supervised clustering analysis according to signalling

(A, B) Supervised cluster analysis of Z-scores according to the PTEN expression status and differential effects between normal PTEN and lost PTEN expression in the breast epithelial cells under (A) normoxia and (B) hypoxia were identified using the Mann-Whitney-U test. Statistically significant effects of siRNAs targeting specific genes are displayed ($p \leq 0.05$). (C, D) Supervised cluster analysis of Z-scores according to the AKT activity status and differential effects between high vs low AKT activity of all breast epithelial cells under (C) normoxia and (D) hypoxia were identified using the Mann-Whitney-U test. Statistically significant effects of siRNAs targeting specific genes are displayed ($p \leq 0.05$).

Figure 4.18

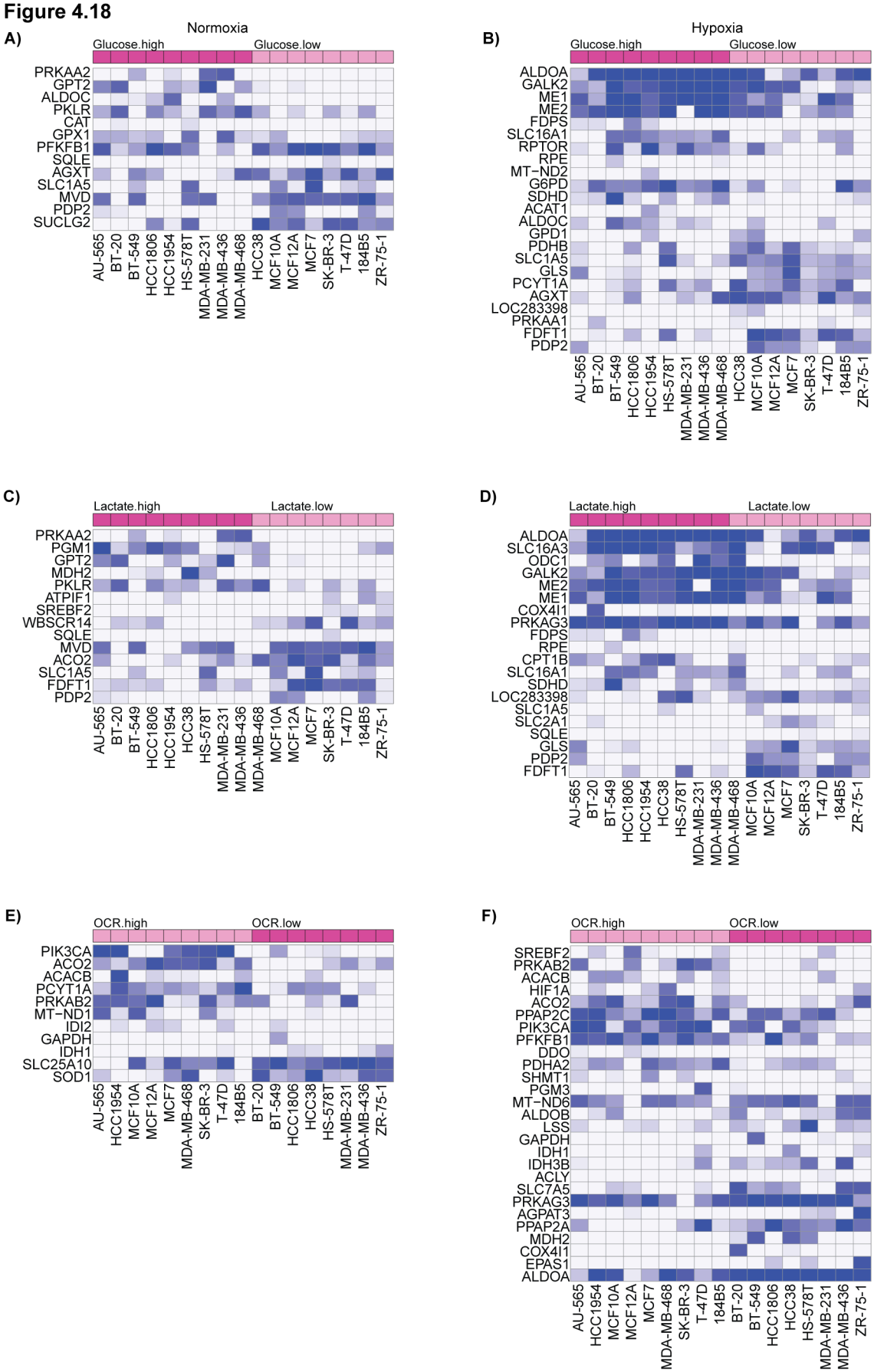
A)
Normoxia
Glucose.high
Glucose.low
PRKAA2
GPT2
ALDOC
PKLR
CAT
GPX1
PFKFB1
SQLE
AGXT
SLC1A5
MVD
PDP2
SUCLG2
AU-565
BT-20
BT-549
HCC1806
HCC1954
HS-578T
MDA-MB-231
MDA-MB-436
MDA-MB-468
HCC38
MCF10A
MCF12A
MCF7
SK-BR-3
T-47D
184B5
ZR-75-1
B)
Hypoxia
Glucose.high
Glucose.low
ALDOA
GALK2
ME1
ME2
FDPS
SLC16A1
RPTOR
RPE
MT−ND2
G6PD
SDHD
ACAT1
ALDOC
GPD1
PDHB
SLC1A5
GLS
PCYT1A
AGXT
LOC283398
PRKAA1
FDFT1
PDP2
C)
Lactate.high
Lactate.low
PRKAA2
PGM1
GPT2
MDH2
PKLR
ATPIF1
SREBF2
WBSCR14
SQLE
MVD
ACO2
SLC1A5
FDFT1
PDP2
D)
Lactate.high
Lactate.low
ALDOA
SLC16A3
ODC1
GALK2
ME2
ME1
COX4I1
PRKAG3
FDPS
RPE
CPT1B
SLC16A1
SDHD
LOC283398
SLC1A5
SLC2A1
SQLE
GLS
PDP2
FDFT1
E)
OCR.high
OCR.low
PIK3CA
ACO2
ACACB
PCYT1A
PRKAB2
MT−ND1
IDI2
GAPDH
IDH1
SLC25A10
SOD1
F)
OCR.high
OCR.low
SREBF2
PRKAB2
ACACB
HIF1A
ACO2
PPAP2C
PIK3CA
PFKFB1
DDO
PDHA2
SHMT1
PGM3
MT−ND6
ALDOB
LSS
GAPDH
IDH1
IDH3B
ACLY
SLC7A5
PRKAG3
AGPAT3
PPAP2A
MDH2
COX4I1
EPAS1
ALDOA

Figure 4-18 Supervised clustering analysis according to metabolic phenotypes

(A, B) Supervised cluster analysis of Z-scores according to the glucose consumption status and differential effects between high vs low glucose consuming breast epithelial cells under (A) normoxia and (B) hypoxia were identified using the Mann-Whitney-U test. Statistically significant effects of siRNAs targeting specific genes are displayed ($p \leq 0.05$). (C, D) Supervised cluster analysis of Z-scores according to the lactate secretion status and differential effects between high vs low lactate secreting breast epithelial cells under (C) normoxia and (D) hypoxia were identified using the Mann-Whitney-U test. Statistically significant effects of siRNAs targeting specific genes are displayed ($p \leq 0.05$). (E, F) Supervised cluster analysis of Z-scores according to the oxygen consumption and differential effects between high vs low oxygen consuming breast epithelial cells under (E) normoxia and (F) hypoxia were identified using the Mann-Whitney-U test. Statistically significant effects of siRNAs targeting specific genes are displayed ($p \leq 0.05$).

Figure 4.19

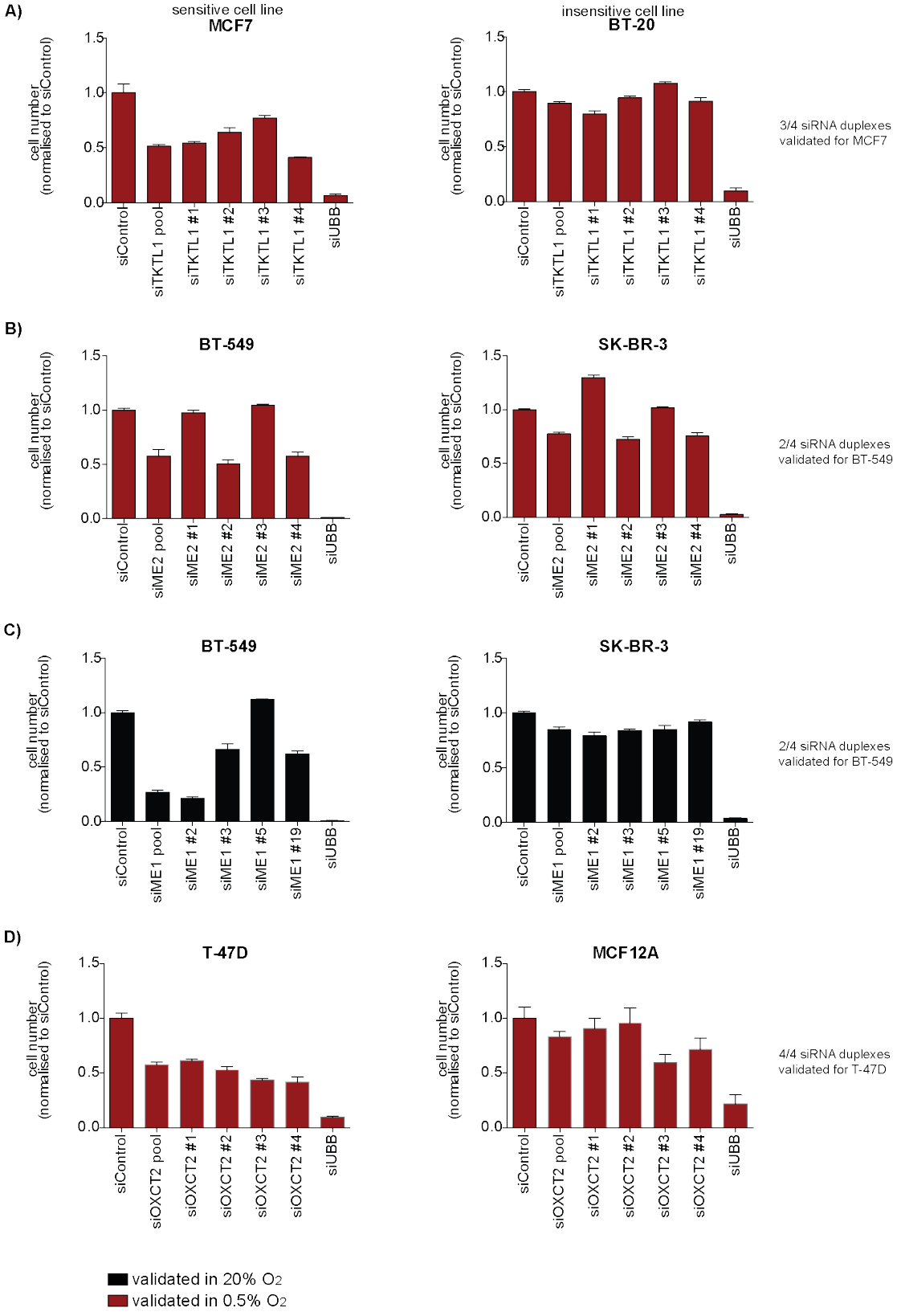
A)
sensitive cell line
MCF7
insensitive cell line
BT-20
cell number (normalised to siControl)
1.5
1.0
0.5
0.0
siControl
siTKTL1 pool
siTKTL1 #1
siTKTL1 #2
siTKTL1 #3
siTKTL1 #4
siUBB
3/4 siRNA duplexes validated for MCF7
B)
BT-549
SK-BR-3
siME2 pool
siME2 #1
siME2 #2
siME2 #3
siME2 #4
2/4 siRNA duplexes validated for BT-549
C)
BT-549
SK-BR-3
siME1 pool
siME1 #2
siME1 #3
siME1 #5
siME1 #19
2/4 siRNA duplexes validated for BT-549
D)
T-47D
MCF12A
siOXCT2 pool
siOXCT2 #1
siOXCT2 #2
siOXCT2 #3
siOXCT2 #4
4/4 siRNA duplexes validated for T-47D
validated in 20% O2
validated in 0.5% O2

Figure 4.19

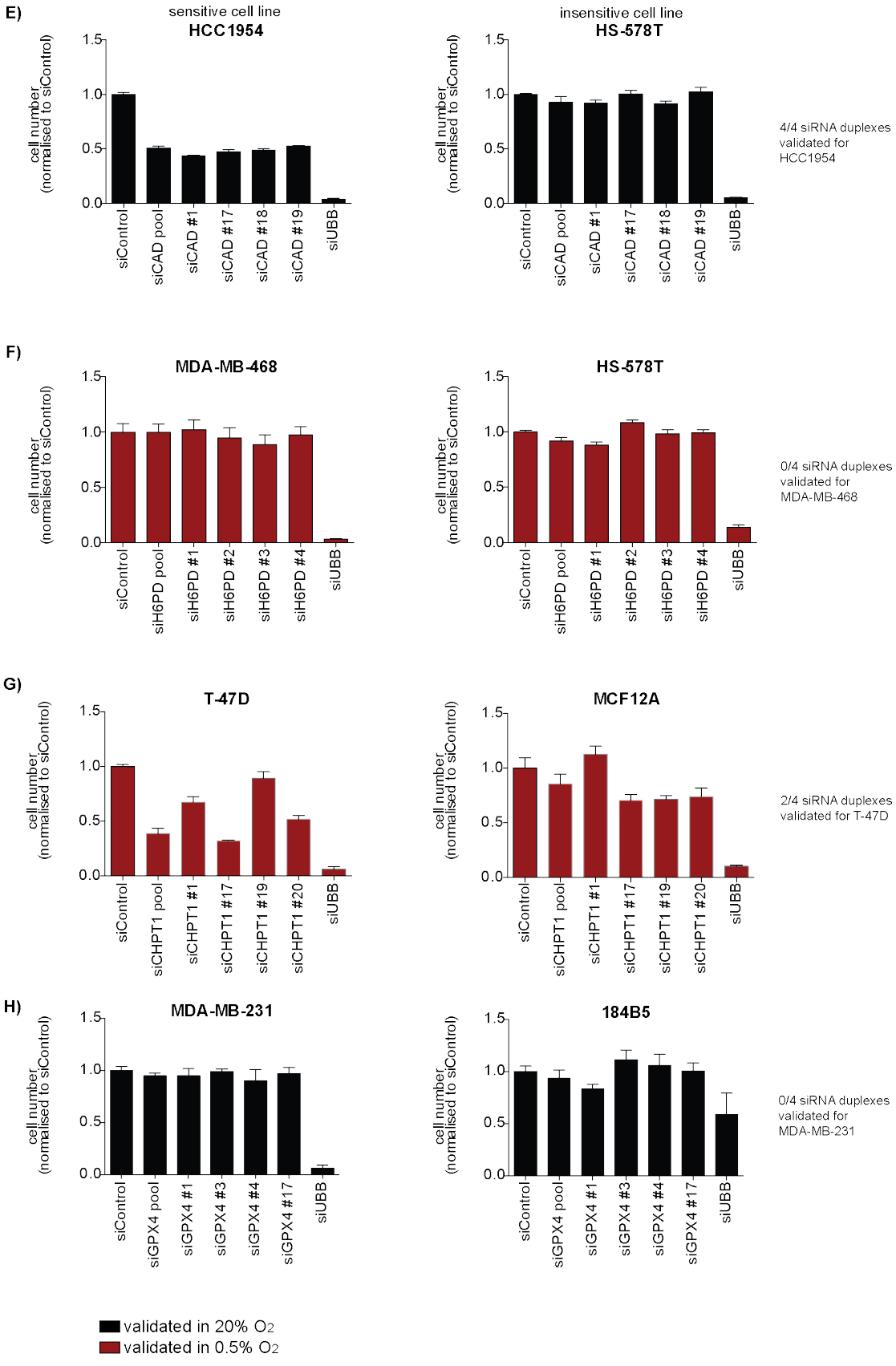
E)
sensitive cell line
HCC1954
insensitive cell line
HS-578T
cell number (normalised to siControl)
1.5
1.0
0.5
0.0
siControl
siCAD pool
siCAD #1
siCAD #17
siCAD #18
siCAD #19
siUBB
4/4 siRNA duplexes validated for HCC1954
F)
MDA-MB-468
HS-578T
siH6PD pool
siH6PD #1
siH6PD #2
siH6PD #3
siH6PD #4
0/4 siRNA duplexes validated for MDA-MB-468
G)
T-47D
MCF12A
siCHPT1 pool
siCHPT1 #1
siCHPT1 #17
siCHPT1 #19
siCHPT1 #20
2/4 siRNA duplexes validated for T-47D
H)
MDA-MB-231
184B5
siGPX4 pool
siGPX4 #1
siGPX4 #3
siGPX4 #4
siGPX4 #17
0/4 siRNA duplexes validated for MDA-MB-231
validated in 20% O2
validated in 0.5% O2

Figure 4.19

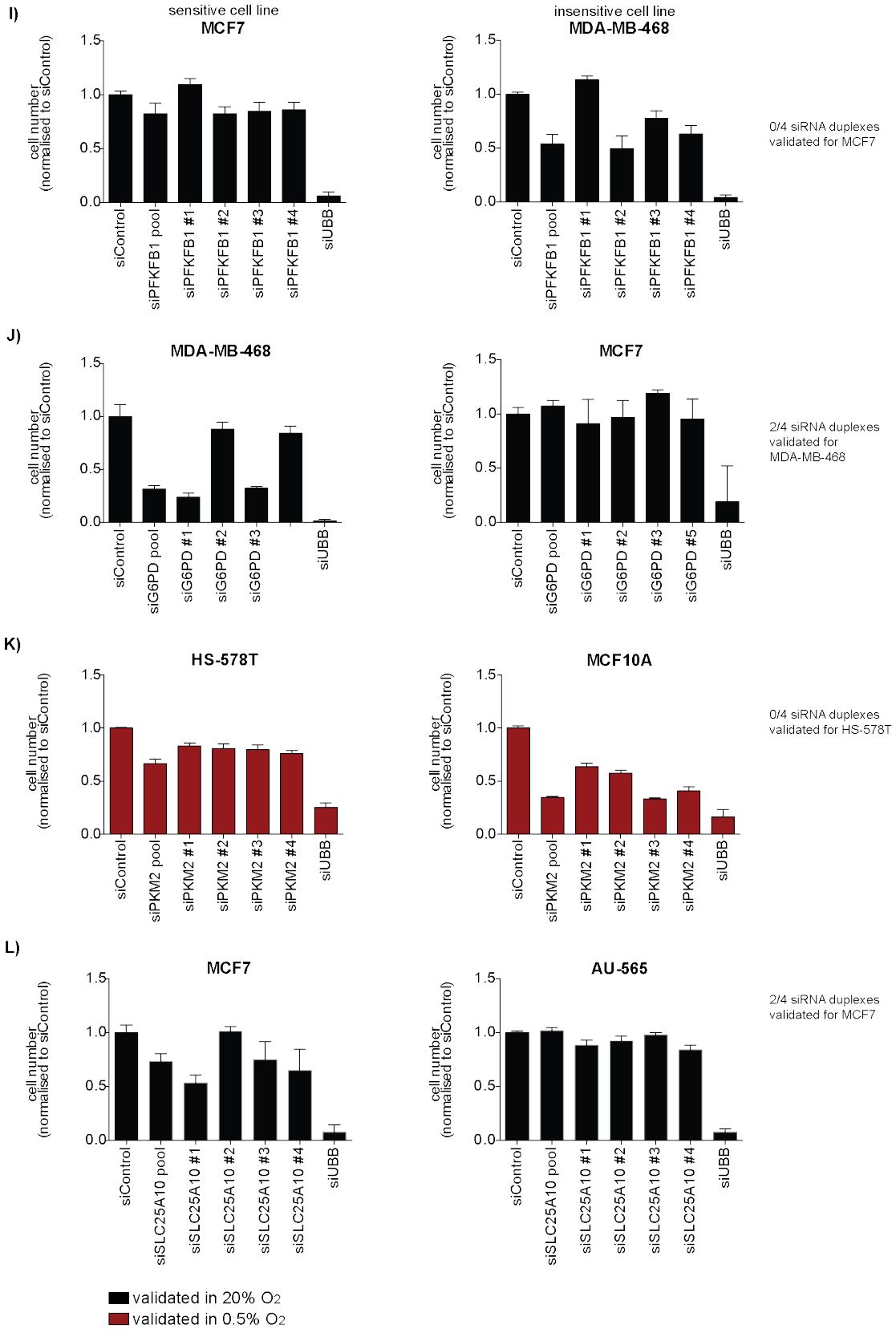
I)
sensitive cell line
MCF7
insensitive cell line
MDA-MB-468
cell number (normalised to siControl)
1.5
1.0
0.5
0.0
siControl
siPFKFB1 pool
siPFKFB1 #1
siPFKFB1 #2
siPFKFB1 #3
siPFKFB1 #4
siUBB
0/4 siRNA duplexes validated for MCF7
J)
MDA-MB-468
MCF7
siG6PD pool
siG6PD #1
siG6PD #2
siG6PD #3
siG6PD #5
2/4 siRNA duplexes validated for MDA-MB-468
K)
HS-578T
MCF10A
siPKM2 pool
siPKM2 #1
siPKM2 #2
siPKM2 #3
siPKM2 #4
0/4 siRNA duplexes validated for HS-578T
L)
MCF7
AU-565
siSLC25A10 pool
siSLC25A10 #1
siSLC25A10 #2
siSLC25A10 #3
siSLC25A10 #4
2/4 siRNA duplexes validated for MCF7
validated in 20% O2
validated in 0.5% O2

Figure 4.19

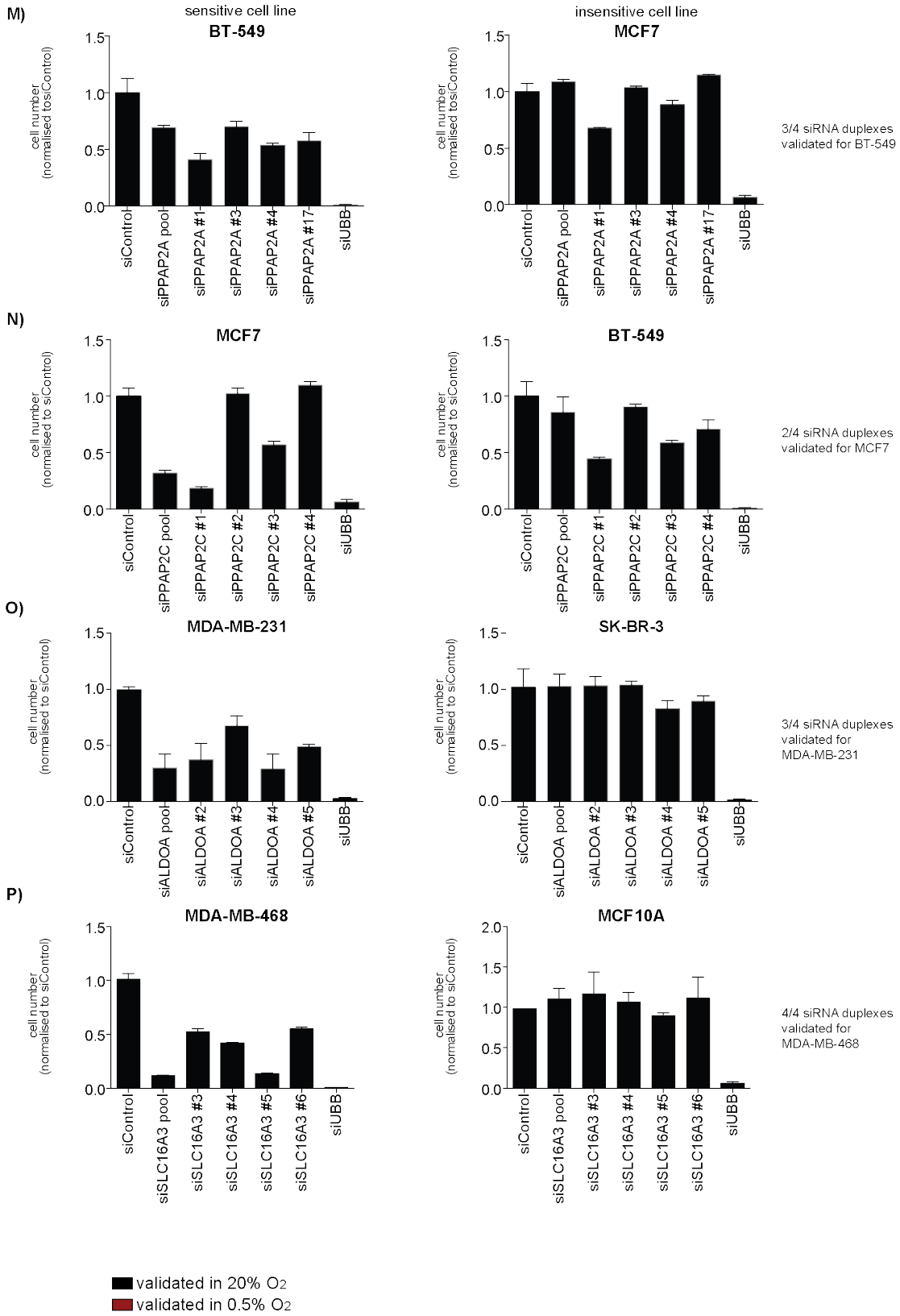
M)
sensitive cell line
BT-549
insensitive cell line
MCF7
cell number (normalised tosiControl)
siControl
siPPAP2A pool
siPPAP2A #1
siPPAP2A #3
siPPAP2A #4
siPPAP2A #17
siUBB
3/4 siRNA duplexes validated for BT-549
N)
MCF7
BT-549
cell number (normalised to siControl)
siPPAP2C pool
siPPAP2C #1
siPPAP2C #2
siPPAP2C #3
siPPAP2C #4
2/4 siRNA duplexes validated for MCF7
O)
MDA-MB-231
SK-BR-3
siALDOA pool
siALDOA #2
siALDOA #3
siALDOA #4
siALDOA #5
3/4 siRNA duplexes validated for MDA-MB-231
P)
MDA-MB-468
MCF10A
siSLC16A3 pool
siSLC16A3 #3
siSLC16A3 #4
siSLC16A3 #5
siSLC16A3 #6
4/4 siRNA duplexes validated for MDA-MB-468
validated in 20% O2
validated in 0.5% O2

Figure 4-19 Deconvolution of candidate genes on cell number

Bar graphs of pooled and individual siRNAs targeting a specific genes and its effect on cell number in a sensitive (left) and insensitive breast cell line (right). Data was normalised to siControl and siUBB was used as a positive control to determine transfection efficiency. Black bars indicate deconvolution under normoxia while red bars indicate deconvolution under hypoxia. Following siRNAs were used for deconvolution: (A) TKTL1, (B) ME2, (C) ME1, (D) OXCT2, (E) CAD, (F) H6PD, (G) CHPT1, (H) GPX4, (I) PFKFB1, (J) G6PD, (K) PKM2, (L) SLC25A10, (M) PPAP2A, (N) PPAP2C, (O) ALDOA, (P) SLC16A3.

Figure 4.20

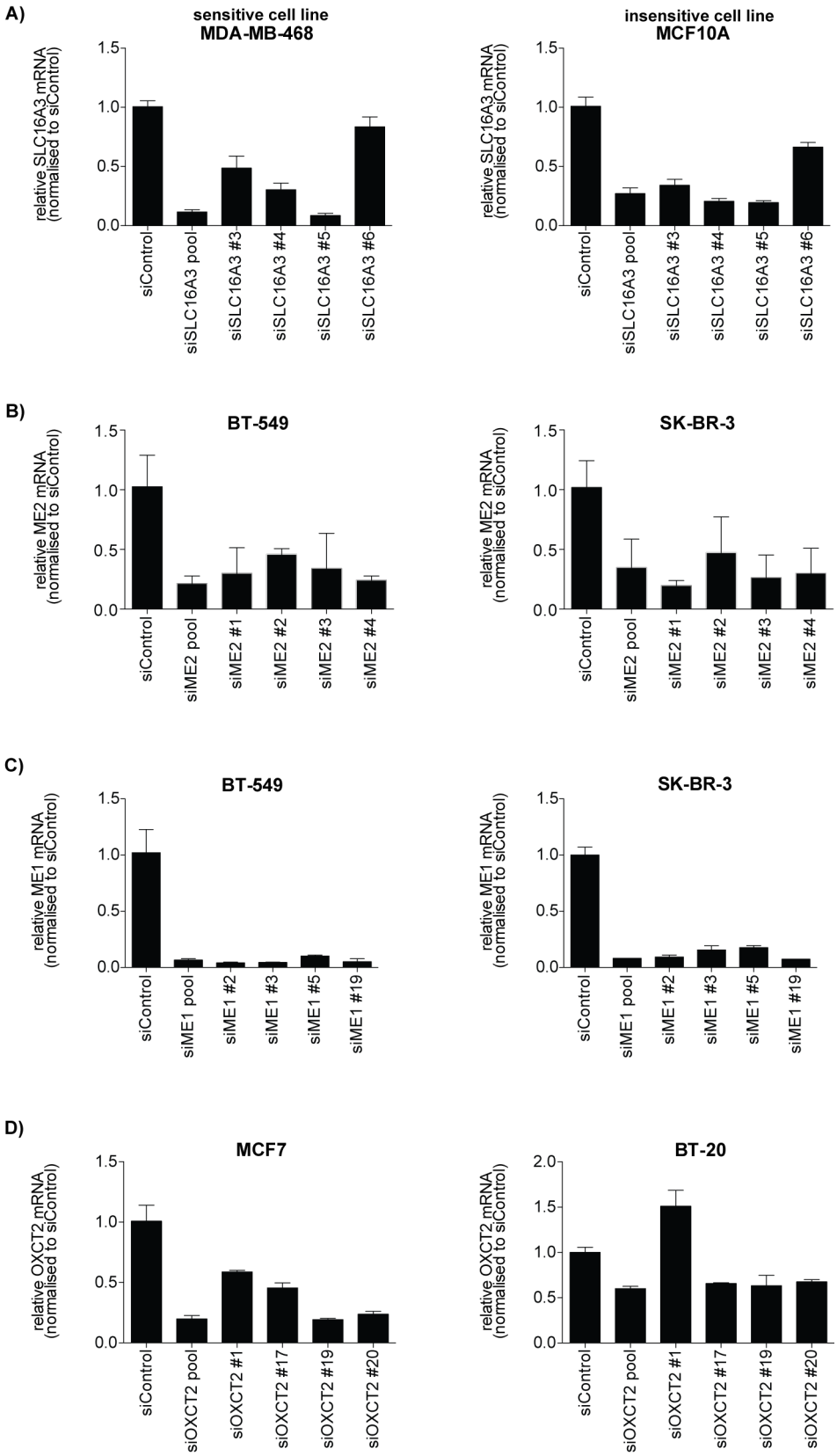
A)
sensitive cell line
MDA-MB-468
insensitive cell line
MCF10A
relative SLC16A3 mRNA (normalised to siControl)
siControl
siSLC16A3 pool
siSLC16A3 #3
siSLC16A3 #4
siSLC16A3 #5
siSLC16A3 #6
B)
BT-549
SK-BR-3
relative ME2 mRNA (normalised to siControl)
siControl
siME2 pool
siME2 #1
siME2 #2
siME2 #3
siME2 #4
C)
BT-549
SK-BR-3
relative ME1 mRNA (normalised to siControl)
siControl
siME1 pool
siME1 #2
siME1 #3
siME1 #5
siME1 #19
D)
MCF7
BT-20
relative OXCT2 mRNA (normalised to siControl)
siControl
siOXCT2 pool
siOXCT2 #1
siOXCT2 #17
siOXCT2 #19
siOXCT2 #20

Figure 4.20

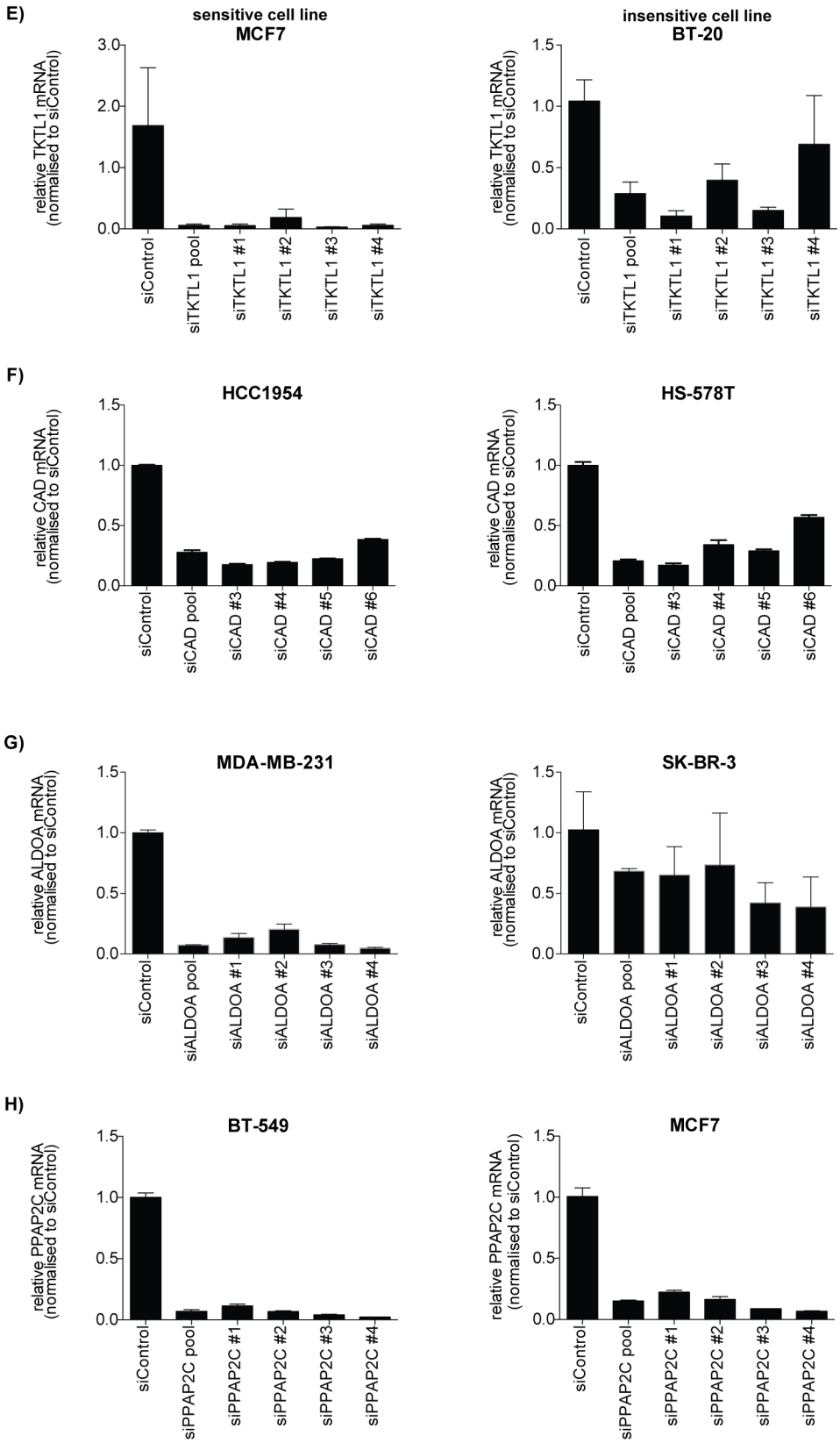
E)
sensitive cell line
MCF7
insensitive cell line
BT-20
relative TKTL1 mRNA (normalised to siControl)
siControl
siTKTL1 pool
siTKTL1 #1
siTKTL1 #2
siTKTL1 #3
siTKTL1 #4
F)
HCC1954
HS-578T
relative CAD mRNA (normalised to siControl)
siCAD pool
siCAD #3
siCAD #4
siCAD #5
siCAD #6
G)
MDA-MB-231
SK-BR-3
relative ALDOA mRNA (normalised to siControl)
siALDOA pool
siALDOA #1
siALDOA #2
siALDOA #3
siALDOA #4
H)
BT-549
MCF7
relative PPAP2C mRNA (normalised to siControl)
siPPAP2C pool
siPPAP2C #1
siPPAP2C #2
siPPAP2C #3
siPPAP2C #4

Figure 4.20

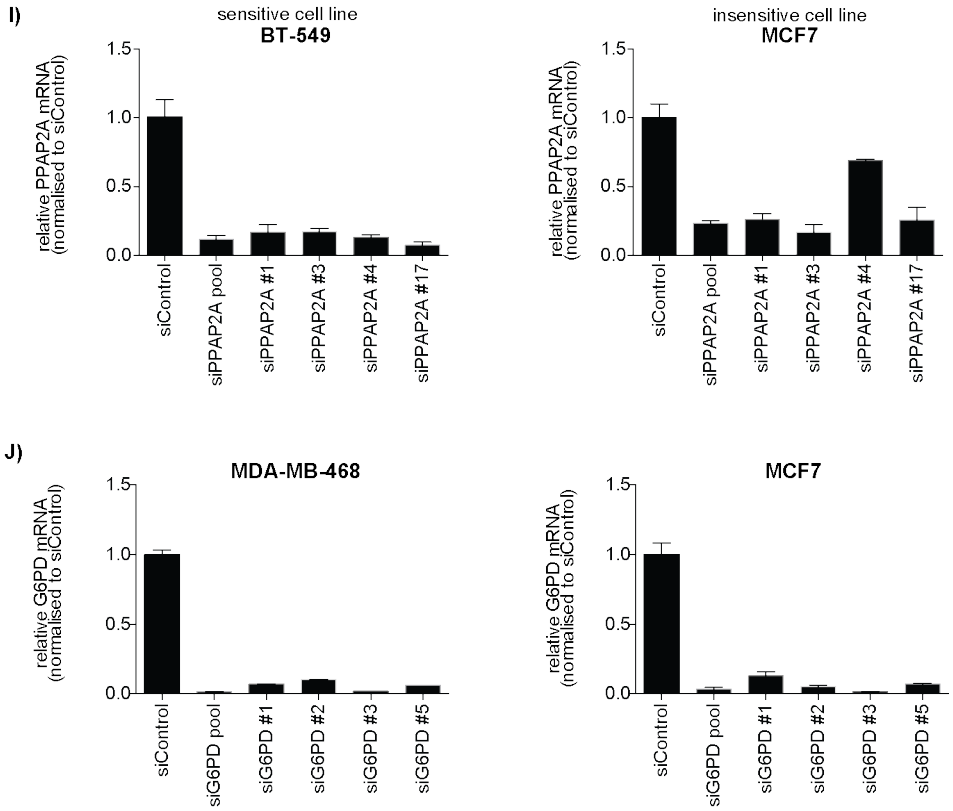

Figure 4-20 Deconvolution on RNA level

Bar graphs of pooled and individual siRNAs targeting a specific gene and their effect on mRNA levels in a sensitive (left) and insensitive breast cell line (right). Data was normalised to siControl. Following siRNAs were used for deconvolution: (A) SLC16A3, (B) ME2, (C) ME1, (D) OXCT2, (E) TKTL1, (F) CAD, (G) ALDOA, (H) PPAP2C, (I) PPAP2A, (J) G6PD.

5 Monocarboxylate transporter 4 is essential for the survival of ER-negative breast cancer

5.1 SLC16A gene family

Cancer cell metabolism is not only influenced by metabolite concentrations and metabolic signalling processes within the cell, but also by the microenvironment. Cells exchange signals as well as metabolites with their surroundings to increase proliferation and to promote survival. To exchange metabolites, cells have different transporters that transport nutrients (such as amino acids and sugars), remove metabolic end products, and exchange ions and protons (Ganapathy et al., 2009).

This chapter focuses on the role and function of the human monocarboxylate transporters (MCTs). The name MCT derives from their role in carrying molecules with one carboxylate group ($R\text{-}COO^-$) across membranes. Lactate, pyruvate, ketone bodies such as acetoacetate and hydroxybutyrate as well as specific amino acids (e.g. aspartate) are known substrates of different MCTs (Halestrap and Meredith, 2004). This family is encoded by the solute carrier 16 gene family (*SLC16*) and is very well conserved. All MCTs are predicted to be 12 trans-membrane proteins. Currently fourteen different members are known in mammals (Halestrap and Meredith, 2004; Kennedy and Dewhirst, 2010). Only four members of the MCT family, MCT1 (SLC16A1), MCT2 (SLC16A8), MCT3 (SLC16A4) and MCT4 (SLC16A3), facilitate the proton-linked symport of monocarboxylates (Halestrap and Price, 1999). The direction of the flux is dependent on the concentration gradient of monocarboxylates and protons across the membranes. Each MCT1-4 has specific substrates and is affected by different inhibitors. Moreover, MCTs show different expression levels across different tissues. These can be partially explained by their regulators and co-chaperones, while other regulating mechanisms still need to be discovered. MCT1 is constitutively expressed in almost all tissues (Garcia et al., 1995) and its main role is to transport lactic acid across the plasma membrane (Dimmer et al., 2000). The gene *SLC16A1* codes for MCT1 and has been suggested to be a direct transcriptional target of c-Myc (Kang et al., 2009). The promoter of *SLC16A1* contains many CpG islands that are necessary for epigenetic regulation through methylation. The methylation of CpG islands might prevent certain

transcription factors to bind to the DNA and could thereby suppress the expression of MCT1 in certain tissues or under certain metabolic situations (Cross and Bird, 1995). MCT1 has been shown to be overexpressed in many cancers (Pinheiro et al., 2010a; Pinheiro et al., 2012). It has been demonstrated that MCT1 expression correlates with the glycolytic phenotype observed in cancer cells (Birsoy et al., 2012b).

MCT4 is strongly expressed in glycolytic tissue such as the heart and skeletal muscle (Bonen, 2001; Juel and Halestrap, 1999). MCT4 is important for lactate export in these tissues as it displays lower affinity to lactate compared to MCT1 (Dimmer et al., 2000). MCT1 and MCT4 have also been suggested to be part of the coupled metabolism between cancer cells (Sonveaux et al., 2008). Other studies have followed demonstrating that lactate can be used as an alternative carbon source for cancer cells to allow them to proliferate when glucose is scarce (Brooks, 2009; Feron, 2009; Whitaker-Menezes et al., 2011). The regulation of *SLC16A3* is HIF1α dependent and two hypoxic response elements (HRE) were found in its promotor (Ullah et al., 2006). Pouyssegur and colleagues have demonstrated that both MCT1 and MCT4 are more important for pH regulation and tumour growth (Chiche et al., 2010a).
There are numerous studies suggesting a role for MCT1 and MCT4 in cancer. However, conflicting results regarding the transport of lactate or pyruvate by these two MCTs have been reported (Bonen, 2001; Dimmer et al., 2000; Garcia et al., 1994; Gerlinger et al., 2012; Koukourakis et al., 2006; Sonveaux et al., 2008; Vegran et al., 2011). It has also been proposed that MCT4 is not important for cancer cells under normoxic conditions as pyruvate is used as a substrate for mitochondrial respiration (Halestrap and Wilson, 2012).

MCT1 and MCT4 function in association with the ancillary protein basigin (BSG), a member of the immunoglobulin superfamily (Biswas et al., 1995). BSG is necessary for trafficking of MCT1 and MCT4 to the plasma membrane and its expression on the plasma membrane (Kennedy and Dewhirst, 2010; Kirk et al., 2000; Pinheiro et al., 2010b). BSG is also implied to be important for tumorigenesis (Davidson et al., 2003; Marionnet et al., 2003; Riethdorf et al., 2006) and its depletion has been shown to reduce tumour growth (Le Floch et al., 2011; Schneiderhan et al., 2009).

5.2 Ablation of *SLC16A3* results in loss of cell viability

The results of the siRNA screen, showed that depletion of *SLC16A3* caused differential loss of cell viability under the following criteria: Cell lines with amplified HER2 and ER-negative/HER2-negative cell lines are more sensitive towards *SLC16A3* ablation under both oxygen conditions. Furthermore, most cancer cell lines were highly sensitive to the abrogation of *SLC16A3* compared to the non-malignant cell lines (Fig 5.1A).

To confirm the screen results, four breast epithelial cell lines were taken forward for validation and deconvolution studies. The non-malignant cell line MCF10A and the ER-negative/HER2-negative cell line MDA-MB-231 were both resistant to siRNA-mediated abrogation of *SLC16A3* (Fig 5.1B,C). In contrast, silencing of SLC16A3 in MDA-MB-468 and HCC1954 cells induced substantial loss of cell number. These effects were also observed under hypoxic conditions (Fig 5.1D,E). The deconvolution of SLC16A3 siRNA sequences revealed the strongest effects with siRNA duplexes #4 and #5 (see chapter 4, Fig 4.19P, Fig 4.20A).

To investigate if the reduction in cell number is caused by induction of apoptosis, cleaved caspase activity was determined. Indeed, MDA-MB-468 cells (Fig 5.2A) and HCC1954 cells (Fig 5.2B) showed significant increases in cleaved caspases 3 and 7 after depletion of SLC16A3 under normoxic conditions. Interestingly, no induction of cleaved caspases was observed in MDA-MB-468 and HCC1954 cells in hypoxia (Fig 5.2A,B). Furthermore, no increase in caspase activity was found in the non-malignant cell line MCF10A (Fig 5.2C) and the cancer cell line MDA-MB-231 (Fig 5.2D) under both oxygen conditions. This might suggest a different mechanism that results in the observed reduction in cell number.

To confirm the apoptosis in these cells under normoxic conditions, MCF10A and MDA-MB-468 cells were reversed transfected with pooled and individual siRNA targeting *SLC16A3* and whole cell lysates were analysed for the cleavage of Poly (ADP-ribose) polymerase (PARP) (Fig 5.2E). MCF10A showed no induction of PARP cleavage after depletion of *SLC16A3*. MDA-MB-468, however, showed elevated levels of cleaved PARP in the pooled siRNAs and siRNA duplexes #4 and #5. This correlated with the silencing efficiency on RNA (see chapter 4, Fig 4.20A) and protein level (Fig 5.2E).

Given that the culture medium of MCF10A cells is supplemented with growth factors and 5% horse serum compared to that of the cancer cell lines grown in 10% standard serum, it was assessed if the growth conditions of MCF10A played a protective role against SLC16A3 silencing. To test this, MCF10A cells were cultured with the medium of the cancer cell lines and the sensitive cell lines HCC1954 and MDA-MB-468 were culture under the conditions of the non-malignant cells (Fig 5.3A). Despite the reduced proliferation of the cancer cell lines under the growth conditions of non-malignant cells, a reduction in cell number was still observed (Fig 5.3A). The non-malignant cell line MCF10A showed minor growth impairment in the cancer cell medium after silencing of SLC16A3 but not to the same extent as the cancer cells.

In summary, *SLC16A3* is selectively important for the survival of ER-negative breast cancer cells *in-vitro*. The cause of reduced cell viability seems to be the induction of programmed cell death in normoxia but not in hypoxia. Moreover, it was established that the growth factor supplementation of MCF10A is not protecting the cells from undergoing cell death after silencing of *SLC16A3*.

5.3 *SLC16A3* silencing-mediated loss of viability can be rescued using a siRNA resistant SLC16A3 construct

To investigate if the reduced viability after depletion of *SLC16A3* can be rescued by re-expression of the protein, an expression construct for *SLC16A3* with a mutated sequence within the site that is complementary to the siRNA binding sites (siRNA duplexes #4 and #5) was generated. Overexpression of wild-type *SLC16A3* only slightly diminished the effect of siRNA transfection in HCC1954 and MDA-MB-468 cells. In contrast, the siRNA-resistant SLC16A3 mutant prevented the reduction in cell number after siRNA transfection (Fig 5.4A). Equal expression of wild-type and mutant SLC16A3 was confirmed by immunoblot analysis.

Taken together, loss of cell viability after depletion of *SLC16A3* can be rescued with a siRNA resistant construct.

5.4 Differential expression of *SLC16A3*/MCT4 in breast cancer cell lines

To examine a potential correlation between the observed cell death after *SLC16A3* silencing and the genetic background of the breast epithelial cell lines, RNA and protein expression was determined. In Figure 5.5, the expression levels of both mRNA and protein revealed differential expression of SLC16A3 across the panel of breast cell lines. HER2-positive cell lines expressed higher levels of *SLC16A3* on mRNA level compared to the ER-positive/HER2-negative and ER-negative/HER2-negative cell lines (Fig 5.5A). The pattern of *SLC16A3* mRNA corresponded to the MCT4 protein expression in these cell lines (Fig 5.3B). Of note, the observed phenotype after *SLC16A3* depletion did not correlate with the RNA or protein expression.

Given that HER2-positive cell lines express high levels of SLC16A3, it was assessed whether *SLC16A3* expression is regulated by HER2 signalling. Therefore, the sensitive HER2-positive cell lines HCC1954 and the ER-negative/HER2-negative cell line MDA-MB-468, that overexpresses EGFR and showed very low basal MCT4 expression (see Fig 5.5), were exposed to the HER ligands EGF and neuregulin 1β (NRG1β) or the dual inhibitor Lapatinib, that targets HER2 and EGFR. HCC1954 cells only showed minor induction of MCT4 expression after treatment with high concentrations of EGF while treatment with NRG1β had no effect (Fig 5.6A). In contrast, treatment with the inhibitor Lapatinib slightly reduced the levels of MCT4 expression (Fig 5.6A). The weak induction of MCT4 in HCC1954 cells might be due to the low affinity of HER2 for ligands and the ligand-independent activation of HER2 in these cells due to amplified *ERBB2*. MDA-MB-468 cells weak MCT4 expression showed weak basal MCT4 expression but a stronger increase in MCT4 expression after treatment with increasing amounts of EGF. However, NRG1β and Lapatinib did not affect MCT4 expression in these cells (Fig 5.6B). Of note, NRG1β stimulation of MDA-MB-468 cells might not trigger ERBB signalling given that NRG1β is not a ligand for EGFR. The different levels of inhibition of EGFR/HER2 signalling by Lapatinib in breast cancer cells lines has been established and HCC1954 cells are more sensitive towards Lapatinib compared to MDA-MB-468 cells (Konecny et al., 2006).

To further investigate HER2 signalling in SLC16A3 regulation, MCF10A cells that show the highest levels of SLC16A3 expression (see Fig 5.5) and MCF10A cells overexpressing *ERBB2* (MCF10A-*ERBB2*) were analysed for SLC16A3 expression under normoxic and hypoxic conditions (Fig 5.7). MCF10A-*ERBB2* cells were a generous gift from Dr. Eyal Gottlieb (Beatson Institute, Glasgow). MCF10A cells showed induction of *SLC16A3* mRNA after exposure to hypoxia ($p<0.0001$). However, MCF10A-*ERBB2* cells had significantly lower *SLC16A3* mRNA levels under normoxic conditions compared to MCF10A cells ($p<0.0001$). However, these cells also showed a strong induction of *SLC16A3* under hypoxia, even though the final levels were slightly lower than in MCF10A cells (Fig 5.7A). A similar result was obtained when *LDHA* expression was determined as a positive control for HIF-dependent signalling (Fig 5.7B). Similar observation was found when looked at the MCT4 expression at protein level (Fig 5.7C).

Next, it was aimed to determine whether *SLC16A3* expression is influenced when cells are cultured in matrigel for 3D growth. Acini of MCF10A cells with their characteristic hollow lumen showed distinct MCT4 expression on the cell membranes that face towards the outside of the acinar structure. However, the disorganised structures of MCF10A-ERBB2 cells with cell remaining in the lumen displayed stronger staining of MCT4, particularly in the cells that are located within the lumen of these structures (Fig 5.7C).

Taken together, this preliminary data suggests that MCT4 expression is regulated by activation of HER/ERBB signalling. To elucidate the mechanism of regulation of *SLC16A3* by the ERBB family, further experiments are needed.

5.5 Exposure to hypoxia induces *SLC16A3*/MCT4 expression in some breast cancer cells

It has been shown that *SLC16A3* expression can be regulated directly by HIF1α (Ullah et al., 2006). To investigate whether its expression changes after exposure to low oxygen in the panel of breast epithelial cell lines, SLC16A3 expression in these cell lines was determined on RNA and protein level after exposure to low oxygen for 24

hours. This revealed that *SLC16A3* is strongly upregulated on mRNA (Fig 5.8A) and protein level (Fig 5.8B) under hypoxic conditions compared to normoxic conditions in most cell lines. However, MCF7, HCC1806 and 184B5 cells lacked the induction of SLC16A3 after exposure to hypoxia on RNA and protein levels (Fig 5.8).

To further determine the role of *SLC16A3* and its association to cell survival under hypoxia, four cell lines were exposed to hypoxia in a time dependent manner and the expression of *SLC16A3* was assessed (Fig 5.9). To assure that the observed changes correlate with the activation of HIF in hypoxia, *VEGFA* expression was used as a positive control.

The non-malignant cell line MCF10A, that was insensitive to depletion of *SLC16A3*, showed only a minor increase in SLC16A3 expression, after an initial downregulation of *SLC16A3* mRNA after 2 hours of hypoxia, while a strong reduction of *VEGFA* expression was observed with prolonged exposure to hypoxia (Fig 5.9A). In contrast, the sensitive cell line MDA-MB-468 strongly upregulated *SLC16A3* under hypoxia. This correlated with *VEGFA* expression (Fig 5.9B). Analysis of the sensitive cell line HCC1954 revealed strong induction of *SLC16A3* and *VEGFA* (Fig 5.9C).

To determine whether the hypoxic survival of the breast epithelial cell lines is predictive for their sensitivity towards *SLC16A3* ablation, a Pearson correlation was performed (Fig 5.10). A Pearson r factor of 1 indicates a strong positive correlation, whereas -1 indicates a negative correlation. Analysis of the Z-scores of each cell line with the level of cell survival under hypoxia resulted in a Pearson r factor of -0.45 indicating that a weak negative linear correlation exists (Fig. 5.10).

In summary, HIF dependent upregulation of *SLC16A3* mRNA was observed in MDA-MB-468 and HCC1954 cells. The insensitive cell line MCF10A however only showed a weak induction of *SLC16A3* expression. This might partially explain the observed insensitivity to *SLC16A3* depletion in these cells under hypoxia. Moreover, the sensitivity towards *SLC16A3* silencing point to a weak correlation with the survival under hypoxic conditions of breast cell lines.

5.6 *SLC16A3* silencing results in decreased intracellular pH

MCT4 is involved in the transport of monocarboxylates and protons across membranes. This requires the presence of its co-chaperone BSG that translocates MCT4 to the membrane. The ablation of *SLC16A3* might thereby result in changes in the intracellular pH (Kirk et al., 2000). To determine whether *SLC16A3* depletion influences the pH homeostasis in these cells, intracellular pH was measured using the fluorescent probe SNARF. MCF10A cells showed no change in intracellular pH under normoxic conditions after silencing of *SLC16A3* or when *BSG* was depleted (Fig 5.11A). The cell lines HCC1954 and MDA-MB-468, that showed impairment of cell viability after abrogation of *SLC16A3,* exhibited decreased pH_i after silencing of *SLC16A3* under normoxic conditions (Fig 5.11B,C). In addition, HCC1954 cells showed a significant decrease in pH_i not only in *SLC16A3* silenced cells, but also in *BSG* silenced cells under hypoxia (Fig 5.11B). MDA-MB-468 reduced their pH_i after *SLC16A3* silencing, but ablation of *BSG* did not cause a reduction in pH_i (Fig 5.11C). Analysis of pH_i in MDA-MB-231 revealed no changes under normoxic conditions, while an increase in pH_i was observed after *SLC16A3* depletion under hypoxic conditions (Fig 5.11D).

To investigate if the altered pH_i in some of these cells is due to accumulation of lactate, intracellular lactate levels were determined in both oxygen conditions (Fig 5.11E-H). Analysis of the cells under normoxia showed that there was no increase in intracellular lactate. Under hypoxic condition, however, intracellular lactate was increased in BSG silenced HCC1954 and MDA-MB468 cells, but not after ablation of *SLC16A3* in any of the cell lines.

To further investigate the cause of a reduction in pH_i, supernatants of control and *SLC16A3* silenced MDA-MB-468 cells were analysed by mass spectrometry to assess if there are changes in the rates of metabolite import or export after abrogation of *SLC16A3* (Fig 5.12). In normoxia (Fig 5.12A), the export of lactate, malate, and isocitrate/citrate was reduced after ablation of *SLC16A3*. It should be noted, however, that the amount of lactate exported by control cells was 10-times higher compared to the amount of citrate/isocitrate. This confirms that MCT4 is involved in the export of lactate from these cells. Moreover, cells with silenced *SLC16A3* showed increased uptake of the amino acids glutamine, isoleucine/leucine, lysine and arginine. Mass spectrometry analysis of the supernatants from hypoxic cells showed that *SLC16A3*

silencing caused a strong reduction in lactate and isocitrate/citrate export, suggesting that lactate is accumulating in these cells (Fig 5.12B). In contrast, glutamate export increased in *SLC16A3* silenced MDA-MB-468 cells compared to control transfected cells. In addition, besides the decreased import of several amino acids (e.g. glutamine, arginine, phenylalanine, lysine), glucose import showed a strong reduction after ablation of *SLC16A3* under hypoxia (Fig 5.12B). It should be noted, however, that the detection of glucose by the technique used here is not very accurate.

To assess whether the export of pyruvate and lactate after *SLC16A3* silencing has an effect on mitochondrial activity, the oxygen consumption rate (OCR) and extracellular acidification rate (ECAR) was investigated in three cell lines cultured under standard medium conditions in normoxia (Fig 5.13). The non-malignant cell line MCF10A showed no changes in OCR after depletion of *SLC16A3* compared to control transfected, accompanied by decreased ECAR levels (Fig 5.13A). In contrast, MDA-MB-468 breast cancer cells showed increased OCR but displayed only a minor increase in ECAR levels (Fig 5.13B). MDA-MB-231 showed no change in OCR after SLC16A3 depletion although the ECAR was increased after silencing of *SLC16A3* (Fig 5.13C).

Next, it was aimed to rescue the effect of *SLC16A3* silencing on cell number in MDA-MB-468 and HCC1954 cell lines by perturbation of metabolic processes (Fig 5.14). MDA-MB-468 and HCC1954 cells showed a reduction of cell number after treatment with 2-DG or glutamine withdrawal, while treatment with dichloroacetate (DCA), an inhibitor of PDHK1, or glucose withdrawal only had minor effects under normoxia. Silencing of *SLC16A3* resulted in a 50% reduction of cell number in DMSO-treated cells and this was not enhanced by treatment with 2-DG or glutamine withdrawal (Fig 5.14A,B). However, in hypoxic cells, treatment with 2-DG in both cell lines or withdrawal of glucose in HCC1954 reduced cell number in control transfected cells. This was not further enhanced by *SLC16A3* silencing in both cell lines after treatment with 2-DG (Fig 5.14A,B), suggesting that SLC16A3 ablation targets the metabolic pathways also affected by 2-DG treatment. It was surprising that glucose withdrawal of *SLC16A3* depleted HCC1954 cells had a pronounced effect compared to DMSO treated cells after *SLC16A3* silencing under hypoxia.

Collectively, these results indicate that *SLC16A3* influences pH homeostasis by affecting lactate transport. Moreover, cancer cells depleted of *SLC16A3* seem to import more amino acids under normoxic conditions. Under hypoxic conditions, the import of several metabolites, including the carbon sources glucose and glutamine was decreased after silencing of *SLC16A3*. It could be hypothesised that this indicates that cells respond to *SLC16A3* silencing by entering a state of starvation. This has to be further investigated. In addition, the fate of lactate in the absence of *SLC16A3* needs to be elucidated, as no accumulation of intracellular lactate was observed. However the OCR and ECAR data suggests that MDA-MB-468 cells indeed try to use their mitochondrial activity to cope with increased levels of lactate, pyruvate, aspartate and malate under normoxic conditions.

5.7 Ablation of *SLC16A3* increases ROS levels

To investigate if *SLC16A3* affects intracellular ROS, the ROS levels in four cell lines following *SLC16A3* depletion under normoxic conditions were determined. The non-malignant cell line MCF10A showed a minor increase in ROS levels (Fig 5.15A), while MDA-MB-231 showed no change in ROS levels compared to the control transfected MDA-MB-231 cells (Fig 5.15B). In contrast, the sensitive cell line MDA-MB-468 increased its ROS levels significantly after silencing of *SLC16A3*compared to the control silenced cells ($p<0.0001$). This was also observed in the second sensitive cell line HCC1954 ($p=0.004$).

These results indicate that *SLC16A3* might be important for the cellular redox balance. The sensitive cell line MDA-MB468 increased its OCR after *SLC16A3* ablation, while ECAR was reduced. This could indicate increased mitochondrial metabolism resulting in enhanced production of ROS. In addition, MDA-MB-468 cells showed decreased serine uptake and increased levels of glutamine and glutamate uptake, suggesting that the serine biosynthesis pathway could be upregulated to compensate for increased ROS levels in *SLC16A3* depleted cells. However, the mechanism why these cells increase ROS after *SLC16A3* depletion is still under investigation.

5.8 *SLC16A3* depletion affects cell viability in an *in-vivo* like system

To assess whether *SLC16A3* depletion shows similar phenotypes in a more *in-vivo* like situation, 3D cultures and spheroid formation after transient siRNA transfection were established and analysed. MDA-MB-468 embedded in matrigel showed that *SLC16A3* silencing affected cell viability, while *BSG* silencing did not have an effect on cell viability (Fig 5.16A). The same was observed for HCC1954 cells (Fig 5.16B). Depletion of *BSG*, however, reduced cell viability in HCC1954. In contrast to the sensitive cell lines MDA-MB-468 and HCC1954, 3D cultures of MDA-MB-231 cells were not impaired in their viability after silencing of *SLC16A3* or *BSG* (Fig 5.16C). These observations were also confirmed by spheroid formation assays (Fig 5.17). Clusters of HCC1954 and MDA-MB-468 cells transfected with siSLC16A3 were smaller in size compared to control transfected cells (Fig 5.17 A,B). In contrast, MDA-MB-231 showed no changes in the size or appearance of the 3D cell clusters after depletion of SLC16A3 (Fig 5.17C).

Collectively, these findings indicate that SLC16A3 could play a role in the growth of breast cancer cell lines *in-vivo.*

5.9 Depletion of *SLC16A3* using shRNA results in decreased cell viability

To confirm SLC16A3 as an essential mediator of cell survival in ER-negative cancer cells lines (HER2-positive, ER-negative/HER2-negative), four cell lines were taken forward for lentiviral infection with TET-pLKO constructs, each containing a different shRNA sequence targeting *SLC16A3*. The expression of these shRNAs is under the control of the Tet-operator and can be induced by doxycycline administration.
First, silencing efficiency of the different shRNAs was tested. Effective silencing on RNA and protein expression upon doxycycline treatment was observed in all four cell lines with at least one sequence (Fig 5.18).

To establish if shRNA-mediated silencing also affects cell viability, colony assays were carried out. The sensitive cell line MDA-MB-468 and the insensitive cell line MDA-MB-231, both expressing shRNAs targeting *SLC16A3*, were cultured for 10 days in the

presence or absence of doxycyline (Fig 5.19). Loss of cell viability was observed in doxycycline treated MDA-MB-468 cells containing shRNA sequences #74 and #88 compared to their untreated counterparts (Fig 5.19A) and this was confirmed by quantified measurements (Fig 5.19B). In contrast, MDA-MB-231 cells displayed no effect in all samples treated with doxycycline compared to the non-doxycyline treated samples and no significant effect of silencing of *SLC16A3*/MCT4 was observed (Fig 5.19B, D).

To investigate the cause of the reduction in cell viability, the metabolic state of the cells was investigated. To do this, the acute effect of glucose and glutamine on oxygen consumption was investigated using the Seahorse Bioanalyser (Fig 5.20). Cells were initially depleted of glucose and glutamine and basic OCR was determined. Both metabolites were then sequentially injected into the plate and changes in OCR over the baseline were recorded. After titration of glucose into the glucose- and glutamine-depleted medium, MDA-MB-468 cells (either expressing a scrambled shRNA or in the absence of doxycycline) displayed a decrease in oxygen consumption after injection of glucose (Fig 5.20). Ablation of *SLC16A3* by doxycycline administration reduced the ability of the cells to decrease their OCR following glucose injection. This effect was even more pronounced when glutamine was subsequently injected into the now glucose-containing medium (Fig 5.20A). In contrast, the insensitive cell line MDA-MB-231 showed a small increase in OCR after glucose or glutamine injection and this was not affected by depletion of *SLC16A3* (Fig 5.20B).

In summary, these results suggest that the ablation of *SLC16A3* leads to decreased long-term viability only in sensitive breast cancer cell lines. Furthermore, in sensitive cell lines depletion of *SLC16A3* prevents cell from reducing their OCR in the presence of glucose. Increased mitochondrial metabolism in the absence of *SLC16A3* could cause enhanced oxidative stress and cell death.

5.10 *SLC16A3* is important for tumour formation and progression *in-vivo*

Given that silencing with shRNA promotes long-term silencing compared to siRNA, and to further characterise *SLC16A3* as a regulator of cell survival in a more *in-vivo* like

situation, spheroid formation assays were performed over a period of 12 days with MDA-MB-231 and MDA-MB-468 cells containing shRNA sequence #88 (Fig 5.21A). Immunohistochemical analysis was performed on spheroid sections to show diminished MCT4 expression after doxycycline treatment. Staining for active caspase 3 was used to detect apoptotic cells. Transduced MDA-MB-468 cells formed spheroids with a necrotic inner core shown by the hematoxylin and eosin staining. Moreover, the expression of MCT4 was mainly located in an area between the outer cell layers and the necrotic core. In this area, MCT4 showed stronger staining on the plasma membrane (Fig 5.21A). The staining of cleaved caspase correlated with MCT4 expression in untreated cells. Depletion of *SLC16A3* reduced spheroid size and expression of MCT4 in the inner core and only weak staining was detected on the plasma membranes of the spheroid cells. Moreover, it appeared that the cleaved caspase staining was not as pronounced compared to the untreated sample (Fig 5.21A). The spheroids of MDA-MB-468 were phenotypically different from those of MDA-MB-231 cells with no defined necrotic core (Fig 5.21B). In addition, light patches were distributed within the spheroid. The detection of MCT4 in the control cells displayed strong membranous staining especially in the cells at the border between the spheroid and the medium. In contrast, the inner core showed more cytoplasmic staining of MCT4. The light patches were negative for MCT4 staining. There was only weak staining for cleaved caspase with no distinct pattern. After doxycyline induced silencing of *SLC16A3*, it was noted that the spheroids were larger and this is mainly due to an increase in size of the lighter patches. There was also a clear reduction in MCT4 expression visible and no cleaved caspase staining of any distinct area.

To establish whether *SLC16A3* is important for tumour growth, cells of the sensitive breast cancer cell line MDA-MB-468 transduced with the shRNA construct #88 were orthotopically injected into the mammary fat pad of 8-week old female immuno-compromised mice (nu/nu). After initial tumour formation (10 days post-injection) mice were separated and one cohort was given doxycycline in their diet to initiate the depletion of *SLC16A3* whereas the other cohort was kept on a standard diet. Tumours of the mice in the different cohorts were measured twice per week and tumour volume was calculated with the ellipsoidal volume formula: ½ x length x $(\text{width})^2$. After 65 days,

depletion of *SLC16A3* showed a strong impairment of tumour growth in the doxycycline treated mice compared to the cohort on a standard diet. However, at the time of this thesis being written, this experiment was still ongoing (Fig 5.21C).
To further determine a potential link between tumour growth and *SLC16A3*, different slides from a *MMTV-PyMT* transgenic mouse model (Guy et al., 1992) (provided by Dr. Erik Sahai) were probed for MCT4 expression. The expression of MCT4 in normal tissue was low and increased with the grade of neoplastic transformation (Fig 5.22). Remarkably, the expression of MCT4 in the mouse carcinoma was very distinct. In the adenocarcinoma/early carcinoma tissues, MCT4 expression was observed in tumour cells as well as in the surrounding fibroblasts. The carcinoma stage exhibited strong MCT4 expression in cancer cells on the border of the tumour with the stroma (Fig 5.22). This raises the interesting hypothesis that MCT4 expression could be important for the exchange of metabolites between the tumour and the stroma.

Taken together, *SLC16A3* expression is essential for tumour growth in breast cancer cells. Ablation of *SLC16A3* impaired spheroid growth in MDA-MB-468 cells and reduced tumour formation of MDA-MB-468 cells in an orthotopic mouse model. The expression of MCT4 also correlated with tumour progression in a *MMTV-PyMT* mouse model. Moreover, breast cancer cell lines show a distinct response to *SLC16A3* depletion, suggesting that some breast cancer cells (e.g. MDA-MB-231) are not dependent on the function of *SLC16A3*.

5.11 *SLC16A3* expression is upregulated in human breast cancer

To evaluate if *SLC16A3* might be important for the biology of breast cancer, expression of its mRNA in breast cancer tumour specimen was assessed using the publically available platform Oncomine (Rhodes et al., 2004) (Fig 5.23). The TCGA dataset showed elevated expression of *SLC16A3* in invasive carcinomas of the breast (Fig 5.23A). A similar observation was found in the datasets of Zhao et al (Fig 5.23B) and Richardson et al (Fig 5.23C). Moreover, *SLC16A3* expression differed between the normal and tumour stroma (Fig 5.23D). This might indicate the coupled metabolism between stroma and tumour cells (Brooks, 2007; Sonveaux et al., 2008). *SLC16A3*

expression was also found to be a predictor for the recurrence of breast cancer in the study by Finak et al (Fig 5.23E).

Moreover, a tissue microarray of 75 breast specimen in duplicates was used to examine if the clinically defined subtypes show differential expression of MCT4 (Fig 5.24). The different staining intensities were determined by two different pathologists (Prof. Gordon Stamp, Dr. Daniel N. Rodrigues). Normal tissue cores showed low expression of MCT4 protein, whereas breast cancer cores showed higher expression. HER2-positive breast cancer cores showed higher staining intensity in the tumour cells compared to the ER-positive/HER2-negative and ER-negative/HER2-negative subtypes (Fig 5.24A).

Interestingly, GOBO, a online portal for gene expression data, can be used to find correlations between gene expression and breast cancer outcome (Ringner et al., 2011) showed that the overall survival (OS) of HER2-positive breast cancers is dependent on the expression levels of *SLC16A3* (Fig 5.24B). HER2-positive tumours with high expression of *SLC16A3* had an OS of 30-35% after 5 years whereas HER2-positive cancers with low or medium *SLC16A3* expression showed an OS of 70% after 5 years of diagnosis (Fig 5.24B).

Taken together, the data from Oncomine and GOBO as well as the TMA analysis support a role of *SLC16A3*/MCT4 in HER2-positive breast cancer. However, the regulation of SLC16A3 by the HER2 signalling axis and the molecular mechanisms underlying the dependence of these tumours on this transporter still needs to be elucidated.

5.12 Discussion

Patients with ER-negative breast cancer including HER2-positive and ER-negative/HER2-negative subtypes show the worst overall survival (Owens et al., 2004; Slamon et al., 1987). This is due to the lack of personalised therapeutics in ER-negative/HER2-negative breast cancer, highly aggressive tumours accompanied by high incidences of recurrence or the development of resistance against systemic therapy (Fan et al., 2006). In this chapter, the monocarboxylate transporter MCT4 was identified to be important for cancer cell survival of ER-negative breast cancers. Depletion of

SLC16A3 using siRNA and shRNA demonstrated reduced cell viability *in-vitro* and *in-vivo*. This is primarily due to apoptosis supported by increased activity of effector-caspases and enhanced PARP cleavage that was observed after *SLC16A3* silencing under normoxic conditions. Interestingly, the cause of reduced cell viability and induction of cell death under hypoxia appeared to be different to that in normoxia as no activation of caspases was observed. This could indicate that the abrogation of *SLC16A3* induces necrotic cell death in hypoxic cells, potentially via metabolic catastrophe. This hypothesis is supported by the impaired lactate export and decrease in intracellular pH found after *SLC16A3* depletion. Reduced import of amino acids and glucose was also observed. Interestingly, this study showed that citrate and malate export are also influenced as a consequence of *SLC16A3* depletion, suggesting that perturbing the activity of discrete nodes could have wide-ranging effects on the metabolic network.

Using a commercially available tissue microarray, different invasive ductal carcinomas were probed for MCT4 expression and higher staining intensity for HER2-positive tumours was revealed. This is in line with increased expression of MCT4 in the HER2-positive cell lines used in this study. A similar observation by Whitaker-Menezes and colleagues showed that 14 patients with HER2-positive breast cancer had increased *SLC16A3* levels and this is associated with decreased OS (Whitaker-Menezes et al., 2011). This is further supported by the results from the GOBO analysis, that showed a statistically significant reduction in overall survival in HER2-positive tumours with high *SLC16A3* expression compared to normal/low expression tumours (see 5.24). However, there are other studies indicating that *SLC16A3*/MCT4 expression is not preferentially higher in HER2-positive tumours (McCleland et al., 2012; Pinheiro et al., 2010a).

Recent studies also demonstrated that another monocarboxylate transporter is important for the survival of ER-negative/HER2-negative and basal-like breast cancers (Pinheiro et al., 2010a). MCT1 expression has been shown to correlate with high glucose consumption and glycolytic activity in cancer cells (Birsoy et al., 2012a). Another study linked MCT1 to LDHB, an enzyme important for survival of breast cancer cells, arguing that these enzymes are co-upregulated (McCleland et al., 2012; Porporato et al., 2011). However, this study also included MCT4 expression showing an inverse

correlation to high LDHB expression. This might indicate that LDHA and MCT4 function together (Hussien and Brooks, 2011). Both enzymes are upregulated by HIF1α and are important for lactate production and secretion. Moreover, numerous studies demonstrated co-localisation between LDHA, MCT4, HIF1α and other glycolytic enzymes (e.g GLUT1) in breast tumours (Rademakers et al., 2011).

New interesting data from Sonveaux and colleagues propose a coupled metabolism of different cells within tumours, suggesting that metabolites are exchanged between glycolytic and oxidative cells within a tumour (Sonveaux et al., 2008). It is possible that some tumour cells that are highly dependent on glucose express high levels of MCT1 to facilitate the export of pyruvate/lactate, which can then be used by highly glycolytic cells to generate energy and biomass.

Interestingly, cells depleted of *SLC16A3* showed a higher rate of glutamine and amino acid uptake. However, this was restricted to normoxic conditions. In hypoxia, glutamine uptake was reduced after *SLC16A3* depletion. It has been shown that *LDHA* as well as glutamine are important for cell survival under hypoxia (Fantin et al., 2006; Wise et al., 2008). To postulate a connection between MCT4 and glutamine metabolism needs further investigation. Surprisingly, only a weak dependency of breast cell lines on MCT1 in different oxygen conditions was observed (cells with high glucose uptake). Moreover, the panel of cell lines displayed no sensitivity to an MCT1 inhibitor (unpublished observation). This suggests that the dependency of cancer cells on different monocarboxylate transporters could be complex and might dependent on specific conditions, such as metabolite composition of the medium. However, the effect of *SLC16A3* depletion on tumour growth clearly demonstrates that this transporter is required under physiological nutrient conditions. This confirms that the importance of the MCT family of proteins as a whole is unquestionable.

Immunohistochemistry data from *MMTV-PyMT* suggests that increased expression of MCT4 correlates with tumour progression. Both the early stages of the mouse tumour progression model and the normal tissue cores of the human TMA showed low or absent expression of MCT4. Several studies have indicated MCT4 to be important for higher-grade tumours or proposed a role for MCT4 in cell invasion and metastasis (Chiche et al., 2012; Gallagher et al., 2009; Parks et al., 2011). A study in ccRCC cell lines and expression data from ccRCC tumours showed a strong link between MCT4

expression and dependency to hypoxia/HIF as these cells lack functional VHL (Gerlinger et al., 2012). Here, it is shown that cell lines sensitive to *SLC16A3* depletion strongly upregulate its expression after exposure to low oxygen. Hypoxia also causes extracellular acidosis and this feature of the tumour microenvironment can promote cancer cell invasion and metastasis formation. It will be interesting to investigate whether MCT4 is also involved in the metastasis formation in the breast cancer cells used here.

Figure 5.1

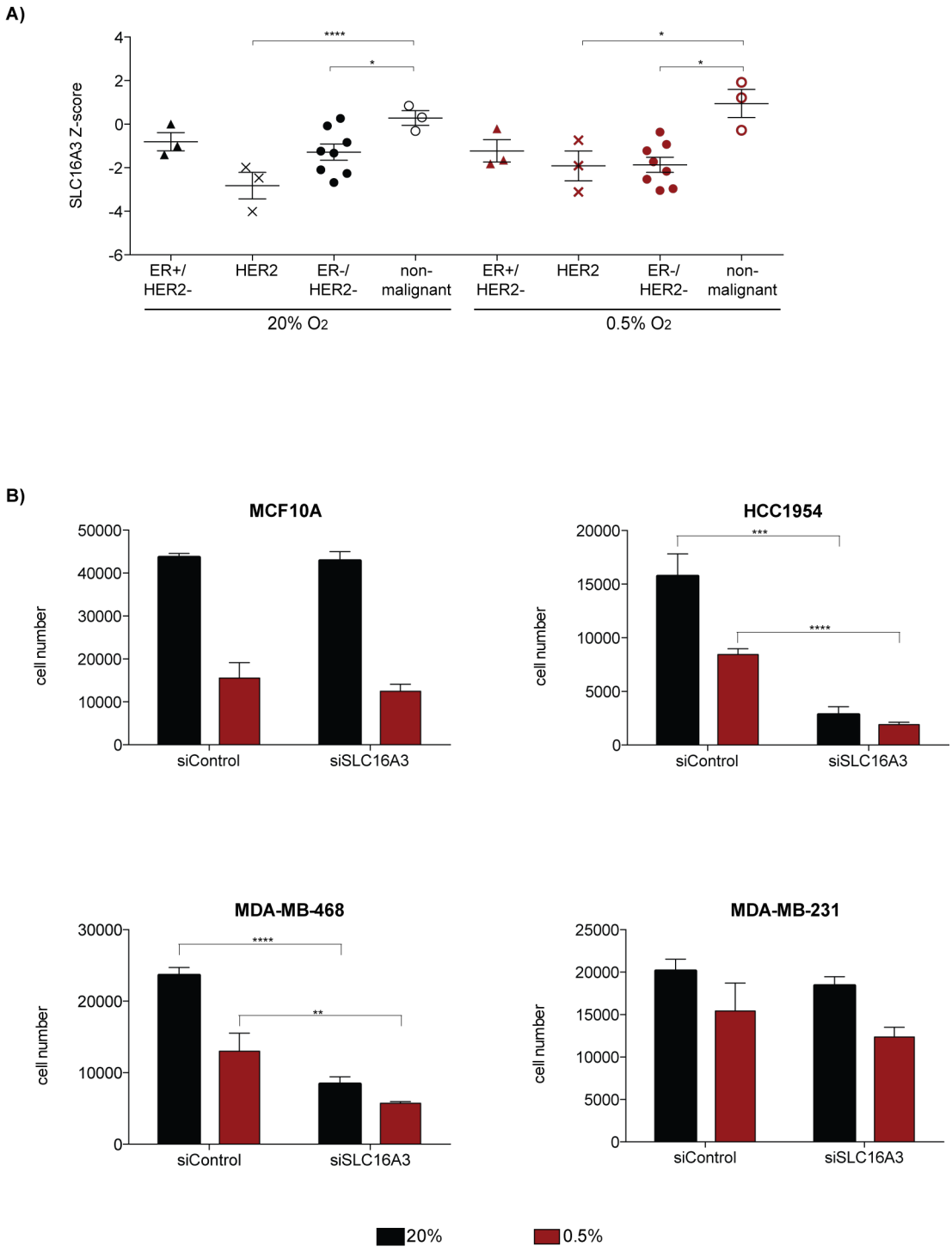

Figure 5-1 *SLC16A3* important for most breast cancer cells

(A) Supervised cluster analysis identified *SLC16A3* as a candidate gene for cell lines negative for hormone receptor expression. (*=p≤0.05, ***=p≤0.001). (B-E) MCF10A, HCC1954, MDA-MB-468 and MDA-MB-231 cells were reverse transfected with siRNA targeting *SLC16A3*. 96 hours post-transfection, cells were stained with DAPI and analysed for cell number under normoxic (black bars) and hypoxic conditions (red bars). Values show mean and SD of two independent experiments with three independent replicates each.

Figure 5.2

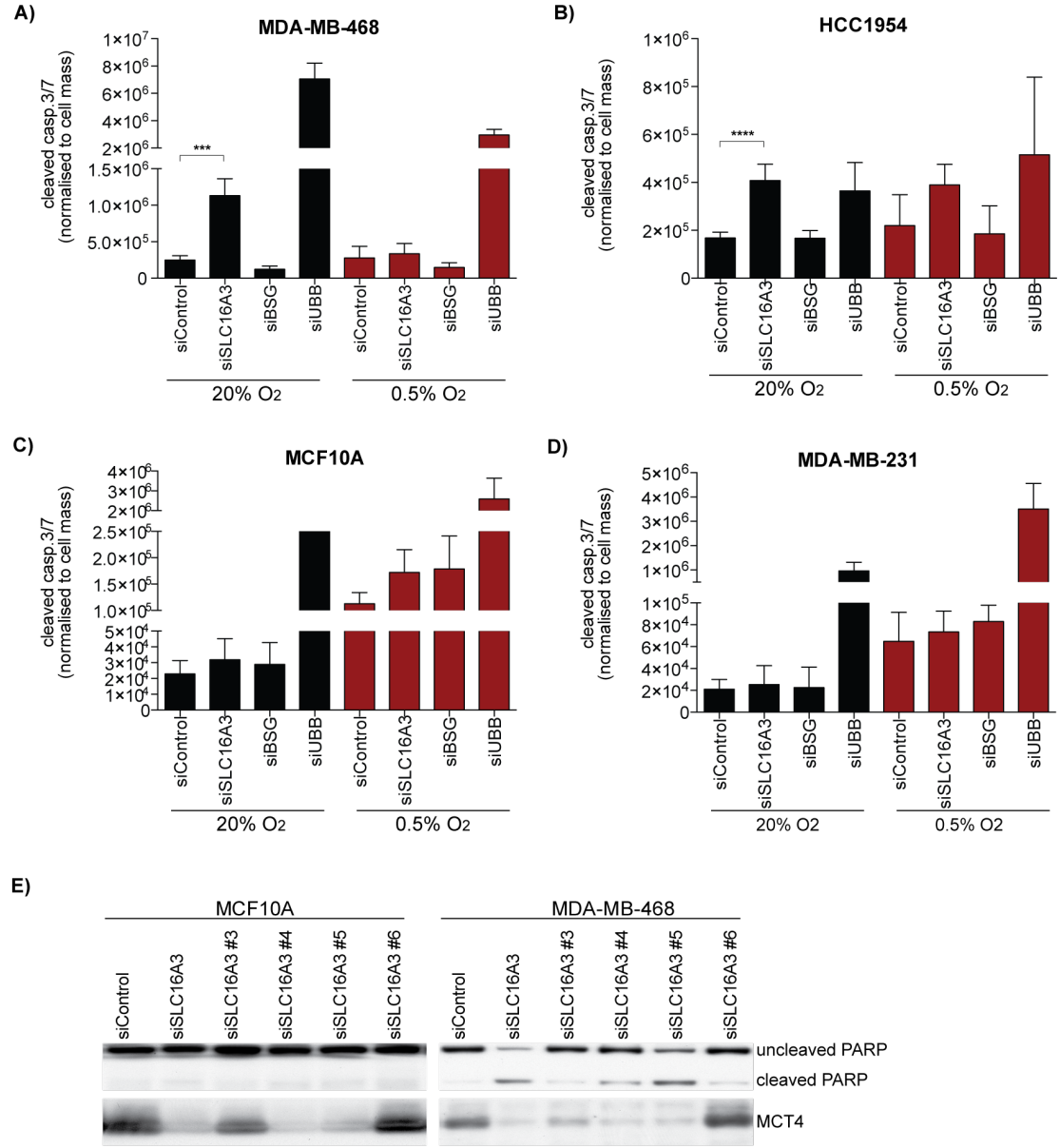

Figure 5-2 *SLC16A3* silencing induces apoptosis only under normoxic conditions

Four breast epithelial breast cell lines MCF10A (A,), HCC1954 (B), MDA-MB-468 (C), and MDA-MB-231 (D) were reverse transfected with siRNA targeting *SLC16A3* and cultured under normoxic (black bars) and hypoxic conditions (red bars). (A-D) 96 hours post-transfection, cells were analysed for caspase activity. Results were normalised to protein content. Values show mean and SD of two independent experiments with three independent replicates each (***=p≤0.001, ****=p≤0.0001) (E) Three days post-transfection, whole cell lysates of MCF10A and MDA-MB-468 cells were harvested and analysed for PARP cleavage and MCT4 expression.

Figure 5.3

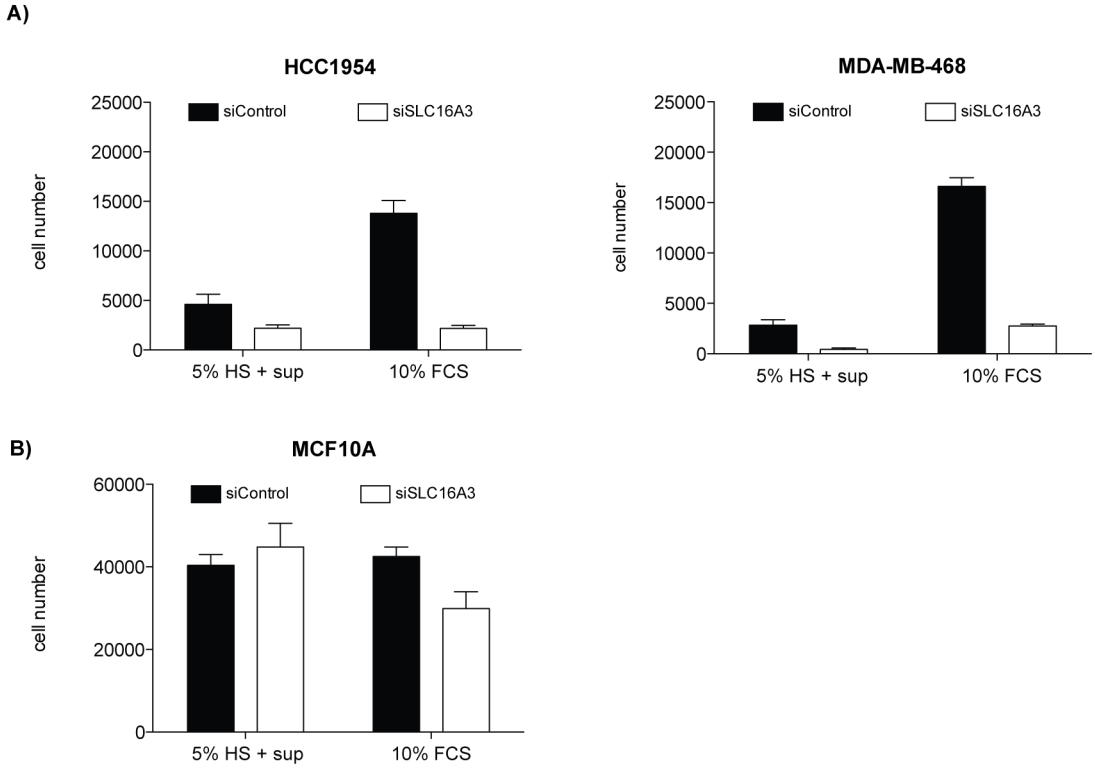

Figure 5-3 Growth factors in MCF10A medium are not protective after depletion of *SLC16A3*

The sensitive cell lines HCC1954 and MDA-MB-468 (A) and the non-malignant insensitive MCF10A cell line (B) were reverse transfected with siControl or siSLC16A3 and cultured for 12 hours, before being placed in the indicated medium conditions. Cell number was determined by DAPI staining. Values show mean and SD of three independent replicates

Figure 5.4

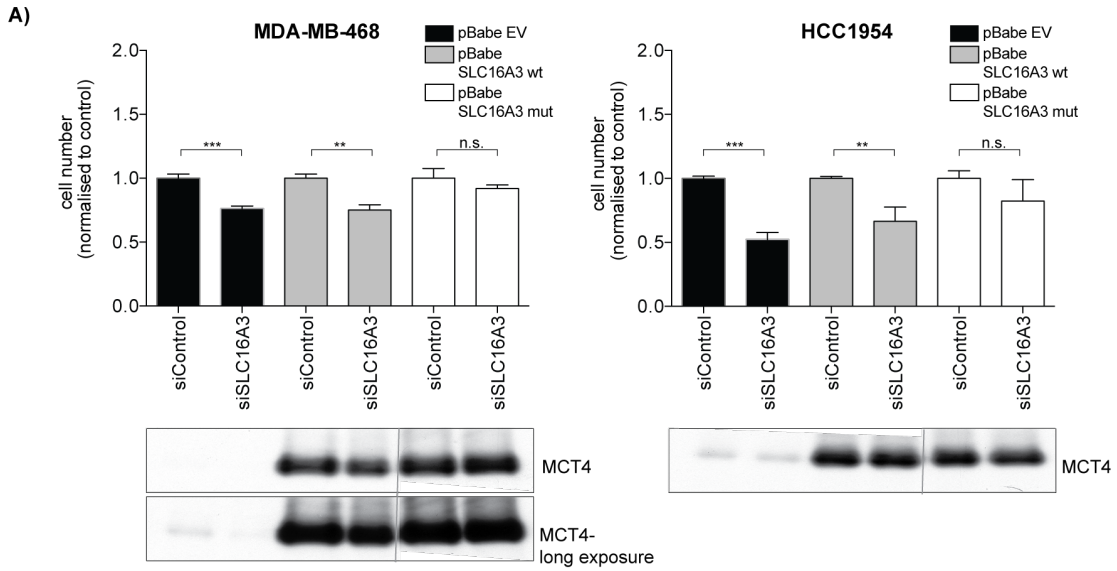

Figure 5-4 Overexpression of mutant SLC16A3 constructs rescue siRNA mediated reduction in cell number

The sensitive cell lines MDA-MB-468 and HCC1954 expressing empty vector (pBABE EV), wildtype SLC16A3 (pBABE SLC16A3 wt) or mutant SLC16A3 (pBABE SLC16A3 mut) were reverse transfected with siControl or siSLC16A3 duplexes #4 and #5, and cultured for 96 hours, before cell number was assessed. Whole protein lysates of the cells 72 post-transfection were harvested and analysed for MCT4 expression. Values show mean and SD of a single experiment performed with three independent replicates. Unpaired t-test was used for significance calculation (**=p≤0.01, ***=p≤0.001). Constructs were generated with the help of Beatrice Griffiths.

Figure 5.5

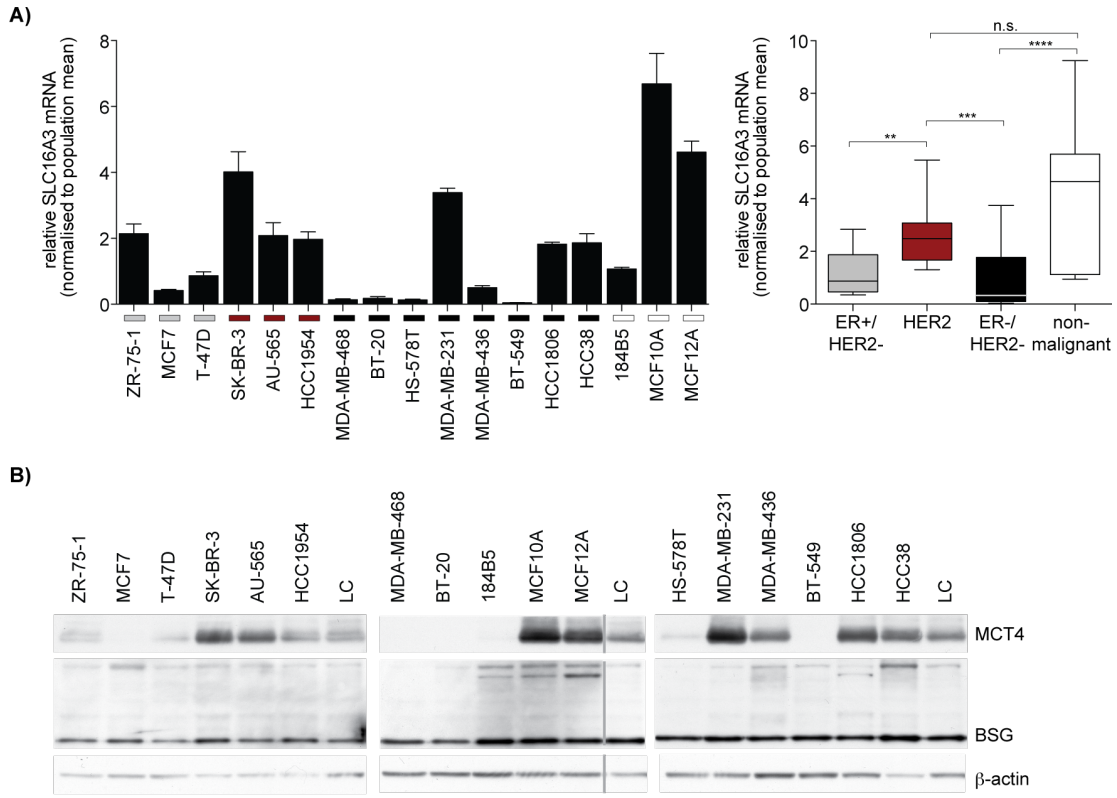

Figure 5-5 Differential expression of *SLC16A3*/MCT4 in breast epithelial cell lines

Breast epithelial cell lines were seeded 24 hours prior to harvesting whole cell lysates for protein and RNA analyses. (A+B) Expression of SLC16A3 was determined by (A) qPCR on mRNA level and (B) for protein expression. Unpaired t-test was used to determine p-values. Values in (A) show mean and SD of two independent experiments with two biological replicates each (**=p≤0.01, ***=p0.001, ****=p≤0.0001).

Figure 5.6

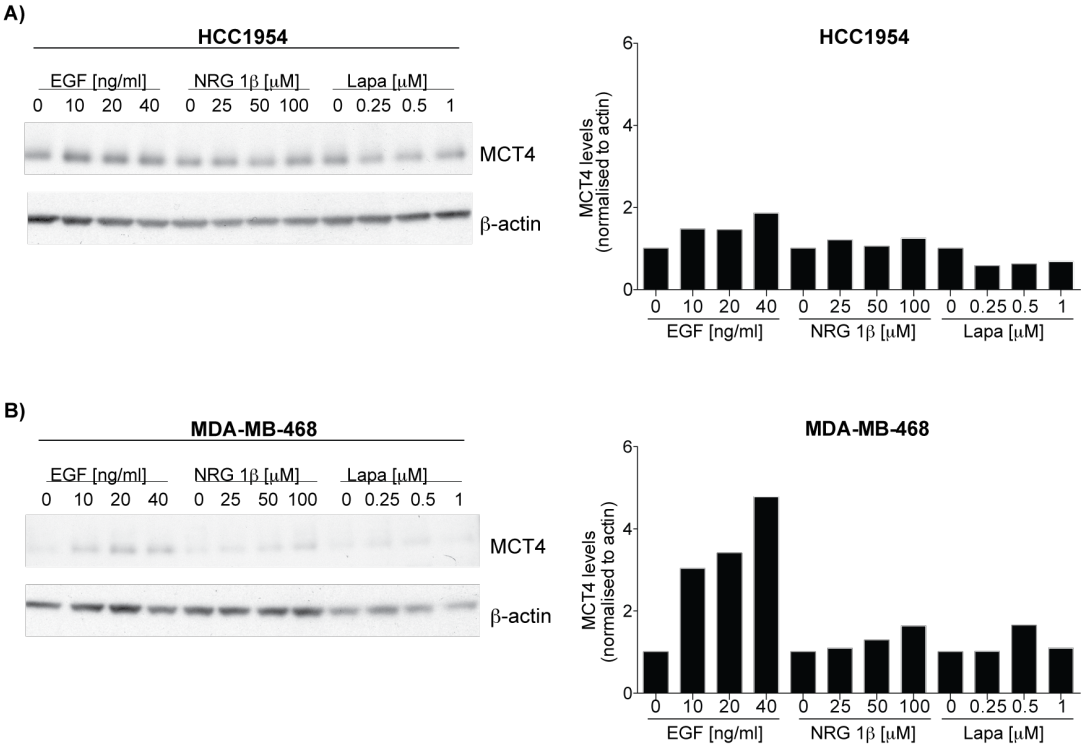

Figure 5-6 Influence of HER signalling on MCT4 expression

HER2-positive cell lines HCC1954 and *EGFR*-amplified/ER-negative/HER2-negative MDA-MB-468 were seeded 24 hours prior to treatment with different ligands (EGF and NRG1β) or the dual HER2 and EGFR inhibitor Lapatinib for 24 hours before whole cell lysates were harvested and used for protein analyses. (A) Expression of MCT4 and β-actin in HCC1954 lysates was determined by immunoblot and quantified using ImageJ. (B) Expression of MCT4 and β-actin of HCC1954 lysates was determined by immunoblot and quantified using ImageJ. This experiment has been performed once.

Figure 5.7

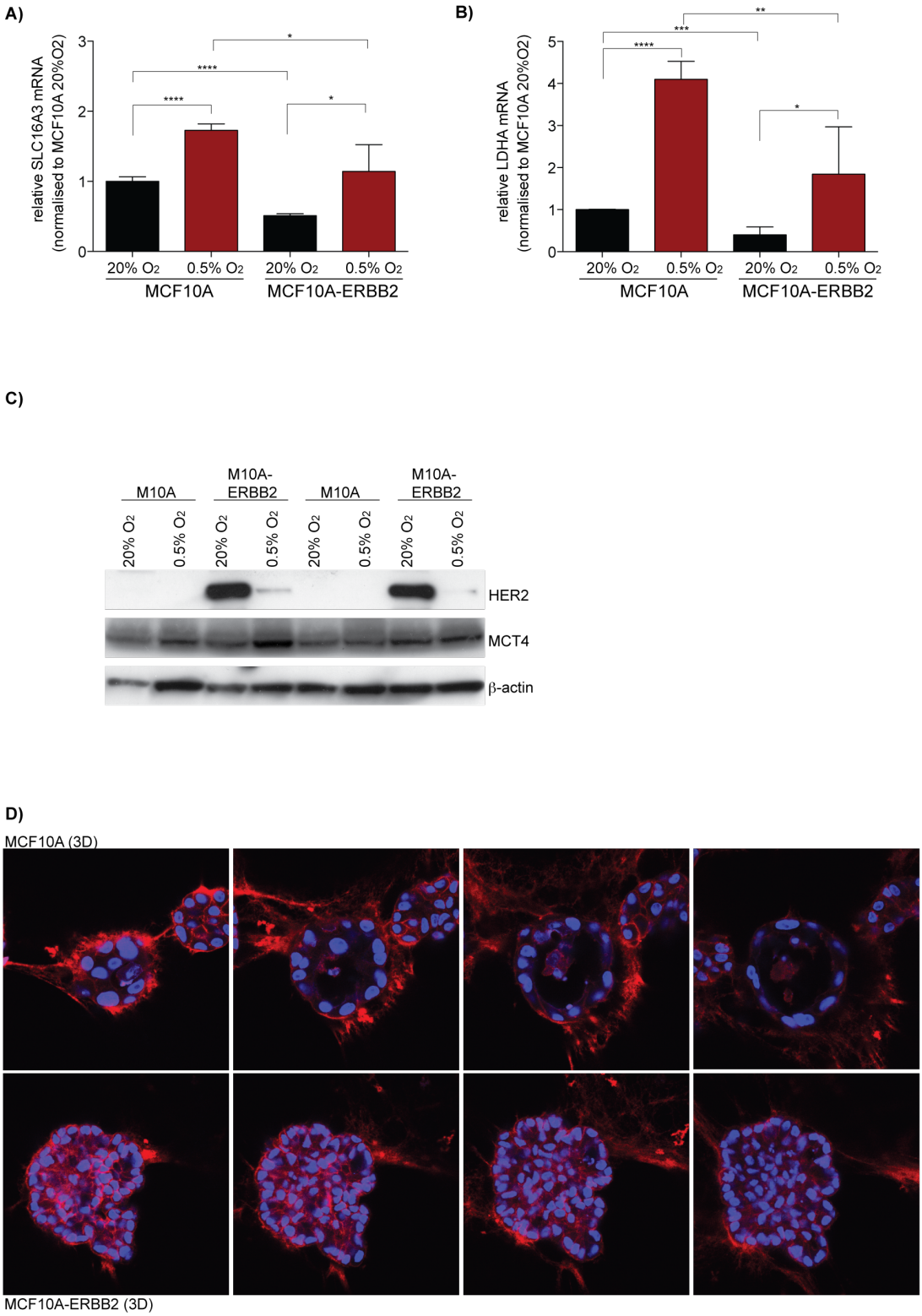
A)
relative SLC16A3 mRNA (normalised to MCF10A 20%O2)
0
1
2
3
****
****
*
*
20% O2
0.5% O2
20% O2
0.5% O2
MCF10A
MCF10A-ERBB2
B)
relative LDHA mRNA (normalised to MCF10A 20%O2)
0
1
2
3
4
5
****
***
**
*
20% O2
0.5% O2
20% O2
0.5% O2
MCF10A
MCF10A-ERBB2
C)
M10A
M10A-ERBB2
M10A
M10A-ERBB2
20% O2
0.5% O2
20% O2
0.5% O2
20% O2
0.5% O2
20% O2
0.5% O2
HER2
MCT4
β-actin
D)
MCF10A (3D)
MCF10A-ERBB2 (3D)

Figure 5-7 *ERBB2* overexpression in MCF10A cells alters *SLC16A3*/MCT4 expression

The non-malignant MCF10A breast epithelial cells and *ERBB2*-overexpressing MCF10A cells were seeded in 2D for 12 hours prior to exposure to hypoxia for further 24 hours. Whole cell lysates were harvested for protein and RNA analyses. Expression of *SLC16A3* (A) and *LDHA* (B) was determined by qPCR on mRNA level. Values show mean and SD of two independent experiments with two biological replicates each. Unpaired t-test was used to determine p-values. (*=p≤0.05, **=p≤0.01, ***=p0.001, ****=p≤0.0001). (C) Expression of MCT4 and β-actin were determined by immunoblot. (D) Non-malignant MCF10A breast epithelial cells and *ERBB2*-overexpressing MCF10A cells were embedded in matrigel for 3D culture for 15 days. Cells were then fixed and stained according to a protocol provided by Prof. Joan Brugge (Harvard Medical School, Boston, MA, USA) and immuno-fluorescent staining of MCT4 and DAPI was assessed by confocal microscopy. Images show a series of confocal sections along the z-axis.

Figure 5.8

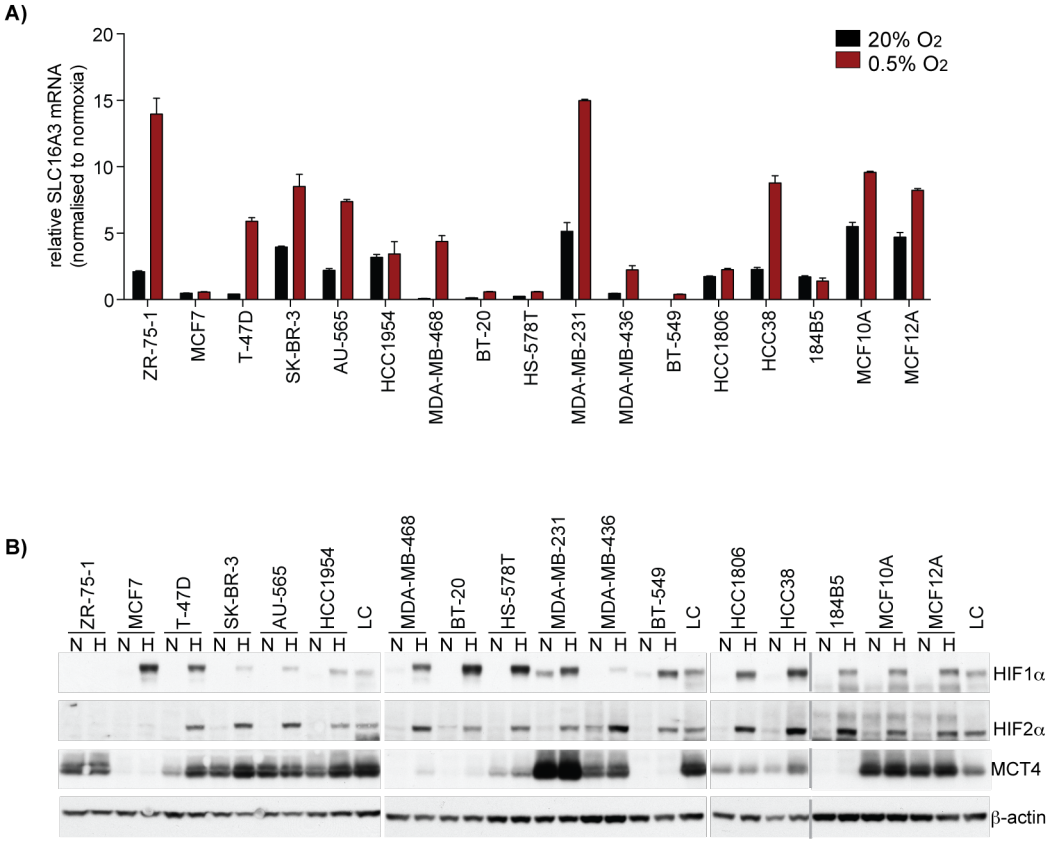

Figure 5-8 *SLC16A3*/MCT4 upregulation under hypoxic conditions

(A) Cells of breast epithelial cell lines were seeded for 24 hours before exposure to hypoxia for further 24 hours. Whole cell lysates were harvested for total RNA and analysed for *SLC16A3* and β-actin expression by qPCR. Graph shows SLC16A3 mRNA levels normalised to β-actin from cells under normoxic (black bars) and hypoxic (red bars) conditions. Values show mean and SD of one independent experiment with two biological replicates each. (B) Cells of breast epithelial cell lines were seeded for 24 hours before exposure to hypoxia for further 24 hours. Whole cell lysates were harvested for protein analysis of HIF1α, HIF2α, MCT4 and β-actin expression for cells cultured in normoxia (N) and hypoxia (H).

Figure 5.9

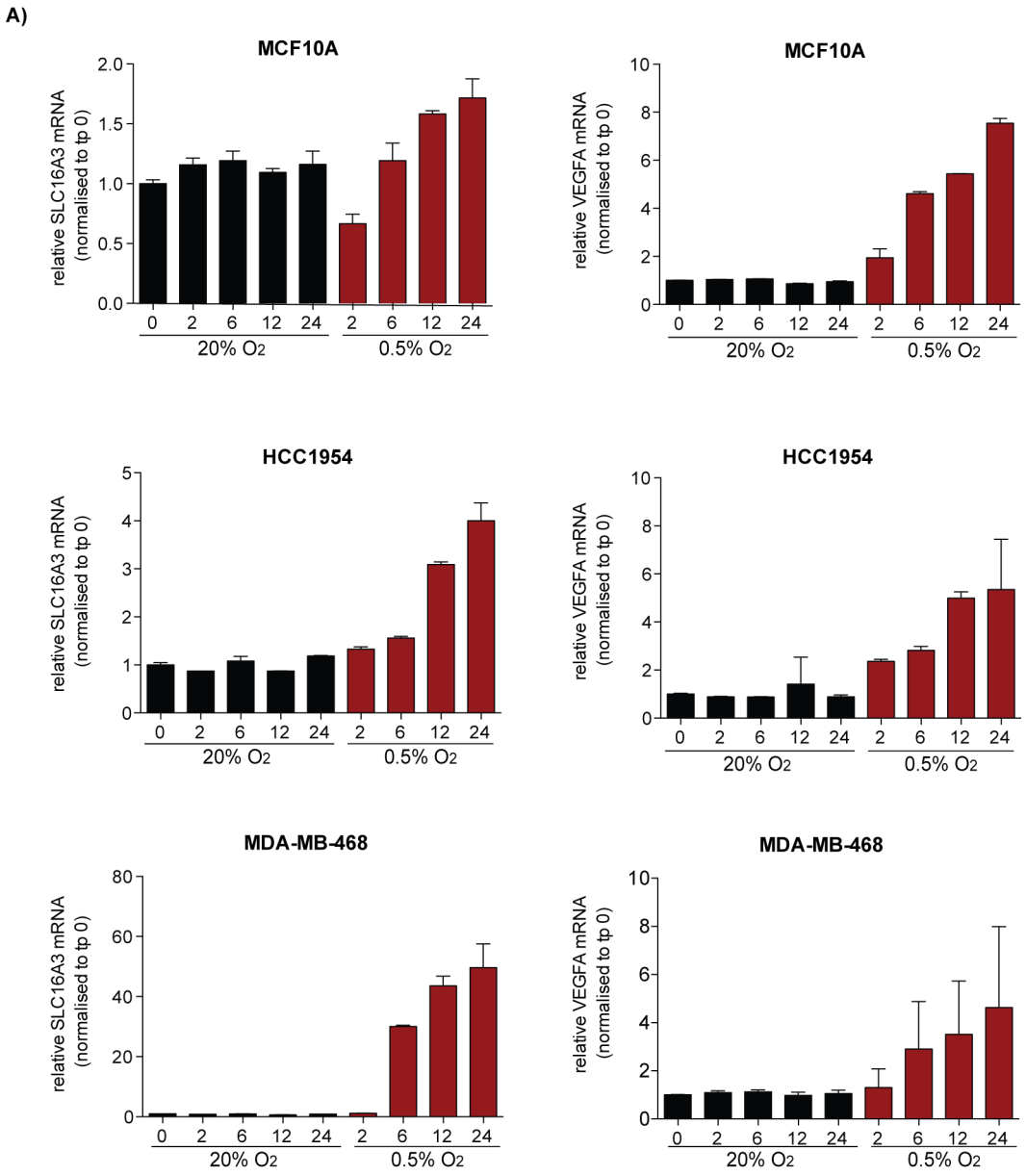

Figure 5-9 Induction of *SLC16A3* in hypoxia

MCF10A cells (A), HCC1954 cells (B) and MDA-MB-468 cells (C) were seeded 12 hours prior to being placed in hypoxia for 0-24 hours. Whole cell lysates were harvested for RNA analyses. Expression of SLC16A3 and β-actin was determined by qPCR. Values show mean and SD of an independent experiment with two biological replicates each.

Figure 5.10

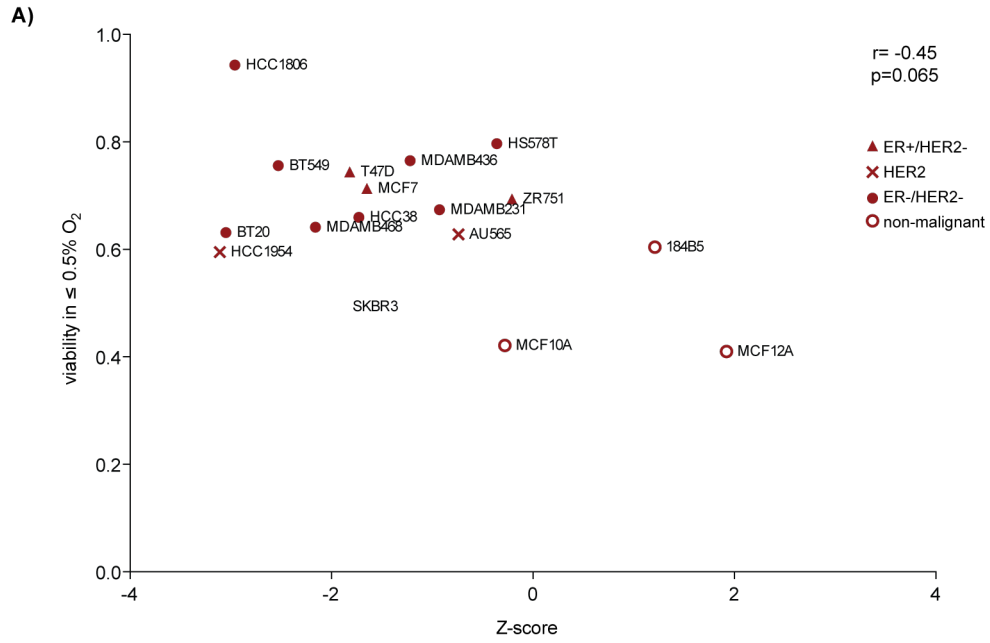

Figure 5-10 Cell viability of breast cell line panel in hypoxia shows weak correlation with sensitivity towards *SLC16A3* silencing

Data from Figure 3.7 was used for the Pearson correlation with data from Figure 5.1.

Figure 5.11

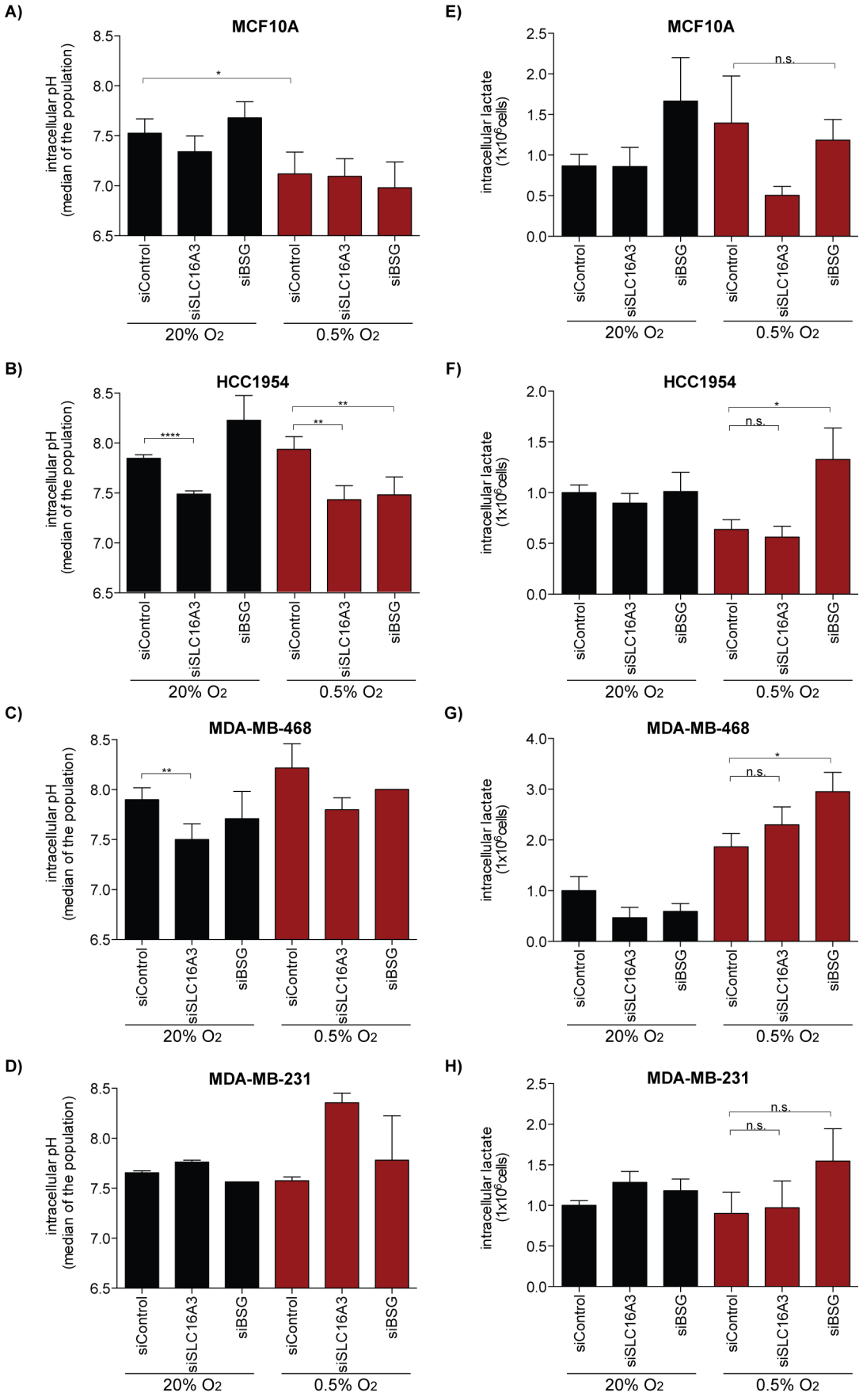
A)
MCF10A
intracellular pH (median of the population)
8.5
8.0
7.5
7.0
6.5
*
siControl
siSLC16A3
siBSG
siControl
siSLC16A3
siBSG
20% O2
0.5% O2
E)
MCF10A
intracellular lactate (1x10^6cells)
2.5
2.0
1.5
1.0
0.5
0.0
n.s.
siControl
siSLC16A3
siBSG
siControl
siSLC16A3
siBSG
20% O2
0.5% O2
B)
HCC1954
intracellular pH (median of the population)
8.5
8.0
7.5
7.0
6.5
****
**
**
siControl
siSLC16A3
siBSG
siControl
siSLC16A3
siBSG
20% O2
0.5% O2
F)
HCC1954
intracellular lactate (1x10^6cells)
2.0
1.5
1.0
0.5
0.0
n.s.
*
siControl
siSLC16A3
siBSG
siControl
siSLC16A3
siBSG
20% O2
0.5% O2
C)
MDA-MB-468
intracellular pH (median of the population)
8.5
8.0
7.5
7.0
6.5
**
siControl
siSLC16A3
siBSG
siControl
siSLC16A3
siBSG
20% O2
0.5% O2
G)
MDA-MB-468
intracellular lactate (1x10^6cells)
4.0
3.0
2.0
1.0
0.0
n.s.
*
siControl
siSLC16A3
siBSG
siControl
siSLC16A3
siBSG
20% O2
0.5% O2
D)
MDA-MB-231
intracellular pH (median of the population)
8.5
8.0
7.5
7.0
6.5
siControl
siSLC16A3
siBSG
siControl
siSLC16A3
siBSG
20% O2
0.5% O2
H)
MDA-MB-231
intracellular lactate (1x10^6cells)
2.5
2.0
1.5
1.0
0.5
0.0
n.s.
n.s.
siControl
siSLC16A3
siBSG
siControl
siSLC16A3
siBSG
20% O2
0.5% O2

Figure 5-11 Depletion of *SLC16A3* decreases intracellular pH levels

Four breast epithelial breast cell lines MCF10A (A,E), HCC1954 (B,F), MDA-MB-468 (C,G), and MDA-MB-231 (D,H) were reverse transfected with siRNA targeting SLC16A3 and cultured under normoxic (black bars) and hypoxic conditions (red bars). (A-D) Three days post-transfection, cells were loaded with SNARF-4F, trypsinised and analysed by FACS to determine the intracellular pH. Displayed is the mean and standard deviation of 2 independent experiments with two independent replicates. (E-F) Three days post-transfection, cells were trypsinised and counted. Of each cell line, $0.5x10^6$ cells were lysed with ddH_2O before intracellular lactate levels were determined using the Biovision lactate detection kit. Displayed is the mean and standard deviation of 2 independent experiments with three biological replicates. Unpaired t-test was used for significance calculations. (*=p≤0.05, **=p≤0.01, ****=p≤0.0001).

Figure 5.12

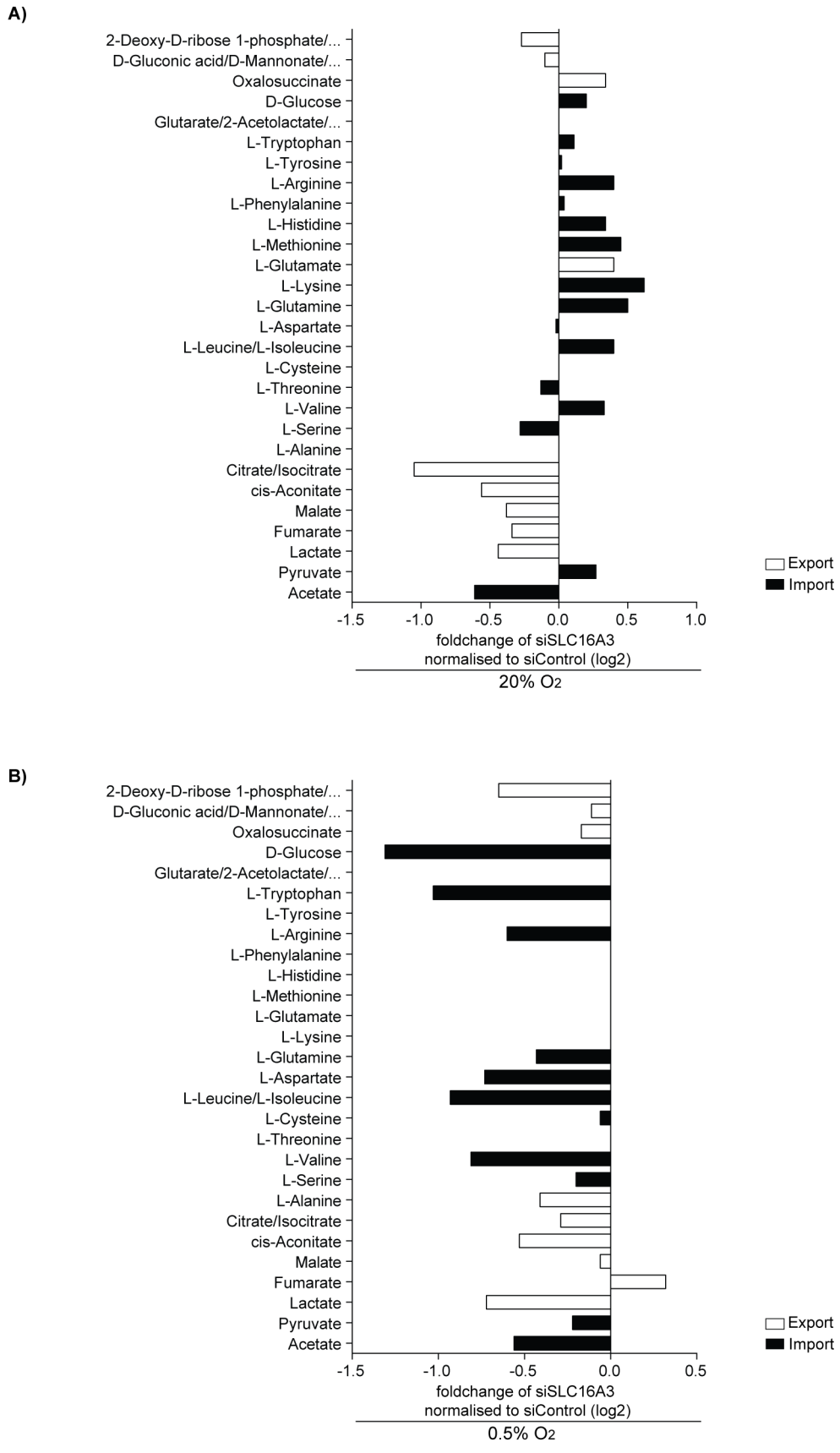
A)
2-Deoxy-D-ribose 1-phosphate/...
D-Gluconic acid/D-Mannonate/...
Oxalosuccinate
D-Glucose
Glutarate/2-Acetolactate/...
L-Tryptophan
L-Tyrosine
L-Arginine
L-Phenylalanine
L-Histidine
L-Methionine
L-Glutamate
L-Lysine
L-Glutamine
L-Aspartate
L-Leucine/L-Isoleucine
L-Cysteine
L-Threonine
L-Valine
L-Serine
L-Alanine
Citrate/Isocitrate
cis-Aconitate
Malate
Fumarate
Lactate
Pyruvate
Acetate
-1.5
-1.0
-0.5
0.0
0.5
1.0
foldchange of siSLC16A3
normalised to siControl (log2)
20% O2
Export
Import
B)
2-Deoxy-D-ribose 1-phosphate/...
D-Gluconic acid/D-Mannonate/...
Oxalosuccinate
D-Glucose
Glutarate/2-Acetolactate/...
L-Tryptophan
L-Tyrosine
L-Arginine
L-Phenylalanine
L-Histidine
L-Methionine
L-Glutamate
L-Lysine
L-Glutamine
L-Aspartate
L-Leucine/L-Isoleucine
L-Cysteine
L-Threonine
L-Valine
L-Serine
L-Alanine
Citrate/Isocitrate
cis-Aconitate
Malate
Fumarate
Lactate
Pyruvate
Acetate
-1.5
-1.0
-0.5
0.0
0.5
foldchange of siSLC16A3
normalised to siControl (log2)
0.5% O2
Export
Import

Figure 5-12 Analysis of metabolite import and export in MDA-MB-468 after *SLC16A3* ablation

MDA-MB-468 cells were reverse transfected with control and SLC16A3 siRNA in triplicate and cultured for 70 hours. Cells were placed in normoxia or hypoxia. Medium was collected at equal time points over a period of 24 hours and used to determine metabolite levels using mass spectrometry (Sebastien Dubuis, ETH, Zurich, Switzerland). The slope of the change in concentration for each metabolite over time was calculated to generate import/export rates and normalised to control transfected cells. Values shown represent the log2-transformed fold change in import/export rate for each metabolite in normoxic (A) and hypoxic (B) cells.

Figure 5.13

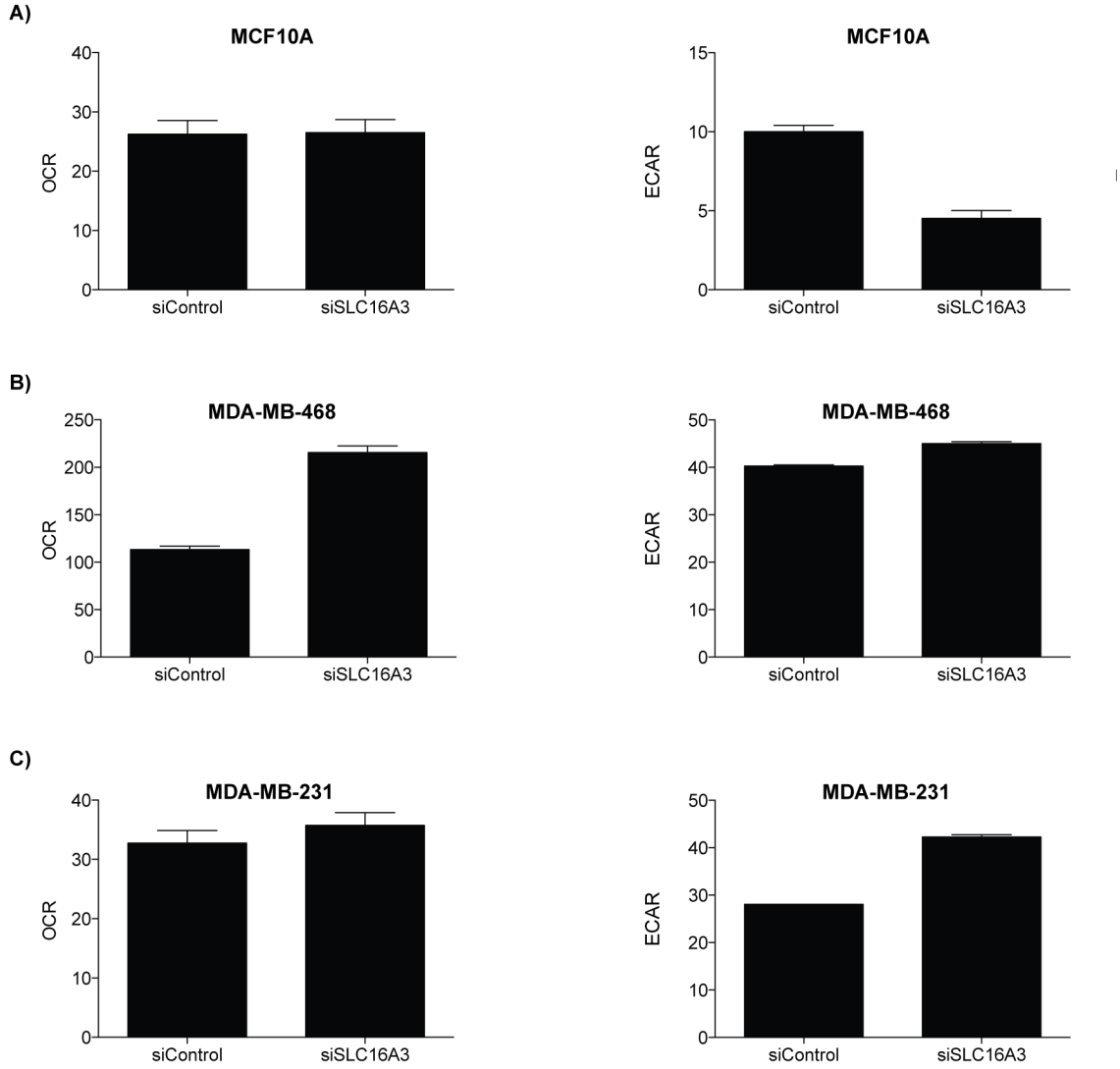

Figure 5-13 OCR and ECAR are influenced by *SLC16A3* abrogation

Three breast epithelial cell lines MCF10A (A), MDA-MB-468 (B), and MDA-MB-231 (C) were reverse transfected with siRNA targeting *SLC16A3* or controls. Two days post-transfection, cells were trypsinised, counted and seeded into Seahorse analysis plates. Basal OCR and ECAR were assessed. Values show mean and SD of one independent experiment with five independent replicates each.

Figure 5.14

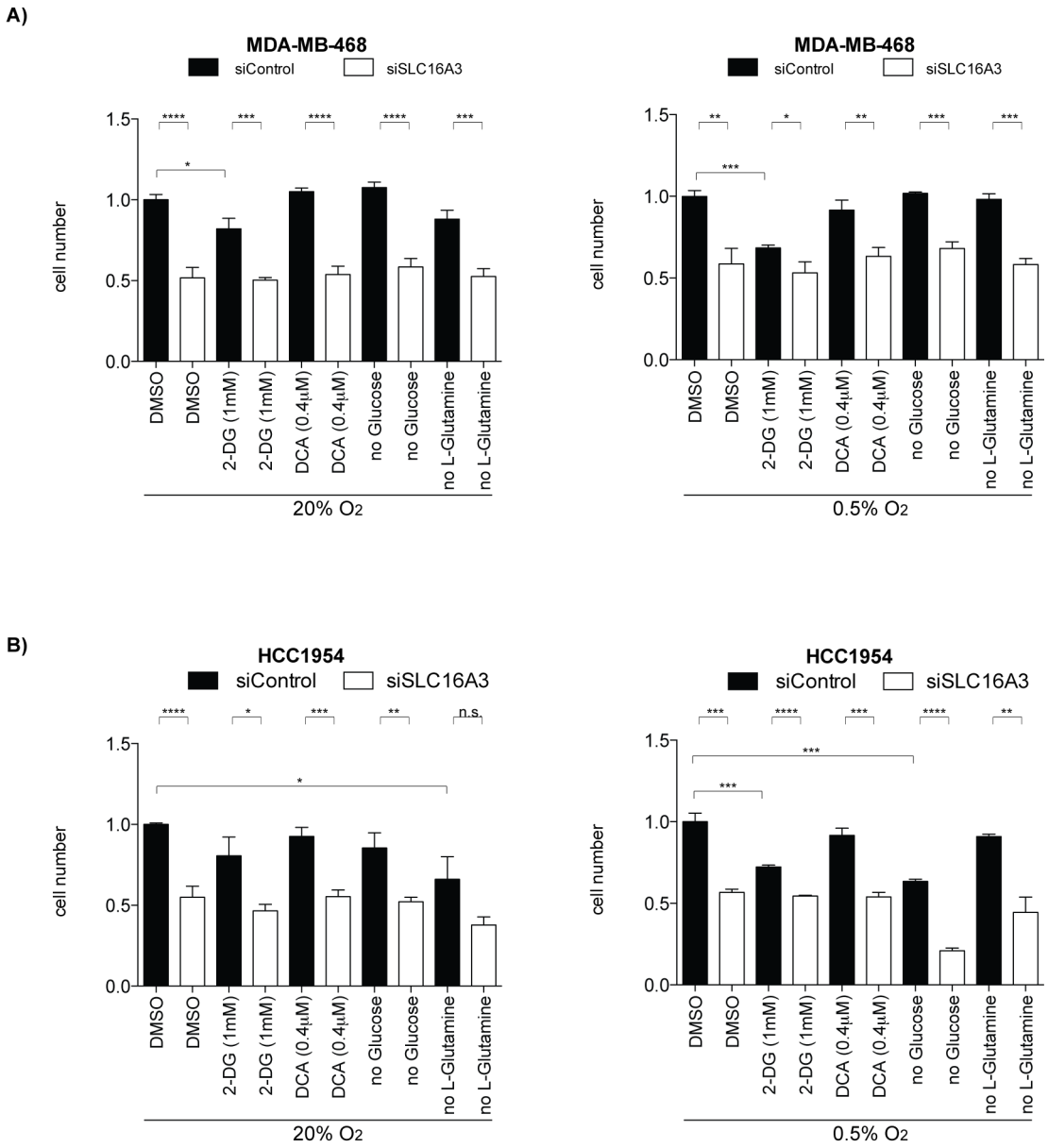

Figure 5-14 Metabolic dependency of the effect of *SLC16A3* depletion on cell viability

The sensitive breast cancer cell lines MDA-MB-468 (A) and HCC1954 (B) were reverse transfected with siRNA targeting *SLC16A3* or controls and cultured under normoxic and hypoxic conditions. Twelve hours post-transfection, cells were treated with different inhibitors or depleted of either glucose or glutamine. 96 hours post-transfection, cells were stained with DAPI and analysed for cell number. Cell number was normalised to siControl-transfected cells. Values show mean and SEM of six independent experiments with one biological replicate each. Unpaired t-test was used (*=p≤0.05, **=p≤0.01, ***=p≤0.001, ****=p≤0.0001)

Figure 5.15

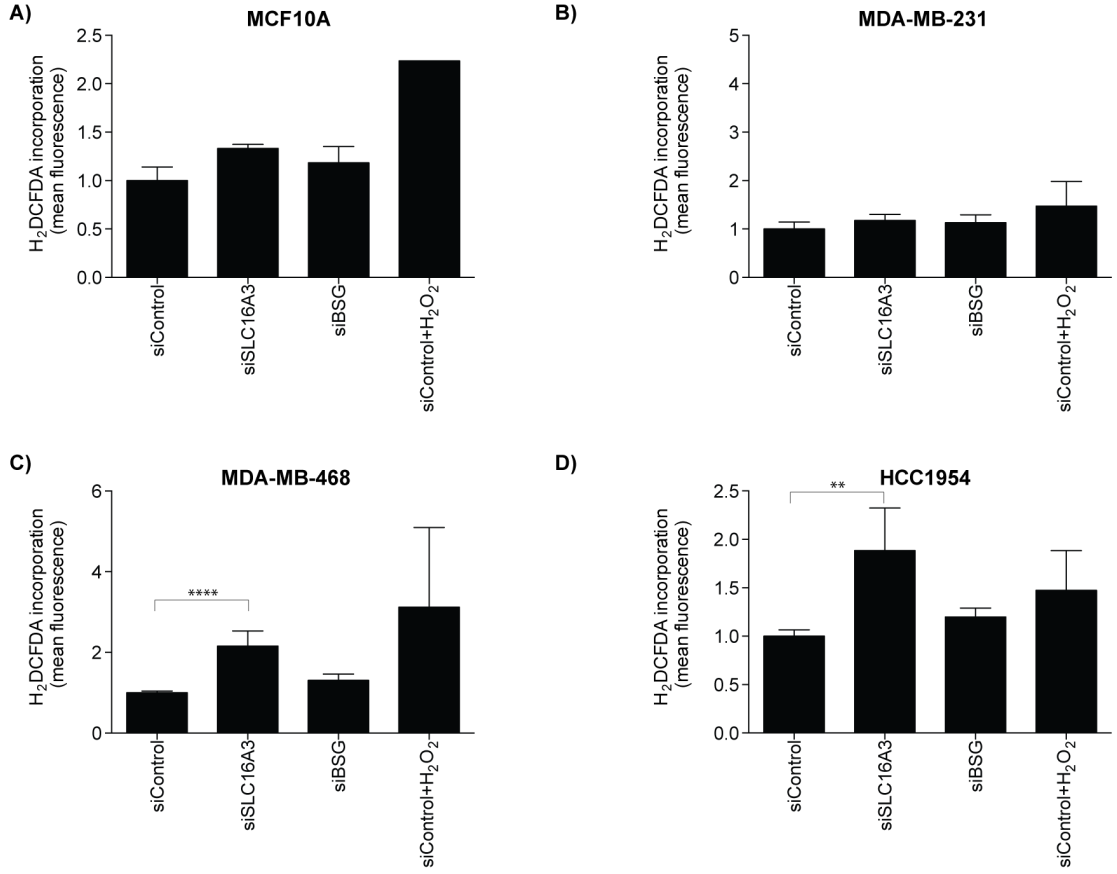

Figure 5-15 ROS levels increase in *SLC16A3* depleted cells

The breast cell lines MCF10A (A), MDA-MB-231 (B), MDA-MB-468 (C) and HCC1954 (D) were reverse transfected with siRNA targeting *SLC16A3* or controls and cultured under normoxic conditions. 72 hours post-transfection, cells were treated with H_2DCFDA and its incorporation was measured by FACS. Mean fluorescence intensity was normalised to that of siControl transfected cells. Values show mean and SEM of three independent experiments with two independent replicates each. Unpaired t-test was used to determine significance. (**=p≤0.01, ****=p≤0.0001)

Figure 5.16

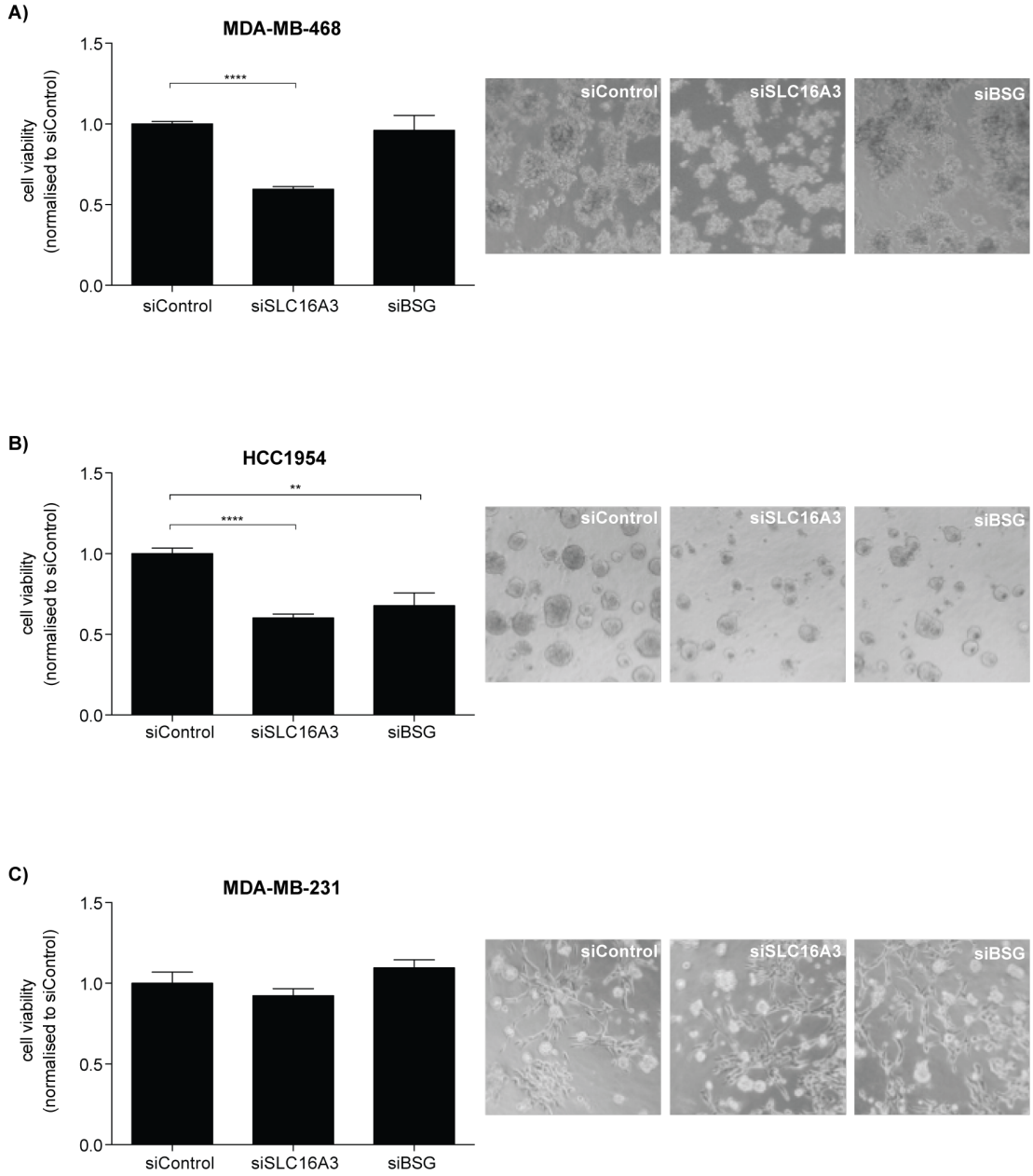

Figure 5-16 Matrigel cultures of breast cells show reduced cell viability after *SLC16A3* silencing

The breast cell lines MDA-MB-468 (A) HCC1954 (B) and MDA-MB-231 were reverse transfected with siRNA targeting *SLC16A3, BSG* or controls and cultured under normoxic conditions. 12 hours post-transfection, cells were trypsinised, counted and embedded on matrigel. The cell viability of cultured cells was assessed with CellTiterBlue assay. Mean fluorescence was normalised to siControl-transfected cells. Values show mean and SEM of three independent experiments with two independent replicates each. Unpaired t-test was used to determine significance (**=p≤0.01, ****=p≤0.0001)

Figure 5.17

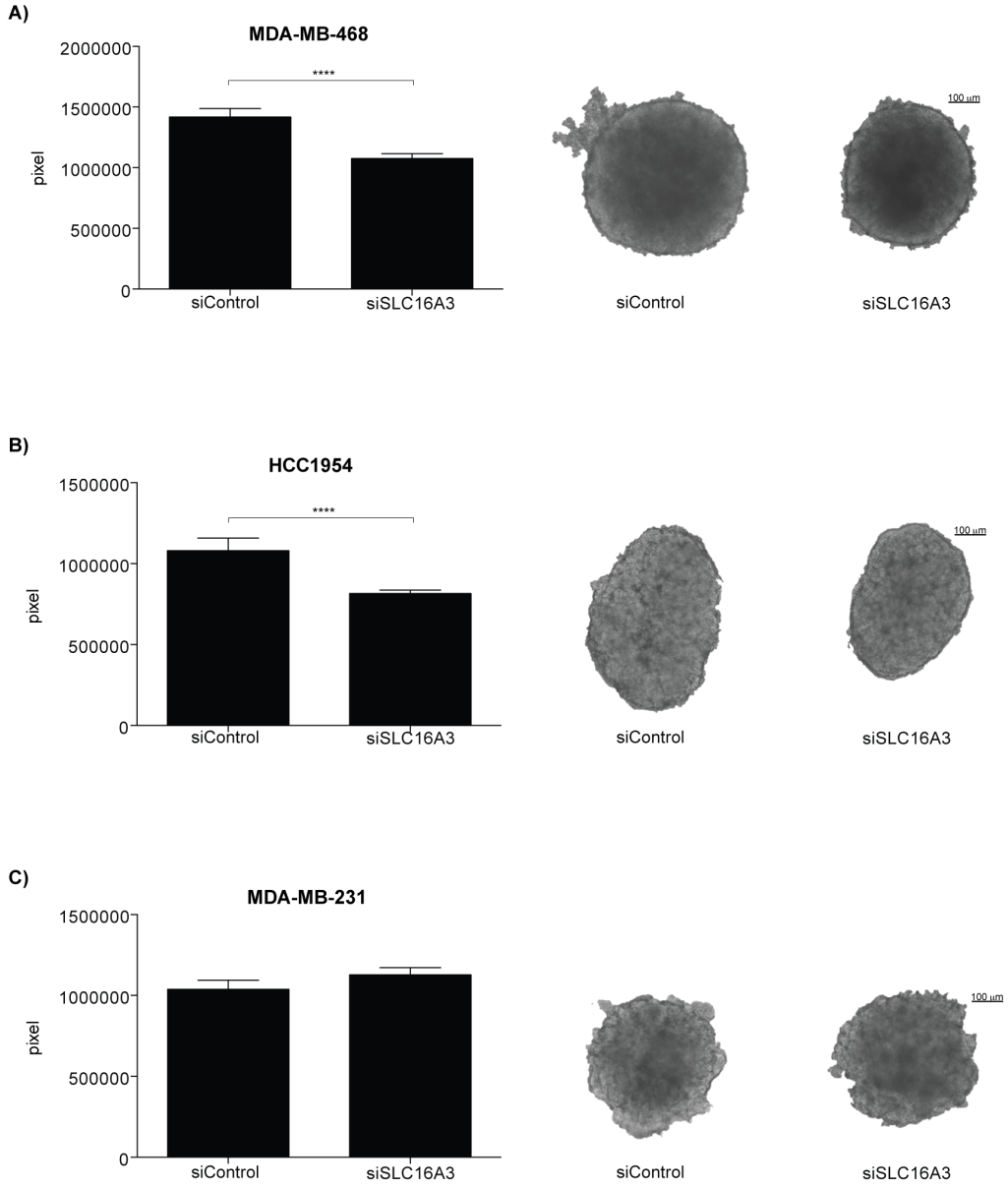

Figure 5-17 Spheroid formation of breast cells shows reduction in size after *SLC16A3* silencing

The breast cell lines MDA-MB-468 (A), HCC1954 (B) and MDA-MB-231 (C) were reverse transfected with siRNA targeting *SLC16A3* or controls and cultured under normoxic conditions. 12 hours post-transfection, cells were trypsinised, counted and incubated with 2% matrigel before centrifugation to initiate spheroid formation. Representative images of spheroids were assessed to determine size and pixel number was quantified with Adobe Photoshop. Mean pixel number of six different spheroids per condition was normalised to spheroids formed by siControl-transfected cells. Unpaired t-test was used to determine significance. (****=p≤0.0001)

Figure 5.18

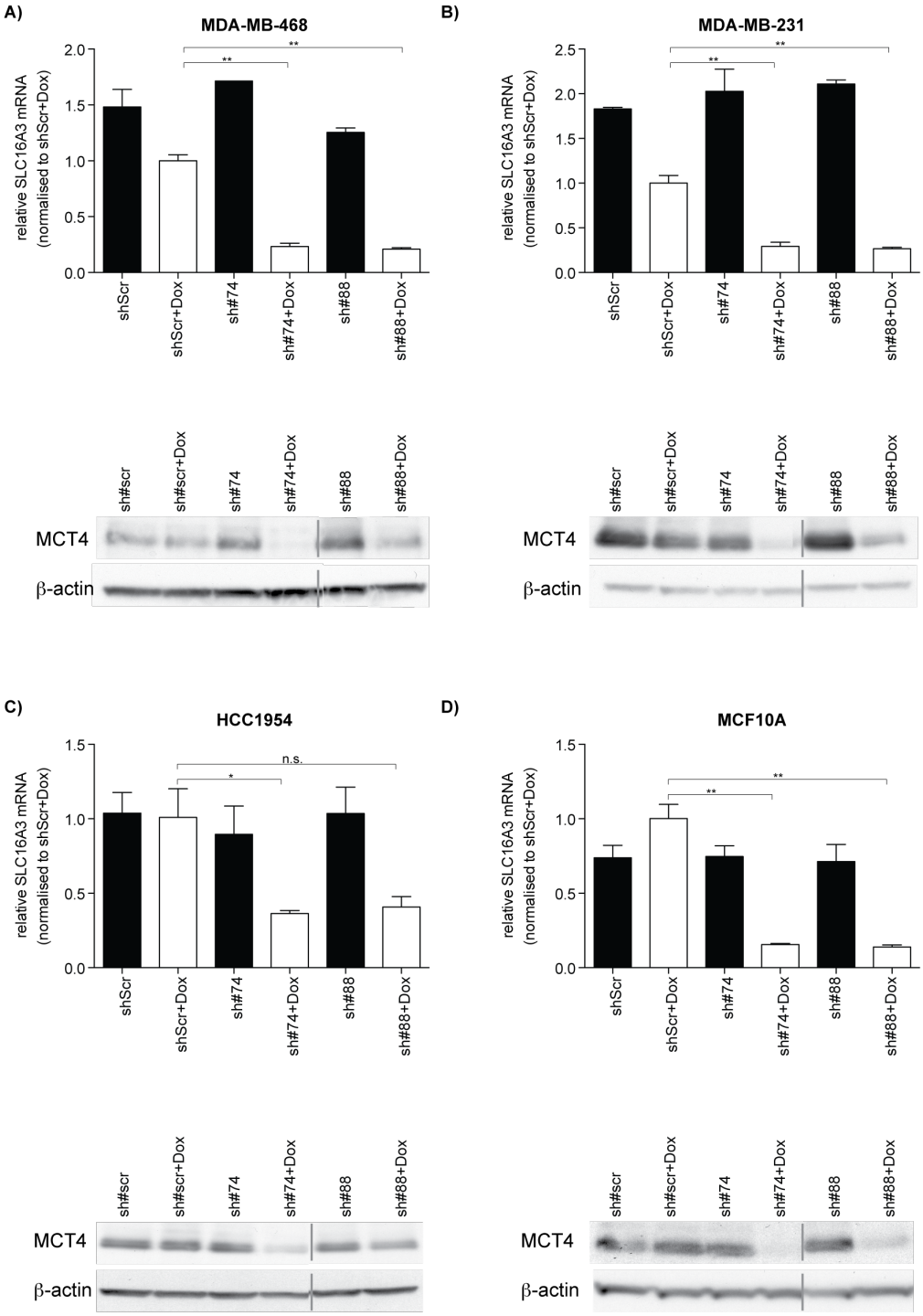

Figure 5-18 *SLC16A3*/MCT4 depletion with shRNA reduces cell viability

The breast cell lines MDA-MB-468 (A), MDA-MB-231 (B), HCC1954 (C), and MCF10A (D) were transduced with lentiviruses expressing two different shRNA sequences targeting *SLC16A3* (#74 and #88) or scrambled control. 12 hours after seeding, cells were treated with doxycycline (dox) or EtOH. Whole cell lysates for total RNA (day 4) and protein (day 6) were harvested and analysed for *SLC16A3*/MCT4 and β-actin expression. Values show mean and SEM of three independent experiments with two biological replicates each. Unpaired t-test was used to determine significance. (*=p≤0.05, **=p≤0.01)

Figure 5.19

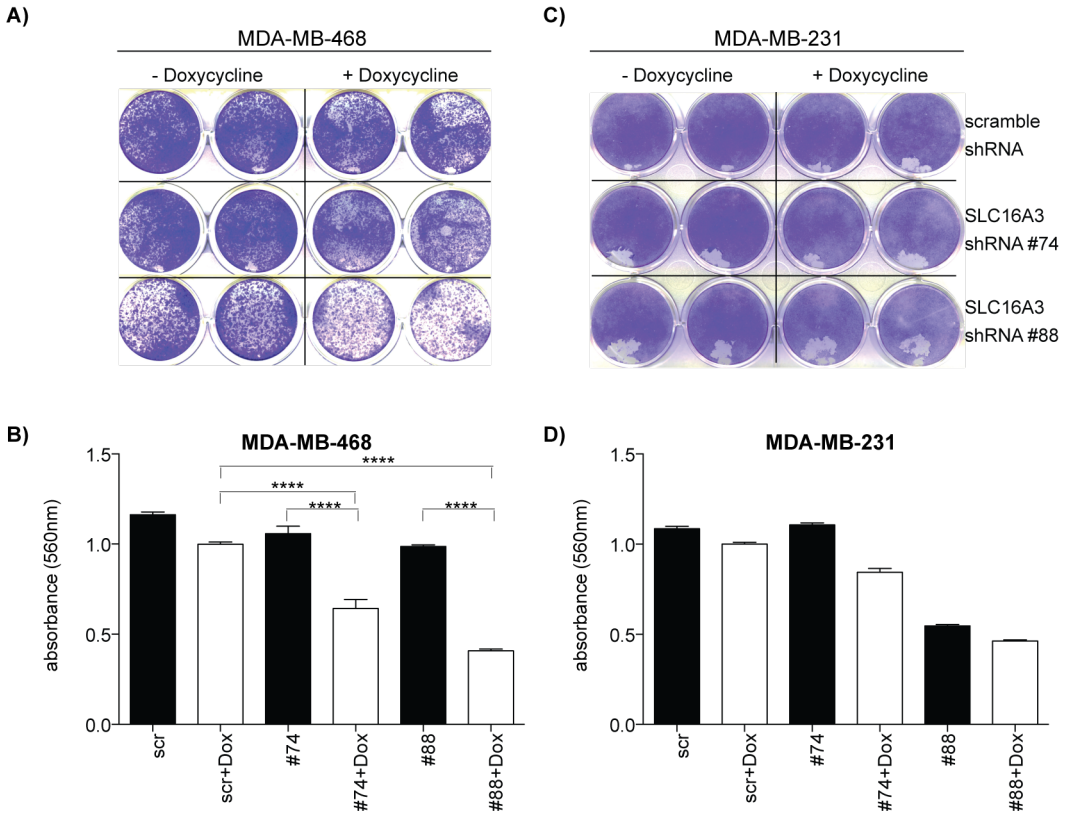

Figure 5-19 Cell viability is reduced in MDA-MB-468 after shRNA-mediated depletion of *SLC16A3*

The breast cell lines MDA-MB-468 (A) and MDA-MB-231 that have been transduced with two different shRNA targeting *SLC16A3* (#74 and #88) or scrambled control were seeded at a density of 10,000 cells per well in a 12-well plate. 12 hours after seeding, cells were either treated with doxycycline (dox) or EtOH. Cell viability was assessed with crystal violet dye at day 10. Representative Images are shown (B) Quantification of staining shown in A. Values show mean and SEM of six independent experiments with three biological replicates each. Unpaired t-test was used to determine significance. (****=p≤0.0001)

Figure 5.20

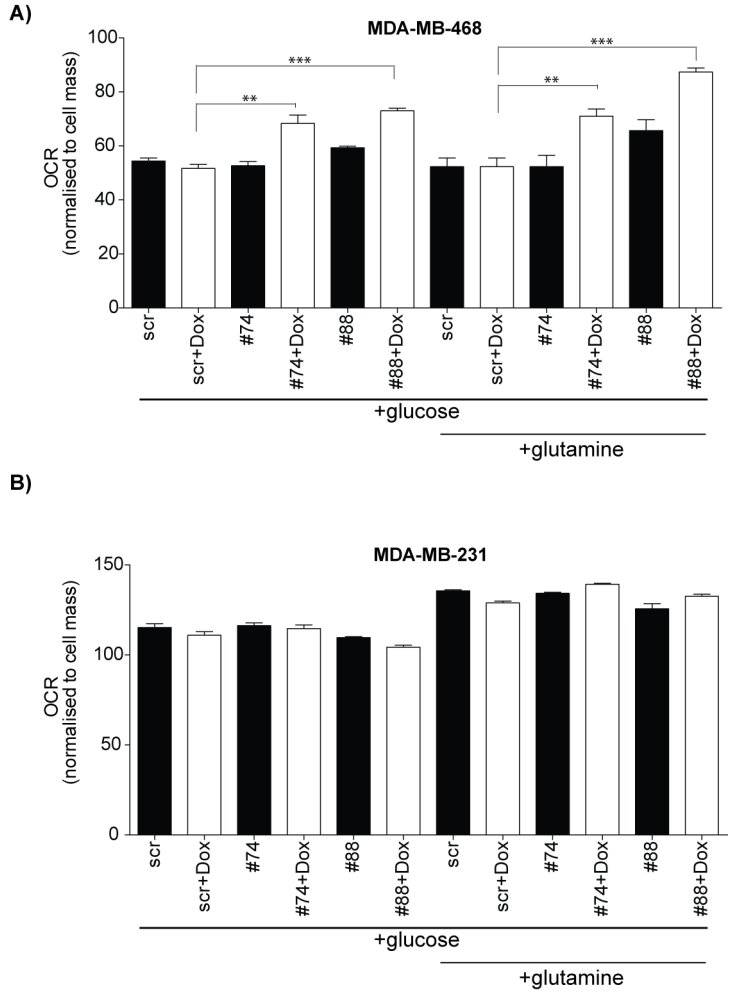

Figure 5-20 *SLC16A3* ablation influences OCR

The breast cell lines MDA-MB-468 (A) and MDA-MB-231 (B) that have been transduced with two different shRNA targeting *SLC16A3* (#74 and #88) or scrambled control were seeded at a density of $0.15x10^6$ cells in a 6-well plate. 12 hours after seeding, cells were treated with either doxycycline (dox) or EtOH. On day 6, cells were trypsinised, counted and plated in Seahorse analysis plates. The following day, cells were deprived of glucose and glutamine for 30 minutes before being placed in Seahorse Bioanalyzer. After measuring the baseline OCR of the cells, 10mM glucose was injected and OCR was measured three times. After this, 2mM glutamine was injected and OCR was measured again three times. Baseline OCR (after glucose and glutamine starvation) was set at 100. All measurements were performed with 6 replicates. Unpaired t-test was used to determine significance. (**=p≤0.01***=p≤0.001)

Figure 5.21

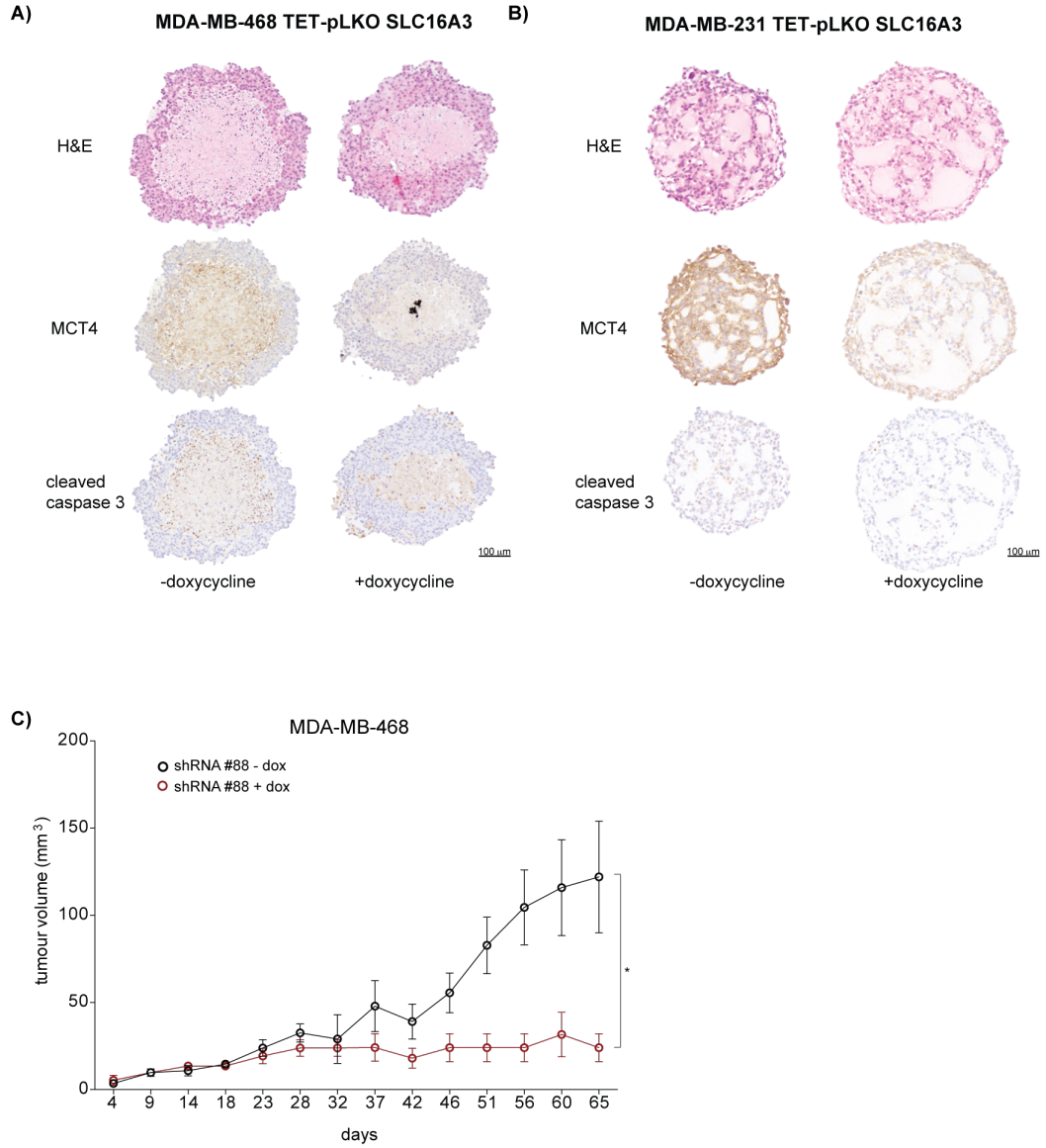

Figure 5-21 SLC16A3 depletion impairs tumour growth *in-vivo*

The breast cell lines MDA-MB-468 (A) and MDA-MB-231 (B) that have been transduced with lentiviruses expressing shRNA targeting SLC16A3 (#88) were incubated with 2% matrigel before centrifugation to initiate spheroid formation and seeded at a density of $0.1x10^4$ cells per well in a low-attachment 96-well plate. 12 hours after seeding, spheroids were either treated with doxycycline (dox) or EtOH. At day 12, spheroids were collected, fixed and processed for H&E and immunohistochemical staining of MCT4 and cleaved caspase 3. Representative images of spheroids are shown here. (C) $1.5x10^6$ cells of the breast cell line MDA-MB-468 transduced with a lentivirus expressing shRNA targeting *SLC16A3* (TET-pLKO SLC16A3 #88) were mixed with with 10% matrigel and injected orthotopically into the mammary fat pad of 8-week old immuno-compromised mice (nu/nu). After tumour initiation (day 10), mice were divided into two cohorts (4 mice in each cohort): one on standard diet while the other cohort was on a doxycycline supplemented diet (0.2g/kg doxycycline in food pellets). Tumours were measured twice per week and growth analysis is plotted here. (*=p≤0.05)

Figure 5.22

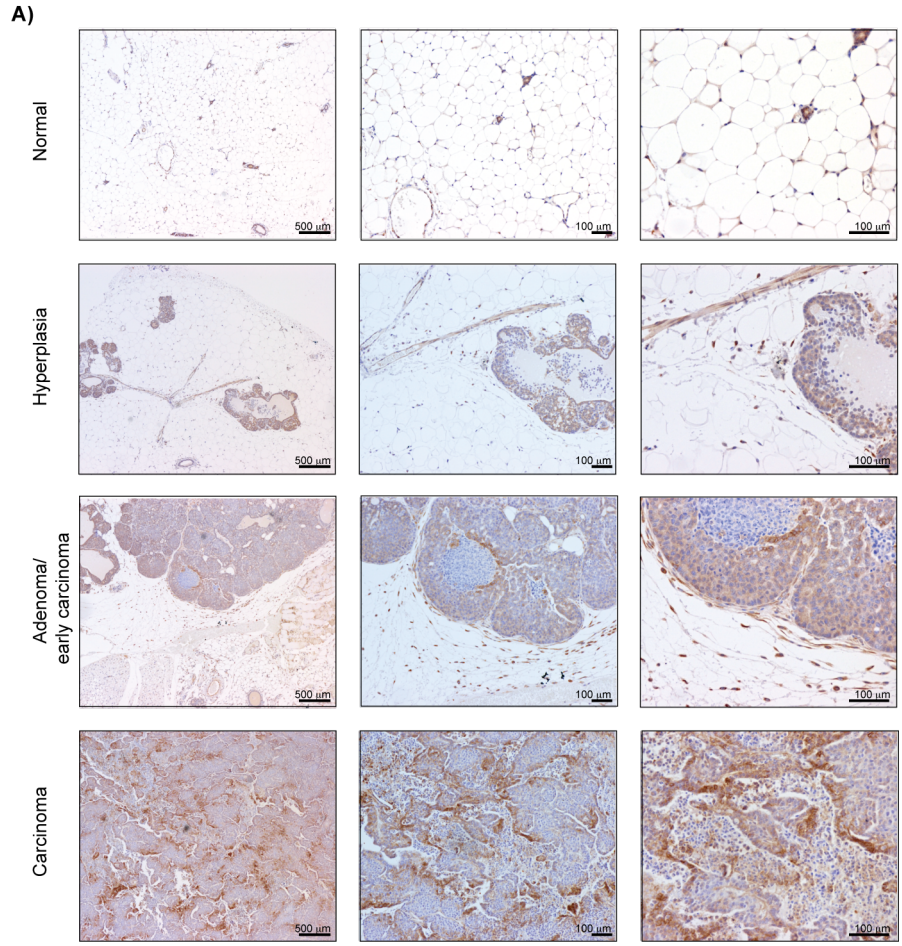

Figure 5-22 MCT4 expression correlates with tumour progression in a *MMTV-PyMT* mouse model

Two slices of the four different stages that develop during *MMTV-PyMT* tumorigenesis were probed with MCT4 according to the staining protocol that was established for the TMA. Here are shown representative pictures of the four different stages at different magnifications.

Figure 5.23

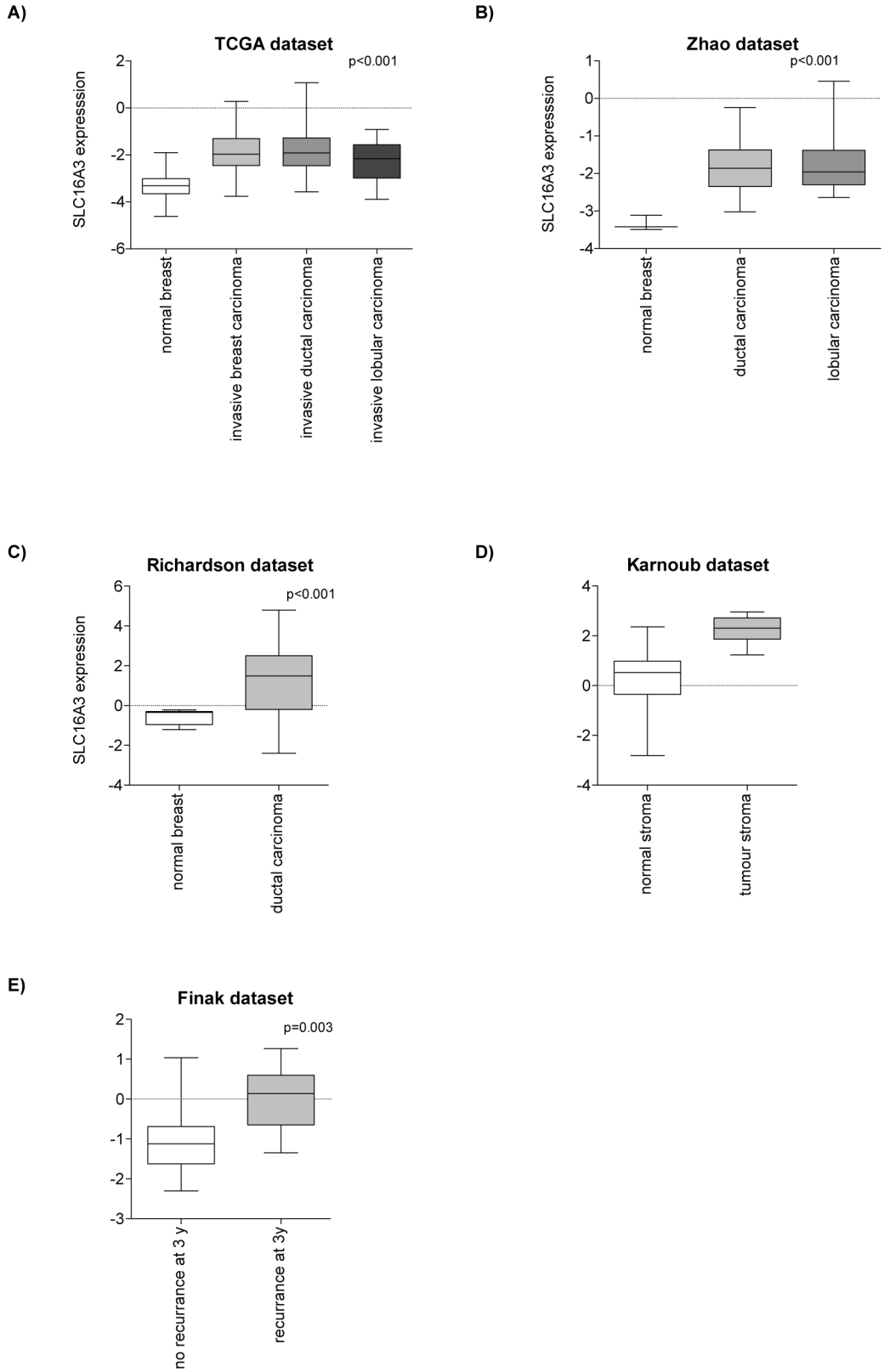
A)
TCGA dataset
p<0.001
SLC16A3 expresssion
2
0
-2
-4
-6
normal breast
invasive breast carcinoma
invasive ductal carcinoma
invasive lobular carcinoma
B)
Zhao dataset
p<0.001
SLC16A3 expresssion
1
0
-1
-2
-3
-4
normal breast
ductal carcinoma
lobular carcinoma
C)
Richardson dataset
p<0.001
SLC16A3 expression
6
4
2
0
-2
-4
normal breast
ductal carcinoma
D)
Karnoub dataset
4
2
0
-2
-4
normal stroma
tumour stroma
E)
Finak dataset
p=0.003
2
1
0
-1
-2
-3
no recurrance at 3 y
recurrance at 3y

Figure 5-23 *SLC16A3* expression in human breast cancer

Oncomine was analysed for studies that included *SLC16A3* expression. The search was based on *SLC16A3* being significantly different between normal and cancer tissue (A-C), cancer vs stroma (D) and recurrence (E).

Figure 5.24

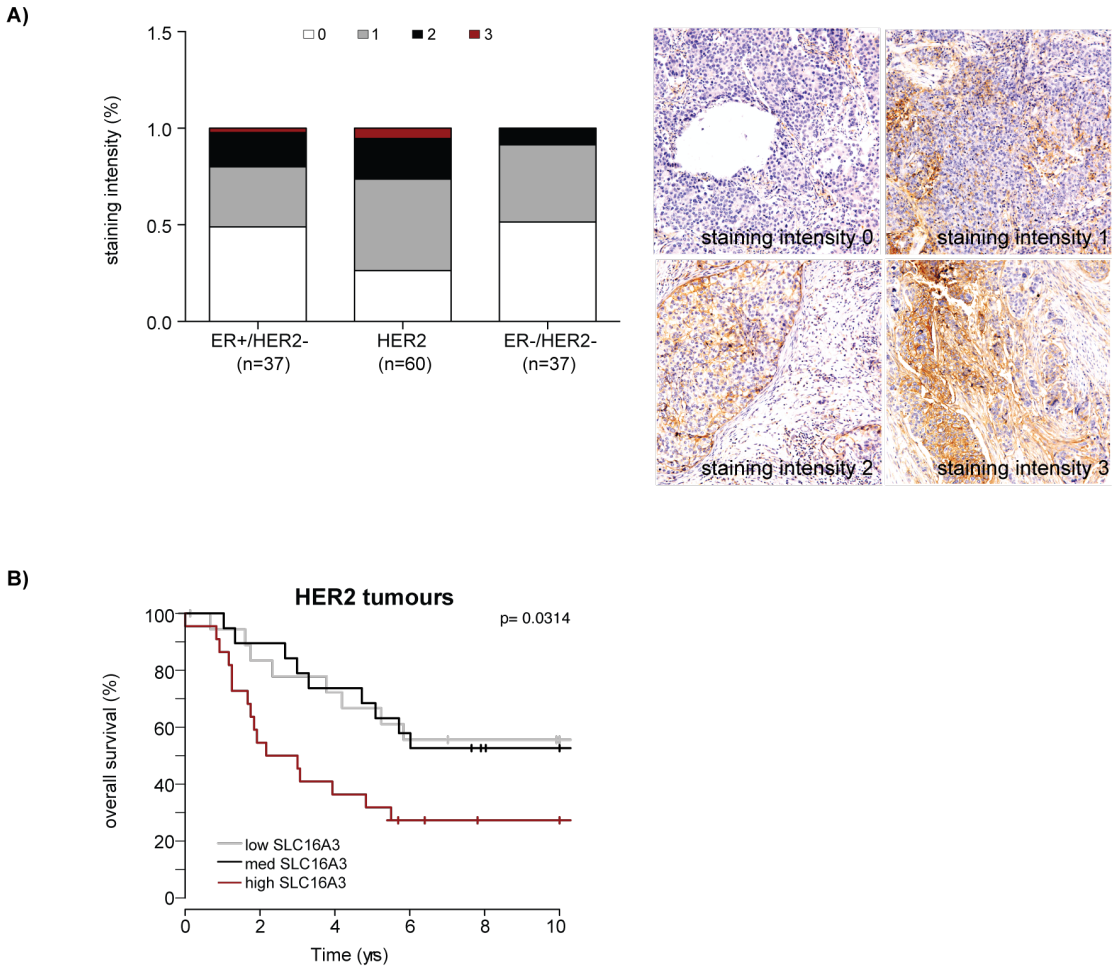

Figure 5-24 SLC16A3 staining in human HER2-positive breast tumours

(A) TMA purchased from BioMax was stained for MCT4 expression and analysed according to the staining intensity. Examples of the different staining intensities are displayed here (from absent 0 to high 3). (B) GOBO analysis of overall survival in HER2-positive tumour samples according to *SLC16A3* expression.

6 Follow up of metabolic genes that are selectively required for the viability of specific subgroups of breast cancer cells

This chapter focuses on preliminary results of six other metabolic enzymes that have been identified by the rank analyses and supervised clustering (see chapter 4). The validated candidate genes were chosen because they occurred in multiple comparisons or of special interest because of isoform specificity in breast cancer subtypes. The ER-positive breast cancer cell lines harbouring *PIK3CA* mutations are sensitive to the ablation of *TKTL1* (see Fig 4.19, whereas ER-negative cell lines showed dependency on *PPAP2A, ME2* and *ALDOA* (see Fig 4.19. The supervised clustering analyses for metabolic parameters (e.g. high glucose utilisation versus low glucose utilisation) identified *PPAP2C* and *ME1* as important genes for cell survival (see Fig 4.19.

6.1 Malic enzyme ablation result in loss of cell number in ER-negative breast cancer cells

Malic enzymes (ME) belong to the family of oxidative decarboxylases. They are highly conserved across different species. The different isoforms of malic enzyme have cofactor specificity and can be also distinguished by their location within the cell. Malic enzyme 1 (ME1) is a $NADP^+$ dependent cytosolic enzyme, whereas malic enzyme 2 (ME2) and malic enzyme 3 (ME3) are located in the mitochondria and utilise NAD^+.
Cytoplasmic malate is converted into pyruvate via ME1. This reaction produces cytosolic NADPH, which is important for the overall NADPH pool. Pyruvate can then re-enter the mitochondria to generate acetyl-CoA via oxidative decarboxylation (MacDonald, 1995). Malate is normally generated in the mitochondria as part of the TCA cycle. The malate-citrate shuttle can transport citrate out of the mitochondria and then further convert it to malate, which can be used for NADPH and pyruvate production (Farfari et al., 2000). Mitochondrial malate can be converted into mitochondrial pyruvate by ME2. This might allow cells to become independent of glucose-derived pyruvate. Other malate consuming enzymes are malate dehydrogenases (MDH1, MDH2) that play roles in oxaloacetate production and the malate-aspartate shuttle. So far, very little is known about the role of malic enzymes in cancer.

6.1.1 Differential expression of malic enzyme 1 and 2 in breast epithelial cell lines

Supervised clustering analysis demonstrated that silencing of *ME1* and *ME2* is detrimental to the survival of some breast cell lines. The comparison of high and low glucose consuming cell lines showed that abrogation for ME1 is necessary for high glucose consuming cell lines under hypoxic conditions (Fig 6.1A). By comparing the different subtypes of breast cancer based on ER expression, *ME2* silencing showed a stronger effect in the ER-negative subgroup under hypoxic conditions compared to normoxic conditions (Fig 6.1B).

Because the silencing of these two isoforms of malic enzyme showed an effect on cell viability (see chapter 4, Fig 4.18B, C), the silencing efficiency was determined for both enzymes after depletion. The silencing efficiency on protein level after depletion of ME1 was good for the siRNA pool as well as each individual sequence in high glucose consuming BT-549 cells and low glucose consuming ER-positive/HER2-negative MCF7 cells. However, the low glucose consuming HER2-positive cell line SK-BR-3 showed only minor silencing efficiency after *ME1* depletion (Fig 6.1C). Comparing the reduction of mRNA with that of protein levels revealed that all four single siRNA duplexes deplete ME1 protein expression but only two sequences silence on mRNA level in BT-549 cells (see chapter 4, Fig 4.19C).

After silencing of *ME2*, a good reduction in protein levels was observed in all three cell lines except for the siRNA oligo #3 in ER-negative/HER2-negative BT-549, ER-positive/HER2-negative MCF7 and HER2-positive SK-BR-3. Of note, MCF7 siControl sample under hypoxia was not blotted correctly onto the membrane due to an air bubble (Fig 6.1D). The protein expression after ME2 depletion did correlate mostly with the RNA profile except for oligo #3 (Fig 4.19B).

To determine the overall expression of both enzymes in the panel of breast epithelial cell lines, expression on mRNA and protein levels were analysed (Fig 6.2). It was observed that the HER2-positive cell lines expressed higher levels of ME1 compared to the other subgroups (Fig 6.2A). This was also observed on protein level (Fig 6.2B). ME2 expression was also higher in the HER2-positive subgroup mainly due to HCC1954 and also in the non-malignant cell lines compared to the ER-positive/HER2-negative and ER-negative/HER2-negative subgroups (Fig 6.2C,D). Of note, *ME2*

mRNA levels were low in BT-549 cells, but their protein expression was high. This might indicate post-transcriptional regulation in these cell lines.

6.1.2 Decrease in cell number after *ME1* silencing is due to apoptosis

To further investigate the reduction in cell number after silencing of *ME1* or *ME2*, caspase activity was determined. In the high glucose consuming cell line BT-549 that is sensitive towards *ME1* depletion, activity of caspases 3 and 7 was observed after *ME1* silencing using ME1 pooled siRNA oligos, or sequences #2 and #3 under normoxic and hypoxic conditions (Fig 6.3A). In contrast, neither MCF7 nor SK-BR-3 that both displayed low glucose consumption showed an induction of apoptosis (Fig 6.3B-C). Ablation of *ME2* under normoxic conditions induced no increase in caspase activity when the pool of four siRNA duplexes was used. However, ME2 siRNA duplexes #2 and #4 caused a small increase in cleaved caspases 3 and 7 in two of the three cell lines (Fig 6.4). Under hypoxic conditions, only the ER-negative/HER2-negative cell line BT-549 showed increased caspase activity after transfection of ME2 siRNA pool or in each of the four individual siRNA duplexes (Fig 6.4A).

Taken together, *ME1* as well as *ME2* ablation causes cells to undergo apoptosis.

6.1.3 Effect of malic enzyme ablation on cellular redox balance

Given that ME1 functions in the cytoplasm to generate NADPH, which is important for glutathione-mediated redox homeostasis, treatment with ROS scavengers was used to investigate whether loss of cell viability after *ME1* depletion is caused by oxidative damage. To demonstrate whether ROS accumulation is compromising cell viability, two ROS scavengers, N-acetylcysteine (NAC) and 4-hydroxy-TEMPO (TEMPO), were therefore tested for their effect on caspase activity (Fig 6.5). Increasing amounts of the anti-oxidant TEMPO diminished the effect of *ME1* depletion on cell viability in BT-549 cells (Fig 6.5A), but not in MCF7 and SK-BR-3 cells as no increase in caspase activity following *ME1* depletion was observed (Fig 6.5C,E). In contrast, the second antioxidant NAC showed no effect on reducing caspase activity after silencing of *ME1* in any of these cell lines (Fig 6.5B,D and F). This might be explained by the different mechanisms of these ROS scavengers. TEMPO is a ROS scavenger that mimics

superoxide dismutase 2 (Sledzinski et al., 1995), whereas NAC is a precursor of L-cysteine and glutathione (Ziment, 1988).

Because of the effect on cell viability after TEMPO treatment, the ROS levels in all three cell lines following *ME1* depletion under both oxygen conditions were determined. BT-549 cells showed elevated ROS levels under hypoxic conditions (Fig 6.6A). No increased ROS levels were detected in MCF7 and SK-BR-3 cells (Fig 6.6B,C).
To evaluate if TEMPO reduces ROS levels, BT-549 cells were cultured under hypoxic conditions and treated with 2 μM TEMPO every 24 h before detecting ROS levels (Fig 6.7). Indeed, BT-549 showed a reduction in ROS levels when treated with TEMPO after *ME1* ablation.
These preliminary experiments indicate that *ME1* is important for cellular redox balance. However, it could be argued that the minor increase in ROS levels might not be sufficient to influence cell survival. An explanation for this could be that the cell death is due to other forms of oxidative damage that were not investigated here. This study only used H_2DCFDA for the detection of ROS. Moreover, the impairment of cell viability might be a result of cumulative ROS over time, rather than an acute effect.

6.1.4 Ablation of ME2 influences the NAD^+/NADH ratio

ME2 is important to generate NADH in the mitochondria for oxidation to produce energy via the electron transport chain. Since *ME2* is a NAD^+-dependent enzyme, it was investigated whether siRNA-mediated depletion of ME2 might cause an increase in the NAD^+/NADH ratio. NAD^+/NADH levels were determined in two independent experiments in the three representative cell lines. Silencing of *ME2* in BT-549 cells resulted in a significant increase of NAD^+/NADH compared to control-transfected cells (Fig 6.8A). This increase was absent or not significant in SK-BR-3 and MCF7 cells (Fig 6.8B,C). The increased NAD^+ levels affected the overall ratio of NAD^+/NADH in the sensitive cell line and might therefore influence other metabolic processes that depend on NADH.

6.1.5 Ablation of *ME1* and *ME2* causes changes in intracellular metabolite levels

The flux of metabolites through enzymatic reactions is regulated by the activity of the enzyme, but also by the availability of the substrate and the concentration of the product. Ablation of an enzyme might lead to a depletion of the product and an accumulation of the substrate. To assess whether ablation of *ME1* and *ME2* causes altered metabolite levels, intracellular metabolites were extracted and analysed by mass spectrometry. Unsupervised clustering of the significant fold changes (log2) are displayed in Figure 6.9. Overall, the cluster analysis distinguished two main sub-clusters across the cell lines after depletion of *ME1* or *ME2* compared to the controls. The first cluster contained intracellular metabolites that show no clear effect or are downregulated, while the second cluster included metabolites that are upregulated in *ME1* and *ME2* silenced cells compared to the controls. Surprisingly, the three metabolites in this cluster are all associated with the TCA cycle. Depletion of *ME2* showed an effect on malate, fumarate, and aspartate in all cell lines under both oxygen conditions. However, *ME1* silencing only affected these metabolites in BT-549 cells under hypoxia. SK-BR-3 cells displayed only a minor increase in these metabolites compared to BT-549 (Fig 6.9).

Collectively, this preliminary data indicate that *ME1* is necessary for cellular redox homeostasis in high glucose consuming cells such as BT-549, but not for the low glucose consuming cell lines. This might lead to growth inhibition via the accumulation of ROS. The ablation of *ME1* affected metabolite levels only under hypoxic conditions, which could suggest impaired cell viability due to increased accumulation of malate, fumarate and aspartate. Interestingly, *ME2* was required for ER-negative/HER2-negative cell lines. Abrogation of *ME2* caused increased NAD^+/NADH levels in BT-549 cells, but all cell lines showed elevated levels of three TCA cycle metabolites. This might suggest that mitochondrial metabolism plays a role in the response to *ME2* silencing. Further experiments are required to understand the role of *ME1* and *ME2* in these breast cancer cell lines.

6.2 ER-driven breast cancer cells harbouring a *PIK3CA* mutation are sensitive to *TKTL1* ablation

Multiple metabolic processes are involved to secure the demand in biomolecules for proliferating cancer cells including the pentose phosphate pathway (PPP). In mammalian cells, the PPP reactions take place in the cytoplasm. There are two main forms of the PPP: the oxidative and the non-oxidative pathway. The oxidative pathway generates approximately two thirds of all NADPH available in a cell. NADPH acts as a reducing power required for biosynthetic reactions such as lipogenesis and is also important to maintain the cellular redox balance. The non-oxidative process is responsible for the generation of pentoses and hexosamines, which are fundamental building blocks for aromatic amino acids and nucleotides.

Transketolase-like 1, an enzyme involved in the non-oxidative PPP, is a homodimer encoded by the *TKTL1* gene. It drives the conversion of sedoheptulose-7-phosphate and D-glyceraldehyde-3-phosphate to D-ribose-5-phosphate and D-xylulose-5-phosphate. This reaction connects the glycolytic pathway with the PPP. Previous work has shown that *TKTL1* is overexpressed in lung, breast and gastrointestinal cancers (Foldi et al., 2007; Kayser et al., 2011; Langbein et al., 2006). The ablation of *TKTL1* led to decrease cell viability in cancer cells (Xu et al., 2009; Yuan et al., 2010). However there are contradictory studies about the role of *TKTL1* and its influence on metabolic processes such as glycolysis (Mayer et al., 2010; Sun et al., 2010). In addition, mutated forms of *TKTL1* have been discovered with a potential role in cancer (Coy et al., 2005).

The supervised clustering analysis of the screen data revealed that the ER-positive breast cancer cells MCF7 and T-47D are more sensitive to *TKTL1* silencing as both cell lines carry a *PIK3CA* mutation. Based on the screen data it was particularly interesting to investigate the role of *TKTL1* under hypoxia. To confirm whether *TKTL1* is selectively required for the survival of ER-expressing breast cancer cells harbouring a *PIK3CA* mutation under hypoxic conditions, the ER-positive/HER2-negative cell lines MCF7 and T-47D and the ER-negative/HER2-negative cell line BT-20, which also harbours a *PIK3CA* mutation, were used to deconvolute the four single siRNA duplexes

for *TKTL1*. The samples were analysed for knockdown efficiency on mRNA level as well as loss of cell number under normoxia and hypoxia (see chapter 4, Fig 18.A, Fig 4.19E). Indeed, MCF7 and T-47D showed a reduction in cell number under hypoxia whereas BT-20 showed no loss of viability despite effective knockdown on mRNA level. This suggests that expression of ER is important for the sensitivity to *TKTL1* silencing.

Given that ER-positive/HER2-negative breast cancers are mostly driven by the expression of *ESR1* and estrogen regulated genes, it was aimed to elucidate the contribution of *ESR1* and estrogen regarding the *TKTL1* dependency in these cell lines. At first, *ESR1*, the gene encoding the estrogen receptor was ablated using siRNA. Silencing of *ESR1* in MCF7 and T-47D cells under normoxic and hypoxic conditions caused a reduction in cell number by 25-30% in MCF7 and T-47D cells. BT-20 cells showed only a minor response to *TKTL1* silencing. There was no additive effect of co-silencing *TKTL1* and *ESR1* they both genes affect the same pathway. This might propose that *TKTL1* is downstream of ER.

To investigate this possibility, *TKTL1* expression in the ER-positive/HER2-negative cell lines MCF7 and T-47D was determined by using an antagonist of estrogen, 4-hydroxy-tamoxifen, that inhibits the transcriptional activity of ER and promotes its proteasomal degradation (Osborne and McGuire, 1979). Treatment with 4-hydroxy-tamoxifen caused a reduction in TKTL1 mRNA expression in MCF7 and T-47D under hypoxia, but not under normoxia (Fig 6.11). To further assess if TKTL1 expression is dependent on ER, MCF7 and T-47D were treated with the ER ligand 17β-estradiol. In MCF7 cells, treatment with 17β-estradiol, which downregulates ERα through ligand-mediated proteasomal degradation (Fan et al., 2004), led to the downregulation of *TKTL1* expression on mRNA level (Fig 6.11B). However, the response to 17β-estradiol in T-47D was not conclusive (Fig 6.11D). Further experiments are needed to determine if *TKTL1* is regulated by an ER-dependent mechanism and to elucidate the role of TKTL1 in ER-positive breast cancer cells.

Collectively, these findings indicate that *TKTL1* is a candidate gene for ER-positive breast cancer cell lines harbouring a *PIK3CA* mutation. *TKTL1* expression was repressed by treatment with the estrogen antagonist 4-hydroxy-tamoxifen. Moreover,

TKTL1 expression was decreased after 17β−estradiol stimulation. However, *TKTL1* was not among the genes identified to contain an estrogen response element (ERE) in their promotors (Carroll et al., 2006). This might suggest a more complex mechanism rather than a direct regulation.

It should be noted that the ER-positive cell lines that are sensitive to *TKTL1* ablation also harboured *PIK3CA* mutations. ZR-75-1 cells belonging to the ER-positive/HER2-negative subtype but do not carry a *PIK3CA* mutation were insensitive to *TKTL1* silencing. It is therefore possible that *PIK3CA* and ER act in combination to induce the observed phenotype.

6.3 Aldolase A

Altered glycolytic flux is one hallmark of cancer metabolism and metabolic enzymes involved in glycolysis are upregulated in many different cancer types. One of these is Aldolase A, which converts 6-carbon-metabolites (F-1,6-BP, F-1-P or sedoheptulose-1,7-phosphate) into the 3-carbon-molecules dihydroxyacetonphosphate and glycerate-3-phosphate.

There are three different genes coding for aldolases (A, B, and C) in mammals. The expression of aldolase isoforms varies across different tissues. *ALDOA* is constitutively expressed in most tissues, *ALDOB* is expressed mainly in hepatic, renal and small intestinal tissue (Lebherz and Rutter, 1969) whereas *ALDOC* is found in smooth muscle tissue and the brain (Baron et al., 1969) (Penhoet et al., 1969)
Aldolase A has been identified as a direct transcriptional target of HIF1α. Moreover its substrate F-1,6-BP shares its binding to *ALDOA* with a inositol-3-phosphate (IP3) binding site (Koppitz et al., 1986).

Studies in *saccharomyces cerevisae* demonstrated that mutants in *ALDOA* show severe growth defects and are not viable (Giaever et al., 2002). Moreover, *ALDOA* is overexpressed in malignant tumours (Tomonaga et al., 2004; Tsunematsu et al., 1968).
Interestingly, human aldolases have also been linked to be involved in other cellular functions that are distinct from its role in metabolism (‘moonlighting’) (Waingeh et al.,

2006). Aldolase has been shown to interact with actin *in-vitro* and *in-vivo* independent from its metabolic function (Wang et al., 1996; Wang et al., 1997).

6.3.1 Aldolase A is important for the survival of ER-negative/HER2-negative cell lines under hypoxic conditions

One of the candidate genes identified through supervised clustering analysis using ER and HER2 as a parameter was Aldolase A (see chapter 4). Depletion of *ALDOA* was selectively detrimental to ER-negative/HER2-negative cell lines under normoxia and hypoxia (Fig 6.12A).

To confirm the effect of *ALDOA* ablation in these cells, the non-malignant cell line MCF12A, the HER2-positive cell line SK-BR-3 and the ER-negative/HER2-negative cell lines MDA-MB-231 were used to test different siRNA sequences targeting *ALDOA*. ALDOA protein levels were substantially reduced after siRNA transfection in MCF12A and MDA-MB-231 cells, while SK-BR-3 cells only showed minor effects. To confirm the on-target effect of ALDOA siRNA, ALDOA siRNA duplexes from another provider were used and similar results were obtained (Fig 6.12B).

To investigate if the expression of ALDOA across the panel of breast epithelial cell lines caused the different levels of reduction in protein, RNA and protein expression was determined (Fig 6.13). Interestingly, overexpression of *ALDOA* was observed in the ER-negative/HER2-negative and non-malignant cell lines compared to the other subtypes (Fig 6.13A). However, the protein expression profile did not correlate with the mRNA expression levels, raising the possibility of post-transcriptional regulation (Fig 6.13B).

Because *ALDOA* has been identified as a HIF1α target (Duvel et al., 2010), all breast cell lines were cultured under normoxic and hypoxic conditions to investigate if *ALDOA* is induced under hypoxia. Indeed, preliminary results show that 16 out of 17 breast epithelial cell lines upregulated *ALDOA* expression under low oxygen conditions. However, HCC38 did not show this induction (Fig 6.12C). Further studies are required to confirm this finding.

In summary, *ALDOA* was identified as a candidate gene that was selectively required for the survival of ER-negative/HER2-negative cell lines. Deconvolution confirmed that 3 out of 4 siRNA duplexes show this effect. ER-positive/HER2-negative and HER2-positive cell lines were less sensitive to the depletion of *ALDOA* despite efficient knockdown of expression. These findings suggest that *ALDOA* inhibition could potentially target only ER-negative/HER2-negative cell lines. However, the mechanism by which *ALDOA* supports cell viability still needs to be elucidated.

6.4 Lipid phosphate phosphatases

Lipid phosphate phosphatases (LPPs) belong to the phosphatase super family. These integral membrane proteins are dephosphorylating various lipid phosphates such as sphingosine-1-phosphate (S-1-P), ceramide-1-phosphate and phosphatic acid (PA). LPPs regulate lipid components that can act as signalling molecules. They generate active second messenger signalling molecules (e.g. ceramide, sphingosine and diacylglycerol) that affect cell proliferation, migration and cell survival (Roberts and Morris, 2000; Sciorra and Morris, 2002).

There are three different isoforms of LPP (Waggoner et al., 1999). Each isoform is encoded by a separate gene: *PPAP2A* encodes LPP1 (Kai et al., 1996), *PPAP2B* codes for LPP3 and *PPAP2C* codes for LPP2 (Brindley et al., 2002). The three isoforms have different substrate specificity and are expressed in a tissue specific manner. LPP1 and LPP3 are constitutively expressed in most tissues. These two isoforms show high affinity towards PA and lysophosphatic acid (LPA), whereas LPP2 shows higher affinity towards S-1-P. LPP2 expression has been shown to be restricted to brain, placenta and pancreatic tissue (Pyne et al., 2004).

The effect of ablation of LPPs has been demonstrated in different studies. Deletion of LPP3 mice is embryonic lethal (Escalante-Alcalde et al., 2003). In contrast, mice deficient for LPP2 are viable and fertile and show no abnormal phenotype (Zhang et al., 2000). The role of LPP1 during development has not been elucidated. However, LPP1 expression in transgenic mice resulted in a different phenotype. These mice are smaller and show abnormal fur growth (Yue et al., 2004).
It is has been proposed that some LPP isoforms may play a role in cancer. A study by Imai and colleagues showed that overexpression of LPP3 reduces growth of ovarian cancer cells (Imai et al., 2000). Moreover, LPP1 is involved in platelet-derived growth factor (PDGF) mediated induction of cell migration in mouse embryo fibroblasts (Long et al., 2006) and has been shown to affect ERK signalling and cell division (Jasinska et al., 1999).

6.4.1 Lipid phosphate phosphatases 1 and 2 are necessary for the survival of breast cancer cells

PPAP2A and *PPAP2C* have been identified as candidate genes in the siRNA screen (see chapter 4) in breast cell lines under normoxic and hypoxic conditions. Sensitivity to PPAP2A depletion was more prevalent in the ER-negative/HER2-negative subtype under normoxia (Fig 6.14A). In contrast, resistance towards *PPAP2A* ablation was observe in the ER-positive/HER2-negative cell lines under normoxic conditions (see chapter 4, Fig 4.14C). Silencing of *PPAP2C* showed a stronger effect in high oxygen consuming cells (mostly ER-positive and HER2-positive cell lines) compared to low oxygen consuming cell lines (mostly ER-negative/HER2-negative cancer cell lines) under hypoxic conditions (Fig 6.14B).

To test if *PPAP2A* and *PPAP2C* are differentially expressed across the breast epithelial cell lines, mRNA levels were analysed. *PPAP2A* and *PPAP2C* display strong differences in their expression across the cell line panel. However, the cancer cell lines BT-549, MDA-MB-468, MDA-MB-231, HCC1806, T-47D and HCC38 show high levels of *PPAP2A* mRNA (Fig 6.14C). *PPAP2C* expression was low across all cell lines except for HCC38 (Fig 6.14D).

6.4.2 Loss of cell number after *PPAP2A* or *PPAP2C* silencing is accompanied by PARP cleavage

Next, it was aimed to elucidate if the decrease in cell number is due to apoptosis. Therefore, whole protein lysates were analysed for cleaved PARP. The abrogation of *PPAP2A* induced PARP cleavage only in the ER-negative/HER2-negative cell line BT-549, but not in the non-malignant cell line MCF12A and the ER-positive/HER2-negative cell line MCF7. It should be noted that BT-549 cells show minor levels of PARP cleavage even in the mock or siControl transfected samples (Fig 6.15).
Interestingly, reduction of cell number after *PPAP2C* silencing correlated with induction of cleaved PARP as BT-549 and MCF7, the two cell lines sensitive to *PPAP2C* ablation, show increased PARP cleavage (Fig 6.15).

This preliminary data indicates that *PPAP2A* might be important for the survival of some ER-negative/HER2-negative cell lines and *PPAP2C* for high oxygen consuming

cells. This is in line with a study from Flanagan and colleagues suggesting *PPAP2C* to be a putative therapeutic target in cancer (Flanagan et al., 2009). However, further studies are needed to investigate the mechanism by which *PPAP2A* and *PPAP2C* support cancer cell growth and survival, and how the differential sensitivity of some cancer cell lines is determined.

6.4.3 Discussion

This study aimed to identify discreet metabolic dependencies by ablation of metabolic enzymes that are necessary for the survival of distinct subgroups of breast cancer cell lines. By using the siRNA screen (see chapter 4), 7 genes have been taken forward for further evaluation. It was found that two isoforms of malic enzyme (ME) play an important role in distinct subgroups of breast epithelial cell lines. *ME1* and *ME2* were validated and it was found that these isoform are highly expressed in HER2-positive cells compared to other cell lines within the panel. *ME1* was selectively required for the survival of cell lines with high glucose uptake, while *ME2* was mainly important for the survival of ER-negative cell lines (HER2-positive and ER-negative/HER2-negative) but was also found in several other comparisons. The preliminary results show that ablation of *ME1* in BT-549 results in increased caspase activity, suggesting that the cell death in response to *ME1* ablation involves apoptosis. *ME1* is one of the enzymes that contribute to the cellular NADPH pool. This is important for biosynthetic processes and for sequestering of ROS, including mitochondrial superoxide. Indeed, induction of ROS levels after *ME1* silencing was rescued when cells were supplemented with the ROS scavenger TEMPOL, a mimetic of mitochondrial superoxide dismutase, inhibiting the induction of apoptosis, supporting cell survival.

In this study, it was also postulated that depletion of ME2 could be important for the survival of different cancer subgroups. It was found that *ME2* is selectively required for ER-negative, ER-negative/HER2-negative and high glucose consuming cell lines. However, the mechanism by which *ME2* contributes to cell viability is likely to be different to that of *ME1*, given that *ME2* is a NAD^+-dependent enzyme compared to the $NADP^+$- dependent *ME1*. Furthermore, both enzymes have different localisation within

the cell with ME1 being cytoplasmic while ME2 is localised to the mitochondria. Interestingly, depletion of *ME2* in BT-549 cells increased the cellular NAD^+/NADH ratio, confirming its enzymatic function.

When publicly available datasets of breast cancer were studied (i.e. Oncomine) no significant overexpression of either *ME1* or *ME2* was found (either between the differing subgroups or cancer to non-cancer samples). This might suggest that the activity of these enzymes is more important than their mRNA expression levels. It would be of great interest to investigate the effect of *ME1* or *ME2* silencing over a longer period of time using shRNA to determine their role in long-term cell survival and to study their contribution to tumour cell growth in an *in-vivo* setting (i.e. xenograft). Although not much is known about the different isoforms of malic enzyme in cancer, it would be of significant interest to determine if these enzymes can compensate for each other.

The siRNA screen used was biased towards hormone receptor negative breast cancer cell lines (ER-negative/HER2-negative), as breast tumours from this subtype (triple negative) are generally difficult to treat and have the least favourable clinical outcome.

While many studies have addressed the role of glycolytic enzymes in cancer, few studies have investigated the dependency of cancer cells on the activity of the PPP. The siRNA screen identified enzymes of this pathway that were selectively required for the survival of ER-positive/HER2-negative breast cancer cells. Of particular interest is *TKTL1*, an isoform of transketolase, which is part of the non-oxidative arm of the PPP. *TKTL1* was selectively required for the survival under hypoxia of ER-positive/HER2-negative breast cancer cells harbouring a *PIK3CA* mutation. Although the molecular mechanism by which *TKTL1* supports cell survival still needs to be elucidated, it can be hypothesised that *TKTL1* depletion could result in reduced levels of glyceraldehyde-3-phosphate and F-6-P, which are required to maintain glycolytic flux and provide intermediates for lipid synthesis during cell growth. *TKTL1* depletion might also lead to a reduction in cellular pyruvate that is necessary for biosynthetic processes and energy production. It is also notable that the non-oxidative PPP is necessary for the synthesis of ribose-5-phosphate required for nucleotide biosynthesis (Tong et al., 2009).

It would be of great interest to investigate other breast cell lines derived from ER-positive breast cancer to see if they exhibit a similar dependency on *TKTL1*, given that over two thirds of diagnosed breast cancer patients in the UK present with ER-positive disease. Moreover, other cancer types such as ovarian and endometrial cancers are also driven by estrogen and could show similar dependencies. Many of these gynaecological cancers also harbour *PIK3CA* mutations, and *TKTL1* might also play a role in these cancers (Krockenberger et al., 2007). Previous immunohistochemical studies have found a correlation between AKT expression and TKTL1 levels (Volker et al., 2008).

The glycolytic enzyme *ALDOA* was identified to be selectively required for ER-negative/HER2-negative cell lines. *ALDOA* is known to be a downstream target of mTOR/HIF signalling. Given that the ER-negative/HER2-negative cell lines display high proliferative capacity compared to the other breast cancer subtypes, it might be expected that these cell lines are highly dependent on *ALDOA* expression. ALDOA may be important to maintain the flux from 6-carbon- to 3-carbon-metabolites within the glycolytic process. Depletion of *ALDOA* may therefore arrest cells as not enough metabolic intermediates are generated to support rapid proliferation. This hypothesis has to be further investigated.

Other interesting candidate genes were the two isoforms of an enzyme involved in lipid signalling. The lipid phosphate phosphatase *PPAP2A* was selectively required for viability of ER-negative cell lines in normoxia, while *PPAP2C* was selectively required for cell lines that show high oxygen consumption. These enzymes are important for the generation of specific lipid species (i.e. DAG), which are important in the activation of second messenger signalling molecules, such as PKC family members, that are known to be activated in cancers and promote tumour progression. Perturbation of the downstream signalling of these signalling intermediates might prevent the communication between extracellular stimuli and intracellular signalling cascades. Moreover, lipid biosynthesis, membrane fluidity and architecture might be altered resulting in cells not having enough lipids for proliferation. This is very speculative, and investigating the effect of *PPAP2A/C* isoforms on processes such as ER-stress, which is

activated when lipid synthesis is disrupted, would be of significant interest, although this requires further study.

In summary, the siRNA screen revealed a number of different metabolic dependencies in breast cancer cell lines. Further work is needed to elucidate the molecular mechanisms by which these enzymes support the viability of cells within the different clinical, genetic and phenotypic subtypes of breast cancer.

Figure 6.1

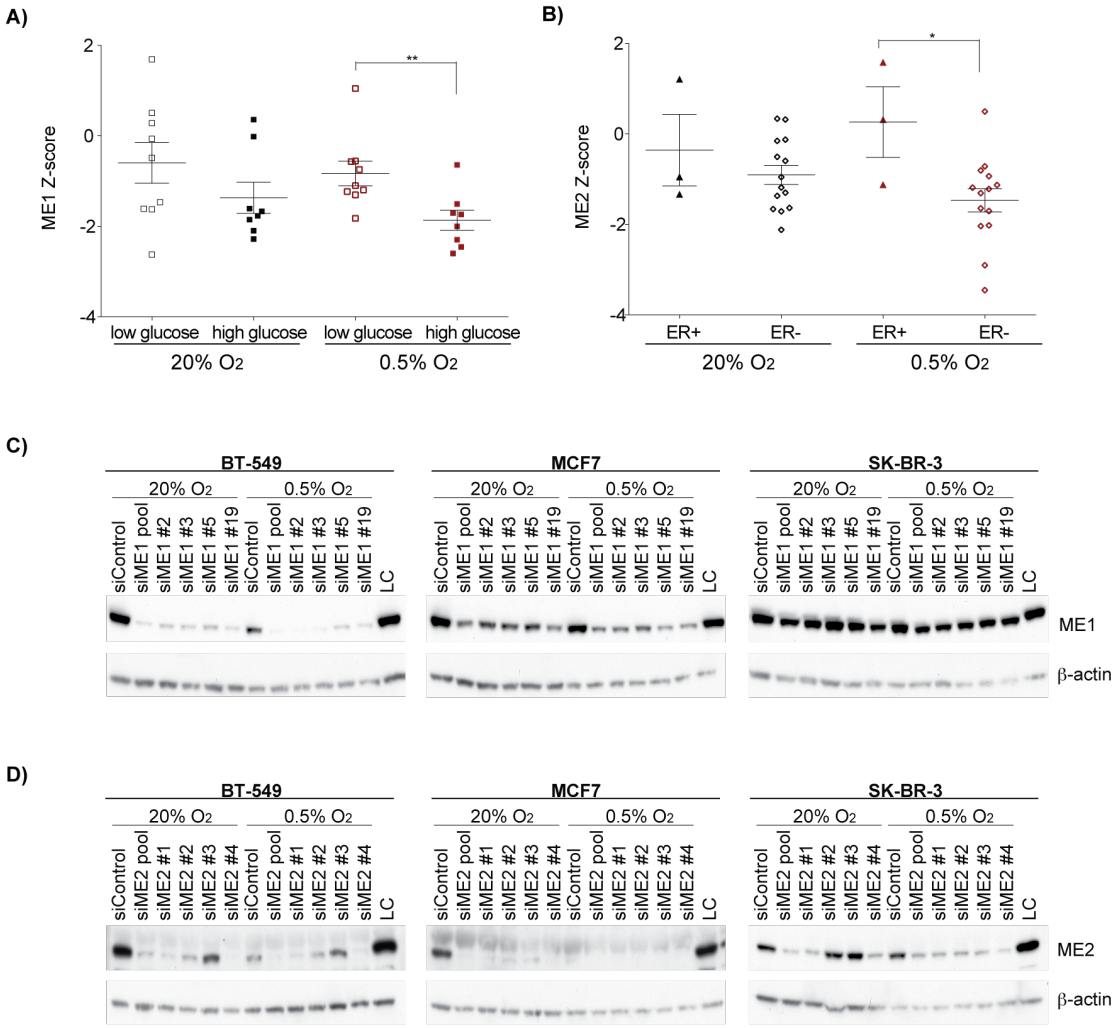

Figure 6-1 Malic enzyme 1 and malic enzyme 2 are detrimental to the ER-negative breast cell lines

(A) Supervised cluster analysis identified *ME1* as a candidate gene for cell lines exhibiting high glucose utilisation under hypoxia. (**=p≤0.01). (B) Supervised cluster analysis identified *ME2* as a candidate gene for ER-negative cell lines under hypoxia. (*=p≤0.05). (C) Whole protein lysates were harvested after siRNA transfection of *ME1* in these cell lines for 72 hours and analysed for ME1 and β–actin. (D) Whole protein lysates were harvested after siRNA transfection of *ME2* in these cell lines for 72 hours and analysed for ME2 and β–actin.

Figure 6.2

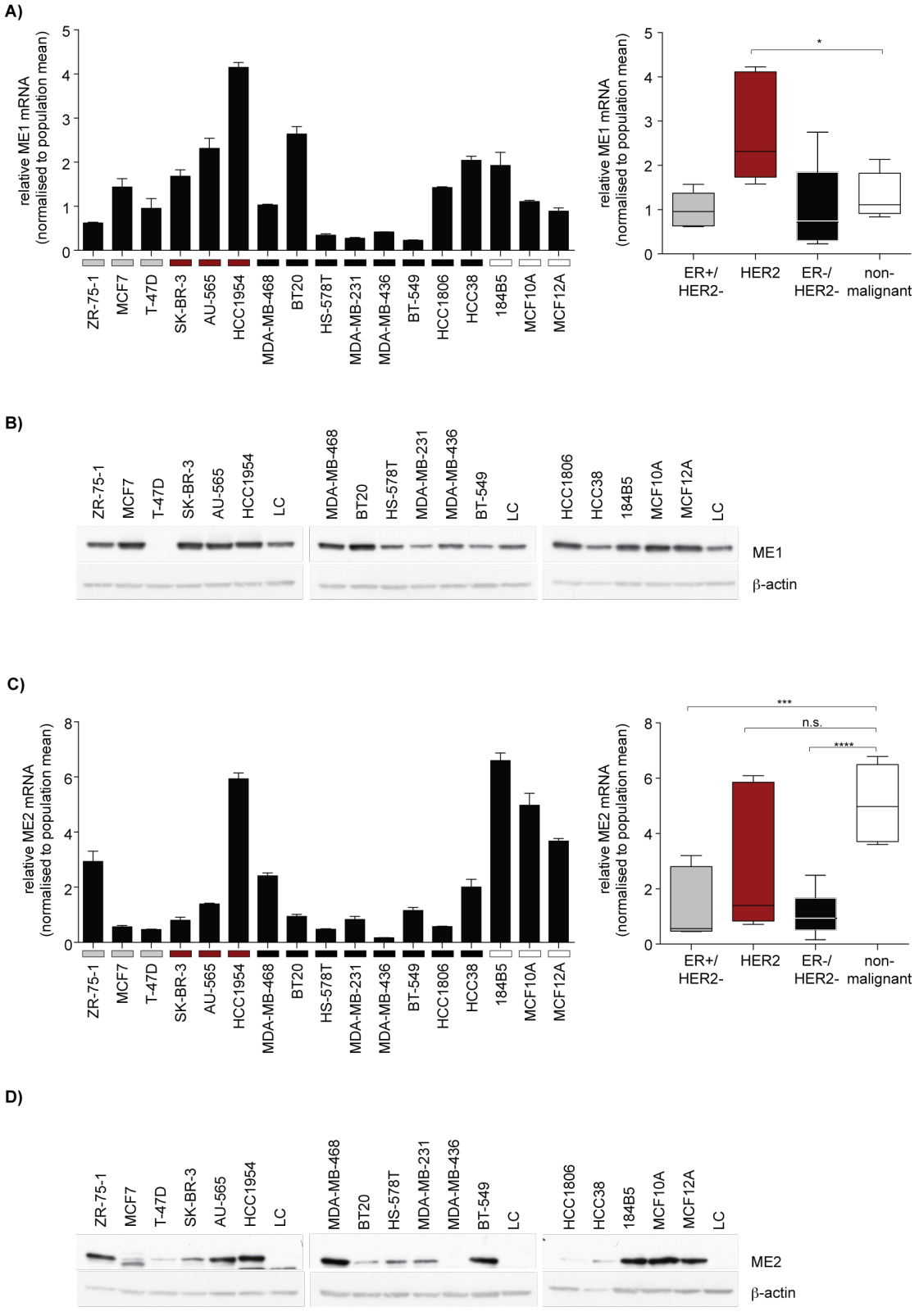
A)
relative ME1 mRNA (normalised to population mean)
ZR-75-1
MCF7
T-47D
SK-BR-3
AU-565
HCC1954
MDA-MB-468
BT20
HS-578T
MDA-MB-231
MDA-MB-436
BT-549
HCC1806
HCC38
184B5
MCF10A
MCF12A
*
ER+/ HER2-
HER2
ER-/ HER2-
non-malignant
B)
LC
ME1
β-actin
C)
relative ME2 mRNA (normalised to population mean)
***
n.s.
****
D)
ME2

Figure 6-2 Differential expression of ME 1 and ME2 in breast epithelial cell lines

Breast epithelial cell lines were seeded 24 hours prior harvesting whole cell lysates for protein and RNA analyses. (A+B) Expression of ME1 was determined by (A) qPCR on mRNA level and (B) for protein expression. (C+D) Expression of ME2 was determined by (C) qPCR on mRNA level and (D) for protein expression. LC is the control lysate to cross-compare immunoblots. Actin is shown as loading control. (*=p≤0.05, ***=p≤0.001, ****=p≤0.0001)

Figure 6.3

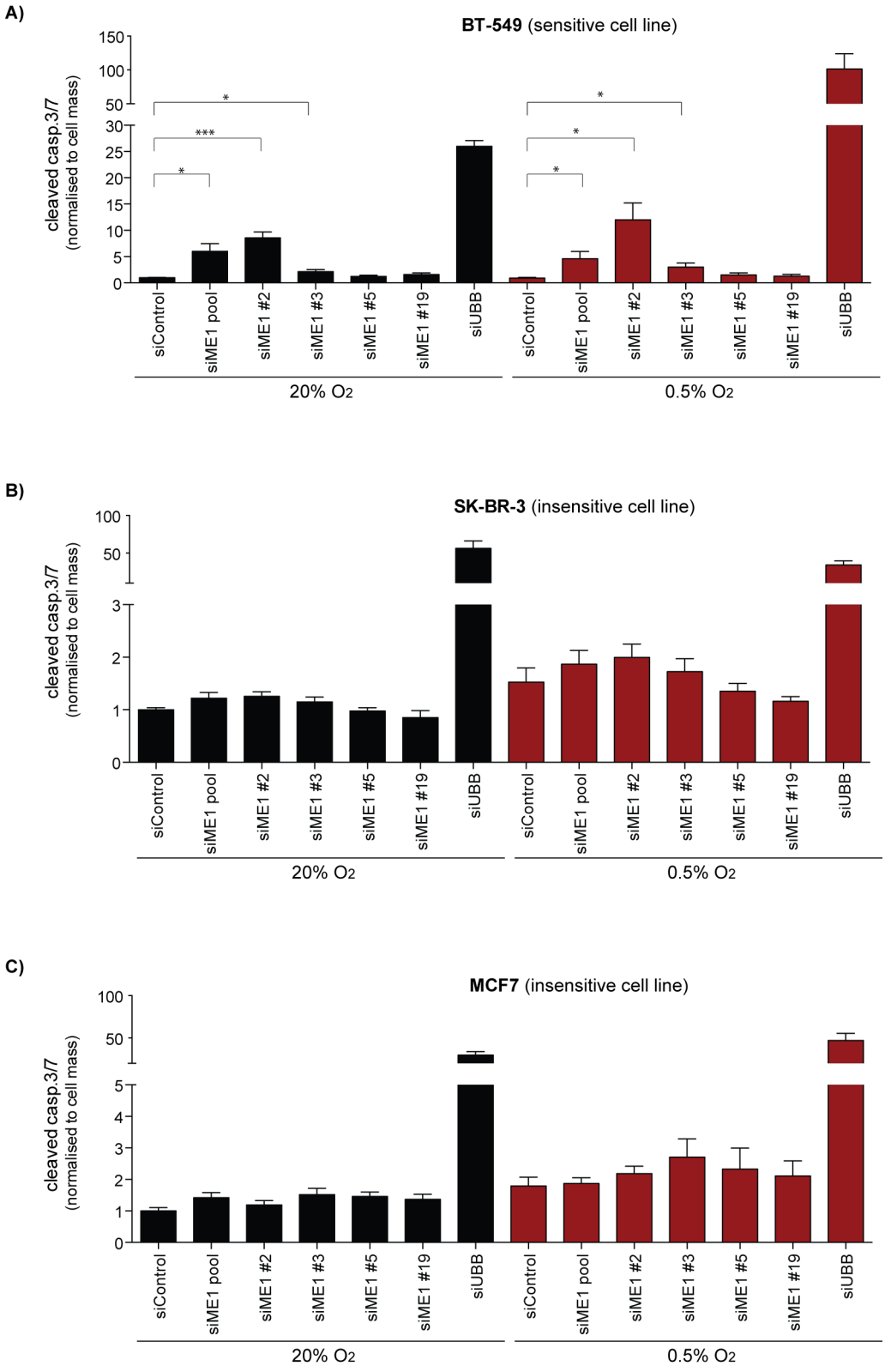
A)
BT-549 (sensitive cell line)
cleaved casp.3/7 (normalised to cell mass)
150
100
50
30
25
20
15
10
5
0
*
***
*
*
*
*
siControl
siME1 pool
siME1 #2
siME1 #3
siME1 #5
siME1 #19
siUBB
20% O2
0.5% O2
B)
SK-BR-3 (insensitive cell line)
cleaved casp.3/7 (normalised to cell mass)
100
50
3
2
1
0
C)
MCF7 (insensitive cell line)
cleaved casp.3/7 (normalised to cell mass)
100
50
5
4
3
2
1
0

Figure 6-3 Loss of cell number after *ME1* ablation is due to apoptosis

(A) BT-549, (B) SK-BR-3 and (C) MCF7 cells were reverse transfected with non-targeting siControls, pooled or individual siRNAs targeting *ME1*. siUBB was used the positive control. Cells were cultured in a 96-well format under normoxic or hypoxic conditions. After 96 hours of culture, cells and supernatants were analysed for the activity of caspases 3 and 7 using an enzymatic fluorescent assay. This assay was incubated 1.5 hours prior to measurement. Values were normalised to protein content (cell mass). Data shown is based on two independent experiments each done in triplicates. P-values were calculated using the unpaired t-test (*=p≤0.05, **=p≤0.01, ***=p≤0.001).

Figure 6.4

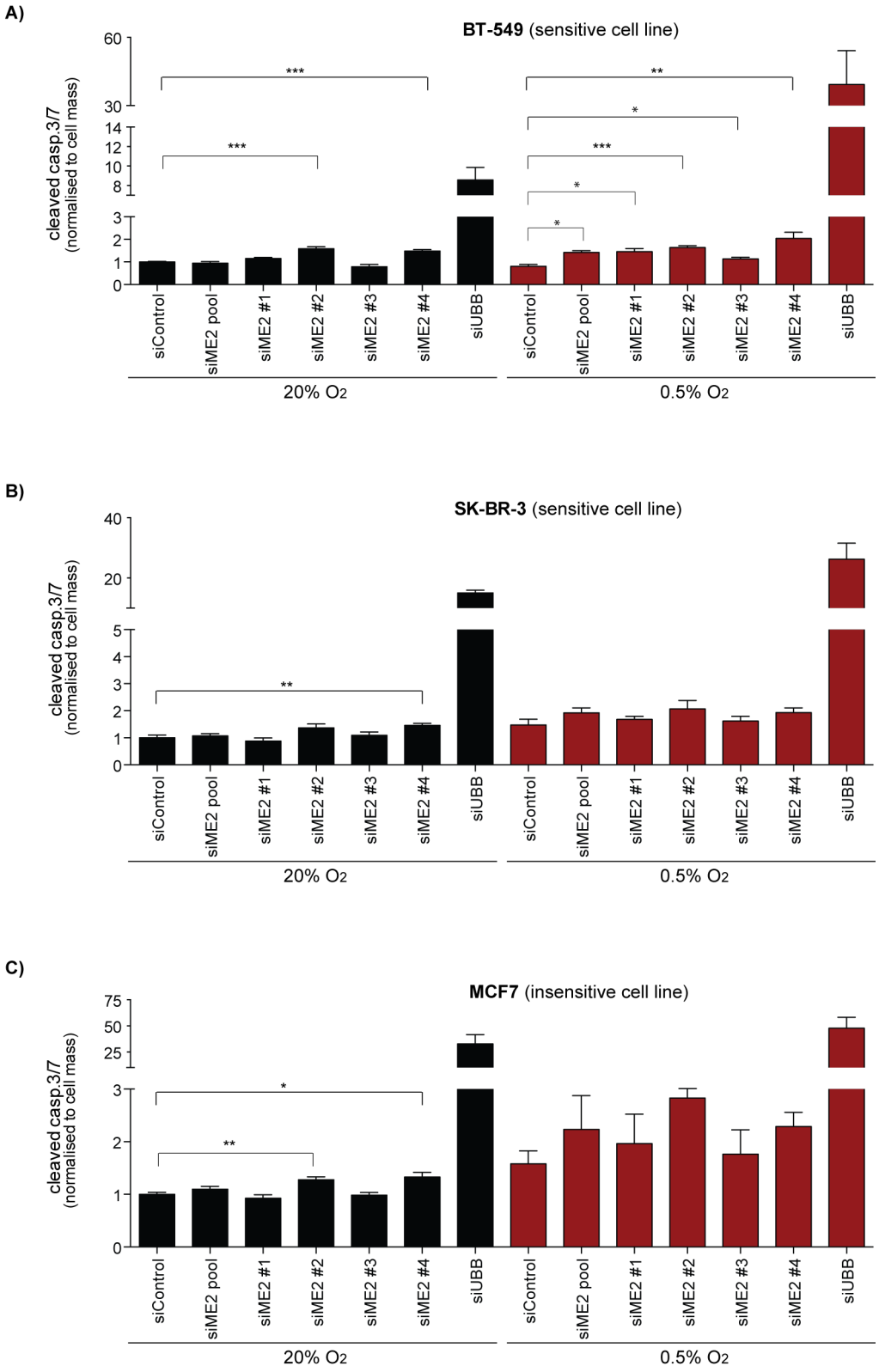
A)
BT-549 (sensitive cell line)
cleaved casp.3/7 (normalised to cell mass)
siControl
siME2 pool
siME2 #1
siME2 #2
siME2 #3
siME2 #4
siUBB
20% O2
0.5% O2
B)
SK-BR-3 (sensitive cell line)
C)
MCF7 (insensitive cell line)

Figure 6-4 Loss of cell number after *ME2* silencing leads to apoptosis

(A) BT-549, (B) SK-BR-3 and (C) MCF7 cells were reverse transfected with non-targeting siControls, pooled or individual siRNAs targeting *ME2*. siUBB was used the positive control. Cells were cultured in a 96-well format under normoxic or hypoxic conditions. After 96 hours of culture, cells and supernatants were analysed for the activity of caspases 3 and 7 using an enzymatic fluorescent assay. This assay was incubated 1.5 hours prior to measurement. Values were normalised to protein content (cell mass). Data shown is based on two independent experiments each done in triplicates. P-values were calculated using the unpaired t-test (*=p≤0.05, **=p≤0.01, ***=p≤0.001).

Figure 6.5

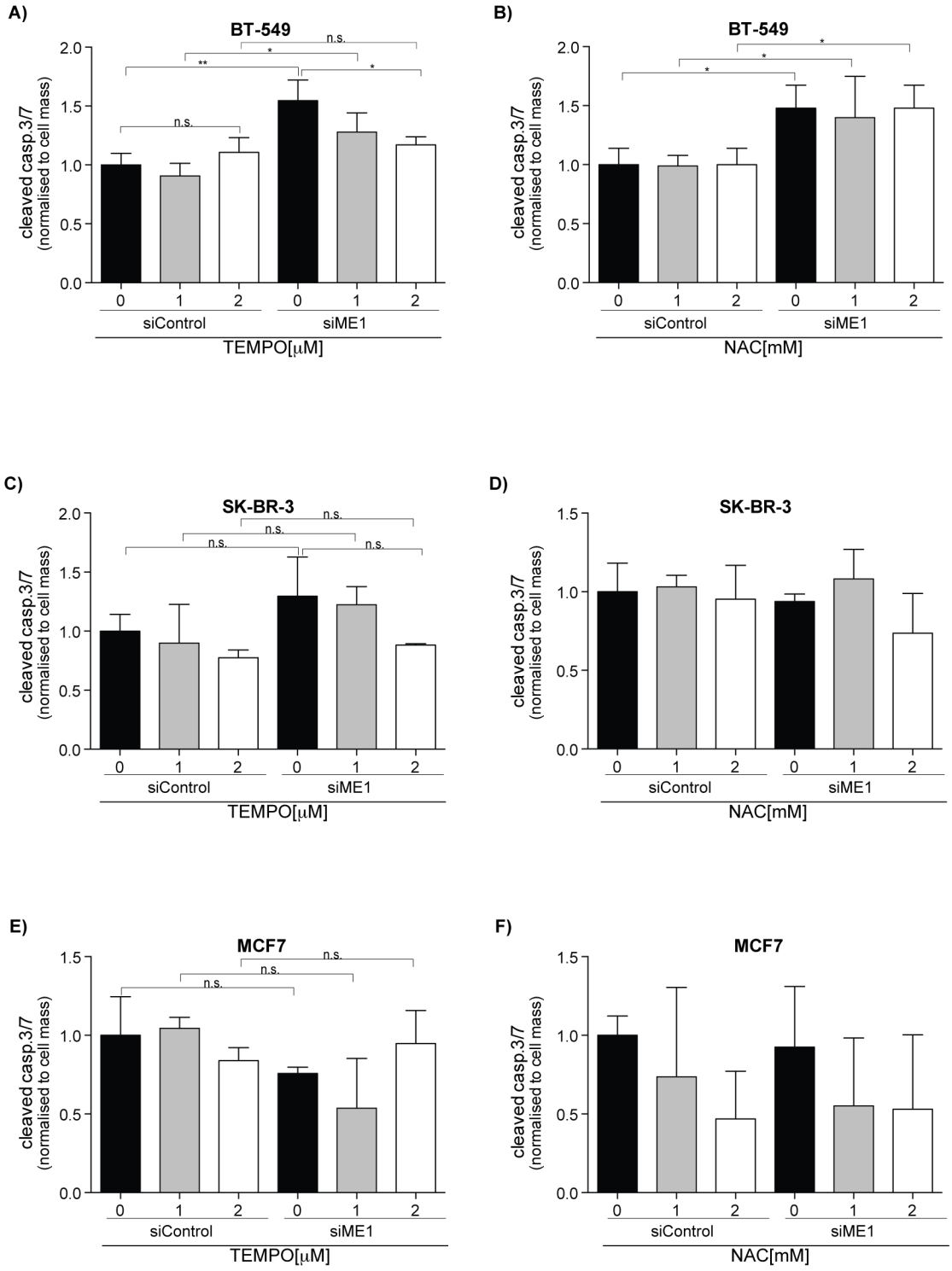
A)
BT-549
cleaved casp.3/7 (normalised to cell mass)
n.s.
*
**
*
n.s.
0 1 2 0 1 2
siControl siME1
TEMPO[μM]
B)
BT-549
cleaved casp.3/7 (normalised to cell mass)
*
*
*
0 1 2 0 1 2
siControl siME1
NAC[mM]
C)
SK-BR-3
cleaved casp.3/7 (normalised to cell mass)
n.s.
n.s.
n.s.
n.s.
0 1 2 0 1 2
siControl siME1
TEMPO[μM]
D)
SK-BR-3
cleaved casp.3/7 (normalised to cell mass)
0 1 2 0 1 2
siControl siME1
NAC[mM]
E)
MCF7
cleaved casp.3/7 (normalised to cell mass)
n.s.
n.s.
n.s.
0 1 2 0 1 2
siControl siME1
TEMPO[μM]
F)
MCF7
cleaved casp.3/7 (normalised to cell mass)
0 1 2 0 1 2
siControl siME1
NAC[mM]

Figure 6-5 ROS scavenger diminish effect of cleaved caspase activity

(A) BT-549 cells, (B) SK-BR-3 and (C) MCF7 cells were reverse transfected with siRNA targeting *ME1* or the non-targeting siControl in a 96-well format and cultured under normoxic conditions. The indicated doses of NAC and TEMPOL were added repeatedly at 12, 24, 48 and 72 hours after transfection. After 96 hours of culture, cells and supernatants were analysed for the activity of caspases 3 and 7 using an enzymatic fluorescent dye. Apo-one was incubated 1.5 hours prior to its measurement and normalised to protein content (cell mass). Data shown here is based on one experiment done in triplicates. P-values were calculated using the unpaired t-test (*=p≤0.05, **=p≤0.01).

Figure 6.6

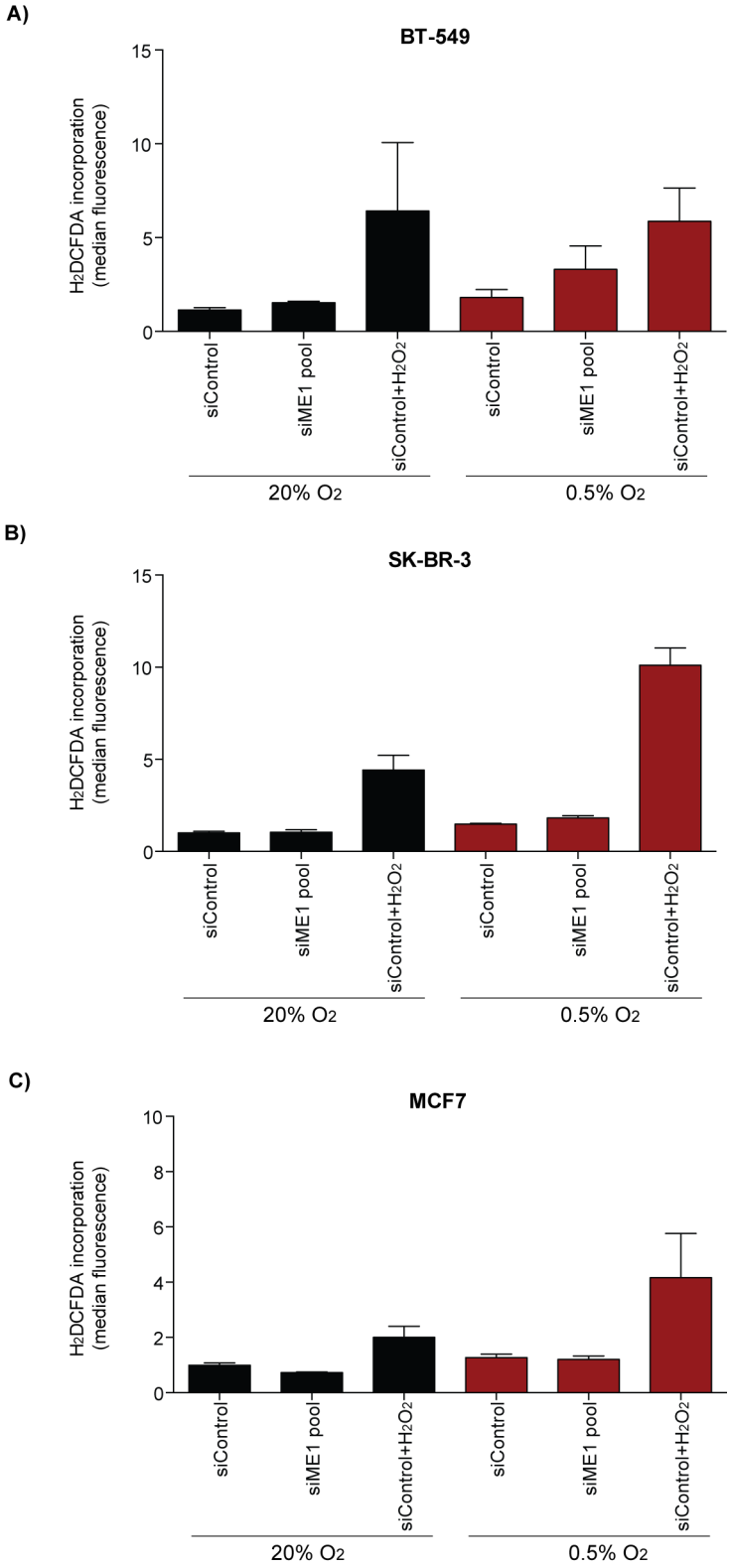
A)
BT-549
H2DCFDA incorporation (median fluorescence)
15
10
5
0
siControl
siME1 pool
siControl+H2O2
siControl
siME1 pool
siControl+H2O2
20% O2
0.5% O2
B)
SK-BR-3
H2DCFDA incorporation (median fluorescence)
15
10
5
0
siControl
siME1 pool
siControl+H2O2
siControl
siME1 pool
siControl+H2O2
20% O2
0.5% O2
C)
MCF7
H2DCFDA incorporation (median fluorescence)
10
8
6
4
2
0
siControl
siME1 pool
siControl+H2O2
siControl
siME1 pool
siControl+H2O2
20% O2
0.5% O2

Figure 6-6 *ME1* abrogation increases ROS levels in BT-549 under hypoxia

(A) BT-549 cells, (B) SK-BR-3 and (C) MCF7 were reverse transfected with siRNA targeting *ME1* or the non-targeting siControl and cultured under normoxic and hypoxic conditions. After 72 hours the incorporation of H_2DCFDA was measured by using FACS. H_2O_2 was added 1 hour before starting of the H_2DCFDA incorporation as a positive control for determining ROS levels

Figure 6.7

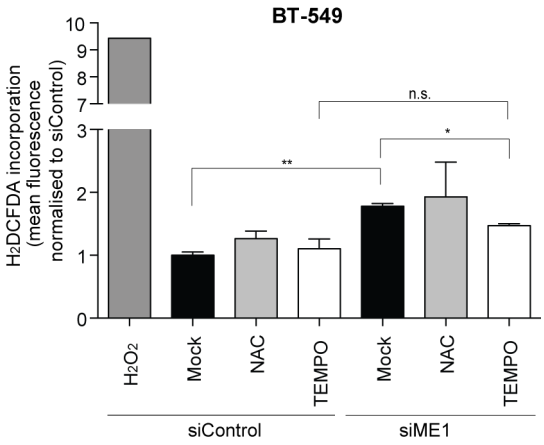

Figure 6-7 ROS scavenger rescues effect after *ME1* depletion

BT-549 cells were reverse transfected with siRNA targeting ME1 or the non-targeting siControl and cultured under hypoxic conditions. The indicated doses of NAC and TEMPOL were added repeatedly at 12, 24 and 48 hours after transfection before the incorporation of H_2DCFDA was measured 72 hours post-transfection. H_2O_2 was added 1 hour before starting the H_2DCFDA incorporation as a positive control. Data shown here represent one experiment performed in triplicates. P-values were calculated using the unpaired t-test (*=p≤0.05, **=p≤0.01).

Figure 6.8

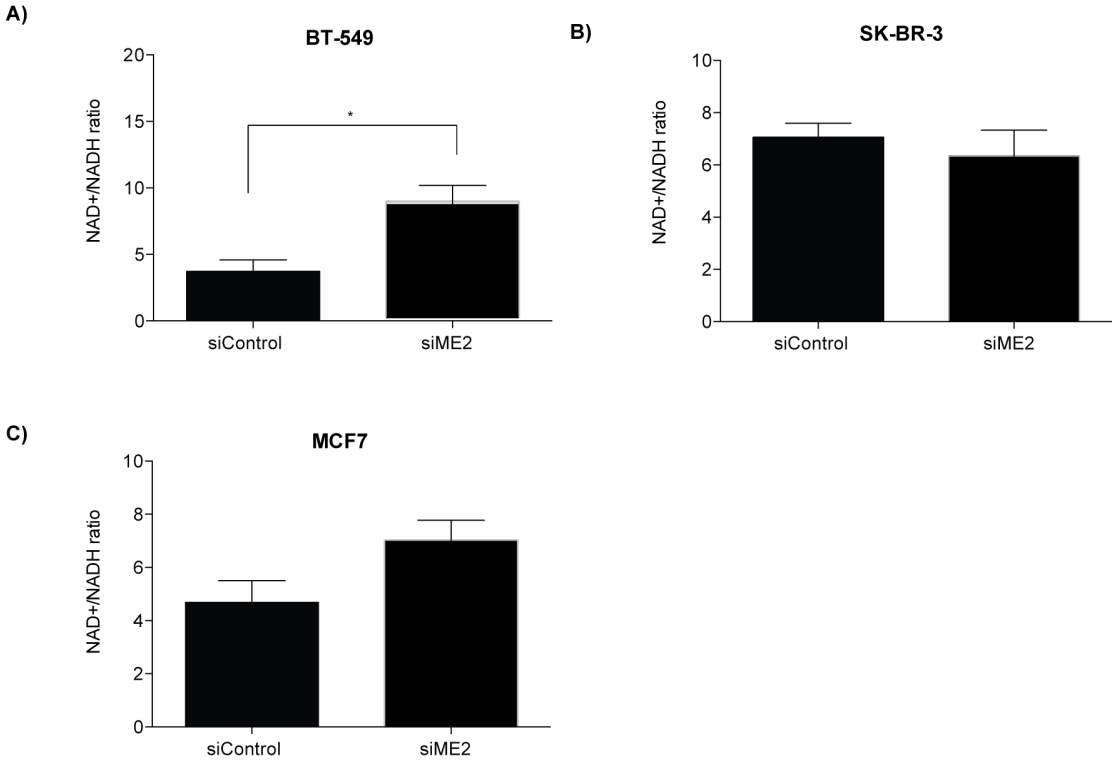

Figure 6-8 NAD^+/NADH levels are affected after *ME2* silencing

(A) BT-549, (B) SK-BR-3 and (C) MCF7 cells were transiently transfected with ME2 siRNA or siControl and cultured for 72 hours under normoxic conditions. $0.2x10^6$ cells per condition were used for analysis of the NAD^+/NADH ratio. Data shown represents two independent experiments performed in duplicates Significance was calculated with unpaired t-test (*=p≤0.05).

Figure 6.9

A)

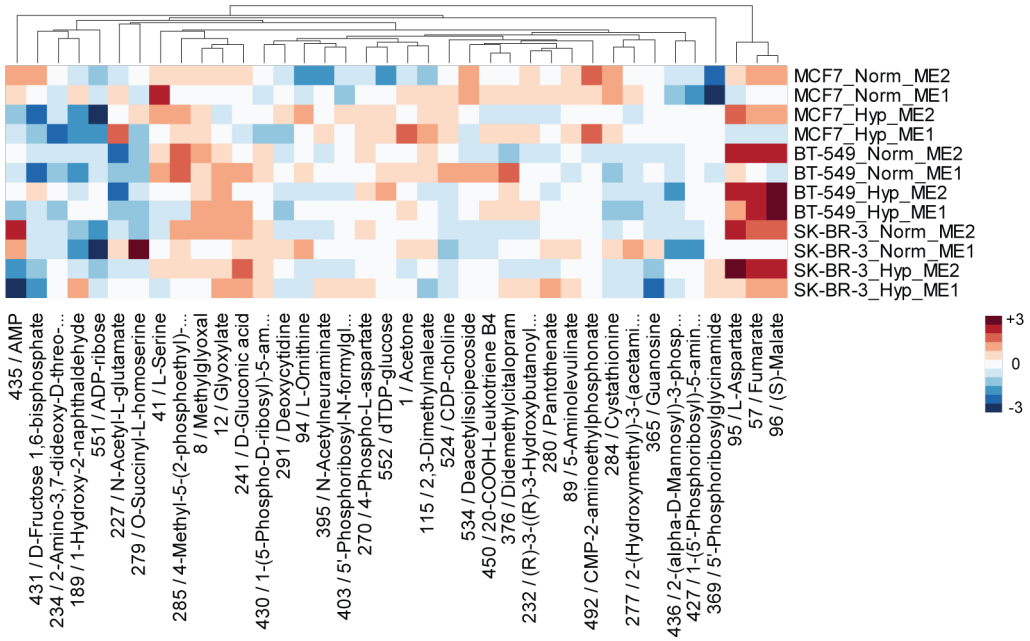

Figure 6-9 Perturbation of *ME1* or *ME2* results in significant changes in succinate, fumarate and malate levels

Cells of MCF7, SK-BR-3 and BT-549 cells were transiently transfected with ME1, ME2 siRNA or siControls in 6-well plates in triplicate. Cells were then cultured under normoxic and hypoxic conditions for 72 hours. Cells were then snap frozen in liquid nitrogen prior to metabolite extraction and analysed by mass spectrometry. Here shown is the log2 fold change of significant intracellular metabolite levels in log2 *ME1* ablated and *ME2* ablated samples that have been normalised to siControl.

Figure 6.10

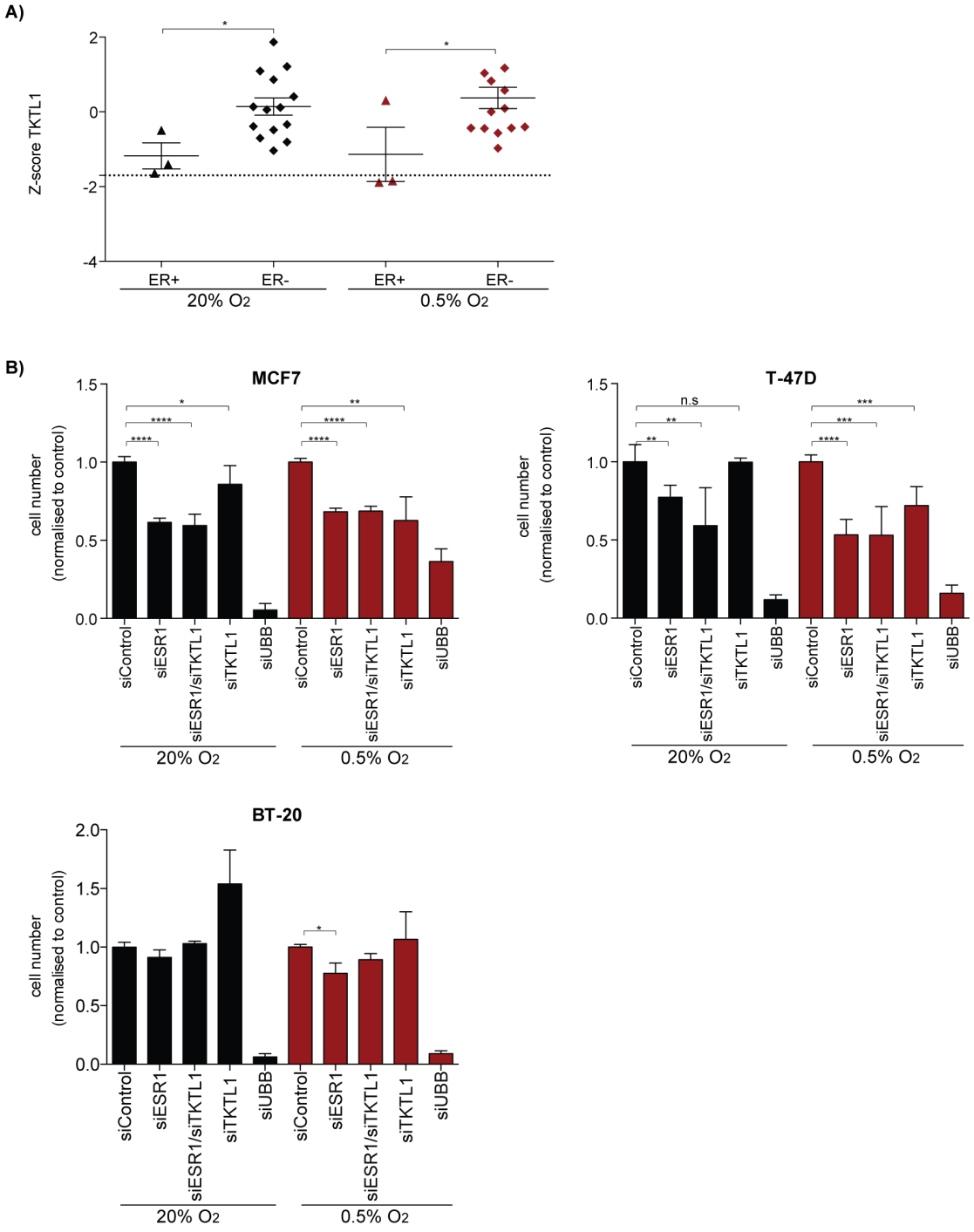

Figure 6-10 *TKTL1* silencing is detrimental in ER-positive breast cancer cells under hypoxia

(A) Supervised cluster analysis identified *TKTL1* as a candidate gene for ER-positive/HER2-negative cell lines under normoxic and hypoxic conditions (*=p≤0.05). (B) ER-positive cell lines MCF7, T-47D and the ER-negative cell line BT-20 were transiently transfected with *ESR1* or *TKTL1* alone, or in combination under normoxic (black bars) and hypoxic conditions (red bars). Cells were analysed after 96 hours culture for changes in cell number. Data shown here are from two independent experiments. Unpaired t-test was used for testing significance. (*=p≤0.05, **=p≤0.01, ***=p≤0.001, ****=p≤0.0001)

Figure 6.11

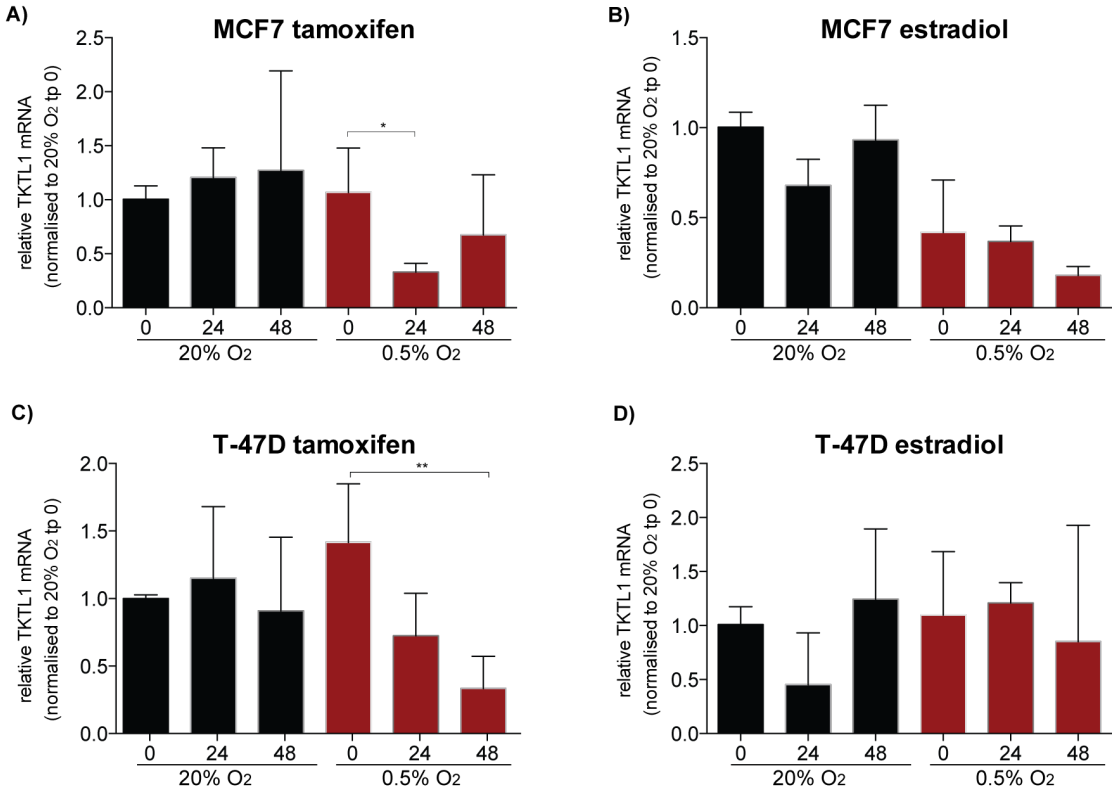

Figure 6-11 *TKTL1* is potentially regulated by the ER signalling

MCF7 and T-47D were cultured under normoxic and hypoxic condition in phenol red free DMEM/F12 supplemented with 10% charcoal-treated FCS 24 hours prior treatment with (A+C) 4-hydroxy-tamoxifen and (B+D) 17β-estradiol for 24 and 48 hours. Cell lysates were harvested for total RNA. Expression of TKTL1 on mRNA level was analysed by qPCR and normalised to β–actin. Data from two independent experiments are shown. (*=p≤0.05, **=p≤0.01)

Figure 6.12

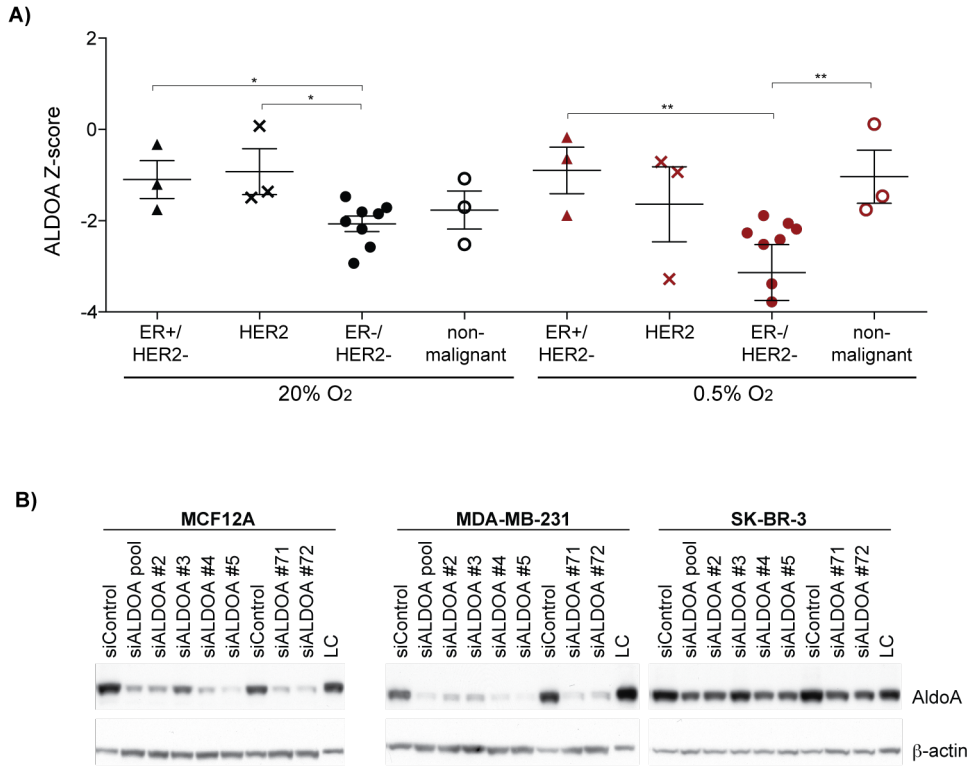

Figure 6-12 *ALDOA* is important for the survival of ER-negative breast cancer cell lines under hypoxia

(A) Supervised cluster analysis identified *ALDOA* as a candidate gene for ER-negative/HER2-negative cell lines under normoxic and hypoxic conditions (*=p≤0.05, **=p≤0.01). (B) Effects of *ALDOA* silencing with different siRNA sequences. Cells were reverse transfected with ALDOA siRNA and harvested for whole cell protein lysates after 72 hours and analysed for ALDOA and β-actin.

Figure 6.13

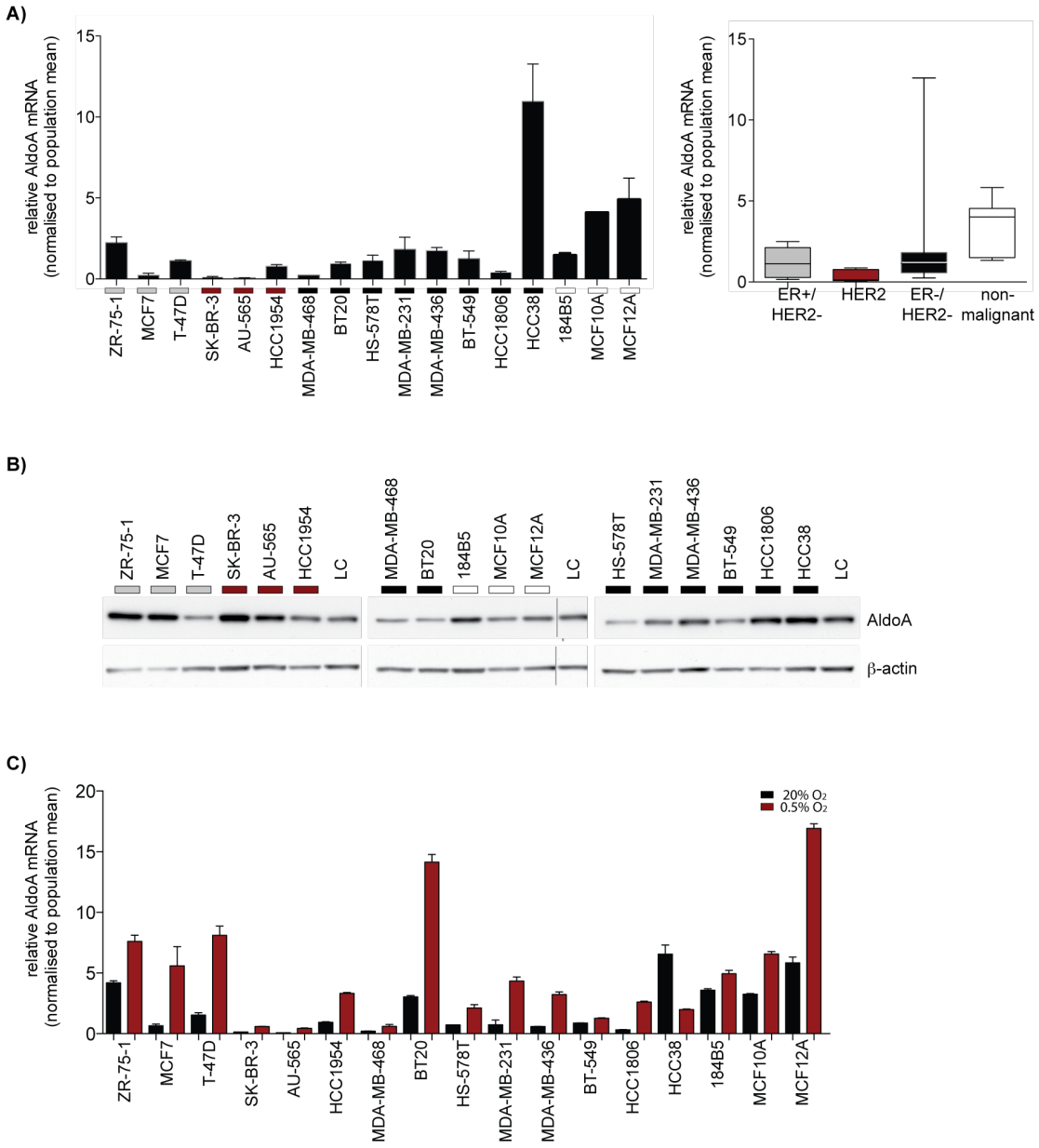

Figure 6-13 *ALDOA* expression is more prevalent in ER-negative breast cancer cells

Expression of ALDOA in the panel of 17 breast epithelial cell lines. (A) Cells were seeded for 24 hours before total RNA was extracted and analysed for *ALDOA* and β-actin by qPCR. (B) Cells of breast epithelial cell lines were seeded for 24 hours before whole cell lysates for protein were harvested and analysed for ALDOA and β-actin. (C) Cells were seeded for 24 hours before exposure to hypoxia for 24 hours. Whole cell lysates were harvested for total RNA and mRNA was then analysed for *ALDOA* and β-actin by qPCR. Normoxia (black bars) Hypoxia (red bars).

Figure 6.14

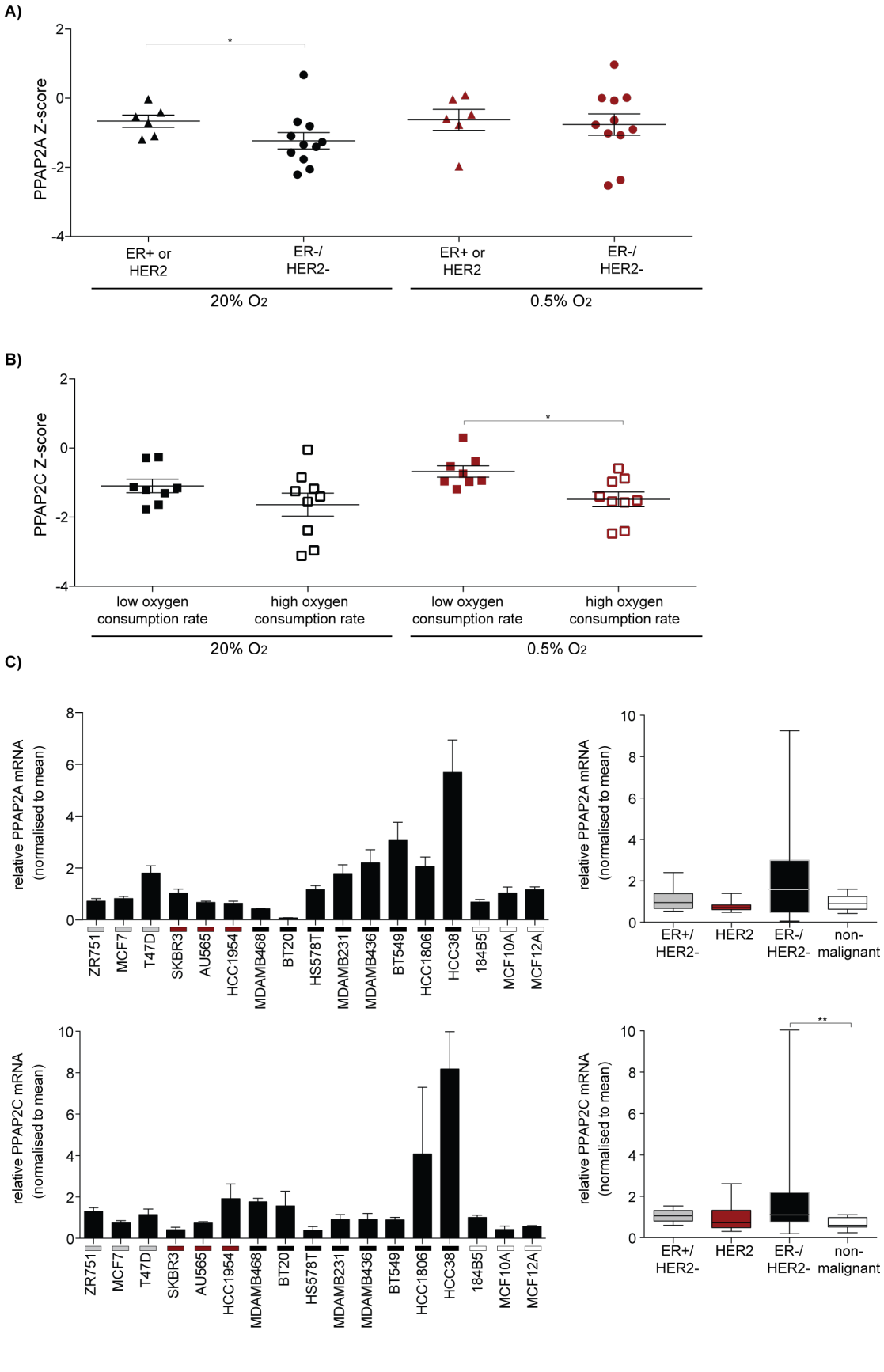
A)
PPAP2A Z-score
2
0
-2
-4
*
ER+ or HER2
ER-/ HER2-
ER+ or HER2
ER-/ HER2-
20% O2
0.5% O2
B)
PPAP2C Z-score
2
0
-2
-4
*
low oxygen consumption rate
high oxygen consumption rate
low oxygen consumption rate
high oxygen consumption rate
20% O2
0.5% O2
C)
relative PPAP2A mRNA (normalised to mean)
ZR751
MCF7
T47D
SKBR3
AU565
HCC1954
MDAMB468
BT20
HS578T
MDAMB231
MDAMB436
BT549
HCC1806
HCC38
184B5
MCF10A
MCF12A
ER+/ HER2-
HER2
ER-/ HER2-
non-malignant
relative PPAP2C mRNA (normalised to mean)
**

Figure 6-14 *PPAP2A* and *PPAP2C* are important for survival of breast cell lines

(A) Supervised cluster analysis identified *PPAP2A* as a candidate gene for ER-negative/HER2-negative cell lines under normoxic conditions. (*=p≤0.05). (B) Supervised cluster analysis identified *PPAP2C* as a candidate gene for supporting the survival of cell lines exhibiting high oxygen consumption under hypoxia. (*=p≤0.05). (C) Cells were seeded for 24 hours before total RNA was extracted. mRNA was then analysed for PPAP2A and PPAP2C and β-actin by qPCR.

Figure 6.15

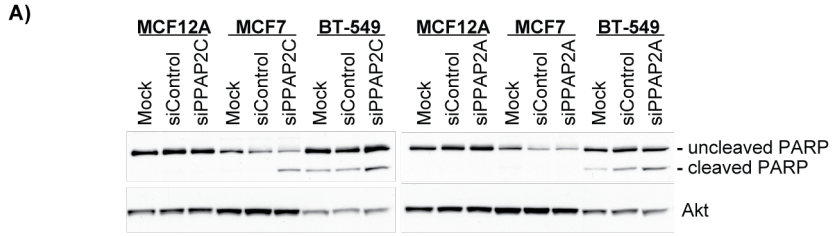

Figure 6-15 *PPAP2A* and *PPAP2C* silencing results in PARP cleavage

(A) Cells of the above breast epithelial cell lines were reverse transfected with PPAP2A or PPAP2C siRNA and cultured for 72 hours before being harvested for protein analyses. Supernatant as well as whole cell lysates were collected and analysed for PARP cleavage. AKT is shown as loading control.

7 Discussion

7.1 Cancer metabolism

Cancer is defined as a collection of complex and heterogeneous diseases depending on the tissue origin and the specific genetic repertoire of each tumour. Nevertheless, distinct phenotypic characteristics have been described that encompass the broad nature of cancer (Hanahan and Weinberg, 2011). One hallmark has been the rewired metabolism of cancer cells (Cantor and Sabatini, 2012). Within the last couple of years, the field of cellular metabolism in cancer was revived substantially. The initial finding of aerobic glycolysis was by Otto Warburg, who showed that cancer cells display increased glucose uptake, which is predominantly being converted into lactate even in the presence of oxygen. Nowadays, it is established that glucose dependency is one aspect of cancer cell metabolism. Experimental models of tumour progression *in-vitro* and *in-vivo* have shown that with increased transformation the cells become more reliant on glycolysis rather than mitochondrial respiration for energy production (Ramanathan et al., 2005). Glucose consumption studies in an *in-vivo* mammary mouse model have also monitored increased glucose uptake with FDG-PET during tumour progression from an *in-situ* ductal carcinoma to invasive carcinomas (Abbey et al., 2004).

However, it becomes more and more obvious, that this was just the tip of the iceberg given that genetic reprogramming of the metabolism by oncogenes and tumour suppressors, communication with the microenvironment to cope with limited supplies of oxygen and nutrient, homeostasis of pH and cellular redox potential all need to work together to facilitate the proliferative capacity of tumour cells (Cantor and Sabatini, 2012; Vander Heiden et al., 2009). Not only are these processes highly complex, it is now established that cancer cell metabolism differs between different tissues in which tumours arise in and this is linked to the effects of the genetic alterations that drive these tumours (Yuneva et al., 2012). *In-vivo* analysis with stable isotope labelling in mice also illustrated site-specific cancer cell metabolism (Marin-Valencia et al., 2012).

This study aimed to elucidate the metabolic capacity of a panel of breast epithelial cell lines and to understand whether their dependency on specific metabolic processes could be exploited. Nowadays, breast cancer is a more generic term of different diseases that show distinct histopathological, molecular and clinical features. Despite the numerous subtypes, the main classification it is often referred to as ER-positive or ER-negative breast cancer, as gene expression studies have shown that ER-negative and ER-positive breast cancers show substantial differences leading to the conclusion that these represent different diseases (Perou et al., 2000; Sorlie et al., 2001).

Clinically, breast cancer is differentiated by the expression of hormone receptors, receptor tyrosine kinase HER2 and tumours that lack the expression of these receptors. The development of molecular therapies such as endocrine therapy and inhibition of HER2 by targeted therapies, such as Tamoxifen for ER-positive and Trastuzumab and Lapatinib for HER2-positive breast cancer patients, have translated into improved overall survival. In contrast, patients who have breast tumours that do not display the expression of these extracellular receptors (ER-negative/HER2-negative) have to date only limited therapeutic options and their disease is treated with agents such as Anthracyclines that perturb DNA synthesis, which are less efficacious and toxic to all highly proliferative cells, not just cancer cells.

7.2 Metabolic classification of breast cancer

In chapter 3 it was established that the metabolism in different breast cancer cell lines shows distinct features. It was demonstrated that the ER-negative/HER2-negative subtype of highly proliferative breast cancer cells exhibit high aerobic glycolysis. Interestingly, these breast cancer cells also showed low mitochondrial activity and pseudo-hypoxic features. This has been recently confirmed by a study with multiple breast cancer cell lines which investigated the role of an isoform of LDH in cancer cell survival (McCleland et al., 2012). Altered mitochondrial metabolism can influence tumour growth. Silencing of the mitochondrial genes MRPL28 and MRPL12 that are involved in mitochondrial activity resulted in increased glycolysis and enhanced tumour growth (Chen et al., 2009). Moreover, genetic alterations that impaired mitochondrial respiration induce NADH levels and suppressed PTEN function leading to increased

AKT activity (Pelicano et al., 2006). The activation of AKT has been demonstrated to shift cell metabolism towards biosynthetic processes (Bauer et al., 2005; Hatzivassiliou et al., 2005). In chapter 3, it was also shown that high AKT activity correlates with PTEN and HER2 status in these cell lines. Therefore, it can be hypothesised that cancer cells harbouring loss of PTEN or amplified HER2 depend on lipogenesis as AKT signals through mTORC1 and induces the transcription factor *SREBP1* (Duvel et al., 2010; Porstmann et al., 2008). This might have clinical relevance for ER-negative/HER2-negative tumours as they could benefit from dual inhibitors of mTORC1/AKT signalling, compounds that impede SREBP activity or the use of agents that inhibit lipid synthesis.

The ER-positive/HER2-negative and HER2-positive cell lines were similar to each other when glucose utilisation and lactate secretion was investigated. Moreover, these cell lines displayed an oxidative phenotype compared to the ER-negative/HER2-negative subtype. This was somewhat surprising as these subtypes differ in their clinical parameters including overall survival and aggressiveness.

The results of the work described in chapter 3 also shows that breast epithelial cells displayed specific dependencies on glucose and glutamine, demonstrating that the non-malignant cell lines were highly sensitive towards growth factor, glucose and glutamine withdrawal. Cancer cells were more resistant to growth factor or nutrient withdrawal. However, how starvation affects the metabolic processes and which metabolites are utilised for which process in these cells needs further investigation.

To further characterise the differences in metabolism, metabolite analyses were carried out shown in chapter 3. ER-negative/HER2-negative cells were distinct from most other cell type with significant differences in amino acid metabolism when compared to the other subtypes. Previous studies analysed the metabolite repertoire of cancer cells under normoxic conditions (Jain et al., 2012; Sreekumar et al., 2009) and identified certain metabolites such as sarcosine and glycine as markers for tumorigenesis. These studies also determined that glucose utilisation correlates with the export of lactate. Not only lactate was secreted but also other metabolites (e.g. malate, isocitrate/citrate and

pyruvate) were also incompletely catabolised and secreted into the culture medium. Increased consumption of amino acids was also noticed in the cancer cells studied here. To better characterise amino acid metabolism in ER-negative/HER2-negative cells, tracing of isotope-labelled amino acids to evaluate their contribution to biochemical processes would be of great interest. Moreover, investigating whether ablation of specific amino acid transporters cause decreased cell viability or how amino acid starvation impact breast cancer survival are all interesting question remaining open as this study here did not focus on amino acid transporter in detail. Metabolite profiling within this study provides a foundation for the future studies.

7.3 Functional studies

Global siRNA and shRNA screens have been used successfully to identify drivers of tumorigenesis in multiple cell lines. (Toyoshima et al., 2012; Zuber et al., 2011). Small-scale siRNA screens targeting the kinome or metabolic processes have shown to be valid approaches to identify particular dependencies (Brough et al., 2011; Possemato et al., 2011; Ros et al., 2012). Moreover, targeted siRNA screens performed using 2D cultures which recapitulate a component of the tumour microenvironment, such as low serum, have been validated *in-vivo* and shown to have a striking effect on tumour growth (Possemato et al., 2011; Ros et al., 2012).

In the present study, a functional analysis using RNAi across 17 breast epithelial cell lines under normoxic and hypoxic conditions was performed. A small-scale siRNA library of 231 pooled siRNA duplexes targeting genes associated to metabolic processes was used. This has led to the identification of metabolic dependencies, which can be categorised according to the established breast cancer subtypes (chapter 4).
The optimisation process that was undertaken was important for reducing non-specific/off-target effects. A non-biased approach to screen transfection reagents for low toxicity and good siRNA delivery was performed. The screening conditions under hypoxia were used to recapitulate a feature of solid breast tumours, which can be found *in-vivo* that is associated with poor prognosis and decreased survival in patients. In chapter 4, a workflow for the identification of candidate genes was followed. Spearman analysis suggested robust screening data in most of the breast epithelial cells as the

controls behaved as expected and the replicates were similar to each other in most cases. Different analysis strategies were used to identify candidate genes, and, initially, genes that showed effects in more than two cell lines/ conditions were identified. Among these candidates were genes previously identified or mentioned in relation to cancer metabolism. ODC1 was predicted to be important in cancer cells (Hayes et al., 2006). Interestingly, some genes identified here were also found in other screens such as *PIK3CA* (Brough et al., 2011; Iorns et al., 2009), *PFKFB1* (Iorns et al., 2009) and *SLC16A3* (Possemato et al., 2011) suggesting reliable screening results in these cells. Moreover, non-malignant cells also displayed metabolic dependencies that were distinct from those of cancer cells (e.g. PDP2), indicating that cancer cells have specifically adapted their metabolism. However, it should be noted that the non-malignant cell lines were also highly proliferative under the 2D culture conditions used here. This is in contrast to the normal cells within living tissues as these are mostly in a differentiated state.

The difficulty of modelling normal cells within an *in-vitro* system is a common experimental problem. However, 3D cultures of these cells better mimic the behaviour of different cell types *in-vivo*.

7.4 Candidate genes

In chapter 5, the role of the monocarboxylate transporter 4 (MCT4), which has been found to disturb pH homeostasis of ER-negative breast cancer cells, is described. It was demonstrated that cells after ablation of MCT4 increase their mitochondrial activity to compensate for reduced export of lactate. This might have detrimental effects if these cancer cells are normally not using their mitochondria. One of the main drivers of aggressive cancer phenotypes is acidosis (Gatenby et al., 2007). Therefore MCT4 might be an interesting candidate to be exploited therapeutically. The observations in chapter 3 showed that most of the ER-negative cells are highly glycolytic and display pseudohypoxic features. This supports the role of MCT4 as an important lactate transporter in breast cancer suggested in chapter 5. This was confirmed by the analysis of metabolites of the supernatant. However, previous studies have suggested that MCT4 is not important under normoxic conditions and that both MCT1 and MCT4 have to be inhibited to reduce cell viability (Le Floch et al., 2011). This is in contrast to the

findings described in this thesis as it is demonstrated that *SLC16A3* is also important for HER2-positive breast cancer cells under normoxia. Moreover, silencing of *SLC16A3* alone was sufficient to impair cell growth. This was further supported by the *in-vivo*-like analyses indicating that inhibition of MCT4 might be sufficient to prevent proliferation and survival in some cancer cells. Perturbing lactate metabolism via inhibition of MCT resulted in cell death (necrosis) in a study by Colen and colleagues that investigated highly glycolytic glioblastoma cells and the role of lactate in supporting their survival (Colen et al., 2011). This study also showed reduced survival of matrigel cultures when lactate secretion was impaired. Another isoform, MCT1, was identified for highly glycolytic cells, but the differential was quite weak and not further followed up.

HER2-positive breast cancer tissue showed stronger immunohistological staining for MCT4. MCT1, which has been shown to be upregulated in basal-like and ER-negative/HER2-negative breast cancer cells, was used as positive control. In fact, the same staining protocol previously established by Pinheiro et al was used for this analysis (Pinheiro et al., 2010a). However, MCT1 expression was found not to be increased in ER-negative/HER2-negative breast cancer tissues (data not shown). This might be due to different fixation methods of the tumour material and differences in antigen retrieval. Therefore, larger studies are needed to evaluate the significance of different MCT expression levels across different breast cancer subtypes.

In summary, it is still not known why some cancer cells depend on MCT1, MCT4 or both transporters. MCT1 has been shown recently to be involved in the coupled metabolism between cancer cells (Sonveaux et al., 2008). This study suggested that MCT1 takes up lactate that is secreted from cancer cells that express MCT4. Moreover, MCT1 has been implicated to be important for cells with mutant p53 under hypoxia as MCT1 is upregulated in a p53-dependent way to adapt to metabolic needs (Boidot et al., 2012). Together with the work described here, these findings delineate that highly glycolytic cancer cells may be able to use either MCT1 or MCT4 for exporting lactate. However, the relative importance of these two transporters may depend on the genetic

background of the cancer cell and their relative position within the tumour microenvironment.

It can also be hypothesised that cancer cells with increased lactate secretion have less pyruvate available for mitochondrial metabolism. Hypoxia and HIF activation can rewire mitochondrial metabolism and induce aerobic glycolysis by the induction of *PDHK, PKM2, LDHA* and *SLC16A3*. This might suggest a network of different enzymes and transporters supporting one specific process: induction of glycolysis and enhanced export of lactate. In contrast, MCT1 has been suggested to work together with LDHB, which would support lactate import that is then converted to pyruvate via LDHB (Hussien and Brooks, 2011; McCleland et al., 2012). However, the relative use of different transporters and the direction of metabolite flux need further investigation.

Lactate export from cancer cells might also be important for modification of the tumour microenvironment as inhibition of proton and lactate transport affect the pH homeostasis. Given that some enzymes such as MMPs and cathepsins need a more acidic environment to function (Hirschhaeuser et al., 2011), the ablation of MCTs would cause a more alkaline extracellular pH. Moreover, MCTs have also been implicated as targets in immunosuppression (Murray et al., 2005; Vegran et al., 2011). As the microenvironment contributes to the metabolic heterogeneity of cancer cells (Almendro et al., 2012; Marusyk et al., 2012), the interference of metabolic processes that influence the microenvironment might be highly important.

It could be argued that with the here presented data the importance of MCT4 in ER-negative breast cancers is underlined but whether *in-vivo* MCT1 or MCT4 is responsible for facilitating cancer progression needs further investigation, however the importance of the MCT family of proteins is irrefutable, and the work in this thesis contributes strongly to this statement.

As well as SLC16A3, the screen also identified other metabolic enzymes that were found to be important mainly for ER-negative breast cell lines. ALDOA, a direct downstream target of mTORC1 (Duvel et al., 2010), has been suggested to have a

similar role as PKM2 in cancer as it is important for the provision of glycolytic intermediates for cell growth (Mazurek et al., 2002).

Moreover, malic enzymes 1 and 2 have also been identified as important enzyme for cancer cell survival. ME2 was mainly important for ER-negative cell lines, whereas ME1 was selectively required for highly glycolytic cells. The roles of ME isoforms in cancer have not been studied extensively. While several reviews have predicted a role of malic enzyme in cancer cells, this has previously not been supported by experimental evidence. A study by Vander Heiden suggested that $NADP^+$-dependent ME1 should be a promising enzyme for the targeting of cancer because glutamine catabolism to pyruvate or lactate could generate NADPH via this enzyme (Vander Heiden et al., 2009). The induction of glutaminolysis by Myc allows the cancer cells to generate additional NADPH for nucleotide and fatty acid synthesis. Therefore the regulation of NADPH production in rapidly proliferating cancer cells is crucial for biomass production (Wise et al., 2008). The modulation of abundant pyruvate in glutamine dependent cancer cells via ablation of *ME1* might be important. These studies all imply that ME are good candidates that could be exploited for cancer therapy (Deberardinis et al., 2008; Wise et al., 2008). Furthermore, a study has demonstrated that *ME1* is a target of the transcription factor SREBP1 (Amemiya-Kudo et al., 2002). It is postulated that cancer cells with high SREBP activity display higher ME1 expression. Regulation of SREBP by upstream signalling components such as AKT, mTORC1 and HIF might therefore also influence ME1 levels.

Interestingly, *ME2* was important for ER-negative/HER2-negative breast cancer cells that have exhibited low oxygen consumption and mitochondrial capacity in the metabolic characterisation described in chapter 3. It could be postulated that these cells depend on glutaminolysis, as they cannot completely rely on glucose-derived pyruvate. Therefore, pyruvate generated from malate might give these cells a survival benefit. Perturbation of this reaction is not compensated by pyruvate produced by ME1 and/or glucose. However, whether isoform compensation as shown by Mueller and colleagues (Muller et al., 2012) might play a role in breast cancer cells needs to be further investigated.

7.5 Hypoxia

Beside acidosis, hypoxia is considered to be the second main driver of aggressive and advanced diseases. Breast cancers exhibit a median pO2 of 10 mm HG with an overall hypoxia coverage of 25% with less than ≤2.5mm HG (Ward et al., 2013). Therefore, it has been proposed that detection of hypoxia would be a good tool for patient selection (Vaupel et al., 2007). A third of all breast cancers display hypoxic areas with an oxygen concentration below 0.3%. In 40-50% of all primary and locally advanced breast cancers, hypoxic heterogeneity within the tumour has been observed (Ward et al., 2013). This heterogeneity is due to leaky tumour blood vessels and insufficiently vascularised areas of the tumour. This is not favourable, as breast cancers with hypoxic areas that are below 1% in oxygen display resistance to radiation in 30-40% of all patient cases evaluated.

Moreover, oxygen is also required for non-mitochondrial processes, including fatty acid desaturation. However, even under hypoxic conditions, some amount of oxygen is still available (Evans et al., 2001). The extent of hypoxia is crucial for the metabolic consequences for the tumour cells. Moderate hypoxia might cause a decrease in proliferation (Hockel and Vaupel, 2001a, b), while a severe form of hypoxia, anoxia, is more detrimental to the cells and can lead to necrotic cell death (Papandreou et al., 2005).

The activity of HIF regulates mitochondrial metabolism to allow cells to maintain their proliferative capacity (Kim et al., 2006; Papandreou et al., 2006; Zhang et al., 2007a). Most cancer cells retain active mitochondrial metabolism and only a small percentage of human tumours carry genetic alterations that completely impair mitochondrial activity. Genetic mutations in mitochondrial DNA have been identified in multiple cancers (e.g. prostate and ovarian cancer) (Brandon et al., 2006; Liu et al., 2001; Petros et al., 2005). Additionally, previous studies have shown mutations in metabolic enzymes that lead to the stabilisation of HIF (Gottlieb and Tomlinson, 2005). However, genetic alterations of SDH or FH were not observed in the CCLE data of the breast epithelial cell lines used in the study, suggesting that variations in the mitochondrial activity are caused by different mechanisms.

Most breast cancers belong to the ER–positive/HER2-negative subtype (approximately 70%), and patients are successfully treated with endocrine therapy of different SERM. The RNAi screen described here was biased towards breast cancer cell lines that are representative of the subtype that is difficult to treat (i.e. ER-negative cell lines). However, a candidate gene for ER-positive/HER2-negative cell lines harbouring mutant *PIK3CA*, was identified under hypoxic conditions. ER is an important driver of tumour growth and potential perturbations of ER-mediated metabolic signalling by targeting *TKTL1* might reveal novel insights into ER/*PIK3CA* signalling in general. As discussed in chapter 3, ER-positive/HER2-negative cells display a more oxidative phenotype than the ER-negative cells. Therefore, it could be postulated that these cells when exposed to hypoxia, become more dependent on non-oxidative processes such as the non-oxidative PPP. The hypoxic response evaluated by Hedenfalk and colleagues in three breast cell lines (MCF7, T-47D and MDA-MB-468) demonstrated that the same biological processes can be affected by hypoxia although through different genes (Hedenfalk et al., 2005). HIF suppresses oxidative PPP, but increases activity of PKM2 and transketolases, to compensate for unavailability of oxidative PPP. When *TKTL1* is lost under hypoxia, cells might not cope well with an impaired non-oxidative PPP (Tong et al., 2009). All reactions within non-oxidative PPP are reversible, but under hypoxia the rewiring to other metabolic pathways might be limited (Schenk et al., 1998) and the main source of ribulose-5-phosphate synthesis in tumour cells might not be available ((Boros et al., 2000; Cascante et al., 2000). *TKTL1* has been reported to be overexpressed in metastatic tumours and its inhibition has led to death (Coy et al., 2005) (Zhang et al., 2007b). Another possibility could also be that *TKTL1* was found as a hypoxia-specific candidate gene as hypoxia downregulates ERα and ERβ due to repression of transcription and proteasomal degradation. However, the data shown in chapter 6 suggests ER-mediated signalling and decrease of ER activity by 4-hydroxy tamoxifen and 17β-estradiol causes downregulation of *TKTL1*.

Hypoxia and HIF repress MCT1 expression but increase MCT4 (Ullah et al., 2006). Under hypoxic condition, all cancer cells were sensitive to *SLC16A3* ablation as shown in chapter 5. The cell lines displaying MCT4 sensitivity showed a strong induction of it expression following hypoxia compared to the non-malignant cell line MCF10A.

Moreover, the overexpression of *ERBB2* can induce HIF1α and stabilise it (Semenza, 2002), suggesting a potential mechanism for the MCT4-dependency of HER2-positive cells under normoxia. It has also been shown by next-generation sequencing that some ER-negative cell lines and tumours can harbour specific HER2 mutations, which could explain the dependency on MCT4 of some of the HER2-negative cell lines and extend the potential of MCT4 as a target for cancer treatment.

It has been shown that cancers can also depend on the activity of genes that are not themselves oncogenes. The activity of these genes is required to maintain the oncogenic state. Only a few metabolic enzymes have so far been found to harbour mutations or amplifications in tumours. Nonetheless, metabolic enzymes are regulated by oncogenic signalling cascades and could be a rate-limiting factor in the respective signalling pathway. Targeting the activity of these enzymes could block the growth and survival of cancer cells harbouring oncogenic activations within this pathway.

As demonstrated in this thesis, the use of small-scale siRNA screens is an effective approach to discover novel cancer vulnerabilities. The unbiased approach of testing multiple cell lines that recapitulate the genetic diversity in breast cancer in small-scale screening experiments has brought forward 7 candidate genes. These seem to be mostly required for the survival of ER-negative breast cancer cell lines for which no suitable targeted therapy strategy has been developed yet. Monocarboxylate transporters, malic enzymes and PPAP2A are promising candidates for further investigations into their roles in the biology of HER2-positive and ER-negative/HER2-negative breast cancers, while the dependency of cancer cells on TKTL1, ME1 and PPAP2C was defined by their respective metabolic features, a concept that may become available through advanced diagnostics and requires further study.

7.6 Concluding remarks and future outlook

The continuous work and progress of scientists and clinicians in understanding the biology of cancer has improved the overall survival of cancer patients. Today's knowledge of the sequence of the human genome, RNA interference and next generation sequencing technology has provided extensive knowledge of the genetic landscape of cancer and the role of individual genes. The observed high- and low-frequency of genetic alterations influence the signalling cascades in these tumour cells. As signalling and metabolism are directly linked, it would be of great interest to unravel metabolic dependencies that allow the perturbation of the rewired signalling of these tumour cells. This should selectively impair their ability to fulfil the requirements for rapid proliferation. The complexity of rewired metabolism and signalling in cancer cells is even further extended by tumour heterogeneity. This reinforces the need for a better understanding of the underlying genetic and biochemical processes that support cancer development, tumour progression and recurrence as well as therapy resistance.

8 Appendix

8.1 Plasmid map

A)

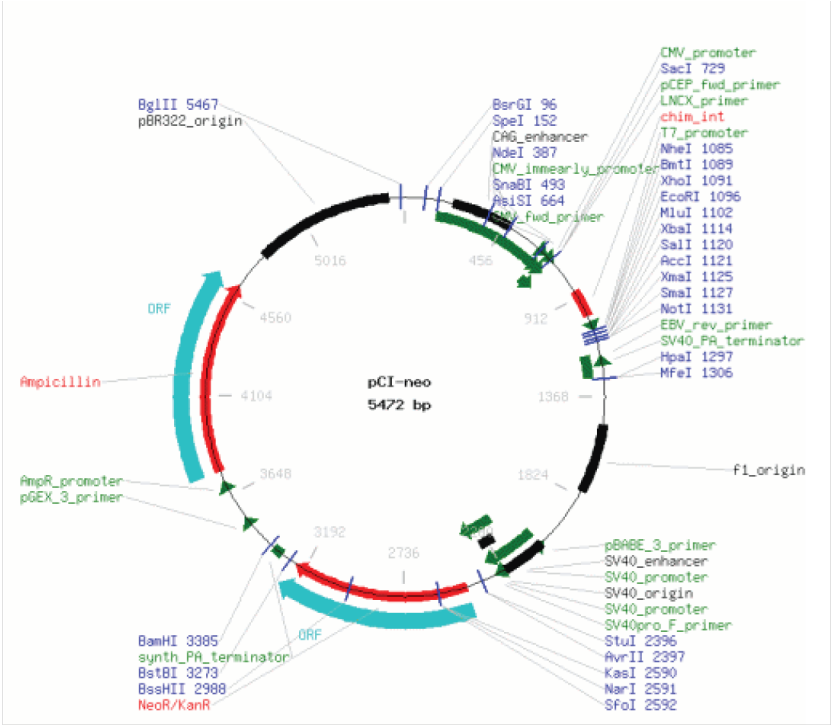

B)

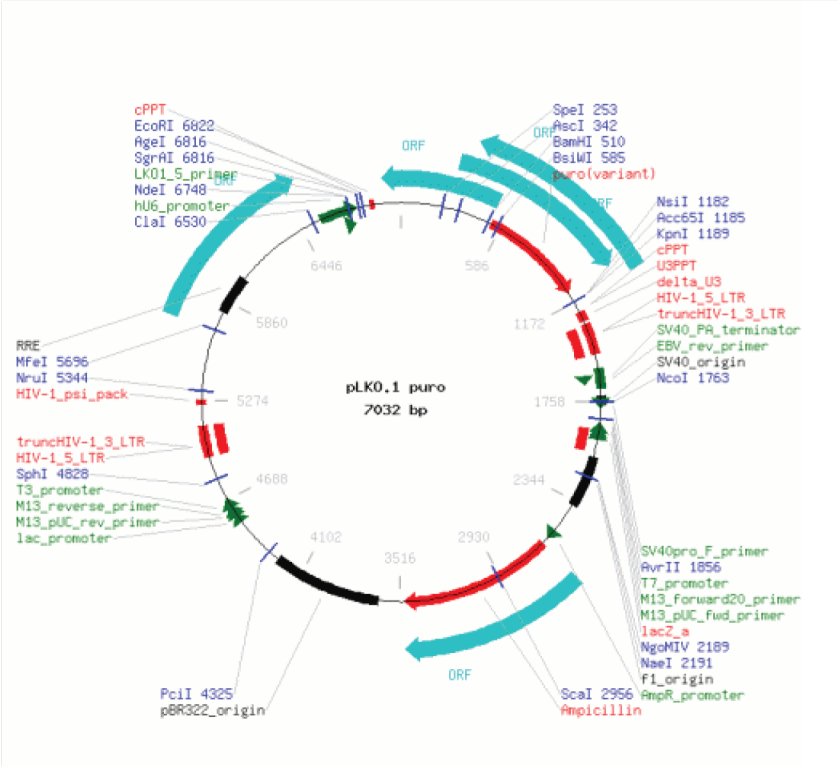

C)

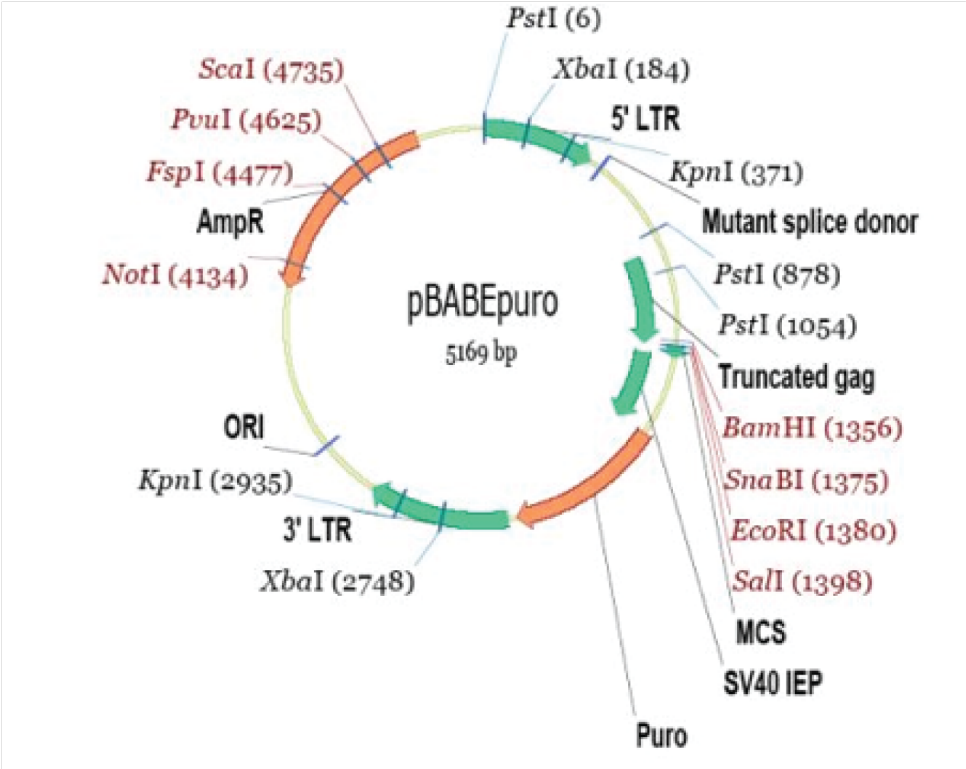
PstI (6)
XbaI (184)
5' LTR
KpnI (371)
Mutant splice donor
PstI (878)
PstI (1054)
Truncated gag
BamHI (1356)
SnaBI (1375)
EcoRI (1380)
SalI (1398)
MCS
SV40 IEP
Puro
ScaI (4735)
PvuI (4625)
FspI (4477)
AmpR
NotI (4134)
pBABEpuro
5169 bp
ORI
KpnI (2935)
3' LTR
XbaI (2748)

8.2 Dharmacon siGenome library

Table 4: siRNA oligonucleotides used in this study

Gene Symbol	Gene Id	Plate	Well	Pool Number	Duplex Number	Sequence
HK1	3098	1	A03	MU-006820-01	D-006820-01	GGAAGGAGAUGAAGAAUGG
					D-006820-03	GAAGUUACCUGUGGGAUUC
					D-006820-04	GCACAACAAUGCCGUGGUU
					D-006820-05	GACCGAGAAUGGUGACUUC
HK2	3099	1	A04	MU-006735-01	D-006735-05	GCGGAUGUGUAUCAAUAUG
					D-006735-02	GAAGUUGGCCUCAUUGUUG
					D-006735-03	GCAGAAGGUUGACCAGUAU
					D-006735-04	CAAGCUACAUCCUCACUUU
GCK	2645	1	A05	MU-010819-01	D-010819-05	CCACGAUGAUCUCCUGCUA
					D-010819-01	GCAAGCAGAUCUACAACAU
					D-010819-02	GCUCAUAGGUGGCAAGUAC
					D-010819-04	GCACGAAGACAUCGAUAAG
PKLR	5313	1	A06	MU-006780-01	D-006780-01	GUGAAGAGGUUUGAUGAAA
					D-006780-02	GGGCAAGCCUGUUGUCUGU
					D-006780-03	GUGGAGAGCUUUGCAGGUU
					D-006780-04	GAAGGACACGGCAUCAAGA
PKM2	5315	1	A07	MU-006781-02	D-006781-05	GCAUUGAGAUUCCUGCAGA
					D-006781-01	GAAAGAACAUCAAGAUUAU
					D-006781-02	UUAGGAAGGUCCUGGGAGA
					D-006781-03	GCAAGAAGGGUGUGAACCU
PC	5091	1	A08	MU-008950-02	D-008950-01	GAAAGCAGAUGAAGCCUAU
					D-008950-03	GAGCUGAUGUGGUGGAUGU
					D-008950-18	GGAUAAUGCUUCCGCCUUC
					D-008950-19	UCUCUGAGCGAGCGGACUU
PDHA1	5160	1	A09	MU-010329-02	D-010329-02	GCUCUAGCCUGUAAGUAUA
					D-010329-04	GCUCACGGCUUUACUUUCA
					D-010329-05	AAGCAGAUCAGCUGUAUAA
					D-010329-06	AAUAAUCGCUAUGGAAUGG
PDHA2	5161	1	A10	MU-023925-01	D-023925-01	UAAGAGGGAUCCUAUAAUA
					D-023925-02	GAUGAGAUCUGUUUGACUU
					D-023925-03	GCAGAUAGCCGAAGCUUUC
					D-023925-04	GCUCAUGGUGUGUGCUAUA
PDHB	5162	1	A11	MU-008803-01	D-008803-01	CAAAUCAUCUUGUAACUGU
					D-008803-02	GGUCAAAGACAUCAUAUUU
					D-008803-03	GAAAGGCAAGGAACACAUA
					D-008803-04	GAGAAUGAAUUGAUGUAUG
DLD	1738	1	A12	MU-009509-01	D-009509-04	GUACAAAGUUGGGAAAUUC
					D-009509-01	GAAGUUCGCUUGAAUUUAG
					D-009509-02	UAUUAAAGCUGCCCAGUUA
					D-009509-03	CAAUGGAUAUGGAAAGAUA
DLAT	1737	1	B03	MU-008490-00	D-008490-01	GCACAGCGAUUAAUGCAAU
					D-008490-02	CAACCGAAGUAACAGAUUU
					D-008490-03	GGAUUGAUCUUACACAAGU
					D-008490-04	GUACGGAAAGAACUUAAUA
ACACA	31	1	B04	MU-004551-02	D-004551-01	GAAAGCAGGUCAACUAUGA
					D-004551-03	CAGCAAACCUGGAUUCUGA
					D-004551-04	GCAGAUGACUUCCCUAAUC
					D-004551-09	GCAAUUAGAUUCGUUGUCA
LDHA	3939	1	B05	MU-008201-01	D-008201-01	GGAGAAAGCCGUCUUAAUU
					D-008201-02	GGCAAAGACUAUAAUGUAA
					D-008201-03	GAAGAGGCCCGUUUGAAGA
					D-008201-04	CUACGUGGCUUGGAAGAUA
LDHB	3945	1	B06	MU-009779-01	D-009779-01	GAAAGUCUCUGGCUGAUGA
					D-009779-02	GGAAGGAAGUGCAUAAGAU
					D-009779-03	GAACUGACAAUGAUAGUGA
					D-009779-04	CAUGGGAGCUUAUUUCUUC
LDHC	3948	1	B07	MU-008759-02	D-008759-01	GGAUUUGGCUGAUGAACUU
					D-008759-03	GUUAAGGGAUUAUAUGGAA
					D-008759-04	GGAAUGGUGUCUCAGAUGU
					D-008759-05	CGUAAUGUGGCUAUAAUGA

Gene Symbol	Gene Id	Plate	Well	Pool Number	Duplex Number	Sequence
CS	1431	1	B08	MU-009334-01	D-009334-01	GCAAAGAUCUACCGAAAUC
					D-009334-03	GGACUGGUCUCACAAUUUC
					D-009334-04	GCAAAGCUACCUUGUGUUG
					D-009334-17	GGAAGACUGAUCCGCGAUA
ACLY	47	1	B09	MU--004915-00	D-004915-01	CCAACGAGCUCAACAAUAU
					D-004915-02	GACCAAAGAUGGAGUCUAU
					D-004915-03	UCAACGAGCUGGCAAACUA
					D-004915-04	CCACUCCUCUGCUCGAUUA
G6PD	2539	1	B10	MU-008181-02	D-008181-05	UGACCUACGGCAACAGAUA
					D-008181-01	GAGAGUGGGUUUCCAGUAU
					D-008181-02	CAACAUCGCCUGCGUUAUC
					D-008181-03	CGUGAGGCCUGGCGUAUUU
FASN	2194	1	B11	MU-003954-04	D-003954-01	GAGCGUAUCUGUGAGAAAC
					D-003954-03	UGACAUCGUCCAUUCGUUU
					D-003954-04	CCAUGGAGCGUAUCUGUGA
					D-003954-08	GCAACUCACGCUCCGGAAA
CHKA	1119	1	B12	MU-006704-01	D-006704-01	GAAUUAAGUUUGCCAGAUA
					D-006704-02	CAGAUGAGGUCCUGUAAUA
					D-006704-03	GAGCAAACAUCCGGAAGUA
					D-006704-04	GAAUACAGCAGUUACAAUU
CHKB	1120	1	C03	MU-006705-00	D-006705-01	GGAAUGGCCUUUCUACAAA
					D-006705-02	GUGAGUGGGUUUAUGAUUA
					D-006705-03	CCACGAAGAUGGCGCAAUU
					D-006705-04	CAUAGAAUUUGGUUACUUG
HMGCS1	3157	1	C04	MU-009808-01	D-009808-01	GAAGACACCUACUUUGAUA
					D-009808-04	GAUAUUAACUCUCUUUGCA
					D-009808-17	GCCAAAUGUACUCGAAUGA
					D-009808-18	CAGAGACAAUCAUCGACAA
HMGCS2	3158	1	C05	MU-010179-01	D-010179-01	AAACUGACCUGGAGAAGUA
					D-010179-02	ACACAAACCAGCUUAUAUA
					D-010179-03	AGAGAGCAAUUCUACCAUA
					D-010179-04	GGGCAUAGAUACCACCAAU
HMGCR	3156	1	C06	MU-009811-02	D-009811-03	UGAAGAAUGUCUACAGAUA
					D-009811-04	CCAGAAAUGUGAUUCAGUA
					D-009811-06	GAGCAGUGACAUUAUAAUU
					D-009811-19	GAUGGAAACUCAUGAGCGU
SLC2A4	6517	1	C07	MU-007517-02	D-007517-01	CAGAUAGGCUCCGAAGAUG
					D-007517-02	GCAUGGGUUUCCAGUAUGU
					D-007517-03	UCAACCAACUGGCCAUUGU
					D-007517-05	ACAGAUAGGCUCCGAAGAU
SLC2A1	6513	1	C08	MU-007509-01	D-007509-02	CCAAGAGUGUGCUAAAGAA
					D-007509-03	CAUCGUGGCUGAACUCUUC
					D-007509-04	GAGCAUCGUGGCCAUCUUU
					D-007509-05	GUAUGUGGGUGAAGUGUCA
SREBF1	6720	1	C09	MU-006891-01	D-006891-01	UGACUUCCCUGGCCUAUUU
					D-006891-02	ACAUUGAGCUCCUCUCUUG
					D-006891-03	GCGCACUGCUGUCCACAAA
					D-006891-04	ACACAGACGUGCUCAUGGA
SREBF2	6721	1	C10	MU-009549-00	D-009549-01	GAGCGGAGCUGGUCUGUGA
					D-009549-02	GAAGAGAGCUGUGAAUUCU
					D-009549-03	GCACAAGUCUGGCGUUCUG
					D-009549-04	AAACUCAGCUGCAACAACA
PRKAA1	5562	1	C11	MU-005027-02	D-005027-01	CAAAGUCGACCAAAUGAUA
					D-005027-02	GUAGAGCAAUCAAACAAUU
					D-005027-03	GACAAGCACUUACUCCAAA
					D-005027-05	ACAAUUGGAUUAUGAAUGG
PRKAA2	5563	1	C12	MU-005361-02	D-005361-02	GUACCUACGUUAUUUAAGA
					D-005361-03	GGAAGGUAGUGAAUGCAUA
					D-005361-04	GACAGAAGAUUCGCAGUUU
					D-005361-05	ACAGAAGAUUCGCAGUUUA
HIF1A	3091	1	D03	MU-004018-05	D-004018-01	GGACACAGAUUUAGACUUG
					D-004018-06	UCACCAAAGUUGAAUCAGA
					D-004018-03	GAUGGAAGCACUAGACAAA
					D-004018-05	CGUGUUAUCUGUCGCUUUG

Gene Symbol	Gene Id	Plate	Well	Pool Number	Duplex Number	Sequence
AKT2	208	1	D05	MU-003001-02	D-003001-05	GUACUUCGAUGAUGAAUUU
					D-003001-06	GCAAAGAGGGCAUCAGUGA
					D-003001-07	GGGCUAAAGUGACCAUGAA
					D-003001-08	GCAGAAUGCCAGCUGAUGA
AKT3	10000	1	D06	MU-003002-02	D-003002-09	GAAAGAUUGUGUACCGUGA
					D-003002-10	GGACUACUGUUAUAGAGAG
					D-003002-11	UGAGACAGAUACUAGAUAU
					D-003002-12	GCUCAUUCAUAGGAUAUAA
ILVBL	10994	1	D07	MU-009658-02	D-009658-03	UGACUGCGGUGAAGAAUGC
					D-009658-20	CCUGGUAUUUAGAGAAUUA
					D-009658-21	CGUCAAUCGUAAUCGGGAA
					D-009658-22	GCUACAGCCUCAUCGAAUU
PHGDH	26227	1	D08	MU-009518-01	D-009518-01	GAACAUCCCUGAAGAAUGC
					D-009518-02	GAACUCACUUGUGGAAUGA
					D-009518-03	GGAAAGACCCUGGGAAUUC
					D-009518-04	GGAAGGGCAUCUUGGUUAU
MDH1	4190	1	D09	MU-009264-00	D-009264-01	CAAAGGAACUGACAGAAGA
					D-009264-02	CAUCAAGGCUCGAAAACUA
					D-009264-03	GUUGAAGGUCUCCCUAUUA
					D-009264-04	AAGGUGAAAUUGCAAGGAA
MDH2	4191	1	D10	MU-008439-00	D-008439-01	CCAGAACAAUGCUAAAGUA
					D-008439-02	CAACACCAAUGCCACGAUU
					D-008439-03	CAAGAAGCAUGGAGUGUAC
					D-008439-04	CCUGAAAGGUUGUGAUGUG
GPD1	2819	1	D11	MU-008782-01	D-008782-02	AGAAAGAGUUGCUGAAUGG
					D-008782-04	GAUCGUGGGUGGCAAUGCA
					D-008782-17	AGAUGAUAGCCUUCGCCAA
					D-008782-18	CCCAUCAGUUCAUCGGCAA
GPD2	2820	1	D12	MU-009843-02	D-009843-01	UGAAUGAAGUGCGUAAUUA
					D-009843-02	GAACCUGGCCUAUGUUAAA
					D-009843-03	GAUAUGAUUUCACGUCGUA
					D-009843-05	GAGAGUGGCCUUAUUACUA
PRPS1	5631	1	E03	MU-006784-00	D-006784-01	GCAAAUAUGCUAUCUGUAG
					D-006784-02	UGGAGGAACUGCACUAUUG
					D-006784-03	GUGAUUGACAUCUCUAUGA
					D-006784-04	CCAUGCAGCUGACAAACUU
PRPS2	5634	1	E04	MU-004877-02	D-004877-05	GAUCUUGGCCGAAGCAAUC
					D-004877-01	AUACAGGGAUUCUUUGAUA
					D-004877-03	CAAAGUGUAUGCUAUCCUU
					D-004877-04	CAGAGUAACUGCCGUGAUC
PPAT	5471	1	E05	MU-006003-01	D-006003-01	GAAAUGGUCUGGAAUGUUU
					D-006003-02	GGUAAAUGCUGCUCGAUUA
					D-006003-03	GGGAAUGGGUCUUGUAAAU
					D-006003-05	GAAUGGGUCUUGUAAAUCA
UMPS	7372	1	E06	MU-009828-01	D-009828-02	GAACUAAGCGUCUUGUAGA
					D-009828-04	GAAGACUCAUGUAGAUAUU
					D-009828-17	AUUUCUGGCUCCCGAGUAA
					D-009828-18	UGAUAUUUGAAGACCGGAA
SLC1A5	6510	1	E07	MU-007429-01	D-007429-02	GGAUGUGGGUUUACUCUUU
					D-007429-03	GUUCUGGUCUCCUGGAUCA
					D-007429-17	GAGAGGAAUAUCACCGGAA
					D-007429-18	CAGUCAACCUCCCGGUCGA
SLC7A5	8140	1	E08	MU-004953-01	D-004953-01	GAUCCCAACUUCUCAUUUG
					D-004953-03	UGACCAACCUGGCCUACUU
					D-004953-17	GUGAACUGCUACAGCGUGA
					D-004953-18	UGAAAACUCUGGUACGAAU
PFKL	5211	1	E09	MU-006822-00	D-006822-01	UGAAGAUGCUGGCACAAUA
					D-006822-02	GCACAAUACCGCAUCAGUA
					D-006822-03	CACAAUACCGCAUCAGUAU
					D-006822-04	UGCUGAAGAUGCUGGCACA
GAPDH	2597	1	E10	MU-004253-02	D-004253-01	CAACGGAUUUGGUCGUAUU
					D-004253-03	GACCUCAACUACAUGGUUU
					D-004253-04	UGGUUUACAUGUUCCAAUA
					D-004253-05	GUCAACGGAUUUGGUCGUA

Gene Symbol	Gene Id	Plate	Well	Pool Number	Duplex Number	Sequence
GAPDS	26330	1	E11	MU-009671-01	D-009671-01	CAAGGGAAGUGUGGAAUUC
					D-009671-02	GGACAACCAUGAGAUCUCU
					D-009671-03	UGGUGUACAUGUUUAAGUA
					D-009671-04	CCAUGAACAUUGUGAGCAA
PGK1	5230	1	E12	MU-006767-01	D-006767-05	GAAGCGGGUCGUUAUGAGA
					D-006767-01	CAAAAUUGAUGAUCCAUUA
					D-006767-02	UUGAUGAUCCAUUAAGUAA
					D-006767-04	GCACAGCAUCUCAGCUCAU
PGK2	5232	1	F03	MU-006768-02	D-006768-05	GGAAUGGGCCGUUAGGAGU
					D-006768-02	GCAGACAAGAUCCAACUUA
					D-006768-03	CAAGAUCCCUCUGGAAAGA
					D-006768-04	UGACAAAUAUUCCUUAGCA
ENO1	2023	1	F04	MU-004034-02	D-004034-03	CAAACUGAUGAUCGAGAUG
					D-004034-04	AAUGAUAAGACUCGCUAUA
					D-004034-01	GAACGUCACAGAACAAGAG
					D-004034-02	GAUAAGACUCGCUAUAUGG
IDH1	3417	1	F05	MU-008296-00	D-008294-03	GUACAUAACUUUGAAGAAG
					D-008294-04	CAAGAUAAGUCAAUUGAAG
					D-008294-01	GAGCAAAGCUUGAUAACAA
					D-008294-02	GGACUUGGCUGCUUGCAUU
IDH2	3418	1	F06	MU-004013-00	D-004013-01	CAAGAACUAUGACGGAGAU
					D-004013-02	GCGCCACUAUGCCGACAAA
					D-004013-03	AACGAGCACUUCCUGAACA
					D-004013-04	GACAUCCAGCUAAAGUAUU
OGDH	4967	1	F07	MU-009679-02	D-009679-03	GCUAGGACAUUUCAACAGA
					D-009679-05	CAGACAAACUUGGGUUCUA
					D-009679-18	UCUAGAAGGCUGCGAGGUA
					D-009679-19	CUGAUGAGGGCUCCGGAGA
SDHA	6389	1	F08	MU-009398-02	D-009398-01	GAGGGAGGCAUUCUCAUUA
					D-009398-03	CGAAGGACCUGGCGUCUAG
					D-009398-04	UGAGAAAGAUCACGUCUAC
					D-009398-14	CGAAAGGUUUAUGGAGCGA
SDHB	6390	1	F09	MU-011773-02	D-011773-01	GGUAUUGGAUGCUUUAAUC
					D-011773-02	GAACAUCAAUGGAGGCAAC
					D-011773-19	GUGAGAAACUGGACGGGCU
					D-011773-20	GCUACUGGUGGAACGGAGA
SDHC	6391	1	F10	MU-011385-01	D-011385-17	GGGCUUAGAUAGAAAGUCU
					D-011385-18	AGUUAAAGCUGUGGGUCGA
					D-011385-19	GAAAAGAAGUGACGCAUGU
					D-011385-20	UCGAAGUAAUGUACCCUUU
SDHD	6392	1	F11	MU-006305-00	D-006305-01	GGACCGACCUAUCCCAGAA
					D-006305-02	GCUUUGCUAUUUCAACUAU
					D-006305-03	ACUUUCAGCUUUAACCUUU
					D-006305-04	CAGACCUGCUCAUAUCUCA
FH	2271	1	F12	MU-009512-00	D-009512-01	GAUCUACGAUGAACUUUAA
					D-009512-02	UCAACAAGCUGAUGAAUGA
					D-009512-03	GCACAGAUCAUCAAGAUUG
					D-009512-04	AGCCAGAGCUCAAAUGAUA
CHPT1	56994	1	G03	MU-009775-02	D-009775-01	GAACUUAUCCUGACUGGUU
					D-009775-06	UUUCAGGCAUGUUGAGAUU
					D-009775-19	GCGCUCAUUGGCAGACUUA
					D-009775-20	CUUCAUUUGAUAUGGUGAU
MVK	4598	1	G04	MU-006749-00	D-006749-01	UGGAAGAGCUCAUUGACAU
					D-006749-02	ACACCAAAGUCCCUCGCAA
					D-006749-03	GCUCAAGUUCCCAGAGAUC
					D-006749-04	ACCAAAGUCCCUCGCAAUA
PMVK	10654	1	G05	MU-006782-01	D-006782-01	UUUAUCCGCUCCAGACUUU
					D-006782-02	CGAGAACCAUGGAGUUGAA
					D-006782-03	GCGAAACCCUGCCAUAUCC
					D-006782-04	AAUGUGGCCUGGACAACUU
MVD	4597	1	G06	MU-006748-00	D-006748-01	GACCGGAUUUGGCUGAAUG
					D-006748-02	ACAUCGCGGUCAUCAAGUA
					D-006748-03	GCCCAUCUCUUACCUCAAU
					D-006748-04	CAGCAUCGCUCGGCAAGUG

Gene Symbol	Gene Id	Plate	Well	Pool Number	Duplex Number	Sequence
FDPS	2224	1	G07	MU-008632-02	D-008632-01	GACCAGAAUUCAGAUGUUU
					D-008632-02	CAGCAGUGUUCUUGCAAUA
					D-008632-05	GAAGACAGUUACAGCCACA
					D-008632-06	GGGUGAAGGCGCUAUAUGA
GGPS1	9453	1	G08	MU-016477-02	D-016477-03	CAAAUUAGGGAUGAUUAUG
					D-016477-04	UAAAACCGCUACUUAAUAC
					D-016477-20	GGGACAAGGCCUAGAUAUU
					D-016477-21	CCAAUUGGGAAGCGGAAAA
LSS	4047	1	G09	MU-008624-00	D-008624-01	GGACUGCGCUCAACUAUGU
					D-008624-02	GCAGAAGGCUCAUGAGUUC
					D-008624-03	GAAGCUGUAUGAACACAUU
					D-008624-04	UGCAGGCGCUUAAGUAUUU
DHCR7	1717	1	G10	MU-020182-01	D-020182-01	GGCCAAGACUCCACCUAUA
					D-020182-02	GAACAAGUAUCAGAUCAAC
					D-020182-03	CAUCAUGGCUUGUGACCAG
					D-020182-04	GCCCAGCUCUAUACCUUGU
PRKAG2	51422	1	G11	MU-009693-01	D-009693-02	GCAAUAAGCUGGAAAUACU
					D-009693-03	CCACAACAUUGCCUUCAUA
					D-009693-17	CGGAGUGACCGCCGUGAAU
					D-009693-18	CCACAGAUUGCCCGUUAUU
PRKAG3	53632	1	G12	MU-009859-01	D-009859-01	UCUAUGAGAUUGAACAACA
					D-009859-02	GGGAAGUGAUCGACAGGAU
					D-009859-03	ACAAACGCCUGCUCAAGUU
					D-009859-05	GCUCCAAGCUAGUCAUCUU
PRKAB1	5564	1	H03	MU-007675-00	D-007675-01	CAGAAGCCACAAUAACUUU
					D-007675-02	CAACAACUGGAGUAAACUU
					D-007675-03	UGUCUGAGCUGUCCAGUUC
					D-007675-04	GGAAGGAGAGCAUCAGUAC
PRKAB2	5565	1	H04	MU-007672-00	D-007672-01	GUUCGAUGCUUUAAAGUUA
					D-007672-02	UAAGAGCCAUAAUGACUUU
					D-007672-03	GCAAGGAGGUCUUCAUCUC
					D-007672-04	GCACCAAGAUUCCACUGAU
PRKAG1	5571	1	H05	MU-009056-01	D-009056-01	GGACAUCUACUCCAAGUUU
					D-009056-02	GAUGCUGUCUCUUCAUUAA
					D-009056-03	CAACAUCGAUCACAUUACU
					D-009056-04	GUGUAUACUUCCUUCAUGA
EPAS1	2034	1	H06	MU-004814-01	D-004814-05	ACACAUCUUUGGAUAACGA
					D-004814-02	GCAAAUGUACCCAAUGAUA
					D-004814-03	GAGCGGGACUUCUUCAUGA
					D-004814-04	AGACGGAGGUGUUCUAUGA
MT-ND1	4535	1	H07	n.a.	D-012827-01	UAACCUCCCUGUUCUUAUG
					D-012827-02	UGAUUUAUCUCCACACUAG
					D-012827-03	CUAAUAAGUGGCUCCUUUA
					D-012827-04	CCGAAUACACAAACAUUAU
MT-ND2	4536	1	H08	n.a.	D-012828-01	GCGCUAAGCUCGCACUGAU
					D-012828-02	UAACCAAUACUACCAAUCA
					D-012828-03	CAAUAUACUCUCCGGACAA
					D-012828-04	CCAUAUCUAACAACGUAAA
MT-ND3	4537	1	H09	n.a.	D-012829-01	CAACUAACCUGCCACUAAU
					D-012829-02	CCGCGUCCCUUUCUCCAUA
					D-012829-03	CUUAGUAGCUAUUACCUUC
					D-012829-04	CAACUCAACGGCUACAUAG
MT-ND4	4538	1	H10	n.a.	D-012830-01	CUAGGCGGCUAUGGUAUAA
					D-012830-02	GACCUAAAAUCGCUCAUUG
					D-012830-03	GAGCCAAUAACUUAAUAUG
					D-012830-04	UAACCACGUUCUCCUGAUC
MT-ND5	4540	1	H11	n.a.	D-012831-01	UGAGAGGGCGUAGGAAUUA
					D-012831-02	GCCUAUAGCACUCGAAUAA
					D-012831-03	CUAGGACUCAUAAUAGUUA
					D-012831-04	CUACUCCACUCAAGCACUA
MT-ND6	4541	1	H12	n.a.	D-012832-01	GGUCGGGUGUGUUAUUAUU
					D-012832-02	GAAUGAUGGUUGUCUUUGG
					D-012832-03	CGAUGGCUAUUGAGGAGUA
					D-012832-04	GAUUAUGGGCGUUGAUUAG

Gene Symbol	Gene Id	Plate	Well	Pool Number	Duplex Number	Sequence
GALK1	2584	2	A03	M-007728-01	D-007728-03	GACCAGUUCAUCUCACUUA
					D-007728-04	GCGCCAAUGUGAAGAAGUG
					D-007728-05	GGGAACACACGGACUACAA
					D-007728-06	GAGCCAAGGUGCUGUGCUU
GALK2	2585	2	A04	M-006725-00	D-006725-01	GCUAAUAACAUCCAGAUUG
					D-006725-02	GCACAACUAUUUCUUAUGU
					D-006725-03	GGAAAUAUCCCACCAAGUU
					D-006725-04	GGACCAGUCUAUAUCAUUU
GALT	2592	2	A05	M-010327-00	D-010327-01	AAACAAAGGUGCCAUGAUG
					D-010327-02	GAUCUAGCCUCCAUCAUGA
					D-010327-03	GAUCUCAGCAGGCCUAUAA
					D-010327-04	GCAAACGACCAUCAGCAUA
PGM1	5236	2	A06	M-010925-00	D-010925-01	CGAAUCGUCUUCCGACUGA
					D-010925-02	GUACAUCGAUAGCUAUGAG
					D-010925-03	CGACUGAAGAUCCGUAUUG
					D-010925-04	GGAAAUUGUGGAUUCGGUA
PGM3	5238	2	A07	M-013912-00	D-013912-01	GAGGUCAAUUCCAUGAUUA
					D-013912-02	GGAUUUAGGUGCUAUUACA
					D-013912-03	GGGCAAACUCAAUCAUUUA
					D-013912-04	GACAAGAUAGCAACGUUAA
GLUD1	2746	2	A08	M-004032-02	D-004032-01	GCAACCAUGUGCUGAGUCU
					D-004032-02	UAAAUCAUGUCAGCUAUGG
					D-004032-05	CAAUGAAGCUUCUUACAUG
					D-004032-19	GAAAUUAAGGUUAGCGGAU
GLUD2	2747	2	A09	M-009067-02	D-009067-01	CAAUGAAGCUUCUUACAUG
					D-009067-04	GGACGCAUCUCUGCUACUG
					D-009067-05	CAAGGGAGGUAUCCGUUAC
					D-009067-18	CUUUAUUGGUCCUGGCGUU
HK3	3101	2	A10	M-006736-00	D-006736-01	GGAAUGCGAUGUCUCCUUA
					D-006736-02	GCAGUUGACUCGUGUCUGA
					D-006736-03	GACAGGAGCACCCUCAUUU
					D-006736-04	UCACGUUCCUGCAGUCAGA
GPI	2821	2	A11	M-004900-01	D-004900-01	GGAAAUACAUCACCAAAUC
					D-004900-03	CAACCAAAGUGAAGGAGUU
					D-004900-04	GAUGAUACCCUGUGACUUC
					D-004900-05	UCACGACGCUUCUACCAAU
PFKM	5213	2	A12	M-006765-01	D-006765-01	UCAAGAAUCUGGUGGUUAA
					D-006765-03	GAUCAUGGAAAUUGUAGAU
					D-006765-04	CAGAAGACAUCAAGAAUCU
					D-006765-05	GGAUAUGACACCCGGGUUA
PFKP	5214	2	B03	M-010253-01	D-010253-01	GAAAUCGGCUGGACAGAUG
					D-010253-02	CAACGUAGCUGUCAUCAAC
					D-010253-03	GAAGAGAUCGCCACACAGA
					D-010253-05	GGAACGGCCAGAUCGAUAA
PFKFB1	5207	2	B04	M-006761-01	D-006761-01	UAAAGAGAAUUGAGUGCUA
					D-006761-03	UAAUGACCCUGGCAUAAUU
					D-006761-04	GCUAUGAGGUCAACUACCA
					D-006761-17	UACCAGAGAACGACGGUCA
PFKFB2	5208	2	B05	M-006762-02	D-006762-01	GAACUUUGCUGAACAGAAU
					D-006762-02	GAACAGAGAGAACGUGAUG
					D-006762-03	CCAAUAUUCUGGAGGUUAA
					D-006762-18	CGGCAUGGAGAAAGCGAGU
PFKFB3	5209	2	B06	M-006763-01	D-006763-01	GGACCUAACCCGCUCAUGA
					D-006763-02	GAGGAUCAGUUGCUAUGAA
					D-006763-03	AAAGCUACCUGGCGAAAGA
					D-006763-17	ACAAGUACUAUUACCGCUA
PFKFB4	5210	2	B07	M-006764-01	D-006764-01	GAGCGACCAUCUUUAAUUU
					D-006764-02	GAAAUGACCUACGAGGAAA
					D-006764-04	CAUCGUAUAUUACCUCAUG
					D-006764-17	GGGACAGGCCUCAGAACGU
ALDOA	226	2	B08	M-010376-01	D-010376-02	GGACAAAUGGCGAGACUAC
					D-010376-03	UUGAAGCGCUGCCAGUAUG
					D-010376-04	GGCGUUGUGUGCUGAAGAU
					D-010376-05	UGACAUCGCUCACCGCAUC

Gene Symbol	Gene Id	Plate	Well	Pool Number	Duplex Number	Sequence
ALDOB	229	2	B09	M-010990-01	D-010990-01	CCAAAGCCCUGGAAACUAA
					D-010990-02	GGACAUGCCUGCACCAAGA
					D-010990-04	GAAGAAGGAGCUCUCAGAA
					D-010990-05	CCAAAGGACAGUAUGUUCA
ALDOC	230	2	B10	M-012697-01	D-012697-01	GAAAGAUGAUAAUGGUGUU
					D-012697-02	GCGCUUACCUUCUCCUAUG
					D-012697-03	GCACAGUCACUCUACAUUG
					D-012697-04	AAACGUUGUCAGUAUGUUA
TPI1	7167	2	B11	M-009776-02	D-009776-01	GCAAGGUCGUCCUGGCCUA
					D-009776-02	GCUCAGAGCACCCGUAUCA
					D-009776-05	AGAGAGAAGGCAUGUCUUU
					D-009776-06	GAUCAAAGACUGCGGAGCC
PGAM4	441531	2	B12	M-034271-00	D-034271-13	GCACAGGUUCUCAGUCUAA
					D-034271-14	CCUCAUACCAAUAUAGGAU
					D-034271-15	CAUGCUAAGCCACGACCAA
					D-034271-16	CAGAAGAGAGUGAUCCGGA
PGAM1	5223	2	C03	M-008883-01	D-008883-02	GGACAAGAACUUGAAGCCU
					D-008883-03	CCAUGCAGUUUCUGGGGGA
					D-008883-04	UGAAGAGACGGUGCGCAAA
					D-008883-05	GGUCUAACCGGUCUCAAUA
PGAM2	5224	2	C04	M-008712-02	D-008712-01	GAUCAAGGCCGGCAAGCGA
					D-008712-03	CCAAGAUGGAGUUUGACAU
					D-008712-18	UGUCAGACCAGGCGAUCAU
					D-008712-19	GGAUGUCAGACCAGGCGAU
BPGM	669	2	C05	M-008917-02	D-008917-02	GAAAGCUCCUGGCGUCUAA
					D-008917-03	GGAAUAAGGAGAACCGUUU
					D-008917-04	GGAGGAAGCUCGGAACUGU
					D-008917-18	CAACUGCCACGGUCGGAAA
ENO2	2026	2	C06	M-009777-01	D-009777-04	CUGAACGUCUGGCUAAAUA
					D-009777-17	GGACAUAACUUCCGUAAUC
					D-009777-18	CCACUGAUCCUUCCCGAUA
					D-009777-19	CCUCAGAGUUUUAUCGUGA
ENO3	2027	2	C07	M-009718-02	D-009718-02	CUAUGAGGCUCUGGAACUA
					D-009718-03	GGGUGAACAUCCAGAUUGU
					D-009718-04	GCAAUGGGAAGUACGAUCU
					D-009718-05	CGGAGCGUCUGGCCAAAUA
LDHAL6A	160287	2	C08	M-008760-01	D-008760-01	GGAGAAACACGCCUUGAUU
					D-008760-02	CCAGAUAUAGGAACUGAUA
					D-008760-03	GGAGUGGUGUGAACAUUGC
					D-008760-04	GAAGAGGAGGCCAUUCAUC
LDHAL6B	92483	2	C09	M-008908-02	D-008908-01	UGGAAUAGAUGAAGAAGUA
					D-008908-03	AGUAAGGUCUCCAUCAUAG
					D-008908-04	GACGAUGGAUCUUCAACAU
					D-008908-17	GAGUGAGCUUAUUGAGCGU
PDK3	5165	2	C10	M-005021-02	D-005021-02	GUUGGUAUAUGCAGAGUUU
					D-005021-03	UAAGAUCAGUGACCUAGGU
					D-005021-05	CGGGAGAGAUAAUGCAUGU
					D-005021-06	GUUCAGAGUUGGUAUAUGC
PDK4	5166	2	C11	M-019425-02	D-019425-01	AAAGAAGACCUUACCAUUA
					D-019425-02	GAAAUAGACACCAUAAUGU
					D-019425-03	CGACAAGAAUUGCCUGUGA
					D-019425-04	GACCGCCUCUUUAGUUAUA
PDP1	54704	2	C12	M-008718-00	D-008718-01	CGACUGAUAUUGAUGUUAA
					D-008718-02	GAACUGAGCAGGAUCUAUG
					D-008718-03	GCAUCCAAAUUGUACUUUA
					D-008718-04	GCAAGUUGGUGAUCCUAAU
PDP2	57546	2	D03	M-022572-00	D-022572-01	CAACAGAGGAAGAUGAUUU
					D-022572-02	GCAAACCAAUGGACUGAUG
					D-022572-03	GGAACAGCAUUGCCACAUU
					D-022572-04	GAAGAAGCAUUAAUGUACU
ACO1	48	2	D04	M-010037-00	D-010037-01	GCAAACAGGUCGUGAUGAA
					D-010037-02	GAACAUAGAAGUGCCAUUU
					D-010037-03	GUAGGAAUGUUUCGAGAUU
					D-010037-04	GAGAUUCGGUAACAACUGA

Gene Symbol	Gene Id	Plate	Well	Pool Number	Duplex Number	Sequence
ACO2	50	2	D05	M-009566-00	D-009566-01	CAAUCUAGCUGAUGAAUUC
					D-009566-02	CCACUUCCGUGUUCCCUUA
					D-009566-03	GCAGUGCCCUCAACAGAAU
					D-009566-04	GGACGGCUAUGCACAGAUC
LOC441996	441996	2	D06	M-035153-01	D-035153-09	CAGGCAAGGAUGGCAAGAA
					D-035153-10	GGUCAGUUGCACAGAAAGG
					D-035153-11	GCAGGAGAAGAACAUAAUU
					D-035153-12	GCAGAUCCGUGCCUCCAUU
IDH3A	3419	2	D07	M-008753-00	D-008753-01	GCAGAAAGCUGUAAAGAUA
					D-008753-02	GAACGUCACUGCCAUUCAA
					D-008753-03	GGAAAGAGCUUGACAAAAG
					D-008753-04	GCUAAAGAGUCCAUGGAUA
IDH3B	3420	2	D08	M-009596-00	D-009596-01	UGAAGAAGGUGAUCAAAGU
					D-009596-02	GCAUCUUAAUCUUGAGUAU
					D-009596-03	GCAGUGGGCAGGAAUAUAG
					D-009596-04	UUGAGACAAUGAUCAUAGA
IDH3G	3421	2	D09	M-009361-00	D-009361-01	GCAAGAGUAUCGCCAAUAA
					D-009361-02	GGACAUAGACAUCCUCAUU
					D-009361-03	GCACGUGAGUUCCAAUGCU
					D-009361-04	GAACACAGAGGGCGAGUAC
DLST	1743	2	D10	M-009941-02	D-009941-01	GCAGGAAGGUUGUCAUUAA
					D-009941-02	GCAGAGAGGCUGUGACUUU
					D-009941-05	GAUGAGGGCUCGGCACAAA
					D-009941-19	CAAAAUCAAGGCAGCGGUA
LOC283398	283398	2	D11	M-026908-01	D-026908-01	UAAAGGAAGCUCAAGUAUA
					D-026908-02	CAAAUUACGAAGCUGUAUA
					D-026908-03	GGACGACAAAUCAGAGAAU
					D-026908-04	ACUAGAAACUUCCAGUCAA
SUCLG2	8801	2	D12	M-008918-01	D-008918-01	AAAGGAAGCUCAAGUAUAU
					D-008918-02	AAAUGAAGCUGCCAAAUAU
					D-008918-04	GGACUAGAUGGGAACAUUG
					D-008918-17	GGUACAAUCUAGCGACAAA
SUCLG1	8802	2	E03	M-008677-01	D-008677-01	GAAAUUCCCUUGGUUGUGU
					D-008677-02	AGAGAAUGCUGCAGAAUUU
					D-008677-03	GGGCUUACCUGUCUUUAAU
					D-008677-04	GAUCUGGCACCCUGACUUA
SUCLA2	8803	2	E04	M-008237-00	D-008237-01	GCAAAGGAAUCUCUCACUA
					D-008237-02	GGAUGAAGCUGCUAGAAUG
					D-008237-03	UCAAGGUCCUGUAUUAAUA
					D-008237-04	GGGAAGUUCUGGAUUGUUU
GOT1	2805	2	E05	M-011673-01	D-011673-01	GAGCAUAUCGCACGGAUGA
					D-011673-02	UUAAAGACAUUCGGUCCUA
					D-011673-03	UAGCCUAAAUCACGAGUAU
					D-011673-17	GAACAGGUGCACUUCGAAU
GOT2	2806	2	E06	M-011674-02	D-011674-01	GCAUGCAGCUACAAGGUUA
					D-011674-03	AACAUGGGCUUAUAUGGUG
					D-011674-04	CUUGAAGAGUGGCCGGUUU
					D-011674-18	UGAGAAACAGCACACGUUA
SLC25A11	8402	2	E07	M-007470-00	D-007470-01	GGACUCAGGCUACUUCUCU
					D-007470-02	GGGAUGGGAGCUACAGUUU
					D-007470-03	CAGAACAUGCGGAUGAUUG
					D-007470-04	UCUAUACCGUGCUGUUUGA
GPD1L	23171	2	E08	M-008514-01	D-008514-01	GGAAGACCAUUGAAGAGUU
					D-008514-02	GGCUGAAGCUCAUUUCUGA
					D-008514-03	GUUGCCAUGUCAAAUCUUA
					D-008514-04	GCAGACCAGUUCAAGAGAU
ME3	10873	2	E09	M-008499-01	D-008499-01	CAACAAUGCUGAAUUCUUG
					D-008499-02	ACAAAUACCGUAACAAGUA
					D-008499-03	GGAGCCACCUGAACCAUGA
					D-008499-04	CUAAAGGGCUCAUUGUCAA
GLUL	2752	2	E10	M-008228-01	D-008228-01	GCACGUGUCUUCUCAAUGA
					D-008228-02	GAAGAAGGGUUACUUUGAA
					D-008228-03	GCACACCUGUAAACGGAUA
					D-008228-04	CAUGAAACCUCCAACAUCA

Gene Symbol	Gene Id	Plate	Well	Pool Number	Duplex Number	Sequence
GPT	2875	2	E11	M-031622-00	D-031622-01	GAAGAAGCCUUUCACCGAG
					D-031622-02	GAACAUGGACGCUGCAGUG
					D-031622-03	GCGCAGUGCAGGUGGAUUA
					D-031622-04	CCGAGCAGGUCUUCAAUGA
GPT2	84706	2	E12	M-004173-02	D-004173-01	UCAAAUGGCUCCAGACAUG
					D-004173-03	GUGAAAGACUUCCACAUCA
					D-004173-04	UCAAGAAGGUGCUGUACGA
					D-004173-18	GUGAAAAGGUUAAAUCGUA
DDO	8528	2	F03	M-009311-01	D-009311-02	CAGCACGGAUUGCAGUUGU
					D-009311-03	UCAGAGAAACCUUUAAUCA
					D-009311-17	GGACCUAUGCAGAUUUAUA
					D-009311-18	GGUGUAACAUGUAAGCUGA
AGXT	189	2	F04	M-008925-01	D-008925-01	GGAGAGACAUCGUCAGCUA
					D-008925-02	GCAAGGAUAUGUACCAGAU
					D-008925-04	UAGACCACUUCGACAUUGA
					D-008925-05	GGUCAUCUCUGGCUCGGGA
AGXT2	64902	2	F05	M-009818-00	D-009818-01	GGAAAGAAGAGCUAAGUAA
					D-009818-02	GGACCUACAUGUUACUAAA
					D-009818-03	GGAAGCAGAUACCUGGAUU
					D-009818-04	CAUAACCACUCCAGAGAUU
PSAT1	29968	2	F06	M-010398-02	D-010398-21	UUUAAGAGUGCCAGGCGAA
					D-010398-22	GAGAAUCUUGUGCGGGAAU
					D-010398-23	GCGCAAAUGAGACGGUGCA
					D-010398-24	GGACUAUAAAUAUCGUUCA
CAD	790	2	F07	M-009471-01	D-009471-01	GAGGGUCUCUUCUUAAGUA
					D-009471-17	GGAAGGAGAUUGAGUACGA
					D-009471-18	CCAACAGAUAAGCGGAUUU
					D-009471-19	AUUAAGACUCCACGGGUAU
ODC1	4953	2	F08	M-006668-00	D-006668-01	GAGCAGACCUUUAUGUAUU
					D-006668-02	CGAAAGAGCUAAAUAUCGA
					D-006668-03	GAAGUUGAGUUGAUGAAAG
					D-006668-04	GAAGAGAUCACCGGCGUAA
SHMT1	6470	2	F09	M-004617-00	D-004617-01	GAGCUGGCAUGAUCUUCUA
					D-004617-02	GGAGAACGCACGCCUCUUC
					D-004617-03	CCUAGGCUCUUGCUUAAAU
					D-004617-04	UACGGAAGAUUGCAGAUGA
SHMT2	6472	2	F10	M-004906-01	D-004906-01	GGAGAUCCCUUACACAUUU
					D-004906-02	GGUCAGGGCUCAUCUUCUA
					D-004906-03	GGACAGUGAUCCUGAGAUG
					D-004906-04	AAACUGGCCUCAUUGACUA
TKT	7086	2	F11	M-004734-01	D-004734-01	GAAAAUGCCAUCAUCUAUA
					D-004734-03	GAACUAGCCGCCAAUACAA
					D-004734-04	CUGCCGAACUGCUGAAGAA
					D-004734-05	GGAACUAGCCGCCAAUACA
TKTL1	8277	2	F12	M-004736-01	D-004736-01	GCAAGUACCGCUCUAAUUU
					D-004736-02	GGAAUUCCCUUCGCUGUUU
					D-004736-03	GCAGAAAGUUGGCAUGCAA
					D-004736-04	GGAAUUAGUGCCAGACAUA
DKFZP 434L1717	84076	2	G03	M-004735-01	D-004735-01	CGACAGAGCAUGCUAUUUA
					D-004735-02	GUGAAUUGCUGGAUAUGUU
					D-004735-03	GAUAAAGUCACAGUAAUUG
					D-004735-04	GUAAUUGGAGCUGGAGUUA
PGLS	25796	2	G04	M-020023-00	D-020023-01	GAUUGUGGCUCCCAUCAGU
					D-020023-02	CACACUACCUGUCCUGAAU
					D-020023-03	GCAAGGCAGCUGUUCUGAA
					D-020023-04	CGGCUGAGGACUACGCCAA
H6PD	9563	2	G05	M-004692-01	D-004692-01	CCGAGGAGCUGAUCUCUAA
					D-004692-02	GCAGCCCUCUGUCCGAUUA
					D-004692-03	GGACAUGUCUCCAUAAUCC
					D-004692-04	GGGCUACGCUCGGAUCUUG
PGD	5226	2	G06	M-008371-00	D-008371-01	GAUCAUCUCUUACGCUCAA
					D-008371-02	UAAUAGGACUGUCUCCAAA
					D-008371-03	GAAAUCACAGCCAAUAUUC
					D-008371-04	GAAAUUGGUACCAUUGUUG

Gene Symbol	Gene Id	Plate	Well	Pool Number	Duplex Number	Sequence
RPIA	22934	2	G07	M-016428-01	D-016428-01	GGAAGUGGUUCUACAAUUG
					D-016428-02	GCGAAUAGCUGAAAGGGUG
					D-016428-03	GCUAGUCGCUUCAUCGUGA
					D-016428-04	CAAAUGGAGUGAAGUGAAU
PRPS1L1	221823	2	G08	M-006804-00	D-006804-01	GCAAAUAUGCUCUCUAUAG
					D-006804-02	GAAAUCAACGACAGUCUAA
					D-006804-03	CAACACUGCAUGCUUUGAA
					D-006804-04	CAACCAGAGUUUAUGCUAU
GPAM	57678	2	G09	M-009946-01	D-009946-01	GGAAAGAUGUUCUCUAUAG
					D-009946-02	GAUAAUACCUGUUGGAAUC
					D-009946-03	GUUCAUAGAUCCCAUAUUG
					D-009946-04	AGAAAGAAAUGUUGCAGUA
AGPAT1	10554	2	G10	M-003810-01	D-003810-01	AUGAAGAUCUUGCGUCUAA
					D-003810-03	CGUGGCGCCUUCCAUCUUG
					D-003810-04	UCGAGAACAUGAAGAUCUU
					D-003810-05	UCAAAUACCUGUACGGGAU
AGPAT2	10555	2	G11	M-003811-02	D-003811-01	GUGCGAAGCUUCAAGUACU
					D-003811-03	GCCGGACGGUGGAGAACAU
					D-003811-21	CGGCCGAGUUCUACGCCAA
					D-003811-22	GCGCUGUGCUUCACGGUGU
AGPAT6	137964	2	G12	M-010300-00	D-010300-01	GAAAUUGGAGCCACAGUUU
					D-010300-02	UUAAGGAGUUCAUGAGUAA
					D-010300-03	GAACCUGCAUCAAUAAUAC
					D-010300-04	GAGAAGAACCACCAGCUUU
UNQ1849	253558	2	H03	M-010307-00	D-010307-01	GGAAUUGCCUGAUGCGAUA
					D-010307-02	UCGAAGACAUGAUUGAUUA
					D-010307-03	GCCUAUAUCUUCAUUCAUA
					D-010307-04	GAAAGAAGUGUCAUUAUCA
AGPAT3	56894	2	H04	M-008620-00	D-008620-01	GCUCCAAGGUCCUCGCUAA
					D-008620-02	GGGAGCAGCUUCCUUUGGA
					D-008620-03	UCCAGGAGAUAUAUAAUCA
					D-008620-04	GCAGCUGUCUAUGAUGUAA
AGPAT4	56895	2	H05	M-009283-01	D-009283-01	AGAAAGAGCUGGCCUAUGU
					D-009283-02	GGAGUUCGAUGGAUGAUUG
					D-009283-03	GCACACGGUUCACGGAGAA
					D-009283-04	AAAUGUAGUUUCAGCUGUA
PPAP2A	8611	2	H06	M-019098-01	D-019098-01	GAGGAGGACUCUCAUACAA
					D-019098-03	CUACAUAUGUCGAGGGAAU
					D-019098-04	CAACAACUGGGAAUCACUA
					D-019098-17	CUGUAUAUGUAUCGGAUUU
PPAP2C	8612	2	H07	M-011500-00	D-011500-01	UGACAGACCUGGCCAAGUA
					D-011500-02	GCACGACUCUGUUGGAAGU
					D-011500-03	GCUCGGACUUCAACAACUA
					D-011500-04	CCGCGUGUCUGAUUACAAA
PPAP2B	8613	2	H08	M-017312-01	D-017312-01	GGGACUGUCUCGCGUAUCA
					D-017312-02	UCUAUUACCUGAAGAAGUC
					D-017312-03	CAGUUCACCUUGAUCAUGA
					D-017312-05	GGAAUUCUACCGGAUCUAU
PCYT1A	5130	2	H09	M-008642-01	D-008642-01	GGAGAGGGUUGACAAAGUA
					D-008642-02	UGAAACAUAUGCUGAAAGA
					D-008642-04	GGAGAAGUCCCGAGAAUUC
					D-008642-17	UGUGAGAGUUUAUGCCGAU
PCYT1B	9468	2	H10	M-009611-01	D-009611-02	GGACAUCAUUACCAGAAUU
					D-009611-03	AAAGAGCCAUGAUCUAAUU
					D-009611-17	GGAAAUAACUAAUGCCUAU
					D-009611-18	CUUAGUCACCUGUGCGAAA
PLD1	5337	2	H11	M-009413-00	D-009413-01	UAACUGAGCUUAUCUAUGU
					D-009413-02	GAAGAACAAUUCCUUGGUA
					D-009413-03	GAAGAUUACUUGACAAAGA
					D-009413-04	GGUAAUCAGUGGAUAAAUU

Gene Symbol	Gene Id	Plate	Well	Pool Number	Duplex Number	Sequence
PLD2	5338	2	H12	M-005064-01	D-005064-01	GGACAACCAAGAAGAAAUA
					D-005064-02	GGACCGGCCUUUCGAAGAU
					D-005064-03	GACCUGCACUACCGACUGA
					D-005064-04	CAGCAUGGCGGGACUAUAU
ACAS2L	84532	3	A03	M-008549-00	D-008549-01	CCACCAAGAUCGCCAAAUA
					D-008549-02	GAUCGGAGCUGUCCACACA
					D-008549-03	GAAGAUCAAUCAGUUCUAU
					D-008549-04	UGAGGAAGAUCAUCACUAG
ACAS2	55902	3	A04	M-010396-00	D-010396-01	GAGAAGGGUUUCCCAGUAA
					D-010396-02	GAGACAACCUACUUUAAGA
					D-010396-03	CCACAACCUUCAAGUAUGU
					D-010396-04	GCACCUGGCUUGCCUAAAA
ACACB	32	3	A05	M-004759-02	D-004759-01	GAACAUCCCUGCACAGAAA
					D-004759-05	CCACAAAGGAUUUAAAUAC
					D-004759-18	GAACUUAACCGGAUGCGUA
					D-004759-19	AGAUACAUGAUCACGGAUA
MT	27349	3	A06	M-014204-01	D-014204-01	GAAGAAUUCCUCUAAGUUU
					D-014204-02	UAAAGGCAGUCGACAUUAA
					D-014204-04	AGACGAUGCAUGCCAUAUA
					D-014204-17	GCUGGCCGCUGUCGAGAAA
THEDC1	55301	3	A07	M-004796-01	D-004796-01	GGGCAGAUCUGAACAUUGU
					D-004796-02	GGAUAAACCAUUUGCAUUU
					D-004796-04	CCAAGGAAUUUGUGAAACA
					D-004796-17	GGAUCCUGCGAACGAGAAA
FLJ20604	54995	3	A08	M-031860-00	D-031860-01	GGAGACUCAUUUAGAUUUA
					D-031860-02	GGUCAGCAUUCGAUAUAAA
					D-031860-03	GCAAUUGGCAUGGGAAUGA
					D-031860-04	UCUCAACUAUGUUCCACUA
ELOVL6	79071	3	A09	M-008861-01	D-008861-01	CAAUGGACCUGUCAGCAAA
					D-008861-02	GGUCGGCACCUAAUGAAUA
					D-008861-03	CGAACUAGGAGAUACAAUA
					D-008861-17	GGGUGUAUAUCUAGAACGA
SCD	6319	3	A10	M-005061-01	D-005061-02	GAUAUGCUGUGGUGCUUAA
					D-005061-04	AGAAUGAUGUCUAUGAAUG
					D-005061-05	CGACAUUCGCCCUGAUAUA
					D-005061-06	GGAGUACGCUAGACUUGUC
SCD5	79966	3	A11	M-008416-03	D-008416-03	CAUAUUGGGUGGCUGUUUG
					D-008416-20	AGAACAUCGUCUGGAGGAA
					D-008416-21	GAGAAAGCUUGACGUCACU
					D-008416-22	CAGAAUGACAUCUUCGAGU
ACAT1	38	3	A12	M-009408-00	D-009408-01	GAAAUGAACAGGACGCUUA
					D-009408-02	GGGUAAAGCUUGAAGAUUU
					D-009408-03	GCAAAGAAGCUGAAUAUUG
					D-009408-04	GCGAAGAGGCUCAAUGUUA
ACAT2	39	3	B03	M-010001-01	D-010001-01	UCACUUGGCUUACUUGAGA
					D-010001-02	GGAAUUCCCUACUCUGUUC
					D-010001-03	GAAGCCAUGUCCAAGCUAA
					D-010001-04	GCAUCUGGCUGUCGAAUUC

Gene Symbol	Gene Id	Plate	Well	Pool Number	Duplex Number	Sequence
AACS	65985	3	B04	M-009458-01	D-009458-02	CGAAAGGAAUCGCAGAUGU
					D-009458-04	GGCAAGAAGUGGCUUUGUU
					D-009458-17	CGUAUACGCUCAACGGCAA
					D-009458-18	GGAACGAUGAGAACGGCAA
IDI1	3422	3	B05	M-009357-00	D-009357-01	GAACAUUGAGAAAGGAUUA
					D-009357-02	GAGGAAGAAUGUAACUUUG
					D-009357-03	UAAGAUAACGCCAUGGUUU
					D-009357-04	UAAAUGGUGGGAUAACUUA
IDI2	91734	3	B06	M-008463-00	D-008463-01	GUAGUAGCCACCCAUUAUA
					D-008463-02	GGAAUUGCCAUCUGAACGA
					D-008463-03	UGGAGGAAAUGCUGAUUGU
					D-008463-04	UCACGUUUCCUGGGUAUUU
FDFT1	2222	3	B07	M-009442-02	D-009442-01	GGAAGAGAUUUAUCAUAGA
					D-009442-03	GGACAAGUACUGCCACUAU
					D-009442-04	CCACUUUGGCUGCCUGUUA
					D-009442-05	GUUUGGAGCAGGUAUGUUA
SQLE	6713	3	B08	M-009646-01	D-009646-04	UAUUGAAGGUGUUGUGUUA
					D-009646-17	UUUCAAACUUGGUGGCGAA
					D-009646-18	CAAACUUGGUGGCGAAUGU
					D-009646-19	GAGAUACAGUGGAAGGUCU
CYP51A1	1595	3	B09	M-009215-01	D-009215-01	CAGCAUACAUCCUCAACUA
					D-009215-02	CCACUAUGCUUCGUUUAUA
					D-009215-03	GAAGGGAGUUGCAUACGAU
					D-009215-17	GGUAGGGAAUAAUCGAACA
NSDHL	50814	3	B10	M-008448-00	D-008448-01	UGACAGGCCUCAAUUAUGA
					D-008448-02	GCCAAGAGAUGCACAGUGA
					D-008448-03	GAUAUGCUGUCAAUGUAUU
					D-008448-04	GCAGUUAGCGAGCCAAUGA
HSD17B7	51478	3	B11	M-008140-02	D-008140-02	GAAGAUGGACCUAGAUGAA
					D-008140-03	GGAAUUCUGCCUCCGUUUA
					D-008140-18	CAAUAUUGCUACUUCGCUU
					D-008140-19	GCAUUCACUUUGACACCAU
EBP	10682	3	B12	M-012282-01	D-012282-01	GAAAGAGUAUGCCAAGGGA
					D-012282-03	GCCGAUACAUCCUGGGUGA
					D-012282-04	ACGAAGACCUGCUUGGAGA
					D-012282-17	CCCACAGUUUGGAGGGACA
SC5DL	6309	3	C03	M-009745-01	D-009745-01	CAAAUUACAUGAUGACCUA
					D-009745-02	GAAGAUUCCUACUCCAUUU
					D-009745-03	GGAAGGGACCGCUCAGUUA
					D-009745-04	GUGCAACACUGAGCUAUUA
DHCR24	1718	3	C04	M-010222-01	D-010222-01	CAACACAUCUGCACUGCUU
					D-010222-02	GAAAUGAGGCAGAGCUCUA
					D-010222-03	GGAGUACAUUCCCUUGAGA
					D-010222-04	CAUCAUCCCUGCCAAGAAG
SOD1	6647	3	C05	M-008364-01	D-008364-05	UCGUUUGGCUUGUGGUGUA
					D-008364-06	ACAAAGAUGGUGUGGCCGA
					D-008364-07	GUGCAGGGCAUCAUCAAUU
					D-008364-08	UUAAUCCUCUAUCCAGAAA

Gene Symbol	Gene Id	Plate	Well	Pool Number	Duplex Number	Sequence
SOD2	6648	3	C06	M-009784-02	D-009784-03	AAAGAUACAUGGCUUGCAA
					D-009784-04	GUAAUCAACUGGGAGAAUG
					D-009784-19	ACCAGGAGGCGUUGGCCAA
					D-009784-20	GGAUUGAUGUGUGGGAGCA
SOD3	6649	3	C07	M-009741-01	D-009741-01	GCGCCAAGCUCGACGCCUU
					D-009741-02	ACGCCAAGGUCACGGAGAU
					D-009741-03	GCGGAGUGGAUCCGAGACA
					D-009741-04	AAGAAGCGGCGGCGCGAGA
CAT	847	3	C08	M-010021-01	D-010021-01	CACAUGACAUUACCAAAUA
					D-010021-02	GGAAUCCAGUUAAUUACUU
					D-010021-03	GAGCACAGCAUCCAAUAUU
					D-010021-04	GGACAUCGCCACAUGAAUG
GPX6	257202	3	C09	M-019309-00	D-019309-01	GCAAGCACGUCCUGUUUGU
					D-019309-02	GCAGUUCAAUACCCACUAG
					D-019309-03	GCGAGGAGUACAUCCAAUU
					D-019309-04	AUAGGAAGGUGGAUUGCAA
GPX1	2876	3	C10	M-008982-00	D-008982-01	GCAAGGUACUACUUAUCGA
					D-008982-02	UGAAUUCCCUCAAGUACGU
					D-008982-03	GGAGAACGCCAAGAACGAA
					D-008982-04	GCAACCAGUUUGGGCAUCA
GPX2	2877	3	C11	M-011675-00	D-011675-01	GAACGAGCAUCCUGUCUUC
					D-011675-02	GAAGGUAGAUUUCAAUACG
					D-011675-03	CAGGAGAACUGUCAGAAUG
					D-011675-04	GCAGGGCCGUGCUGAUUGA
GPX3	2878	3	C12	M-006485-01	D-006485-01	GUACGGAGCCCUCACCAUU
					D-006485-02	GGAUGUCAAUGGAGAGAAA
					D-006485-03	AGGAAGAGCUUGCACCAUU
					D-006485-04	GAGGCUUUGUCCCUAAUUU
GPX4	2879	3	D03	M-011676-01	D-011676-01	CAACGUGGCCUCCCAGUGA
					D-011676-03	GUAACGAAGAGAUCAAAGA
					D-011676-04	CGUCAAAUUCGAUAUGUUC
					D-011676-17	GCUGCGUGGUGAAGCGCUA
GPX5	2880	3	D04	M-009445-01	D-009445-03	GCAAGCACAUCCUCUUCGU
					D-009445-04	UGGCGUACUUGAAGCAAUU
					D-009445-17	AGGCCAUCGCACUUAAUAA
					D-009445-18	GGGAGGAUUUGUACCUAGU
GPX7	2882	3	D05	M-009875-01	D-009875-01	GAAGCGAGAAGACUUAUAA
					D-009875-02	ACAAGGAGAUUGAGAGCUU
					D-009875-03	GCACCUACAGUGUCUCAUU
					D-009875-04	GGACUUCUACGACUUCAAG
SCO2	9997	3	D06	M-011987-01	D-011987-01	GCAGAUCGGCUGAGCAGAU
					D-011987-02	GAACAGAAGCCCUGCGCCA
					D-011987-03	GAACCCGGCUGCUGAUCAC
					D-011987-04	ACAGUUACCGCGUGUACUA
ATPIF1	93974	3	D07	M-017220-00	D-017220-01	AAGAAGAAAUCGUUCAUCA
					D-017220-02	AGAGAGAGCAGGCUGAAGA
					D-017220-03	GCCAUAAGCAGAAGAUCAA
					D-017220-04	GGGCGUGAGGACCAUGCAA

Gene Symbol	Gene Id	Plate	Well	Pool Number	Duplex Number	Sequence
COX4I1	1327	3	D08	M-011625-00	D-011625-01	UGUACGAGCUCAUGAAAGU
					D-011625-02	GCAGAAGCACUAUGUGUAC
					D-011625-03	CGAGUUGUAUCGCAUUAAG
					D-011625-04	CCAAGUGGGACUACGAAAA
COX4I2	84701	3	D09	M-013590-00	D-013590-01	GCACAGAACUCAACGCUGA
					D-013590-02	UCGCAGCUCUGGUGAUUUG
					D-013590-03	GCAGCGGGUCUACGUAUUU
					D-013590-04	GAUGAACCGUCGCUCCAAU
COX5A	9377	3	D10	M-011940-00	D-011940-01	GAACUUAGACCAACUUUAA
					D-011940-02	ACACACUUGUUACCUAUGA
					D-011940-03	GCAUGCAGACGGUUAAAUG
					D-011940-04	GAUAUAGAUGCCUGGGAAU
C12ORF5	57103	3	D11	M-020597-01	D-020597-01	AAUCACAGCUCUAAAGUUA
					D-020597-02	GAUAUGACGGUAAAGUAUG
					D-020597-03	GAAAUACGGGGUUGUAGAA
					D-020597-04	GAGUCACGGUGCUUACAUG
OXCT1	5019	3	D12	M-004045-00	D-004045-01	GAACGACAGUACUUAUCUG
					D-004045-02	UUAUGUACAUCGCCUUAUA
					D-004045-03	UGUGUCAACCGCAUUAUUA
					D-004045-04	UCAACCGCAUUAUUACUGA
OXCT2	64064	3	E03	M-013881-00	D-013881-01	UUAUGUAGAUCGCGUGAUA
					D-013881-02	CCAAGAUCAUGGAGAAAUG
					D-013881-03	ACGCGCAGCUCUGGAAUUU
					D-013881-04	GCGCUUAACGAUCCUGAAA
SLC16A7	9194	3	E04	M-007409-01	D-007409-01	GGAUUUAACUGGAGAAUAU
					D-007409-02	GAUAGCAGGAGGCUUAUUA
					D-007409-04	CAGCAAAUAUUCCACACUA
					D-007409-17	CGGAAGAUGUUAACGUCAA
SLC16A3	9123	3	E05	M-005126-03	D-005126-03	GGCAACUUCUUCUGCAUUA
					D-005126-04	CGACCCACGUCUACAUGUA
					D-005126-05	CAUGGUGGCUGCGUCCUUU
					D-005126-06	GCUCACCUCCUCCCUGAUU
SLC16A8	23539	3	E06	M-007410-01	D-007410-02	GCACGUCCCGUAUCUGUUC
					D-007410-03	CCAAAGCCGUGAGCGUCUU
					D-007410-04	UGUACGCCGUCACCAAGUU
					D-007410-17	CUGCCUGCGUUGUGCUAAA
SLC16A4	9122	3	E07	M-007406-00	D-007406-01	GACAGGAGCCCUUAUAUUA
					D-007406-02	GAAACACACUGCCAUGAGA
					D-007406-03	GAAGAAAGUGAUAAGGUUA
					D-007406-04	UGACAUACUUGGAGAGAAA
TALDO1	6888	3	E08	M-008996-02	D-008996-01	GAGCAGAAAUACUAAAGAA
					D-008996-02	CAGCACAGAUGCCCGCUUA
					D-008996-05	CACAAGAGGACCAGAUUAA
					D-008996-18	CCACAGAAGUAGACGCAAG
RPE	6120	3	E09	M-012767-00	D-012767-01	GGGCUAAUCAGAUAGAUAU
					D-012767-02	GAGCUAACAUGAUUGUGUC
					D-012767-03	GUUCCCAUCUUUGGAUAUA
					D-012767-04	CCAUAAAUGUGCAGAGGCA

Gene Symbol	Gene Id	Plate	Well	Pool Number	Duplex Number	Sequence
GFPT1	2673	3	E10	M-008833-01	D-008833-02	GGACGAGGCUAUCAUUAUG
					D-008833-03	UGAAACGGCUGCCUGAUUU
					D-008833-17	GAGCAUGGAUGACGAAAUU
					D-008833-18	CAUGCAAGAAAGACGCAAA
GFPT2	9945	3	E11	M-010390-01	D-010390-01	UCGCCAAGCUGAUUAAAUA
					D-010390-03	GAUCAUCCGUGGCUUGAGA
					D-010390-04	AGACAAAGGCAACGAAUUU
					D-010390-17	CGAUGGGAAUAAUCACGAA
GNPNAT1	64841	3	E12	M-005239-01	D-005239-02	CGGCAACUCUGAUUAUAGA
					D-005239-03	CUACAUGUGUCGGAGGUUU
					D-005239-04	GUACUGCUGACUUAAAUAG
					D-005239-17	GGAUUACAUAUGUCGGCUA
UAP1	6675	3	F03	M-017160-01	D-017160-01	GAACAAAGUUUCUAUGGCU
					D-017160-02	UGAGAGAUGUUGUCAAUGU
					D-017160-03	CUACUACGUUUCUGGAAUG
					D-017160-04	ACCCAAGGACAGUUAAUUA
OGT	8473	3	F04	M-019111-00	D-019111-01	GCAGUUCGCUUGUAUCGUA
					D-019111-02	CGACAUGCAUUGCGUCUCA
					D-019111-03	GAUUAAGCCUGUUGAAGUC
					D-019111-04	CCGAGAAAUUGGCUUAUAU
PGM1	5236	3	F05	M-010925-00	D-010925-01	CGAAUCGUCUUCCGACUGA
					D-010925-02	GUACAUCGAUAGCUAUGAG
					D-010925-03	CGACUGAAGAUCCGUAUUG
					D-010925-04	GGAAAUUGUGGAUUCGGUA
PGM3	5238	3	F06	M-013912-00	D-013912-01	GAGGUCAAUUCCAUGAUUA
					D-013912-02	GGAUUUAGGUGCUAUUACA
					D-013912-03	GGGCAAACUCAAUCAUUUA
					D-013912-04	GACAAGAUAGCAACGUUAA
WBSCR14	51085	3	F07	MU-009253-00	D-009253-01	GACACUCUCUUCACCAUGAUU
					D-009253-02	ACAAGUGGCGCAUCUACUAUU
					D-009253-03	GGGCACAUCUACCAGUAUCUU
					D-009253-04	GCCCAUGCCUUCAAACUUCUU
SLC25A10	1468	3	F08	MU-007469-00	D-007469-01	GCAGACAGAUGACCUACUCUU
					D-007469-02	GUACCUCUCUGACAACAUCUU
					D-007469-03	CCGCGUAGCUCGUGAAGAGUU
					D-007469-04	CUGAAGACUCGCCUGAUGUU
ME1	4199	3	F09	MU-009348-02	D-009348-02	CAUCUGACAUUGAGAAAUU
					D-009348-03	AGUAAGAGGUUCUGAAUAU
					D-009348-19	CCUUGCAGCUCUUCGAAUA
					D-009348-05	GGUAAAUUGGCUCUAUAUA
ME2	4200	3	F10	MU-009461-00	D-009461-01	GAAGAAGCAUAUACACUUAUU
					D-009461-02	UGAAAGGCCUGUAAUAUUUUU
					D-009461-03	GAACAUGGCGGAGUGAAUAUU
					D-009461-04	GAAACGAGAUCGCACACAAUU
GLS	2744	3	F11	MU-004548-00	D-004548-01	AGACAUGGUUGGUAUAUUAUU
					D-004548-02	UGAAUAAGAUGGCUGGUAAUU
					D-004548-03	GGUGGUUUCUGCCCAAUUAUU
					D-004548-04	GAAUAACACUCCCAUGGAUUU

Gene Symbol	Gene Id	Plate	Well	Pool Number	Duplex Number	Sequence
GLS2	27165	3	F12	MU-012500-00	D-012500-01	UCAAACUGCUUCAAGAUUAUU
					D-012500-02	GAACUUAGAAAGCAUGGUAUU
					D-012500-03	CAAGUGGCCUGCGCUACAAUU
					D-012500-04	GCCAUCGGCUAUUAUCUCAUU
PIK3CA	5290	3	G03	MU-003018-03	D-003018-07	GGACAACUGUUUCAUAUAG
					D-003018-08	GCCAGUACCUCAUGGAUUA
					D-003018-24	CUUGAAGAGUGUCGAAUUA
					D-003018-25	GCUUGAAGAGUGUCGAAUU
MYLCD	23417	3	G04	MU-009626--01	D-009626-01	GGAAUGAACUCUUUACAGA
					D-009626-02	GAACAUCCUCCAUCAGAAA
					D-009626-03	UGAAAGGAAUGCUCUCAGA
					D-009626-04	UCAACUGGAUGGCGGAUGU
IRS1	3667	3	G08	MU-003015-01	D-003015-05	AAAGAGGUCUGGCAAGUGA
					D-003015-06	GAACCUGAUUGGUAUCUAC
					D-003015-07	CCACGGCGAUCUAGUGCUU
					D-003015-08	GUCAGUCUGUCGUCCAGUA
PTEN	5728	3	G12	MU-003023-01	D-003023-05	GUGAAGAUCUUGACCAAUGUU
					D-003023-06	GAUCAGCAUACACAAAUUAUU
					D-003023-07	GGCGCUAUGUGUAUUAUUAUU
					D-003023-08	GUAUAGAGCGUGCAGAUAAUU
MYC	4609	3	H03	MU-003282-07	D-003282-14	AACGUUAGCUUCACCAACA
					D-003282-15	GGAACUAUGACCUCGACUA
					D-003282-16	GAACACACAACGUCUUGGA
					D-003282-35	CUACCAGGCUGCGCGCAAA
RPTOR	57521	3	H04	MU-004107-00	D-004107-01	GAAACCAUCGGUGCAAAUUUU
					D-004107-02	AGAAGGGCAUUACGAGAUUUU
					D-004107-03	UGGAGAAGCGUGUCAGAUAUU
					D-004107-04	GCCCGUCGAUCUUCGUCUAUU
RICTOR	253260	3	H05	MU-016984-01	D-016984-01	UCAACGAGCUCACAUAUGAUU
					D-016984-02	GUACGAAGACUACUUUAUUUU
					D-016984-03	UGACCGAUCUGGACCCAUAUU
					D-016984-04	GUACUUGGGCUCAUAGCUAUU
SLC16A1	6566	3	H06	MU-007402-02	D-007402-01	GCAGUAUCCUGGUGAAUAA
					D-007402-02	AGAGGAAGCUUUCUAAUUC
					D-007402-05	GGUAAUUGGAGCUUUCAUU
					D-007402-18	GCCAAUAAGACCUCGAAUU
SLC25A1	6576	3	H07	MU-007468-01	D-007468-01	CCAUAGUGUUUGUCAUCUA
					D-007468-02	GCCUGGAGGCGCACAAAUA
					D-007468-05	GCGCACAAAUACCGGAACA
					D-007468-06	UGAAGCUGCUCAACAAAGU
PDK1	5163	3	H08	MU-005019-00	D-005019-01	GGAAGUCCAUCUCAUCGAAUU
					D-005019-02	GGAACACCAUGCCAACAGAUU
					D-005019-03	GAUCAGAAACCGACACAAUUU
					D-005019-04	GAUCAGUGAAUGCUUGUGAUU
PDK2	5164	3	H09	MU-005020-00	D-005020-01	CAAAGAUGCCUACGACAUGUU
					D-005020-02	GCACGGAGCCCAAGAACACUU
					D-005020-03	GCUCCUGUGUGACAAGUAUUU
					D-005020-04	CCAGCACACCCUCAUCUUUUU

Gene Symbol	Gene Id	Plate	Well	Pool Number	Duplex Number	Sequence
CPT1a	1374	3	H10	MU-009749-02	D-009749-01	GAGAGAACCUCAUCAAUUU
					D-009749-02	GAAGAAGGAUACAGAAGUG
					D-009749-05	GGACAGCUACGCCAAAUCU
					D-009749-18	UGACAACGAUGUACGCCAA
CPT1b	1375	3	H11	MU-010266-01	D-010266-04	CAAGUAACUAUGUGAGUGA
					D-010266-17	GAUCAUGUAUCGCCGUAAA
					D-010266-18	GGACUGAGACUGUGCGUUC
					D-010266-19	CAUGAUUGCAGGCGAGAAC
AKT1	207	3	H12	MU-003000-03	D-003000-05	GACAAGGACGGGCACAUUA
AKT2	208			MU-003001-02	D-003000-07	GCUACUUCCUCCUCAAGAA
AKT3	209			MU-003002-02	D-003000-08	GACCGCCUCUGCUUUGUCA
					D-003000-22	GGCAGCACGUGUACGAGAA
					D-003001-05	GUACUUCGAUGAUGAAUUU
					D-003001-07	GGGCUAAAGUGACCAUGAA
					D-003001-08	GCAGAAUGCCAGCUGAUGA
					D-003001-21	GAGUAGAAUAAUCGUCUUU
					D-003002-09	GAAAGAUUGUGUACCGUGAUU
					D-003002-10	GGACUACUGUUAUAGAGAGUU
					D-003002-11	UGAGACAGAUACUAGAUAUUU
					D-003002-12	GCUCAUUCAUAGGAUAUAAUU

8.3 Transfection reagent

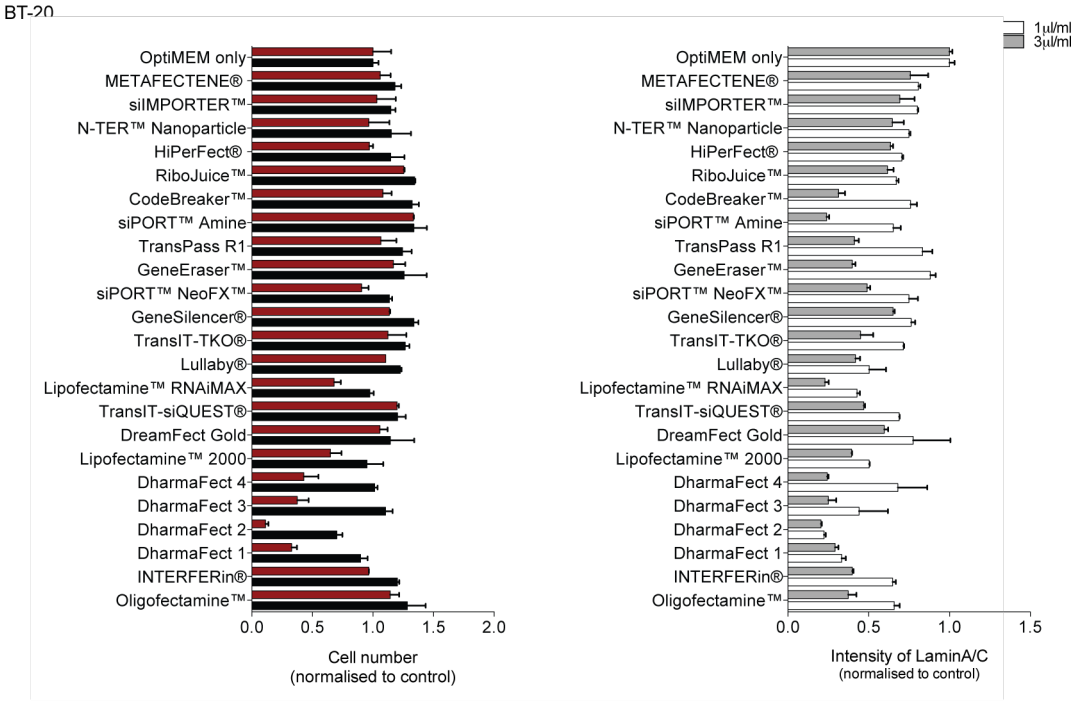

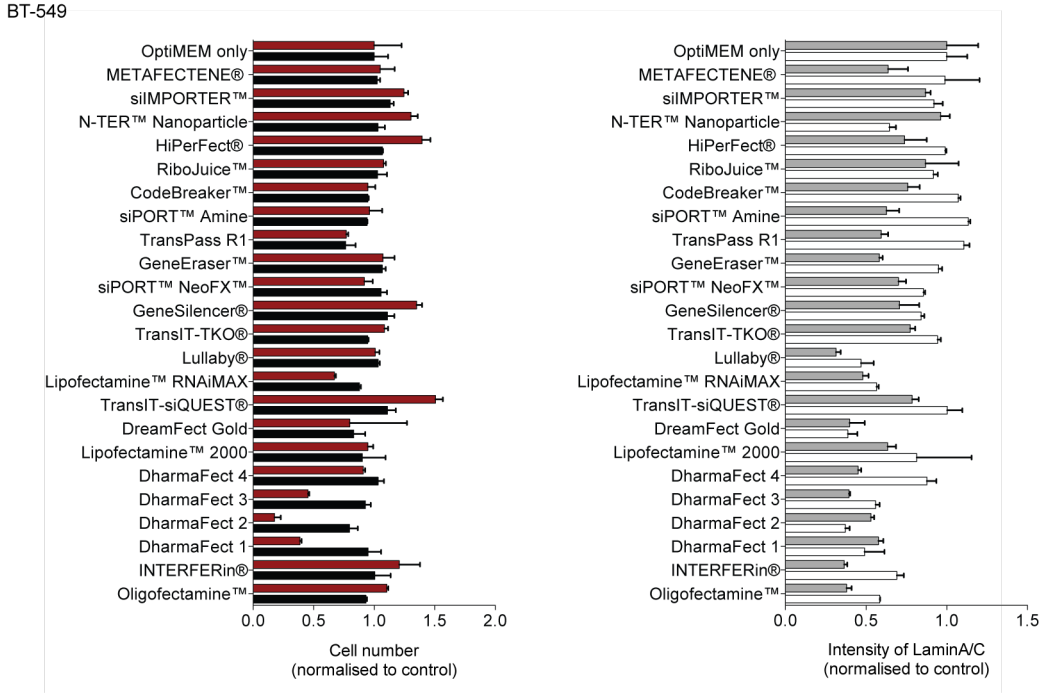

HS-578T

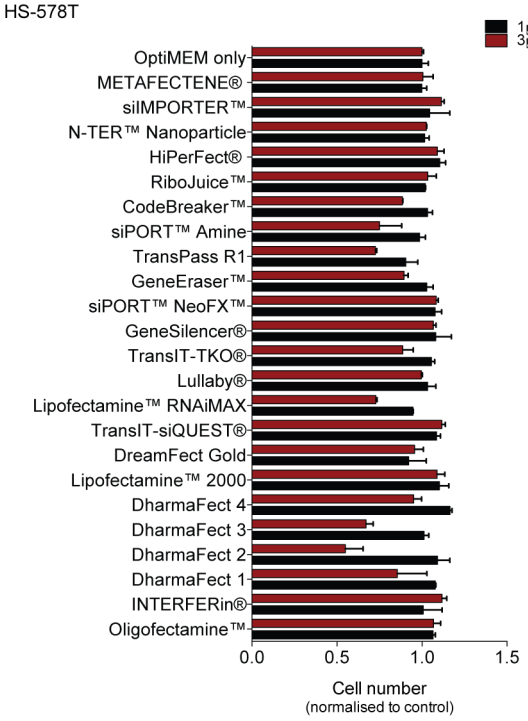
1μl/ml
3μl/ml
OptiMEM only
METAFECTENE®
siIMPORTER™
N-TER™ Nanoparticle
HiPerFect®
RiboJuice™
CodeBreaker™
siPORT™ Amine
TransPass R1
GeneEraser™
siPORT™ NeoFX™
GeneSilencer®
TransIT-TKO®
Lullaby®
Lipofectamine™ RNAiMAX
TransIT-siQUEST®
DreamFect Gold
Lipofectamine™ 2000
DharmaFect 4
DharmaFect 3
DharmaFect 2
DharmaFect 1
INTERFERin®
Oligofectamine™
0.0
0.5
1.0
1.5
Cell number
(normalised to control)

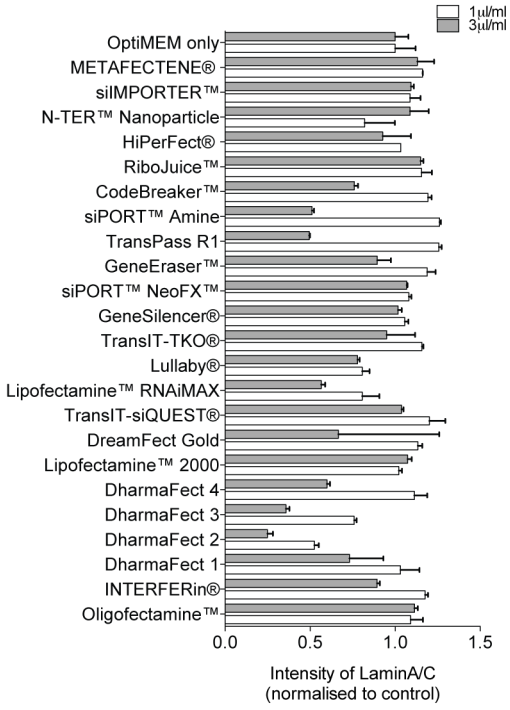
1μl/ml
3μl/ml
OptiMEM only
METAFECTENE®
siIMPORTER™
N-TER™ Nanoparticle
HiPerFect®
RiboJuice™
CodeBreaker™
siPORT™ Amine
TransPass R1
GeneEraser™
siPORT™ NeoFX™
GeneSilencer®
TransIT-TKO®
Lullaby®
Lipofectamine™ RNAiMAX
TransIT-siQUEST®
DreamFect Gold
Lipofectamine™ 2000
DharmaFect 4
DharmaFect 3
DharmaFect 2
DharmaFect 1
INTERFERin®
Oligofectamine™
0.0
0.5
1.0
1.5
Intensity of LaminA/C
(normalised to control)

MCF7

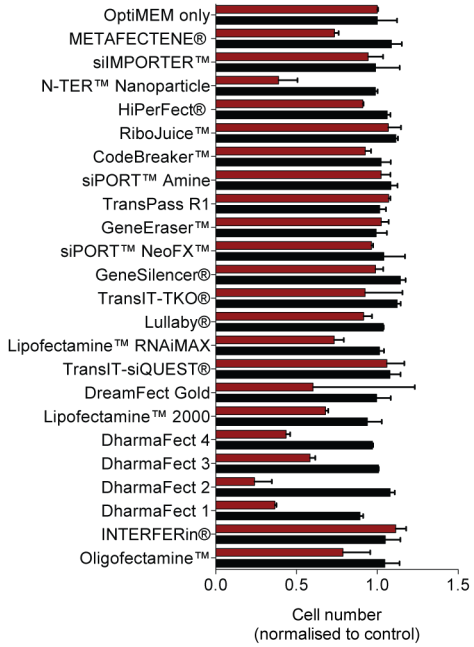
OptiMEM only
METAFECTENE®
siIMPORTER™
N-TER™ Nanoparticle
HiPerFect®
RiboJuice™
CodeBreaker™
siPORT™ Amine
TransPass R1
GeneEraser™
siPORT™ NeoFX™
GeneSilencer®
TransIT-TKO®
Lullaby®
Lipofectamine™ RNAiMAX
TransIT-siQUEST®
DreamFect Gold
Lipofectamine™ 2000
DharmaFect 4
DharmaFect 3
DharmaFect 2
DharmaFect 1
INTERFERin®
Oligofectamine™
0.0
0.5
1.0
1.5
Cell number
(normalised to control)

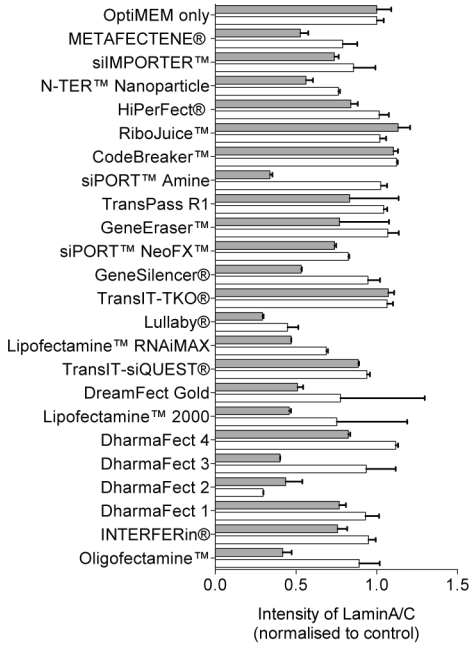
OptiMEM only
METAFECTENE®
siIMPORTER™
N-TER™ Nanoparticle
HiPerFect®
RiboJuice™
CodeBreaker™
siPORT™ Amine
TransPass R1
GeneEraser™
siPORT™ NeoFX™
GeneSilencer®
TransIT-TKO®
Lullaby®
Lipofectamine™ RNAiMAX
TransIT-siQUEST®
DreamFect Gold
Lipofectamine™ 2000
DharmaFect 4
DharmaFect 3
DharmaFect 2
DharmaFect 1
INTERFERin®
Oligofectamine™
0.0
0.5
1.0
1.5
Intensity of LaminA/C
(normalised to control)

MCF10A

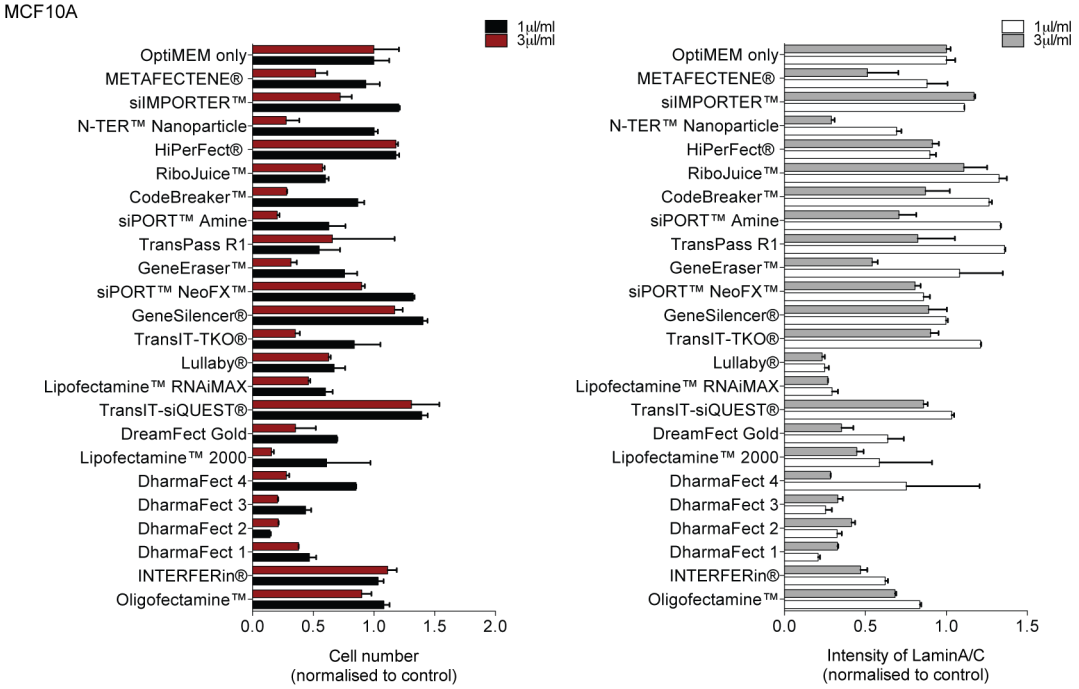

MDA-MB-231

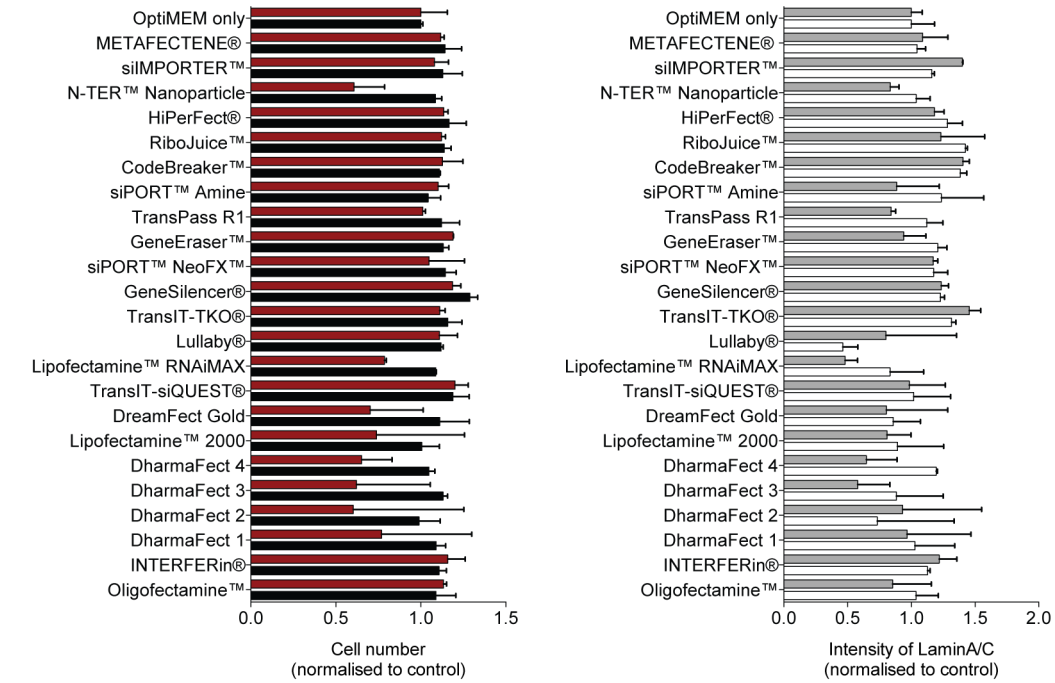

MDA-MB-468

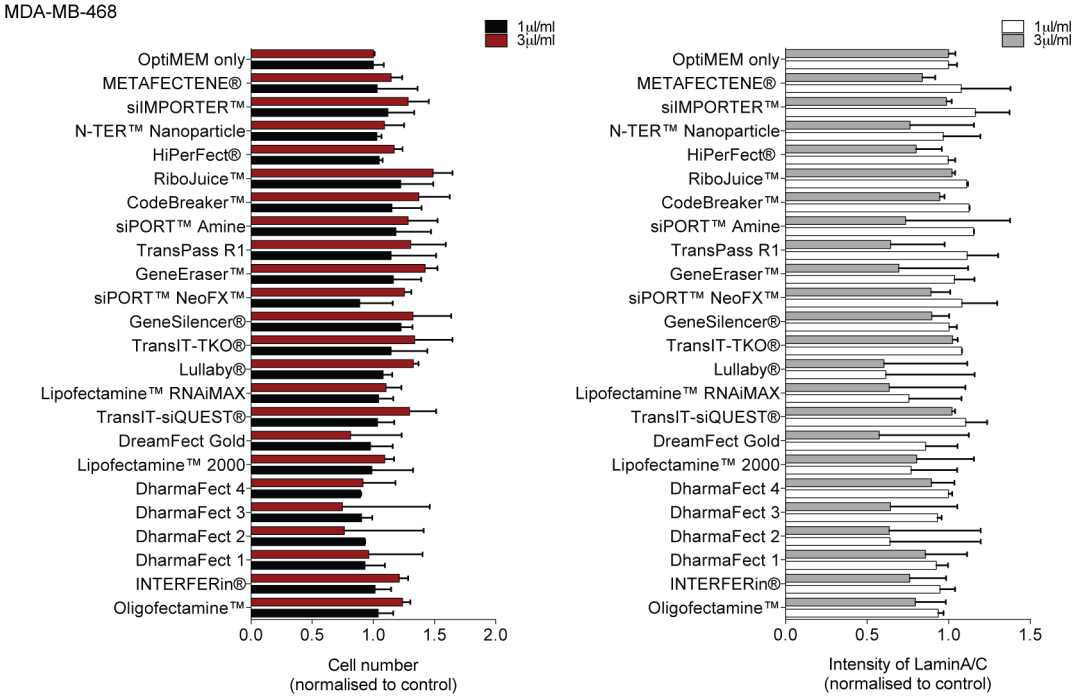

SK-BR-3

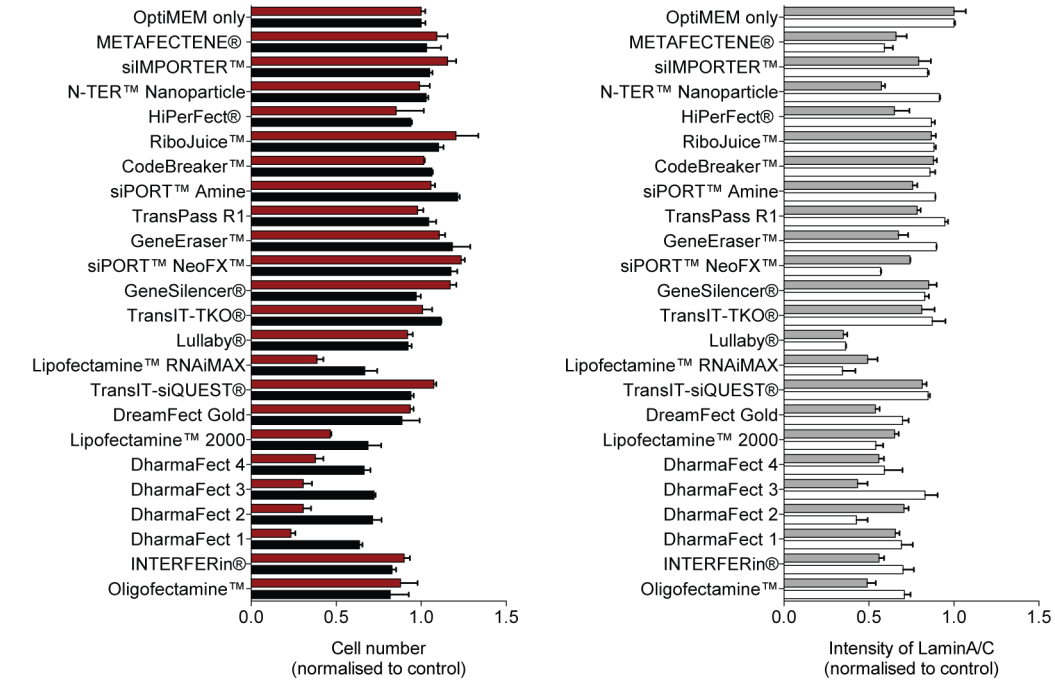

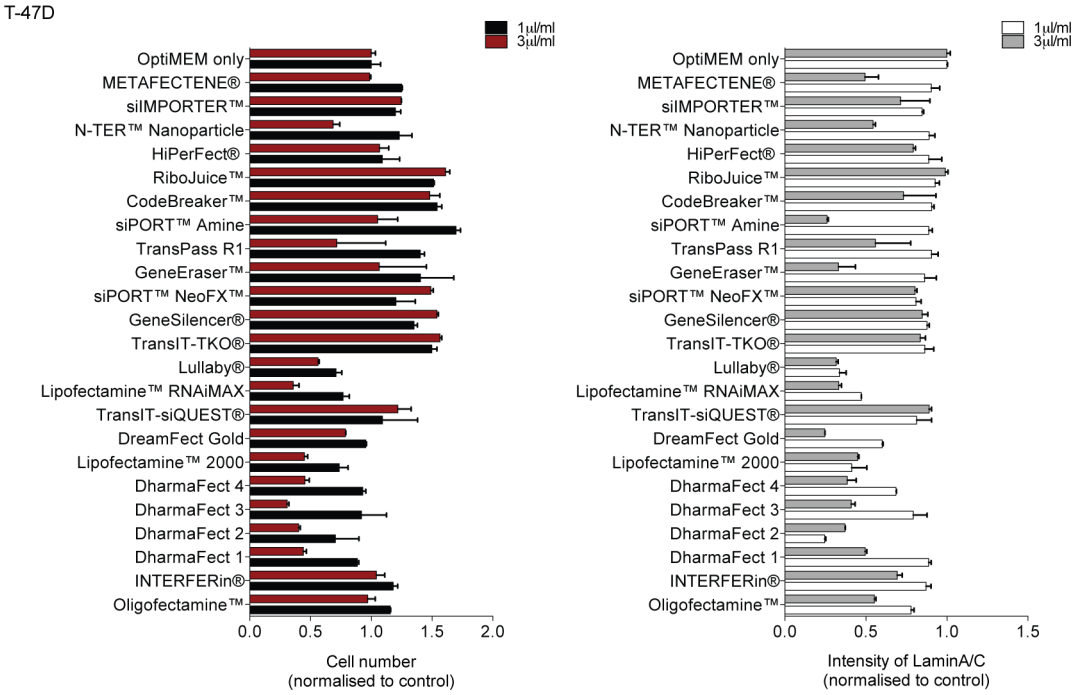
T-47D
1µl/ml
3µl/ml
OptiMEM only
METAFECTENE®
siIMPORTER™
N-TER™ Nanoparticle
HiPerFect®
RiboJuice™
CodeBreaker™
siPORT™ Amine
TransPass R1
GeneEraser™
siPORT™ NeoFX™
GeneSilencer®
TransIT-TKO®
Lullaby®
Lipofectamine™ RNAiMAX
TransIT-siQUEST®
DreamFect Gold
Lipofectamine™ 2000
DharmaFect 4
DharmaFect 3
DharmaFect 2
DharmaFect 1
INTERFERin®
Oligofectamine™
0.0
0.5
1.0
1.5
2.0
Cell number
(normalised to control)
1µl/ml
3µl/ml
Intensity of LaminA/C
(normalised to control)

Reference List

Abbey, C.K., Borowsky, A.D., McGoldrick, E.T., Gregg, J.P., Maglione, J.E., Cardiff, R.D., and Cherry, S.R. (2004). In vivo positron-emission tomography imaging of progression and transformation in a mouse model of mammary neoplasia. Proc Natl Acad Sci U S A *101*, 11438-11443.

Abe, A., Miyanohara, A., and Friedmann, T. (1998). Polybrene increases the efficiency of gene transfer by lipofection. Gene therapy *5*, 708-711.

Acharyya, S., Oskarsson, T., Vanharanta, S., Malladi, S., Kim, J., Morris, P.G., Manova-Todorova, K., Leversha, M., Hogg, N., Seshan, V.E.*, et al.* (2012). A CXCL1 paracrine network links cancer chemoresistance and metastasis. Cell *150*, 165-178.

Almendro, V., Marusyk, A., and Polyak, K. (2012). Cellular Heterogeneity and Molecular Evolution in Cancer. Annu Rev Pathol.

Alroy, I., and Yarden, Y. (2000). Biochemistry of HER2 oncogenesis in breast cancer. Breast Dis *11*, 31-48.

Amemiya-Kudo, M., Shimano, H., Hasty, A.H., Yahagi, N., Yoshikawa, T., Matsuzaka, T., Okazaki, H., Tamura, Y., Iizuka, Y., Ohashi, K.*, et al.* (2002). Transcriptional activities of nuclear SREBP-1a, -1c, and -2 to different target promoters of lipogenic and cholesterogenic genes. J Lipid Res *43*, 1220-1235.

Anastasiou, D., Poulogiannis, G., Asara, J.M., Boxer, M.B., Jiang, J.K., Shen, M., Bellinger, G., Sasaki, A.T., Locasale, J.W., Auld, D.S.*, et al.* (2011). Inhibition of pyruvate kinase M2 by reactive oxygen species contributes to cellular antioxidant responses. Science *334*, 1278-1283.

Arriola, E., Marchio, C., Tan, D.S., Drury, S.C., Lambros, M.B., Natrajan, R., Rodriguez-Pinilla, S.M., Mackay, A., Tamber, N., Fenwick, K.*, et al.* (2008). Genomic analysis of the HER2/TOP2A amplicon in breast cancer and breast cancer cell lines. Lab Invest *88*, 491-503.

Ashrafian, H., O'Flaherty, L., Adam, J., Steeples, V., Chung, Y.L., East, P., Vanharanta, S., Lehtonen, H., Nye, E., Hatipoglu, E.*, et al.* (2010). Expression profiling in progressive stages of fumarate-hydratase deficiency: the contribution of metabolic changes to tumorigenesis. Cancer Res *70*, 9153-9165.

Bae, S.N., Arand, G., Azzam, H., Pavasant, P., Torri, J., Frandsen, T.L., and Thompson, E.W. (1993). Molecular and cellular analysis of basement membrane invasion by human breast cancer cells in Matrigel-based in vitro assays. Breast Cancer Res Treat *24*, 241-255.

Bando, H., Atsumi, T., Nishio, T., Niwa, H., Mishima, S., Shimizu, C., Yoshioka, N., Bucala, R., and Koike, T. (2005). Phosphorylation of the 6-phosphofructo-2-kinase/fructose 2,6-bisphosphatase/PFKFB3 family of glycolytic regulators in human cancer. Clin Cancer Res *11*, 5784-5792.

Bardos, J.I., and Ashcroft, M. (2004). Hypoxia-inducible factor-1 and oncogenic signalling. Bioessays *26*, 262-269.

Baron, D.N., Buck, G.M., and Foxwell, C.J. (1969). Multiple forms of aldolase in mammalian brain, gonads, fetal tissue and muscle. Adv Enzyme Regul *7*, 325-336.

Barretina, J., Caponigro, G., Stransky, N., Venkatesan, K., Margolin, A.A., Kim, S., Wilson, C.J., Lehar, J., Kryukov, G.V., Sonkin, D.*, et al.* (2012). The Cancer Cell Line Encyclopedia enables predictive modelling of anticancer drug sensitivity. Nature *483*, 603-607.

Barthel, A., Schmoll, D., Kruger, K.D., Bahrenberg, G., Walther, R., Roth, R.A., and Joost, H.G. (2001). Differential regulation of endogenous glucose-6-phosphatase and phosphoenolpyruvate carboxykinase gene expression by the forkhead transcription factor FKHR in H4IIE-hepatoma cells. Biochem Biophys Res Commun *285*, 897-902.
Baselga, J. (2011). Targeting the phosphoinositide-3 (PI3) kinase pathway in breast cancer. Oncologist *16 Suppl 1*, 12-19.
Basu, S., Chen, W., Tchou, J., Mavi, A., Cermik, T., Czerniecki, B., Schnall, M., and Alavi, A. (2008). Comparison of triple-negative and estrogen receptor-positive/progesterone receptor-positive/HER2-negative breast carcinoma using quantitative fluorine-18 fluorodeoxyglucose/positron emission tomography imaging parameters: a potentially useful method for disease characterization. Cancer *112*, 995-1000.
Bauer, D.E., Hatzivassiliou, G., Zhao, F., Andreadis, C., and Thompson, C.B. (2005). ATP citrate lyase is an important component of cell growth and transformation. Oncogene *24*, 6314-6322.
Bengoechea-Alonso, M.T., and Ericsson, J. (2007). SREBP in signal transduction: cholesterol metabolism and beyond. Curr Opin Cell Biol *19*, 215-222.
Bensaad, K., Cheung, E.C., and Vousden, K.H. (2009). Modulation of intracellular ROS levels by TIGAR controls autophagy. EMBO J *28*, 3015-3026.
Bensaad, K., Tsuruta, A., Selak, M.A., Vidal, M.N., Nakano, K., Bartrons, R., Gottlieb, E., and Vousden, K.H. (2006). TIGAR, a p53-inducible regulator of glycolysis and apoptosis. Cell *126*, 107-120.
Berg, J.M., Tymoczko, J.L., and Stryer, L. (2002). Biochemistry, 5th edition edn (New York, W H Freeman).
Bergamaschi, A., Tagliabue, E., Sorlie, T., Naume, B., Triulzi, T., Orlandi, R., Russnes, H.G., Nesland, J.M., Tammi, R., Auvinen, P.*, et al.* (2008). Extracellular matrix signature identifies breast cancer subgroups with different clinical outcome. J Pathol *214*, 357-367.
Berwick, D.C., Hers, I., Heesom, K.J., Moule, S.K., and Tavare, J.M. (2002). The identification of ATP-citrate lyase as a protein kinase B (Akt) substrate in primary adipocytes. J Biol Chem *277*, 33895-33900.
Bhargava, R., Gerald, W.L., Li, A.R., Pan, Q., Lal, P., Ladanyi, M., and Chen, B. (2005). EGFR gene amplification in breast cancer: correlation with epidermal growth factor receptor mRNA and protein expression and HER-2 status and absence of EGFR-activating mutations. Mod Pathol *18*, 1027-1033.
Birsoy, K., Wang, T., Possemato, R., Yilmaz, O.H., Koch, C.E., Chen, W.W., Hutchins, A.W., Gultekin, Y., Peterson, T.R., Carette, J.E.*, et al.* (2012a). MCT1-mediated transport of a toxic molecule is an effective strategy for targeting glycolytic tumors. Nat Genet.
Birsoy, K., Wang, T.Y., Possemato, R., Yilmaz, O.H., Koch, C.E., Chen, W.W., Hutchins, A.W., Gultekin, Y., Peterson, T.R., Carette, J.E.*, et al.* (2012b). MCT1-mediated transport of a toxic molecule is an effective strategy for targeting glycolytic tumors. Nature Genetics.
Bissell, M.J., Radisky, D.C., Rizki, A., Weaver, V.M., and Petersen, O.W. (2002). The organizing principle: microenvironmental influences in the normal and malignant breast. Differentiation *70*, 537-546.
Biswas, C., Zhang, Y., DeCastro, R., Guo, H., Nakamura, T., Kataoka, H., and Nabeshima, K. (1995). The human tumor cell-derived collagenase stimulatory factor

(renamed EMMPRIN) is a member of the immunoglobulin superfamily. Cancer Res *55*, 434-439.
Boidot, R., Vegran, F., Meulle, A., Le Breton, A., Dessy, C., Sonveaux, P., Lizard-Nacol, S., and Feron, O. (2012). Regulation of monocarboxylate transporter MCT1 expression by p53 mediates inward and outward lactate fluxes in tumors. Cancer Res *72*, 939-948.
Bonen, A. (2001). The expression of lactate transporters (MCT1 and MCT4) in heart and muscle. Eur J Appl Physiol *86*, 6-11.
Boros, L.G., Torday, J.S., Lim, S., Bassilian, S., Cascante, M., and Lee, W.N. (2000). Transforming growth factor beta2 promotes glucose carbon incorporation into nucleic acid ribose through the nonoxidative pentose cycle in lung epithelial carcinoma cells. Cancer Res *60*, 1183-1185.
Borsi, L., Allemanni, G., Gaggero, B., and Zardi, L. (1996). Extracellular pH controls pre-mRNA alternative splicing of tenascin-C in normal, but not in malignantly transformed, cells. Int J Cancer *66*, 632-635.
Boutros, M., Bras, L.P., and Huber, W. (2006). Analysis of cell-based RNAi screens. Genome Biol *7*, R66.
Brandon, M., Baldi, P., and Wallace, D.C. (2006). Mitochondrial mutations in cancer. Oncogene *25*, 4647-4662.
Brindley, D.N., English, D., Pilquil, C., Buri, K., and Ling, Z.C. (2002). Lipid phosphate phosphatases regulate signal transduction through glycerolipids and sphingolipids. Biochim Biophys Acta *1582*, 33-44.
Brooks, G.A. (2007). Lactate: link between glycolytic and oxidative metabolism. Sports Med *37*, 341-343.
Brooks, G.A. (2009). Cell-cell and intracellular lactate shuttles. J Physiol *587*, 5591-5600.
Brough, R., Frankum, J.R., Sims, D., Mackay, A., Mendes-Pereira, A.M., Bajrami, I., Costa-Cabral, S., Rafiq, R., Ahmad, A.S., Cerone, M.A.*, et al.* (2011). Functional viability profiles of breast cancer. Cancer Discov *1*, 260-273.
Burris, H.A., 3rd (2004). Dual kinase inhibition in the treatment of breast cancer: initial experience with the EGFR/ErbB-2 inhibitor lapatinib. Oncologist *9 Suppl 3*, 10-15.
Buscher, J.M., Czernik, D., Ewald, J.C., Sauer, U., and Zamboni, N. (2009). Cross-platform comparison of methods for quantitative metabolomics of primary metabolism. Anal Chem *81*, 2135-2143.
Buzzai, M., Jones, R.G., Amaravadi, R.K., Lum, J.J., DeBerardinis, R.J., Zhao, F., Viollet, B., and Thompson, C.B. (2007). Systemic treatment with the antidiabetic drug metformin selectively impairs p53-deficient tumor cell growth. Cancer Res *67*, 6745-6752.
Cairns, R.A., Harris, I.S., and Mak, T.W. (2011). Regulation of cancer cell metabolism. Nat Rev Cancer *11*, 85-95.
CancerGenomeAtlasNetwork (2012). Comprehensive molecular portraits of human breast tumours. Nature *490*, 61-70.
Canto, C., Gerhart-Hines, Z., Feige, J.N., Lagouge, M., Noriega, L., Milne, J.C., Elliott, P.J., Puigserver, P., and Auwerx, J. (2009). AMPK regulates energy expenditure by modulating NAD+ metabolism and SIRT1 activity. Nature *458*, 1056-1060.
Canto, C., Houtkooper, R.H., Pirinen, E., Youn, D.Y., Oosterveer, M.H., Cen, Y., Fernandez-Marcos, P.J., Yamamoto, H., Andreux, P.A., Cettour-Rose, P.*, et al.* (2012).

The NAD(+) precursor nicotinamide riboside enhances oxidative metabolism and protects against high-fat diet-induced obesity. Cell Metab *15*, 838-847.
Cantor, J.R., and Sabatini, D.M. (2012). Cancer cell metabolism: one hallmark, many faces. Cancer Discov *2*, 881-898.
Carpenter, A.E., and Sabatini, D.M. (2004). Systematic genome-wide screens of gene function. Nat Rev Genet *5*, 11-22.
Carpten, J.D., Faber, A.L., Horn, C., Donoho, G.P., Briggs, S.L., Robbins, C.M., Hostetter, G., Boguslawski, S., Moses, T.Y., Savage, S.*, et al.* (2007). A transforming mutation in the pleckstrin homology domain of AKT1 in cancer. Nature *448*, 439-444.
Carroll, J.S., Meyer, C.A., Song, J., Li, W., Geistlinger, T.R., Eeckhoute, J., Brodsky, A.S., Keeton, E.K., Fertuck, K.C., Hall, G.F.*, et al.* (2006). Genome-wide analysis of estrogen receptor binding sites. Nat Genet *38*, 1289-1297.
Cascante, M., Centelles, J.J., Veech, R.L., Lee, W.N., and Boros, L.G. (2000). Role of thiamin (vitamin B-1) and transketolase in tumor cell proliferation. Nutr Cancer *36*, 150-154.
Cendan, J.C., Souba, W.W., Copeland, E.M., 3rd, and Lind, D.S. (1996). Increased L-arginine transport in a nitric oxide-producing metastatic colon cancer cell line. Ann Surg Oncol *3*, 501-508.
Cheang, M.C., van de Rijn, M., and Nielsen, T.O. (2008). Gene expression profiling of breast cancer. Annu Rev Pathol *3*, 67-97.
Chen, C., Pore, N., Behrooz, A., Ismail-Beigi, F., and Maity, A. (2001). Regulation of glut1 mRNA by hypoxia-inducible factor-1. Interaction between H-ras and hypoxia. J Biol Chem *276*, 9519-9525.
Chen, Y., Cairns, R., Papandreou, I., Koong, A., and Denko, N.C. (2009). Oxygen consumption can regulate the growth of tumors, a new perspective on the Warburg effect. PLoS One *4*, e7033.
Chi, J.T., Wang, Z., Nuyten, D.S., Rodriguez, E.H., Schaner, M.E., Salim, A., Wang, Y., Kristensen, G.B., Helland, A., Borresen-Dale, A.L.*, et al.* (2006). Gene Expression Programs in Response to Hypoxia: Cell Type Specificity and Prognostic Significance in Human Cancers. PLoS Med *3*, e47.
Chiarugi, A., Dolle, C., Felici, R., and Ziegler, M. (2012). The NAD metabolome - a key determinant of cancer cell biology. Nat Rev Cancer *12*, 741-752.
Chiche, J., Brahimi-Horn, M.C., and Pouyssegur, J. (2010a). Tumour hypoxia induces a metabolic shift causing acidosis: a common feature in cancer. J Cell Mol Med *14*, 771-794.
Chiche, J., Ilc, K., Brahimi-Horn, M.C., and Pouyssegur, J. (2010b). Membrane-bound carbonic anhydrases are key pH regulators controlling tumor growth and cell migration. Adv Enzyme Regul *50*, 20-33.
Chiche, J., Ilc, K., Laferriere, J., Trottier, E., Dayan, F., Mazure, N.M., Brahimi-Horn, M.C., and Pouyssegur, J. (2009). Hypoxia-inducible carbonic anhydrase IX and XII promote tumor cell growth by counteracting acidosis through the regulation of the intracellular pH. Cancer Res *69*, 358-368.
Chiche, J., Le Fur, Y., Vilmen, C., Frassineti, F., Daniel, L., Halestrap, A.P., Cozzone, P.J., Pouyssegur, J., and Lutz, N.W. (2012). In vivo pH in metabolic-defective Ras-transformed fibroblast tumors: key role of the monocarboxylate transporter, MCT4, for inducing an alkaline intracellular pH. Int J Cancer *130*, 1511-1520.

Chowdhury, R., Yeoh, K.K., Tian, Y.M., Hillringhaus, L., Bagg, E.A., Rose, N.R., Leung, I.K., Li, X.S., Woon, E.C., Yang, M.*, et al.* (2011). The oncometabolite 2-hydroxyglutarate inhibits histone lysine demethylases. EMBO Rep *12*, 463-469.
Christofk, H.R., Vander Heiden, M.G., Harris, M.H., Ramanathan, A., Gerszten, R.E., Wei, R., Fleming, M.D., Schreiber, S.L., and Cantley, L.C. (2008a). The M2 splice isoform of pyruvate kinase is important for cancer metabolism and tumour growth. Nature *452*, 230-233.
Christofk, H.R., Vander Heiden, M.G., Wu, N., Asara, J.M., and Cantley, L.C. (2008b). Pyruvate kinase M2 is a phosphotyrosine-binding protein. Nature *452*, 181-186.
Chung, N., Zhang, X.D., Kreamer, A., Locco, L., Kuan, P.F., Bartz, S., Linsley, P.S., Ferrer, M., and Strulovici, B. (2008). Median absolute deviation to improve hit selection for genome-scale RNAi screens. J Biomol Screen *13*, 149-158.
Clem, B., Telang, S., Clem, A., Yalcin, A., Meier, J., Simmons, A., Rasku, M.A., Arumugam, S., Dean, W.L., Eaton, J.*, et al.* (2008). Small-molecule inhibition of 6-phosphofructo-2-kinase activity suppresses glycolytic flux and tumor growth. Mol Cancer Ther *7*, 110-120.
Colen, C.B., Shen, Y., Ghoddoussi, F., Yu, P., Francis, T.B., Koch, B.J., Monterey, M.D., Galloway, M.P., Sloan, A.E., and Mathupala, S.P. (2011). Metabolic targeting of lactate efflux by malignant glioma inhibits invasiveness and induces necrosis: an in vivo study. Neoplasia *13*, 620-632.
Cori, C.F. (1981). The glucose-lactic acid cycle and gluconeogenesis. Curr Top Cell Regul *18*, 377-387.
Coy, J.F., Dressler, D., Wilde, J., and Schubert, P. (2005). Mutations in the transketolase-like gene TKTL1: clinical implications for neurodegenerative diseases, diabetes and cancer. Clin Lab *51*, 257-273.
Cross, D.A., Alessi, D.R., Cohen, P., Andjelkovich, M., and Hemmings, B.A. (1995). Inhibition of glycogen synthase kinase-3 by insulin mediated by protein kinase B. Nature *378*, 785-789.
Cross, S.H., and Bird, A.P. (1995). CpG islands and genes. Curr Opin Genet Dev *5*, 309-314.
Curtis, C., Shah, S.P., Chin, S.F., Turashvili, G., Rueda, O.M., Dunning, M.J., Speed, D., Lynch, A.G., Samarajiwa, S., Yuan, Y.*, et al.* (2012). The genomic and transcriptomic architecture of 2,000 breast tumours reveals novel subgroups. Nature *486*, 346-352.
Dang, C.V. (2009). MYC, microRNAs and glutamine addiction in cancers. Cell Cycle *8*, 3243-3245.
Dang, C.V. (2012). MYC on the path to cancer. Cell *149*, 22-35.
Dang, C.V., Hamaker, M., Sun, P., Le, A., and Gao, P. (2011). Therapeutic targeting of cancer cell metabolism. J Mol Med *89*, 205-212.
Dang, L., White, D.W., Gross, S., Bennett, B.D., Bittinger, M.A., Driggers, E.M., Fantin, V.R., Jang, H.G., Jin, S., Keenan, M.C.*, et al.* (2009). Cancer-associated IDH1 mutations produce 2-hydroxyglutarate. Nature *462*, 739-744.
Dang, L., White, D.W., Gross, S., Bennett, B.D., Bittinger, M.A., Driggers, E.M., Fantin, V.R., Jang, H.G., Jin, S., Keenan, M.C.*, et al.* (2010). Cancer-associated IDH1 mutations produce 2-hydroxyglutarate. Nature *465*, 966.
Davidson, B., Goldberg, I., Berner, A., Kristensen, G.B., and Reich, R. (2003). EMMPRIN (extracellular matrix metalloproteinase inducer) is a novel marker of poor outcome in serous ovarian carcinoma. Clin Exp Metastasis *20*, 161-169.

DeBerardinis, R.J., Mancuso, A., Daikhin, E., Nissim, I., Yudkoff, M., Wehrli, S., and Thompson, C.B. (2007). Beyond aerobic glycolysis: transformed cells can engage in glutamine metabolism that exceeds the requirement for protein and nucleotide synthesis. Proc Natl Acad Sci U S A *104*, 19345-19350.
Deberardinis, R.J., Sayed, N., Ditsworth, D., and Thompson, C.B. (2008). Brick by brick: metabolism and tumor cell growth. Curr Opin Genet Dev *18*, 54-61.
DeRisi, J., Penland, L., Brown, P.O., Bittner, M.L., Meltzer, P.S., Ray, M., Chen, Y., Su, Y.A., and Trent, J.M. (1996). Use of a cDNA microarray to analyse gene expression patterns in human cancer. Nat Genet *14*, 457-460.
Deroo, B.J., and Korach, K.S. (2006). Estrogen receptors and human disease. J Clin Invest *116*, 561-570.
Dimmer, K.S., Friedrich, B., Lang, F., Deitmer, J.W., and Broer, S. (2000). The low-affinity monocarboxylate transporter MCT4 is adapted to the export of lactate in highly glycolytic cells. Biochem J *350 Pt 1*, 219-227.
Doane, A.S., Danso, M., Lal, P., Donaton, M., Zhang, L., Hudis, C., and Gerald, W.L. (2006). An estrogen receptor-negative breast cancer subset characterized by a hormonally regulated transcriptional program and response to androgen. Oncogene *25*, 3994-4008.
Duvel, K., Yecies, J.L., Menon, S., Raman, P., Lipovsky, A.I., Souza, A.L., Triantafellow, E., Ma, Q., Gorski, R., Cleaver, S.*, et al.* (2010). Activation of a metabolic gene regulatory network downstream of mTOR complex 1. Mol Cell *39*, 171-183.
Elbashir, S.M., Harborth, J., Lendeckel, W., Yalcin, A., Weber, K., and Tuschl, T. (2001). Duplexes of 21-nucleotide RNAs mediate RNA interference in cultured mammalian cells. Nature *411*, 494-498.
Ely, J.O.J.o.t.F.I. (1954). 2-Deoxy-D-glucose as an inhibitor of cancerous growth in animals. Journal of the Franklin Institute, 157–160.
Engelman, J.A., Luo, J., and Cantley, L.C. (2006). The evolution of phosphatidylinositol 3-kinases as regulators of growth and metabolism. Nat Rev Genet *7*, 606-619.
Escalante-Alcalde, D., Hernandez, L., Le Stunff, H., Maeda, R., Lee, H.S., Jr Gang, C., Sciorra, V.A., Daar, I., Spiegel, S., Morris, A.J.*, et al.* (2003). The lipid phosphatase LPP3 regulates extra-embryonic vasculogenesis and axis patterning. Development *130*, 4623-4637.
Evans, S.M., Hahn, S.M., Magarelli, D.P., and Koch, C.J. (2001). Hypoxic heterogeneity in human tumors: EF5 binding, vasculature, necrosis, and proliferation. Am J Clin Oncol *24*, 467-472.
Ewald, B., Sampath, D., and Plunkett, W. (2008). Nucleoside analogs: molecular mechanisms signaling cell death. Oncogene *27*, 6522-6537.
Falschlehner, C., Steinbrink, S., Erdmann, G., and Boutros, M. (2010). High-throughput RNAi screening to dissect cellular pathways: a how-to guide. Biotechnol J *5*, 368-376.
Fan, C., Oh, D.S., Wessels, L., Weigelt, B., Nuyten, D.S., Nobel, A.B., van't Veer, L.J., and Perou, C.M. (2006). Concordance among gene-expression-based predictors for breast cancer. N Engl J Med *355*, 560-569.
Fan, M., Nakshatri, H., and Nephew, K.P. (2004). Inhibiting proteasomal proteolysis sustains estrogen receptor-alpha activation. Mol Endocrinol *18*, 2603-2615.

Fantin, V.R., St-Pierre, J., and Leder, P. (2006). Attenuation of LDH-A expression uncovers a link between glycolysis, mitochondrial physiology, and tumor maintenance. Cancer Cell *9*, 425-434.
Farfari, S., Schulz, V., Corkey, B., and Prentki, M. (2000). Glucose-regulated anaplerosis and cataplerosis in pancreatic beta-cells: possible implication of a pyruvate/citrate shuttle in insulin secretion. Diabetes *49*, 718-726.
Farmer, P., Bonnefoi, H., Becette, V., Tubiana-Hulin, M., Fumoleau, P., Larsimont, D., Macgrogan, G., Bergh, J., Cameron, D., Goldstein, D.*, et al.* (2005). Identification of molecular apocrine breast tumours by microarray analysis. Oncogene *24*, 4660-4671.
Favaro, E., Lord, S., Harris, A.L., and Buffa, F.M. (2011). Gene expression and hypoxia in breast cancer. Genome Med *3*, 55.
Fedorov, Y., King, A., Anderson, E., Karpilow, J., Ilsley, D., Marshall, W., and Khvorova, A. (2005). Different delivery methods-different expression profiles. Nat Methods *2*, 241.
Feron, O. (2009). Pyruvate into lactate and back: from the Warburg effect to symbiotic energy fuel exchange in cancer cells. Radiother Oncol *92*, 329-333.
Fire, A., Xu, S., Montgomery, M.K., Kostas, S.A., Driver, S.E., and Mello, C.C. (1998). Potent and specific genetic interference by double-stranded RNA in Caenorhabditis elegans. Nature *391*, 806-811.
Flanagan, J.M., Funes, J.M., Henderson, S., Wild, L., Carey, N., and Boshoff, C. (2009). Genomics screen in transformed stem cells reveals RNASEH2A, PPAP2C, and ADARB1 as putative anticancer drug targets. Mol Cancer Ther *8*, 249-260.
Foldi, M., Stickeler, E., Bau, L., Kretz, O., Watermann, D., Gitsch, G., Kayser, G., Zur Hausen, A., and Coy, J.F. (2007). Transketolase protein TKTL1 overexpression: A potential biomarker and therapeutic target in breast cancer. Oncol Rep *17*, 841-845.
Forbes, S.A., Bindal, N., Bamford, S., Cole, C., Kok, C.Y., Beare, D., Jia, M., Shepherd, R., Leung, K., Menzies, A.*, et al.* (2011). COSMIC: mining complete cancer genomes in the Catalogue of Somatic Mutations in Cancer. Nucleic Acids Res *39*, D945-950.
Foulkes, W.D., Smith, I.E., and Reis-Filho, J.S. (2010). Triple-negative breast cancer. N Engl J Med *363*, 1938-1948.
Freed-Pastor, W.A., Mizuno, H., Zhao, X., Langerod, A., Moon, S.H., Rodriguez-Barrueco, R., Barsotti, A., Chicas, A., Li, W., Polotskaia, A.*, et al.* (2012). Mutant p53 disrupts mammary tissue architecture via the mevalonate pathway. Cell *148*, 244-258.
Frezza, C., Tennant, D.A., and Gottlieb, E. (2010). IDH1 mutations in gliomas: when an enzyme loses its grip. Cancer Cell *17*, 7-9.
Frezza, C., Zheng, L., Folger, O., Rajagopalan, K.N., MacKenzie, E.D., Jerby, L., Micaroni, M., Chaneton, B., Adam, J., Hedley, A.*, et al.* (2011). Haem oxygenase is synthetically lethal with the tumour suppressor fumarate hydratase. Nature *477*, 225-228.
Fuhrer, T., Heer, D., Begemann, B., and Zamboni, N. (2011). High-throughput, accurate mass metabolome profiling of cellular extracts by flow injection-time-of-flight mass spectrometry. Anal Chem *83*, 7074-7080.
Gaglio, D., Metallo, C.M., Gameiro, P.A., Hiller, K., Danna, L.S., Balestrieri, C., Alberghina, L., Stephanopoulos, G., and Chiaradonna, F. (2011). Oncogenic K-Ras decouples glucose and glutamine metabolism to support cancer cell growth. Mol Syst Biol *7*, 523.
Gallagher, E.J., and LeRoith, D. (2011). Diabetes, cancer, and metformin: connections of metabolism and cell proliferation. Ann N Y Acad Sci *1243*, 54-68.

Gallagher, S.M., Castorino, J.J., and Philp, N.J. (2009). Interaction of monocarboxylate transporter 4 with beta1-integrin and its role in cell migration. Am J Physiol Cell Physiol *296*, C414-421.
Gambhir, S.S., Czernin, J., Schwimmer, J., Silverman, D.H., Coleman, R.E., and Phelps, M.E. (2001). A tabulated summary of the FDG PET literature. J Nucl Med *42*, 1S-93S.
Ganapathy, V., Thangaraju, M., and Prasad, P.D. (2009). Nutrient transporters in cancer: relevance to Warburg hypothesis and beyond. Pharmacol Ther *121*, 29-40.
Garcia, C.K., Brown, M.S., Pathak, R.K., and Goldstein, J.L. (1995). cDNA cloning of MCT2, a second monocarboxylate transporter expressed in different cells than MCT1. J Biol Chem *270*, 1843-1849.
Garcia, C.K., Goldstein, J.L., Pathak, R.K., Anderson, R.G., and Brown, M.S. (1994). Molecular characterization of a membrane transporter for lactate, pyruvate, and other monocarboxylates: implications for the Cori cycle. Cell *76*, 865-873.
Garcia-Cao, I., Song, M.S., Hobbs, R.M., Laurent, G., Giorgi, C., de Boer, V.C., Anastasiou, D., Ito, K., Sasaki, A.T., Rameh, L.*, et al.* (2012). Systemic Elevation of PTEN Induces a Tumor-Suppressive Metabolic State. Cell *149*, 49-62.
Gatenby, R.A., Smallbone, K., Maini, P.K., Rose, F., Averill, J., Nagle, R.B., Worrall, L., and Gillies, R.J. (2007). Cellular adaptations to hypoxia and acidosis during somatic evolution of breast cancer. Br J Cancer *97*, 646-653.
Gerlinger, M., Santos, C.R., Spencer-Dene, B., Martinez, P., Endesfelder, D., Burrell, R.A., Vetter, M., Jiang, M., Saunders, R.E., Kelly, G.*, et al.* (2012). Genome-wide RNA interference analysis of renal carcinoma survival regulators identifies MCT4 as a Warburg effect metabolic target. J Pathol *227*, 146-156.
Giaever, G., Chu, A.M., Ni, L., Connelly, C., Riles, L., Veronneau, S., Dow, S., Lucau-Danila, A., Anderson, K., Andre, B.*, et al.* (2002). Functional profiling of the Saccharomyces cerevisiae genome. Nature *418*, 387-391.
Goidts, V., Bageritz, J., Puccio, L., Nakata, S., Zapatka, M., Barbus, S., Toedt, G., Campos, B., Korshunov, A., Momma, S.*, et al.* (2012). RNAi screening in glioma stem-like cells identifies PFKFB4 as a key molecule important for cancer cell survival. Oncogene *31*, 3235-3243.
Goldstein, J.L., DeBose-Boyd, R.A., and Brown, M.S. (2006). Protein sensors for membrane sterols. Cell *124*, 35-46.
Gottlieb, E., and Tomlinson, I.P. (2005). Mitochondrial tumour suppressors: a genetic and biochemical update. Nat Rev Cancer *5*, 857-866.
Gottlob, K., Majewski, N., Kennedy, S., Kandel, E., Robey, R.B., and Hay, N. (2001). Inhibition of early apoptotic events by Akt/PKB is dependent on the first committed step of glycolysis and mitochondrial hexokinase. Genes Dev *15*, 1406-1418.
Graus-Porta, D., Beerli, R.R., Daly, J.M., and Hynes, N.E. (1997). ErbB-2, the preferred heterodimerization partner of all ErbB receptors, is a mediator of lateral signaling. EMBO J *16*, 1647-1655.
Griffin, J.L., and Shockcor, J.P. (2004). Metabolic profiles of cancer cells. Nat Rev Cancer *4*, 551-561.
Groheux, D., Giacchetti, S., Moretti, J.L., Porcher, R., Espie, M., Lehmann-Che, J., de Roquancourt, A., Hamy, A.S., Cuvier, C., Vercellino, L.*, et al.* (2011). Correlation of high 18F-FDG uptake to clinical, pathological and biological prognostic factors in breast cancer. Eur J Nucl Med Mol Imaging *38*, 426-435.

Guedj, M., Marisa, L., de Reynies, A., Orsetti, B., Schiappa, R., Bibeau, F., MacGrogan, G., Lerebours, F., Finetti, P., Longy, M*., et al.* (2012). A refined molecular taxonomy of breast cancer. Oncogene *31*, 1196-1206.
Guppy, A., Jamal-Hanjani, M., and Pickering, L. (2011). Anticancer effects of metformin and its potential use as a therapeutic agent for breast cancer. Future Oncol *7*, 727-736.
Guy, C.T., Cardiff, R.D., and Muller, W.J. (1992). Induction of mammary tumors by expression of polyomavirus middle T oncogene: a transgenic mouse model for metastatic disease. Mol Cell Biol *12*, 954-961.
Gwinn, D.M., Shackelford, D.B., Egan, D.F., Mihaylova, M.M., Mery, A., Vasquez, D.S., Turk, B.E., and Shaw, R.J. (2008). AMPK phosphorylation of raptor mediates a metabolic checkpoint. Mol Cell *30*, 214-226.
Halestrap, A.P., and Meredith, D. (2004). The SLC16 gene family-from monocarboxylate transporters (MCTs) to aromatic amino acid transporters and beyond. Pflugers Arch *447*, 619-628.
Halestrap, A.P., and Price, N.T. (1999). The proton-linked monocarboxylate transporter (MCT) family: structure, function and regulation. Biochem J *343 Pt 2*, 281-299.
Halestrap, A.P., and Wilson, M.C. (2012). The monocarboxylate transporter family--role and regulation. IUBMB Life *64*, 109-119.
Hanahan, D., and Weinberg, R.A. (2011). Hallmarks of cancer: the next generation. Cell *144*, 646-674.
Hannon, G.J. (2002). RNA interference. Nature *418*, 244-251.
Hardie, D.G. (2011). AMP-activated protein kinase: an energy sensor that regulates all aspects of cell function. Genes Dev *25*, 1895-1908.
Harley, W., Floyd, C., Dunn, T., Zhang, X.D., Chen, T.Y., Hegde, M., Palandoken, H., Nantz, M.H., Leon, L., Carraway, K.L., 3rd*, et al.* (2010). Dual inhibition of sodium-mediated proton and calcium efflux triggers non-apoptotic cell death in malignant gliomas. Brain Res *1363*, 159-169.
Harris, A.L., Nicholson, S., Sainsbury, J.R., Farndon, J., and Wright, C. (1989). Epidermal growth factor receptors in breast cancer: association with early relapse and death, poor response to hormones and interactions with neu. J Steroid Biochem *34*, 123-131.
Hartmaier, R.J., Priedigkeit, N., and Lee, A.V. (2012). Who's driving anyway? Herculean efforts to identify the drivers of breast cancer. Breast Cancer Res *14*, 323.
Hatzivassiliou, G., Zhao, F., Bauer, D.E., Andreadis, C., Shaw, A.N., Dhanak, D., Hingorani, S.R., Tuveson, D.A., and Thompson, C.B. (2005). ATP citrate lyase inhibition can suppress tumor cell growth. Cancer Cell *8*, 311-321.
Hayes, C.S., DeFeo, K., Lan, L., Paul, B., Sell, C., and Gilmour, S.K. (2006). Elevated levels of ornithine decarboxylase cooperate with Raf/ERK activation to convert normal keratinocytes into invasive malignant cells. Oncogene *25*, 1543-1553.
Hedenfalk, I., Glarner, N., Kronblad, A., Veerla, S., Ringner, M., and Landberg, G. (2005). Microarray-Based Analyses of Hypoxia-Induced Transcriptional Changes in Breast Cancer Cell Lines. Cancer genomics and proteomics
.
Hirschhaeuser, F., Sattler, U.G., and Mueller-Klieser, W. (2011). Lactate: a metabolic key player in cancer. Cancer Res *71*, 6921-6925.

Hitosugi, T., Kang, S., Vander Heiden, M.G., Chung, T.W., Elf, S., Lythgoe, K., Dong, S., Lonial, S., Wang, X., Chen, G.Z.*, et al.* (2009). Tyrosine phosphorylation inhibits PKM2 to promote the Warburg effect and tumor growth. Sci Signal *2*, ra73.
Hockel, M., and Vaupel, P. (2001a). Biological consequences of tumor hypoxia. Semin Oncol *28*, 36-41.
Hockel, M., and Vaupel, P. (2001b). Tumor hypoxia: definitions and current clinical, biologic, and molecular aspects. J Natl Cancer Inst *93*, 266-276.
Hollander, M.C., Blumenthal, G.M., and Dennis, P.A. (2011). PTEN loss in the continuum of common cancers, rare syndromes and mouse models. Nat Rev Cancer *11*, 289-301.
Horsman, M.R., Mortensen, L.S., Petersen, J.B., Busk, M., and Overgaard, J. (2012). Imaging hypoxia to improve radiotherapy outcome. Nat Rev Clin Oncol *9*, 674-687.
Hu, W., Zhang, C., Wu, R., Sun, Y., Levine, A., and Feng, Z. (2010). Glutaminase 2, a novel p53 target gene regulating energy metabolism and antioxidant function. Proc Natl Acad Sci U S A *107*, 7455-7460.
Hu, Z., Fan, C., Oh, D.S., Marron, J.S., He, X., Qaqish, B.F., Livasy, C., Carey, L.A., Reynolds, E., Dressler, L.*, et al.* (2006). The molecular portraits of breast tumors are conserved across microarray platforms. BMC Genomics *7*, 96.
Hudis, C.A. (2007). Trastuzumab--mechanism of action and use in clinical practice. N Engl J Med *357*, 39-51.
Hussien, R., and Brooks, G.A. (2011). Mitochondrial and plasma membrane lactate transporter and lactate dehydrogenase isoform expression in breast cancer cell lines. Physiol Genomics *43*, 255-264.
Hynes, N.E., and Stern, D.F. (1994). The biology of erbB-2/neu/HER-2 and its role in cancer. Biochim Biophys Acta *1198*, 165-184.
Imai, A., Furui, T., Tamaya, T., and Mills, G.B. (2000). A gonadotropin-releasing hormone-responsive phosphatase hydrolyses lysophosphatidic acid within the plasma membrane of ovarian cancer cells. J Clin Endocrinol Metab *85*, 3370-3375.
Inoki, K., Li, Y., Zhu, T., Wu, J., and Guan, K.L. (2002). TSC2 is phosphorylated and inhibited by Akt and suppresses mTOR signalling. Nat Cell Biol *4*, 648-657.
Inoki, K., Ouyang, H., Zhu, T., Lindvall, C., Wang, Y., Zhang, X., Yang, Q., Bennett, C., Harada, Y., Stankunas, K.*, et al.* (2006). TSC2 integrates Wnt and energy signals via a coordinated phosphorylation by AMPK and GSK3 to regulate cell growth. Cell *126*, 955-968.
Iorns, E., Lord, C.J., Grigoriadis, A., McDonald, S., Fenwick, K., Mackay, A., Mein, C.A., Natrajan, R., Savage, K., Tamber, N.*, et al.* (2009). Integrated functional, gene expression and genomic analysis for the identification of cancer targets. PLoS One *4*, e5120.
Isaacs, J.S., Jung, Y.J., Mole, D.R., Lee, S., Torres-Cabala, C., Chung, Y.L., Merino, M., Trepel, J., Zbar, B., Toro, J.*, et al.* (2005). HIF overexpression correlates with biallelic loss of fumarate hydratase in renal cancer: novel role of fumarate in regulation of HIF stability. Cancer Cell *8*, 143-153.
Jaakkola, P., Mole, D.R., Tian, Y.M., Wilson, M.I., Gielbert, J., Gaskell, S.J., Kriegsheim, A., Hebestreit, H.F., Mukherji, M., Schofield, C.J.*, et al.* (2001). Targeting of HIF-alpha to the von Hippel-Lindau ubiquitylation complex by O2-regulated prolyl hydroxylation. Science *292*, 468-472.
Jackson, J.G., Pant, V., Li, Q., Chang, L.L., Quintas-Cardama, A., Garza, D., Tavana, O., Yang, P., Manshouri, T., Li, Y.*, et al.* (2012). p53-mediated senescence impairs the

apoptotic response to chemotherapy and clinical outcome in breast cancer. Cancer Cell *21*, 793-806.
Jacobetz, M.A., Chan, D.S., Neesse, A., Bapiro, T.E., Cook, N., Frese, K.K., Feig, C., Nakagawa, T., Caldwell, M.E., Zecchini, H.I.*, et al.* (2012). Hyaluronan impairs vascular function and drug delivery in a mouse model of pancreatic cancer. Gut.
Jain, M., Nilsson, R., Sharma, S., Madhusudhan, N., Kitami, T., Souza, A.L., Kafri, R., Kirschner, M.W., Clish, C.B., and Mootha, V.K. (2012). Metabolite profiling identifies a key role for glycine in rapid cancer cell proliferation. Science *336*, 1040-1044.
Jasinska, R., Zhang, Q.X., Pilquil, C., Singh, I., Xu, J., Dewald, J., Dillon, D.A., Berthiaume, L.G., Carman, G.M., Waggoner, D.W.*, et al.* (1999). Lipid phosphate phosphohydrolase-1 degrades exogenous glycerolipid and sphingolipid phosphate esters. Biochem J *340 (Pt 3)*, 677-686.
Jeon, S.M., Chandel, N.S., and Hay, N. (2012). AMPK regulates NADPH homeostasis to promote tumour cell survival during energy stress. Nature *485*, 661-665.
Jiang, P., Du, W., Wang, X., Mancuso, A., Gao, X., Wu, M., and Yang, X. (2011). p53 regulates biosynthesis through direct inactivation of glucose-6-phosphate dehydrogenase. Nat Cell Biol *13*, 310-316.
Jiralerspong, S., Palla, S.L., Giordano, S.H., Meric-Bernstam, F., Liedtke, C., Barnett, C.M., Hsu, L., Hung, M.C., Hortobagyi, G.N., and Gonzalez-Angulo, A.M. (2009). Metformin and pathologic complete responses to neoadjuvant chemotherapy in diabetic patients with breast cancer. J Clin Oncol *27*, 3297-3302.
Johnston, S.R. (2010). New strategies in estrogen receptor-positive breast cancer. Clin Cancer Res *16*, 1979-1987.
Jones, N.P., and Schulze, A. (2012). Targeting cancer metabolism--aiming at a tumour's sweet-spot. Drug Discov Today *17*, 232-241.
Juel, C., and Halestrap, A.P. (1999). Lactate transport in skeletal muscle - role and regulation of the monocarboxylate transporter. J Physiol *517 (Pt 3)*, 633-642.
Kai, M., Wada, I., Imai, S., Sakane, F., and Kanoh, H. (1996). Identification and cDNA cloning of 35-kDa phosphatidic acid phosphatase (type 2) bound to plasma membranes. Polymerase chain reaction amplification of mouse H2O2-inducible hic53 clone yielded the cDNA encoding phosphatidic acid phosphatase. J Biol Chem *271*, 18931-18938.
Kan, Z., Jaiswal, B.S., Stinson, J., Janakiraman, V., Bhatt, D., Stern, H.M., Yue, P., Haverty, P.M., Bourgon, R., Zheng, J.*, et al.* (2010). Diverse somatic mutation patterns and pathway alterations in human cancers. Nature *466*, 869-873.
Kanehisa, M., Goto, S., Sato, Y., Furumichi, M., and Tanabe, M. (2012). KEGG for integration and interpretation of large-scale molecular data sets. Nucleic Acids Res *40*, D109-114.
Kang, K.W., Im, Y.B., Go, W.J., and Han, H.K. (2009). C-myc amplification altered the gene expression of ABC- and SLC-transporters in human breast epithelial cells. Mol Pharm *6*, 627-633.
Katso, R., Okkenhaug, K., Ahmadi, K., White, S., Timms, J., and Waterfield, M.D. (2001). Cellular function of phosphoinositide 3-kinases: implications for development, homeostasis, and cancer. Annu Rev Cell Dev Biol *17*, 615-675.
Kaufman, L., and Rousseeuw, P.J. (1990). Finding Groups in Data: An Introduction to Cluster Analysis.
Kawauchi, K., Araki, K., Tobiume, K., and Tanaka, N. (2008). p53 regulates glucose metabolism through an IKK-NF-kappaB pathway and inhibits cell transformation. Nat Cell Biol *10*, 611-618.

Kayser, G., Sienel, W., Kubitz, B., Mattern, D., Stickeler, E., Passlick, B., Werner, M., and Zur Hausen, A. (2011). Poor outcome in primary non-small cell lung cancers is predicted by transketolase TKTL1 expression. Pathology *43*, 719-724.
Keith, B., Johnson, R.S., and Simon, M.C. (2012). HIF1alpha and HIF2alpha: sibling rivalry in hypoxic tumour growth and progression. Nat Rev Cancer *12*, 9-22.
Kennedy, K.M., and Dewhirst, M.W. (2010). Tumor metabolism of lactate: the influence and therapeutic potential for MCT and CD147 regulation. Future Oncol *6*, 127-148.
Kenny, P.A., Lee, G.Y., Myers, C.A., Neve, R.M., Semeiks, J.R., Spellman, P.T., Lorenz, K., Lee, E.H., Barcellos-Hoff, M.H., Petersen, O.W.*, et al.* (2007). The morphologies of breast cancer cell lines in three-dimensional assays correlate with their profiles of gene expression. Mol Oncol *1*, 84-96.
Kerbel, R.S. (2009). Issues regarding improving the impact of antiangiogenic drugs for the treatment of breast cancer. Breast *18 Suppl 3*, S41-47.
Kim, J.W., Tchernyshyov, I., Semenza, G.L., and Dang, C.V. (2006). HIF-1-mediated expression of pyruvate dehydrogenase kinase: a metabolic switch required for cellular adaptation to hypoxia. Cell Metab *3*, 177-185.
Kirk, P., Wilson, M.C., Heddle, C., Brown, M.H., Barclay, A.N., and Halestrap, A.P. (2000). CD147 is tightly associated with lactate transporters MCT1 and MCT4 and facilitates their cell surface expression. EMBO J *19*, 3896-3904.
Knowles, L.M., Yang, C., Osterman, A., and Smith, J.W. (2008). Inhibition of fatty-acid synthase induces caspase-8-mediated tumor cell apoptosis by up-regulating DDIT4. J Biol Chem *283*, 31378-31384.
Kohn, A.D., Barthel, A., Kovacina, K.S., Boge, A., Wallach, B., Summers, S.A., Birnbaum, M.J., Scott, P.H., Lawrence, J.C., Jr., and Roth, R.A. (1998). Construction and characterization of a conditionally active version of the serine/threonine kinase Akt. J Biol Chem *273*, 11937-11943.
Kondoh, H., Lleonart, M.E., Gil, J., Wang, J., Degan, P., Peters, G., Martinez, D., Carnero, A., and Beach, D. (2005). Glycolytic enzymes can modulate cellular life span. Cancer Res *65*, 177-185.
Konecny, G.E., Pegram, M.D., Venkatesan, N., Finn, R., Yang, G., Rahmeh, M., Untch, M., Rusnak, D.W., Spehar, G., Mullin, R.J.*, et al.* (2006). Activity of the dual kinase inhibitor lapatinib (GW572016) against HER-2-overexpressing and trastuzumab-treated breast cancer cells. Cancer Res *66*, 1630-1639.
Koppitz, B., Vogel, F., and Mayr, G.W. (1986). Mammalian aldolases are isomer-selective high-affinity inositol polyphosphate binders. Eur J Biochem *161*, 421-433.
Koukourakis, M.I., Giatromanolaki, A., Harris, A.L., and Sivridis, E. (2006). Comparison of metabolic pathways between cancer cells and stromal cells in colorectal carcinomas: a metabolic survival role for tumor-associated stroma. Cancer Res *66*, 632-637.
Kovacina, K.S., Park, G.Y., Bae, S.S., Guzzetta, A.W., Schaefer, E., Birnbaum, M.J., and Roth, R.A. (2003). Identification of a proline-rich Akt substrate as a 14-3-3 binding partner. J Biol Chem *278*, 10189-10194.
Krockenberger, M., Honig, A., Rieger, L., Coy, J.F., Sutterlin, M., Kapp, M., Horn, E., Dietl, J., and Kammerer, U. (2007). Transketolase-like 1 expression correlates with subtypes of ovarian cancer and the presence of distant metastases. Int J Gynecol Cancer *17*, 101-106.

Kuhajda, F.P. (2000). Fatty-acid synthase and human cancer: new perspectives on its role in tumor biology. Nutrition *16*, 202-208.
Laemmli, U.K. (1970). Cleavage of structural proteins during the assembly of the head of bacteriophage T4. Nature *227*, 680-685.
Lagarde, A.E., Franchi, A.J., Paris, S., and Pouyssegur, J.M. (1988). Effect of mutations affecting Na+: H+ antiport activity on tumorigenic potential of hamster lung fibroblasts. J Cell Biochem *36*, 249-260.
Lakhani, S.R., Ellis, I.O., Schnitt, S.J., Tan, P.H., and J., v.d.V.M. (2012). WHO Classification of Tumours of the Breast., Fourth edition edn (Lyon, WHO).
Lala, P.K., and Chakraborty, C. (2001). Role of nitric oxide in carcinogenesis and tumour progression. Lancet Oncol *2*, 149-156.
Langbein, S., Zerilli, M., Zur Hausen, A., Staiger, W., Rensch-Boschert, K., Lukan, N., Popa, J., Ternullo, M.P., Steidler, A., Weiss, C.*, et al.* (2006). Expression of transketolase TKTL1 predicts colon and urothelial cancer patient survival: Warburg effect reinterpreted. Br J Cancer *94*, 578-585.
Le, A., Lane, A.N., Hamaker, M., Bose, S., Gouw, A., Barbi, J., Tsukamoto, T., Rojas, C.J., Slusher, B.S., Zhang, H.*, et al.* (2012). Glucose-independent glutamine metabolism via TCA cycling for proliferation and survival in B cells. Cell Metab *15*, 110-121.
Le Floch, R., Chiche, J., Marchiq, I., Naiken, T., Ilk, K., Murray, C.M., Critchlow, S.E., Roux, D., Simon, M.P., and Pouyssegur, J. (2011). CD147 subunit of lactate/H+ symporters MCT1 and hypoxia-inducible MCT4 is critical for energetics and growth of glycolytic tumors. Proc Natl Acad Sci U S A *108*, 16663-16668.
Lebherz, H.G., and Rutter, W.J. (1969). Distribution of fructose diphosphate aldolase variants in biological systems. Biochemistry *8*, 109-121.
Lee, G.Y., Kenny, P.A., Lee, E.H., and Bissell, M.J. (2007). Three-dimensional culture models of normal and malignant breast epithelial cells. Nat Methods *4*, 359-365.
Lehmann, B.D., Bauer, J.A., Chen, X., Sanders, M.E., Chakravarthy, A.B., Shyr, Y., and Pietenpol, J.A. (2011). Identification of human triple-negative breast cancer subtypes and preclinical models for selection of targeted therapies. J Clin Invest *121*, 2750-2767.
Li, J., Yen, C., Liaw, D., Podsypanina, K., Bose, S., Wang, S.I., Puc, J., Miliaresis, C., Rodgers, L., McCombie, R.*, et al.* (1997). PTEN, a putative protein tyrosine phosphatase gene mutated in human brain, breast, and prostate cancer. Science *275*, 1943-1947.
Li, Y., Xu, S., Mihaylova, M.M., Zheng, B., Hou, X., Jiang, B., Park, O., Luo, Z., Lefai, E., Shyy, J.Y.*, et al.* (2011). AMPK phosphorylates and inhibits SREBP activity to attenuate hepatic steatosis and atherosclerosis in diet-induced insulin-resistant mice. Cell Metab *13*, 376-388.
Lim, J.H., Lee, Y.M., Chun, Y.S., Chen, J., Kim, J.E., and Park, J.W. (2010). Sirtuin 1 modulates cellular responses to hypoxia by deacetylating hypoxia-inducible factor 1alpha. Mol Cell *38*, 864-878.
Lin, Y., Wang, J., Jin, W., Wang, L., Li, H., Ma, L., Li, Q., and Pang, T. (2011). NHE1 mediates migration and invasion of HeLa cells via regulating the expression and localization of MT1-MMP. Cell Biochem Funct.
Liu, V.W., Shi, H.H., Cheung, A.N., Chiu, P.M., Leung, T.W., Nagley, P., Wong, L.C., and Ngan, H.Y. (2001). High incidence of somatic mitochondrial DNA mutations in human ovarian carcinomas. Cancer Res *61*, 5998-6001.

Livak, K.J., and Schmittgen, T.D. (2001). Analysis of relative gene expression data using real-time quantitative PCR and the 2(-Delta Delta C(T)) Method. Methods (San Diego, Calif *25*, 402-408.
Locasale, J.W., Grassian, A.R., Melman, T., Lyssiotis, C.A., Mattaini, K.R., Bass, A.J., Heffron, G., Metallo, C.M., Muranen, T., Sharfi, H.*, et al.* (2011). Phosphoglycerate dehydrogenase diverts glycolytic flux and contributes to oncogenesis. Nat Genet *43*, 869-874.
Lock, F.E., McDonald, P.C., Lou, Y., Serrano, I., Chafe, S.C., Ostlund, C., Aparicio, S., Winum, J.Y., Supuran, C.T., and Dedhar, S. (2012). Targeting carbonic anhydrase IX depletes breast cancer stem cells within the hypoxic niche. Oncogene.
Locke, G.A., Cheng, D., Witmer, M.R., Tamura, J.K., Haque, T., Carney, R.F., Rendina, A.R., and Marcinkeviciene, J. (2008). Differential activation of recombinant human acetyl-CoA carboxylases 1 and 2 by citrate. Arch Biochem Biophys *475*, 72-79.
Loftus, T.M., Jaworsky, D.E., Frehywot, G.L., Townsend, C.A., Ronnett, G.V., Lane, M.D., and Kuhajda, F.P. (2000). Reduced food intake and body weight in mice treated with fatty acid synthase inhibitors. Science *288*, 2379-2381.
Long, J.S., Yokoyama, K., Tigyi, G., Pyne, N.J., and Pyne, S. (2006). Lipid phosphate phosphatase-1 regulates lysophosphatidic acid- and platelet-derived-growth-factor-induced cell migration. Biochem J *394*, 495-500.
Lunt, S.Y., and Vander Heiden, M.G. (2011). Aerobic glycolysis: meeting the metabolic requirements of cell proliferation. Annu Rev Cell Dev Biol *27*, 441-464.
Lupu, R., and Menendez, J.A. (2006). Targeting fatty acid synthase in breast and endometrial cancer: An alternative to selective estrogen receptor modulators? Endocrinology *147*, 4056-4066.
MacDonald, M.J. (1995). Feasibility of a mitochondrial pyruvate malate shuttle in pancreatic islets. Further implication of cytosolic NADPH in insulin secretion. J Biol Chem *270*, 20051-20058.
Macheda, M.L., Rogers, S., and Best, J.D. (2005). Molecular and cellular regulation of glucose transporter (GLUT) proteins in cancer. J Cell Physiol *202*, 654-662.
Maddams, J., Utley, M., and Moller, H. (2012). Projections of cancer prevalence in the United Kingdom, 2010-2040. Br J Cancer.
Mahon, P.C., Hirota, K., and Semenza, G.L. (2001). FIH-1: a novel protein that interacts with HIF-1alpha and VHL to mediate repression of HIF-1 transcriptional activity. Genes Dev *15*, 2675-2686.
Majewski, N., Nogueira, V., Robey, R.B., and Hay, N. (2004). Akt inhibits apoptosis downstream of BID cleavage via a glucose-dependent mechanism involving mitochondrial hexokinases. Mol Cell Biol *24*, 730-740.
Majmundar, A.J., Wong, W.J., and Simon, M.C. (2010). Hypoxia-inducible factors and the response to hypoxic stress. Mol Cell *40*, 294-309.
Majumder, P.K., Febbo, P.G., Bikoff, R., Berger, R., Xue, Q., McMahon, L.M., Manola, J., Brugarolas, J., McDonnell, T.J., Golub, T.R.*, et al.* (2004). mTOR inhibition reverses Akt-dependent prostate intraepithelial neoplasia through regulation of apoptotic and HIF-1-dependent pathways. Nat Med *10*, 594-601.
Malo, N., Hanley, J.A., Cerquozzi, S., Pelletier, J., and Nadon, R. (2006). Statistical practice in high-throughput screening data analysis. Nat Biotechnol *24*, 167-175.
Malone, K.E., Daling, J.R., Doody, D.R., Hsu, L., Bernstein, L., Coates, R.J., Marchbanks, P.A., Simon, M.S., McDonald, J.A., Norman, S.A.*, et al.* (2006). Prevalence and predictors of BRCA1 and BRCA2 mutations in a population-based

study of breast cancer in white and black American women ages 35 to 64 years. Cancer Res *66*, 8297-8308.
Maltzman, W., and Czyzyk, L. (1984). UV irradiation stimulates levels of p53 cellular tumor antigen in nontransformed mouse cells. Molecular and cellular biology *4*, 1689-1694.
Marchio, C., Natrajan, R., Shiu, K.K., Lambros, M.B., Rodriguez-Pinilla, S.M., Tan, D.S., Lord, C.J., Hungermann, D., Fenwick, K., Tamber, N.*, et al.* (2008). The genomic profile of HER2-amplified breast cancers: the influence of ER status. J Pathol *216*, 399-407.
Marcotte, R., Brown, K.R., Suarez, F., Sayad, A., Karamboulas, K., Krzyzanowski, P.M., Sircoulomb, F., Medrano, M., Fedyshyn, Y., Koh, J.L.*, et al.* (2012). Essential gene profiles in breast, pancreatic, and ovarian cancer cells. Cancer Discov *2*, 172-189.
Marcucci, G., Maharry, K., Wu, Y.Z., Radmacher, M.D., Mrozek, K., Margeson, D., Holland, K.B., Whitman, S.P., Becker, H., Schwind, S.*, et al.* (2010). IDH1 and IDH2 gene mutations identify novel molecular subsets within de novo cytogenetically normal acute myeloid leukemia: a Cancer and Leukemia Group B study. J Clin Oncol *28*, 2348-2355.
Marin-Hernandez, A., Gallardo-Perez, J.C., Ralph, S.J., Rodriguez-Enriquez, S., and Moreno-Sanchez, R. (2009). HIF-1alpha modulates energy metabolism in cancer cells by inducing over-expression of specific glycolytic isoforms. Mini Rev Med Chem *9*, 1084-1101.
Marin-Valencia, I., Yang, C., Mashimo, T., Cho, S., Baek, H., Yang, X.L., Rajagopalan, K.N., Maddie, M., Vemireddy, V., Zhao, Z.*, et al.* (2012). Analysis of tumor metabolism reveals mitochondrial glucose oxidation in genetically diverse human glioblastomas in the mouse brain in vivo. Cell Metab *15*, 827-837.
Marionnet, C., Lalou, C., Mollier, K., Chazal, M., Delestaing, G., Compan, D., Verola, O., Vilmer, C., Cuminet, J., Dubertret, L.*, et al.* (2003). Differential molecular profiling between skin carcinomas reveals four newly reported genes potentially implicated in squamous cell carcinoma development. Oncogene *22*, 3500-3505.
Marusyk, A., Almendro, V., and Polyak, K. (2012). Intra-tumour heterogeneity: a looking glass for cancer? Nat Rev Cancer *12*, 323-334.
Maschek, G., Savaraj, N., Priebe, W., Braunschweiger, P., Hamilton, K., Tidmarsh, G.F., De Young, L.R., and Lampidis, T.J. (2004). 2-deoxy-D-glucose increases the efficacy of adriamycin and paclitaxel in human osteosarcoma and non-small cell lung cancers in vivo. Cancer Res *64*, 31-34.
Matoba, S., Kang, J.G., Patino, W.D., Wragg, A., Boehm, M., Gavrilova, O., Hurley, P.J., Bunz, F., and Hwang, P.M. (2006). p53 regulates mitochondrial respiration. Science *312*, 1650-1653.
Mayer, A., Von Wallbrunn, A., and Vaupel, P. (2010). Glucose metabolism of malignant cells is not regulated by transketolase-like (TKTL)-1. Int J Oncol *37*, 265-271.
Mazurek, S., Grimm, H., Boschek, C.B., Vaupel, P., and Eigenbrodt, E. (2002). Pyruvate kinase type M2: a crossroad in the tumor metabolome. Br J Nutr *87 Suppl 1*, S23-29.
McCleland, M.L., Adler, A.S., Shang, Y., Hunsaker, T., Truong, T., Peterson, D., Torres, E., Li, L., Haley, B., Stephan, J.P.*, et al.* (2012). An Integrated Genomic Screen Identifies LDHB as an Essential Gene for Triple-Negative Breast Cancer. Cancer Res *72*, 5812-5823.

Medes, G., Thomas, A., and Weinhouse, S. (1953). Metabolism of neoplastic tissue. IV. A study of lipid synthesis in neoplastic tissue slices in vitro. Cancer Res *13*, 27-29.
Mendoza, E.E., Pocceschi, M.G., Kong, X., Leeper, D.B., Caro, J., Limesand, K.H., and Burd, R. (2012). Control of Glycolytic Flux by AMP-Activated Protein Kinase in Tumor Cells Adapted to Low pH. Transl Oncol *5*, 208-216.
Menendez, J.A., and Lupu, R. (2007). Fatty acid synthase and the lipogenic phenotype in cancer pathogenesis. Nat Rev Cancer *7*, 763-777.
Metallo, C.M., Gameiro, P.A., Bell, E.L., Mattaini, K.R., Yang, J., Hiller, K., Jewell, C.M., Johnson, Z.R., Irvine, D.J., Guarente, L.*, et al.* (2012). Reductive glutamine metabolism by IDH1 mediates lipogenesis under hypoxia. Nature *481*, 380-384.
Michael, D., and Oren, M. (2003). The p53-Mdm2 module and the ubiquitin system. Seminars in cancer biology *13*, 49-58.
Michelakis, E.D., Webster, L., and Mackey, J.R. (2008). Dichloroacetate (DCA) as a potential metabolic-targeting therapy for cancer. Br J Cancer *99*, 989-994.
Migita, T., Ruiz, S., Fornari, A., Fiorentino, M., Priolo, C., Zadra, G., Inazuka, F., Grisanzio, C., Palescandolo, E., Shin, E.*, et al.* (2009). Fatty acid synthase: a metabolic enzyme and candidate oncogene in prostate cancer. J Natl Cancer Inst *101*, 519-532.
Mihaylova, M.M., and Shaw, R.J. (2011). The AMPK signalling pathway coordinates cell growth, autophagy and metabolism. Nat Cell Biol *13*, 1016-1023.
Mimura, I., Nangaku, M., Kanki, Y., Tsutsumi, S., Inoue, T., Kohro, T., Yamamoto, S., Fujita, T., Shimamura, T., Suehiro, J.*, et al.* (2012). Dynamic change of chromatin conformation in response to hypoxia enhances the expression of GLUT3 (SLC2A3) by cooperative interaction of hypoxia-inducible factor 1 and KDM3A. Mol Cell Biol *32*, 3018-3032.
Minchenko, A., Leshchinsky, I., Opentanova, I., Sang, N., Srinivas, V., Armstead, V., and Caro, J. (2002). Hypoxia-inducible factor-1-mediated expression of the 6-phosphofructo-2-kinase/fructose-2,6-bisphosphatase-3 (PFKFB3) gene. Its possible role in the Warburg effect. J Biol Chem *277*, 6183-6187.
Moasser, M.M. (2007). The oncogene HER2: its signaling and transforming functions and its role in human cancer pathogenesis. Oncogene *26*, 6469-6487.
Montgomery, N., Hill, A., McFarlane, S., Neisen, J., O'Grady, A., Conlon, S., Jirstrom, K., Kay, E.W., and Waugh, D.J. (2012). CD44 enhances invasion of basal-like breast cancer cells by upregulating serine protease and collagen-degrading enzymatic expression and activity. Breast Cancer Res *14*, R84.
Moreno-Sanchez, R., Rodriguez-Enriquez, S., Marin-Hernandez, A., and Saavedra, E. (2007). Energy metabolism in tumor cells. FEBS J *274*, 1393-1418.
Morgenstern, J.P., and Land, H. (1990). Advanced mammalian gene transfer: high titre retroviral vectors with multiple drug selection markers and a complementary helper-free packaging cell line. Nucleic Acids Res *18*, 3587-3596.
Moscatello, D.K., Holgado-Madruga, M., Godwin, A.K., Ramirez, G., Gunn, G., Zoltick, P.W., Biegel, J.A., Hayes, R.L., and Wong, A.J. (1995). Frequent expression of a mutant epidermal growth factor receptor in multiple human tumors. Cancer Res *55*, 5536-5539.
Mullen, A.R., Wheaton, W.W., Jin, E.S., Chen, P.H., Sullivan, L.B., Cheng, T., Yang, Y., Linehan, W.M., Chandel, N.S., and DeBerardinis, R.J. (2012). Reductive carboxylation supports growth in tumour cells with defective mitochondria. Nature *481*, 385-388.

Muller, F.L., Colla, S., Aquilanti, E., Manzo, V.E., Genovese, G., Lee, J., Eisenson, D., Narurkar, R., Deng, P., Nezi, L.*, et al.* (2012). Passenger deletions generate therapeutic vulnerabilities in cancer. Nature *488*, 337-342.
Murray, C.M., Hutchinson, R., Bantick, J.R., Belfield, G.P., Benjamin, A.D., Brazma, D., Bundick, R.V., Cook, I.D., Craggs, R.I., Edwards, S.*, et al.* (2005). Monocarboxylate transporter MCT1 is a target for immunosuppression. Nat Chem Biol *1*, 371-376.
Mycielska, M.E., Patel, A., Rizaner, N., Mazurek, M.P., Keun, H., Ganapathy, V., and Djamgoz, M.B. (2009). Citrate transport and metabolism in mammalian cells: prostate epithelial cells and prostate cancer. Bioessays *31*, 10-20.
Nakae, J., Kitamura, T., Silver, D.L., and Accili, D. (2001). The forkhead transcription factor Foxo1 (Fkhr) confers insulin sensitivity onto glucose-6-phosphatase expression. J Clin Invest *108*, 1359-1367.
Neve, R.M., Chin, K., Fridlyand, J., Yeh, J., Baehner, F.L., Fevr, T., Clark, L., Bayani, N., Coppe, J.P., Tong, F.*, et al.* (2006). A collection of breast cancer cell lines for the study of functionally distinct cancer subtypes. Cancer Cell *10*, 515-527.
Nicklin, P., Bergman, P., Zhang, B., Triantafellow, E., Wang, H., Nyfeler, B., Yang, H., Hild, M., Kung, C., Wilson, C.*, et al.* (2009). Bidirectional transport of amino acids regulates mTOR and autophagy. Cell *136*, 521-534.
Nik-Zainal, S., Alexandrov, L.B., Wedge, D.C., Van Loo, P., Greenman, C.D., Raine, K., Jones, D., Hinton, J., Marshall, J., Stebbings, L.A.*, et al.* (2012a). Mutational processes molding the genomes of 21 breast cancers. Cell *149*, 979-993.
Nik-Zainal, S., Van Loo, P., Wedge, D.C., Alexandrov, L.B., Greenman, C.D., Lau, K.W., Raine, K., Jones, D., Marshall, J., Ramakrishna, M.*, et al.* (2012b). The life history of 21 breast cancers. Cell *149*, 994-1007.
Ntambi, J.M., and Miyazaki, M. (2004). Regulation of stearoyl-CoA desaturases and role in metabolism. Prog Lipid Res *43*, 91-104.
Olayioye, M.A., Neve, R.M., Lane, H.A., and Hynes, N.E. (2000). The ErbB signaling network: receptor heterodimerization in development and cancer. EMBO J *19*, 3159-3167.
Oliver, S.G. (2002). Functional genomics: lessons from yeast. Philos Trans R Soc Lond B Biol Sci *357*, 17-23.
Opdam, F.L., Guchelaar, H.J., Beijnen, J.H., and Schellens, J.H. (2012). Lapatinib for advanced or metastatic breast cancer. Oncologist *17*, 536-542.
Osborne, C.K., and McGuire, W.L. (1979). Therapy for cancer of the breast. Current status of steroid hormone receptors. West J Med *130*, 401-407.
Owens, M.A., Horten, B.C., and Da Silva, M.M. (2004). HER2 amplification ratios by fluorescence in situ hybridization and correlation with immunohistochemistry in a cohort of 6556 breast cancer tissues. Clin Breast Cancer *5*, 63-69.
Papaldo, P., Lopez, M., Cortesi, E., Cammilluzzi, E., Antimi, M., Terzoli, E., Lepidini, G., Vici, P., Barone, C., Ferretti, G.*, et al.* (2003). Addition of either lonidamine or granulocyte colony-stimulating factor does not improve survival in early breast cancer patients treated with high-dose epirubicin and cyclophosphamide. J Clin Oncol *21*, 3462-3468.
Papandreou, I., Cairns, R.A., Fontana, L., Lim, A.L., and Denko, N.C. (2006). HIF-1 mediates adaptation to hypoxia by actively downregulating mitochondrial oxygen consumption. Cell Metab *3*, 187-197.

Papandreou, I., Krishna, C., Kaper, F., Cai, D., Giaccia, A.J., and Denko, N.C. (2005). Anoxia is necessary for tumor cell toxicity caused by a low-oxygen environment. Cancer Res *65*, 3171-3178.
Papelard, H., de Bock, G.H., van Eijk, R., Vliet Vlieland, T.P., Cornelisse, C.J., Devilee, P., and Tollenaar, R.A. (2000). Prevalence of BRCA1 in a hospital-based population of Dutch breast cancer patients. Br J Cancer *83*, 719-724.
Parker, J.S., Mullins, M., Cheang, M.C., Leung, S., Voduc, D., Vickery, T., Davies, S., Fauron, C., He, X., Hu, Z*., et al.* (2009). Supervised risk predictor of breast cancer based on intrinsic subtypes. J Clin Oncol *27*, 1160-1167.
Parks, S.K., Chiche, J., and Pouyssegur, J. (2011). pH control mechanisms of tumor survival and growth. J Cell Physiol *226*, 299-308.
Parsons, D.W., Jones, S., Zhang, X., Lin, J.C., Leary, R.J., Angenendt, P., Mankoo, P., Carter, H., Siu, I.M., Gallia, G.L*., et al.* (2008). An integrated genomic analysis of human glioblastoma multiforme. Science *321*, 1807-1812.
Pear, W.S., Nolan, G.P., Scott, M.L., and Baltimore, D. (1993). Production of high-titer helper-free retroviruses by transient transfection. Proceedings of the National Academy of Sciences of the United States of America *90*, 8392-8396.
Pedersen, P.L. (2012). 3-Bromopyruvate (3BP) a fast acting, promising, powerful, specific, and effective "small molecule" anti-cancer agent taken from labside to bedside: introduction to a special issue. J Bioenerg Biomembr *44*, 1-6.
Pelicano, H., Xu, R.H., Du, M., Feng, L., Sasaki, R., Carew, J.S., Hu, Y., Ramdas, L., Hu, L., Keating, M.J*., et al.* (2006). Mitochondrial respiration defects in cancer cells cause activation of Akt survival pathway through a redox-mediated mechanism. J Cell Biol *175*, 913-923.
Penhoet, E.E., Kochman, M., and Rutter, W.J. (1969). Molecular and catalytic properties of aldolase C. Biochemistry *8*, 4396-4402.
Perez, E.A., Suman, V.J., Davidson, N.E., Sledge, G.W., Kaufman, P.A., Hudis, C.A., Martino, S., Gralow, J.R., Dakhil, S.R., Ingle, J.N*., et al.* (2008). Cardiac safety analysis of doxorubicin and cyclophosphamide followed by paclitaxel with or without trastuzumab in the North Central Cancer Treatment Group N9831 adjuvant breast cancer trial. J Clin Oncol *26*, 1231-1238.
Perez-Tenorio, G., Alkhori, L., Olsson, B., Waltersson, M.A., Nordenskjold, B., Rutqvist, L.E., Skoog, L., and Stal, O. (2007). PIK3CA mutations and PTEN loss correlate with similar prognostic factors and are not mutually exclusive in breast cancer. Clin Cancer Res *13*, 3577-3584.
Perou, C.M. (2011). Molecular stratification of triple-negative breast cancers. Oncologist *16 Suppl 1*, 61-70.
Perou, C.M., Sorlie, T., Eisen, M.B., van de Rijn, M., Jeffrey, S.S., Rees, C.A., Pollack, J.R., Ross, D.T., Johnsen, H., Akslen, L.A*., et al.* (2000). Molecular portraits of human breast tumours. Nature *406*, 747-752.
Petros, J.A., Baumann, A.K., Ruiz-Pesini, E., Amin, M.B., Sun, C.Q., Hall, J., Lim, S., Issa, M.M., Flanders, W.D., Hosseini, S.H*., et al.* (2005). mtDNA mutations increase tumorigenicity in prostate cancer. Proc Natl Acad Sci U S A *102*, 719-724.
Phang, J.M., Liu, W., Hancock, C., and Christian, K.J. (2012). The proline regulatory axis and cancer. Front Oncol *2*, 60.
Pinheiro, C., Albergaria, A., Paredes, J., Sousa, B., Dufloth, R., Vieira, D., Schmitt, F., and Baltazar, F. (2010a). Monocarboxylate transporter 1 is up-regulated in basal-like breast carcinoma. Histopathology *56*, 860-867.

Pinheiro, C., Longatto-Filho, A., Azevedo-Silva, J., Casal, M., Schmitt, F.C., and Baltazar, F. (2012). Role of monocarboxylate transporters in human cancers: state of the art. J Bioenerg Biomembr *44*, 127-139.
Pinheiro, C., Longatto-Filho, A., Ferreira, L., Pereira, S.M., Etlinger, D., Moreira, M.A., Jube, L.F., Queiroz, G.S., Schmitt, F., and Baltazar, F. (2008a). Increasing expression of monocarboxylate transporters 1 and 4 along progression to invasive cervical carcinoma. Int J Gynecol Pathol *27*, 568-574.
Pinheiro, C., Longatto-Filho, A., Scapulatempo, C., Ferreira, L., Martins, S., Pellerin, L., Rodrigues, M., Alves, V.A., Schmitt, F., and Baltazar, F. (2008b). Increased expression of monocarboxylate transporters 1, 2, and 4 in colorectal carcinomas. Virchows Arch *452*, 139-146.
Pinheiro, C., Reis, R.M., Ricardo, S., Longatto-Filho, A., Schmitt, F., and Baltazar, F. (2010b). Expression of monocarboxylate transporters 1, 2, and 4 in human tumours and their association with CD147 and CD44. J Biomed Biotechnol *2010*, 427694.
Pollard, P.J., Briere, J.J., Alam, N.A., Barwell, J., Barclay, E., Wortham, N.C., Hunt, T., Mitchell, M., Olpin, S., Moat, S.J.*, et al.* (2005). Accumulation of Krebs cycle intermediates and over-expression of HIF1alpha in tumours which result from germline FH and SDH mutations. Hum Mol Genet *14*, 2231-2239.
Ponchel, F., Toomes, C., Bransfield, K., Leong, F.T., Douglas, S.H., Field, S.L., Bell, S.M., Combaret, V., Puisieux, A., Mighell, A.J.*, et al.* (2003). Real-time PCR based on SYBR-Green I fluorescence: an alternative to the TaqMan assay for a relative quantification of gene rearrangements, gene amplifications and micro gene deletions. BMC biotechnology *3*, 18.
Porporato, P.E., Dhup, S., Dadhich, R.K., Copetti, T., and Sonveaux, P. (2011). Anticancer targets in the glycolytic metabolism of tumors: a comprehensive review. Front Pharmacol *2*, 49.
Porstmann, T., Griffiths, B., Chung, Y.L., Delpuech, O., Griffiths, J.R., Downward, J., and Schulze, A. (2005). PKB/Akt induces transcription of enzymes involved in cholesterol and fatty acid biosynthesis via activation of SREBP. Oncogene *24*, 6465-6481.
Porstmann, T., Santos, C.R., Griffiths, B., Cully, M., Wu, M., Leevers, S., Griffiths, J.R., Chung, Y.L., and Schulze, A. (2008). SREBP activity is regulated by mTORC1 and contributes to Akt-dependent cell growth. Cell Metab *8*, 224-236.
Possemato, R., Marks, K.M., Shaul, Y.D., Pacold, M.E., Kim, D., Birsoy, K., Sethumadhavan, S., Woo, H.K., Jang, H.G., Jha, A.K.*, et al.* (2011). Functional genomics reveal that the serine synthesis pathway is essential in breast cancer. Nature *476*, 346-350.
Prat, A., Parker, J.S., Karginova, O., Fan, C., Livasy, C., Herschkowitz, J.I., He, X., and Perou, C.M. (2010). Phenotypic and molecular characterization of the claudin-low intrinsic subtype of breast cancer. Breast Cancer Res *12*, R68.
Pylayeva-Gupta, Y., Grabocka, E., and Bar-Sagi, D. (2011). RAS oncogenes: weaving a tumorigenic web. Nat Rev Cancer *11*, 761-774.
Pyne, S., Kong, K.C., and Darroch, P.I. (2004). Lysophosphatidic acid and sphingosine 1-phosphate biology: the role of lipid phosphate phosphatases. Semin Cell Dev Biol *15*, 491-501.
Qing, G., and Simon, M.C. (2009). Hypoxia inducible factor-2alpha: a critical mediator of aggressive tumor phenotypes. Curr Opin Genet Dev *19*, 60-66.

Rademakers, S.E., Lok, J., van der Kogel, A.J., Bussink, J., and Kaanders, J.H. (2011). Metabolic markers in relation to hypoxia; staining patterns and colocalization of pimonidazole, HIF-1alpha, CAIX, LDH-5, GLUT-1, MCT1 and MCT4. BMC Cancer *11*, 167.
Rafn, B., Nielsen, C.F., Andersen, S.H., Szyniarowski, P., Corcelle-Termeau, E., Valo, E., Fehrenbacher, N., Olsen, C.J., Daugaard, M., Egebjerg, C.*, et al.* (2012). ErbB2-driven breast cancer cell invasion depends on a complex signaling network activating myeloid zinc finger-1-dependent cathepsin B expression. Mol Cell *45*, 764-776.
Ramanathan, A., Wang, C., and Schreiber, S.L. (2005). Perturbational profiling of a cell-line model of tumorigenesis by using metabolic measurements. Proc Natl Acad Sci U S A *102*, 5992-5997.
Rapisarda, A., and Melillo, G. (2012). Overcoming disappointing results with antiangiogenic therapy by targeting hypoxia. Nat Rev Clin Oncol *9*, 378-390.
Razandi, M., Pedram, A., Park, S.T., and Levin, E.R. (2003). Proximal events in signaling by plasma membrane estrogen receptors. J Biol Chem *278*, 2701-2712.
Reis-Filho, J.S., and Pusztai, L. (2011). Gene expression profiling in breast cancer: classification, prognostication, and prediction. Lancet *378*, 1812-1823.
Rhodes, D.R., Yu, J., Shanker, K., Deshpande, N., Varambally, R., Ghosh, D., Barrette, T., Pandey, A., and Chinnaiyan, A.M. (2004). ONCOMINE: a cancer microarray database and integrated data-mining platform. Neoplasia *6*, 1-6.
Richardson, A.D., Yang, C., Osterman, A., and Smith, J.W. (2008). Central carbon metabolism in the progression of mammary carcinoma. Breast Cancer Res Treat *110*, 297-307.
Riethdorf, S., Reimers, N., Assmann, V., Kornfeld, J.W., Terracciano, L., Sauter, G., and Pantel, K. (2006). High incidence of EMMPRIN expression in human tumors. Int J Cancer *119*, 1800-1810.
Riley, T., Sontag, E., Chen, P., and Levine, A. (2008). Transcriptional control of human p53-regulated genes. Nat Rev Mol Cell Biol *9*, 402-412.
Ringner, M., Fredlund, E., Hakkinen, J., Borg, A., and Staaf, J. (2011). GOBO: gene expression-based outcome for breast cancer online. PLoS One *6*, e17911.
Roberts, R.Z., and Morris, A.J. (2000). Role of phosphatidic acid phosphatase 2a in uptake of extracellular lipid phosphate mediators. Biochim Biophys Acta *1487*, 33-49.
Robey, I.F., Baggett, B.K., Kirkpatrick, N.D., Roe, D.J., Dosescu, J., Sloane, B.F., Hashim, A.I., Morse, D.L., Raghunand, N., Gatenby, R.A.*, et al.* (2009). Bicarbonate increases tumor pH and inhibits spontaneous metastases. Cancer Res *69*, 2260-2268.
Robey, R.B., and Hay, N. (2006). Mitochondrial hexokinases, novel mediators of the antiapoptotic effects of growth factors and Akt. Oncogene *25*, 4683-4696.
Robey, R.B., and Hay, N. (2009). Is Akt the "Warburg kinase"?-Akt-energy metabolism interactions and oncogenesis. Semin Cancer Biol *19*, 25-31.
Rolo, A.P., Palmeira, C.M., and Cortopassi, G.A. (2009). Biosensor plates detect mitochondrial physiological regulators and mutations in vivo. Anal Biochem *385*, 176-178.
Romond, E.H., Perez, E.A., Bryant, J., Suman, V.J., Geyer, C.E., Jr., Davidson, N.E., Tan-Chiu, E., Martino, S., Paik, S., Kaufman, P.A.*, et al.* (2005). Trastuzumab plus adjuvant chemotherapy for operable HER2-positive breast cancer. N Engl J Med *353*, 1673-1684.
Ros, S., Santos, C.R., Moco, S., Baenke, F., Kelly, G., Howell, M., Zamboni, N., and Schulze, A. (2012). Functional metabolic screen identifies 6-phosphofructo-2-

kinase/fructose-2,6-biphosphatase 4 as an important regulator of prostate cancer cell survival. Cancer Discov *2*, 328-343.
Rozhin, J., Sameni, M., Ziegler, G., and Sloane, B.F. (1994). Pericellular pH affects distribution and secretion of cathepsin B in malignant cells. Cancer Res *54*, 6517-6525.
Saal, L.H., Holm, K., Maurer, M., Memeo, L., Su, T., Wang, X., Yu, J.S., Malmstrom, P.O., Mansukhani, M., Enoksson, J.*, et al.* (2005). PIK3CA mutations correlate with hormone receptors, node metastasis, and ERBB2, and are mutually exclusive with PTEN loss in human breast carcinoma. Cancer Res *65*, 2554-2559.
Salmena, L., Carracedo, A., and Pandolfi, P.P. (2008). Tenets of PTEN tumor suppression. Cell *133*, 403-414.
Samuels, Y., Wang, Z., Bardelli, A., Silliman, N., Ptak, J., Szabo, S., Yan, H., Gazdar, A., Powell, S.M., Riggins, G.J.*, et al.* (2004). High frequency of mutations of the PIK3CA gene in human cancers. Science *304*, 554.
Sansal, I., and Sellers, W.R. (2004). The biology and clinical relevance of the PTEN tumor suppressor pathway. J Clin Oncol *22*, 2954-2963.
Sauter, G., Maeda, T., Waldman, F.M., Davis, R.L., and Feuerstein, B.G. (1996). Patterns of epidermal growth factor receptor amplification in malignant gliomas. Am J Pathol *148*, 1047-1053.
Schafer, Z.T., Grassian, A.R., Song, L., Jiang, Z., Gerhart-Hines, Z., Irie, H.Y., Gao, S., Puigserver, P., and Brugge, J.S. (2009). Antioxidant and oncogene rescue of metabolic defects caused by loss of matrix attachment. Nature *461*, 109-113.
Schenk, G., Duggleby, R.G., and Nixon, P.F. (1998). Properties and functions of the thiamin diphosphate dependent enzyme transketolase. Int J Biochem Cell Biol *30*, 1297-1318.
Scheuner, M.T., McNeel, T.S., and Freedman, A.N. (2010). Population prevalence of familial cancer and common hereditary cancer syndromes. The 2005 California Health Interview Survey. Genet Med *12*, 726-735.
Schneiderhan, W., Scheler, M., Holzmann, K.H., Marx, M., Gschwend, J.E., Bucholz, M., Gress, T.M., Seufferlein, T., Adler, G., and Oswald, F. (2009). CD147 silencing inhibits lactate transport and reduces malignant potential of pancreatic cancer cells in in vivo and in vitro models. Gut *58*, 1391-1398.
Schwartzenberg-Bar-Yoseph, F., Armoni, M., and Karnieli, E. (2004). The tumor suppressor p53 down-regulates glucose transporters GLUT1 and GLUT4 gene expression. Cancer Res *64*, 2627-2633.
Sciorra, V.A., and Morris, A.J. (2002). Roles for lipid phosphate phosphatases in regulation of cellular signaling. Biochim Biophys Acta *1582*, 45-51.
Selak, M.A., Armour, S.M., MacKenzie, E.D., Boulahbel, H., Watson, D.G., Mansfield, K.D., Pan, Y., Simon, M.C., Thompson, C.B., and Gottlieb, E. (2005). Succinate links TCA cycle dysfunction to oncogenesis by inhibiting HIF-alpha prolyl hydroxylase. Cancer Cell *7*, 77-85.
Semenza, G. (2002). Signal transduction to hypoxia-inducible factor 1. Biochem Pharmacol *64*, 993-998.
Semenza, G.L. (2010a). Defining the role of hypoxia-inducible factor 1 in cancer biology and therapeutics. Oncogene *29*, 625-634.
Semenza, G.L. (2010b). Oxygen homeostasis. Wiley Interdiscip Rev Syst Biol Med *2*, 336-361.
Sena, L.A., and Chandel, N.S. (2012). Physiological roles of mitochondrial reactive oxygen species. Mol Cell *48*, 158-167.

Shackelford, D.B., Vasquez, D.S., Corbeil, J., Wu, S., Leblanc, M., Wu, C.L., Vera, D.R., and Shaw, R.J. (2009). mTOR and HIF-1alpha-mediated tumor metabolism in an LKB1 mouse model of Peutz-Jeghers syndrome. Proc Natl Acad Sci U S A *106*, 11137-11142.
Shah, S.P., Roth, A., Goya, R., Oloumi, A., Ha, G., Zhao, Y., Turashvili, G., Ding, J., Tse, K., Haffari, G.*, et al.* (2012). The clonal and mutational evolution spectrum of primary triple-negative breast cancers. Nature *486*, 395-399.
Shimoda, L.A., Fallon, M., Pisarcik, S., Wang, J., and Semenza, G.L. (2006). HIF-1 regulates hypoxic induction of NHE1 expression and alkalinization of intracellular pH in pulmonary arterial myocytes. Am J Physiol Lung Cell Mol Physiol *291*, L941-949.
Slamon, D.J., Clark, G.M., Wong, S.G., Levin, W.J., Ullrich, A., and McGuire, W.L. (1987). Human breast cancer: correlation of relapse and survival with amplification of the HER-2/neu oncogene. Science *235*, 177-182.
Slamon, D.J., Godolphin, W., Jones, L.A., Holt, J.A., Wong, S.G., Keith, D.E., Levin, W.J., Stuart, S.G., Udove, J., Ullrich, A.*, et al.* (1989). Studies of the HER-2/neu proto-oncogene in human breast and ovarian cancer. Science *244*, 707-712.
Slattery, M.L., and Kerber, R.A. (1993). A comprehensive evaluation of family history and breast cancer risk. The Utah Population Database. JAMA *270*, 1563-1568.
Sledzinski, Z., Wozniak, M., Antosiewicz, J., Lezoche, E., Familiari, M., Bertoli, E., Greci, L., Brunelli, A., Mazera, N., and Wajda, Z. (1995). Protective effect of 4-hydroxy-TEMPO, a low molecular weight superoxide dismutase mimic, on free radical toxicity in experimental pancreatitis. Int J Pancreatol *18*, 153-160.
Soh, H., Wasa, M., and Fukuzawa, M. (2007). Hypoxia upregulates amino acid transport in a human neuroblastoma cell line. J Pediatr Surg *42*, 608-612.
Song, S., Kim, S.Y., Hong, Y.M., Jo, D.G., Lee, J.Y., Shim, S.M., Chung, C.W., Seo, S.J., Yoo, Y.J., Koh, J.Y.*, et al.* (2003). Essential role of E2-25K/Hip-2 in mediating amyloid-beta neurotoxicity. Mol Cell *12*, 553-563.
Sonveaux, P., Vegran, F., Schroeder, T., Wergin, M.C., Verrax, J., Rabbani, Z.N., De Saedeleer, C.J., Kennedy, K.M., Diepart, C., Jordan, B.F.*, et al.* (2008). Targeting lactate-fueled respiration selectively kills hypoxic tumor cells in mice. J Clin Invest *118*, 3930-3942.
Sorlie, T., Perou, C.M., Tibshirani, R., Aas, T., Geisler, S., Johnsen, H., Hastie, T., Eisen, M.B., van de Rijn, M., Jeffrey, S.S.*, et al.* (2001). Gene expression patterns of breast carcinomas distinguish tumor subclasses with clinical implications. Proc Natl Acad Sci U S A *98*, 10869-10874.
Sorlie, T., Tibshirani, R., Parker, J., Hastie, T., Marron, J.S., Nobel, A., Deng, S., Johnsen, H., Pesich, R., Geisler, S.*, et al.* (2003). Repeated observation of breast tumor subtypes in independent gene expression data sets. Proc Natl Acad Sci U S A *100*, 8418-8423.
Soussi, T., and Lozano, G. (2005). p53 mutation heterogeneity in cancer. Biochem Biophys Res Commun *331*, 834-842.
Spankuch-Schmitt, B., Bereiter-Hahn, J., Kaufmann, M., and Strebhardt, K. (2002). Effect of RNA silencing of polo-like kinase-1 (PLK1) on apoptosis and spindle formation in human cancer cells. J Natl Cancer Inst *94*, 1863-1877.
Sreekumar, A., Poisson, L.M., Rajendiran, T.M., Khan, A.P., Cao, Q., Yu, J., Laxman, B., Mehra, R., Lonigro, R.J., Li, Y.*, et al.* (2009). Metabolomic profiles delineate potential role for sarcosine in prostate cancer progression. Nature *457*, 910-914.

Stacpoole, P.W., Nagaraja, N.V., and Hutson, A.D. (2003). Efficacy of dichloroacetate as a lactate-lowering drug. J Clin Pharmacol *43*, 683-691.
Stein, W.H., and Moore, S. (1954). The free amino acids of human blood plasma. J Biol Chem *211*, 915-926.
Stemke-Hale, K., Gonzalez-Angulo, A.M., Lluch, A., Neve, R.M., Kuo, W.L., Davies, M., Carey, M., Hu, Z., Guan, Y., Sahin, A.*, et al.* (2008). An integrative genomic and proteomic analysis of PIK3CA, PTEN, and AKT mutations in breast cancer. Cancer Res *68*, 6084-6091.
Stephens, P.J., Tarpey, P.S., Davies, H., Van Loo, P., Greenman, C., Wedge, D.C., Nik-Zainal, S., Martin, S., Varela, I., Bignell, G.R.*, et al.* (2012). The landscape of cancer genes and mutational processes in breast cancer. Nature *486*, 400-404.
Straussman, R., Morikawa, T., Shee, K., Barzily-Rokni, M., Qian, Z.R., Du, J., Davis, A., Mongare, M.M., Gould, J., Frederick, D.T.*, et al.* (2012). Tumour micro-environment elicits innate resistance to RAF inhibitors through HGF secretion. Nature *487*, 500-504.
Sun, W., Liu, Y., Glazer, C.A., Shao, C., Bhan, S., Demokan, S., Zhao, M., Rudek, M.A., Ha, P.K., and Califano, J.A. (2010). TKTL1 is activated by promoter hypomethylation and contributes to head and neck squamous cell carcinoma carcinogenesis through increased aerobic glycolysis and HIF1alpha stabilization. Clin Cancer Res *16*, 857-866.
Sunpaweravong, P., Sunpaweravong, S., Puttawibul, P., Mitarnun, W., Zeng, C., Baron, A.E., Franklin, W., Said, S., and Varella-Garcia, M. (2005). Epidermal growth factor receptor and cyclin D1 are independently amplified and overexpressed in esophageal squamous cell carcinoma. J Cancer Res Clin Oncol *131*, 111-119.
Swietach, P., Hulikova, A., Vaughan-Jones, R.D., and Harris, A.L. (2010). New insights into the physiological role of carbonic anhydrase IX in tumour pH regulation. Oncogene *29*, 6509-6521.
Tchou, J., Sonnad, S.S., Bergey, M.R., Basu, S., Tomaszewski, J., Alavi, A., and Schnall, M. (2010). Degree of tumor FDG uptake correlates with proliferation index in triple negative breast cancer. Mol Imaging Biol *12*, 657-662.
Telang, S., Yalcin, A., Clem, A.L., Bucala, R., Lane, A.N., Eaton, J.W., and Chesney, J. (2006). Ras transformation requires metabolic control by 6-phosphofructo-2-kinase. Oncogene *25*, 7225-7234.
Tennant, D.A., Duran, R.V., and Gottlieb, E. (2010). Targeting metabolic transformation for cancer therapy. Nat Rev Cancer *10*, 267-277.
Thompson, C.B., Bauer, D.E., Lum, J.J., Hatzivassiliou, G., Zong, W.X., Zhao, F., Ditsworth, D., Buzzai, M., and Lindsten, T. (2005). How do cancer cells acquire the fuel needed to support cell growth? Cold Spring Harb Symp Quant Biol *70*, 357-362.
Tomonaga, T., Matsushita, K., Yamaguchi, S., Oh-Ishi, M., Kodera, Y., Maeda, T., Shimada, H., Ochiai, T., and Nomura, F. (2004). Identification of altered protein expression and post-translational modifications in primary colorectal cancer by using agarose two-dimensional gel electrophoresis. Clin Cancer Res *10*, 2007-2014.
Tong, X., Zhao, F., and Thompson, C.B. (2009). The molecular determinants of de novo nucleotide biosynthesis in cancer cells. Curr Opin Genet Dev *19*, 32-37.
Toyoshima, M., Howie, H.L., Imakura, M., Walsh, R.M., Annis, J.E., Chang, A.N., Frazier, J., Chau, B.N., Loboda, A., Linsley, P.S.*, et al.* (2012). Functional genomics identifies therapeutic targets for MYC-driven cancer. Proc Natl Acad Sci U S A *109*, 9545-9550.

Tsunematsu, K., Yokota, S., and Shiraishi, T. (1968). Changes in aldolase isozyme patterns of human cancerous tissues. Gann *59*, 415-419.
Ullah, M.S., Davies, A.J., and Halestrap, A.P. (2006). The plasma membrane lactate transporter MCT4, but not MCT1, is up-regulated by hypoxia through a HIF-1alpha-dependent mechanism. J Biol Chem *281*, 9030-9037.
Vander Heiden, M.G. (2010). Targeting cell metabolism in cancer patients. Sci Transl Med *2*, 31ed31.
Vander Heiden, M.G. (2011). Targeting cancer metabolism: a therapeutic window opens. Nat Rev Drug Discov *10*, 671-684.
Vander Heiden, M.G., Cantley, L.C., and Thompson, C.B. (2009). Understanding the Warburg effect: the metabolic requirements of cell proliferation. Science *324*, 1029-1033.
Vander Heiden, M.G., Lunt, S.Y., Dayton, T.L., Fiske, B.P., Israelsen, W.J., Mattaini, K.R., Vokes, N.I., Stephanopoulos, G., Cantley, L.C., Metallo, C.M*., et al.* (2011). Metabolic pathway alterations that support cell proliferation. Cold Spring Harb Symp Quant Biol *76*, 325-334.
Vander Heiden, M.G., Lunt, S.Y., Dayton, T.L., Fiske, B.P., Israelsen, W.J., Mattaini, K.R., Vokes, N.I., Stephanopoulos, G., Cantley, L.C., Metallo, C.M*., et al.* (2012). Metabolic Pathway Alterations that Support Cell Proliferation. Cold Spring Harb Symp Quant Biol.
Vanhaesebroeck, B., Guillermet-Guibert, J., Graupera, M., and Bilanges, B. (2010). The emerging mechanisms of isoform-specific PI3K signalling. Nat Rev Mol Cell Biol *11*, 329-341.
Vaupel, P., Hockel, M., and Mayer, A. (2007). Detection and characterization of tumor hypoxia using pO2 histography. Antioxid Redox Signal *9*, 1221-1235.
Vaupel, P., Kallinowski, F., and Okunieff, P. (1989). Blood flow, oxygen and nutrient supply, and metabolic microenvironment of human tumors: a review. Cancer Res *49*, 6449-6465.
Vegran, F., Boidot, R., Michiels, C., Sonveaux, P., and Feron, O. (2011). Lactate influx through the endothelial cell monocarboxylate transporter MCT1 supports an NF-kappaB/IL-8 pathway that drives tumor angiogenesis. Cancer Res *71*, 2550-2560.
Vichai, V., and Kirtikara, K. (2006). Sulforhodamine B colorimetric assay for cytotoxicity screening. Nat Protoc *1*, 1112-1116.
Volker, H.U., Hagemann, C., Coy, J., Wittig, R., Sommer, S., Stojic, J., Haubitz, I., Vince, G.H., Kammerer, U., and Monoranu, C.M. (2008). Expression of transketolase-like 1 and activation of Akt in grade IV glioblastomas compared with grades II and III astrocytic gliomas. Am J Clin Pathol *130*, 50-57.
Vousden, K.H., and Ryan, K.M. (2009). p53 and metabolism. Nat Rev Cancer *9*, 691-700.
Waggoner, D.W., Xu, J., Singh, I., Jasinska, R., Zhang, Q.X., and Brindley, D.N. (1999). Structural organization of mammalian lipid phosphate phosphatases: implications for signal transduction. Biochim Biophys Acta *1439*, 299-316.
Waingeh, V.F., Gustafson, C.D., Kozliak, E.I., Lowe, S.L., Knull, H.R., and Thomasson, K.A. (2006). Glycolytic enzyme interactions with yeast and skeletal muscle F-actin. Biophys J *90*, 1371-1384.
Walker, R.A., and Dearing, S.J. (1999). Expression of epidermal growth factor receptor mRNA and protein in primary breast carcinomas. Breast Cancer Res Treat *53*, 167-176.

Wang, G.L., and Semenza, G.L. (1995). Purification and characterization of hypoxia-inducible factor 1. J Biol Chem *270*, 1230-1237.
Wang, J., Morris, A.J., Tolan, D.R., and Pagliaro, L. (1996). The molecular nature of the F-actin binding activity of aldolase revealed with site-directed mutants. J Biol Chem *271*, 6861-6865.
Wang, J., Tolan, D.R., and Pagliaro, L. (1997). Metabolic compartmentation in living cells: structural association of aldolase. Exp Cell Res *237*, 445-451.
Warburg, O. (1956). On the origin of cancer cells. Science *123*, 309-314.
Warburg, O., Wind, F., and Negelein, E. (1927). The Metabolism of Tumors in the Body. J Gen Physiol *8*, 519-530.
Ward, C., Langdon, S.P., Mullen, P., Harris, A.L., Harrison, D.J., Supuran, C.T., and Kunkler, I.H. (2013). New strategies for targeting the hypoxic tumour microenvironment in breast cancer. Cancer Treat Rev *39*, 171-179.
Weigelt, B., Warne, P.H., and Downward, J. (2011). PIK3CA mutation, but not PTEN loss of function, determines the sensitivity of breast cancer cells to mTOR inhibitory drugs. Oncogene *30*, 3222-3233.
Weinstein, I.B., and Joe, A. (2008). Oncogene addiction. Cancer Res *68*, 3077-3080; discussion 3080.
Whitaker-Menezes, D., Martinez-Outschoorn, U.E., Lin, Z., Ertel, A., Flomenberg, N., Witkiewicz, A.K., Birbe, R.C., Howell, A., Pavlides, S., Gandara, R.*, et al.* (2011). Evidence for a stromal-epithelial "lactate shuttle" in human tumors: MCT4 is a marker of oxidative stress in cancer-associated fibroblasts. Cell Cycle *10*, 1772-1783.
Wiederschain, D., Wee, S., Chen, L., Loo, A., Yang, G., Huang, A., Chen, Y., Caponigro, G., Yao, Y.M., Lengauer, C.*, et al.* (2009). Single-vector inducible lentiviral RNAi system for oncology target validation. Cell Cycle *8*, 498-504.
Wilson, W.R., and Hay, M.P. (2011). Targeting hypoxia in cancer therapy. Nat Rev Cancer *11*, 393-410.
Wise, D.R., DeBerardinis, R.J., Mancuso, A., Sayed, N., Zhang, X.Y., Pfeiffer, H.K., Nissim, I., Daikhin, E., Yudkoff, M., McMahon, S.B.*, et al.* (2008). Myc regulates a transcriptional program that stimulates mitochondrial glutaminolysis and leads to glutamine addiction. Proc Natl Acad Sci U S A *105*, 18782-18787.
Wise, D.R., and Thompson, C.B. (2010). Glutamine addiction: a new therapeutic target in cancer. Trends Biochem Sci *35*, 427-433.
Wolf, A., Agnihotri, S., Micallef, J., Mukherjee, J., Sabha, N., Cairns, R., Hawkins, C., and Guha, A. (2011). Hexokinase 2 is a key mediator of aerobic glycolysis and promotes tumor growth in human glioblastoma multiforme. J Exp Med *208*, 313-326.
Wolf, K., and Friedl, P. (2009). Mapping proteolytic cancer cell-extracellular matrix interfaces. Clin Exp Metastasis *26*, 289-298.
Xing, F., Saidou, J., and Watabe, K. (2010). Cancer associated fibroblasts (CAFs) in tumor microenvironment. Front Biosci *15*, 166-179.
Xu, W., Yang, H., Liu, Y., Yang, Y., Wang, P., Kim, S.H., Ito, S., Yang, C., Xiao, M.T., Liu, L.X.*, et al.* (2011). Oncometabolite 2-hydroxyglutarate is a competitive inhibitor of alpha-ketoglutarate-dependent dioxygenases. Cancer Cell *19*, 17-30.
Xu, X., Zur Hausen, A., Coy, J.F., and Lochelt, M. (2009). Transketolase-like protein 1 (TKTL1) is required for rapid cell growth and full viability of human tumor cells. Int J Cancer *124*, 1330-1337.

Yahagi, N., Shimano, H., Hasegawa, K., Ohashi, K., Matsuzaka, T., Najima, Y., Sekiya, M., Tomita, S., Okazaki, H., Tamura, Y.*, et al.* (2005). Co-ordinate activation of lipogenic enzymes in hepatocellular carcinoma. Eur J Cancer *41*, 1316-1322.
Yamada, K.M., and Cukierman, E. (2007). Modeling tissue morphogenesis and cancer in 3D. Cell *130*, 601-610.
Yamamoto, T., Seino, Y., Fukumoto, H., Koh, G., Yano, H., Inagaki, N., Yamada, Y., Inoue, K., Manabe, T., and Imura, H. (1990). Over-expression of facilitative glucose transporter genes in human cancer. Biochem Biophys Res Commun *170*, 223-230.
Yan, H., Parsons, D.W., Jin, G., McLendon, R., Rasheed, B.A., Yuan, W., Kos, I., Batinic-Haberle, I., Jones, S., Riggins, G.J.*, et al.* (2009). IDH1 and IDH2 mutations in gliomas. N Engl J Med *360*, 765-773.
Yarden, Y., and Pines, G. (2012). The ERBB network: at last, cancer therapy meets systems biology. Nat Rev Cancer *12*, 553-563.
Yarden, Y., and Sliwkowski, M.X. (2001). Untangling the ErbB signalling network. Nat Rev Mol Cell Biol *2*, 127-137.
Yi, W., Clark, P.M., Mason, D.E., Keenan, M.C., Hill, C., Goddard, W.A., 3rd, Peters, E.C., Driggers, E.M., and Hsieh-Wilson, L.C. (2012). Phosphofructokinase 1 glycosylation regulates cell growth and metabolism. Science *337*, 975-980.
Yoon, S., Lee, M.Y., Park, S.W., Moon, J.S., Koh, Y.K., Ahn, Y.H., Park, B.W., and Kim, K.S. (2007). Up-regulation of acetyl-CoA carboxylase alpha and fatty acid synthase by human epidermal growth factor receptor 2 at the translational level in breast cancer cells. J Biol Chem *282*, 26122-26131.
Yoshii, Y., Furukawa, T., Yoshii, H., Mori, T., Kiyono, Y., Waki, A., Kobayashi, M., Tsujikawa, T., Kudo, T., Okazawa, H.*, et al.* (2009). Cytosolic acetyl-CoA synthetase affected tumor cell survival under hypoxia: the possible function in tumor acetyl-CoA/acetate metabolism. Cancer Sci *100*, 821-827.
Yoshimura, H., Dhar, D.K., Kohno, H., Kubota, H., Fujii, T., Ueda, S., Kinugasa, S., Tachibana, M., and Nagasue, N. (2004). Prognostic impact of hypoxia-inducible factors 1alpha and 2alpha in colorectal cancer patients: correlation with tumor angiogenesis and cyclooxygenase-2 expression. Clin Cancer Res *10*, 8554-8560.
Yuan, W., Wu, S., Guo, J., Chen, Z., Ge, J., Yang, P., and Hu, B. (2010). Silencing of TKTL1 by siRNA inhibits proliferation of human gastric cancer cells in vitro and in vivo. Cancer Biol Ther *9*, 710-716.
Yue, J., Yokoyama, K., Balazs, L., Baker, D.L., Smalley, D., Pilquil, C., Brindley, D.N., and Tigyi, G. (2004). Mice with transgenic overexpression of lipid phosphate phosphatase-1 display multiple organotypic deficits without alteration in circulating lysophosphatidate level. Cell Signal *16*, 385-399.
Yuneva, M., Zamboni, N., Oefner, P., Sachidanandam, R., and Lazebnik, Y. (2007). Deficiency in glutamine but not glucose induces MYC-dependent apoptosis in human cells. J Cell Biol *178*, 93-105.
Yuneva, M.O., Fan, T.W., Allen, T.D., Higashi, R.M., Ferraris, D.V., Tsukamoto, T., Mates, J.M., Alonso, F.J., Wang, C., Seo, Y.*, et al.* (2012). The metabolic profile of tumors depends on both the responsible genetic lesion and tissue type. Cell Metab *15*, 157-170.
Zhang, H., Gao, P., Fukuda, R., Kumar, G., Krishnamachary, B., Zeller, K.I., Dang, C.V., and Semenza, G.L. (2007a). HIF-1 inhibits mitochondrial biogenesis and cellular respiration in VHL-deficient renal cell carcinoma by repression of C-MYC activity. Cancer Cell *11*, 407-420.

Zhang, N., Sundberg, J.P., and Gridley, T. (2000). Mice mutant for Ppap2c, a homolog of the germ cell migration regulator wunen, are viable and fertile. Genesis *27*, 137-140.
Zhang, S., Yang, J.H., Guo, C.K., and Cai, P.C. (2007b). Gene silencing of TKTL1 by RNAi inhibits cell proliferation in human hepatoma cells. Cancer Lett *253*, 108-114.
Zhao, J.J., Liu, Z., Wang, L., Shin, E., Loda, M.F., and Roberts, T.M. (2005). The oncogenic properties of mutant p110alpha and p110beta phosphatidylinositol 3-kinases in human mammary epithelial cells. Proc Natl Acad Sci U S A *102*, 18443-18448.
Zhong, H., De Marzo, A.M., Laughner, E., Lim, M., Hilton, D.A., Zagzag, D., Buechler, P., Isaacs, W.B., Semenza, G.L., and Simons, J.W. (1999). Overexpression of hypoxia-inducible factor 1alpha in common human cancers and their metastases. Cancer Res *59*, 5830-5835.
Ziment, I. (1988). Acetylcysteine: a drug that is much more than a mucokinetic. Biomed Pharmacother *42*, 513-519.
Zuber, J., Shi, J., Wang, E., Rappaport, A.R., Herrmann, H., Sison, E.A., Magoon, D., Qi, J., Blatt, K., Wunderlich, M.*, et al.* (2011). RNAi screen identifies Brd4 as a therapeutic target in acute myeloid leukaemia. Nature *478*, 524-528.
Zwerschke, W., Mazurek, S., Massimi, P., Banks, L., Eigenbrodt, E., and Jansen-Durr, P. (1999). Modulation of type M2 pyruvate kinase activity by the human papillomavirus type 16 E7 oncoprotein. Proc Natl Acad Sci U S A *96*, 1291-1296.